



**HAL**  
open science

# Biodiversity of the marine ecosystem and carbon flux around Kerguelen (Southern Ocean) : role of small phytoplankton at the single cell level

Solène Irion

► **To cite this version:**

Solène Irion. Biodiversity of the marine ecosystem and carbon flux around Kerguelen (Southern Ocean) : role of small phytoplankton at the single cell level. Biodiversity. Université du Littoral Côte d'Opale, 2020. English. NNT : 2020DUNK0570 . tel-03178263

**HAL Id: tel-03178263**

**<https://theses.hal.science/tel-03178263v1>**

Submitted on 23 Mar 2021

**HAL** is a multi-disciplinary open access archive for the deposit and dissemination of scientific research documents, whether they are published or not. The documents may come from teaching and research institutions in France or abroad, or from public or private research centers.

L'archive ouverte pluridisciplinaire **HAL**, est destinée au dépôt et à la diffusion de documents scientifiques de niveau recherche, publiés ou non, émanant des établissements d'enseignement et de recherche français ou étrangers, des laboratoires publics ou privés.

Présentée par

**Solène Irion**

Pour l'obtention du grade de :  
Docteur de l'Université du Littoral Côte d'Opale

École doctorale : Sciences de la Matière, du Rayonnement et de l'Environnement (ED SMRE, 104)  
Discipline: Agronomie, productions animale et végétale, agroalimentaire. Biologie de l'environnement, des populations, écologie.

Unité de Recherche : Laboratoire d'Océanologie et de Géosciences

---

**Biodiversité de l'écosystème marin et flux de carbone autour de Kerguelen  
(océan Austral): le rôle du petit phytoplancton à l'échelle de la cellule**

**Biodiversity of the marine ecosystem and carbon flux around Kerguelen  
(Southern Ocean): role of small phytoplankton at the single cell level**

---

Soutenance prévue le 19 novembre 2020 devant le jury composé de :

**Pr. Aud Larsen**

Research director (Molecular Biology), NORCE  
Professor, University of Bergen / rapporteuse

**Pr. David Scanlan**

Professor, University of Warwick / rapporteur

**Dr. Ingrid Obernosterer**

DR CNRS, Laboratoire d'Océanographie Microbienne (LOMIC) / examinatrice

**Pr. Sébastien Monchy**

PR ULCO, Laboratoire d'Océanologie et de Géosciences (LOG) / examinateur

**Dr. David Moreira**

DR CNRS, Laboratoire d'Ecologie, Systématique Evolution (ESE) / examinateur

**Pr. Urania Christaki**

PR ULCO, Laboratoire d'Océanologie et de Géosciences (LOG) / directrice de thèse

**Pr. Ludwig Jardillier**

PR Université Paris-Saclay, Laboratoire d'Ecologie, Systématique Evolution (ESE) / directeur de thèse



## Remerciements

Cette thèse a été menée au Laboratoire d'Océanologie et de Géosciences (Wimereux) et financée par l'Université du Littoral Côte d'Opale, la Région Hauts-de-France et le projet MOBYDICK (LEFE-CYBER 2017-2018, ANR 2018-2021).

Mes premiers remerciements s'adressent à mes deux directeurs de thèse. Merci pour la qualité scientifique de votre encadrement, vous avez écrit un projet de thèse novateur et ambitieux qui m'a immédiatement séduite. Merci pour la confiance que vous m'avez accordée, vous avez su m'accompagner avec bienveillance.

Merci à Hugo pour tes précieux conseils et ta bonne humeur lors des sessions NanoSIMS ; sans tes compétences, la partie NanoSIMS aurait été bien plus laborieuse.

Merci à l'équipe du LOG, en particulier à Ingrid et Ioli avec lesquelles j'ai toujours pris plaisir à travailler et discuter.

Merci à tous les participants à la campagne MOBYDICK, qui ont été d'une grande aide en mer et ont permis de partager un jeu de données de qualité. Je tiens à remercier en particulier Céline Dimer, qui a réalisé tous les prélèvements et traitements en laboratoire pour les analyses HPLC. Merci également à Bernard Quéguiner et Ingrid Obernosterer pour avoir porté le projet MOBYDICK.

Merci à toute l'équipe de l'ESE, qui m'a toujours accueillie chaleureusement, tout particulièrement à Purificación López-García et David Moreira pour avoir mis l'équipement de la plateforme UNICELL à ma disposition, ainsi qu'à Paola Bertolino, Hélène Timpano et Maria Ciobanu dont l'aide m'a été précieuse pour me former à la préparation des bibliothèques de séquençage ou dans l'utilisation du cytomètre en flux.

Merci à Peter Magee pour les relectures et corrections des manuscrits en anglais.

Merci à mes stagiaires, Océane et Sébastien pour m'avoir aidée dans les comptages FISH et dans l'analyse de certaines images NanoSIMS.

Enfin, merci à tous mes proches sans qui cette thèse n'aurait pas été possible. Merci notamment à toutes les personnes qui ont pris soin de mon fils, Léandre, quand je n'étais pas disponible. Vous m'avez permis de profiter pleinement de cette expérience enrichissante, je vous en suis infiniment reconnaissante.

## Résumé

Cette thèse s'intéresse à la diversité du petit phytoplancton ( $<20 \mu\text{m}$ ) et à sa contribution à la fixation du carbone dans des écosystèmes marins contrastés : la région productive du plateau de Kerguelen d'une part et les zones à faible productivité en dehors du plateau, d'autre part. Le petit phytoplancton domine les communautés phytoplanctoniques tout au long de l'année en dehors du plateau, où les faibles concentrations en fer limitent la production primaire. Le plateau de Kerguelen, naturellement fertilisé en fer, est quant à lui caractérisé par le développement au printemps-été de blooms massifs de diatomées en chaîne et de grande taille. Depuis la découverte du mécanisme de fertilisation naturelle en fer sur le plateau, l'attention de la communauté scientifique s'est focalisée sur les diatomées de grande taille, qui favoriseraient la séquestration du carbone sur la zone. Toutefois, les données satellitaires suggéraient que le petit phytoplancton dominait les communautés phytoplanctoniques en dehors du bloom sur l'ensemble de la zone.

Le premier objectif de ce travail visait à obtenir une image fine de la diversité du petit et grand phytoplancton après le bloom de diatomées (Mars 2018). Un fragment de l'ADNr 18S des communautés planctoniques de petite ( $0.2\text{-}20 \mu\text{m}$ ) et grande taille ( $20\text{-}100 \mu\text{m}$ ), collectées à plusieurs profondeurs, a été séquencé par la méthode Illumina MiSeq. Les séquences ainsi obtenues ont permis de déterminer la diversité taxonomique moléculaire du petit et grand phytoplancton. En surface, les diatomées étaient majoritaires dans la grande fraction de taille tandis que *Phaeocystis antarctica* était particulièrement important dans la petite fraction sur l'ensemble de la zone d'étude. Dans leur ensemble, les communautés de petit phytoplancton différaient sur et en dehors du plateau. Des concentrations élevées en acide silicique en dehors du plateau favorisaient la présence d'un assemblage varié de diatomées de petite taille, tandis que de fortes concentrations en ammonium sur le plateau pourraient favoriser le développement de picophytoplancton du genre *Micromonas*. L'utilisation de marqueurs pigmentaires chémotaxonomiques a permis de décrire la succession temporelle des communautés phytoplanctoniques sur le plateau, dominées par les diatomées du début au déclin du bloom, tandis que la contribution du petit phytoplancton augmentait fortement après le bloom (moins de 10% à 53% de la chlorophylle).

Le deuxième objectif de cette thèse était d'établir la contribution relative de différents groupes phytoplanctoniques à la fixation globale de carbone, en prenant en compte les différences inter- et intra-groupe dans l'activité métabolique de cellules individuelles. Pour ce faire, des communautés planctoniques naturelles ont été incubées en présence d'un traceur isotopique ( $\text{NaH}^{13}\text{CO}_3$ ) en reproduisant les conditions *in situ*. La fixation du carbone au niveau cellulaire a été mesurée par imagerie NanoSIMS et SIMS. Les grandes diatomées ( $> 20 \mu\text{m}$ ) montraient des taux de croissance faibles et variables d'une cellule à l'autre, avec  $19 \pm 13\%$  de diatomées inactives. Inversement, les petites cellules, appartenant à des taxons phylogénétiques éloignés (prymnesiophytes, prasinophytes et petites diatomées) étaient majoritairement en croissance active ( $>98\%$ ). Par conséquent, le petit phytoplancton contribuait de 41 à 70% à la fixation du carbone sur l'ensemble de la zone après le bloom.

Tandis que le petit phytoplancton contribuait de façon importante à la fixation de carbone et à la biomasse chlorophyllienne en surface, les diatomées dominaient dans les données pigmentaires et de séquençage en dessous de 200 m, indiquant leur export préférentiel par sédimentation directe. Cependant, un faisceau d'indices suggère que le phytoplancton de petite taille, en particulier *Phaeocystis*, pourrait participer à l'export de carbone par agrégation, ainsi que via les réseaux trophiques et la production de pelotes fécales des brouteurs.

## Abstract

This thesis focuses on small phytoplankton diversity (<20  $\mu\text{m}$ ) and its contribution to  $\text{CO}_2$ -fixation in contrasted marine ecosystems: the productive Kerguelen Plateau (KP) on the one hand and low productive surrounding waters on the other hand. Iron-limited phytoplankton communities off-plateau are dominated by small cells all year long, whereas natural iron-fertilization over the KP promotes the seasonal development of chain-forming or large diatom blooms in spring and summer. Since the demonstration of natural iron fertilization on-plateau, the scientific community focused on large diatoms, assumed to promote carbon sequestration in the area. However, satellite data suggest that small phytoplankton dominate the phytoplankton communities outside of the bloom period on- and off-plateau. Consequently, this thesis had two main objectives.

The first objective of this work was to obtain a precise image of the diversity of small and large phytoplankton after the diatom bloom (March 2018). A fragment of the 18S rRNA gene from small (0.2-20  $\mu\text{m}$ ) and large (20-100  $\mu\text{m}$ ) planktonic communities collected at discrete depths (down to 300 m), was sequenced (Illumina MiSeq) and used as an identity marker gene to determine the taxonomic diversity of small and large phytoplankton. At the surface, diatoms were dominant in the large-size fraction, while *Phaeocystis antarctica* was particularly abundant in the small-size fraction, over the entire study area. As a whole, small phytoplankton communities were significantly different on- and off- plateau. High concentrations of silicic acid off-plateau favored the presence of a diverse assemblage of small diatoms, while high concentrations of ammonium on-plateau likely promoted the development of pico-sized *Micromonas*. Using chemotaxonomic pigments markers allowed the description of the temporal succession of phytoplankton communities on-plateau, dominated by diatoms from the onset to the decline of the bloom, while the contribution of small phytoplankton increased sharply after the bloom (less than 10% to 53% chlorophyll).

The second objective of this thesis was to establish the relative contribution of different phytoplankton groups to bulk  $\text{CO}_2$ -fixation, considering inter- and intra-group differences in the metabolic activity of individual cells. To do so, natural planktonic communities were incubated mimicking *in situ* conditions in the presence of an isotopic tracer ( $\text{NaH}^{13}\text{CO}_3$ ).  $\text{CO}_2$ -fixation by small and large cells was then measured at the single cell level by NanoSIMS and SIMS imaging (mass spectrometry with lateral resolution of 50 nm and 1  $\mu\text{m}$ , respectively). Large diatoms (> 20  $\mu\text{m}$ ) showed highly variable growth rates with  $19 \pm 13\%$  inactive diatoms, whereas small cells, affiliated to distant phylogenetic taxa (prymnesiophytes, prasinophytes and small diatoms) were actively growing (> 98%). This showed that small phytoplankton contributed to 41-70% of  $\text{CO}_2$ -fixation over the entire area after the bloom.

While small phytoplankton contributed significantly to  $\text{CO}_2$ -fixation and chlorophyll biomass at the surface, diatoms dominated in pigment and sequencing data below 200 m, indicating their preferential export by direct sedimentation. However, a body of evidence suggests that small phytoplankton, in particular *Phaeocystis*, may contribute to carbon export through aggregation, as well as via the production of fecal pellets from grazers.

## Table of contents

<b>RESUME DETAILLE EN FRANÇAIS .....</b>	<b>5</b>
<b><u>A. INTRODUCTION.....</u></b>	<b>17</b>
<b>1. PHYTOPLANKTON DIVERSITY.....</b>	<b>18</b>
1.1 EVOLUTION AND DIVERSITY OF PHYTOPLANKTON.....	18
1.2 ECOLOGICAL TRAITS OF SMALL AND LARGE PHYTOPLANKTON CELLS .....	19
1.3 PHYTOPLANKTON DIVERSITY IN THE SOUTHERN OCEAN.....	21
<b>2. PHYTOPLANKTON IN THE CARBON CYCLE .....</b>	<b>27</b>
2.1 THE BIOLOGICAL CARBON PUMP (BCP) .....	27
2.2 IMPACT OF PHYTOPLANKTON COMMUNITY SIZE STRUCTURE ON THE BCP .....	27
2.3 PREDICTED INCREASE IN SMALL PHYTOPLANKTON DOMINATED COMMUNITIES .....	29
<b>3. SOUTHERN OCEAN PHYTOPLANKTON AND THE C-CYCLE.....</b>	<b>30</b>
3.1 CONTROL OF SOUTHERN OCEAN PRODUCTIVITY.....	30
3.2 IMPACT OF FE-FERTILIZATION ON PHYTOPLANKTON COMMUNITIES AND C-EXPORT .....	31
3.3 INVERSE RELATIONSHIP BETWEEN PRIMARY PRODUCTION AND EXPORT .....	33
<b>4. SCIENTIFIC CONTEXT AND PHD OBJECTIVES .....</b>	<b>34</b>
4.1 OCEANIC CIRCULATION IN THE STUDY AREA.....	34
4.2 KEOPS AND MOBYDICK CUISES.....	34
4.3 PHD OBJECTIVES.....	36
<b><u>B. MATERIAL AND METHODS.....</u></b>	<b>37</b>
<b>1. DESCRIPTION OF SMALL PHYTOPLANKTON COMMUNITY COMPOSITION.....</b>	<b>37</b>
1.1 MOLECULAR EXPLORATION OF SMALL PHYTOPLANKTON DIVERSITY WITH 18S rDNA METABARCODING.....	38
1.2 CARD-FISH.....	41
1.3 CHEMOTAXONOMY .....	42
<b>2. CONTRIBUTION OF SPECIFIC GROUPS OF SMALL PHYTOPLANKTON TO CO<sub>2</sub>-FIXATION.....</b>	<b>43</b>
2.1 INCUBATION WITH CARBON ISOTOPES: PRINCIPLES AND LIMITATIONS.....	43
2.2 GROUP SPECIFIC CO <sub>2</sub> -FIXATION .....	44
2.3 CELL-SPECIFIC CO <sub>2</sub> -FIXATION.....	45
<b><u>C. RESULTS.....</u></b>	<b>47</b>
<b>1. SMALL PHYTOPLANKTON DIVERSITY AROUND KERGUELEN .....</b>	<b>47</b>
PAPER 1: MARKED SPATIOTEMPORAL VARIATIONS IN SMALL PHYTOPLANKTON STRUCTURE IN CONTRASTED WATERS OF THE SOUTHERN OCEAN (KERGUELEN AREA) .....	49
62	
PERSPECTIVES.....	73
APPENDIX.....	76
<b>2. CO<sub>2</sub>-FIXATION BY SMALL PHYTOPLANKTON AROUND KERGUELEN.....</b>	<b>80</b>
INTRODUCTION .....	80
PAPER 2: SMALL PHYTOPLANKTON CONTRIBUTE GREATLY TO CO <sub>2</sub> -FIXATION AFTER THE DIATOM BLOOM IN THE SOUTHERN OCEAN .....	81
PERSPECTIVES.....	115

<b>D. SUMMARY AND DISCUSSION.....</b>	<b>117</b>
1. FIRST INSIGHTS INTO SMALL PHYTOPLANKTON DIVERSITY AROUND KERGUELEN.....	118
2. SEASONALITY AND INTERANNUAL VARIABILITY OF PHYTOPLANKTON COMMUNITIES AROUND KERGUELEN.....	121
2.1. SEASONAL SUCCESSION FROM DIATOMS TO SMALL NON-SILICIFIED CELLS.....	121
2.2. INTERANNUAL VARIABILITY OF THE DIATOM BLOOM.....	123
2.3. ECOLOGICAL CONSEQUENCES OF A SHIFT TOWARDS SMALLER CELLS.....	123
3. IMPACT OF SURFACE PHYTOPLANKTON COMMUNITY STRUCTURE AND PRODUCTIVITY REGIME ON THE BIOLOGICAL CARBON PUMP .....	124
4. OUTLOOK FOR FUTURE STUDIES ON THE ROLE OF SMALL PHYTOPLANKTON IN THE MARINE C-CYCLE.....	129
 <b>RELATED PAPERS AS CO-AUTHOR.....</b>	 <b>132</b>
 <b>PAPER 3: MICROZOOPLANKTON DIVERSITY AND ROLE IN CARBON CYCLE IN CONTRASTING SOUTHERN OCEAN PRODUCTIVITY REGIMES (CHRISTAKI ET AL., SUBMITTED TO JOURNAL OF MARINE SYSTEMS).....</b>	 <b>133</b>
135	
<b>PAPER 4: PROTIST INTERACTIONS AND COMMUNITY STRUCTURE DURING EARLY AUTUMN IN THE KERGUELEN REGION (SOUTHERN OCEAN) (SASSENHAGEN ET AL., 2020).....</b>	<b>174</b>
175	
<b>PAPER 5: SEASONAL MICROBIAL FOOD WEB DYNAMICS IN CONTRASTING SOUTHERN OCEAN PRODUCTIVITY REGIMES (CHRISTAKI ET AL., 2020) .....</b>	<b>199</b>
 <b>REFERENCES .....</b>	 <b>214</b>



## Résumé détaillé en français

### Introduction

#### 1. La diversité du phytoplancton

Les organismes phytoplanctoniques sont des microbes photoautotrophes qui vivent dans la couche euphotique des eaux douces ou des milieux marins. Au cours de la photosynthèse oxygénique, ils utilisent l'énergie lumineuse pour convertir le carbone inorganique en molécules de carbone organique riches en énergie. Ainsi, ils modulent activement les concentrations atmosphériques de dioxyde de carbone et d'oxygène. Le phytoplancton est composé d'une large gamme de taxons, des cyanobactéries aux eucaryotes, dont la taille varie considérablement (<1 à >100  $\mu\text{m}$ ), avec des représentants dans 4 des 6 super-groupes de l'arbre de vie eucaryote décrit par Adl et al. (2005) (Fig. A2). Les diversités phylogénétique, de taille et de métabolisme des communautés de phytoplancton affectent la structure du réseau trophique et le cycle biogéochimique du carbone dans les océans.

Historiquement, 4 000 à 25 000 espèces de phytoplancton ont été décrites par observation morphologique au microscope (Sournia et al., 1991 ; Falkowski, 2004). Ce nombre sous-estime probablement largement l'étendue réelle de la diversité du phytoplancton et les approches moléculaires basées sur le séquençage du gène ARNr 18S ont révélé que le nombre réel de taxons de phytoplancton est systématiquement environ 10 fois plus élevé que les estimations basées sur la morphologie (Pierella Karlusich et al., 2020). Compte tenu de l'étendue de la complexité liée à l'évaluation de la diversité taxonomique du phytoplancton, le phytoplancton est souvent classé en fonction de la taille des cellules. La taille des cellules du phytoplancton s'étend sur au moins 9 ordres de grandeur, d'un volume cellulaire d'environ 0,1  $\mu\text{m}^3$  pour les plus petites cyanobactéries à plus de 10<sup>8</sup>  $\mu\text{m}^3$  pour les plus grandes diatomées (Fig. A3).

La taille des cellules de phytoplancton est un critère très utile à la modélisation des cycles biogéochimiques, car les processus de croissance et de mortalité du phytoplancton dépendent fortement de la taille (Marañón et al., 2009). Schématiquement, on considère que les petites cellules phytoplanctoniques sont avantagées par rapport aux grandes pour l'acquisition de la lumière et des nutriments grâce à des ratios surface/volume avantageux. Inversement, la grande taille de certaines cellules leur offrirait une meilleure défense, au moins de façon temporaire, contre les brouteurs microzooplanctoniques. Ces principes généraux de croissance et mortalité déterminent la structure de taille des communautés phytoplanctoniques et expliquent la dominance globale du petit phytoplancton dans les eaux tropicales oligotrophes, à l'inverse des cellules plus grandes, qui tendent à dominer la biomasse dans les upwellings ou les eaux côtières riches en nutriments (Fig. A4).

Au sein du phytoplancton de petite et grande taille, les différentes lignées taxonomiques sont caractérisées par des traits écologiques particuliers (sensibilité à la qualité de la luminosité reçue, qualité/quantité des nutriments nécessaires à la croissance, mécanismes défensifs face aux prédateurs, pour n'en citer que quelques-uns Glibert, 2016). Par conséquent, les groupes de phytoplancton présentent des différences dans leurs niches écologiques (Brun et al., 2015). L'océan Austral abrite des communautés phytoplanctoniques généralement dominées par le pico- et le nanophytoplancton eucaryote, auxquels se superposent ponctuellement des blooms de diatomées et colonies de *Phaeocystis* (haptophyte) (par exemple, Wright et al., 2010 ; Wolf et al., 2014). Les grandes diatomées, du fait de leur capacité à former des blooms très productifs ont été considérées comme le groupe phytoplanctonique le plus important pour la production primaire de l'océan Austral. Cependant, le petit phytoplancton semble contribuer davantage à la production primaire en dehors des blooms de diatomées, notamment en hiver (Fig. A5). De nombreuses incertitudes et controverses persistent sur la composition et la contribution respective du petit et grand phytoplancton à la production primaire dans l'océan Austral. Les mesures *in situ* sont ponctuelles et restreintes à certaines zones du fait de l'éloignement de cet océan. Par ailleurs, les observations satellite sont souvent rendues impossibles par la couverture nuageuse persistante, ce qui conduit à des données hivernales rares (Losa et al., 2019). Parmi les taxons les plus importants du petit phytoplancton de l'océan Austral, les haptophytes, les petites diatomées, les cryptophytes et, dans une moindre mesure, les prasinophytes ont été décrits comme des acteurs clés des communautés phytoplanctoniques (Moline et al., 2004 ; Uitz et al., 2009 ; Georges et al., 2014 ; Iida et Odate, 2014). L'identification précise des genres représentatifs importants au sein de ces grands groupes taxonomiques, ainsi que des facteurs écologiques responsables de leur succès, est toutefois rare.

Les grandes cellules phytoplanctoniques sont principalement représentées par les diatomées, dont la croissance est favorisée par d'importantes concentrations en fer dissous, acide silicique et une stratification élevée de la colonne d'eau (Arrigo et al., 2010 ; Mills et al., 2010). Parmi le petit phytoplancton, les haptophytes, dont *Phaeocystis antarctica*, dominent parfois la biomasse phytoplanctonique. Sa capacité à croître à faible luminosité lui permet de se développer tôt dans la saison ou sous la glace de mer (Peperzak et al., 1998 ; Hilst et Jr, 2002 ; Boyd et al., 2010). *P. antarctica* bénéficie également de constantes de demi-saturation en fer plus faibles que les diatomées (Alderkamp et al., 2012). En général, on observe une alternance entre forme coloniale et forme flagellée solitaire au fil des saisons (Smith et al., 2003). La formation de colonies de *Phaeocystis* nécessite de fortes concentrations en fer (Bender et al., 2018). La grande taille des colonies semble réduire les taux de broutage par rapport aux cellules solitaires, qui sont facilement consommées par le microzooplancton (Caron et al., 2000 ; Tang et al., 2008). Par conséquent, les formes coloniales de *Phaeocystis* augmenteraient l'export de carbone par sédimentation de grands agrégats mucilagineux riches en carbone, tandis que les formes solitaires alimenteraient le réseau

trophique microbien et seraient rapidement recyclées au sein de la couche de mélange (Smith et al., 2003). Les prasinophytes et les cryptophytes ont également été identifiés dans des études pigmentaires comme des contributeurs majeurs à la Chl *a* dans certains secteurs de l'océan Austral (Moline et al., 2004 ; Iida et Odate, 2014). Les prasinophytes sont des algues vertes caractérisées par une préférence disproportionnée pour l'ammonium par rapport au nitrate (Litchman et Klausmeier, 2008) mais semblent avoir des exigences en fer plus élevées que les autres groupes de phytoplancton (Quigg *et al.*, 2003). Récemment, il a été suggéré que la bactériovorie pourrait constituer une ressource complémentaire importante pour les algues vertes dans des conditions de faible teneur en nutriments, même à de faibles concentrations bactériennes (McKie-Krisberg et Sanders, 2014 ; McKie-Krisberg et al., 2015 ; Anderson et al., 2018). L'importance des cryptophytes a été principalement signalée dans les eaux côtières de l'Antarctique occidental, où les blooms sont historiquement dominés par les diatomées. L'importance croissante des cryptophytes au détriment des diatomées de grande taille, en lien avec une forte stratification de la colonne d'eau et de fortes luminosités (Ducklow et al., 2013 ; Mendes et al., 2018) affecterait la composition des communautés de zooplancton et pourrait entraîner une diminution du flux de carbone vers l'océan profond (Moline et al., 2004).

En conclusion, peu d'informations sont actuellement disponibles sur la diversité du petit phytoplancton et ses déterminants écologiques, bien que certains modèles de production primaire de l'océan Austral estiment que le petit phytoplancton contribuerait davantage à la production primaire annuelle (2,5 Gt C an<sup>-1</sup>) que le microphytoplancton (0,9 Gt C an<sup>-1</sup>, Uitz et al. 2010).

## 2. Le phytoplancton dans le cycle du carbone

Historiquement, la diversité du phytoplancton a profondément influencé le cycle du carbone. Par exemple, le succès écologique grandissant des grandes cellules phytoplanctoniques eucaryotes au Mésozoïque a augmenté l'export de carbone organique et de nutriments vers l'intérieur de l'océan (Katz et al., 2007). Ainsi, la composition taxonomique et la taille des cellules phytoplanctoniques contrôlent potentiellement le flux d'export de carbone vers l'océan intérieur et influencent la concentration à long terme du CO<sub>2</sub> dans l'atmosphère.

On considère usuellement que le carbone produit par le phytoplancton de petite ou de grande taille suit différentes voies : le réseau trophique microbien pour les petites cellules et l'intégration vers la chaîne alimentaire classique pour les plus grandes (Legendre et Le Fèvre, 1995 ; Laender et al., 2010). Dans le réseau microbien, la production autotrophe est dominée par de petites cellules et rapidement respirée dans la boucle microbienne en surface (par exemple, Michaels & Silver 1988), ce qui entraîne un faible export de carbone. Inversement, les grandes cellules phytoplanctoniques seraient associées à des chaînes alimentaires courtes et directes (par exemple diatomées-krill-baleines dans l'océan Austral ; Smetacek et al., 2004). On pense généralement que cette chaîne alimentaire classique alimente la pompe biologique à carbone par sédimentation directe de

grandes cellules phytoplanctoniques, ainsi que par production de grandes pelotes fécales par les niveaux trophiques supérieurs (Michaels et Silver, 1988 ; Fig. A9). Cependant, ce paradigme classique selon lequel les grandes cellules contribuent de manière disproportionnée à l'export de carbone est de plus en plus débattu, avec des preuves indirectes et directes croissantes que le petit phytoplancton peut être un contributeur majeur à l'export de carbone, notamment via des mécanismes d'agrégation (Richardson and Jackson, 2007). Avec le réchauffement climatique et l'oligotrophisation des eaux de surface, l'abondance du petit phytoplancton va connaître une forte hausse et il paraît d'autant plus nécessaire d'explorer davantage les routes possibles d'export des petites cellules vers l'océan profond (Bopp et al., 2001 ; Sarmiento et al., 2004).

### 3. Le phytoplancton et le cycle du carbone dans l'océan Austral

L'océan Austral comptabilise  $43\% \pm 3\%$  ( $42 \pm 5$  Pg C) du puit océanique de carbone anthropogénique de 1861-2005 (Frölicher et al., 2014). L'océan Austral devrait prochainement connaître de profonds bouleversements (réchauffement accru, renforcement des vents, augmentation de l'acidification, de la stratification des eaux de surface, diminution des remontées d'eaux profondes, de la glace de mer, de la salinité et migration vers le sud des principaux fronts océaniques ; Deppeler et Davidson, 2017). Tous ces changements soulèvent des incertitudes majeures concernant les assemblages phytoplanctoniques futurs, leur productivité et le devenir de la pompe biologique à carbone.

L'océan Austral est la plus grande zone HNLC (High nutrient Low Chlorophyll), où les macronutriments abondants (N, P, Si) ne sont pas utilisés par le phytoplancton de surface du fait d'une limitation par des micronutriments, principalement le fer (de Baar et al., 2005; Blain et al., 2007; Boyd et al., 2007). Le fer est en effet un micronutriment essentiel pour le phytoplancton, nécessaire notamment au fonctionnement des chaînes de transport d'électrons utilisées lors de la photosynthèse (par exemple par le PSI, PSII, le complexe cytochrome b6-f-FeS; Behrenfeld et Milligan, 2013). Par conséquent, la production primaire reste faible dans l'essentiel de l'océan Austral à l'exception de quelques zones où des blooms de larges cellules sont observés à proximité d'îles, dans des eaux profitant d'une fertilisation naturelle en fer.

Les expériences explorant l'effet d'une fertilisation artificielle ou naturelle en fer au cours des deux dernières décennies ont montré sans équivoque que cette dernière favorisait une croissance accrue du phytoplancton (Boyd et al., 2001 ; Coale et al., 2004). Au Sud du Front Polaire, dans les eaux riches en acide silicique, la fertilisation en fer favorisait la prolifération de diatomées de grande taille, tandis qu'au Nord du Front Polaire, un assemblage mixte de petites cellules était observé (Boyd et al., 2000; Buesseler et al., 2005; Martin et al., 2013), en lien avec une plus forte limitation en acide silicique des diatomées. L'augmentation de la biomasse phytoplanctonique était plus faible dans les assemblages dominés par les petites cellules, du fait de leur importante régulation par les prédateurs microzooplanctoniques (Schulz et al., 2018). L'impact sur l'export de carbone

des changements occasionnés par la fertilisation en fer était variable selon les expériences. L'augmentation de la production ne s'accompagnait pas pour chaque expérience d'une augmentation significative de l'export, sans lien systématique entre export mesuré et composition des assemblages phytoplanctoniques de surface (Blain et al., 2007; Pollard et al., 2009; Smetacek et al., 2012).

#### 4. Contexte scientifique et objectifs de la thèse

Le plateau des Kerguelen est un plateau océanique antarctique s'étendant de 46°S à 64°S à l'isobathe des 3000 m. Il forme une barrière à l'écoulement vers l'est du Courant Circumpolaire Antarctique (ACC) (Fig. A11 ; Park et al., 2008). Dans cette région, le Front Polaire est une zone frontale majeure, marquant la limite entre des eaux subtropicales au Nord et les eaux antarctiques au sud. La position du Front Polaire présente de grandes variations saisonnières, se déplaçant vers le sud du printemps à l'été, poussé vers le sud par des eaux plus chaudes et plus douces amenées du nord-ouest par l'ACC (Pauthenet et al., 2018). Sur le plateau, la circulation entre les îles Kerguelen et Heard est plutôt stagnante,  $<5 \text{ cm}^2 \text{ s}^{-1}$  en moyenne (Robinson et al., 2016).

Cette thèse s'inscrit dans le cadre du projet MOBYDICK (Marine Ecosystem Biodiversity and Dynamics of Carbon around Kerguelen ; <https://mobydick.mio.osupytheas.fr/>), qui visait à évaluer les liens entre la biodiversité pélagique marine, le transfert du carbone dans le réseau trophique et l'export de carbone vers l'océan intérieur au large des îles Kerguelen. Par rapport aux études précédentes, l'originalité de MOBYDICK réside dans l'étude simultanée de la biodiversité pélagique à tous les niveaux trophiques, et de chaque groupe fonctionnel, du picoplancton aux prédateurs supérieurs, dans des environnements contrastés sur et en dehors du plateau. De précédentes campagnes océanographiques dans la région ont montré que le plateau naturellement fertilisé en fer était dominé par le microphytoplancton (principalement des diatomées), qui contribuait à 80-90% de la production primaire totale, alors que la région HNLC était principalement (65 - 74 %) dominée par les nano-flagellés, notamment *Phaeocystis antarctica*, et les petites diatomées (Uitz et al., 2009 ; Lasbleiz et al., 2016 ; Georges et al., 2014).

Avant MOBYDICK, aucun projet n'avait exploré en détails la structure des communautés de phytoplancton sur le plateau des Kerguelen en dehors de la période du bloom de diatomées. Cependant, les données satellitaires et les prélèvements effectués juste avant le bloom semblaient indiquer que les petites cellules constituaient un élément important des communautés phytoplanctoniques en dehors du bloom (Rembauville et al., 2017 ; Penna et al., 2018). L'étude de la diversité et de l'importance du phytoplancton de petite taille dans la fixation du CO<sub>2</sub> sur et autour des eaux naturellement fertilisées en fer du plateau après le bloom des diatomées constitue une étape importante dans la compréhension du fonctionnement des écosystèmes et du cycle du carbone dans cette région où la production de phytoplancton est fortement saisonnière.

Les deux principaux objectifs de cette thèse étaient les suivants :

1. Décrire la diversité du petit phytoplancton après le bloom de diatomées dans des écosystèmes habituellement caractérisés par des régimes de productivité contrastés sur et en dehors du plateau fertilisé en fer,
2. Évaluer la contribution de différents groupes de taille du phytoplancton à la fixation du CO<sub>2</sub> après le bloom, en prenant en compte la variabilité intra-groupe au niveau cellulaire.

L'évaluation de la variabilité de la fixation du CO<sub>2</sub> entre et au sein de différents groupes devrait aider à comprendre comment la diversité taxonomique et de taille du phytoplancton affecte le cycle du carbone dans l'océan Austral. La comparaison de ces résultats avec les données collectées en début et fin de bloom apportera des informations précieuses sur les facteurs écologiques déterminant l'équilibre entre le petit phytoplancton et les diatomées au fil des saisons, et sur la manière dont les communautés phytoplanctoniques affectent le fonctionnement de la pompe biologique à carbone.

## Matériel et méthodes

Différentes approches ont été utilisées au cours de cette thèse pour étudier les liens entre diversité du phytoplancton et fixation du CO<sub>2</sub>. La composition taxonomique du phytoplancton de petite et grande taille a été étudiée en combinant différentes méthodes (métabarcoding, CARD-FISH et chemotaxonomie pigmentaire ; Tableau B1) afin d'obtenir une compréhension qualitative et quantitative de la diversité du phytoplancton dans la zone d'étude. Le rôle du phytoplancton de petite et grande taille dans la fixation du CO<sub>2</sub> a été étudié grâce à des incubations des communautés phytoplanctoniques en présence de DI<sup>13</sup>C. L'incorporation du carbone marqué (<sup>13</sup>C) dans le carbone organique particulaire (POC) total, ainsi qu'au niveau cellulaire, a ensuite été évaluée par spectrométrie de masse EA-IRMS (POC total) NanoSIMS (cellules < 20µm) et IMS1280 (cellules >20µm). Les instruments NanoSIMS et IMS1280 utilisent un faisceau d'ions primaires (Cs<sup>+</sup>), pour éroder lentement la couche superficielle d'un échantillon plat. Les ions secondaires ainsi créés sont ensuite transportés dans un spectromètre de masse, permettant la création de cartes isotopiques, où le rapport entre le nombre d'ions rares (par exemple <sup>13</sup>C) et les ions naturels plus abondants (par exemple <sup>12</sup>C) peut être visualisé (Fig. B4).

L'utilisation d'outils complémentaires de biologie moléculaire, de chemotaxonomie pigmentaire et de spectrométrie de masse au niveau cellulaire nous a ainsi permis d'explorer de manière originale la diversité et l'importance dans la fixation du CO<sub>2</sub> du petit et grand phytoplancton.

## Résultats

### 1. La diversité du petit phytoplancton autour de Kerguelen

Dans l'océan Austral, les blooms de diatomées ont attiré beaucoup d'attention, tandis que la diversité taxonomique des cellules phytoplanctoniques de petite taille a été très peu étudiée. Cette étude examine la diversité du petit phytoplancton, défini ici comme l'ensemble des cellules <20 µm (petites diatomées et petit phytoplancton non silicifié), sur deux zones contrastées : le plateau productif de Kerguelen et les eaux environnantes à faible productivité. Pour évaluer la diversité et la structure spatiale du phytoplancton après le bloom de diatomées, des échantillons de plancton ont été prélevés à des profondeurs distinctes (de 0 à 300 m) pour deux fractions de taille (<20 et 20 à 100 µm), puis analysés par metabarcoding Illumina de l'ADNr 18S. La succession saisonnière du phytoplancton a été décrite en combinant des données pigmentaires, de cytométrie en flux et environnementales de deux campagnes précédentes sur cette même zone, au début et lors du déclin du bloom de diatomées.

Dans la couche de mélange, le petit phytoplancton non silicifié représentait moins de 10% de la chlorophylle a (Chl *a*) en début et fin de bloom sur le plateau, mais il contribuait pour 53–70% de Chl *a* après le bloom. Cette augmentation relative du petit phytoplancton dans la biomasse phytoplanctonique après le bloom pourrait principalement être liée à l'épuisement de l'acide silicique sur le plateau durant le bloom, limitant la croissance de nombreuses espèces de diatomées.

Au sein du petit phytoplancton, *Phaeocystis antarctica* (sous sa forme de flagellé solitaire) était relativement abondant à toutes les stations échantillonnées après le bloom, mais la distribution spatiale des autres groupes présentait des différences marquées sur et en dehors du plateau. Des concentrations plus élevées en NH<sub>4</sub><sup>+</sup> sur le plateau pourraient favoriser la présence de *Micromonas*, tandis que les pélagophytes étaient principalement séquencés en dehors du plateau. Un assemblage diversifié de petites diatomées était également observé au large du plateau, où les concentrations en acide silicique étaient encore élevées.

En profondeur, les diatomées contribuaient dans l'ensemble d'avantage au nombre de séquences que le petit phytoplancton non-silicifié. Cependant, *P. antarctica* représentait jusqu'à 25% du nombre de séquences à 300 m de profondeur en dehors du plateau dans la fraction de plus grande taille, ce qui suggère qu'il pourrait contribuer de façon significative, probablement sous forme d'agrégats, à l'export de carbone dans les eaux peu productives de cette région.

### 2. Contribution du petit phytoplancton à la fixation du CO<sub>2</sub> autour de Kerguelen

Le phytoplancton est composé de micro-organismes aux tailles et appartenances phylogénétiques très variées. Cette diversité influence le métabolisme, et par là, la capacité de différents groupes de phytoplancton à fixer le CO<sub>2</sub> lors de la photosynthèse, ainsi que le devenir dans la pompe

biologique du carbone fixé en surface. Afin d'améliorer notre compréhension du fonctionnement de la pompe à carbone, il faut donc évaluer la variabilité dans la fixation du CO<sub>2</sub> entre différents groupes, mais également au sein de chaque groupe de phytoplancton. Seules ces mesures complémentaires permettront de déterminer la contribution respective des différents groupes, et si tous les individus au sein de ces groupes participent de façon égale ou non à la fixation du carbone. Pour ce faire, nous avons mesuré à l'échelle cellulaire la fixation du CO<sub>2</sub> par différents groupes de phytoplancton autour du plateau de Kerguelen, naturellement fertilisé en fer (océan Austral). Cette zone était principalement connue pour ses importants blooms de diatomées au printemps-été, favorisant l'export de carbone vers l'océan profond.

Notre étude a montré qu'après le bloom, les petites cellules phytoplanctoniques (<20 µm), composées de taxons éloignés sur le plan phylogénétique (prymnesiophytes, prasinophytes et petites diatomées) présentaient des taux de croissance supérieurs (0,22 ± 0,09 division j<sup>-1</sup> en dehors du plateau et 0,37 ± 0,13 division j<sup>-1</sup> sur le plateau) à ceux des grandes diatomées (0,11 ± 0,14 sur le plateau et 0,09 ± 0,11 en dehors du plateau). Du fait des faibles taux de croissance des grandes diatomées, le petit phytoplancton (principalement non silicifié) pourrait représenter 41 à 61% de la fixation totale de CO<sub>2</sub> sur le plateau de Kerguelen, bien plus que ce qui est habituellement mesuré dans les régions naturellement fertilisées en fer de l'océan Austral (Tableau 2). Sur le plateau, la contribution élevée du petit phytoplancton à la fixation de carbone était principalement attribuable à des petites cellules (<5µm) non-silicifiées. Autour du plateau, les petites diatomées (3,8 ± 1,5 µm) étaient également abondantes et actives (Fig. 4b). Beaucoup de diatomées de plus grande taille (>20 µm) étaient inactives (19 ± 13%) à ce moment de la saison, tandis que quelques cellules très actives seulement au sein de ce groupe assuraient la majeure partie de la fixation du CO<sub>2</sub> (Fig. 4c). Il est possible que certains groupes de grandes diatomées possèdent des caractéristiques avantageuses qui leur permettent de continuer à croître dans les conditions environnementales défavorables après le bloom. Ainsi, les diatomées pennées, possédant la ferritine, pourraient être avantagées dans les zones où le fer est limitant, tandis que *Corethron inerme* serait avantagé sur le plateau par sa capacité à se développer dans des environnements où les concentrations en acide silicique sont faibles.

L'analyse de la distribution verticale des pigments dans la colonne d'eau suggère que les diatomées participent le plus à la sédimentation directe de phytoplancton, mais souligne également qu'aux stations les plus productives, une importante part du petit phytoplancton pourrait être consommée en surface, puis exportée en profondeur sous forme de pelotes fécales. De façon générale, cette étude met en évidence la nécessité d'explorer davantage le rôle des petites cellules dans la fixation et l'export du CO<sub>2</sub>.



## Discussion générale

Révéler le rôle fonctionnel des micro-organismes et les facteurs environnementaux qui contrôlent la fonction qu'ils assurent dans l'écosystème est l'une des tâches les plus difficiles de l'écologie microbienne (Madsen, 2005; Gutierrez-Zamora et Manefield, 2010). Les deux principaux objectifs de cette thèse - explorer la diversité du petit phytoplancton et sa contribution à la fixation du CO<sub>2</sub> dans des environnements contrastés - s'inscrivent dans ce cadre conceptuel.

Trois questions ont été abordées dans cette thèse pour répondre à ces deux objectifs :

1. La composition du petit phytoplancton diffère-t-elle sur et en dehors de la zone naturellement fertilisée en fer après le bloom de diatomées ?
2. Quels sont les facteurs environnementaux qui déterminent la dominance des petites cellules et des grandes diatomées au fil des saisons ?
3. Quelle est la contribution du petit phytoplancton à la fixation du CO<sub>2</sub> après le bloom et quelles en sont les implications pour la pompe biologique à carbone dans la région ?

### 1. Premier aperçu de la diversité du petit plancton autour de Kerguelen

Cette thèse a clairement mis en évidence la contribution importante du petit phytoplancton - *Phaeocystis antarctica* - en particulier, à la biomasse et production phytoplanctonique sur et en dehors du plateau après le bloom de diatomées (article 1 ; Fig. 3, Fig. 6). Le succès de *P. antarctica* peut être lié au polymorphisme de ses différents stades de vie (cellules flagellées individualisées ou grandes colonies), qui constituent différentes stratégies d'adaptation à des contrôles environnementaux contrastés au fil des saisons. Dans les eaux fertilisées en fer, la capacité à former de grandes colonies permet à *P. antarctica* d'échapper en partie à la forte prédation par le microzooplancton (Schoemann et al., 2005). La formation des colonies est en effet déclenchée par la disponibilité du fer (Bender et al., 2018), mais la taille des colonies peut augmenter de 30% en présence de prédateurs, ce qui tend à confirmer l'importance écologique de la formation de colonies comme mécanisme de défense (Tang et al., 2008). Sous la forme de cellules flagellées individualisées, cette espèce peut s'acclimater à la limitation en fer en réduisant sa taille, son taux de croissance, sa concentration en chlorophylle *a* et sa production de carbone organique particulaire (Bender et al., 2018 ; Koch et al., 2019). L'importance de *Phaeocystis* va d'ailleurs probablement continuer à augmenter avec les changements attendus dans l'océan Austral (Zhu et al., 2016 ; Koch et al., 2019). La distribution d'autres taxons de petit phytoplancton semblait dans notre étude influencée par des concentrations contrastées en silice, ammonium et fer sur et autour du plateau (article 1 ; fig. 5). Comme aucune étude n'a exploré en détail la structure taxonomique des communautés de petit phytoplancton tout au long de l'année, nous ne pouvons pas exclure que différents groupes de petit phytoplancton puissent prévaloir plus tard dans la saison. Ainsi, d'autres groupes de petit phytoplancton pourraient être aussi, voire même davantage compétitifs

en automne et en hiver, notamment lorsque la luminosité est faible quand la couche de mélange est beaucoup plus profonde (jusqu'à 185 m) en hiver. En dehors du plateau, la position du Front Polaire semble également fortement influencer la composition du petit phytoplancton à petite échelle spatiale. La limitation en acide silicique au nord du Front Polaire semble limiter la croissance des diatomées de petite taille, très présentes au sud de ce front. D'autres facteurs, en lien possible avec la circulation océanique et la distribution biogéographique de certains groupes pourraient également influencer la composition taxonomique des prasinophytes de part et d'autre du Front Polaire. Etant donné que des espèces spécifiques de ce groupe, comme *Micromonas*, pourraient servir de "sentinelles" du réchauffement des océans (Demory et al., 2019), il pourrait être intéressant d'explorer davantage la composition taxonomique détaillée des taxons de petit phytoplancton dans les zones frontales de l'océan Austral.

## 2. Saisonnalité et variabilité interannuelle des communautés phytoplanctoniques autour de Kerguelen

En comparant les campagnes MOBYDICK, KEOPS I et II, il a été possible de décrire la succession saisonnière des communautés phytoplanctoniques sur le plateau, du bloom de diatomées à la dominance par les petites cellules non-silicifiées après le bloom (article 1, fig. 6).

Au début du bloom, la stabilisation de la colonne d'eau et les fortes concentrations en nutriments inorganiques majeurs et en fer (maximum de 0,6 nM, réduit à 0,05 nM en été) profite à la fois aux diatomées et au petit phytoplancton sur le plateau (Mongin et al., 2008). Cependant, le petit phytoplancton est efficacement brouté par le microzooplancton, ce qui empêche l'accumulation de sa biomasse en début de bloom. Bien au contraire, une forte diminution des pigments associés au petit phytoplancton (prymnesiophytes et prasinophytes) est observée sur le plateau en début de bloom (article 1 ; fig. 6), période durant laquelle la biomasse des ciliés était multipliée par 7 (Christaki et al., 2015), contrôlant fortement le petit phytoplancton. Pendant MOBYDICK, des expériences ont également montré que le taux de croissance net du phytoplancton était inférieur au taux de broutage par le microzooplancton après le bloom (article 3; Christaki et al., en révision). Le microzooplancton était alors cependant fortement contrôlé par les copépodes (Fig. D2). Cela peut expliquer pourquoi les abondances de phytoplancton de petite taille restaient supérieures à  $10^6$  cellules  $L^{-1}$  malgré la forte prédation par le microzooplancton après le bloom (article 1 ; Fig. 6). Au fil du bloom, l'épuisement en acide silicique ( $<2 \mu\text{mol } L^{-1}$ ) est probablement le facteur principal limitant la croissance des diatomées. De surcroît, les interactions biotiques, comme la prédation et le parasitisme, peuvent accélérer le déclin du bloom. Pendant MOBYDICK, une forte proportion de parasites Syndiniales (55-70% des séquences) a été séquencée dans la petite fraction de taille au cours des deux premières visites sur le plateau. Ces séquences pourraient correspondre à des spores de Syndiniales libérées après la mort de l'hôte, reflétant potentiellement la fin d'une infection parasitaire d'importance en fin de bloom (article 4 ; Sassenhagen et al. 2020).

Le bloom de diatomées est caractérisé par une grande variabilité interannuelle (article 1, figure 6a), en lien probable avec de fortes variations des apports d'acide silicique et de fer dans cette région caractérisée par des fronts dynamiques (Mongin et al., 2008; Robinson et al., 2016). Dans ce contexte, la position du Front Polaire au nord ou au sud du plateau des Kerguelen pourrait être cruciale, car les eaux subantarctiques au nord du Front Polaire sont pauvres en acide silicique nécessaire aux diatomées. Le déplacement saisonnier du Front Polaire vers le sud du plateau est d'ores et déjà plus prononcé lorsque des anomalies de température de surface des eaux chaudes se produisent (Moore et al., 1999) et s'intensifiera à mesure que les eaux se réchaufferont et se stratifieront davantage en raison du changement climatique (Moore et al., 1999 ; Deppeler et Davidson, 2017 ; Freeman et al., 2018). Cela pourrait favoriser les petites cellules de phytoplancton au détriment des grosses diatomées, à l'instar de la situation observée pendant MOBYDICK. Des changements dans la fréquence et l'ampleur des blooms de diatomées sur le plateau sont susceptibles d'avoir un impact sur l'ensemble de la chaîne alimentaire, provoquant un déclin des populations de krill et une augmentation des salpes gélatineuses (Moline et al., 2004), qui pourrait en conséquence avoir des conséquences négatives sur les consommateurs de krill, comme les manchots et les phoques (Atkinson et al., 2004).

### 3. Impact de la structure des communautés phytoplanctoniques de surface et du régime de productivité sur la pompe biologique à carbone

En théorie, quand les petites cellules dominent le phytoplancton, l'export de carbone est faible, en raison du recyclage rapide de la majeure partie de la matière organique dans la zone euphotique (Smetacek et al., 2004). Une réduction de l'export de carbone à 200 m a été observée après le bloom par rapport à l'export mesuré en fin de bloom (KEOPS1), mais l'export demeurait plus élevé après le bloom qu'en début de bloom (KEOPS2) (7, 25 et 4 mmol m<sup>-2</sup> j<sup>-1</sup>, respectivement) (article 5 ; Christaki et al. 2020). Cela suggère que le petit phytoplancton contribue à l'export de carbone, par agrégation ou broutage par les niveaux trophiques supérieurs et export sous forme de pelotes fécales, comme le suggèrent plusieurs résultats de cette thèse. La forte proportion de *Phaeocystis* hors du plateau à 300 m dans la fraction de grande taille (article 1 ; fig. 3) indique que *Phaeocystis* pourrait être incorporé dans la neige marine sous forme d'agrégats. L'étude de la distribution verticale des pigments suggère en outre que les petits taxons non-silicifiés sont rapidement ingérés par les brouteurs, en particulier sur le plateau et à M1, où se trouvent des populations denses de salpes (article 2 ; fig. 2). Pendant MOBYDICK, les diatomées du genre *Odontella*, *Eucampia* et *Chaetoceros* étaient bien représentées dans les données de séquençage en dessous de 125m sur le plateau, ce qui suggère que les espèces productrices de spores et formes de résistance y sont efficacement exportées. En dehors du plateau, les grandes diatomées lourdement silicifiées comme *Fragilariopsis* et *Thalassiosira* étaient également courantes dans les résultats de séquençage à 300m (Paper 1 ; Fig. 7). Ainsi, même lorsque le petit phytoplancton contribue

grandement à la biomasse du phytoplancton et à la production primaire en surface, certaines grandes diatomées semblent contribuer de façon disproportionnée à l'export de carbone.

La qualité de la matière organique exportée au cours des différentes saisons reflète la succession des assemblages de phyto- et zooplancton. Les agrégats de phytoplancton dominaient le flux descendant au début du bloom (Laurenceau-Cornec et al., 2015b), lorsque les brouteurs étaient encore dans une phase de développement. Le régime de productivité était alors élevé (BPC 344 mmol m<sup>-2</sup> j<sup>-1</sup>) mais l'efficacité de l'export très faible (1 %), ce qui suggère un système de rétention caractérisé par une forte reminéralisation bactérienne et une accumulation de biomasse en surface (Laurenceau-Cornec et al., 2015b ; Christaki et al., 2020). En revanche, en fin de bloom les grosses pelotes fécales (>100 µm) dominaient le flux d'export, du fait du développement d'importantes communautés de mésozooplancton (Ebersbach et Trull, 2008). À cette période, l'efficacité de l'export sur le plateau était maximale (26 %). Après le bloom (MOBYDICK), les particules < 50 µm représentaient la quasi-totalité de la biomasse du POC jusqu'à 300 m (Planchon, communication personnelle). Cette caractéristique suggère que les pelotes fécales des petits brouteurs (microzooplancton et petits copépodes) et des salpes jouent alors un rôle plus important l'export. L'efficacité de l'export après le bloom n'était plus que de 5 % (article 3 ; Christaki et al., 2020), ce qui tend à confirmer que l'efficacité de l'export est plus faible lorsque les organismes de petite taille dominent le phyto- et zooplancton.

Compte tenu de cette saisonnalité marquée, il pourrait être tentant d'associer des assemblages caractéristiques de phyto- et zooplancton à des régimes d'export spécifiques, puis d'extrapoler ces mesures à un cycle annuel. Cependant, l'utilisation de pièges à sédiments déployés sur une année a montré que les spores de *Chaetoceros* spp. et *Thalassiosira antarctica* étaient responsables de plus de 60% du flux annuel de POC lors de pulses d'export brefs (Rembauville, Blain, et al., 2015). Ces évènements ponctuels majeurs soulignent la dimension idiosyncrasique des liens entre écologie pélagique et biogéochimie des océans et soulignent la difficulté pour des campagnes océanographiques ponctuelles d'utiliser des expériences de fertilisation naturelle ou artificielle en fer pour comprendre le fonctionnement de la pompe biologique à carbone. Compte tenu de l'éloignement et du rôle central de l'océan Austral dans le cycle global du carbone, cela souligne la nécessité de développer des dispositifs d'échantillonnage automatisés pour explorer la saisonnalité, la récurrence et les liens environnementaux entre les communautés phytoplanctoniques de surface et l'export qui leur est associé.

## A. Introduction

Phytoplankton are photoautotrophic microorganisms that live in the euphotic layer of freshwaters or marine environments. During oxygenic photosynthesis, they use the light energy to oxidize inorganic carbon and convert it to energy-rich organic carbon molecules. As the main marine primary producer community, phytoplankton provide food, directly or indirectly, to virtually every other marine creature. At a global scale, they account for less than 1% of Earth's photosynthetic biomass but are responsible for more than 45% of the global annual net primary production (Field *et al.*, 1998; Bar-On *et al.*, 2018). Thus, they modulate actively atmospheric carbon dioxide and oxygen concentrations. Within the phytoplankton, functional groups (characterized by distinct traits associated to size or taxonomy) have variable impacts on carbon and other major biogeochemical cycles, such as nitrogen, phosphorus and silica (Litchman *et al.*, 2015). Phytoplankton are composed of a broad suite of taxa, from cyanobacteria to eukaryotes, that vary considerably in size (<1 to >100  $\mu\text{m}$ ). The diversity in size and metabolism of phytoplankton communities affects food web structure and biogeochemical cycling of major elements.

In the first part of this introduction, I will briefly provide an overview of the origin of the major phytoplanktonic lineages and discuss what is known on their physiology, metabolism and ecology of broad size- and taxonomic groups, focusing on phytoplankton of the Southern Ocean (SO). I will then discuss how phytoplankton size and taxonomy affect the marine carbon cycle with a focus on the SO. The SO is the most important sink of anthropogenic carbon dioxide and thus a key region in understanding the role of marine biogeochemical carbon cycling (Frölicher *et al.*, 2014). It is the largest high nutrient, low chlorophyll (HNLC) area of the global ocean, where primary production is limited by iron availability despite high concentrations of macronutrients (Martin, 1990; de Baar *et al.*, 2005). The "Iron hypothesis" proposed by Martin, (1990) suggested that relief from iron deficiency via increased dust deposition enhanced phytoplankton primary production in the SO during the Last Glacial Maximum (20 000 years ago), lowering atmospheric  $\text{CO}_2$  by as much as 100 ppm in comparison with preindustrial times ( $\sim 280$  ppm).

Since the discovery of the essential role of iron in the productivity of the SO and potential effect in mitigation of  $\text{CO}_2$  emissions, many studies focused on the influence of artificial or natural iron fertilization on phytoplankton communities,  $\text{CO}_2$ -fixation and carbon export (reviewed by Yoon *et al.*, 2018). In the SO, large phytoplankton blooms occur in spring and summer in naturally iron-fertilized waters downstream of island plateaus, such as those of Kerguelen, Crozet and South Georgia. These blooms are usually characterized by different phytoplankton communities than surrounding low productive HNLC waters and enhanced carbon export to the deep ocean (Blain *et al.*, 2007; Pollard *et al.*, 2009; Korb *et al.*, 2012). Thus, these contrasted ecosystems on and off

naturally-fertilized waters constitute unique natural laboratories to explore the influence of contrasted phytoplankton communities and productivity regimes on the marine carbon cycle.

## 1. Phytoplankton diversity

*“Phytoplankton is a nineteenth century ecological construct for a biologically diverse group of pelagic photoautotrophs that share common metabolic functions but not evolutionary histories.”* (Quigg *et al.*, 2003)

### 1.1 Evolution and diversity of phytoplankton

The first marine photoautotrophs appeared about 3.8 Ga years ago in the Archaean period with the origin of photosynthesis in prokaryotic Cyanobacteria (Katz *et al.*, 2007; Nutman *et al.*, 2016), which led to the rise of oxygen on Earth ~2.3 billion years ago (Bekker *et al.*, 2004).

Oxygenic photosynthesis is supposed to have evolved only once in an ancestral Cyanobacteria, but it subsequently spread via endosymbiosis to a wide variety of eukaryotic clades (Delwiche, 1999). The engulfment of a cyanobacteria by a heterotrophic eukaryote ~1 900 to 900 Myr ago marked the origin of eukaryotic phytoplankton (Sánchez-Baracaldo *et al.*, 2017). This primary endosymbiosis gave rise to the Archaeplastida lineage, a monophyletic group that includes Glaucophyta, Rhodophyta (red algae), Chlorophyta (green algae) and streptophyta (land plants) (Fig. A1). In turn, secondary endosymbioses involving archaeplastid lineages (red or green algae) spread photosynthesis to the haptophytes, cryptophytes, dinoflagellates, stramenopiles, euglenids (red lineage) and chlorarachniophyte rhizarians (Gentil *et al.*, 2017). In modern oceans, the red lineage (especially haptophytes, dinoflagellates and diatoms) is extremely successful and groups the most common bloom-forming species (Falkowski, 2004).

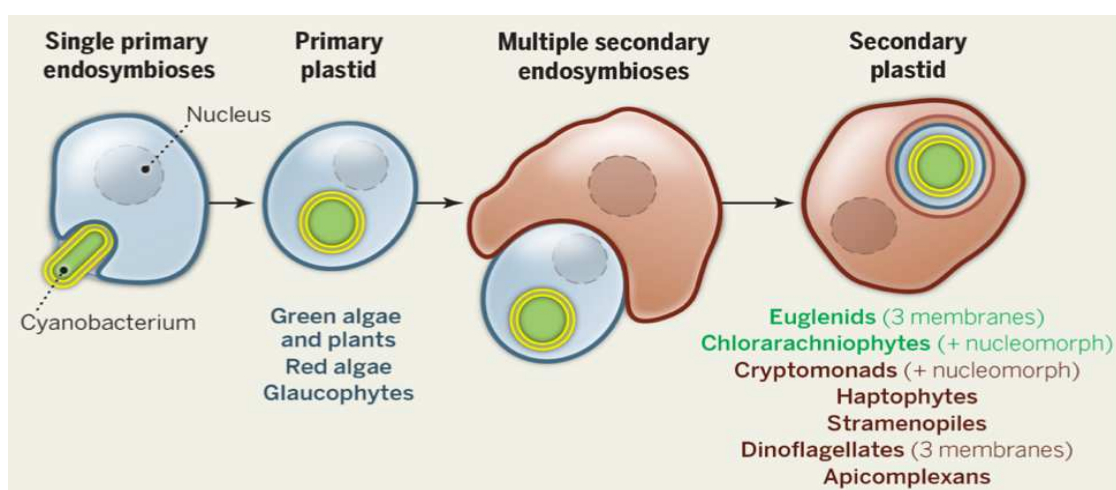


Fig. A1: Evolution and diversification of eukaryotic autotrophic lineages. Taxa that inherited their plastids from a secondary endosymbiosis with green algae or red algae are labeled in green and red, respectively (Source: Worden *et al.*, 2015)

Phytoplankton has now representatives in 4 of the 6 super-groups of in the eukaryotic tree of life described by Adl et al. (2005) (Fig. A2).

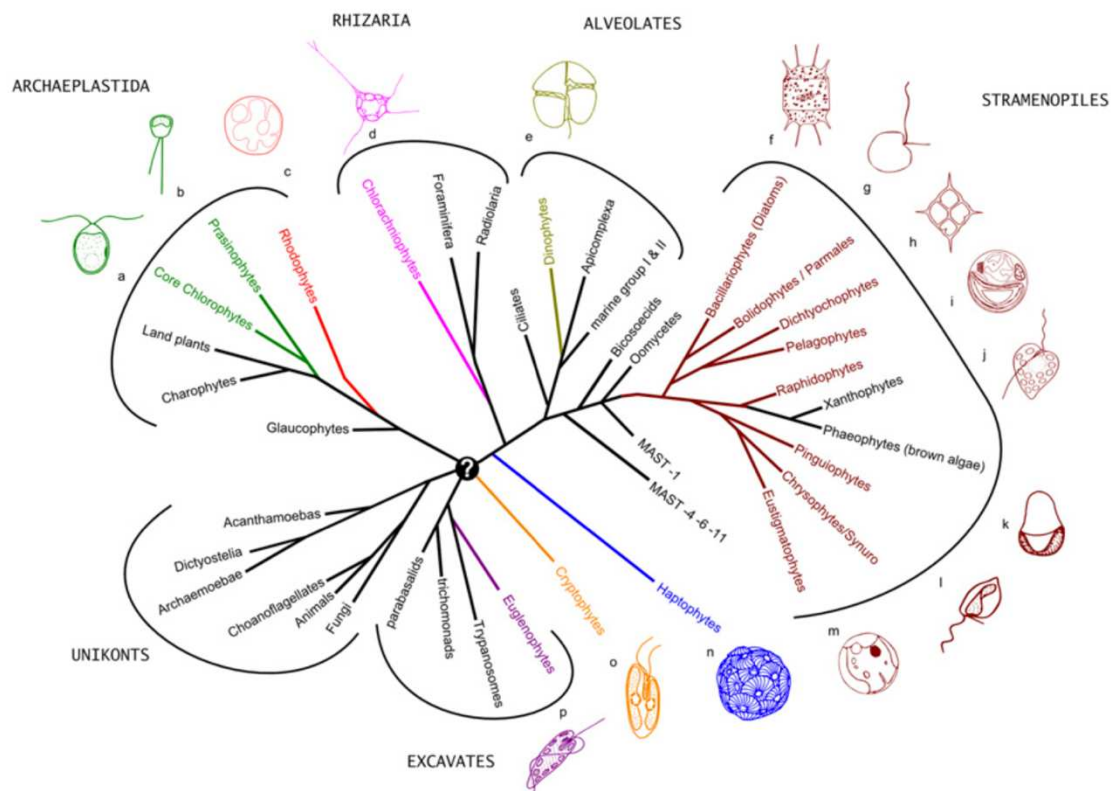


Fig. A2: Schematic phylogenetic tree representing the distribution of phytoplanktonic taxa across eukaryote lineages (in color). Illustrations of (a) Chlorophyceae, (b) Pseudoscurfieldia sp., (c) Porphyridium cruentum, (d) Gymnochlora dimorpha, (e) Dinoflagellates, (f) Odontella sp. (g) Bolidomonas pacifica, (h) Dictyocha sp., (i) Aureococcus anophagefferens, (j) Heterosigma akashiwa, (k) Pinguicoccus pyriformis, (l) Ochromonas sp., (m) Nannochloropsis salina, (n) Calcidiscus sp., (o) Cryptomonas sp., (p) Euglenids. (Source : Not et al., 2012)

Historically, the diversity of eukaryotic phytoplankton has been assessed by microscope-based description of morphological features and approximately 4 000-25 000 phytoplankton morpho-species were described this way (Sournia *et al.*, 1991; Falkowski, 2004). This number probably largely underestimates the real extent of phytoplankton diversity and molecular approaches keep unveiling new uncultured lineages (e.g. Moreira and López-García, 2002; Massana and Pedrés-Alió, 2008; Massana *et al.*, 2014) and the existence of cryptic species (Sáez *et al.*, 2003; Amato *et al.*, 2007). Extensive molecular surveys of phytoplankton diversity based on sequencing of the 18S rRNA gene (V9 region) revealed that the actual numbers of phytoplankton taxa based on operational taxonomic units (OTUs, a proxy for species in molecular surveys) are consistently approximately 10-fold higher than morphology-based estimates (Pierella Karlusich *et al.*, 2020).

## 1.2 Ecological traits of small and large phytoplankton cells

As phytoplankton taxonomic diversity is large, phytoplankton taxa are often classified based on cell size. The cell size of phytoplankton spans over at least 9 orders of magnitude, from a cell volume

around  $0.1 \mu\text{m}^3$  for the smallest cyanobacteria to more than  $10^8 \mu\text{m}^3$  for the largest diatoms (Fig. A3).

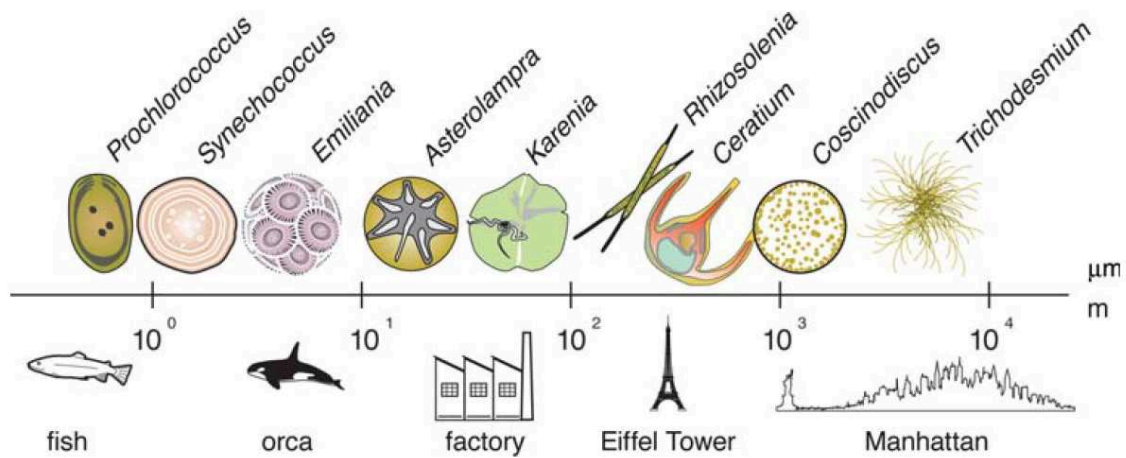


Fig. A3: A comparison of the size range of phytoplankton relative to macroscopic objects (Source: Finkel *et al.*, 2010)

The arbitrary size ranges of  $0.2$  to  $2 \mu\text{m}$ ,  $>2$  to  $20 \mu\text{m}$ , and  $>20$  to  $200 \mu\text{m}$ , are historically referred to as picophytoplankton, nanophytoplankton, and microphytoplankton, respectively. In this thesis, I will use the definition from Richardson (2018) and consider cells  $<20 \mu\text{m}$  to be small and cells  $>20 \mu\text{m}$  to be large.

The distinction between small and large cells is particularly useful as phytoplankton growth and loss process are strongly size dependent (reviewed in Mara $\acute{o}$ n *et al.*, 2009). Small cells are in theory advantaged over larger ones in nutrients and light uptake. They are characterized by higher surface to volume ratio, resulting in increased diffusion capability of nutrients through the cell membrane (e.g Chisholm, 1992; Raven, 1998). The amount of light absorbed per pigment unit also decreases with increasing cell size, as high intracellular pigment concentration creates self-shading among the different pigment molecules (the “package effect”; Finkel, 2001). Moreover, a large cell size increases the cell’s sinking velocity (mechanism also known as Stokes’ law), which implies a reduction of their residence time in the euphotic layer unless they have a way to regulate their position in the water column (e.g. active swimming, gas vacuoles). These advantages of being small are particularly relevant in strongly stratified water columns, where nutrients input from deep waters are scarce and large cells are less likely to return to the photic layer in the absence of water mixing.

While being small is advantageous in terms of resource and light acquisition, large cell size is assumed to lower, or at least offset the predation pressure. The main reason is that the generation time of predators increases with body size more rapidly than the generation time of phytoplankton. Small phytoplankton are typically consumed by microzooplankton like dinoflagellates and ciliates,



which have generation times similar to those of phytoplankton (in the order of hours to days) and exert a strong control on their biomass. In contrast, large cells may accumulate biomass temporarily by their ability to escape high predation rates (Smetacek *et al.*, 2004; Irigoien *et al.*, 2005). This theoretical approach of allometric relationship between prey size and its grazing mortality is however oversimplified as it appears that heterotrophic protists with short generation times (in particular dinoflagellates) are important consumers of large cells such as diatoms (Sherr and Sherr, 2009). Consequently, although some studies have found that small phytoplankton suffer higher grazing losses than larger cells (Latasa *et al.*, 1997; Landry *et al.*, 2000; Strom *et al.*, 2007), others have reported similar grazing pressure on phytoplankton groups of markedly different mean cell size (Latasa *et al.*, 2005; Gutiérrez-Rodríguez *et al.*, 2011; Chang *et al.*, 2013).

These general growth and loss patterns play a role in determining the size structure of phytoplankton communities in contrasting marine environments and explain the overall dominance of small phytoplankton in oligotrophic tropical waters, whereas larger cells dominate the chlorophyll *a* biomass in upwellings or nutrient-rich coastal waters (Fig. A4).

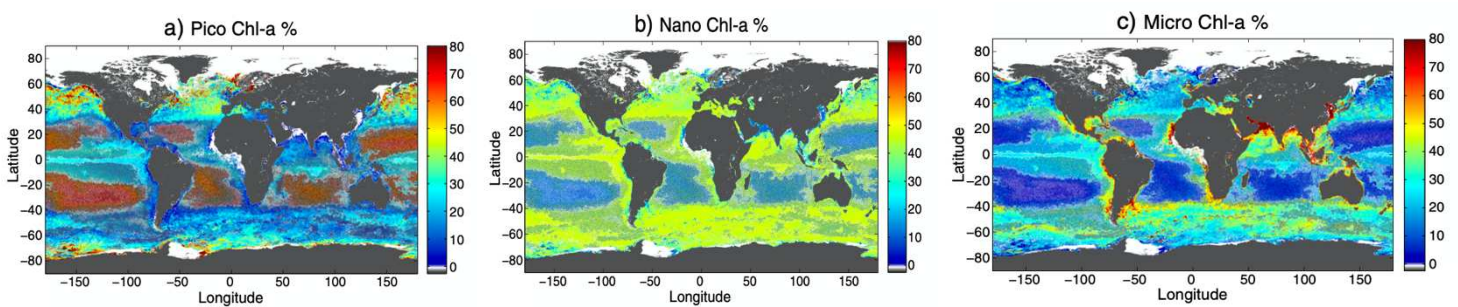


Fig. A4: Estimated contribution of phytoplankton size-groups to Chl *a* for the period of winter 2010–2011. (Source: Roy *et al.*, 2013)

Within small and large phytoplankton, specific taxonomic lineages are characterised by particular ecological traits (e.g. light and nutrient quality/quantity requirements or grazer avoidance, to cite only a few Glibert, 2016). Consequently, phytoplankton groups feature differences in their ecological niches (Brun *et al.*, 2015).

In the next paragraph, I will briefly review the specific ecological characteristics determining the fitness and success of important “small” and “large” phytoplankton groups that thrive in the ocean, with a focus on emblematic groups of the SO.

### 1.3 Phytoplankton diversity in the Southern Ocean

The SO harbours phytoplankton communities typically dominated by diatoms and haptophytes, superimposed upon a background of pico- and nanophytoplankton (e.g. Wright *et al.*, 2010; Wolf *et al.*, 2014). For decades, large diatoms have been considered as the most important

phytoplankton group for primary production in the SO, because of their ability to form large blooms. Estimates from remote sensing studies considered that diatoms could account for 89% of the primary production of the SO (Rousseaux and Gregg, 2013). This important role of diatoms in SO primary production constitutes the foundation of the emblematic “food chain of the giants” (diatoms-krill-whales) (Smetacek, 2008). However, large disagreements still exist between the models regarding the distribution and contribution to production of major phytoplankton groups of the SO (Fig. A5). *In situ* measurements to calibrate models are sparse in space and time in this remote ocean and satellite observations require cloud-free scenes which leads to sparse winter data in the often cloud-covered SO (Losa *et al.*, 2019).

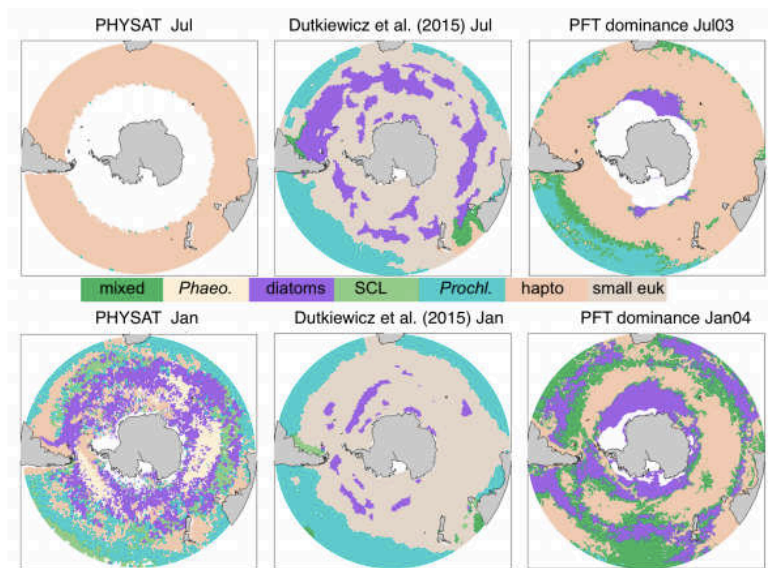


Fig. A5: Surface dominance (fraction of total Chl a > 55%) of phytoplankton groups for July 2003 and January 2004 according to three different models (PHYSAT; Alvain *et al.*, 2008), the Darwin-MITgcm version of (Dutkiewicz *et al.*, 2015) and (Losa *et al.*, 2019). “SCL” represents *Synechococcus* like prokaryotic phytoplankton. Simulated haptophytes include *coccolithophores* and *Phaeocystis*. The dominance between diatoms and small phytoplankton (haptophytes, Phaeo and small eukaryotes) varies greatly between models. However, in all models, the dominance of small phytoplankton over diatoms is observed during winter months (July).

Among the most important groups of small phytoplankton of the SO, haptophytes, small diatoms, cryptophytes and to a lesser extent prasinophytes have been described as key players of phytoplankton communities (Moline *et al.*, 2004; Uitz *et al.*, 2009; Georges *et al.*, 2014; Iida and Odate, 2014). Precise identification of important representative genera within these broad taxonomic groups, as well as the ecological drivers of their success is, however, scarce.

### Diatoms

Diatoms (Bacillariophyceae), are photoautotrophic stramenopiles, characterized by a silica cell wall, the frustule. Sarthou *et al.* (2005) reported that diatoms may contribute up to 40% of oceanic primary productivity. This group exerts a major influence upon the biogeochemical cycles of carbon, silicon, nitrate, and iron in the open ocean (Tréguer *et al.*, 2018). Diatoms tend to have significantly

higher maximum uptake rates of nutrients than any other group and relatively high maximum growth rates (Litchman *et al.*, 2007; Litchman and Klausmeier, 2008). Large diatoms are able to effectively utilize nutrient pulses by storing nutrients in disproportionately large vacuoles compared to smaller diatoms (Sicko-Goad *et al.*, 1984; Raven, 1987).

In the SO, iron and silicic acid availability are critical for diatoms to sustain high relative growth rates and biomass. They are able to form large seasonal blooms in iron-enriched regions in summer in high macronutrient regions such as the Ross Sea, the Kerguelen Plateau and South Georgia (Korb and Whitehouse, 2004; Blain *et al.*, 2007). Diatom dominance also seems to be favored by high water column stratification as they are characterized by higher tolerance to photoinhibition as compared to *P. antarctica* populations in high light conditions (Arrigo *et al.*, 2010; Mills *et al.*, 2010). In addition to iron availability, the supply of silicate, required for diatoms to build their silica frustules, is also considered to be an important factor controlling the dominance of diatoms in the SO. The silicate concentrations show a decreasing northward gradient, in particular on either side of the Antarctic Polar Front, with low silicate concentrations ( $< 5 \mu\text{M}$ ) in the sub-Antarctic waters north of the Polar Front and high silicate concentrations ( $> 60 \mu\text{M}$ ) to the south of the Polar Front (Tréguer, 2014; Fig. A6). As a result, diatoms typically dominate phytoplankton communities in summer South of the Polar Front in iron-enriched, stratified waters like marginal ice zones (Wang *et al.*, 2014) or over naturally iron-fertilized areas near islands (Korb and Whitehouse, 2004; Blain *et al.*, 2007).

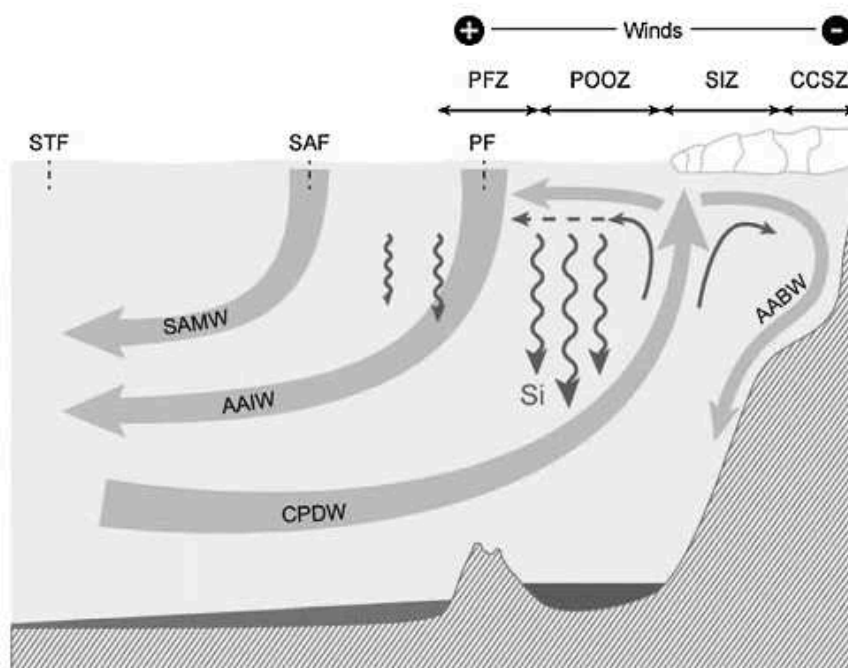


Fig. A6: Schematic representation of water masses, frontal systems and transport of nutrients in the SO. PF: Polar Front, STF: Sub-Tropical Front.

Through the upwelling of the Circumpolar Deep Water (CPDW) at the Antarctic Divergence, the surface waters are enriched in nutrients (nitrate, phosphate and silicic acid in particular). This favors the growth of diatoms and intense biogenic silica production, which triggers abundant export of biogenic silica to deep waters, ultimately depositing opal on abyssal sediments (mostly south of the PF). Unused nutrients are exported to the rest of the world ocean through the Sub-Antarctic Mode Water (SAMW), the Antarctic Intermediate Water (AAIW), and the Antarctic Bottom Water (AABW). (Source: Tréguer, 2014)

Iron availability can greatly influence diatoms' size, chain length and taxonomic composition. Typically, adding iron to iron-limited surface waters particularly stimulate growth of large and chain-forming diatoms (Boyd *et al.*, 2007). Inversely, most diatoms decrease their cell volumes by as much as 50% when grown under iron-limited conditions (Sunda and Huntsman, 1997; Leynaert *et al.*, 2004) and tend to be present as solitary cells or form very short chains (Hoffmann *et al.*, 2008). Different diatom taxonomic compositions were observed on and off naturally iron-fertilized areas (Armand *et al.*, 2008; Lasbleiz *et al.*, 2016). This likely results from species-specific responses to iron availability and some diatom families like pennate diatoms, *Pseudo-nitzschia* in particular, consistently thrive when iron is non-limiting (de Baar *et al.*, 2005; Marchetti *et al.*, 2009).

### Haptophytes

Haptophytes constitute a widespread lineage, dominating the Chl *a*-normalized phytoplankton standing stock in modern oceans and possibly accounting for 30–50% of total Chl *a* biomass in the global ocean (Liu *et al.*, 2009). Their success in diverse environments (open-ocean, shelf, upwelling, coastal, littoral, brackish and freshwater environments) has been attributed to their ability to complement photosynthesis with other particulate (bacteria mostly) and/or dissolved organic food sources (Kawachi *et al.*, 1991; Nygaard and Tobiesen, 1993; Liu *et al.*, 2009).

Molecular evidence support the division of the Haptophyta into two main classes, the Pavlovophyceae and the Prymnesiophyceae (Edvardsen *et al.*, 2000). The vast majority of the known diversity of haptophytes occurs in the Prymnesiophyceae, which comprises two orders of non-calcifying (Phaeocystales and Prymnesiales) and one calcifying taxa (coccolithophores containing four orders: Isochrysidales, Coccolithales, Syracosphaerales and Zygodiscales; Fig. A7).

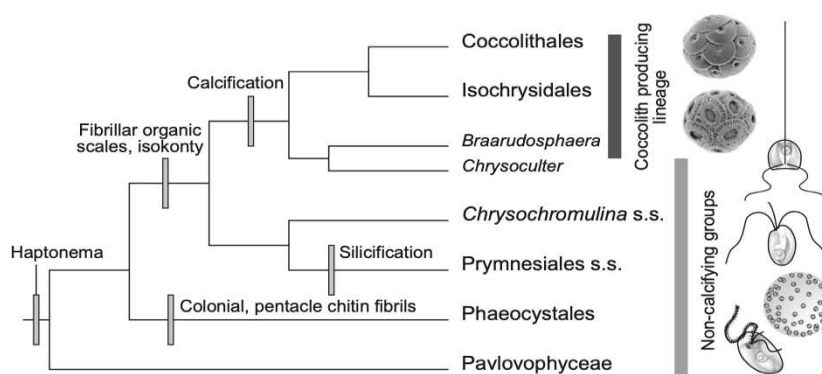


Fig. A7: Phylogenetic tree of haptophyte algae showing major groups. (Source: Tsuji and Yoshida, 2017)

Haptophytes include famous bloom-forming taxa, such as the famous calcifying species (coccolithophore) *Emiliana huxleyi*, as well as *Chrysochromulina*, *Prymnesium* and *Phaeocystis* (Gjøsæter *et al.*, 2000; Tyrrell and Merico, 2004; Schoemann *et al.*, 2005; Granéli *et al.*, 2012). *Phaeocystis* is an ubiquitous marine genus that contains three bloom-forming species with typical

geographic distributions: *P. pouchetii* dominating in the Arctic Ocean, *P. globosa* in temperate coastal seas and *P. antarctica* in the SO, respectively (Schoemann *et al.*, 2005). The divergence of the “cold-water forms” (*P. pouchetii* and *P. antarctica*) from the “warm-water forms” (*P. globosa*) was estimated to happen about 30 Mya and the divergence of *P. antarctica* and *P. pouchetii* to be about 15 Mya (Lange *et al.*, 2002). Ecological success of bloom-forming *Phaeocystis* was attributed to its polymorphic life cycle alternating free-living cells (3–9  $\mu\text{m}$  in diameter) and gelatinous colonies usually reaching several millimeters (Schoemann *et al.*, 2005; Fig. A8).

In the SO, *P. antarctica* colonies regularly form huge blooms in the seasonal ice zone and coastal Antarctic waters, that can lead to rapid carbon export through the formation of fast sinking aggregates (DiTullio *et al.*, 2000). Nutrients such as nitrate and phosphate appear to have little influence on *P. antarctica* growth, as they remain at relatively high concentrations over the annual cycle. Its ability to grow at low irradiance allows it to bloom early in the season or under the sea ice (Peperzak *et al.*, 1998; Hilst and Jr, 2002; Boyd *et al.*, 2010). *P. antarctica* also benefits from lower iron half-saturation constants for growth than diatoms (Alderkamp *et al.*, 2012). However, iron availability triggers *Phaeocystis* colony formation which can result in the bloom in the Ross Sea for example (Bender *et al.*, 2018). Typically, a switch from colony to solitary forms is observed throughout the season as a consequence of more severe micronutrient limitation for the colonies relative to solitary cells (Smith *et al.*, 2003). The large size of colonies appear to lower the grazing rates in comparison to solitary cells, which are easily consumed by microzooplankton (Caron *et al.*, 2000; Tang *et al.*, 2008). Consequently, colonial forms of *Phaeocystis* are assumed to enhance carbon export by direct sinking of large ungrazed mucilaginous aggregates rich in carbon, whereas solitary forms are assumed to fuel the microbial network and be quickly recycled within the mixed layer (Smith *et al.*, 2003).

### Other phytoplanktonic groups of the SO

Prasinophytes and cryptophytes have been identified in pigment studies as major contributors to Chl *a* in some sectors of the SO (Moline *et al.*, 2004; Iida and Odate, 2014 and references therein). Prasinophytes form a paraphyletic group belonging to division Chlorophyta (“Green algae”), represented by flagellated small cells characterized by chlorophylls *a* and *b* as the major photosynthetic pigments (reviewed in Leliaert *et al.*, 2012). Mamiellophyceae is the largest lineage

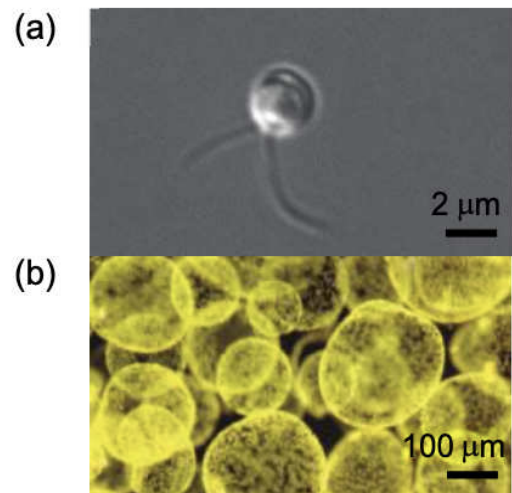


Fig. A8: Pictures of (a) a single *Phaeocystis* in cell culture and (b) *Phaeocystis* colonies in a Ross Sea bloom. (Source: Bender *et al.*, 2018)

of prasinophytes, including some of the smallest eukaryotes known (e.g., *Ostreococcus*, *Micromonas*; < 2  $\mu\text{m}$ ).

Prasinophytes are characterized by intermediate values of nutrient uptake and growth parameters, except for ammonium, for which they have a disproportionately high preference over nitrate (Litchman and Klausmeier, 2008). This high preference for ammonium may be linked to the higher availability of ammonium under lower  $\text{pO}_2$  conditions 1.5 billion years ago, when prasinophytes likely appeared (Litchman and Klausmeier, 2008). Furthermore, at this time, iron concentrations in the water were more elevated than at the present time, which may explain their higher iron requirements than phytoplankton cells from the red lineage (Quigg *et al.*, 2003). These two characteristics could partly explain why they dominate the eukaryotic picoplankton in coastal eutrophic areas especially, reaching  $10^5$  cells  $\text{ml}^{-1}$  (O'Kelly *et al.*, 2003; Guillou *et al.*, 2004; Not *et al.*, 2004). Recently, it has been suggested that bacterivory could be a significant complementary resource acquisition strategy for green algae under low nutrient conditions, even at low bacterial concentrations (McKie-Krisberg and Sanders, 2014; McKie-Krisberg *et al.*, 2015; Anderson *et al.*, 2018). In the SO, pigment analyses have reported the presence of prasinophytes mostly north in the sub-Antarctic zone north of the Polar Front (Wright *et al.*, 1996; Iida and Odate, 2014; Wolf *et al.*, 2014; van Leeuwe *et al.*, 2015). However, classical pigment and microscopy analyses are not adapted to reveal the taxonomic identity of these prasinophytes as these tiny cells lack easily identifiable morphological features. Recently, a genetic study demonstrated that *Micromonas* was present in the SO and that Antarctic *Micromonas* may be connected to Arctic *Micromonas* through deep-sea currents (Simmons *et al.*, 2015). *Micromonas* also represented a major fraction of the sequences of the pico- and nanoplankton community within an artificially Fe-fertilized patch (Thiele *et al.*, 2014).

The importance of cryptophytes has been mostly reported in coastal waters of West Antarctica, where blooms are usually dominated by diatoms. Some studies have noted the increasing importance of cryptophytes that can prevail over diatoms in association with highly illuminated conditions in shallow upper mixed layers and strong water column stratification (Ducklow *et al.*, 2013; Mendes *et al.*, 2018). Such a recurrent transition from diatoms to cryptophytes represents a fundamental decrease in the size spectrum of the phytoplankton community, which can impact grazing efficiencies of different zooplankton species, enhancing microbial activity in the region and, consequently, promoting changes in carbon fluxes within the water column (Moline *et al.*, 2004).

Concluding, even though models of primary production in the SO estimates that small phytoplankton contributes more to annual primary production ( $2.5 \text{ Gt C yr}^{-1}$ ) than microphytoplankton ( $0.9 \text{ Gt C yr}^{-1}$ , Uitz *et al.* 2010), little information is currently available on small phytoplankton diversity and ecological drivers in the SO. This knowledge gap partly originates from the timing of most cruises exploring phytoplankton community composition during spring and summer diatom blooms, a period where small cells represent a small fraction of the biomass.

## 2. Phytoplankton in the carbon cycle

Historically, the evolution and diversity of phytoplankton deeply influenced the carbon cycle. For instance, the radiation of large-celled eukaryotic marine phytoplankton enhanced the export of organic carbon and nutrients to the ocean interior through the Mesozoic (Katz *et al.*, 2007). This established stronger lateral, vertical and temporal variations of nutrient levels that further advantaged eukaryotic phytoplankton relative to cyanobacteria, because of their larger nutrient storage capacity and complex behavioral and trophic strategies (Worden *et al.*, 2015). Therefore, taxonomic composition and size-structure of phytoplankton communities potentially control carbon export flux and influence the long-term concentration of CO<sub>2</sub> in the atmosphere.

### 2.1 The Biological Carbon Pump (BCP)

Currently, phytoplankton in the global ocean is responsible for the photosynthetic fixation of around 45-50.10<sup>15</sup> g C annually, which represents almost half of global net primary production on Earth (Field *et al.*, 1998). Some 20% of phytoplankton net primary production (5-10 Gt C) is exported toward the ocean's interior, either in the form of sinking particles or as dissolved material (Falkowski *et al.*, 1998; Palmer and Totterdell, 2001). The vertical transfer processes include passive sinking of organic particles, physical mixing of particulate and dissolved organic carbon (POC and DOC, respectively), and active transport by zooplankton migration. The mineralization of the organic matter increases with depth the concentration of dissolved inorganic carbon. The net effect of this phytoplankton-fueled biological pump, is the transport of CO<sub>2</sub> from the atmosphere to the deep ocean, where it may be sequestered over the timescales of deep-ocean circulation (10<sup>2</sup>–10<sup>3</sup> years). A small fraction (<1%) of the organic matter transported toward the deep ocean escapes mineralization and is buried in the ocean sediments, where it is retained over timescales of >10<sup>6</sup> years. It is predicted that if the biological pump stops pumping carbon down to the ocean interior, atmospheric levels of CO<sub>2</sub> would in time rise by another 100-200 ppm thereby accelerating global warming (Field *et al.*, 1998; Ito and Follows, 2005). Thus, phytoplankton play a role in the regulation of the atmospheric content of CO<sub>2</sub> and therefore affect climate variability.

Several studies have demonstrated that regional differences exist in the strength, overall export efficiency and depth-dependent export efficiency of the biological pump (Henson *et al.*, 2012). These differences are driven by the structure of pelagic communities, which ultimately determine the magnitude of the biological sequestration of carbon in the deep ocean and sediments (Turner, 2015).

### 2.2 Impact of phytoplankton community size structure on the BCP

Size-structure of phytoplankton communities is often considered as an important determinant of the magnitude of the BCP. Classically, it is considered that the carbon produced by small or large phytoplankton follow different pathways: the microbial food web for small cells and classical food

chain for larger ones (Legendre and Le Fèvre, 1995; Laender *et al.*, 2010). In the microbial food web, autotrophic production is dominated by small cells and rapidly respired within the microbial loop in the euphotic layer (e.g. Michaels & Silver 1988), resulting in little export. In contrast, the dominance of larger phytoplanktonic cells is thought to be associated with short, direct food chains (e.g. “diatoms-krill-whales” in the SO; Smetacek *et al.*, 2004). This classical food chain is generally thought to fuel the BCP through direct sinking of large phytoplankton cells and the production of large fast-sinking fecal pellets by higher trophic levels, with a high carbon content (Michaels and Silver, 1988) (Fig. A9).

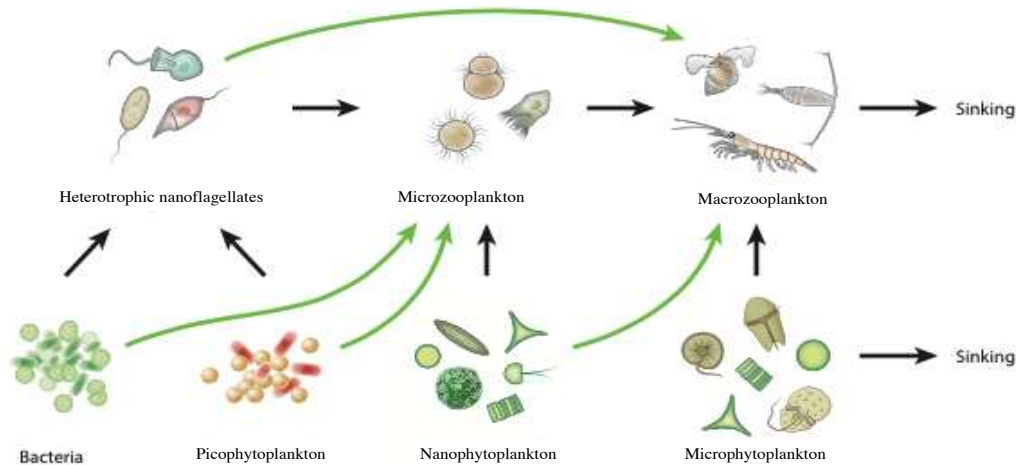


Fig. A9: The two-level food web of Michaels & Silver (1988), which was a modification of the basic food web (black arrows) with the size of prey ingested by zooplankton expanded (green arrows). In this scheme, only large phytoplankton can directly sink and their export pathway through grazing is more direct (only one step, than for small phytoplankton). (Source: Richardson, 2018)

These general ecological and biogeochemical features associated with small and large phytoplankton marine communities (Table A1) have motivated the development of marine ecosystem and biogeochemistry models integrating different phytoplankton size classes (Poulin and Franks, 2010; Ward *et al.*, 2012).

Table A1: General ecological and biogeochemical properties of plankton communities in which phytoplankton are dominated by small vs large cells (Marañón *et al.*, 2009)

Dominant size-class	Small cells	Large cells
Total phytoplankton biomass	Low	High
Total primary production	Low	High
Dominant trophic pathway	Microbial food web	Classical food chain
Main loss process for phytoplankton	Grazing by protists	Sedimentation and grazing by metazoans
Photosynthesis:respiration ratio	Appr. 1	>1
Export efficiency	5-15%	>40%
Main fate of primary production	Recycling within the euphotic layer	Export toward deep waters

However, the classical view that large cells contribute disproportionately to export is increasingly debated with growing indirect and direct evidences that small phytoplankton can be a major contributor to C-export. The debate started in 2007 when Richardson and Jackson advanced that the relative direct and indirect contribution of picoplankton to export were proportional to their total



net primary production, despite their small size (Richardson and Jackson, 2007). Their conclusion, based on inverse modelling and network analyses, underlined the importance of aggregation that made small cells available to mesozooplankton grazers and allowed them after transformation in fecal pellets to reach relatively high sinking rates. Indeed, direct observations from sinking aggregates confirmed that small cells could make substantial contributions to export production via the production of fecal pellets by mesozooplankton or salps grazers (e.g. Sutherland *et al.*, 2010; Wilson and Steinberg, 2010; Ebersbach *et al.*, 2014). Interestingly, intact *Prochlorococcus* cells at concentrations of  $10^2$ – $10^4$  cells mL<sup>-1</sup> were reported as deep as 800 m in the Pacific (Jiao *et al.*, 2014). These observations suggest that small phytoplankton could play an important role in C-export. Overall, direct observations based on modern underwater particle imaging combined with field POC flux data estimated that higher mass fluxes were measured for large phytoplankton-dominated communities than in systems dominated by small phytoplankton. However, small phytoplankton-dominated communities were characterized by lower remineralization rates, resulting in higher export efficiency than in systems dominated by larger cells (Guidi *et al.*, 2009).

### 2.3 Predicted increase in small phytoplankton dominated communities

Ongoing climate warming is expected to increase ocean stratification, and hence reduce nutrient input from deep waters to the upper mixed layer, with an overall negative effect on phytoplankton primary production (Bopp *et al.*, 2001; Sarmiento *et al.*, 2004). Such a change is already taking place and oceanic areas exhibiting the lowest chlorophyll concentrations ( $<0.07$  mg L<sup>-1</sup>) are expanding at annual rates varying between 0.8% and 4.3% (Polovina *et al.*, 2008). For the reasons explained in part 1.2., this scenario is thought to favor small phytoplankton at the expense of diatoms (Bopp *et al.*, 2005; Li *et al.*, 2009).

Resulting changes in phytoplankton community structure are expected to have a cascading effect on structure of marine food webs and biogeochemical cycling of carbon (Finkel *et al.*, 2010). Using a coupled oceanic biogeochemical model and climate model, a large decrease in export production as a result of this shift, by as much as 25% at in case of a four-fold increase of CO<sub>2</sub> concentrations was predicted (Bopp *et al.*, 2005). However, treatment of plankton communities is relatively simple in these models, with 1–3 phytoplankton functional types and typically one zooplankton group (Bopp *et al.*, 2013). The models including both large and small phytoplankton, assume a higher export efficiency (by a factor of 3 or more) for the large phytoplankton (Aumont and Bopp, 2006). Consequently, it is not surprising that these models predicted that a shift towards smaller phytoplankton cells is expected to decrease C-export. Other models combining inverse modeling and ecological network analysis predicted that a shift from large to small phytoplankton-dominated communities would alter the pathways of carbon flow, but result in minimal changes in carbon export (Vernet *et al.*, 2017). In this inverse model, high export in nanoflagellates dominated community was possible, if a link between the classical and microbial food webs develops through

the consumption of microzooplankton and detritus by copepods. More integrative *in situ* studies are needed to study the effects of a shift from large to small phytoplankton communities and settle this debate.

### 3. Southern Ocean phytoplankton and the C-cycle

The SO (south of 30°S), occupies 30% of global surface ocean area and is estimated to account for 43%±3% (42±5 Pg C) of anthropogenic CO<sub>2</sub> and 75%±22% of heat uptake by the ocean over 1861-2005 (Frölicher *et al.*, 2014). The SO holds a special place in view of its possible impact on the biogeochemistry of the world ocean. The circulation of Antarctic Intermediate Water, formed in the Polar Frontal Zone, redistributes major nutrients to lower latitudes and controls the dynamics of primary producers over large regions of the world ocean, directly influencing the biological pump at the global scale (see Fig. A8).

Over the last century, large decadal variations in the SO carbon sink have raised several concerns regarding to the future capacity of the SO carbon sink (Quéré *et al.*, 2007; Landschützer *et al.*, 2015; Sitch *et al.*, 2015). Climate of the SO is predicted to experience increased warming, strengthening wind, acidification, shallowing mixed layer depths, increasing light, changes in upwelling and nutrient replenishment, declining sea ice, reduced salinity, and the southward migration of major fronts (Deppeler and Davidson, 2017). All these changes raise major uncertainties concerning the response of phytoplankton communities and the impact of SO productivity on the BCP.

#### 3.1 Control of Southern Ocean productivity

##### *The Southern Ocean paradox*

The SO is the largest upwelling region of the globe. Remarkably, major nutrients (N, P, Si) brought to surface waters by the upwelling of deep waters on the Antarctic shelf are not fully used and the SO is the largest high-nutrient, low-chlorophyll (HNLC) region of the world. The fact that macronutrients were not used up was termed the “Antarctic paradox” since the 1930s (Hart, 1934). Several hypotheses have been ventured to explain this paradox: growth limitation due to unfavorable light (because of deep mixing and light limitation in winter), trace element deficiency, and high mortality due to intense grazing pressure by micro- and microzooplankton, limiting the accumulation of phytoplankton biomass. Smetacek *et al.*, (1990) described the Antarctic ecosystem as a “retention type system”, in which relatively high abundances of zooplankton are sustained in an ecosystem despite low phytoplankton biomass. The recycling of the bulk of zooplankton faeces in the surface layer would provide the essential nutrients to maintain phytoplankton growth (González, 1992). The relative importance of these mutually inclusive explanations is still under debate, however there is strong evidence that the key factor limiting phytoplankton production in vast areas of the SO is iron availability (de Baar *et al.*, 2005; Blain *et al.*, 2007; Boyd *et al.*, 2007).

### The Iron hypothesis

The Iron hypothesis formulated by Martin in 1990 suggested that the higher productivity observed in the SO during glacial periods may have been stimulated by greater inputs of dust-bearing iron. This, in turn, would have increased the strength of the biological pump and explain the strong decrease of atmospheric CO<sub>2</sub> during cold times (Fig. A10).

Iron is indeed a vital micronutrient for phytoplankton because of its requirement in photosynthetic electron transport chains (e.g. PSI, PSII, the Cytochrome b6-f-FeS complex; Behrenfeld and Milligan, 2013). As a consequence of the lack of iron, phytoplankton cannot completely utilize the available macronutrients (particularly nitrate) for photosynthesis, and the primary

production is relatively low in vast areas of the SO, despite high availability of macronutrients. The implications of the “iron hypothesis” in a context of climate change are huge. After John Martin stated during a lecture, “give me a half tanker of iron, and I will give you an ice age”, iron-addition to HNLC waters has been debated as a solution to mitigate the effects of anthropogenic CO<sub>2</sub> by stimulating phytoplankton production (e.g. Chisholm, 2000; Buesseler and Boyd, 2003). These events marked the begin of the “iron age” in oceanography (de Baar *et al.*, 2005; Stoll, 2020), with many cruises and experiments trying to disentangle the interplay between Fe-fertilization, plankton community structure, food webs and their effects on the BCP.

### 3.2 Impact of Fe-fertilization on phytoplankton communities and C-export

Artificial iron fertilization experiments in HNLC waters conducted over the past two decades have unequivocally led to enhanced phytoplankton growth in iron limited regions (Boyd *et al.*, 2001; Coale *et al.*, 2004). In the SO, seven artificial iron fertilization experiments, namely SOIREE (Southern Ocean Iron Release Experiment; Boyd, 2002), EisenEx (Eisen Experiment; Assmy *et al.*, 2007), SOFeX (Southern Ocean Iron Experiment; Coale *et al.*, 2004), SOLAS-SAGE (Surface Ocean Lower Atmosphere Studied-Sea Air Gas Exchange Experiment; Harvey *et al.*, 2011), EIFEX (European Iron Fertilization Experiment; Smetacek *et al.*, 2012) and LOHAFEX (Loha Fertilization

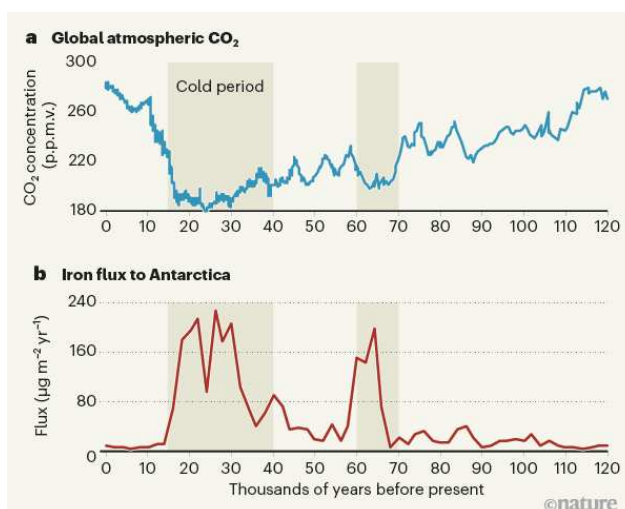


Fig. A10: The anti-correlated data that inspired the iron hypothesis. (a) Measurements of air bubbles trapped in cores drilled from the Antarctic ice sheet show that atmospheric levels of carbon dioxide were significantly lower during the coldest periods (shaded regions) than during modern times (CO<sub>2</sub> concentrations are shown in parts per million by volume; p.p.m.v.). (b) The ice-core records also reveal that more iron was transported to the Southern Ocean in wind-blown dust during the coldest periods than during warmer times (iron flux is measured in micrograms per square metre per year). (Source:Stoll 2020)

Experiment; Martin *et al.*, 2013) have been carried out so far. During SOIREE (February 1999) and EisenEx (November 2000), increased growth rates, as well as a floristic change from piconano-flagellates to large chain-forming diatoms was observed over the first days of fertilization, with no measurable change in the downward POC flux with the  $^{234}\text{Th}$  method (Boyd *et al.*, 2000; Assmy *et al.*, 2007). The short observational periods (13 and 27 days), as well as other intrinsic limits and artefacts of the small-scale fertilization technique, may have prevented a clear assessment of carbon export and explain why no increase in the C-export was observed during these experiments. During EIFEX, Fe-fertilization led to a massive diatom bloom and it was estimated that at least half the bloom biomass sank far below a depth of 1,000 metres (Smetacek *et al.*, 2012). SoFEX compared the effects of iron fertilization in low Si sub-Antarctic ( $\text{Si}[\text{OH}]_4 < 3 \mu\text{mol L}^{-1}$ ) waters north of the Polar Frontal and in high silicate waters south of the Southern Antarctic Circumpolar Current Front ( $\text{Si}[\text{OH}]_4 > 60 \mu\text{mol L}^{-1}$ ). A mixed community of dinoflagellates, *Phaeocystis* and large diatoms (genus *Pseudo nitzschia*), benefited the most from the fertilization in the low-silicate “North Patch”, whereas in the high-silicate “South Patch”, up to 65% of the phytoplankton in the bloom were diatoms (Buesseler *et al.*, 2005). Increased C-export was observed in both patches. Although northern production and biomass were dominated by nonsilicious phytoplankton, the communities driving export production shifted toward diatoms in the north, but remained diatom-dominated in the south (Coale *et al.*, 2004). SOLAS-SAGE and LOHAFEX also explored the effect of Fe-fertilization in Si-limited waters. During SOLAS-SAGE, a modest increase in picophytoplankton biomass was observed, but without an increase in particulate organic carbon (POC) at the surface or in C-export. Phytoplankton growth was thought to have been kept in check by the resident microzooplankton grazers with the increase in POC being recycled through the microbial food web (Harvey *et al.*, 2011). LOHAFEX was a three-weeks experiment in the productive south-west Atlantic sector of the Southern Ocean depleted in Si in late summer 2009. Chlorophyll levels tripled and the biomass of autotrophic pico- and nanoflagellates doubled (Martin *et al.*, 2013). The biomass levels of almost all other groups of the phyto- and microzooplankton (heterotrophic nanoflagellates, dinoflagellates and ciliates) remained remarkably stable throughout the experiment both inside and outside the fertilized patch (Schulz *et al.*, 2018). Fe-fertilization during LOHAFEX didn't enhance downward export of particles, but many small flagellates and coccoid cells were found in the sediment traps, and it was suggested that these small cells probably contributed the majority of downward POC flux (Ebersbach *et al.*, 2014).

Other studies analyzed the effect of natural iron fertilization near land mass (Crozet and Kerguelen Plateau, South Georgia) on phytoplankton communities and C-export. CROZEX established that *Phaeocystis* represented 78% of phytoplankton biomass in Fe-fertilized subantarctic waters north of the Crozet Plateau, whereas HNLC waters South of the plateau were characterized by large diatoms (Poulton *et al.*, 2007). Primary production was 3 to 5 times higher and C-export two to

three times larger in naturally iron-fertilized waters by the Crozet plateau than in the adjacent HNLC area (Pollard *et al.*, 2009). KEOPS 1 and 2 studied respectively the decline (February 2005) and onset (November 2011) of a large diatom bloom over the Kerguelen Plateau. Phytoplankton communities on the Plateau were largely dominated by diatoms, whereas small phytoplankton (flagellates and small diatoms) were abundant off-plateau (Uitz *et al.*, 2009; Lasbleiz *et al.*, 2016). POC export over the plateau was approximately twice larger than in HNLC waters off-plateau during both cruises (Blain *et al.*, 2007; Planchon *et al.*, 2015). Sinking material contained a mixture of phytodetrital aggregates and fecal pellets at bloom onset and mainly fecal pellets at bloom decline, highlighting temporal variations in ecosystem structure and export pathways throughout the season (Laurenceau-Cornec *et al.*, 2015a).

Near South Georgia, diatoms were dominant in and out of iron replete waters, but diatoms were larger and primary production rates were three times higher at stations situated within the main bloom compared to those outside of the bloom (Korb *et al.*, 2008). C-export was more than five times greater in Fe-fertilized areas, with a greater contribution of fecal pellets (Manno *et al.*, 2015). In conclusion, these experiments showed unequivocally that Fe-fertilization enhanced primary production rates. However, a shift to diatom-dominated phytoplankton community was only observed in Si-replete ecosystems. Increased C-export in Fe-fertilized waters was not observed during all experiments, but could involve both diatoms as well as small flagellates dominated surface assemblages (Blain *et al.*, 2007; Pollard *et al.*, 2009; Smetacek *et al.*, 2012).

### 3.3 Inverse relationship between primary production and export

In most of the global ocean, export efficiency is positively correlated to primary production (Laws *et al.*, 2011). However, in the SO, the use in models of this global relationship has been shown to overestimate two to fourfold the export production in comparison with *in situ* export rates (Maiti *et al.*, 2013). Maiti *et al.* (2013) concluded that one of the main reasons for this overestimation was that ecosystems of the SO were characterized by decreasing export efficiency with increasing production which is contrary to existing export models.

Numerous *in situ* measurements confirmed this inverse relationship between primary production and export efficiency (e.g. Froneman *et al.*, 2004; Cavan *et al.*, 2015; Le Moigne *et al.*, 2016). To mention only data collected in our study area, export efficiency at 100 m was on average lower (28%) above the plateau, than in surrounding HNLC waters (58%)(Savoie *et al.*, 2008) during the bloom decline (KEOPS1) although primary production was more than 3 times higher on the plateau (Uitz *et al.*, 2009). At bloom onset (KEOPS1), export efficiency was 37% at HNLC reference station and only 1-2% on the plateau (Planchon *et al.*, 2015).

Several studies have investigated the possible causes for this inverse relationship, suggesting that bacteria and zooplankton may play an important role in the regulation of export efficiency through grazing, remineralization of organic matter, and production/export of fecal pellets (Cavan *et al.*,

2015; Le Moigne *et al.*, 2016). Around Kerguelen, it was also suggested that direct export of heavy-silicified, grazing resistant diatoms found intact in sediment traps may favor the high export efficiency observed in HNLC waters (Laurenceau-Cornec *et al.*, 2015a).

As phytoplankton communities in low productive waters are mostly dominated by small cells, further exploration of the taxonomic and functional diversity of small phytoplankton, as well as direct estimates of their C-fixation with *in situ* measurements are needed to shed light on the drivers of the high export efficiency observed in HNLC waters of the SO.

#### 4. Scientific context and PhD objectives

##### 4.1 Oceanic circulation in the study area

The Kerguelen Plateau (southeast of the Kerguelen Island) is a major bathymetry feature within the Indian Ocean sector of the Southern Ocean, extending from 46°S to 64°S at the 3000 m isobath. It forms a major barrier to the eastward flowing Antarctic Circumpolar Current (ACC), with most of the flow being deflected by the topography to the north of the plateau, and the substantial remainder to the south (Fig. A11)(Park *et al.*, 2008). The Polar Front is a major circulation feature within the region, flowing close to the southeast Kerguelen Island. The position of the Polar Front presents large seasonal variations, shifting southward from spring to summer, being pushed south by warmer and fresher waters brought from the northwest by the ACC (Pauthenet *et al.*, 2018). The circulation over the plateau between the Kerguelen and Heard islands is rather stagnant,  $<5 \text{ cm}^2 \text{ s}$  on average (Robinson *et al.*, 2016).

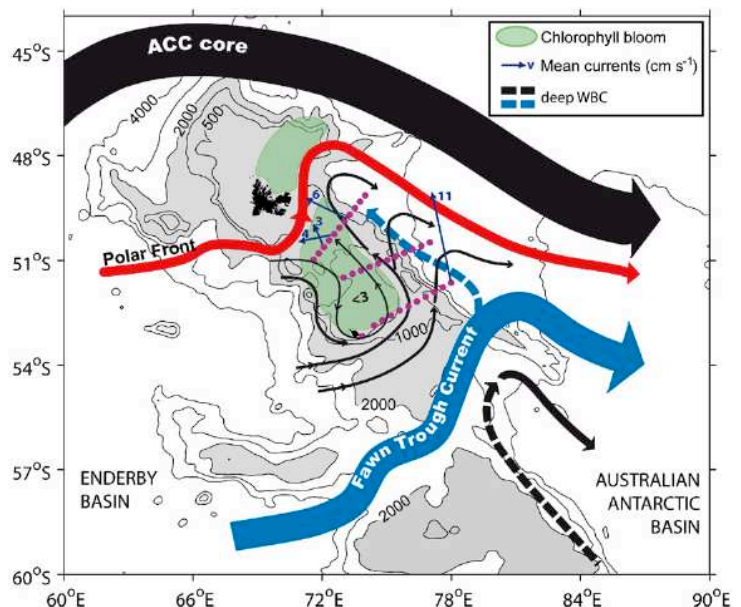


Fig. A11: Schematic of the geostrophic circulation over and around the Kerguelen Plateau based on the synthesis of our major findings. Thin arrows with Arabic numerals stand for directly measured time-mean current vectors averaged over the upper 500 m layer. (Source: Park *et al.*, 2008)

##### 4.2 KEOPS and MOBYDICK cruises

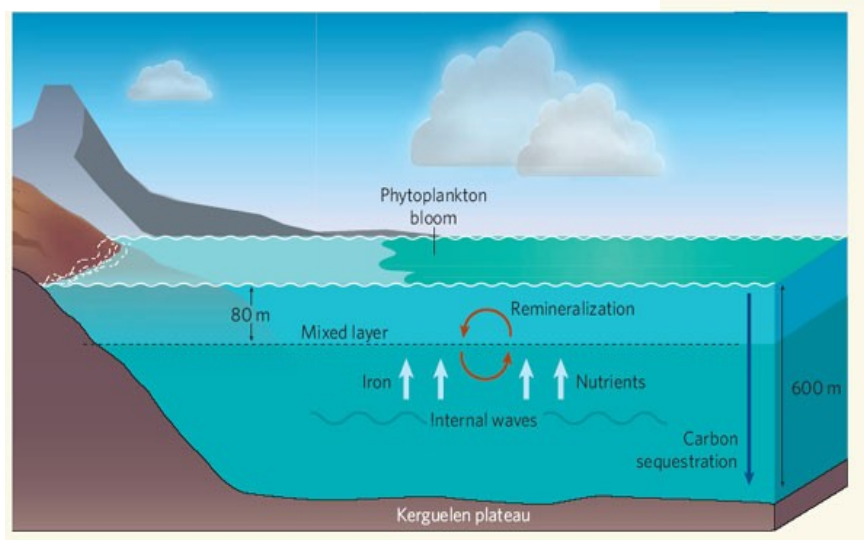
This thesis is part of the MOBYDICK project (Marine Ecosystem Biodiversity and Dynamics of Carbon around Kerguelen; <https://mobydick.mio.osupytheas.fr/>), which aimed at evaluating the links between marine pelagic biodiversity and the carbon sequestration and transfer along the food

web continuum, off Kerguelen islands. Compared to previous studies, the originality of MOBYDICK is the concurrent investigation of pelagic biodiversity at all trophic levels and of every functional group from picoplankton to top predators, together with data acquisition of environmental drivers including dissolved and particulate nutrients. MOBYDICK is a follow-up of two previous cruises in the area: KEOPS 1 at the end of summer (19 January to 13 February 2005) and centered on the plateau and KEOPS 2 (10 October–20 November 2011) at the beginning of spring, which tracked the bloom onset on a fertilized plume in the wake of Kerguelen.

The bloom area is characterized by a narrow plume that extends north- east of the island and north of the Polar Front, that shows high mesoscale and temporal variability, and a larger bloom (45 000 km<sup>2</sup>) southeast of the island and south of the Polar Front, constrained to the bathymetry of the plateau (Blain *et al.*, 2007). Results from the KEOPS cruises unveiled the mechanism of natural iron fertilization on the plateau (Box 1).

### Box 1: Mechanism of iron fertilization over the Kerguelen Plateau

Waters surrounding the Kerguelen area are enriched with macronutrients and trace elements from the crustal interface with the plateau. The interactions between geostrophic current disturbances due to the presence of the island, the tidal activity over the plateau, and strong winds generate internal waves, eddies, jets, Ekman pumping, and a complex hydrodynamical environment (Park *et al.*, 2008; Gille *et al.*, 2014). These characteristics enhance the vertical mixing of the deep waters above the plateau, characterized by high iron and nutrient concentrations, and stimulate higher productivities and C-export above the Plateau in comparison to HNLC surrounding waters (Blain *et al.*, 2007)



*Mechanism of iron and nutrients supply over the Kerguelen Plateau (Source: Boyd 2007)*

KEOPS1 cruise further demonstrated that the iron-enriched bloom region was dominated by microphytoplankton (mainly diatoms), which contributed 80–90% to the total primary production, whereas the HNLC area was mainly (65%) dominated by nano-flagellates and small diatoms (Uitz *et al.*, 2009). The importance of small phytoplankton was also highlighted during KEOPS2 at the HNLC reference station, where autotrophic pico- and nanoeukaryotes represented 74% of the plankton biomass (Lasbleiz *et al.*, 2016). High throughput sequencing of planktonic communities further identified *P. antarctica* as the dominant small phytoplankton taxa (Georges *et al.*, 2014). On-plateau, it was suggested, that diatoms growth were co-limited by iron and silicic acid during the bloom decline (Mosseri *et al.*, 2008). Diatom community composition and succession

throughout the season were studied in details. On-plateau, diatoms evolved from a chain-forming *Chaetoceros* bloom to a remnant *Eucampia antarctica* assemblage, whereby off-plateau, heavy silicified *Fragilariopsis kerguelensis* dominated throughout the season (Armand *et al.*, 2008; Lasbleiz *et al.*, 2016).

#### 4.3 PhD objectives

Before MOBYDICK, no project explored thoroughly the structure of phytoplankton communities on the Kerguelen Plateau outside of the bloom period. However, satellite data and sampling just before the bloom seemed to indicate that small cells were an important component of phytoplankton communities outside of the bloom period (Rembauville *et al.*, 2017; Penna *et al.*, 2018). Investigating small phytoplankton diversity and importance in CO<sub>2</sub>-fixation on and around naturally iron-fertilized waters of the SO when the diatom bloom is over will constitute a milestone in understanding ecosystem functioning and C-cycling in this region where phytoplankton production is highly seasonal.

The two main objectives of this thesis were:

1. To describe the diversity of small phytoplankton after the diatom bloom in ecosystems usually characterized by different productivity regimes on and off the naturally iron-fertilized plateau of Kerguelen.
2. To evaluate the contribution of different taxonomic and size groups of phytoplankton to CO<sub>2</sub>-fixation after the bloom, considering intra-group variability at the single cell level.

Assessing CO<sub>2</sub>-fixation variability between and within different phytoplankton groups should help understanding how phytoplankton taxonomic and size diversity affects the C-cycle within these ecosystems. Comparing these results to the description of phytoplankton communities and productivity regimes at bloom onset and decline will bring valuable insights into the ecological drivers determining the balance between small phytoplankton and diatoms throughout the season and how this affects the functioning of the biological carbon pump.



## B. Material and methods

One of the most exciting challenge for microbial ecologists consist in linking identity of the microorganisms to functions. Over the past two decades, the development of molecular tools such as genomics has completely changed our qualitative understanding of microbial taxonomic and functional diversity in the marine environment (Moran, 2015; Sunagawa *et al.*, 2015). In parallel, new methodologies, like NanoSIMS have been used to directly quantify the role specific microbial populations in biogeochemical processes (e.g. Orphan *et al.*, 2001; Musat *et al.*, 2012; Nuñez *et al.*, 2017).

Different approaches have been used during this thesis to study phytoplankton diversity and link this diversity to CO<sub>2</sub>-fixation. Small and large phytoplankton community composition have been studied by combining different methods (metabarcoding, CARD-FISH and chemotaxonomy) to gain a qualitative and quantitative understanding of phytoplankton's diversity in the study area. The role of small and large phytoplankton in CO<sub>2</sub>-fixation at the single cell-level has then been assessed with NanoSIMS and large geometry SIMS. In this chapter, I will briefly review the principles, interests and limits of these methods.

### 1. Description of small phytoplankton community composition

We combined molecular methods (metabarcoding and CARD-FISH) and chemotaxonomy to investigate the diversity, abundance and structure of phytoplankton communities, focusing on small phytoplankton taxa (Table B1).

*Table B1: Summary of the objectives and methods used to describe the diversity, abundance and biomass of phytoplankton communities, focusing on small phytoplankton groups*

Objectives	Method	Sampling
1. Molecular diversity of small (<20 $\mu\text{m}$ ) and large (>20 $\mu\text{m}$ ) phytoplankton	- Metabarcoding (18S rRNA gene)	- 2 size fractions (0.2-20 $\mu\text{m}$ and 20-100 $\mu\text{m}$ ) - 4 depths (10, 60, 125, 300 m) - After the bloom (MOBYDICK)
2. Abundance of specific taxonomic groups of small phytoplankton	- CARD-FISH labelling of prymnesiophytes, prasinophytes and pelagophytes	- Surface only - After the bloom (MOBYDICK)
3. Biomass of small cells and importance in phytoplankton communities throughout the season	- HPLC and CHEMTAX analysis	- Surface down to 50 m - 3 cruises: Bloom onset (KEOPS 2) Bloom decline (KEOPS 1) After the bloom (MOBYDICK)

## 1.1 Molecular exploration of small phytoplankton diversity with 18S rDNA metabarcoding

Environmental rDNA metabarcoding has opened a new way of assessing the diversity of the smallest organisms in natural environments. The method provides diversity data on many organisms that are difficult to identify by microscopy observation, hard to grow in culture, fragile, or rare. Consequently, metabarcoding studies have revealed previously hidden taxonomic richness, including rare species and parasites (Pedrós-Alió, 2007; Logares *et al.*, 2014), and provided much higher biodiversity estimates than traditional microscopy-based methods (Bachy *et al.*, 2013).

### Process

In our study, 10L of seawater was filtered successively on 20  $\mu\text{m}$  and 0.2  $\mu\text{m}$  to collect large and small planktonic organisms, respectively. After extracting the DNA present on the filter, an identity-gene marker, in our case the short variable regions V4 or V9 of the RNA of the small subunit of the ribosome (18S rRNA gene), was amplified by polymerase chain reaction (PCR). The 18S rRNA gene comprises both conserved and hypervariable regions. Primers targeting conserved regions enable to amplify almost all eukaryotes, while sequencing of hypervariable regions enable to assign the taxonomic affiliation of the different organisms within the sample. We used general eukaryotic primers biased against metazoan to mainly target unicellular eukaryotes (Bower *et al.*, 2004). Informatic processing of the sequences obtained from the pool of amplicons makes it possible to describe the molecular diversity present in the environmental sample (Fig. B1).

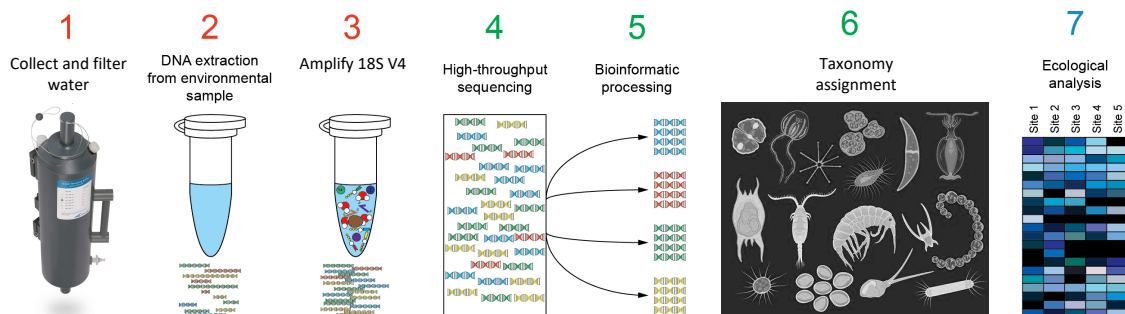


Fig. B1: Overview of the different steps involved in metabarcoding of planktonic communities. Adapted from <http://www.naturemetrics.co.uk>

### Limits

The first applications of metabarcoding attempted to provide quantitative data (based on the assumption that reads obtained from a sequencing run correlate with biomass in the original sample) (Symondson and Harwood, 2014). However, the quantitative relationship between the biomass and sequences produced is not accurate in all cases (Lamb *et al.*, 2019). Each step of the metabarcoding method, from sampling to bio-informatic data analysis is indeed associated with potential biases that can distort the community picture (Table B2).

Table B2: Overview of the factors that can create quantitative biases at each step of the metabarcoding process. Adapted and completed from Lamb *et al.*, (2019).

Stage of protocol	Potential biases
Sample collection	-Presence of PCR inhibitors -Gathering enough material to be representative of the community
DNA extraction	-Differential DNA extraction success between different species
PCR	-Different amplification rates between different species -PCR amplification errors
Sequencing	-Different quantitative estimates between sequencers and runs -Sequencing errors
Bio-informatics	-Different pipelines and data cleaning procedures can yield different community composition

These biases may lead to over- or underestimation of specific taxa. Indeed, amplification rates may differ between species as a result from the difficulty to find universal primers matching with the same efficiency a wide range of divergent lineages (Elbrecht and Leese, 2015). For example, diplomonad flagellates have been revealed as very diverse and abundant using the v9 region, while they are barely detected with conventional v4 approaches (Flegontova *et al.*, 2016). Moreover, the number of rRNA gene copies per cell varies among eukaryotes from one to several thousand (Gong and Marchetti, 2019). Specific taxonomic groups, dinoflagellates for example, have a high number of gene copies (Wisecaver and Hackett, 2011) and are likely overrepresented in molecular data. The number of copies also depends on cell size and while picoeukaryotes have one or a few copies per cell (Rodríguez-Martínez *et al.*, 2009), larger eukaryotes show variations up to several orders of magnitude among taxa (Biard *et al.*, 2017) leading to a higher representation of large organisms in sequencing datasets. To avoid contamination by larger organisms with high rRNA gene content, we used size-fractionated sequencing to access the diversity of small and large protists. A prefiltration on 100  $\mu\text{m}$  was chosen to remove large metazoans and focus on protist communities. We didn't use a prefiltration on 200  $\mu\text{m}$  -considered as a common threshold to define mesoplankton- as this threshold is too high and results in high contamination by large metazoans (Liu *et al.*, 2017). The 20  $\mu\text{m}$  size-fractionation removed most of the larger cells and allowed to have a more in-depth sequencing of the small eukaryotes that we focused on in this study. However, size fractionation only allowed us to infer that the sequence-linked organism was probably smaller than the prefilter pore-size (<20  $\mu\text{m}$ ), but it is possible that some of the sequences obtained from small size-fraction samples derive from larger organisms, which could have broken during the prefiltration step. Alternatively, certain life-stages of larger organisms (e.g., swarmers, resting spores) could be small enough to pass through the prefilter. These concerns highlight the interest of completing the molecular description of phytoplankton communities by microscopic observations to assess the reliability of the data in case sequencing results are unexpected.

In addition to the methodological concerns linked with organisms biology described in the above paragraph, PCR artifacts, sequencing errors and PCR chimeras (sequences formed from two or more biological sequences joined together) are known to artificially inflate diversity estimates

(Kunin *et al.*, 2010; Lee *et al.*, 2012). Discriminating between natural amplicons and technical artifacts is a challenge that has to be addressed by the informatic pipeline for accurate interpretation of diversity estimates. Customarily, the analysis of metabarcoding data begins with the construction of molecular operational taxonomic units (OTUs), i.e. clusters of reads that differ by less than a fixed sequence dissimilarity threshold, most commonly 3% or 1% (Caron *et al.*, 2009). The taxonomic composition of a sample then lists the number of reads of each OTU, which are often treated alike 'species' in diversity analysis. Using dissimilarity thresholds allows to reduce the artificial inflation of diversity resulting from the technical artifacts mentioned above. Nevertheless, these thresholds are arbitrary and the resulting sequences do not always correspond to exact biological sequences. In an attempt to overcome this issue, new methods try to infer the biological sequences in the sample prior to the introduction of amplification and sequencing errors, and distinguish sequence variants differing by as little as one nucleotide (Quince *et al.*, 2011; Callahan *et al.*, 2016). It is the case of the DADA2 pipeline, an open-source R package implementing a full amplicon workflow for Illumina sequencing denoising: filtering, dereplication, sample inference, chimera identification, and merging of paired-end reads (Callahan *et al.*, 2016). To discriminate biological sequences from sequencing errors, DADA2 builds an error model on the basis of the expectation that biological sequences are more likely to be repeatedly observed than are error-containing sequences. Sequencing quality is also considered to determine the likelihood of a new amplicon sequence variant (ASV) to result from a sequencing error. Although metabarcoding methods can't be considered as quantitative for the reasons exposed in the next paragraph, ASV have been shown to be more accurate than conventional OTU methods in representing a sample's diversity and they constitute consistent labels that can be used to compare Illumina datasets using the same marker-gene (Callahan *et al.*, 2017; Caruso *et al.*, 2019). In spite of these advantages, DADA2 can also introduce spurious ASVs, but these spurious ASVs account for a low proportion (<4%) of read numbers (Prodan *et al.*, 2020). In this case, ASVs can be grouped based on similarity or abundance thresholds (Needham *et al.*, 2017).

The last major limitation of sequencing comes from the under-representation of uncultured organisms in databases, resulting in a consequent number of unidentified organisms, for which the taxonomic identification is restricted to a low taxonomic resolution (class or order). Although being the most comprehensive database, using NCBI's GenBank is not recommended to classify 18S rRNA gene sequences due to large amount of wrongly annotated sequences (Geisen *et al.*, 2019). At least two curated databases are dedicated to the 18S rRNA gene, Silva (Pruesse *et al.*, 2007) and PR<sup>2</sup> (Guillou *et al.*, 2013). We decided to use PR<sup>2</sup> as it implements more specialized databases designed for specific taxonomic groups, e.g. foraminifera (Morard *et al.*, 2015) or dinoflagellates (Mordret *et al.*, 2018).

## 1.2 CARD-FISH

Considering the biases described above, marker-gene sequencing needs to be completed with quantitative methods. The most straightforward quantitative monitoring technique available for the specific detection of active small phytoplanktonic cells consists in whole-cell fluorescence in situ hybridization (FISH) of the ribosomal RNA (rRNA). Fluorescently labelled groups can subsequently be visualized under an epifluorescence microscope (DeLong *et al.*, 1989). FISH can be used to detect, identify, and enumerate active microorganisms without requiring culture. The probe can be selected to bind organisms at different taxonomic levels, e.g. group-specific to species-specific, and/or multiple probes can be used to locate multiple taxonomic groups. Fluorochromes are attached to the probe, so that when the probe binds to its target, the cells belonging to the target taxa will become fluorescent when observed at a particular wave length with an epifluorescence microscope (Fig. B2). Standard FISH is not always sufficient to detect pico-sized cells with low rRNA copy numbers, and as such, CARD-FISH (Catalysed Reporter Deposition-FISH), also known as Tyramide Signal Amplification CARD-FISH, is preferably used when studying the composition of marine plankton communities (Pernthaler *et al.*, 2002).

Most probes designed for phytoplankton target broad taxonomic groups, however species-specific probes also exist (Not *et al.*, 2004). Developing probes for finer taxonomic levels is possible, but is time consuming and requires many cultures of closely related taxonomic groups to test the sensitivity and specificity of the probes developed.

In our study, we used results from metabarcoding of the small size fraction to choose the primers that would target most organisms sequenced within Prymnesiophyceae, Pelagophyceae, Mamiellophyceae (Table B3). *In silico* validity of these probes was recently re-assessed and showed that they were indeed specific to their target groups, with some exceptions such as PRAS04 that do not hybridize with 17 targeted taxa (Riou *et al.*, 2017). Abundances obtained in this study should thus be considered as minima.

Table B3: FISH probes used in this study

Probe name	Target group	Source
PRAS04	Mamiellophyceae with a few exception (e.g. <i>Dolichomatix</i> )	(Not <i>et al.</i> , 2004)
PELA01	Pelagophyceae	(Simon <i>et al.</i> , 2000)
PRYM02	Haptophyta	(Simon <i>et al.</i> , 2000)
Euk1209+NChlo01+Chlo02	Eukarya	(Not <i>et al.</i> , 2002)

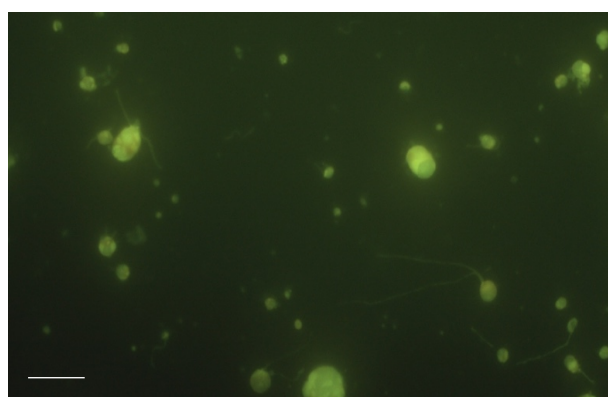


Fig. B2: Epifluorescence microscopy of small phytoplankton sampled during MOBYDICK. Hybridization with a combination of EUK 1209R, NCHLO01 and CHLO01 aimed at targeting all eukaryotes. Scale bar = 10  $\mu$ m.

### 1.3 Chemotaxonomy

Chemotaxonomy was used to complete CARD-FISH quantitative approach and evaluate the contribution of a few small phytoplankton broad taxonomic groups to the chlorophyll *a* (Chl *a*) pool. Chl *a* is the most common index to estimate the biomass of phytoplankton. In some cases, the biomass of Chl *a* can in turn be used as a proxy of phytoplankton carbon biomass using a conversion factor C:Chl *a*. Classically, ratios ranging from 35 to 60 (mean value=50) are used. However, these ratios can be highly variable (e.g. from 6 to 333) depending on the season, light, temperature, depth and nutrient availability (Geider, 1987; Harrison *et al.*, 1990; Jakobsen and Markager, 2016). Consequently, the measure of Chl *a*, often used as a proxy of phytoplankton biomass, remains particularly challenging to convert to carbon.

In addition to the use of Chl *a* as a general proxy for phytoplankton biomass, other pigments, characteristic of specific broad taxonomic groups can be used to estimate the contribution of these groups to Chl *a*. Pigment analyses by high-performance liquid chromatography (HPLC) are widely applied to study algal distributions on a large scale (e.g. Roy *et al.*, 2011). The development of softwares designed to convert pigment patterns into algal groups (CHEMical TAXonomy: CHEMTAX) has further promoted the application of HPLC analyses (Mackey *et al.*, 1996). CHEMTAX is a tool that derives the quantitative contributions of phytoplankton taxonomic groups to the total chlorophyll pool by using the likely pigment:Chl *a* ratios of each group. Expected composition of taxonomic groups in the sample is needed to choose which groups must be included in the pigment:Chl *a* ratio matrix. Then, pigment:Chl *a* ratios are ideally obtained directly from local cultures, or based on published literature data. Indeed, in addition to geographic variations, pigment:Chl *a* ratios of the different groups can vary according to species, light, depth or nutrients, so that they cannot be known beforehand. To avoid introducing strong biases in the results due to the initial pigment ratio matrix used for predicting the contribution of the different groups to Chl *a*, it is highly recommended to modify iteratively the initial ratios to successively reduce the amount of unexplained Chl *a* of the produced model (Coupel *et al.*, 2015).

In our study, samples were first clustered according to their similarity in pigment:Chl *a* ratios, as CHEMTAX requires to run the analysis on homogeneous pigment:Chl *a* ratios to reach an optimal solution. The initial ratio matrix was based on the literature available on pigment composition of Southern Ocean phytoplankton (Wright *et al.*, 2010; van Leeuwe *et al.*, 2014). The ratio matrix was then randomized a minimum of 60 times for each cluster of samples to achieve root mean square of the residuals <0.1, considered as the threshold for checking model accuracy. The average contribution of each taxonomic group to Chl *a* was obtained by averaging the six best runs.

## 2. Contribution of specific groups of small phytoplankton to CO<sub>2</sub>-fixation

Once the diversity of small phytoplankton and its contribution to biomass were evaluated, we investigated the contribution of specific phytoplankton groups to CO<sub>2</sub>-fixation. To understand how phytoplankton size structure and taxonomic diversity affected CO<sub>2</sub>-fixation, it was necessary to combine the measurements of CO<sub>2</sub>-fixation at different levels: at the community, specific size-ranges, taxa, and single cell scale. The latter was essential to assess if all cells contributed equally to CO<sub>2</sub>-fixation or if the function depended mainly on a few individual cells.

### 2.1 Incubation with carbon isotopes: principles and limitations

The first experiments measuring phytoplankton CO<sub>2</sub>-fixation using isotopic tracers (<sup>14</sup>C or <sup>13</sup>C) date back to the 1950s, when Steemann Nielsen (1952) established the principles of <sup>14</sup>C radiotracer labelling. The method developed then is still the same and consists in incubating a phytoplankton community for several hours in the presence of a known quantity of <sup>13</sup>C or <sup>14</sup>C-DIC. At the end of the experiment, the metabolic activity of phytoplankton is stopped, and the incorporated labeled carbon (<sup>13</sup>C or <sup>14</sup>C-POC) is measured into particulate organic matter. The initial DIC concentration of the sample being known as well as the added amount of <sup>14</sup>C-DIC, the measurement of labeled POC makes it possible to determine the amount of DIC fixed during the experiment. This method assumes that the fixation of <sup>13</sup>C or <sup>14</sup>C during an incubation is proportional to the fixation of dissolved inorganic carbon (DIC) naturally present in the water column. The fixation rate of DIC into particulate organic carbon (POC) is then considered as a proxy of primary production.

This method is relatively easy to implement but faces methodological and conceptual limitations. Methodological concerns can be regrouped in the so-called “bottle effect”, a term describing how the incubation bottle could affect metabolic processes of the community sampled. These effects are more pronounced over long incubations into small volumes (<1L). They arise from different factors, like contamination with trace metals from the bottle walls, loss of turbulence, changes in the community composition or damage to organisms due to incubation conditions (e.g. Gieskes *et al.*, 1979; Fitzwater *et al.*, 1982; Mine Berg *et al.*, 1999; Calvo-Díaz *et al.*, 2011). Additionally to bottle effects problems, it remained unclear from the very beginning if the <sup>14</sup>C method was measuring net or gross primary production or an intermediate between net and gross (Steemann Nielsen, 1955; Marra, 2009). No consensus has been reached over the years. It is established that <sup>13</sup>C or <sup>14</sup>C-based estimates of photosynthesis would considerably underestimate gross production (Grande *et al.*, 1989). This conclusion is unsurprising and based on the assumption that phytoplankton respire recently fixed, i.e. labelled carbon, so that the measure at the end of the incubation already incorporates part of the respiratory loss of labelled carbon. For Marra (2009), <sup>14</sup>C uptake is a proxy of net production since phytoplankton would respire labelled carbon as they incorporate it. Nevertheless, Pei and Laws (2013) showed that this assumption wasn't always true and that some species would respire preferentially old unlabelled carbon. In this case, using

labelled carbon fixation would overestimate net production. Despite these shortcomings, labelling techniques with  $^{13}\text{C}$  and  $^{14}\text{C}$  remain useful key methods to evaluate phytoplankton  $\text{CO}_2$ -fixation. In this study, plankton communities were incubated mimicking *in situ* temperature and light conditions in  $^{13}\text{C}$ -enriched water from dawn to dusk (Fig. B3). Bulk  $\text{CO}_2$ -fixation was measured by conventional mass spectrometry (EA-IRMS). Detailed description of the incubations and calculations performed are available in Paper 2.



Fig. B3: Picture of the on-deck incubators in the vicinity of the Kerguelen islands. *In situ* temperature was reproduced in the incubator by a constant flow of sub-surface seawater. *In situ* light intensity of the sampling depth (10 m) was mimicked using blue light screens attenuating direct sunlight by approximately 50%.

## 2.2 Group specific $\text{CO}_2$ -fixation

Bulk measurements don't provide any information on the functional groups responsible for  $\text{CO}_2$ -fixation. Regarding the major diversity of natural phytoplankton communities, measuring the carbon uptake of different phytoplankton groups is paramount to explain ecosystem functioning.

To establish the relative contribution of different groups to  $\text{CO}_2$ -fixation, the most common approach consists in measuring  $\text{CO}_2$ -fixation of different size groups. This is most commonly achieved by successive filtration of natural communities incubated with labelled carbon on arbitrary mesh sizes (for example 20  $\mu\text{m}$ , 5  $\mu\text{m}$ , 2  $\mu\text{m}$ ) (e.g. Teira *et al.*, 2005; Poulton *et al.*, 2006; Pérez *et al.*, 2006; Tilstone *et al.*, 2017), or by flow cytometry sorting of populations characterized by homogeneous fluorescence and forward scatter, a proxy of cell size (Li, 1994; Jardillier *et al.*, 2010; Rii *et al.*, 2016). Flow cytometry enables the rapid counting and sorting of small autotrophic prokaryotes and pico- and nano-eukaryotes. Radiocarbon ( $^{14}\text{C}$ ) incorporated in sorted cells can subsequently be quantified using a liquid scintillation cocktail (e.g. Li, 1994). Studies exploring contribution of different size groups to primary production showed that their contribution wasn't proportional to their abundance, reflecting different cell-specific  $\text{CO}_2$ -fixation rates of specific size or phylogenetic groups (Li, 1994; Jardillier *et al.*, 2010; Hartmann *et al.*, 2014; Rii *et al.*, 2016). These differences in cell-specific  $\text{CO}_2$ -fixation rates could be linked with taxonomic affiliations or size-specific nutrient



requirements of the different groups (Jardillier *et al.*, 2010). Cell biomass could be an important determinant of CO<sub>2</sub>-fixation rates as biomass-specific CO<sub>2</sub>-fixation rates were equivalent in several studies, independently of taxonomic affiliation or nutrient concentration (Grob *et al.*, 2015). This isometric relationship between biomass and CO<sub>2</sub>-fixation rates goes against the assumption that rates of metabolism decrease universally with increasing organism size, also known as the Kleiber's law (Kleiber, 1947). For phytoplankton, different studies have found contradictory results regarding the universality of this rule (e.g. Huete-Ortega *et al.*, 2012; Ward *et al.*, 2017; Zaoli *et al.*, 2019), underlying the need to further explore this question in different natural environments.

Studies combining flow cytometry sorting of radiolabelled phytoplankton groups paved the way in linking phytoplankton diversity to CO<sub>2</sub>-fixation. However, they measured average CO<sub>2</sub>-fixation on a group of cells and did not inform on the actual dispersion of CO<sub>2</sub>-fixation by individual cells around that average. As microbial communities are characterized by high genetic, metabolic and phenotypic heterogeneity of single cells (Ackermann, 2013), understanding how the group average is constructed can help to understand whether all individual cells contribute equally or not to CO<sub>2</sub>-fixation.

### 2.3 Cell-specific CO<sub>2</sub>-fixation

Recently, secondary ion mass spectrometry (large-geometry SIMS and NanoSIMS) has emerged in marine science as one of the most valuable approaches to quantitatively link microbial identity of single cells to function (reviewed by Mayali, 2020). SIMS can provide spatially resolved information about uptake and transfer between organisms of isotopically-labelled compounds in environmental samples. SIMS instruments use a primary ion beam (Cs<sup>+</sup> in our case), that rasters across a flat and dry sample, slowly eroding the surface layer of that sample and creating secondary ions that are then transported into a mass spectrometer. Images of the detected ions allow the creation of isotope maps, where the ratio between counts of rare ions (e.g., <sup>13</sup>C) and more abundant natural ions (e.g., <sup>12</sup>C) can be visualized (Fig. B4). In simple words, SIMS combines the qualities of a microscope with those of a mass spectrometer and reveals elemental and isotopic compositions at a spatial resolution of 1 μm (SIMS) or even 50 nm (NanoSIMS) (Musat *et al.*, 2012).

As far as phytoplankton is concerned, SIMS was used to investigate virus-host interactions (Sheik *et al.*, 2013; Pasulka *et al.*, 2017), transfers between phytoplankton and heterotrophic bacteria (de-Bashan *et al.*, 2016; Arandia-Gorostidi *et al.*, 2017, 2017), symbioses between nitrogen N<sub>2</sub>-fixing prokaryotes and photosynthetic eukaryotes (Thompson *et al.*, 2012) and contribution of specific size and taxonomic groups to CO<sub>2</sub>- or N-fixation (e.g. Ploug *et al.*, 2010; Bonnet *et al.*, 2016; Berthelot *et al.*, 2019; Olofsson *et al.*, 2019). All NanoSIMS studies highlighted great variability in carbon or nitrate metabolism between and within phytoplankton groups, confirming that single cell studies can shed light on how community composition affects biogeochemical process.

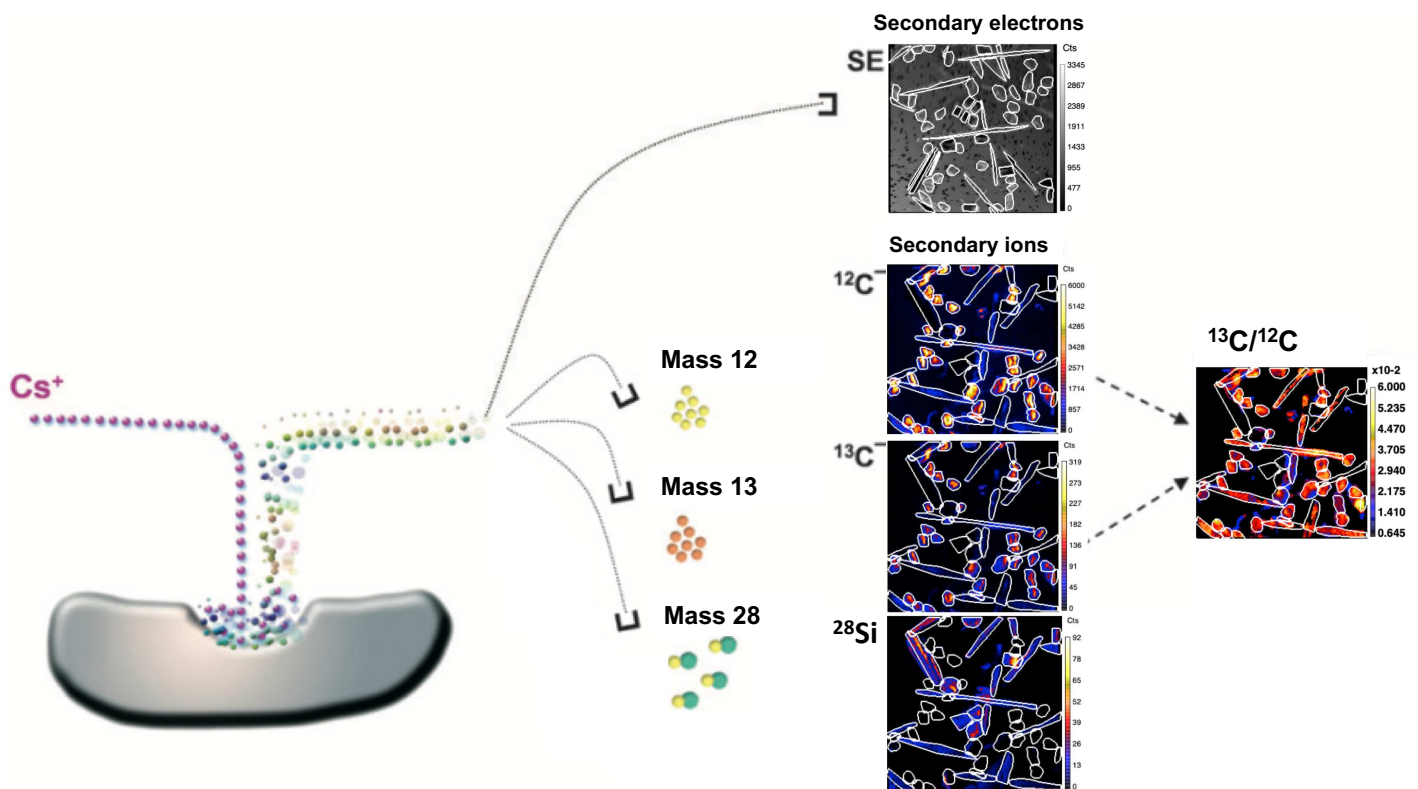


Fig. B4: Principle of SIMS image acquisition. This simplified scheme of SIMS acquisition used during MOBYDICK depicts the sputtering of nano-sized phytoplankton cells by a  $\text{Cs}^+$  primary ion beam and the resulting secondary electron (SE) and secondary ion images of various masses ( $^{12}\text{C}^-$ ,  $^{13}\text{C}^-$ ,  $^{28}\text{Si}^-$ ). In this example, plankton communities were incubated with  $\text{H}^{13}\text{CO}_3^-$  from dawn to dusk. The resulting ratio image of  $^{13}\text{C}/^{12}\text{C}$  was used to quantify  $\text{CO}_2$ -fixation of individual cells sorted by flow cytometry.  $^{28}\text{Si}$  was used to identify the silicified frustule of diatoms. Modified from (Musat *et al.*, 2012).

In our study, large diatoms collected on 20  $\mu\text{m}$  mesh-size filter were measured with large-geometry SIMS and cells  $<20 \mu\text{m}$  with NanoSIMS. Cells  $<20 \mu\text{m}$  were sorted by flow cytometry into 3 different size-groups.  $^{28}\text{Si}$  was used to identify diatoms. Cell C-content was computed from cell biovolume and the conversion factor to carbon from Verity *et al.*, (1992). Finally, the group  $\text{CO}_2$ -fixation was calculated by multiplying mean  $\text{CO}_2$ -fixation of single cells by cell abundance of the group obtained by flow cytometry. We deduced the contribution of different size groups sorted by flow cytometry to total  $\text{CO}_2$ -fixation by comparing the estimates of each groups'  $\text{CO}_2$ -fixation to bulk  $\text{CO}_2$ -fixation measured by conventional mass spectrometry (EA-IRMS). This method enabled to compare  $\text{CO}_2$ -fixation rates of different size groups, of small non-silicified cells and small and large diatoms.

Using complementary tools of molecular biology, chemotaxonomy and SIMS at the single cell level in this thesis allowed us exploring in an original way the diversity and importance in the  $\text{CO}_2$ -fixation of small phytoplankton in comparison to their larger counterparts.

## C. Results

In this section, I will present the results obtained as part of my thesis project. The first chapter addresses the diversity, ecological drivers and importance of small phytoplankton in the structuring of phytoplankton communities during and after the diatom bloom. The second chapter focuses on the contribution of small phytoplankton to CO<sub>2</sub>-fixation after the bloom and its contribution to the functioning of the biological carbon pump in the area.

Chapters begin with a short introduction detailing the objectives of each study. Published or submitted papers offer an in-depth presentation of the context, questions, methods and main findings associated with each chapter. Finally, diverse perspectives for further research are suggested. On that occasion, unpublished results from analysis or methodological developments attempted during this thesis will be discussed.

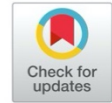
### 1. Small phytoplankton diversity around Kerguelen

The naturally iron-fertilized plateau of Kerguelen has been extensively studied for the occurrence of large diatom blooms during spring and summer (see KEOPS1 and KEOPS2 publications; e.g. Armand *et al.*, 2008; Lasbleiz *et al.*, 2016). Off-plateau, previous studies showed that unidentified pico- and nanoflagellates were the most abundant cells throughout the year (Kopczyńska *et al.*, 1998). On-plateau, the intensity of diatom blooms is highly variable from one year to the other (Robinson *et al.*, 2016) and nano-sized phytoplankton probably dominate phytoplankton communities in the absence of a bloom (Rembauville *et al.*, 2017; Penna *et al.*, 2018). However, small phytoplankton communities on-plateau have never been specifically targeted before this study, and no information was available on their taxonomic composition. Off-plateau, previous studies were mainly based on microscopy observations, not adapted to identify small cells with little morphological characteristics (Fiala *et al.*, 1998; Kopczyńska *et al.*, 1998). These studies highlighted the importance of naked flagellates, most likely prasinophytes, cryptophytes and prymnesiophytes in winter, where the <10 µm size fraction contributed 80% of total Chl *a* biomass (Fiala *et al.*, 1998). Only one metabarcoding study highlighted the importance of *Phaeocystis antarctica* off-plateau (Georges *et al.*, 2014).

This knowledge gap on the composition of small phytoplankton at a fine taxonomic resolution concerns not only the Kerguelen area, but the SO more generally and to date, few studies specifically investigated the composition of small phytoplankton in the SO with modern molecular tools and little information is available on small phytoplankton biogeography and ecological drivers in the SO (Díez *et al.*, 2004; Thiele *et al.*, 2014; Wolf *et al.*, 2014; Clarke and Deagle, 2018).

The objectives of this study were to:

1. Examine the diversity of small and large protists after the bloom, with an emphasis on small phytoplankton, through 18S rDNA metabarcoding of small (<20 $\mu$ m) and large (20-100  $\mu$ m) planktonic communities
2. Determine if small phytoplankton communities were different on and off the naturally iron-fertilized plateau and if so, which environmental drivers could explain the spatial distribution of specific taxa
3. Explore the contribution of small phytoplankton to total chlorophyll throughout and after the diatom bloom. For this, a general overview of the contribution to chlorophyll biomass of broad taxonomic groups over the bloom was assessed by comparing pigment analysis (CHEMTAX) during MOBYDICK with two previous cruises in the area at bloom onset (KEOPS2) and decline (KEOPS1).



## Marked spatiotemporal variations in small phytoplankton structure in contrasted waters of the Southern Ocean (Kerguelen area)

Solène Irion ,<sup>1\*</sup> Ludwig Jardillier ,<sup>2</sup> Ingrid Sassenhagen,<sup>1</sup> Urania Christaki<sup>1</sup>

<sup>1</sup>Laboratoire d'Océanologie et de Géosciences, UMR 8187, Université du Littoral Côte d'Opale, CNRS, Université de Lille, Wimereux, France

<sup>2</sup>Unité d'Ecologie, Systématique et Evolution, Université Paris-Sud, CNRS, AgroParisTech, Université Paris-Saclay, Orsay Cedex, France

### Abstract

In the Southern Ocean, diatom blooms have attracted a lot of attention, while other small nonsilicified phytoplankton groups have been less studied. Here, small phytoplankton (< 20  $\mu\text{m}$ , including small diatoms and nonsilicified small phytoplankton) are focused on in two contrasting areas: the productive Kerguelen plateau and its surrounding low productivity waters. To assess the diversity and spatial structuration of phytoplankton, discrete plankton samples (0–300 m layer) of two size fractions (< 20 and 20–100  $\mu\text{m}$ ) were analyzed with 18S rDNA amplicon sequencing in late summer. Phytoplankton seasonal succession was described using flow cytometry, pigments, and environmental data, from two previous cruises (during the onset and decline of the diatom bloom). In the mixed layer, small nonsilicified phytoplankton represented less than 10% of chlorophyll *a* (Chl *a*) during the onset and late diatom bloom on the plateau, but they increased on and off the plateau after the bloom (53–70% of Chl *a*). *Phaeocystis antarctica* was relatively abundant at all stations after the bloom, but other small phytoplanktonic groups featured marked differences on and off the plateau. Higher  $\text{NH}_4^+$  concentrations on the plateau appeared to stimulate the presence of *Micromonas*, while Pelagophytes were enhanced off the plateau. A diverse assemblage of small diatoms was also promoted off the plateau, where silicate concentration was still high. Interestingly, *P. antarctica* represented up to 25% of all reads at 300 m depth off the plateau in the larger size fraction suggesting a significant contribution to carbon export through aggregation in low productive waters.

Small phytoplankton (< 20  $\mu\text{m}$ ) play key roles in the global carbon cycle and marine food webs (Marañón et al. 2001; Richardson and Jackson 2007; Uitz et al. 2010). Typically, small phytoplankton have an advantage over larger cells in nutrient uptake due to their higher surface to volume ratio (Chisholm 1992; Agawin et al. 2000; Irwin et al. 2006). The Southern Ocean (SO) is the earth's largest high nutrient low chlorophyll (HNLC) area where phytoplankton production is limited by iron despite high concentrations of macronutrients, such as nitrate, silicate, or phosphate (Martin 1990; de Baar et al. 1995). Phytoplankton in these low productive HNLC waters is typically composed of small cells (< 20  $\mu\text{m}$ ), including small nonsilicified phytoplankton and diatoms (Moore

and Abbott 2000; Kopczynska et al. 2001; Uitz et al. 2009, 2010; Lasbleiz et al. 2014). Here, annual primary production of small phytoplankton collectively exceeds the large phytoplankton (herein defined as large-size cells, > 20  $\mu\text{m}$ ) by a factor of 2.7 (2.5 Gt C  $\text{yr}^{-1}$  and 0.9 Gt C  $\text{yr}^{-1}$ , respectively; Uitz et al. 2010). Despite their significant functional role, their diversity and spatiotemporal dynamics have remained overlooked in the SO (e.g., Weber and El-Sayed 1987; Wright et al. 2009; García-Muñoz et al. 2013), when large diatom blooms and the classical Antarctic food chain (diatoms–krill–whales) have received much more attention.

In contrast to HNLC low productive waters, discrete areas of the SO naturally, fertilized in iron and highly productive, are characterized by large diatoms bloom from spring to summer (Blain et al. 2007; Korb et al. 2008; Pollard et al. 2009). This is the case south-east of the Kerguelen archipelago where large diatom blooms appear at this time and result in a chlorophyll-rich area of 45,000  $\text{km}^2$ , constrained by the bathymetry of the plateau (Blain et al. 2007; Mongin et al. 2008). Upward fluxes of deep iron and major nutrients from the shallow continental shelf of the Kerguelen plateau

\*Correspondence: solene.irion@univ-littoral.fr

This is an open access article under the terms of the Creative Commons Attribution License, which permits use, distribution and reproduction in any medium, provided the original work is properly cited.

Additional Supporting Information may be found in the online version of this article.

(< 500 m) sustain these blooms (Blain et al. 2007; Mongin et al. 2008; Park et al. 2008). The blooms over the plateau can be dominated either by small diatoms forming long chains (chain length > 100  $\mu\text{m}$ , e.g., *Pseudo-nitzschia*, *Chaetoceros*) or large diatoms (*Eucampia*, *Corethron*). In contrast, small phytoplankton (mostly *Phaeocystis* and small diatoms) dominates in surrounding HNLC waters and production remains low throughout the year (Fiala et al. 1998; Kopczyńska et al. 1998; Armand et al. 2008; Uitz et al. 2009; Lasbleiz et al. 2016).

Community composition, temporal succession, and contribution to carbon export of diatoms during their blooming period around Kerguelen are well documented (Armand et al. 2008; Rembauville et al. 2015, 2017, 2018; Lasbleiz et al. 2016). Previous cruises KEOPS 1 and 2 (Kerguelen Ocean and Plateau compared Study project) investigated phytoplankton composition and C-cycling during the onset and decline of the bloom. The carbon export efficiency during the onset and decline of the bloom was lower on the plateau than in the HNLC area (e.g., Christaki et al. 2014; Laurenceau-Cornec et al. 2015; Planchon et al. 2015) although the amount of carbon exported at 200 m was twofold higher on the plateau (Blain et al. 2007; Planchon et al. 2015). At a broader scale, this inverse relationship between production and export seems to be a feature of the SO (Maiti et al. 2013; Le Moigne et al. 2016). This pattern could be explained by differences in phytoplankton communities (dominance of either small or large cells) and resulting trophic structures, grazing intensity, and/or microbial mineralization (Maiti et al. 2013; Laurenceau-Cornec et al. 2015; Le Moigne et al. 2016).

As chain-forming and large-diatom blooms occur during relatively short periods, it has been hypothesized that small-size cells are an essential element of Antarctic food webs, especially during winter and periods preceding blooms (Detmer and Bathmann 1997). Satellite data and sampling has indicated that phytoplankton communities on the plateau switch to an ecosystem dominated by small phytoplankton before (Rembauville et al. 2017), and also likely, after the bloom (Penna et al. 2018). As such, the plateau of Kerguelen could also include a persistent and functionally important small phytoplankton community, on which diatom blooms superimpose themselves (Smetacek et al. 1990).

Despite their ecological importance, little is known about the diversity, spatiotemporal dynamics, and environmental drivers of small phytoplankton in the SO. *Phaeocystis antarctica* has been identified as a putative key player in the absence of diatom blooms (Froneman et al. 2004; Hashihama et al. 2008; Iida and Odate 2014; Schulz et al. 2018). Early molecular studies specifically targeting Antarctic small plankton used technologies such as clone libraries or molecular fingerprinting techniques (Díez et al. 2001; Díez et al. 2004; Gast et al. 2004; Piquet et al. 2011). These technologies were unable to depict the full microbial diversity that is dominated by low-abundant taxa (Pedrós-Alio 2007). High-

throughput sequencing of size fractionated samples allowed further description of the diversity of small microbial eukaryotes (Wolf et al. 2014; Clarke and Deagle 2018). However, summer to autumn transition (March) and winter have not been investigated thus far, although these are the periods when the ecosystem most likely relies on primary production by small phytoplankton. Moreover, phytoplankton seasonal dynamics around the Kerguelen Islands has not been fully described yet.

The MOBYDICK (Marine Ecosystem Biodiversity and Dynamics of Carbon) cruise took place in late February and March 2018, a month after the diatom bloom ended. MOBYDICK's two main objectives were: to trace carbon from its initial fixation at the surface to its final export toward the ocean interior, and to explore how diversity influenced the carbon cycle in contrasted marine ecosystems on and off the iron enriched waters of the Kerguelen plateau. The present study focuses on the composition, seasonal variability, and ecology of small phytoplankton on and off the plateau. Molecular diversity of microbial eukaryotes after the bloom (MOBYDICK) is described through 18S rDNA amplicon Illumina Mi-Seq sequencing of small and large-cells size fractions (< 20 and 20–100  $\mu\text{m}$ ). Pigment and flow cytometry data from two previous cruises at the early and late stage of the bloom (KEOPS2 and KEOPS 1, respectively) were also used to complete the seasonal succession of phytoplankton on and off the plateau of Kerguelen. Environmental factors likely governing the balance between small phytoplankton vs. large diatoms throughout the season and potential ecological implications for carbon export are also identified.

## Materials and methods

### Sampling strategy overview

Seawater was collected onboard the R/V *Marion Dufresne* around the plateau of Kerguelen Islands during the MOBYDICK cruise after the diatom bloom (26 February 2018–18 March 2018). We combined samples from the MOBYDICK cruise with data collected during past cruises undertaken at different seasons to describe the seasonal succession. To do so, we restricted the pigment and cytometry data to a similar depth horizon (upper 50 m) and to stations presenting either the same location on the plateau and reference station in the HNLC area off the plateau. KEOPS2 cruise took place during austral spring (15 October 2011–20 November 2011), while KEOPS1 occurred during summer (19 January 2005–13 February 2005) (Table 1). Plateau Sta. A3 of KEOPS1 and 2 corresponds to MOBYDICK Sta. M2 (Fig. 1). This station experiences natural iron enrichment from the plateau resulting in diatom blooms during spring and early summer (Armand et al. 2008; Lasbleiz et al. 2016). Off-plateau stations M1, M3, and M4 (MOBYDICK) were expected to

display HNLC characteristics. Sta. R-2 (KEOPS2) and Sta. C11 (KEOPS1) were the HNLC reference stations (Quéguiner et al. 2007; Cavagna et al. 2015), which will be considered here for the seasonal succession (Fig. 1; Table 1).

**Environmental parameters**

For KEOPS 1 and 2, environmental parameters were described in Mosseri et al. (2008) and Cavagna et al. (2015). For MOBYDICK, temperature, dissolved oxygen, and salinity measurements were collected at all CTD casts using a SeaBird 911-plus.

**Table 1.** Coordinates and dates of samples collected during KEOPS 1 and 2 and MOBYDICK.

Cruise	Station	Date	Longitude (°E)*	Latitude (°S)*
KEOPS 2	A3-1	20 Oct 12	72.1	50.6
	R2	26 Oct 12	66.7	50.4
	A3-2	16 Nov 12	72.1	50.6
KEOPS 1	A3-1	19 Jan 05	72.0	50.4
	A3-2	23 Jan 05	72.0	50.4
	C11-1	26 Jan 05	77.6	51.4
	C11-2	28 Jan 05	77.6	51.4
	A3-3	04 Feb 05	72.0	50.4
MOBYDICK	A3-4	12 Feb 05	72.0	50.4
	M2-1	26 Feb 18	72.0	50.4
	M2-2	06 Mar 18	72.0	50.4
	M2-3	16 Mar 18	72.0	50.5
	M1	09 Mar 18	74.5	49.5
	M3-1	04 Mar 18	68.0	50.4
	M3-3	19 Mar 18	68.0	50.4
	M4-1	01 Mar 18	67.1	52.4
	M4-2	13 Mar 18	67.1	52.4

\*Coordinates and depth of the CTD “stock.”

Ammonium was measured by fluorometry (Holmes et al. 1999). For other dissolved inorganic nutrients ( $PO_4^{3-}$ ,  $Si(OH)_4$ ,  $NO_2^-$ ,  $NO_3^-$ ), samples were collected in 125 mL polyethylene bottles. The samples were then filtered through 0.45  $\mu m$  acetate cellulose filters and preserved with 100  $\mu L$   $HgCl_2$  ( $4 g L^{-1}$ ) in 20 mL. The samples were then stored in the dark at room temperature until analysis in the laboratory with a segmented flow analyzer (Skalar) equipped with colorimetric detection using methods described in Aminot and K erouel (2007).

**Sample collection for DNA extraction and molecular biology**

During the MOBYDICK cruise, four different sites were visited. M2, located on the plateau, was sampled three times during the cruise with about a 10-d interval. Off the plateau, M3 and M4 were sampled twice with a 2-weeks interval, and M1 only once (Table 2). Seawater samples were collected with 12-liter Niskin bottles at all visited stations at four depths (15, 60, 125, and 300 m). The first two depths (15 and 60 m) were chosen to correspond approximately to the surface and bottom of the mixed layer (ML), respectively. Water at 300 m was characteristic of deep nutrient-rich winter water (Park et al. 2008). Water at 125 m corresponded to the “transition layer,” defined as the water mass at the interface between the deep stratified ocean interior and the highly turbulent surface ML (Johnston and Rudnick 2009).

Sampled seawater was first prefiltered using a 100  $\mu m$  nylon mesh (Millipore, U.S.A.) in order to remove Metazoa and large particles. Ten liters of water from each depth were then filtered successively through 20 and 0.2  $\mu m$  pore-size membranes (Millipore) for microbial eukaryote taxonomic composition analyses of large (100–20  $\mu m$ ) and small size-fractions (< 20  $\mu m$ ). This resulted in 64 samples (eight visits at the different stations, four depths, two size fractions). Filters were directly frozen and stored at  $-80^\circ C$  for 18S rDNA

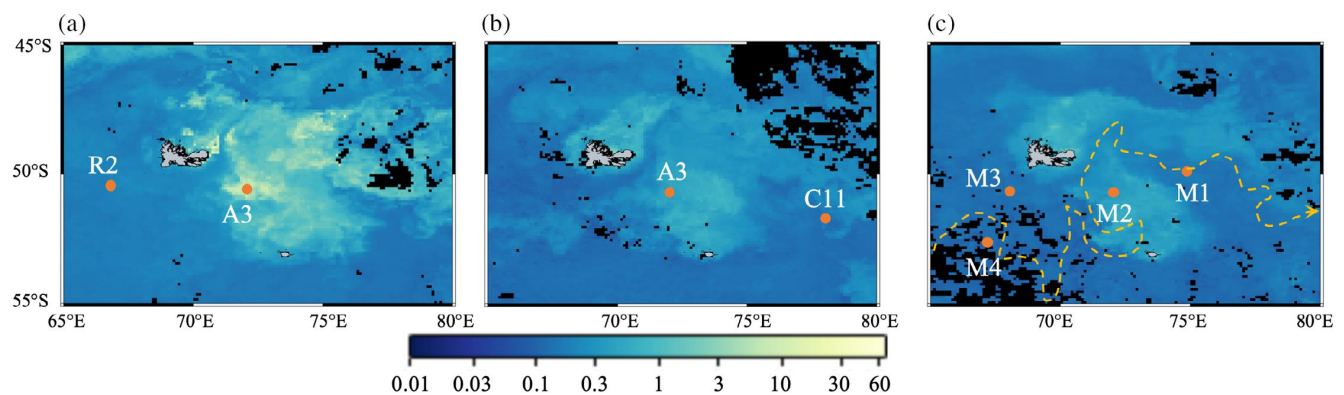


**Fig. 1.** Location of plateau and off-plateau reference stations sampled during KEOPS2 (a), KEOPS1 (b), and MOBYDICK (c). Chl *a* (color scale) represented on the map corresponds to AQUA/MODIS average values ( $\mu g L^{-1}$ ) over the respective cruises’ sampling periods (November 2011 for KEOPS2, January and February 2005 for KEOPS1, and March 2018 for MOBYDICK). The dotted yellow line represents the position of the Polar Front in March 2018 according to Pauthenet et al. (2018).

**Table 2.** Description of MOBYDICK stations. The depth of the mixed layer (ZML) is based on a difference in sigma of 0.02 compared to surface value. The mean ZML is calculated based on all CTD casts performed during the occupation of the stations. Temperature, nutrients, and Chl *a* are mean values of all measures sampled within the ML (2–3 depths depending on the station). The depth of the euphotic layer (Ze) corresponds to the depth where light intensity was at least 1% of incident light at surface during the CTD cast of the sampling for metabarcoding.

Station	Date	Depth (m)	<i>T</i> (°C)	ZML (m)	Ze (m)	Chl <i>a</i> (μg L <sup>-1</sup> )	NO <sub>3</sub> <sup>-</sup> + NO <sub>2</sub> <sup>-</sup> (μmol L <sup>-1</sup> )	NH <sub>4</sub> <sup>+</sup> (μmol L <sup>-1</sup> )	PO <sub>4</sub> <sup>3-</sup> (μmol L <sup>-1</sup> )	Si(OH) <sub>4</sub> (μmol L <sup>-1</sup> )
M2-1	26 Feb 18	520	5.10	62	45	0.27	21.90	0.75	1.47	1.36
M2-2	06 Mar 18	519	5.24	61	46	0.30	21.79	1.1	1.50	1.72
M2-3	16 Mar 18	527	5.11	68	45	0.58	21.90	0.94	1.50	2.75
M1	09 Mar 18	2723	4.99	27	56	0.35	25.20	0.56	1.71	8.38
M3-1	04 Mar 18	1730	5.6	65	75	0.20	23.75	0.50	1.65	2.89
M3-3	19 Mar 18	1730	5.31	79	62	0.14	23.34	0.73	1.08	2.31
M4-1	01 Mar 18	4186	4.45	49	66	0.18	25.70	0.37	1.70	4.36
M4-2	13 Mar 18	4300	4.46	87	64	0.21	24.80	0.48	1.71	4.80

amplicon Illumina Mi-Seq sequencing. Each filter was cut into small pieces before DNA extraction with PowerSoil DNA Isolation Kit (QIAGEN, Germany) following standard manufacturer's protocol. DNA was eluted with 100 μL AE buffer.

#### Polymerase Chain Reaction and Illumina sequencing

To describe protist diversity, the V4 hypervariable region of the 18S rRNA gene was amplified using the primers EK-565F (5'-GCAGTAAAAAGCTCGTAGT) and UNonMet (5'-TTTAA GTTTCAGCCTTGCG) biased against Metazoa (Bower et al. 2004). Different molecular identifiers of 10 bp were added to both forward and reverse primers to tag amplicons and allow to differentiate them after sequencing. Polymerase chain reaction (PCR) mixtures comprised 1–2 μL of DNA, 12.5 μL of DreamTaq Green PCR Master Mix (Thermo Fisher Scientific, U.S.A.), and 1 μL of each primer (10 μmol L<sup>-1</sup>) in a total volume of 25 μL. PCR conditions included an initial step of denaturation at 94°C for 3 min, 25 cycles of denaturation at 94°C for 30 s, annealing at 58°C for 45 s, and extension at 72°C for 90 s, and a final step of extension at 72°C for 10 min. PCR products from at least five different PCR reactions of each sample were then pooled together and purified using the QIAquick PCR purification kit (QIAGEN, Germany), according to the manufacturer's instructions. DNA concentrations were calculated on a Qubit fluorometer with the dsDNA High Sensitivity Assay Kit (Life Technologies Corp., U.S.A.) and identical concentrations of each sample's amplicons were pooled.

Pooled amplicons were then paired-end sequenced on an Illumina MiSeq 2 × 300 platform by Genewiz (U.S.A.).

#### Demultiplexing, quality filtering, and taxonomic affiliation

Paired-end sequences were imported and demultiplexed in Qiime (Caporaso et al. 2010) based on each sample's 10 bp molecular identifier with the functions `extract_barcode.py` (Qiime1) and `demux emp-paired` (Qiime 2-2018.8). Demultiplexed sequences without primers and barcodes were further processed in R-software (R Core Team 2018) using the DADA2 package v.1.10.1 (Callahan et al. 2016) to define amplicon sequence variants (ASVs). Sequences were quality filtered (maximum expected error = 6), trimmed (forward and reverse reads at 270 nt) prior to inferring ASVs and removing chimeric sequences with the DADA2 algorithm. Taxonomy was assigned for each ASV to the best taxonomic level using the RDP naive Bayesian classifier implemented in DADA2 (Wang et al. 2007) in combination with PR<sup>2</sup> database v.4.11.0 (Guillou et al. 2013), a curated database implementing EukRef (del Campo et al. 2018). Taxonomy assigned this way was cross-checked with Sintax algorithm in USEARCH v11 (Edgar 2013). When taxonomy assignment differed between the two algorithms, taxonomy was compared to NCBI blast and/or limited to the highest taxonomic level where both algorithms agreed. All ASVs sequences were aligned in Geneious Prime v.2019 using MAFFT v7.388 plugin (Katoh and Standley 2013) parameterized for FFT-NS-2 analysis to



deal with the large number of sequences. A phylogenetic tree was then built based on this alignment with FastTree 2.1.5 plugin using default parameters (Price et al. 2009). All data for this study are accessible in the MOBYDICK database (<http://www.obs-vlfr.fr/proof/php/mobydick/mobydick.php#SA>). Raw sequencing files in fastq format, as well as ASVs, taxonomy and metadata tables are available at [http://www.obs-vlfr.fr/proof/ftpfree/mobydick/db/DATA/PAR\\_2251/](http://www.obs-vlfr.fr/proof/ftpfree/mobydick/db/DATA/PAR_2251/).

### Statistical analysis

Alpha diversity analyses were conducted in R-software version 3.5.1 (R Core Team 2018) on ASVs with phyloseq v.1.16 (McMurdie and Holmes 2013) and microbiomeSeq (Ssekagiri et al. 2018) after rarefying read depths based on sample with the lowest read count. Observed richness and Pielou's evenness (i.e.,  $J = H'/\ln[S]$  where  $H'$  is Shannon Weiner diversity index and  $S$  is the total number of species in a sample indexes) were compared between size fractions and locations with ANOVA, followed by pairwise tests using Tukey multiple comparisons (Tukey's honestly significant difference test) with 95% confidence interval.

To illustrate community composition differences between samples, phyloseq was used to plot PCoA based on weighted UniFrac distances, that considers the phylogenetic distance between two sample's composition and ASVs relative abundances (Lozupone et al. 2011). Cluster analysis was conducted based on the wUniFrac distance matrix using the hclust function in R-software and Ward classification method (Murtagh and Legendre 2014). Homogeneity of dispersion (variance) within group was calculated with function betadisperser. ANOVA-like test (permutest) was used to determine if the vari-ances differed by groups.

Heatmaps of the 30 most abundant genera were generated using "Ampvis2" R-package (Andersen et al. 2018) after pooling ASVs belonging to the same genus. To test for statistical differences in community composition according to a variable of interest (size fraction, location of the station on or off the plateau), permutational analysis of variance (PERMANOVA) implemented in the function adonis from the "vegan" R-package (Oksanen et al. 2017) was run on weighted UniFrac distances with 1000 permutations. To identify genera differing in abundance between plateau and off-plateau surface samples (10 and 60 m), un-normalized table of ASVs, pooled by genus when possible, representing over 1% of the reads, were transformed using DESeq2 (v1.22.2) (Love et al. 2014). The same package was used to perform the differential analysis. All genera that were significantly different in abundance between plateau and off-plateau surface samples ( $p$  value, adjusted for multiple comparisons using the Benjamini-Hochberg false discovery rate procedure, less than 0.05) were visualized by plotting Log2 fold changes in abundance on and off the plateau in ggplot2 v 2.2.1 (Wickham 2011, 2016).

To explore the influence of abiotic factors on community composition, a canonical correspondence analysis (CCA) was

done with the "vegan" R-package on ASVs relative abundances, pooled by genus when this taxonomic level was available. The same analysis was also run only considering ASVs accounting for over 1% of the reads. Significant environmental variables were selected using function ordistep with 1000 permutations, which performs automatic stepwise model building for constrained ordination methods in both directions (forward and backward) based on pseudo-Akaike Information Criterion. No autocorrelation for selected environmental variables was detected using the vif.cca function. Significance of the final model and the different axis was checked using ANOVA (1000 permutations) and the CCA was plotted using ggplot2.

### Pigment measurements and CHEMTAX analysis

Pigment extractions for KEOPS 1 and 2 cruises are described in Uitz et al. (2009) and Lasbleiz et al. (2014). In brief, from 1 to 2.2 L, based on particle concentrations, were filtered onto Whatman GF/F filters. For the MOBYDICK cruise, 2.32 L of water was sampled and filtered onto Whatman GF/F filters at each station and depth. Filters were then flash-frozen in liquid nitrogen and stored at  $-80^{\circ}\text{C}$ . For all cruises, pigment determination was done using high-performance liquid chromatography (HPLC), following the method of Ras et al. (2008), adapted from Van Heukelem and Thomas (2001). To perform CHEMTAX analysis, HPLC data from all sampling points in the first 50 m were considered.

CHEMTAX v1.95 (Mackey et al. 1996) was used to assess the contribution of seven different taxonomic groups to total chlorophyll  $a$  (Chl  $a$ ): chlorophytes, prasinophytes, cyanobacteria (most likely representative of *Synechococcus*, as *Prochlorococcus* is absent at this latitude), cryptophytes, diatoms, dinoflagellates (with peridinin), and haptophytes (*Phaeocystis* like). This software aims at determining the contribution of different photosynthetic groups to total Chl  $a$  biomass based on each group's characteristic accessory pigment to Chl  $a$  ratio. Pigment composition characteristic of the different groups was assessed using 11 pigments: chlorophyll  $c3$  (Chl  $c3$ ), peridinin (Peri), fucoxanthin (Fuco), prasinoxanthin (Pras), 19'-Hexanoyloxyfucoxanthin (Hex-fuco), zeaxanthin (Zea), alloxanthin (Allo), lutein (Lut), and chlorophyll  $b$  (Chl  $b$ ). An initial matrix of pigment to Chl  $a$  ratios for these seven taxonomic groups was build based on previous chemo-taxonomic studies of phytoplankton in the SO (Wright et al. 2010; van Leeuwe et al. 2014) (Supporting Information Table S1).

Samples were first clustered based on their pigment : Chl  $a$  ratios to form homogeneous bins using R-software, Hierarchical clustering on principle components (HCPC), implemented in the package FactoMineR (Lê et al. 2008). Then, pigment: Chl  $a$  ratios were adjusted for each bin using 60 randomized ratio matrix varying by up to  $\pm 35\%$  of the initial ratio matrix to avoid any bias linked to the ratios chosen from the literature. Taxa composition was then inferred for each sample of every cluster based on the average ratios from the six best

runs, associated with the lowest root mean square of the residuals and hence the lowest amount of unexplained pigment. It was then finally ensured that ratios of each characteristic pigment : Chl *a* obtained in the final ratio matrix for each taxonomic group were still in the range accepted in literature sources used in Higgins et al. (2011).

**Abundance of autotrophic pico- and nanoplankton**

Abundance of pico- and nanoautotrophs was determined by flow cytometry. For all cruises, 4.5 mL of seawater were fixed with glutaraldehyde (1% final concentration). Fixed samples were stored for 30 min at 4°C, flash frozen in liquid nitrogen, and stored at -80°C until analysis (Marie et al. 1999). Counts were performed with BD flow cytometers (FACSCalibur for KEOPS 1, and FACSCanto for KEOPS2 and MOBYDICK cruises) equipped with blue (argon 488 nm) and red (633 nm) lasers. Phytoplankton cells were analyzed according to their natural fluorescence (Chl *a* and phycoerythrin). Approximately 0.75 mL of sample were analyzed at high speed (150  $\mu\text{L min}^{-1}$ ) for 5 min as described in Christaki et al. (2014).

**Results**

**Brief description of the physicochemical parameters (MOBYDICK)**

During MOBYDICK, phosphate and nitrogen were abundant in the ML at all stations (Table 2). On the plateau (M2), silicic acid concentrations were low (< 2  $\mu\text{mol L}^{-1}$ ), especially during the first two visits, but doubled at the last visit after a storm (10 March 2018). M2 was also characterized by the highest ammonium concentrations (0.75–1.1  $\mu\text{mol L}^{-1}$ ). Off-plateau, Sta. M1, M3, and M4, presented different physicochemical characteristics for the ML in relation with their location North or South of the polar front, in subantarctic or

Antarctic waters, respectively (Fig. 1c). Silicate concentrations were lower in subantarctic waters at M3 (minimum of 2.3  $\mu\text{mol L}^{-1}$ ) than in Antarctic waters at M4 and M1 (from 4.36 to 8.38  $\mu\text{mol L}^{-1}$ ). M1 and M4 were located in dynamic water masses near the polar front and were weakly stratified. Consequently, the depth of the ML was shallowest at M1 (27 m) and varied considerably between the two visits at M4 (49 and 87 m). At M2 and M3, ML depth varied between 60 and 80 m and also deepened after the storm (Table 2). Depth of the euphotic layer (Ze) was always shallower at M2 (45 m) than off the plateau (56–75 m). Lowest temperatures were observed at M4 (4.4°C), south of the plateau, and highest temperatures in subantarctic waters at M3 (5.6°C).

**Diversity and community composition of microbial eukaryotes after the diatom bloom**

After DADA2 quality filtering, 8328 ASVs were retrieved from a total of 3,366,966 reads in 64 samples. ASVs not assigned to Eukaryotes or assigned to Metazoa were removed leaving a total of 8164 ASVs and 3,356,832 reads. After removing singletons, 5831 ASVs and 3,355,898 reads were kept for further analysis. One sample with less than 5000 reads was excluded from the analysis (M2-3, 60 m, < 20  $\mu\text{m}$ ).

The number of observed ASVs per sample ranged from 116 (M2-1, 125 m, < 20  $\mu\text{m}$ ) to 648 (M4-2, 125 m, < 20  $\mu\text{m}$ ). The mean observed richness across all stations and depths was significantly higher in the small than in the large size fraction. Richness was not different on and off the plateau for each size fraction. Within the small size fraction, richness differed according to depth and was overall higher at 125 and 300 m than at 10 m (Fig. 2). Highest richness was observed off the plateau at M4 (125 m) with over 600 different ASVs sequenced at each visit and lowest richness on the plateau at M2 (125 m) with only 116 ASVs (Fig. 2). No differences in evenness

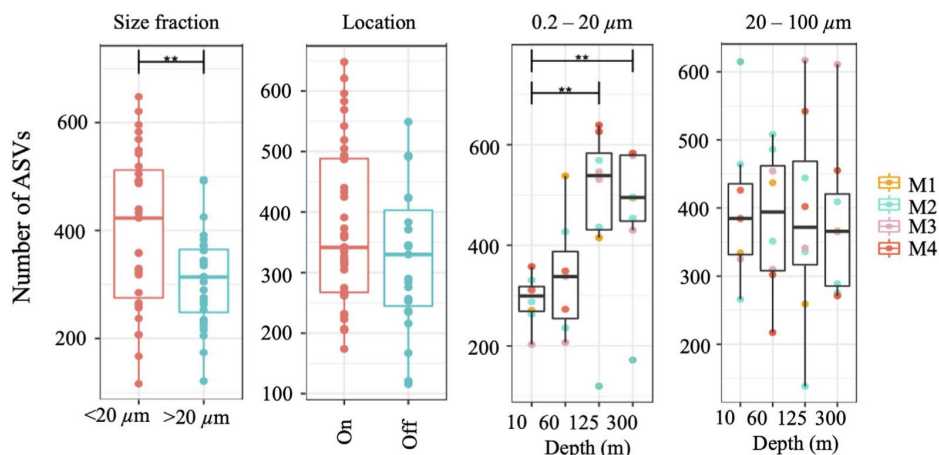


**Fig. 2.** Richness for the entire data set according to different size fractions and locations on or off the plateau, and for each depth of the different size fractions. Pairwise significant differences (Tukey HSD,  $p < 0.05$ ) are indicated.

between the two size fractions could be identified, although it was overall higher off the plateau. Within the small size fraction, evenness was significantly higher at 125 m than at 10 m (Supporting Information Fig. S1). Although all taxonomic orders were found in the two size fractions, small and large size fraction community composition differed significantly at all depths (PERMANOVA,  $p < 0.001$ ).

Surface samples of the  $< 20 \mu\text{m}$  size fraction were dominated either by parasitic Syndiniales (55–78% at M2-1, M2-2, M3-1) or Haptophytes (*Phaeocystis*) (10–46%; Fig. 3). Small diatoms (in the  $< 20 \mu\text{m}$  fraction) were more abundant at Sta. M1 and M4 off-plateau, where they accounted for 21% and up to 30% of the reads, respectively, but represented less than 10% of the reads at M2 and M3. Other phytoplankton, such as

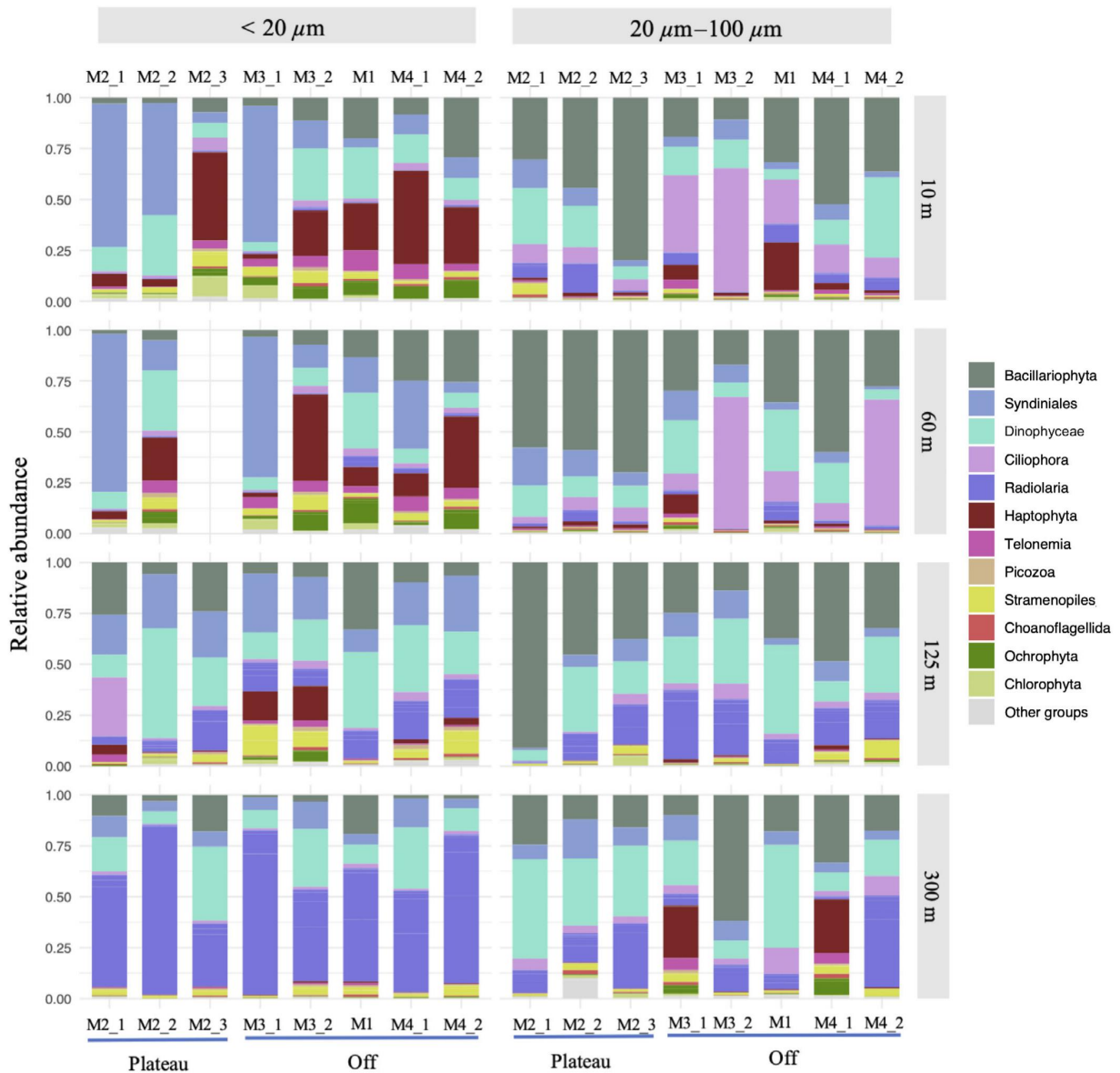


**Fig. 3.** Relative abundance of high-level taxonomic groups at each station and depth for both size fractions. Bacillariophyta have been distinguished from other Ochrophyta and Syndiniales from core dinoflagellates Dinophyceae (Dinoflagellata) to highlight these two taxonomic groups. “Other groups” include rare taxonomic groups representing together less than 0.1% of the reads. Numbers close to each station refer to the order of visits when stations were visited several times (see Table 2).

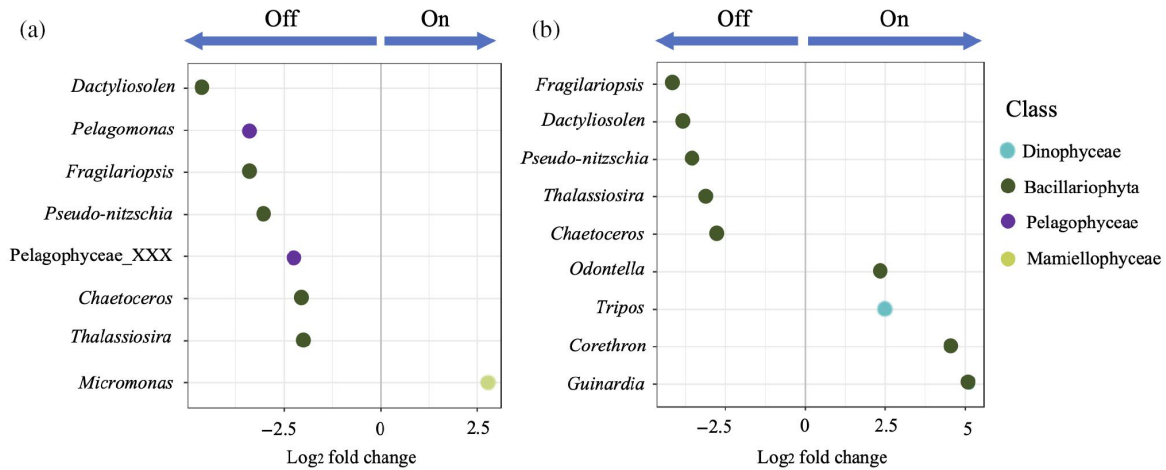


**Fig. 4.** Phytoplankton genera presenting differential read abundances between surface samples collected on and off plateau after Deseq2 analysis ( $p < 0.05$ ) for small (a) and large size-fractions (b). Only most abundant genera ( $> 0.1\%$  of total reads and base mean after Deseq2 normalization superior to 100 reads) are represented. A negative log2 fold change indicates genera that are relatively more abundant off the plateau, while a positive log2 fold change indicates genera relatively more abundant on the plateau.

Ochrophyta (Pelagophyceae) and Chlorophyta (Mamiellophyceae and Prasinococcales), were also present in the small size fraction, but accounted for a low proportion of reads at each station (less than 10%). Picograzers such as Telonemia and Stramenopiles (MAST and MOCH; Fig. 3) were also consistently observed at all surface stations in reduced proportions (less than 10% of the reads). An increase of Dinophyceae and Radiolaria was observed at 125 and 300 m depth. Syndiniales, Stramenopiles, and Haptophytes were also present (Fig. 3). At 300 m, the small size fraction was largely dominated by Radiolaria (31–83%), and Dinophyceae (7–36%).

Surface samples (10 and 60 m) of the large size fraction were dominated by Bacillariophyta (up to 80% at M2-3) or Ciliophora (up to 65% at M3-3, 60 m; Fig. 3). Diatoms were still present (14–91%) deeper at 125 m and contributed up to 91% of the reads at Sta. M2-1 with a marked contribution of *Odontella* and *Eucampia* (Supporting Information Fig. S2). The relative abundance of Dinophyceae and Radiolaria increased at this depth as in the small size fraction. Finally, the large size fraction consisted mainly of an assemblage of dinoflagellates, Radiolaria, Syndiniales, and Bacillariophyta at 300 m depth. Small phytoplanktonic Haptophyta (*Phaeocystis*) represented up to 25% of the reads at 300 m at M3-1 and M4-1 (Fig. 3, Supporting Information Fig. S2) when they were almost absent in this size-fraction in the upper layers.

When looking only at autotrophic taxa of the small size fraction in surface samples (10 and 60 m), phytoplankton communities were different on and off the plateau (PERMANOVA;  $p = 0.04$ ). *Phaeocystis* was present in all surface samples, but a few common autotrophic taxa were enhanced in these distinct regions (DESeq2 analysis; Fig. 4a). *Pelagomonas* and unidentified Pelagophyceae were more

abundant off the plateau in contrast with the prasinophyte *Micromonas* (Mamiellophyceae) that was more abundant on the plateau. Diatoms belonging to the genera *Fragilariopsis*, *Pseudo-nitzschia*, *Dactyliosolen*, *Thalassiosira*, and *Chaetoceros* were enriched off the plateau (Fig. 4a). *Fragilariopsis*, *Pseudo-nitzschia*, *Dactyliosolen*, *Thalassiosira*, and *Chaetoceros* were also enriched off the plateau in the large size fraction, whereas reads of the diatoms *Corethron* and *Guinardia* were more abundant on the plateau (Fig. 4b).

**Relation between environmental variables and community composition in late summer**

CA analyses of surface euphotic layer samples and main environmental variables emphasized a clear distinction between on and off-plateau communities (Fig. 5). *Phaeocystis*, which was abundant in surface waters of all stations, appeared in the middle of the CCA, as it was not related to any particular environmental parameter. Among the environmental variables tested, ammonium, phosphate, temperature, and silicic acid were significant predictors of community composition within the small size fraction when considering all ASVs and/or only the most common ASVs (automatic stepwise model building analysis,  $p < 0.01$ ). None of these variables showed significant auto-correlation and they explained 45.8% of the variance of the entire community composition within the small size fraction (CCA1 = 15.1%; CCA2 = 12.4%; CCA3 = 10.3%; CCA4 = 8.0%). When plotting on the CCA small phytoplankton taxa that were differentially abundant on and off the plateau (cf. Fig. 4a), plateau station M2 was characterized by higher ammonium concentrations along with higher abundances of the prasinophyte *Micromonas* (Mamiellaceae family). Diatoms such as *Fragilariopsis*, *Thalassiosira*, and *Pseudo-nitzschia* were associated off the plateau

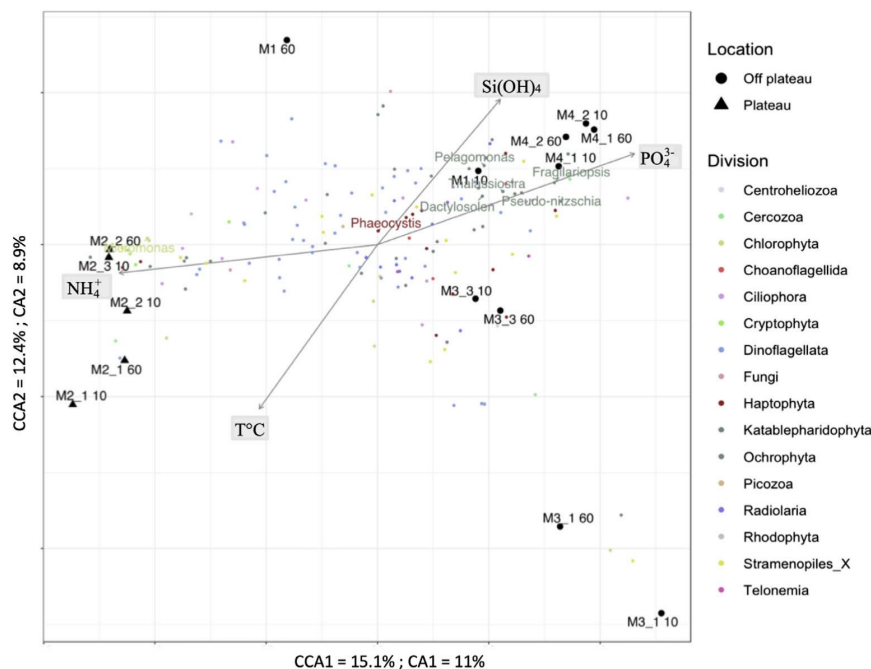


**Fig. 5.** Ordination diagram (CCA) of small protist taxonomic groups at surface (all ASVs) and significant abiotic variables (ammonium [NH<sub>4</sub><sup>+</sup>], phosphate [PO<sub>4</sub><sup>3-</sup>], silicic acid [Si(OH)<sub>4</sub>], and temperature [T, °C]). Black marks are representative of the community composition of each sample, labeled by station and depth. The different genera (or ASVs when this taxonomic level was not available) are represented by dots colored by division. Only the genera/ASVs representing more than 1% of total reads were plotted, to not overload the chart. Only phytoplankton genera considered as differentially abundant between stations on and off plateau according to DESeq2 were labeled. *Phaeocystis* position in the middle of the CCA plot indicated its presence at all stations.

with M1 and M4 as well as the highest concentrations of silicic acid and phosphate (Fig. 5).

**Seasonal changes in phytoplankton assemblages**

CHEMTAX analyses highlighted that phytoplankton communities were contrasted on and off the plateau at the onset and the decline of the Kerguelen bloom (KEOPS 1 and 2, respectively). In late summer (MOBYDICK), small phytoplankton—prymnesiophytes particularly—was important over the entire area (Fig. 6). On the plateau, contribution of the different phytoplankton groups varied markedly over seasons (Fig. 6a,c). Diatoms dominated phytoplankton blooms in spring and summer (KEOPS 2 and 1), while small flagellates represented higher proportions of the phytoplankton community in late summer (MOBYDICK, Fig. 6c). During spring and summer blooms (KEOPS 2 and 1), Chl *a* was sixfold higher on the plateau than off-plateau reference stations (1.21 ± 0.26 μg L<sup>-1</sup> and 0.19 ± 0.05 μg L<sup>-1</sup>, respectively) and diatom pigments represented over 90% of Chl *a* (Fig. 6a,c). Concomitantly, only prymnesiophytes remained at low background levels within small phytoplankton taxa. In late summer (MOBYDICK), Chl *a* on the plateau dropped to values similar to the ones found off the plateau

(0.3 ± 0.02 μg L<sup>-1</sup> at M2-1 and M2-2; Fig. 6a,b). These low Chl *a* concentrations were mainly due to a strong (22-fold) decrease of diatoms' contribution to Chl *a* (from up to 1.8 μg L<sup>-1</sup> in November to 0.08 μg L<sup>-1</sup> end of February). As a consequence of the diatom decline, small nonsilicified phytoplankton's contribution strongly increased on the plateau after the bloom, with prymnesiophytes and prasinophytes accounting for 53–58% of Chl *a* (Fig. 6a,c). The contribution of prasinophytes notably increased from 5.7% to 16.6% between the first and last visit at M2 during late summer (MOBYDICK). They also contributed to 8.9% to Chl *a* biomass at the very early stage of the bloom (KEOPS2, first visit). Total abundances of small phytoplanktonic cells after the bloom (3200–8300 cells mL<sup>-1</sup>) were also much higher after the bloom than during the bloom (700–2000 cells L<sup>-1</sup>).

Off the plateau, Chl *a* was low during the three cruises (0.20 ± 0.05 μg L<sup>-1</sup>; Fig. 6b). Prymnesiophytes, followed by diatoms, were the most represented groups in pigment data, with average relative contribution to Chl *a* of 51.6% and 39.3%, respectively. Pigments characteristic of small nonsilicified phytoplankton dominated at all off-plateau reference stations (Fig. 6b), with the exception of Sta. C11-1

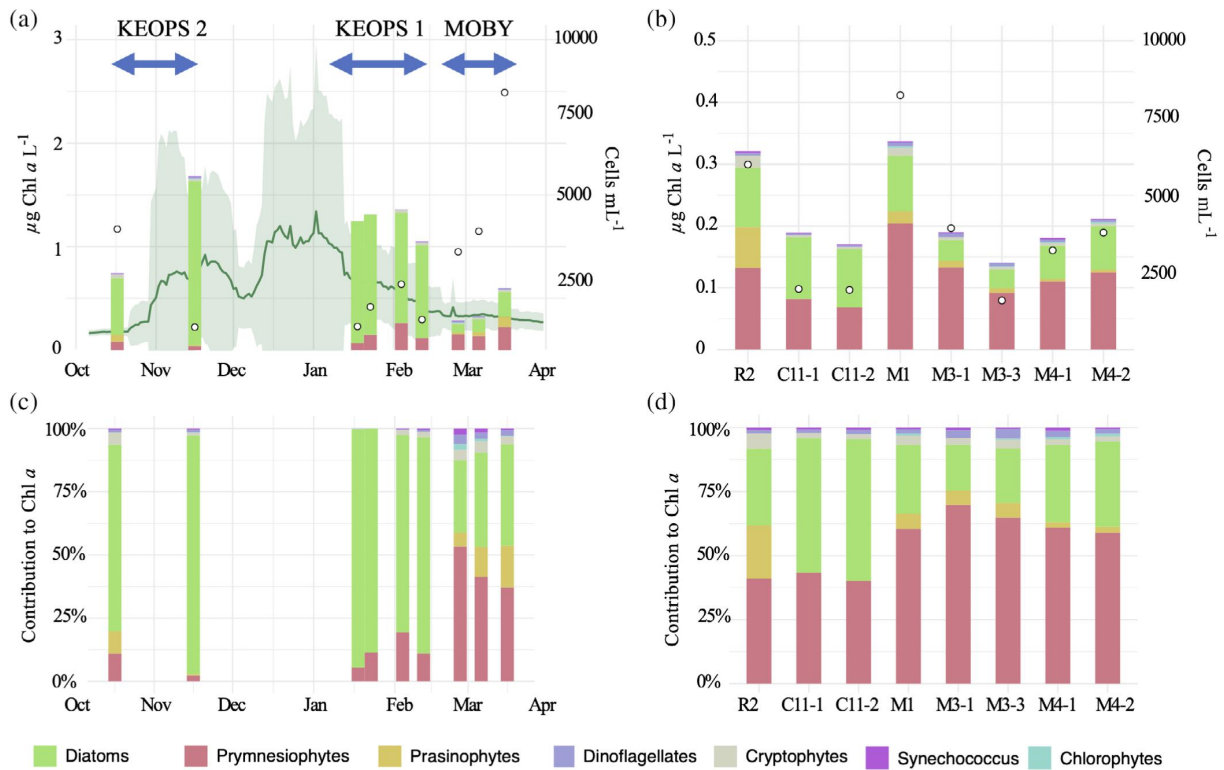


**Fig. 6.** Average estimated contribution of CHEMTAX groups to Chl *a* biomass ( $\mu\text{g L}^{-1}$ ) and abundance of small phytoplankton measured by flow cytometry (open circles,  $\text{cells mL}^{-1}$ ) in the 50 upper meters for plateau station (a) and HNLC reference stations (b) sampled during KEOPS 1-2 and MOBYDICK. Note different scales on Y-axis. In figure (a), average climatological mean (green line) and standard deviation (green area) estimated from satellite data on the plateau are indicated. Relative contribution of the different groups to total Chl *a* for plateau station (c) and HNLC reference stations (d).

(KEOPS1 HNLC reference station) where diatom pigments accounted for 52.1% of Chl *a*. Prymnesiophytes were the most important group and represented up to 70% of Chl *a* (M3-1; Fig. 6d). Other groups were minor contributors to Chl *a*, with the exception of prasinophytes at R2 (20.7%). As a consequence of these contrasted phytoplankton communities on and off the plateau, Chl *a* was significantly correlated with the abundance of small phytoplankton only off the plateau ( $R^2 = 0.89$ ;  $p < 0.0001$ ; Supporting Information Fig. S3).

### Discussion

The MOBYDICK cruise provided first insights into the phytoplankton community around Kerguelen after the summer bloom. Data from this study highlight the dominance of small-sized phytoplankton off the plateau (HNLC) throughout the year and document for the first time their importance in phytoplankton communities in surface waters on the iron-fertilized plateau. The intense diatom blooms on the Kerguelen plateau are thus followed by an increase of small phytoplankton in terms of absolute and relative contribution to

Chl *a* (Fig. 6a,b), displaying a seasonal community succession observed in other regions of the SO (e.g., Moline et al. 1996; Fiala et al. 1998; Wright et al. 2010). This study has further highlighted that small phytoplankton communities differed on and off the plateau in relation with contrasting nutrients concentrations (ammonium and silicic acid) after the bloom (Fig. 7).

### Diversity of pico- and nanophytoplankton and their response to environmental variables

Both CHEMTAX and sequencing analyses suggested that Prymnesiophytes, dominated by *Phaeocystis antarctica*, were the most abundant phytoplankton group in late summer. This phytoplanktonic group represented up to 53% and 70% of the Chl *a* on and off the plateau, respectively (Fig. 6c,d). Contrasted environmental conditions on and off the plateau did not seem to affect their distribution (Fig. 5). The ability of *P. antarctica* to thrive in HNLC waters has been explained by its large phenotypic plasticity, being able to reduce its cell volume and adapt its photo-physiology under Fe-limitation (Alderkamp et al. 2012; Koch et al. 2019). Iron replete conditions are known to trigger

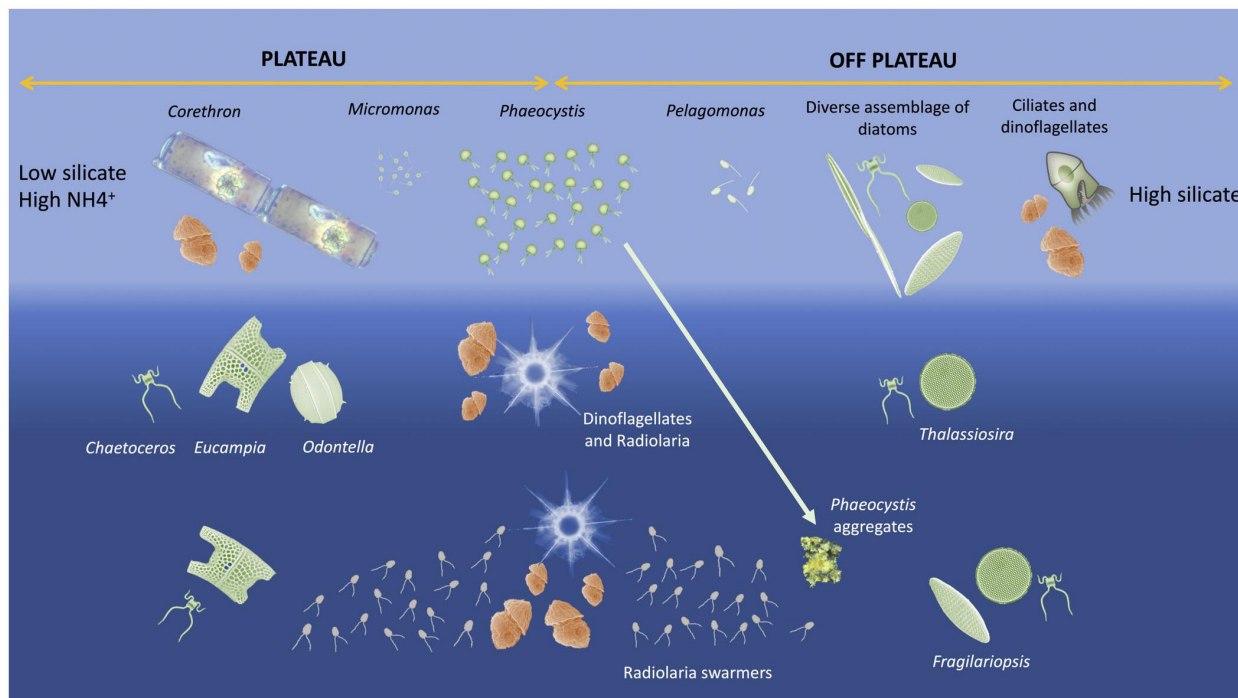


**Fig. 7.** Schematic graph of the dominating microbial eukaryotes after the bloom based on 18s rRNA metabarcoding. At 10 and 60 m (light blue on the figure), *Phaeocystis* was abundant on and off the plateau. On the plateau, where silicate concentrations were low and ammonium concentrations high, phytoplankton community was characterized by the dominance of large and lightly silicified diatom belonging to the genus *Corethron* and the presence of prasinophyte *Micromonas* in the small size-fraction (Fig. 4a). Off the plateau, silicate concentrations were not limiting and promoted a diverse assemblage of diatoms (*Fragilariopsis*, *Thalassiosira*, *Pseudo-nitzschia*, *Chaetoceros*) in both small and large-size fractions (Fig. 4a). Small and large heterotrophic dinoflagellates were well represented everywhere and ciliates were particularly abundant in some samples of the large size fraction off the plateau (Fig. 3). Below the ML (125 m), the relative abundance of heterotrophic dinoflagellates and Radiolaria increased. At 300 m, the small size fraction was largely dominated at all stations by Radiolaria, probably as swimmers stages (Fig. 3). Large, heavily silicified diatoms (*Eucampia* and *Odontella* on the plateau; *Thalassiosira* and *Fragilariopsis* off the plateau) characterized phytoplankton community (Supporting Information Fig. S2). *Chaetoceros* was also present, mostly in the small size fraction on the plateau and at M1. *Phaeocystis*, probably forming aggregates, was detected in large proportions only at 300 m off the plateau (Fig. 3).

*Phaeocystis*' colony formation (Garcia et al. 2009; Bender et al. 2018). Colony formation and size increase could in turn serve as defense mechanisms against small grazers such as copepods and ciliates (Schoemann et al. 2005; Tang et al. 2008). As a consequence, previous studies conducted in the SO observed that *Phaeocystis* population was mostly composed of single cells before and after the phytoplankton bloom. In spring, optimal light and iron concentrations lead to the formation of colonies (Smith et al. 2003). At the onset of the spring bloom (KEOPS2, November), when surface dissolved iron concentration was at its highest (Blain et al. 2007; Bowie et al. 2015), *Phaeocystis* was observed on and off the plateau in small colonies (Georges et al. 2014). This feature probably made them more resistant to grazing by protists than free cells like prasinophytes, as shown by the strong decrease of prasinophytes between the first two visits on the plateau during KEOPS2 (Fig. 6a,c). In late summer (MOBYDICK), *Phaeocystis* was only observed as small flagellated single cells (approximately 3  $\mu\text{m}$ , electron microscopy

observations, Supporting Information Fig. S4) on and off the plateau, in agreement with a potential iron limitation after the phytoplankton bloom (Smith et al. 2003).

While sequencing data indicated that *P. antarctica* was relatively abundant at all stations after the bloom, the structure of the other small phytoplanktonic groups featured marked differences on and off the plateau. Free *Phaeocystis* cells, *Micromonas*, and *Pelagomonas* are mostly grazed by ciliates, whose prey generally falls within the nanophytoplankton size class (Hansen et al. 1994). During MOBYDICK, ciliate communities showed similar structures and abundances on and off the plateau (Christaki, pers comm), suggesting that the observed spatial variability of small phytoplankton was most likely related to the availability of specific nutrients. High  $\text{NH}_4^+$  concentrations on the plateau (0.75–1.1  $\mu\text{mol L}^{-1}$ ) coincided during MOBYDICK with an increase in relative abundance of *Micromonas* (Figs. 5, 7). Increased ammonium concentrations on the plateau have previously been observed during the bloom decay (KEOPS1),

and were attributed to high heterotrophic activity (Mosseri et al. 2008). Ammonium is less energetically costly to assimilate than nitrate and is as such the preferred dissolved nitrogen source for most microalgae (McCarthy 1981; Raven et al. 1992), especially for prasinophytes (Litchman et al. 2007). They are thus able to grow more efficiently than other phytoplanktonic groups when ammonium concentrations are high. Slightly warmer temperatures on the plateau than off the plateau might also represent an advantage for prasinophytes. In the SO, other CHEMTAX studies have reported prasinophytes mostly north of 51°S (Wright et al. 1996), particularly in the Sub Tropical Front, where they could represent up to 10% of Chl *a* biomass (Iida and Odate 2014). In our study area, prasinophytes were mostly found close to the polar front during the onset (R-2, KEOPS2, Georges et al. 2014) and after the bloom (Sta. M2 and M3, MOBYDICK, Fig. 6d). When the Arctic *Micromonas* thrive in a cold and ice-covered ocean (Lovejoy et al. 2007), its close phylogenetic counterpart inhabiting the SO seems to be favored by warmer waters, suggesting differentiation into two distinct ecotypes.

Pelagophytes were enriched in Antarctic waters off the plateau (Figs. 4a, 7). During the LOHAFEX artificial iron experiment, pelagophytes were common in iron limited waters, but their relative abundance in sequencing datasets decreased after iron fertilization, whereas *Micromonas* became more abundant (Thiele et al. 2014). Experimental studies also demonstrated that *Pelagomonas* had higher affinities for dissolved inorganic iron than another prasinophyte *Prasinomonas* (Timmermans et al. 2005). If the same is true for other prasinophytes, *Pelagomonas* could thus be more competitive when iron is limiting, whereas *Micromonas* could be characterized as an opportunistic species, able to rapidly grow on ammonium.

#### Balance between small nonsilicified phytoplankton and diatoms (small and large)

At the bloom onset, when silicate and iron were not limiting, diatoms were able to build up biomass more efficiently than small nonsilicified phytoplankton whose abundance decreased (Fig. 6a; Supporting Information Table S2). Diatom grazers have relatively long generation times, leaving time for diatoms to proliferate until predation pressure control their population (Smetacek et al. 2004). Small nonsilicified phytoplankton are more rapidly controlled by predators, composed of fast growing microzooplankton such as ciliates and dinoflagellates (Coale et al. 1996; Landry et al. 2002, 2011; Smetacek et al. 2004). During the decline and after the bloom on the plateau, the scarcity of silicate ( $18.7 \mu\text{mol L}^{-1}$  in October in KEOPS2 to less than  $2 \mu\text{mol L}^{-1}$  during MOBYDICK; Supporting Information Table S2) and iron likely explains the collapse of diatom populations (Mosseri et al. 2008).

During MOBYDICK, diatom communities differed between on and off-plateau stations. According to sequencing data of the  $< 20 \mu\text{m}$  fraction, a diverse assemblage of small diatoms, such as *Fragilariopsis*, *Pseudo-nitzschia*, *Thalassiosira*, and

*Chaetoceros*, was enriched in Antarctic waters off the plateau (M4 and M1), probably related to higher silicate concentrations (Figs. 5, 7). The same diatom genera were also enriched in the large size fraction (Fig. 4b) and microscopic observations confirmed that their size range overlapped the two size fractions. In contrast, a few large diatoms were enriched on the plateau (Fig. 4b), where the lowest concentrations in  $\text{Si(OH)}_4$  were observed ( $< 2 \mu\text{mol L}^{-1}$  during the first two visits). Silicate requirements as well as Si uptake kinetics can vary from one species to the other. However, Hoffmann et al. (2008) suggested that silicate depletion may limit small diatoms sooner than large diatoms since the amount of silica needed relative to the volume of the cell is higher for small diatoms. In contrast, small diatoms were likely advantaged off the plateau (Sta. M1 and M4), where silicic acid concentration was higher. When silicate concentrations remain sufficient to build the frustules, cell size reduction is a morphological adaptation of diatoms to low iron concentrations, as an increased surface to volume ratio could facilitate iron uptake (Leynaert et al. 2004; Marchetti and Cassar 2009). In addition to their small size, most diatom genera that were enriched off the plateau in our study possess particular physiological adaptations to cope with low iron concentrations. The pennate diatoms *Pseudo-nitzschia* and *Fragilariopsis* use the iron-concentrating protein Ferritin, which allows them to store more iron than centric diatoms (Marchetti et al. 2009). The centric diatom *Thalassiosira* is adapted to low iron concentrations by possessing a modified photosynthetic apparatus, with electron-transport proteins modified to use copper instead of iron (Peers and Price 2006). It is also supposed to have an efficient iron vacuolar storage mechanism (Nuester et al. 2012). Sta. M3 was located in subantarctic waters and differed from the two other Antarctic water influenced off-plateau stations (M1, M4). M3 presented low silicate concentrations and lowest Chl *a* (Table 2). M3 showed the lowest proportion of diatom pigments (25% of Chl *a*) and number of reads in both small and large size fractions suggesting silicate and iron colimitation which disadvantaged growth of all diatoms.

#### Microbial eukaryotes below the ML and potential implications

Surface phytoplankton communities dominated by small cells, as observed during MOBYDICK cruise, are expected to sustain an active microbial loop. This implies little direct export of small phytoplankton production to the deep ocean, most of it being rapidly remineralized (Michaels and Silver 1988; Martin et al. 2013). Molecular analysis showed that the relative contribution of *Phaeocystis* strongly decreased below the ML in the small size fraction. The relative contribution of diatoms to the total amount of reads remained unchanged at 125 m and decreased at 300 m in this size fraction (Fig. 3). In the large size fraction, diatoms still accounted for over 25% of total number of reads in some off-plateau deep samples (M3-2 and M4-1, 300 m). *Thalassiosira* and



*Fragilariopsis*, which were recorded in both small and large size fractions at the surface in off-plateau waters, were found only in the large size fraction at 300 m (Supporting Information Figs. S2, S5). Lightly silicified *Corethron* dominated at the surface on the plateau during MOBYDICK (Supporting Information Fig. S2) while *Chaetoceros*, *Eucampia*, and *Odontella* were the main diatoms detected at 125 m depth (M2-3; Supporting Information Figs. S2, S5b). This suggests that small diatoms are not as efficiently exported as their larger counterparts. It also supports the hypothesis that the higher carbon export efficiency recorded off the plateau in summer (up to 58% of net primary production during KEOPS1) could be due to direct export of large fast sinking heavy silicified diatoms, assumed to be grazing-resistant (Laurenceau-Cornec et al. 2015).

Interestingly, *Phaeocystis* was found in relatively high proportions off the plateau (M3 and M4) at 300 m in the large size-fraction (Fig. 3). Although vertical carbon flux attenuation is higher for *Phaeocystis* than for diatoms (Reigstad and Wassmann 2007), *Phaeocystis* blooms have been shown to greatly contribute to carbon export in the Ross Sea (DiTullio et al. 2000). In our study, only single cells of *Phaeocystis* were observed in surface samples (Supporting Information Fig. S5). Considering the essential role of iron in colony formation, we consider unlikely that the presence of a relatively abundant number of reads at 300 m could result from direct sinking of colonies forms in previous weeks. This suggests that single cells of *Phaeocystis* could be exported directly through aggregation and/or indirectly through grazing (Reigstad and Wassmann 2007; Richardson and Jackson 2007; Richardson 2018). Grazers, such as dinoflagellates and Radiolaria, were the most common organisms in both size-fractions in the deeper samples (Figs. 3, 7). These predators are able to feed on a wide variety of size classes, from small cells to chain-forming diatoms (Swanberg and Caron 1991; Sherr and Sherr 2007). Previous studies have reported their high abundance at the bottom of the ML where they may feed on diatoms and other sinking cells and particles (Christaki et al. 2008, 2015; Gomi et al. 2010). The small fraction of deeper samples was largely dominated on and off-plateau by Radiolaria swimmers belonging to Chaunacanthidae family (cluster 4; Supporting Information Fig. S5b; Fig. 7). This group can form large cysts that can sink from the surface to deep waters where they release thousands of swimmers (< 5  $\mu\text{m}$ ) after the bloom. They may then use surface-produced organic carbon as a nutritional source while ascending through the water column (Martin et al. 2010; Decelle et al. 2013).

Concluding, global-change models project more stratified waters over the plateau of Kerguelen, increasing silicate and iron limitations (Freeman et al. 2018). Iron and silicate depleted waters are known to favor small phytoplankton communities over large ones—as observed during MOBYDICK—and eventually reduce carbon export due to promotion of microbially dominated food webs and greater remineralization (Bowie et al. 2011; Ebersbach et al. 2011; Martin et al. 2013).

Our study has shown contrasting small phytoplankton community structures relative to available nutrients on and off the Kerguelen plateau, and also underlined the capacity of *Phaeocystis* to thrive all over the studied region. In addition, this study has also highlighted that the possible contribution of *Phaeocystis* to carbon export in low productivity conditions deserves to be further studied.

## References

- Agawin, N. S. R., C. M. Duarte, and S. Agustí. 2000. Nutrient and temperature control of the contribution of picoplankton to phytoplankton biomass and production. *Limnol. Oceanogr.* **45**: 591–600. doi:10.4319/lo.2000.45.3.0591
- Alderkamp, A.-C., G. Kulk, A. G. J. Buma, R. J. W. Visser, G. L. Van Dijken, M. M. Mills, and K. R. Arrigo. 2012. The effect of iron limitation on the photophysiology of *Phaeocystis antarctica* (Prymnesiophyceae) and *Fragilariopsis cylindrus* (Bacillariophyceae) under dynamic irradiance. *J. Phycol.* **48**: 45–59. doi:10.1111/j.1529-8817.2011.01098.x
- Aminot, A., and R. K erouel. 2007. Dosage automatique des nutriments dans les eaux marines: M ethodes en flux continu. Editions Quae.
- Andersen, K. S., R. H. Kirkegaard, S. M. Karst, and M. Albertsen. 2018. ampvis2: An R package to analyse and visualise 16S rRNA amplicon data. bioRxiv 299537. doi:10.1101/299537
- Armand, L. K., V. Cornet-Barthaux, J. Mosseri, and B. Qu eguiner. 2008. Late summer diatom biomass and community structure on and around the naturally iron-fertilised Kerguelen Plateau in the Southern Ocean. *Deep-Sea Res. Part II Top. Stud. Oceanogr.* **55**: 653–676. doi:10.1016/j.dsr2.2007.12.031
- Bender, S. J., and others. 2018. Colony formation in *Phaeocystis antarctica*: Connecting molecular mechanisms with iron biogeochemistry. *Biogeosciences* **15**: 4923–4942. doi:10.5194/bg-15-4923-2018
- Blain, S., and others. 2007. Effect of natural iron fertilization on carbon sequestration in the Southern Ocean. *Nature* **446**: 1070–1074. doi:10.1038/nature05700
- Bower, S. M., R. B. Carnegie, B. Goh, S. R. Jones, G. J. Lowe, and M. W. Mak. 2004. Preferential PCR amplification of parasitic protistan small subunit rDNA from metazoan tissues. *J. Eukaryot. Microbiol.* **51**: 325–332. doi:10.1111/j.1550-7408.2004.tb00574.x
- Bowie, A. R., T. W. Trull, and F. Dehairs. 2011. Estimating the sensitivity of the subantarctic zone to environmental change: The SAZ-Sense project. *Deep-Sea Res. Part II Top. Stud. Oceanogr.* **58**: 2051–2058. doi:10.1016/j.dsr2.2011.05.034
- Bowie, A. R., P. van der Merwe, F. Qu erou e, and others. 2015. Iron budgets for three distinct biogeochemical sites around the Kerguelen Archipelago (Southern Ocean) during the

- natural fertilisation study, KEOPS-2. *Biogeosciences* **12**: 4421–4445. doi:<https://doi.org/10.5194/bg-12-4421-2015>
- Callahan, B. J., P. J. McMurdie, M. J. Rosen, A. W. Han, A. J. A. Johnson, and S. P. Holmes. 2016. DADA2: High-resolution sample inference from Illumina amplicon data. *Nat. Methods* **13**: 581–583. doi:[10.1038/nmeth.3869](https://doi.org/10.1038/nmeth.3869)
- Caporaso, J. G., and others. 2010. QIIME allows analysis of high-throughput community sequencing data. *Nat. Methods* **7**: 335–336. doi:[10.1038/nmeth.f.303](https://doi.org/10.1038/nmeth.f.303)
- Cavagna, A. J., and others. 2015. Production regime and associated N cycling in the vicinity of Kerguelen Island, Southern Ocean. *Biogeosciences* **12**: 6515–6528. doi:[10.5194/bg-12-6515-2015](https://doi.org/10.5194/bg-12-6515-2015)
- Chisholm, S. W. 1992. Phytoplankton size, p. 213–237. In P. G. Falkowski, A. D. Woodhead, and K. Vivirito [eds.], *Primary productivity and biogeochemical cycles in the sea*. Springer.
- Christaki, U., I. Obernosterer, F. Van Wambeke, M. Veldhuis, N. Garcia, and P. Catala. 2008. Microbial food web structure in a naturally iron-fertilized area in the Southern Ocean (Kerguelen Plateau). *Deep Sea Research Part II: Topical Studies in Oceanography* **55**: 706–719. doi:[10.1016/j.dsr2.2007.12.009](https://doi.org/10.1016/j.dsr2.2007.12.009)
- Christaki, U., and others. 2014. Microbial food web dynamics during spring phytoplankton blooms in the naturally iron-fertilized Kerguelen area (Southern Ocean). *Biogeosciences* **11**: 6739–6753. doi:[10.5194/bg-11-6739-2014](https://doi.org/10.5194/bg-11-6739-2014)
- Christaki, U., C. Georges, S. Genitsaris, and S. Monchy. 2015. Microzooplankton community associated with phytoplankton blooms in the naturally iron-fertilized Kerguelen area (Southern Ocean). *FEMS Microbiol. Ecol.* **91**: 1–15. doi:[10.1093/femsec/fiv068](https://doi.org/10.1093/femsec/fiv068)
- Clarke, L. J., and B. E. Deagle. 2018. Eukaryote plankton assemblages in the southern Kerguelen Axis region: Ecological drivers differ between size fractions. *Deep-Sea Res. Part II Top. Stud. Oceanogr.* **174**: 1–12. doi:[10.1016/j.dsr2.2018.12.003](https://doi.org/10.1016/j.dsr2.2018.12.003)
- Coale, K. H., and others. 1996. A massive phytoplankton bloom induced by an ecosystem-scale iron fertilization experiment in the equatorial Pacific Ocean. *Nature* **383**: 495–501. doi:[10.1038/383495a0](https://doi.org/10.1038/383495a0)
- de Baar, H. J. W., J. T. M. de Jong, D. C. E. Bakker, B. M. Löscher, C. Veth, U. Bathmann, and V. Smetacek. 1995. Importance of iron for plankton blooms and carbon dioxide drawdown in the Southern Ocean. *Nature* **373**: 412–415. doi:[10.1038/373412a0](https://doi.org/10.1038/373412a0)
- Decelle, J., and others. 2013. Diversity, ecology and biogeochemistry of cyst-forming acantharia (radiolaria) in the oceans. *PLoS One* **8**: e53598. doi:[10.1371/journal.pone.0053598](https://doi.org/10.1371/journal.pone.0053598)
- del Campo, J., and others. 2018. EukRef: Phylogenetic curation of ribosomal RNA to enhance understanding of eukaryotic diversity and distribution. *PLOS Biol.* **16**: e2005849. doi:[10.1371/journal.pbio.2005849](https://doi.org/10.1371/journal.pbio.2005849)
- Detmer, A. E., and U. V. Bathmann. 1997. Distribution patterns of autotrophic pico- and nanoplankton and their relative contribution to algal biomass during spring in the Atlantic sector of the Southern Ocean. *Deep-Sea Res. Part II Top. Stud. Oceanogr.* **44**: 299–320. doi:[10.1016/S0967-0645\(96\)00068-9](https://doi.org/10.1016/S0967-0645(96)00068-9)
- Díez, B., C. Pedrós-Alió, and R. Massana. 2001. Study of genetic diversity of eukaryotic picoplankton in different oceanic regions by small-subunit rRNA gene cloning and sequencing. *Appl. Environ. Microbiol.* **67**: 2932–2941. doi:[10.1128/AEM.67.7.2932-2941.2001](https://doi.org/10.1128/AEM.67.7.2932-2941.2001)
- Díez, B., R. Massana, M. Estrada, and C. Pedrós-Alió. 2004. Distribution of eukaryotic picoplankton assemblages across hydrographic fronts in the Southern Ocean, studied by denaturing gradient gel electrophoresis. *Limnol. Oceanogr.* **49**: 1022–1034. doi:[10.4319/lo.2004.49.4.1022](https://doi.org/10.4319/lo.2004.49.4.1022)
- DiTullio, G. R., and others. 2000. Rapid and early export of *Phaeocystis antarctica* blooms in the Ross Sea, Antarctica. *Nature* **404**: 595–598. doi:[10.1038/35007061](https://doi.org/10.1038/35007061)
- Ebersbach, F., T. W. Trull, D. M. Davies, and S. G. Bray. 2011. Controls on mesopelagic particle fluxes in the Sub-Antarctic and Polar Frontal Zones in the Southern Ocean south of Australia in summer—perspectives from free-drifting sediment traps. *Deep-Sea Res. Part II Top. Stud. Oceanogr.* **58**: 2260–2276.
- Edgar, R. C. 2013. UPARSE: Highly accurate OTU sequences from microbial amplicon reads. *Nat. Methods* **10**: 996–998.
- Fiala, M., E. E. Kopczynska, C. Jeandel, L. Oriol, and G. Vétion. 1998. Seasonal and interannual variability of size-fractionated phytoplankton biomass and community structure at station Kerfix, off the Kerguelen Islands, Antarctica. *J. Plankton Res.* **20**: 1341–1356. doi:[10.1093/plankt/20.7.1341](https://doi.org/10.1093/plankt/20.7.1341)
- Freeman, N. M., N. S. Lovenduski, D. R. Munro, K. M. Krumhardt, K. Lindsay, M. C. Long, and M. MacLennan. 2018. The variable and changing Southern Ocean Silicate Front: Insights from the CESM Large Ensemble. *Global Biogeochem. Cycles* **32**: 752–768. doi:[10.1029/2017GB005816](https://doi.org/10.1029/2017GB005816)
- Froneman, P. W., E. A. Pakhomov, and M. G. Balarin. 2004. Size-fractionated phytoplankton biomass, production and biogenic carbon flux in the eastern Atlantic sector of the Southern Ocean in late austral summer 1997–1998. *Deep-Sea Res. Part II Top. Stud. Oceanogr.* **51**: 2715–2729. doi:[10.1016/j.dsr2.2002.09.001](https://doi.org/10.1016/j.dsr2.2002.09.001)
- García, N. S., P. N. Sedwick, and G. R. DiTullio. 2009. Influence of irradiance and iron on the growth of colonial *Phaeocystis antarctica*: Implications for seasonal bloom dynamics in the Ross Sea, Antarctica. *Aquat. Microb. Ecol.* **57**: 203–220. doi:[10.3354/ame01334](https://doi.org/10.3354/ame01334)
- García-Muñoz, C., L. M. Lubián, C. M. García, Á. Marrero-Díaz, P. Sangrà, and M. Vernet. 2013. A mesoscale study of phytoplankton assemblages around the South Shetland Islands (Antarctica). *Polar Biol.* **36**: 1107–1123. doi:[10.1007/s00300-013-1333-5](https://doi.org/10.1007/s00300-013-1333-5)

- Gast, R. J., M. R. Dennett, and D. A. Caron. 2004. Characterization of protistan assemblages in the Ross Sea, Antarctica, by denaturing gradient gel electrophoresis. *Appl. Environ. Microbiol.* **70**: 2028–2037. doi:10.1128/AEM.70.4.2028-2037.2004
- Georges, C., S. Monchy, S. Genitsaris, and U. Christaki. 2014. Protist community composition during early phytoplankton blooms in the naturally iron-fertilized Kerguelen area (Southern Ocean). *Biogeosciences* **11**: 5847–5863. doi:10.5194/bg-11-5847-2014
- Gomi, Y., M. Fukuchi, and A. Taniguchi. 2010. Diatom assemblages at subsurface chlorophyll maximum layer in the eastern Indian sector of the Southern Ocean in summer. *J. Plankton Res.* **32**: 1039–1050. doi:10.1093/plankt/fbq031
- Guillou, L., and others. 2013. The Protist Ribosomal Reference database (PR2): A catalog of unicellular eukaryote small sub-unit rRNA sequences with curated taxonomy. *Nucleic Acids Res.* **41**: D597–D604. doi:10.1093/nar/gks1160
- Hansen, B., P. K. Bjornsen, and P. J. Hansen. 1994. The size ratio between planktonic predators and their prey. *Limnol. Oceanogr.* **39**: 395–403. doi:10.4319/lo.1994.39.2.0395
- Hashihama, F., T. Hirawake, S. Kudoh, J. Kanda, K. Furuya, Y. Yamaguchi, and T. Ishimaru. 2008. Size fraction and class composition of phytoplankton in the Antarctic marginal ice zone along the 140°E meridian during February–March 2003. *Polar Sci.* **2**: 109–120. doi:10.1016/j.polar.2008.05.001
- Higgins, H. W., S. W. Wright, and L. Schlüter. 2011. Quantitative interpretation of chemotaxonomic pigment data, p. 257–313. *In* *Phytoplankton pigments: Characterization, chemotaxonomy and applications in oceanography*. Cambridge Univ. Press.
- Higgins, H. W., S. W. Wright, and L. Schlüter. 2011. Quantitative interpretation of chemotaxonomic pigment data, p. 257–313. *In* C.A. Llewellyn, E.S. Egeland, G. Johnsen, and S. Roy [eds.], *Phytoplankton Pigments: Characterization, chemotaxonomy and applications in oceanography*. Cambridge University Press.
- Hoffmann, L. J., I. Peeken, and K. Lochte. 2008. Iron, silicate, and light co-limitation of three Southern Ocean diatom species. *Polar Biol.* **31**: 1067–1080. doi:10.1007/s00300-008-0448-6
- Holmes, R. M., A. Aminot, R. Kérouel, B. A. Hooker, and B. J. Peterson. 1999. A simple and precise method for measuring ammonium in marine and freshwater ecosystems. *Can. J. Fish. Aquat. Sci.* **56**: 1801–1808.
- Iida, T., and T. Odate. 2014. Seasonal variability of phytoplankton biomass and composition in the major water masses of the Indian Ocean sector of the Southern Ocean. *Polar Sci.* **8**: 283–297. doi:10.1016/j.polar.2014.03.003
- Irwin, A. J., Z. V. Finkel, O. M. E. Schofield, and P. G. Falkowski. 2006. Scaling-up from nutrient physiology to the size-structure of phytoplankton communities. *J. Plankton Res.* **28**: 459–471. doi:10.1093/plankt/fbi148
- Johnston, T. M. S., and D. L. Rudnick. 2009. Observations of the transition layer. *J. Phys. Oceanogr.* **39**: 780–797. doi:10.1175/2008JPO3824.1
- Katoh, K., and D. M. Standley. 2013. MAFFT multiple sequence alignment software version 7: Improvements in performance and usability. *Mol. Biol. Evol.* **30**: 772–780. doi:10.1093/molbev/mst010
- Koch, F., S. Beszteri, L. Harms, and S. Trimborn. 2019. The impacts of iron limitation and ocean acidification on the cellular stoichiometry, photophysiology, and transcriptome of *Phaeocystis antarctica*. *Limnol. Oceanogr.* **64**: 357–375. doi:10.1002/lno.11045
- Kopczyńska, E. E., M. Fiala, and C. Jeandel. 1998. Annual and interannual variability in phytoplankton at a permanent station off Kerguelen Islands, Southern Ocean. *Polar Biol.* **20**: 342–351. doi:10.1007/s003000050312
- Kopczynska, E. E., F. Dehairs, M. Elskens, and S. Wright. 2001. Phytoplankton and microzooplankton variability between the Subtropical and Polar Fronts south of Australia: Thriving under regenerative and new production in late summer. *J. Geophys. Res. Oceans* **106**: 31597–31609. doi:10.1029/2000JC000278
- Korb, R. E., M. J. Whitehouse, A. Atkinson, and S. E. Thorpe. 2008. Magnitude and maintenance of the phytoplankton bloom at South Georgia: A naturally iron-replete environment. *Mar. Ecol. Prog. Ser.* **368**: 75–91. doi:10.3354/meps07525
- Landry, M. R., and others. 2002. Seasonal dynamics of phytoplankton in the Antarctic Polar Front region at 170°W. *Deep-Sea Res. Part II Top. Stud. Oceanogr.* **49**: 1843–1865. doi:10.1016/S0967-0645(02)00015-2
- Landry, M. R., K. E. Selph, A. G. Taylor, M. Décima, W. M. Balch, and R. R. Bidigare. 2011. Phytoplankton growth, grazing and production balances in the HNLC equatorial Pacific. *Deep-Sea Res. Part II Top. Stud. Oceanogr.* **58**: 524–535. doi:10.1016/j.dsr2.2010.08.011
- Lasbleiz, M., K. Leblanc, S. Blain, J. Ras, V. Cornet-Barthaux, S. Hélias Nunige, and B. Quéguiner. 2014. Pigments, elemental composition (C, N, P, and Si), and stoichiometry of particulate matter in the naturally iron fertilized region of Kerguelen in the Southern Ocean. *Biogeosciences* **11**: 5931–5955. doi:10.5194/bg-11-5931-2014
- Lasbleiz, M., K. Leblanc, L. K. Armand, U. Christaki, C. Georges, I. Obernosterer, and B. Quéguiner. 2016. Composition of diatom communities and their contribution to plankton biomass in the naturally iron-fertilized region of Kerguelen in the Southern Ocean. *FEMS Microbiol. Ecol.* **92**: 1–16. doi:10.1093/femsec/fiw171
- Laurenceau-Cornec, E. C., and others. 2015. The relative importance of phytoplankton aggregates and zooplankton fecal pellets to carbon export: Insights from free-drifting sediment trap deployments in naturally iron-fertilised waters near the Kerguelen Plateau. *Biogeosciences* **12**: 1007–1027. doi:10.5194/bg-12-1007-2015

- Le Moigne, F. A. C., and others. 2016. What causes the inverse relationship between primary production and export efficiency in the Southern Ocean? *Geophys. Res. Lett.* **43**: 4457–4466. doi:10.1002/2016GL068480
- Lê, S., J. Josse, and F. Husson. 2008. FactoMineR: An R package for multivariate analysis. *J. Stat. Softw.* **25**: 1–18.
- Leynaert, A., E. Bucciarelli, P. Claquin, R. C. Dugdale, V. Martin-Jézéquel, P. Pondaven, and O. Ragueneau. 2004. Effect of iron deficiency on diatom cell size and silicic acid uptake kinetics. *Limnol. Oceanogr.* **49**: 1134–1143. doi:10.4319/lo.2004.49.4.1134
- Litchman, E., C. A. Klausmeier, O. M. Schofield, and P. G. Falkowski. 2007. The role of functional traits and trade-offs in structuring phytoplankton communities: Scaling from cellular to ecosystem level. *Ecol. Lett.* **10**: 1170–1181. doi:10.1111/j.1461-0248.2007.01117.x
- Love, M. I., W. Huber, and S. Anders. 2014. Moderated estimation of fold change and dispersion for RNA-seq data with DESeq2. *Genome Biol.* **15**: 550. doi:10.1186/s13059-014-0550-8
- Lovejoy, C., and others. 2007. Distribution, phylogeny, and growth of cold-adapted picoprasinophytes in Arctic Seas. *J. Phycol.* **43**: 78–89. doi:10.1111/j.1529-8817.2006.00310.x
- Lozupone, C., M. E. Lladser, D. Knights, J. Stombaugh, and R. Knight. 2011. UniFrac: An effective distance metric for microbial community comparison. *ISME J.* **5**: 169–172. doi:10.1038/ismej.2010.133
- Mackey, M. D., D. J. Mackey, H. W. Higgins, and S. W. Wright. 1996. CHEMTAX—a program for estimating class abundances from chemical markers: Application to HPLC measurements of phytoplankton. *Mar. Ecol. Prog. Ser.* **144**: 265–283.
- Maiti, K., M. A. Charette, K. O. Buesseler, and M. Kahru. 2013. An inverse relationship between production and export efficiency in the Southern Ocean. *Geophys. Res. Lett.* **40**: 1557–1561. doi:10.1002/grl.50219
- Marañón, E., P. M. Holligan, R. Barciela, N. González, B. Mouriño, M. J. Pazó, and M. Varela. 2001. Patterns of phytoplankton size structure and productivity in contrasting open-ocean environments. *Mar. Ecol. Prog. Ser.* **216**: 43–56. doi:10.3354/meps216043
- Marchetti, A., and N. Cassar. 2009. Diatom elemental and morphological changes in response to iron limitation: A brief review with potential paleoceanographic applications. *Geobiology* **7**: 419–431. doi:10.1111/j.1472-4669.2009.00207.x
- Marchetti, A., and others. 2009. Ferritin is used for iron storage in bloom-forming marine pennate diatoms. *Nature* **457**: 467–470. doi:10.1038/nature07539
- Marie, D., F. Partensky, D. Vaultot, and C. Brussaard. 1999. Enumeration of phytoplankton, bacteria, and viruses in marine samples. *Curr. Protoc. Cytom.* **10**: 11.11.1–11.11.15. doi:10.1002/0471142956.cy1111s10
- Martin, J. H. 1990. Glacial-interglacial CO<sub>2</sub> change: The iron hypothesis. *Paleoceanography* **5**: 1–13. doi:10.1029/PA005i001p00001
- Martin, P., J. T. Allen, M. J. Cooper, D. G. Johns, R. S. Lampitt, R. Sanders, and D. A. H. Teagle. 2010. Sedimentation of acantharian cysts in the Iceland Basin: Strontium as a ballast for deep ocean particle flux, and implications for acantharian reproductive strategies. *Limnol. Oceanogr.* **55**: 604–614. doi:10.4319/lo.2010.55.2.0604
- Martin, P., and others. 2013. Iron fertilization enhanced net community production but not downward particle flux during the Southern Ocean iron fertilization experiment LOHAFEX. *Global Biogeochem. Cycles* **27**: 871–881. doi:10.1002/gbc.20077
- McCarthy, J. 1981. The kinetics of nutrient utilization. *Can. Bull. Fish. Aquat. Sci.* **210**: 211–233.
- McMurdie, P. J., and S. Holmes. 2013. Phyloseq: An R package for reproducible interactive analysis and graphics of microbiome census data. *PLoS One* **8**: e61217. doi:10.1371/journal.pone.0061217
- Michaels, A. F., and M. W. Silver. 1988. Primary production, sinking fluxes and the microbial food web. *Deep-Sea Res. A* **35**: 473–490. doi:10.1016/0198-0149(88)90126-4
- Moline, M. A., B. B. Prezelin, O. Schofield, and R. C. Smith. 1996. Temporal dynamics of coastal Antarctic phytoplankton: Environmental driving forces and impact of 1991/92 summer diatom bloom on the nutrient regimes.
- Moline, M. A., B. B. Prezelin, O. Schofield, and R. C. Smith. 1997. Temporal dynamics of coastal Antarctic phytoplankton: Environmental driving forces and impact of a 1991/92 summer diatom bloom on the nutrient regimes., p. 67–72. In B. Battaglia, H. Valencia, and D. Walton [eds.], *Antarctic communities: Species, structure and survival*. Cambridge University Press.
- Mongin, M., E. Molina, and T. W. Trull. 2008. Seasonality and scale of the Kerguelen plateau phytoplankton bloom: A remote sensing and modeling analysis of the influence of natural iron fertilization in the Southern Ocean. *Deep-Sea Res. Part II Top. Stud. Oceanogr.* **55**: 880–892. doi:10.1016/j.dsr2.2007.12.039
- Moore, J. K., and M. R. Abbott. 2000. Phytoplankton chlorophyll distributions and primary production in the Southern Ocean. *J. Geophys. Res. Oceans* **105**: 28709–28722. doi:10.1029/1999JC000043
- Mosseri, J., B. Quéguiner, L. Armand, and V. Cornet-Barthaux. 2008. Impact of iron on silicon utilization by diatoms in the Southern Ocean: A case study of Si/N cycle decoupling in a naturally iron-enriched area. *Deep-Sea Res. Part II Top. Stud. Oceanogr.* **55**: 801–819. doi:10.1016/j.dsr2.2007.12.003
- Murtagg, F., and P. Legendre. 2014. Ward's hierarchical agglomerative clustering method: Which algorithms implement Ward's criterion? *J. Classif.* **31**: 274–295. doi:10.1007/s00357-014-9161-z

- Nueter, J., S. Vogt, and B. S. Twining. 2012. Localization of iron within centric diatoms of the genus *Thalassiosira*. *J. Phycol.* **48**: 626–634. doi:10.1111/j.1529-8817.2012.01165.x
- Oksanen, J., and others. 2017. vegan: Community ecology package. R package version 2.3-0.2015.
- Pauthenet, E., et al. 2018. Seasonal Meandering of the Polar Front Upstream of the Kerguelen Plateau. *Geophysical Research Letters* **45**: 9774–9781. doi:10.1029/2018GL079614
- Park, Y.-H., F. Roquet, I. Durand, and J.-L. Fuda. 2008. Large-scale circulation over and around the Northern Kerguelen Plateau. *Deep-Sea Res. Part II Top. Stud. Oceanogr.* **55**: 566–581. doi:10.1016/j.dsr2.2007.12.030
- Pedros-Alió, C. 2007. Dipping into the Rare Biosphere. *Science* **315**: 192–193. doi:10.1126/science.1135933
- Peers, G., and N. M. Price. 2006. Copper-containing plastocyanin used for electron transport by an oceanic diatom. *Nature* **441**: 341–344. doi:10.1038/nature04630
- Penna, A. D., T. W. Trull, S. Wotherspoon, S. D. Monte, C. R. Johnson, and F. d'Ovidio. 2018. Mesoscale variability of conditions favoring an iron-induced diatom bloom downstream of the Kerguelen Plateau. *J. Geophys. Res. Oceans* **123**: 3355–3367. doi:10.1029/2018JC013884
- Piquet, A. M.-T., H. Bolhuis, M. P. Meredith, and A. G. J. Buma. 2011. Shifts in coastal Antarctic marine microbial communities during and after melt water-related surface stratification. *FEMS Microbiol. Ecol.* **76**: 413–427. doi:10.1111/j.1574-6941.2011.01062.x
- Planchon, F., and others. 2015. Carbon export in the naturally iron-fertilized Kerguelen area of the Southern Ocean based on the <sup>234</sup>Th approach. *Biogeosciences* **12**: 3831–3848. doi:10.5194/bg-12-3831-2015
- Pollard, R. T., and others. 2009. Southern Ocean deep-water carbon export enhanced by natural iron fertilization. *Nature* **457**: 577–580. doi:10.1038/nature07716
- Price, M. N., P. S. Dehal, and A. P. Arkin. 2009. FastTree: Computing large minimum evolution trees with profiles instead of a distance matrix. *Mol. Biol. Evol.* **26**: 1641–1650. doi:10.1093/molbev/msp077
- Quéguiner, B., S. Blain, and T. Trull. 2007. High primary production and vertical export of carbon over the Kerguelen Plateau as a consequence of natural iron fertilization in a high-nutrient, low-chlorophyll environment, p. 167–172. *In* Proceedings of the The Kerguelen Plateau: Marine ecosystem and fisheries, Proceedings of the 1st international Science Symposium on the Kerguelen Plateau, Société Française d'Ichtyologie. Apr 14-16, 2010, Concarneau
- R Core Team. 2018. R: A language and environment for statistical computing. R Foundation for Statistical Computing.
- Ras, J., H. Claustre, and J. Uitz. 2008. Spatial variability of phytoplankton pigment distributions in the Subtropical South Pacific Ocean: Comparison between in situ and predicted data. *Biogeosciences* **5**: 353–369. doi:10.5194/bg-5-353-2008
- Raven, J. A., B. Wollenweber, and L. L. Handley. 1992. A comparison of ammonium and nitrate as nitrogen sources for photolithotrophs. *New Phytol.* **121**: 19–32. doi:10.1111/j.1469-8137.1992.tb01088.x
- Reigstad, M., and P. Wassmann. 2007. Does *Phaeocystis* spp. contribute significantly to vertical export of organic carbon? p. 217–234. *In* M. A. Van Leeuwe, J. Stefels, S. Belviso, C. Lancelot, P. G. Verity, and W. W. C. Gieskes [eds.], *Phaeocystis*, major link in the biogeochemical cycling of climate-relevant elements. Springer.
- Rembauville, M., S. Blain, L. Armand, B. Quéguiner, and I. Salter. 2015. Export fluxes in a naturally iron-fertilized area of the Southern Ocean – part 2: Importance of diatom resting spores and faecal pellets for export. *Biogeosciences* **12**: 3171–3195. doi:10.5194/bg-12-3171-2015
- Rembauville, M., and others. 2017. Plankton assemblage estimated with BGC-Argo floats in the Southern Ocean: Implications for seasonal successions and particle export. *J. Geophys. Res. Oceans* **122**: 8278–8292. doi:10.1002/2017JC013067
- Rembauville, M., I. Salter, F. Dehairs, J.-C. Miquel, and S. Blain. 2018. Annual particulate matter and diatom export in a high nutrient, low chlorophyll area of the Southern Ocean. *Polar Biol.* **41**: 25–40. doi:10.1007/s00300-017-2167-3
- Richardson, T. L. 2018. Mechanisms and pathways of small-phytoplankton export from the surface ocean. *Ann. Rev. Mar. Sci.* **11**: 57–74. doi:10.1146/annurev-marine-121916-063627
- Richardson, T. L., and G. A. Jackson. 2007. Small phytoplankton and carbon export from the surface ocean. *Science* **315**: 838–840. doi:10.1126/science.1133471
- Schoemann, V., S. Becquevort, J. Stefels, V. Rousseau, and C. Lancelot. 2005. *Phaeocystis* blooms in the global ocean and their controlling mechanisms: A review. *J. Sea Res.* **53**: 43–66. doi:10.1016/j.seares.2004.01.008
- Schulz, I., and others. 2018. Remarkable structural resistance of a nanoflagellate-dominated plankton community to iron fertilization during the Southern Ocean experiment LOHAFEX. *Mar. Ecol. Prog. Ser.* **601**: 77–95. doi:10.3354/meps12685
- Sherr, E. B., and B. F. Sherr. 2007. Heterotrophic dinoflagellates: A significant component of microzooplankton biomass and major grazers of diatoms in the sea. *Mar. Ecol. Prog. Ser.* **352**: 187–197. doi:10.3354/meps07161
- Smetacek, V., P. Assmy, and J. Henjes. 2004. The role of grazing in structuring Southern Ocean pelagic ecosystems and biogeochemical cycles. *Antarct. Sci.* **16**: 541–558. doi:10.1017/S0954102004002317
- Smetacek, V., R. Scharek, and E.-M. Nöthig. 1990. Seasonal and Regional Variation in the Pelagial and its Relationship

- to the Life History Cycle of Krill. Antarctic Ecosystems. Springer Berlin Heidelberg. 103–114.
- Smith, W. O., M. R. Dennett, S. Mathot, and D. A. Caron. 2003. The temporal dynamics of the flagellated and colonial stages of *Phaeocystis antarctica* in the Ross Sea. Deep-Sea Res. Part II Top. Stud. Oceanogr. **50**: 605–617. doi:10.1016/S0967-0645(02)00586-6
- Ssekagiri, A., W. Sloan, and U. Ijaz. 2018. microbiomeSeq: An R package for microbial community analysis in an environmental context. Available at <http://www.github.com/umerijaz/microbiomeSeq>
- Swanberg, N. R., and D. A. Caron. 1991. Patterns of sarcodine feeding in epipelagic oceanic plankton. J. Plankton Res. **13**: 287–312. doi:10.1093/plankt/13.2.287
- Tang, K. W., W. O. Smith Jr., D. T. Elliott, and A. R. Shields. 2008. Colony size of *Phaeocystis antarctica* (prymnesiophyceae) as influenced by zooplankton grazers. J. Phycol. **44**: 1372–1378. doi:10.1111/j.1529-8817.2008.00595.x
- Thiele, S., C. Wolf, I. K. Schulz, P. Assmy, K. Metfies, and B. M. Fuchs. 2014. Stable composition of the nano- and picoplankton community during the ocean iron fertilization experiment LOHAFEX. PLoS One **9**: e113244. doi:10.1371/journal.pone.0113244
- Timmermans, K. R., B. van der Wagt, M. J. W. Veldhuis, A. Maatman, and H. J. W. de Baar. 2005. Physiological responses of three species of marine pico-phytoplankton to ammonium, phosphate, iron and light limitation. J. Sea Res. **53**: 109–120. doi:10.1016/j.seares.2004.05.003
- Uitz, J., H. Claustre, F. B. Griffiths, J. Ras, N. Garcia, and V. Sandroni. 2009. A phytoplankton class-specific primary production model applied to the Kerguelen Islands region (Southern Ocean). Deep-Sea Res. Part I Oceanogr. Res. Pap. **56**: 541–560. doi:10.1016/j.dsr.2008.11.006
- Uitz, J., H. Claustre, B. Gentili, and D. Stramski. 2010. Phytoplankton class-specific primary production in the world's oceans: Seasonal and interannual variability from satellite observations. Global Biogeochem. Cycles **24**: 1–19. doi:10.1029/2009GB003680
- Van Heukelem, L., and C. S. Thomas. 2001. Computer-assisted high-performance liquid chromatography method development with applications to the isolation and analysis of phytoplankton pigments. J. Chromatogr. A **910**: 31–49. doi:10.1016/S0378-4347(00)00603-4
- van Leeuwe, M. A., R. J. W. Visser, and J. Stefels. 2014. The pigment composition of *Phaeocystis antarctica* (Haptophyceae) under various conditions of light, temperature, salinity, and iron. J. Phycol. **50**: 1070–1080. doi:10.1111/jpy.12238
- Wang, Q., G. M. Garrity, J. M. Tiedje, and J. R. Cole. 2007. Naïve Bayesian classifier for rapid assignment of rRNA sequences into the new bacterial taxonomy. Appl. Environ. Microbiol. **73**: 5261–5267. doi:10.1128/AEM.00062-07
- Weber, L. H., and S. Z. El-Sayed. 1987. Contributions of the net, nano- and picoplankton to the phytoplankton standing crop and primary productivity in the Southern Ocean. J. Plankton Res. **9**: 973–994. doi:10.1093/plankt/9.5.973
- Wickham, H. 2011. ggplot2. Wiley Interdiscip. Rev. Comput. Stat. **3**: 180–185.
- Wickham, H. 2016. ggplot2: Elegant graphics for data analysis. Springer.
- Wolf, C., S. Frickenhaus, E. S. Kiliyas, I. Peeken, and K. Metfies. 2014. Protist community composition in the Pacific sector of the Southern Ocean during austral summer 2010. Polar Biol. **37**: 375–389. doi:10.1007/s00300-013-1438-x
- Wright, S. W., D. Thomas, H. Marchant, H. Higgins, M. Mackey, and D. Mackey. 1996. Analysis of phytoplankton of the Australian sector of the Southern Ocean: Comparisons of microscopy and size frequency data with interpretations of pigment HPLC data using the 'CHEMTAX' matrix factorisation program. Mar. Ecol. Prog. Ser. **144**: 285–298. doi:10.3354/meps144285
- Wright, S. W., A. Ishikawa, H. J. Marchant, A. T. Davidson, R. L. van den Eenden, and G. V. Nash. 2009. Composition and significance of picophytoplankton in Antarctic waters. Polar Biol. **32**: 797–808. doi:10.1007/s00300-009-0582-9
- Wright, S. W., R. L. van den Eenden, I. Pearce, A. T. Davidson, F. J. Scott, and K. J. Westwood. 2010. Phytoplankton community structure and stocks in the Southern Ocean (30–80 E) determined by CHEMTAX analysis of HPLC pigment signatures. Deep-Sea Res. Part II Top. Stud. Oceanogr. **57**: 758–778.

#### Acknowledgments

We thank B. Quéguiner, the PI of the MOBYDICK project, for providing us the opportunity to participate to this cruise, the captain, and crew of the R/V *Marion Dufresne* for their enthusiasm and support aboard during the MOBYDICK-THEMISTO cruise (<https://doi.org/10.17600/18000403>) and the chief scientist I. Obernosterer, whose valuable comments considerably improved this manuscript. This work was supported by the French oceanographic fleet (Flotte océanographique française), the French ANR ("Agence Nationale de la Recherche," AAPG 2017 program, MOBYDICK Project number: ANR-17-CE01-0013), and the French Research program of INSU-CNRS LEFE/CYBER ("Les enveloppes fluides et l'environnement"—"Cycles biogéochimiques, environnement et ressources"). We also thank the French Ministry of Higher Education and the Region des Hauts de France for funding the Ph.D. grant to S.I. Diatom pictograms (Fig. 7) were modified from K. Leblanc diatom pictures available on <https://plankton.mio.osupytheas.fr/mobydick-2018/>

#### Conflict of Interest

None declared.

Submitted 17 January 2020

Revised 29 May 2020

Accepted 11 June 2020

Associate editor: Heidi Sosik

Supplementary material

**Table S1.** Initial pigment:Chl *a* ratios used in CHEMTAX analysis of pigment data.

	Chl_c3	Peri	Fuco	Pras	Hex-fuco	Zea	Allo	Lut	Chl_b
<b>Chlorophytes</b>	0	0	0	0	0	0,12	0	0,22	0,15
<b>Cryptophytes</b>	0	0	0	0	0	0	0,22	0	0
<b>Cyanobacteria</b>	0	0	0	0	0	0,586	0	0	0
<b>Diatoms</b>	0	0	0,7	0	0	0	0	0	0
<b>Dinoflagellates</b>	0	0,82	0	0	0	0	0	0	0
<b>Haptophytes (<i>Phaeocystis</i> like)</b>	0,15	0	0,02	0	0,55	0	0	0	0
<b>Prasinophytes</b>	0	0	0	0,09	0	0,017	0	0,006	0,55

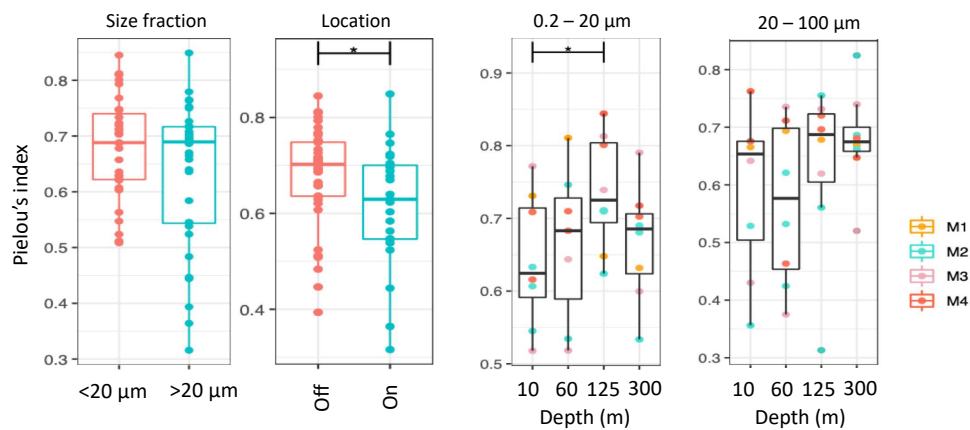


**Fig. S1.** Evenness for the entire dataset according to different size fractions and locations on or off the plateau, and for each depth of the different size fractions. Pairwise significant differences (Tukey HSD,  $P < 0.05$ ) are indicated. Pielou's index is constrained between 0 and 1 (lowest to highest possible evenness).





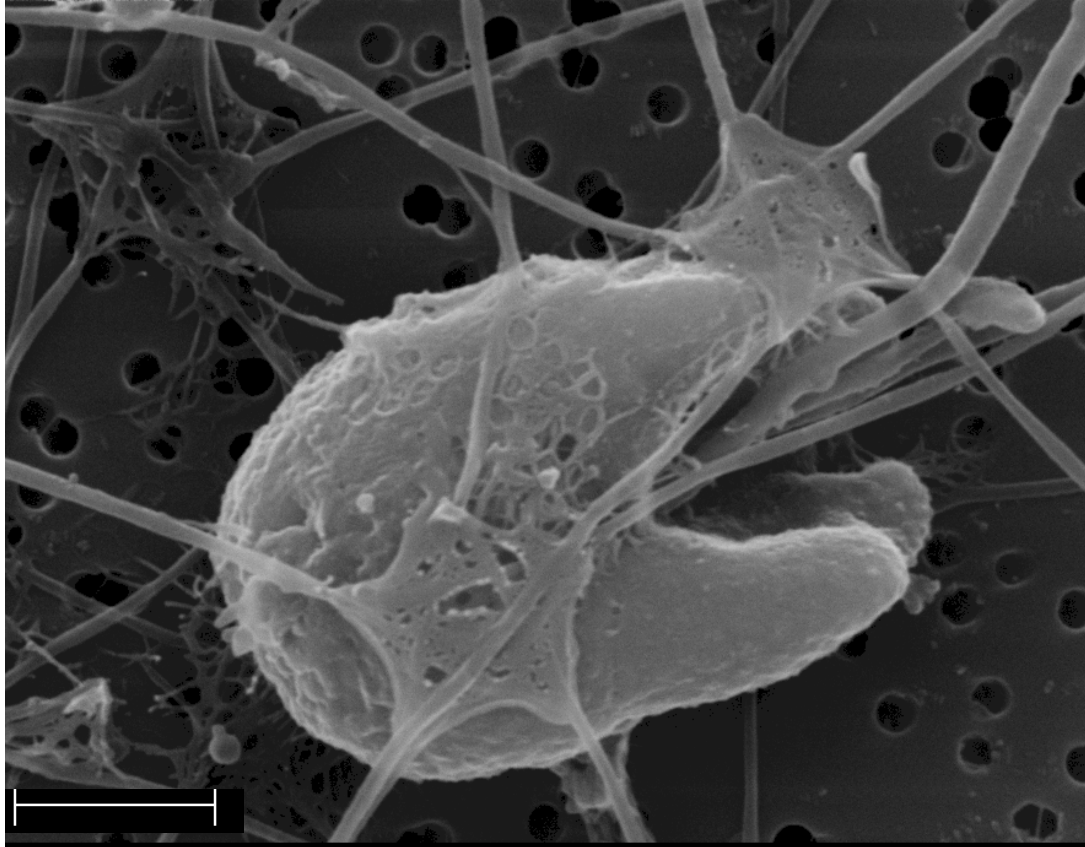


**Fig. S4.** Example of typical *Phaeocystis antarctica* flagellated cell as seen by SEM in MOBYDICK samples. Scale bar = 1  $\mu\text{m}$ . Copyright: Lucie Courcot (LOG)

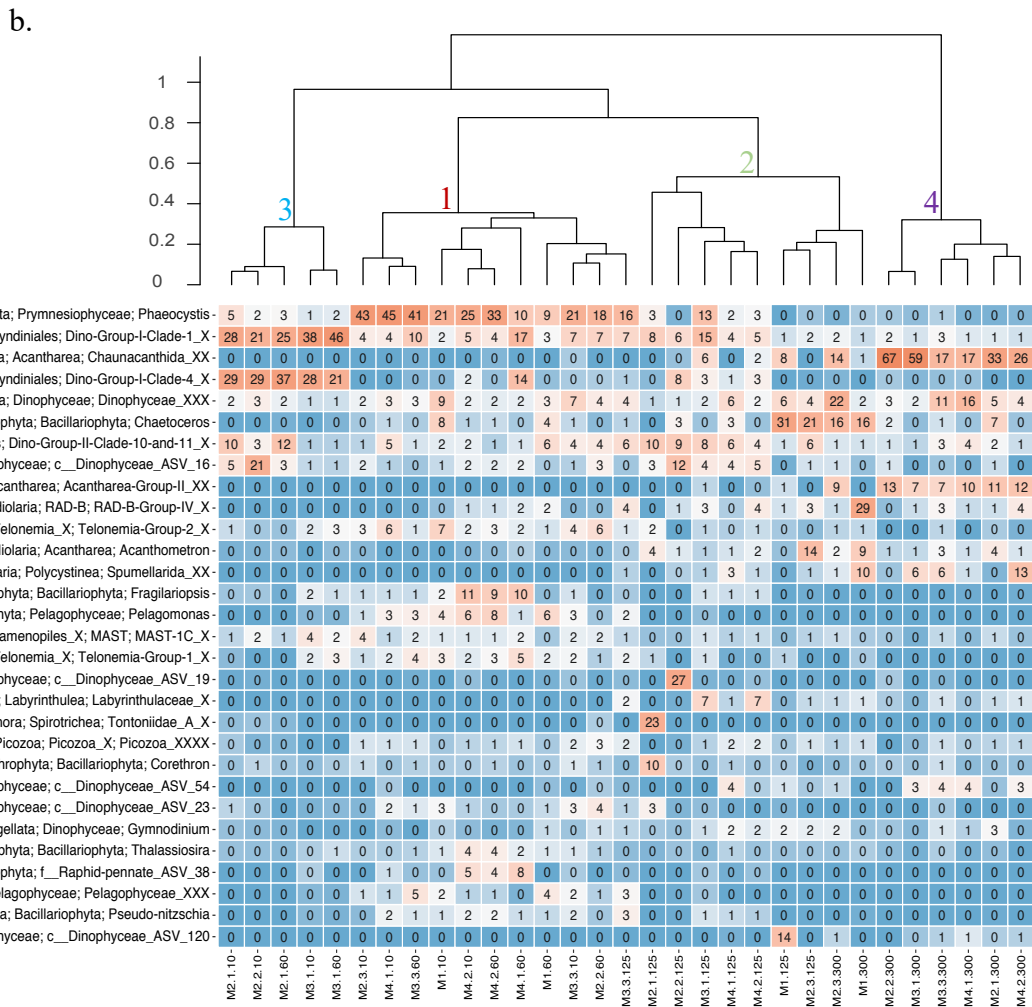
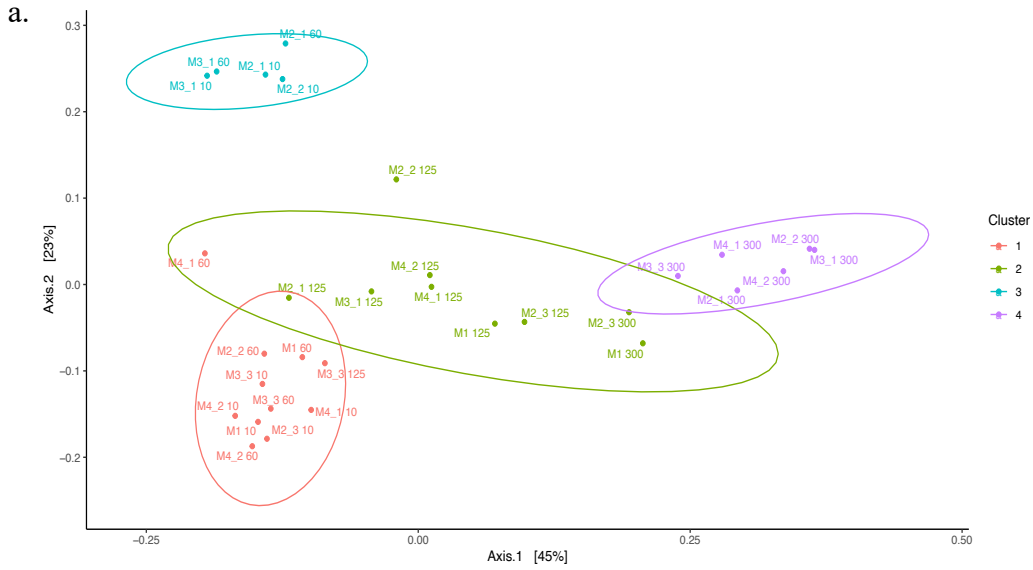


**Fig. S5.** PCoA of communities of the small size-fraction based on weighted UniFrac distances between samples. Each point represents a sampling depth and station (a). Heatmap of the 30 most abundant genera (b). Cluster number is indicated at the root of the dendrogram. In the heatmap, numbers indicate the relative abundance of each genus for each sample. ASVs are labeled by their division, class and genus or best taxonomic classification available (c\_ : class ; f\_ : family). Samples are grouped according to the cluster analysis. Cluster number is indicated at the root of the dendrogram.

Analysis of all samples of the small size fraction showed that on and off-plateau community structures were not different (Permanova,  $P=0.33$ ). Cluster analysis confirmed that samples of the  $< 20 \mu\text{m}$  size fraction were grouped by depth rather than by location (Fig. S5 A, B). Surface samples formed two different clusters (clusters 1 and 3). Cluster 3 corresponded to the first visits at M2 and M3, and was characterized by a high proportion of parasitic Syndiniales reads (Dino-Group 1, clade 1 and 4). In contrast, cluster 1 was dominated by autotrophs, mostly by *Phaeocystis*, and other small autotrophs such as *Pelagomonas* and the diatom *Fragilariopsis* at M4 (Fig. S5 B). Cluster 2 grouped all samples from 125 m and the 300 m samples of M2-3 and M1. Community composition of the samples within this cluster showed higher dispersion than in other clusters (Tukey HSD,  $P<0.05$ ) and constituted a transition between deep samples (cluster 4) and surface samples of clusters 1 and 3 (Fig. S5 A). As a consequence of this heterogeneity, this cluster showed up to 50% dissimilarity between samples whereas other clusters were less than 40% dissimilar (Fig S5 B). In cluster 2, reads of Dinophyceae, Radiolaria and diatoms, in particular *Chaetoceros*, were abundant, which resulted in samples from 300 m depth at M1 and M2-3 also being included in this cluster. The remaining 300 m samples (all but M1 and M2-3) were grouped in cluster 4 and characterized by Radiolaria, mostly belonging to cyst-forming order Chaunacanthida (19-68% of the reads).

**Table S2:** Seasonal drivers and key players of the balance between diatoms and small phytoplankton.

	Diatom silicate limitation	Grazing pressure on small phytoplankton (ciliates biomass ng C l <sup>-1</sup> ) <sup>a</sup>	Balance between diatoms and pico- and nanoflagellates <sup>1</sup>	Key players
Kerguelen bloom				
Early spring :	Non limiting silicate (18.7 μM) <sup>2</sup>	Increasing biomass (101 to 933) <sup>3</sup>	Increasing diatom biomass (0.55 to 1.59 μg Chl <i>a</i> .L <sup>-1</sup> ; 73 to 94% of Chl <i>a</i> ) Picophytoplankton (Prasinophytes) disappearance Decreasing Prymnesiophyte biomass (0.08 to 0.04 μg Chl <i>a</i> .L <sup>-1</sup> )	<i>Chaetoceros</i> , <i>Thalassiosira</i> <sup>4</sup> , some <i>Phaeocystis</i> colonies <sup>5</sup>
Summer :	Limiting silicate (<2 μM) <sup>6</sup>	Decreasing (950 to 520) <sup>7</sup>	High diatom biomass (1.17 to 0.89 μg Chl <i>a</i> .l <sup>-1</sup> ; 94 to 78% of Chl <i>a</i> ) Low Prymnesiophytes biomass (0.07 to 0.12 μg Chl <i>a</i> .l <sup>-1</sup> )	<i>Chaetoceros</i> , <i>Eucampia</i> <sup>8</sup>
Late summer	Limiting silicate (<2 μM) <sup>1</sup>	Increasing (812 to 1318) <sup>9</sup>	Increasing pico- and nanophytoplankton biomass (Prymnesiophytes: 0.15 to 0.22 μg Chl <i>a</i> .l <sup>-1</sup> ; Prasinophytes: 0.02 to 0.1 μg Chl <i>a</i> .l <sup>-1</sup> ) Low diatom biomass (0.08 to 0.24 μg Chl <i>a</i> .l <sup>-1</sup> ; 28 to 40% of Chl <i>a</i> )	<i>Corethron</i> , <i>Phaeocystis</i> free nanoflagellates, <i>Micromonas</i> <sup>1</sup>
HNLC Antarctic waters				
Early Spring	Non limiting (13 μM) <sup>2</sup>	420 <sup>3</sup>	Low but dominant Prymnesiophytes (0.13 μg Chl <i>a</i> .l <sup>-1</sup> ; 41% of Chl <i>a</i> ) and diatoms biomass (0.09 μg Chl <i>a</i> .l <sup>-1</sup> ; 30% of Chl <i>a</i> )	<i>Phaeocystis</i> <sup>5</sup> , <i>Fragilariopsis</i> <sup>4</sup>
Summer	Non limiting (>20 μM) <sup>6</sup>	430 <sup>7</sup>	Low diatom (0.09 μg Chl <i>a</i> .l <sup>-1</sup> ; 53% of Chl <i>a</i> ) and Prymnesiophytes biomass (0.07 μg Chl <i>a</i> .l <sup>-1</sup> ; 41% of Chl <i>a</i> )	<i>Fragilariopsis</i> <sup>8</sup> , small diatoms and nanoflagellates <sup>10</sup>
Late Summer	Non limiting (>4 μM) <sup>1</sup>	540 to 900 <sup>9</sup>	Dominant Prymnesiophytes (0.11 to 0.2 μg Chl <i>a</i> .l <sup>-1</sup> ; 58 to 60%) and diatoms (0.05 to 0.09 μg Chl <i>a</i> .l <sup>-1</sup> ; 26 to 33%)	<i>Phaeocystis</i> , small diatoms and Pelagophytes <sup>1</sup>

<sup>a</sup> For KEOPS2 (early spring) and KEOPS1 (summer), mean integrated biomass are calculated for the ML, for MOBYDICK, they correspond to the first 60m. Ciliates biomass is used here as a proxy of the grazing pressure on pico- and nanophytoplankton.

<sup>1</sup> This study

<sup>2</sup> Closset et al., 2014, <sup>3</sup> Christaki et al., 2015, <sup>4</sup> Lasbleiz et al., 2016, <sup>5</sup> Georges et al., 2014, <sup>6</sup> Mosseri et al., 2008, <sup>7</sup> Christaki et al., 2008, <sup>8</sup> Armand et al., 2008, <sup>9</sup> Christaki, personal communication, <sup>10</sup> Uitz et al., 2009

## Perspectives

### *Complementary approaches are needed to explore phytoplankton diversity*

In this study, we used 18S rDNA metabarcoding of <math><20\ \mu\text{m}</math> cells to provide a detailed description of small phytoplankton species composition and CHEMTAX to gain a more quantitative understanding of the contribution of broad taxonomic groups to the chlorophyll pool. For the moment, size-fractionated metabarcoding studies constitute the best method to explore small phytoplankton diversity, especially for non-silicified small cells lacking characteristic morphological features. For example, the presence of *Micromonas* was documented for the first time in the SO only recently, thanks to metagenomic analyses (Simmons *et al.*, 2015). However, molecular description should be considered as a complementary approach, and not an alternative, to conventional methods such as microscopy observations.

During MOBYDICK, light microscopy counts of phytoplankton and microzooplankton were also performed (Paper 3, Christaki *et al.*, submitted; Lafond *et al.*, submitted). In our study, *Fragilariopsis*, *Chaetoceros*, *Pseudo-nitzschia* and *Dactyliosolen* were enriched in off-plateau samples of the two size fractions (Fig. 4). Contamination by large broken cells in the small size fraction could not be excluded. However, comparison with microscopy observations confirmed that the size range of *Fragilariopsis kerguelensis* (10-93  $\mu\text{m}$ ), *Chaetoceros atlanticus* (7-30  $\mu\text{m}$ ) and *Dactyliosolen antarctica* (14-72  $\mu\text{m}$ ) overlapped the two size fractions and that small specimens were common off-plateau (Lafond *et al.*, submitted). For *Pseudo-nitzschia sp.*, specimens were larger than 20  $\mu\text{m}$  (22-150  $\mu\text{m}$ ), but very thin (2-6  $\mu\text{m}$ ), which could explain their presence in the small size fraction (Lafond *et al.*, submitted). Microscopy also informed on the occurrence of diverse life forms. *Chaetoceros* spores/winter forms were frequently observed during microscopic observations of bottlenet samples, used to sample deep stocks (below 100m) (Leblanc, personal communication). This corroborates the high contribution of *Chaetoceros* reads (up to 31%) observed in this study in the small size fraction at 125 m. Although sequencing results somehow differed with microscopic counts, the two techniques highlighted the same dominant diatom genera, when biomass -and not abundances- were considered (Appendix C1).

In other cases, the discrepancy observed with microscopy highlighted problematic taxonomic affiliations. Maximum likelihood phylogenetic trees were constructed to refine or correct taxonomic assignments that were incongruent with current knowledge of diatom taxa in the SO. The only taxonomic change we made with some confidence was the assignment of *Hemiaulus* sequences to the microscopically observed genus *Dactyliosolen* (Appendix C2). It is necessary to complete existing taxonomic databases by isolating and sequencing organisms, such as *Cylindrotheca*, that were frequently observed with microscopy and were rare, or even missing in sequencing results (Appendix C.1). Phylogenetic trees were also constructed based on the v4 region of the 18S rRNA gene to check visually the taxonomic resolution and coherence of ASVs within lineages containing

a relatively high number of unassigned sequences (e.g up to 25% of unassigned “Dinophyceae” reads). However, in most cases, phylogenetic trees could not help to resolve higher taxonomic affiliation considering the lack of reference sequences from the SO in databases and the limited variability of the sequenced region (Paper 3, Christaki *et al.*, submitted).

#### *From small phytoplankton diversity to functional significance*

In addition to refining the identification of the taxa sequenced, another challenge would be to determine their functional significance. In this study, ASVs affiliated to divisions Chlorophyta, Cryptophyta, Haptophyta, Ochrophyta, and class marine ochrophytes (MOCH), as well as *Tripos* (Dinophyceae), were characterized as photoautotrophs. This classification likely includes ambiguities, such as the classification of certain mixotrophs/heterotrophs in the phytoplankton category. For example, MOCH lineages contain non-pigmented as well as pigmented cells (Massana *et al.*, 2014). To overcome this issue, it was initially planned to establish the composition of autotrophic eukaryotes thanks to the sequencing of the 18S rDNA of pigmented cells sorted by flow cytometry. Stringency in the definition of cytometric populations to avoid contamination with heterotrophic cells skewed the results towards large autotrophic cells, mainly diatoms. As a result, it was decided to work on the diversity of small phytoplankton based on size-fractionated sequencing (0.2-20  $\mu\text{m}$ ) of the whole eukaryotic community.

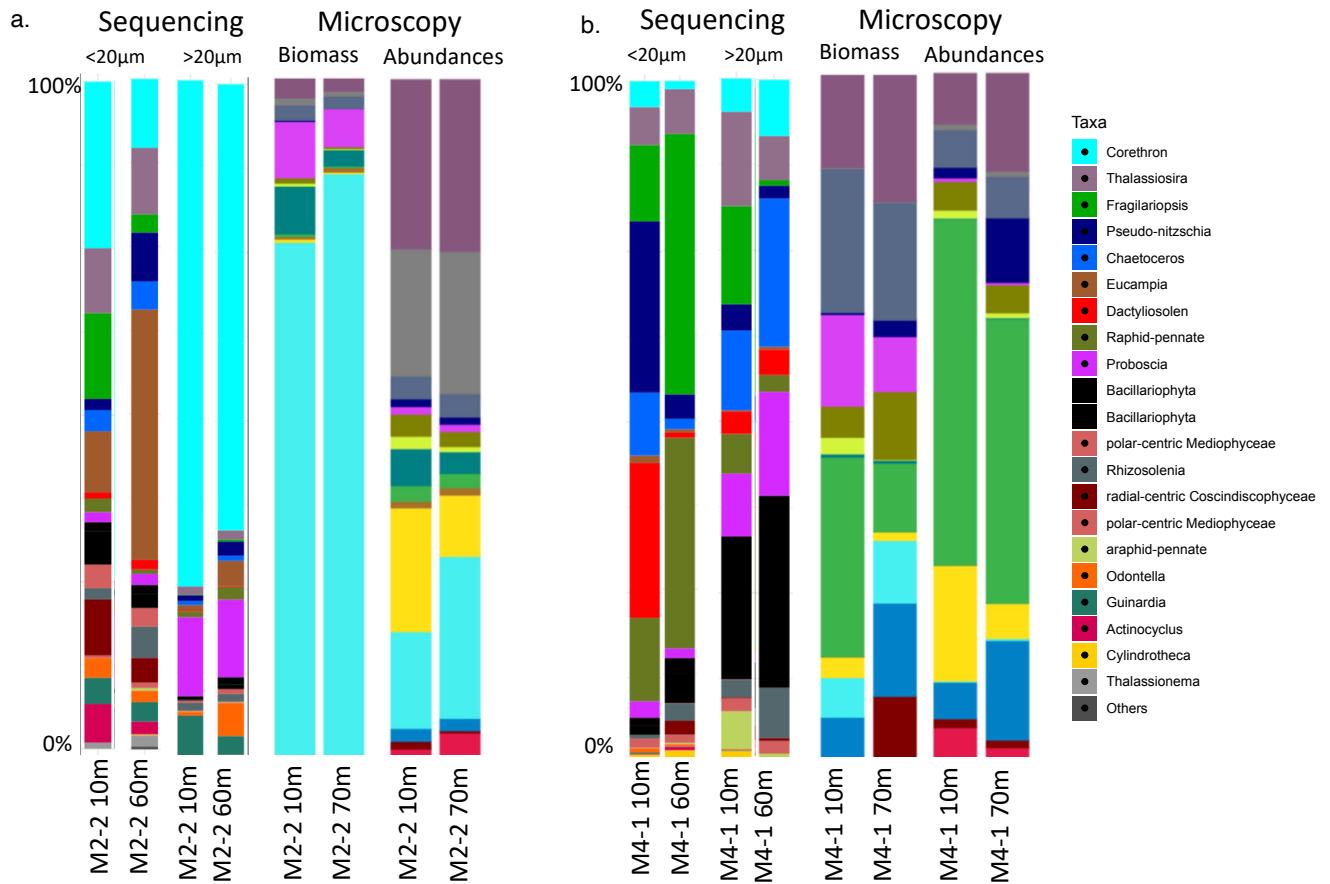
In addition to their role as primary producers, many small phytoflagellates are mixotrophic and major predators of prokaryotes (reviewed by Stoecker *et al.*, 2017). Mixotrophy present a competitive edge over obligate phototrophic cells in nutrient acquisition (Zubkov and Tarran, 2008). For example, incubation experiments showed in the equatorial Pacific, that iron flux through mixotrophic flagellates could amount to 35–58% of the total iron uptake by the entire autotrophic community (Maranger *et al.*, 1998). It would be interesting to run similar experiments in HNLC waters of the SO to see if mixotrophic small phytoplankton can alleviate iron limitation by ingesting bacteria. In our dataset, *Micromonas* contribution to number of reads strongly increased on-plateau over the repeated visits (Fig. S5b). This species has been reported as mixotrophic in the Arctic (McKie-Krisberg and Sanders, 2014). During MOBYDICK, uptake of fluorescently labeled bacteria by small phytoplankton was insignificant (Christaki *et al.*, 2020). However, the fluorescently labeled bacteria may have been too large (appr. 0.8  $\mu\text{m}$ ) to be efficiently grazed by abundant pico-sized phytoplankton such as *Micromonas*, which have been shown to prefer small-sized prey (<0.5  $\mu\text{m}$ ) (McKie-Krisberg and Sanders, 2014).

Mixotrophy is predicted to enhance the transfer of biomass to larger organisms at higher trophic levels and increase the efficiency of the BCP through the production of larger, faster-sinking, and carbon-rich organic detritus, it could be interesting to further explore the trophic status of specific species of small phytoplankton identified in this study as key players in the area.

### *Describing phytoplankton community succession in remote areas*

CHEMTAX analysis over the different cruises established the seasonal succession of phytoplankton communities over the bloom and metabarcoding precised who were the key players of small phytoplankton communities after the bloom. More size-fractionated metabarcoding studies are needed to further explore the spatial and temporal distribution of small phytoplankton taxa in the SO at the species level. This would enable to explore how specific taxonomic groups or species, such as pelagophytes or *Micromonas* respond to nutrient availability throughout the season (iron and ammonium particularly). However, exploring possible seasonal succession within small phytoplankton taxa throughout the season is for the moment impossible due to limited access to this remote ocean. Recently, high-resolution seasonal observations of the prokaryotic community were conducted using a moored remote autonomous sampler (RAS) deployed over 4 months (Liu *et al.*, 2020). In the frame of this project, protist communities were also sequenced. Some promising patterns emerged from the analysis, that could shed light on dynamic interactions between phytoplankton and their grazers or parasites (Appendix C3). However, the fixative used - glutaraldehyde or mercuric chloride ( $\text{HgCl}_2$ )- profoundly affected the picture and diversity of the community sequenced. Preliminary tests showed that glutaraldehyde fixed samples showed 70% similarity with unfixed controls for eukaryotic communities, while similarity dropped to 40% when the samples were preserved with  $\text{HgCl}_2$  (Liu, personal communication). Moreover, sequencing results of diatoms communities were too incongruent with microscopy counts to be confidently interpreted (Liu, personal communication). We tested a kit specifically designed to counterbalance the DNA damages due to the use of fixatives (QIAamp DNA FFPE Tissue Kit, Qiagen, Germany), but sequencing results after extraction using this kit still differed considerably between fixed and unfixed samples (Appendix C4). These major technical obstacles and the difficulty to sample this stormy remote ocean during winter months explain why composition of small phytoplankton communities of the SO remain virtually unexplored during autumn and winter, the seasons when the ecosystems most presumably rely on them.

## Appendix

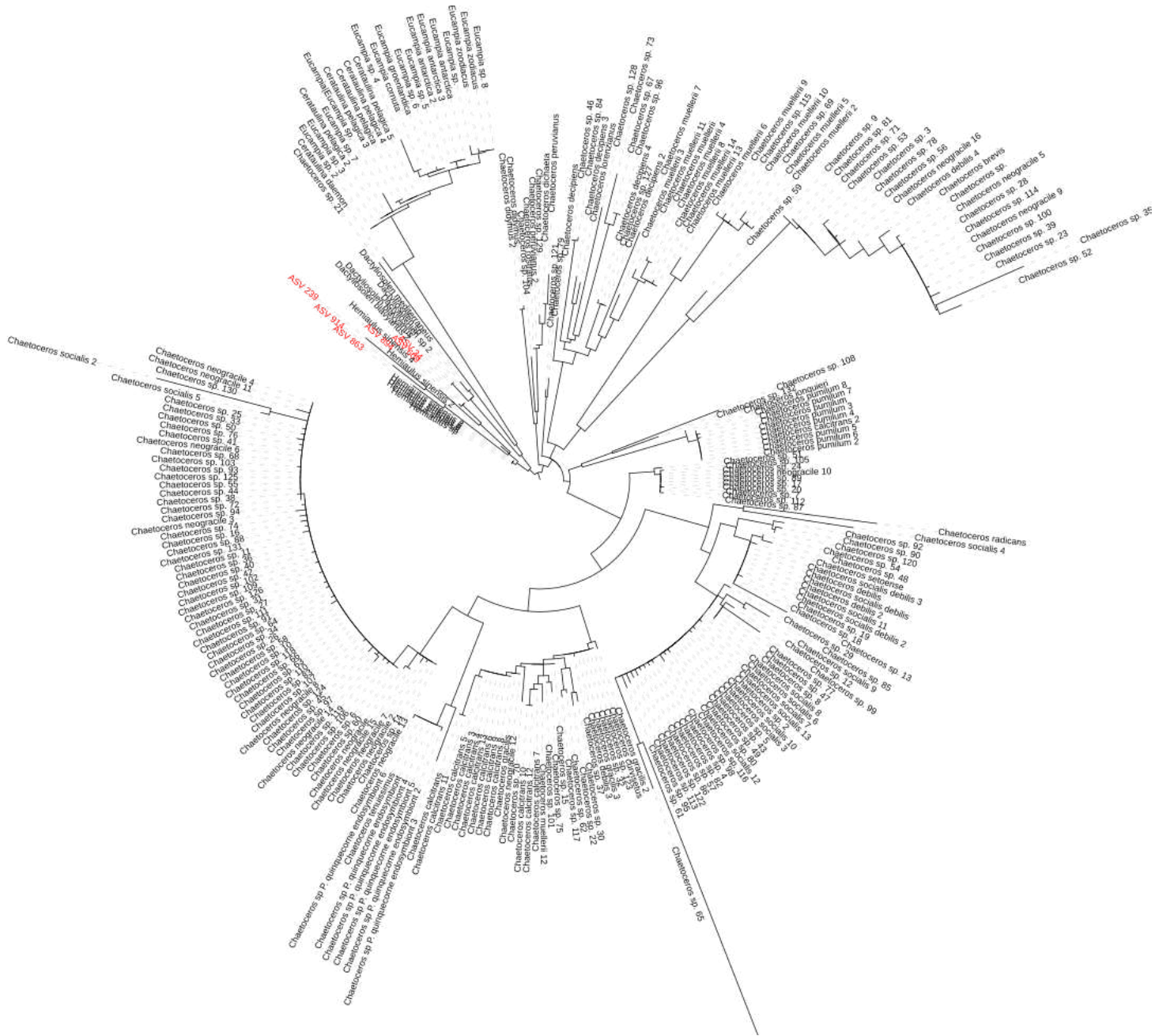


Appendix C1: Example of the comparative analysis of diatom communities obtained with microscopy and sequencing. At station M2-2 (a) Corethron, Proboscia and Guinardia dominated both biomass estimates (microscopy) and sequencing of the >20 µm size fraction. As small diatoms were rare at M2, sequencing of small diatom communities was not congruent with microscopy counts.

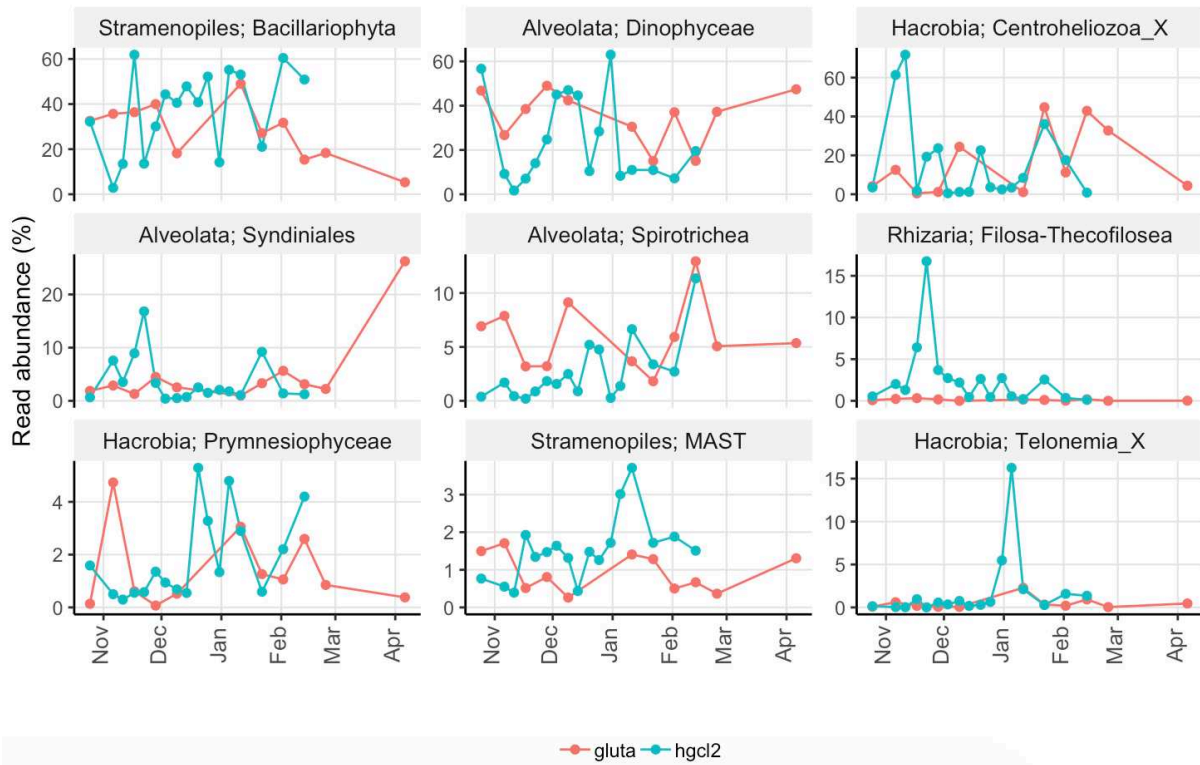
At station M4-1 (b), dominant taxa in microscopy counts were Fragilariopsis, Thalassiosira, Proboscia, Rhizosolenia, Chaetoceros and unidentified raphid pennates. These genera were also dominant in sequencing results of the two size-fraction. Cylindrotheca was abundant in microscopy counts at all stations but rarely sequenced. To note also the important proportion of unidentified "Bacillariophyta" especially in the large size-fraction.

Microscopy counts of diatom communities were conducted at the MIO by Justine Legras and Augustin Lafond.



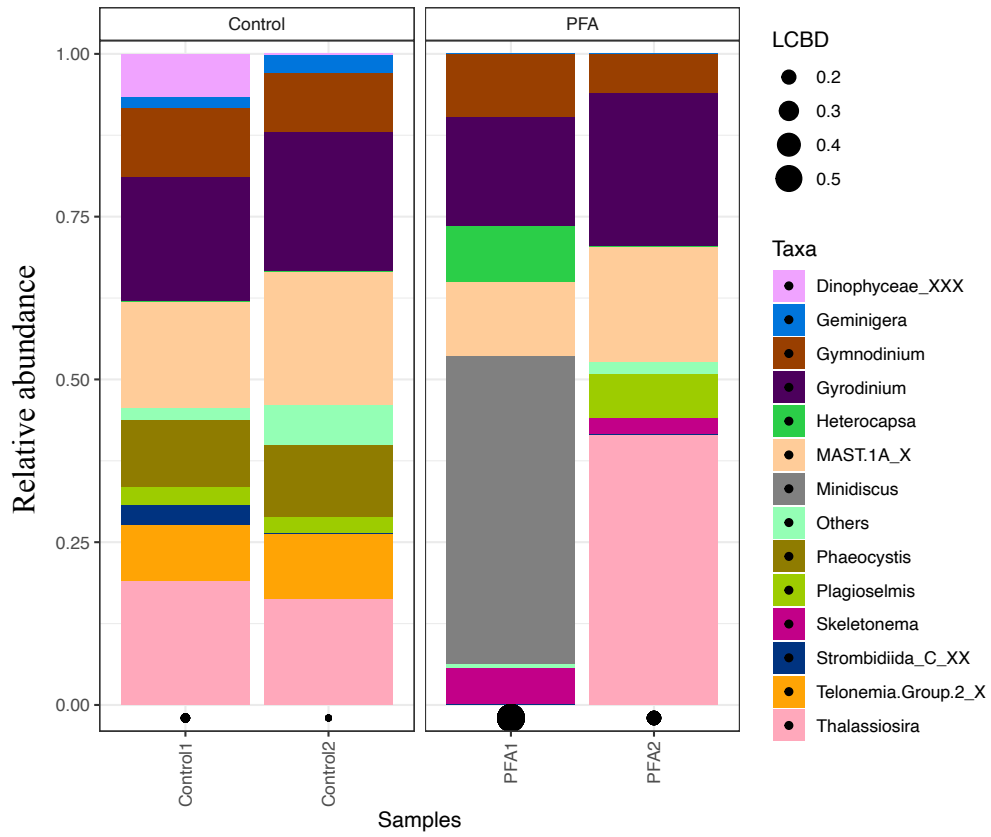


Appendix C2: Maximum Likelihood phylogeny of 18S rRNA gene of diatoms built with RAxML. Sequences marked with ASV in red originate from MOBYDICK community sequencing data. All other sequences represent references from PR2 and NCBI databases. ASVs in red were assigned to Hemiaulus, which is not reported in the SO. Building a tree illustrated the close relatedness of Hemiaulus and Dactyliosolen and supported the adaption of the genus name Dactyliosolen, which was frequently observed by microscopy, for the ASVs in question.



Appendix C3: Seasonal evolution of the relative abundance of the major protist class to total protist community composition determined by Illumina sequencing of 18S rDNA V4 region of RAS samples.

The use of HgCl<sub>2</sub> lead to unexpected and probably erroneous contribution of specific groups, like Centroheliozoa. Samples preserved with glutaraldehyde presented however some interesting patterns. For example, the two peaks in relative abundance of diatoms (Bacillariophyta) corresponded to the two bloom periods, whereas Prymnesiophyceae relative abundance increased before and after the bloom period. Interestingly, the relative abundance of phytoplankton grazers (Dinophyceae and Spirotrichea) increased shortly after the increase of diatoms. The considerable increase of Syndiniales reads after the bloom is also interesting as this group also contributed to a high proportion of reads on-plateau in the small size fraction during MOBYDICK. It was suggested that it could reflect the release of Syndiniales spores after a parasitic infection, which may have played a role in bloom termination (Paper 4; Sassenhagen et al., 2020).



Appendix C4: Comparison of the community composition of samples from the English Channel following DNA extraction with QIAamp DNA FFPE Tissue Kit. Controls correspond to unfixed samples while PFA samples were fixed with 1% PFA (w/V). Local Contributions to Beta Diversity (LCBD) values highlight the dissimilarity of the samples fixed with PFA in terms of community composition.

## 2. CO<sub>2</sub>-fixation by small phytoplankton around Kerguelen

### Introduction

The high abundance and important contribution to Chl *a* of small phytoplankton after the bloom (Paper 1) suggested they could play an important, yet totally overlooked, role in CO<sub>2</sub>-fixation on-plateau. Indeed, previous studies on the Kerguelen Plateau occurred during the bloom onset and decline and established that large diatoms accounted for 80–90% to the total primary production (of 1 g C m<sup>-2</sup> d<sup>-1</sup>) on-plateau, whereas off-plateau production was much lower (0.30 C m<sup>-2</sup> d<sup>-1</sup>) and mainly (65%) achieved by small diatoms and nanoflagellates (Uitz *et al.*, 2009). Diatom-dominated phytoplankton communities on-plateau were characterized by low export efficiency, in contrast to ecosystems dominated by small cells, where export efficiency at 100 m reached 58% (Savoye *et al.*, 2008; Christaki *et al.*, 2014; Planchon *et al.*, 2015).

Moreover, we established in Paper 1 that small phytoplankton communities differed on- and off-plateau, as a result of contrasted post-bloom conditions. Small non-silicified cells, as well as small and large diatoms are associated with unique physiological requirements and ecological characteristics, that are likely to impact CO<sub>2</sub>-fixation and C-export efficiency (Litchman *et al.*, 2015; Tréguer *et al.*, 2018). The seasonal succession and differences in phytoplankton community composition described in Paper 1 are thus expected to have consequences on production and export regime around Kerguelen.

The objectives of this study were to:

1. Evaluate the variability in CO<sub>2</sub>-fixation rates between and within different groups of phytoplankton on- and off-plateau. For this, CO<sub>2</sub>-fixation rates were measured at the single cell level using NanoSIMS for small cells (non-silicified cells and diatoms <20 μm) and large-geometry SIMS for larger diatoms (>20 μm).
2. Establish the contribution of small phytoplankton to community CO<sub>2</sub>-fixation
3. Make hypothesis on the fate of phytoplankton, by looking at grazing indicators and changes in the contribution of broad taxonomic groups to Chl *a* with depth.

Paper 2: Small phytoplankton contribute greatly to CO<sub>2</sub>-fixation after the diatom bloom in the Southern Ocean

Accepted in January 2021 (The ISME Journal)

Solène Irion<sup>1</sup>, Urania Christaki<sup>1</sup>, Hugo Berthelot<sup>2</sup>, Stéphane L'Helguen<sup>2</sup>, Ludwig Jardillier<sup>3</sup>

<sup>1</sup> Univ. Littoral Côte d'Opale, CNRS, Univ. Lille, UMR 8187 - LOG - Laboratoire d'Océanologie et de Géosciences, F-62930 Wimereux, France

<sup>2</sup> Laboratoire des Sciences de l'Environnement Marin (LEMAR), UMR 6539 UBO/CNRS/IRD/IFREMER, Institut Universitaire Européen de la Mer (IUEM), Brest, France

<sup>3</sup>Unité d'Ecologie, Systématique et Evolution, Université Paris-Sud, CNRS, AgroParisTech, Université Paris-Saclay, Orsay Cedex, France

Corresponding author: Solène Irion, LOG 32, avenue Foch, 62930 Wimereux, France, Solene.irion@univ-littoral.fr

Running title: CO<sub>2</sub>-fixation by small phytoplankton in the Southern Ocean

keywords: CO<sub>2</sub>-fixation, NanoSIMS, Southern Ocean, small phytoplankton, diatoms

## Abstract

Phytoplankton is composed of a broad-sized spectrum of phylogenetically diverse microorganisms. Assessing CO<sub>2</sub>-fixation intra- and inter-group variability is crucial in understanding how the carbon pump functions, as each group of phytoplankton may be characterized by diverse efficiencies in carbon fixation and export to the deep ocean. We measured the CO<sub>2</sub>-fixation of different groups of phytoplankton at the single cell level around the naturally iron-fertilized Kerguelen plateau (Southern Ocean), known for intense diatoms blooms suspected to enhance CO<sub>2</sub> sequestration. In our study, small cells (<20 μm) composed of phylogenetically distant taxa (prymnesiophytes, prasinophytes and small diatoms) were growing faster ( $0.37 \pm 0.13$  and  $0.22 \pm 0.09$  division d<sup>-1</sup> on- and off-plateau, respectively) than larger diatoms ( $0.11 \pm 0.14$  and  $0.09 \pm 0.11$  division d<sup>-1</sup> on- and off-plateau, respectively), which showed heterogeneous growth and a large proportion of inactive cells ( $19 \pm 13\%$ ). As a result, small phytoplankton contributed to a large proportion of the CO<sub>2</sub> fixation (41-70%). The analysis of pigment vertical distribution indicated that grazing may be an important pathway of small phytoplankton export. Overall, this study highlights the need to further explore the role of small cells in CO<sub>2</sub>-fixation and export in the Southern Ocean.

## Introduction

Carbon fixation (CO<sub>2</sub>-fixation) by marine phytoplankton accounts for about half the Earth's primary production [1–3]. Some 20% of phytoplankton's net primary production (5-10 Gt C) is exported to the deep ocean via the biological pump [4, 5]. The magnitude and nature of the carbon exported to the deep ocean is impacted by the size-structure of phytoplankton communities [6, 7]. High carbon export (C-export) out of the photic zone is classically linked to the dominance of large phytoplankton (herein defined as >20 μm cells) because of their high sinking velocity or repackaging into dense fecal pellets produced by large grazers [8–10]. Alternatively, it has been suggested that small phytoplankton contribution to export was proportional to their total net primary production through aggregation into larger sinking particles, or, as for their larger counterpart, export as fecal pellets produced by higher trophic levels [11]. Determining the contribution of diverse phytoplankton size-groups to CO<sub>2</sub>-fixation is thus the first step to characterize the functioning of the carbon pump. This is routinely achieved by measuring size-fractionated CO<sub>2</sub>-fixation rates in natural communities using isotopic tracers (<sup>14</sup>C or <sup>13</sup>C labelled substrates) that can be used to model marine production [12, 13]. Defining a general size-scaling relationship for CO<sub>2</sub>-fixation from pico-flagellates to large diatoms based on accurate measurements represents thus a major challenge for models relying on the use of theoretical size-scaling relationships for phytoplankton growth [14, 15]. However, size-based models may be biased due to metabolic variability within a size-class grouping diverse phylogenetic taxa [16, 17]. Including phylogenetic features can further refine phytoplankton production models, but increase drastically their complexity [18–20]. Consequently, it is crucial to determine the degree of complexity required (e.g. size, species, population) and define the descriptors (e.g. biomass, abundances) needed to improve models. To do so, *in situ* measurements are required to appreciate the variability of CO<sub>2</sub>-fixation rates between and within different phytoplankton groups. Diverse studies have previously revealed that the contribution to biogeochemical cycles is not

necessarily proportional to microbial group abundance or biomass. For example, flow cytometry sorting of different small-sized microbial autotrophs has revealed that although picoeukaryotes are far less abundant than cyanobacteria, their contribution to CO<sub>2</sub>-fixation is similar or even greater, relatively [21–23]. More recently, secondary ion mass spectrometry (SIMS) has allowed measurements at the single-cell scale at a resolution of appr. 50 nm (NanosSIMS) or 1 μm (large-geometry SIMS). A pioneer lacustrine study revealed that rare phototrophic bacterial taxa (0.3% of the total cell number) could contribute to more than 70% of the total carbon uptake [24]. Subsequent studies also revealed higher marine phytoplankton contribution to C- or N-fixation than expected from their relative abundance or biomass for diverse microbial groups. This has been observed for example for diazotrophs-associated diatoms [25], chain-forming diatoms [26], or specific pico-phytoplankton groups [27]. This approach also unveiled a high microbial intra-group heterogeneity in C- or N-uptake, likely affecting the group's adaptation potential to changing environments [24, 25, 27–29]. The reasons for this high heterogeneity are unclear but could result from intra-group genetic diversity, intra-group differences in gene expression, or cell life history [24]. Recently, it has been suggested that intra-specific variability in C- or N-uptake is correlated to differences in biovolumes from one cell to the other [30].

The Southern Ocean (SO) is an ideal study area to explore phytoplankton CO<sub>2</sub>-fixation, as it contributes up to 40% ( $42 \pm 5$  Pg C) of the oceanic uptake of anthropogenic CO<sub>2</sub> [31, 32]. Most of the SO is composed of high-nutrient, low-chlorophyll (HNLC) areas, where primary production is limited by iron despite high macronutrients concentrations [33–35]. In these low productive environments, phytoplankton communities and primary production are typically dominated by small cells (<20 μm) [36, 37]. However, large diatoms have attracted most attention because of the enhanced production and C-export observed during diatom blooms in discrete, naturally iron-fertilized regions of the SO such as Kerguelen, Crozet, or South Georgia during spring and summer [38–40]. This study is part of the MOBYDICK cruise (Marine Ecosystem Biodiversity and Dynamics of Carbon around Kerguelen: an integrated view) that aimed at understanding the link between biodiversity and carbon fluxes on and off the naturally iron-fertilized Kerguelen plateau. Off-plateau, phytoplankton biomass and production are dominated throughout the year by small size-groups [12, 41]. On-plateau, spring blooms of chain-forming and large diatoms typically end in February because of silicic acid and iron co-limitation [42]. MOBYDICK was the first study in this area that took place after the diatom bloom (March 2018).

Our main objective was to describe the diversity and assess the role of small phytoplankton in CO<sub>2</sub>-fixation in post-bloom conditions. Surface CO<sub>2</sub>-fixation and division rates of phytoplankton at the single cell level were measured, focusing on small phytoplankton (non-silicified and small diatoms), which have been overlooked so far in this Oceanic region. Changes in the contribution of broad taxonomic groups to chlorophyll *a* (Chl *a*) with depth were used to discuss how small phytoplankton could potentially contribute to C-export.

## Materials and methods

### *Sampling location*

Four different sites were visited on and off the Kerguelen Plateau during the MOBYDICK cruise (Table 1). Station M2, located on the iron-fertilized plateau, was sampled three times at 9 to 10-day intervals. Three off-plateau stations were also sampled (M1, M3, and M4). Station M4 was sampled twice at 2-week intervals, and M1 and M3 was sampled only once. M2, M1 and M4 were located south of the polar front in Antarctic waters. M3 was located south-west of the plateau in subantarctic waters (Fig. 1). Samples were collected with a rosette equipped with Niskin bottles and a CTD probe (SeaBird 911-plus). Three casts were done at all stations for: i) nutrient concentration measurements as well as phytoplankton community composition based on pigment analyses; ii) microbial eukaryote community composition through a metabarcoding approach; and iii) CO<sub>2</sub>-fixation measurements using stable isotope (<sup>13</sup>C) tracer experiments.

### *Water sampling for nutrients and pigment analysis*

Samples for dissolved inorganic nutrients measurements (silicic acid, nitrate, phosphate and ammonium) and pigment analysis were taken at all stations at 9-10 depths (10, 25, 50, 75, 100, 125, 150, 175, 200 and 250 m). Ammonium was measured by fluorometry [43]. Other nutrients were analyzed colorimetrically as described in Aminot and K  rouel [44].

For pigment analysis, 2.3 L of seawater were collected and filtered onto Whatman GF/F filters. Filters were then flash-frozen in liquid nitrogen and stored at -80  C. Pigment determination was done using High Performance Liquid Chromatography (HPLC), following the method of Ras et al. [45]. HPLC data from all sampling points in the first 250 m were considered for CHEMTAX analysis [46]. The contribution to Chl *a* of seven different taxonomic groups (chlorophytes, prasinophytes, cyanobacteria (*Synechococcus* spp.), cryptophytes, diatoms, autotrophic dinoflagellates (with peridinin) and haptophytes (*Phaeocystis* like) was determined based on their characteristic pigment profiles. Samples were first clustered based on their pigment:Chl *a* ratios to form homogeneous bins. Then, pigment:Chl *a* ratios were adjusted for each bin using a 60 randomized ratio matrix varying by up to 35% of the initial ratio matrix to avoid any bias linked to the ratios chosen from the literature [47, 48]. The contribution of the different groups to Chl *a* was determined by averaging the six best runs.

Phaeopigments (the sum of phaeophytin-*a* and phaeophorbide-*a*) are degraded Chl *a* products. Phaeophytin-*a* is traditionally thought to result from grazing, while phaeophorbide-*a* may arise from both phytoplankton senescence and grazing [49]. In this study, it was considered that phaeopigments were mostly likely associated with grazing activity [50], since chlorophyllide-*a*, a degradation pigment associated with cell senescence [47], was only detected at very low concentration (<0.004  $\mu\text{g L}^{-1}$ ) in two samples. The ratio phaeopigments:Chl *a* was determined from the surface down to 250 m. A ratio <1 indicates that phytoplankton material is mostly fresh, whereas a ratio >1 indicates mostly degraded material [51].

### *Water sampling for metabarcoding of phytoplankton communities*



Water samples were collected at 15 m at all stations to describe small and large phytoplankton communities with metabarcoding of 18S rDNA. After pre-filtering through 100  $\mu\text{m}$  mesh to remove most of the metazoans, 10 L of seawater were successively filtered through 20  $\mu\text{m}$  (20-100  $\mu\text{m}$  size-fraction) and 0.2  $\mu\text{m}$  (0.2-20  $\mu\text{m}$  size-fraction). Filters were stored at  $-80^{\circ}\text{C}$  until processing. DNA was extracted following PowerSoil DNA Isolation Kit (QIAGEN, Germany) standard manufacturer's protocol. The 18S rDNA V4 region was amplified using EK-565F (5'-GCAGTTAAAAAGCTCGTAGT) and UNonMet (5'-TTTAAGTTTCAGCCTTGCG) primers [52]. Pooled samples were sequenced on an Illumina MiSeq lane (2 x 300bp) at the company Genewiz (South Plainfield, NJ, USA). Quality filtering of the reads, identification of amplicon sequencing variants (ASV) and taxonomic affiliation based on the PR2 database [53] were done in the R-package DADA2 [54]. ASVs affiliated to divisions Chlorophyta, Cryptophyta, Haptophyta, Ochrophyta, and class marine ochrophytes (MOCH) were filtered to describe phytoplankton communities. Relative abundances of ASVs were normalized to the total number of sequences affiliated to autotrophic phylogenetic taxa to build heatmaps of small (0.2-20  $\mu\text{m}$ ) and large (20-100  $\mu\text{m}$ ) phytoplankton taxa with package ampvis2 [55]. Raw sequencing files in fastq format, as well as ASVs, taxonomy and metadata tables are available on MOBYDICK's public database at [http://www.obs-vlfr.fr/proof/ftpfree/mobydick/db/DATA/PAR\\_2251/](http://www.obs-vlfr.fr/proof/ftpfree/mobydick/db/DATA/PAR_2251/).

#### *Water sampling for stable isotope experiments*

Seawater samples were collected at each site at least one hour before sunrise from surface waters (10 or 15 m depth) to evaluate phytoplankton  $\text{CO}_2$ -fixation. Five HCl-cleaned polycarbonate 12.5 L carboys were filled with 12 L of seawater prefiltered on a 100  $\mu\text{m}$  mesh (Fig. S1). Three carboys were spiked with 12 mL of  $\text{NaH}^{13}\text{CO}_3$  solution (99%  $^{13}\text{C}$ , Cambridge Isotope Laboratories, Inc.), targeting an enrichment of 10% in  $\text{DI}^{13}\text{C}$ . Two carboys were left unspiked as negative control at  $T_0$  and  $T_{\text{final}}$ . Four carboys (one control and three carboys enriched with  $\text{DI}^{13}\text{C}$ ) were incubated on-deck from dawn to dusk (Table S1). *In situ* temperature was reproduced in the incubator by a constant flow of sub-surface seawater. *In situ* light intensity of the sampling depth was mimicked using blue light screens attenuating direct sunlight by approximately 50%. Among the three  $^{13}\text{C}$  enriched carboys, one was left in the dark. Incubations were stopped after sunset by adding paraformaldehyde (PFA; 1% final concentration w/v). After one hour of fixation in the dark, several sub-samples were taken:

- (1) To calculate the bulk  $\text{CO}_2$ -fixation of the community, triplicates from each carboy of 1.5 L were filtered onto precombusted ( $450^{\circ}\text{C}$ , 4 h) GF/F filters, rinsed three times with 20 mL of filtered seawater (0.2  $\mu\text{m}$  pore size membranes) and stored in pre-combusted dark glass tubes at  $-80^{\circ}\text{C}$ . Back in the laboratory, these filters were dried at  $60^{\circ}\text{C}$  overnight, pelletized into tin capsules and analyzed by an elemental analyzer coupled to a continuous flow isotope-ratio mass spectrometer (EA-IRMS).
- (2) To measure the  $\text{CO}_2$ -fixation at the single cell level (large geometry SIMS and NanoSIMS analysis), large ( $>20\mu\text{m}$ ) and small ( $<20\mu\text{m}$ ) cells were collected in duplicates for each treatment by successive filtration of 2 L on 20  $\mu\text{m}$  pore size nylon filter (Millipore, USA) and 0.65  $\mu\text{m}$  pore size PVDF filter (Durapore, Germany) and stored at  $-80^{\circ}\text{C}$ .

(3) To evaluate potential effects of the incubation conditions on plankton community composition, 2 x 5 mL of water were sampled at  $T_0$  and  $T_{\text{final}}$  from each carboy for cytometry analysis of pico-, and nano-phytoplankton abundances.

(4) To determine more precisely the abundance of different taxonomic groups using FISH, 300 mL of water from the  $T_0$  carboy were filtered onto 0.4  $\mu\text{m}$  polycarbonate filters (Nuclepore Track-Etch Membrane, Whatman, USA) and further dehydrated successively with 50%, 70%, and 100% ethanol for 3 minutes each [56] (Supplementary material).

#### *Preparation of samples for secondary ion mass spectrometry (SIMS)*

Single cells  $\text{CO}_2$ -fixation analysis was performed with SIMS. For large cells, the 20  $\mu\text{m}$  nylon filters were placed in 3 mL of 0.01  $\mu\text{m}$  filtered seawater and gently vortexed to detach the cells. The solution was then pipetted onto a 0.2  $\mu\text{m}$  polycarbonate membrane directly connected to a low-vacuum pump ( $< 0.5$  atmosphere) in order to concentrate the cells on a spot of about 2  $\text{mm}^2$  on the filter. No samples were prepared for SIMS analysis of large cells at station M3 since almost no cells were collected on the 20  $\mu\text{m}$  nylon filter during the sampling.

To detach and collect small cells ( $< 20 \mu\text{m}$ ), the 0.65  $\mu\text{m}$  pore size PVDF filters were cut into small pieces, placed in a 3 mL solution composed of 0.01  $\mu\text{m}$  filtered seawater and Pluronic (0.01% w/v final conc., Sigma-Aldrich), and sonicated twice for 1 minute. Small autotrophs were then sorted using BD FACS Aria II flow cytometer (BD Biosciences, San Jose, CA, USA; UNICELL facility). Three different populations were gated at each station based on diverse combinations of red (690/50 nm, for chlorophyll *a* detection) and orange (585/42 nm, for phycoerythrin detection characteristic of *Synechococcus*) fluorescence, forward scatter (FSC, related to cell size) and side scatter (SSC, related to cell structure). *Synechococcus* cells were used as standard to ensure homogeneity in the gating of cells of pico-size from one station to another. *Synechococcus* spp. abundances were low at all stations (45-400 cells  $\text{mL}^{-1}$ ), so that they were sorted together with pico-eukaryotes (pigmented eukaryote cells in the same size range as *Synechococcus*) in a population hereafter called Pico (Fig. S2). Small pigmented nano-eukaryotes were sorted into two groups (Nano1 and Nano2) according to their red fluorescence and forward scatter. Sorted cells were directly collected onto a 0.6  $\mu\text{m}$  polycarbonate membrane (DTTP01300, Millipore) in the sorting chamber using a low-vacuum in order to maximize cell density on the filter [27]. All filters were stored at  $-20 \text{ }^\circ\text{C}$  until analysis. Abundances of the populations sorted were determined in triplicates at the beginning and end of the incubations using a CytoFLEX (Beckman Coulter, Singapore) at a high flow rate (60  $\mu\text{l min}^{-1}$ ) for 3 minutes. Homogeneity in the gating of the populations between the two flow cytometers used was ensured using *Synechococcus* as standard.

#### *SIMS analyses (Large geometry SIMS and NanoSIMS)*

Pieces of the filters prepared for SIMS analyses were placed on double-sided conductive adhesive copper tape and mounted on plots adapted to SIMS samples holders. They were then metalized by sputter deposition of a gold film (20-50 nm thickness).

The  $^{13}\text{C}$ -fixation of large diatoms was measured using a large geometry SIMS (IMS1280, Cameca, Gennevilliers, France) at the Centre de Recherches Pétrographiques et Géochimiques (CRPG, CNRS-

Univ. Lorraine, Nancy, France). Areas of interest (120  $\mu\text{m}$  \* 120  $\mu\text{m}$ ) were pre-sputtered with a primary 10 nA Cs<sup>+</sup> beam for 5 min to remove the silica frustules of most diatoms and access their cellular content. Analyses were conducted on a 100 \* 100  $\mu\text{m}$  field using a 50-100 pA Cs<sup>+</sup> beam with a spatial resolution of approx. 1.5  $\mu\text{m}$  for 80 cycles. Secondary ion images (512 \* 512 pixels) were recorded for <sup>12</sup>C<sup>14</sup>N<sup>-</sup> (2 s per cycle), <sup>13</sup>C<sup>14</sup>N<sup>-</sup> (4 s per cycle) and <sup>28</sup>Si (2 s per cycle) at a mass resolution of 12 000 (M/ $\Delta$ M).

The <sup>13</sup>C-fixation of small pigmented cells sorted by flow cytometry in three populations (Pico, Nano1 and Nano2) was measured using a NanoSIMS 50 (Cameca, Gennevilliers, France) at the Museum National d'Histoire Naturelle (MNHN, Paris, France). NanoSIMS analyses were conducted on a field size of 40 \* 40  $\mu\text{m}$  (255 \* 255 pixels) with a primary Cs<sup>+</sup> ion beam of 1.2 pA with a lateral resolution of 60-120 nm for 1000  $\mu\text{s px}^{-1}$ . A larger field (42 \* 42  $\mu\text{m}$ ) was pre-sputtered with a high primary ion beam current (300 pA) for 2 to 2.5 min. Secondary ions <sup>12</sup>C, <sup>13</sup>C, <sup>12</sup>C<sup>14</sup>N<sup>-</sup>, <sup>13</sup>C<sup>14</sup>N<sup>-</sup> and <sup>28</sup>Si were collected on at least 20 planes. For large geometry SIMS and NanoSIMS images, regions of interest corresponding to single cells were manually defined using Limage software (Larry Nittler, Carnegie Institution of Washington) based on the total <sup>12</sup>C<sup>14</sup>N<sup>-</sup> ion counts. <sup>28</sup>Si was further used to correct the shape of diatoms based on their silica frustule. The equivalent spherical diameter (ESD) was measured on NanoSIMS images and used to estimate biovolumes of small non-silicified cells. For small diatoms, the biovolume was calculated after Sun and Liu [57], taking measures on NanoSIMS images for each silicified cell. The average ESD of Pico, Nano1 and Nano2 cells were 1.6  $\pm$  0.3, 2.5  $\pm$  0.4, and 4.8  $\pm$  1.6  $\mu\text{m}$ , respectively.

A total of 344 cells were analyzed with large geometry SIMS and 2194 with NanoSIMS (1162 Pico, 944 Nano1, and 211 Nano2: Table S2). In addition, 774 non-enriched cells from the control carboys were analyzed to determine natural <sup>13</sup>C isotopic content of phytoplankton cells.

#### *CO<sub>2</sub>-fixation calculations (EA-IRMS, large geometry SIMS and NanoSIMS)*

Bulk CO<sub>2</sub>-fixation rates measured by EA-IRMS ( $\mu\text{mol C L}^{-1} \text{d}^{-1}$ ) were calculated as follows:

$$\text{Bulk CO}_2\text{-fixation} = \frac{A_{\text{sample}}^{\text{POC}} - A_{\text{control}}^{\text{POC}}}{A_{\text{enriched}}^{\text{DIC}} - A_{\text{natural}}^{\text{DIC}}} \times \text{POC}_{\text{sample}}$$

Where A is the <sup>13</sup>C isotopic fractional abundance (in atom%) of the community labeled with <sup>13</sup>C after incubation ( $A_{\text{sample}}^{\text{POC}}$ ) of the T<sub>0</sub> non-enriched samples ( $A_{\text{control}}^{\text{POC}}$ ) of the enriched DIC source pool ( $A_{\text{enriched}}^{\text{DIC}}$ ) and of the natural DIC pool ( $A_{\text{natural}}^{\text{DIC}}$ ).

For each cell analyzed with NanoSIMS, <sup>13</sup>C<sup>14</sup>N<sup>-</sup> and <sup>12</sup>C<sup>14</sup>N<sup>-</sup> ions were counted and specific fractional abundance ( $A_{\text{Cell}}$ ) were calculated where

$$A_{\text{Cell}} = \frac{{}^{13}\text{C}^{14}\text{N}^-_{(\text{Cell})}}{{}^{13}\text{C}^{14}\text{N}^-_{(\text{Cell})} + {}^{12}\text{C}^{14}\text{N}^-_{(\text{Cell})}} \times 100$$

To assess the metabolic activity of individual cells, C-based cell-specific division rates ( $\text{d}^{-1}$ ) were calculated as in Berthelot et al. [27], assuming that DIC was the only carbon source used for growth:

$$\text{C - based cell - specific division rates}(\text{d}^{-1}) = \log_2 \frac{A_{\text{DIC}} - A_{\text{control}}}{A_{\text{DIC}} - A_{\text{Cell}}}$$

with  $A_{Control}$  being the mean  $^{13}C$  cell fractional abundance in non-enriched populations. Cells whose fractional abundance enrichment  $A_{Cell} - A_{Control}$  was less than two times the standard deviation associated with the Poisson distribution parameterized by  $\lambda = A_{Cell} * N_{CNcell}$ , with  $N_{CNcell}$  being the CN-ion counts of the cell, were considered as inactive [27].

Contribution of the different population sorted by flow cytometry was calculated by multiplying the mean cell-specific  $CO_2$ -fixation by the abundance of the population.

For this, the C-based turnover of the cellular C-content was calculated as follows:

$$C - based\ turnover\ of\ the\ cellular\ C - content = \frac{A_{Cell} - A_{Control}}{A_{DIC} - A_{Control}}$$

Cell-specific  $CO_2$ -fixation ( $fmol\ C\ cell^{-1}\ d^{-1}$ ) were obtained by multiplying the C-based turnover of the cellular C-content by the carbon content of the cell, calculated after Verity et al. [58]:

$$C - cell\ content = 0.433 \times Biovolume^{0.863}$$

### Statistical analysis

All statistical analyses were conducted in R [59]. Differences in  $CO_2$ -fixation rates between groups and stations were assessed using the Kruskal Wallis test, followed by pairwise the Mann-Whitney test with Bonferroni correction for multiple comparisons with ggpubr package. Interquartile range (IQR) was used as a measure of statistical dispersion within groups. The package fitdistrplus was used to select the best probability distribution fitting the division rates observed for small and large cells.

## Results

### Study area

Chl *a* was low at all stations and visits (0.18-0.31 and 0.28-0.58  $mg\ m^{-3}$  on- and off-plateau, respectively). Nutrient concentrations were contrasted on- and off-plateau (Table 1). Plateau station M2 was depleted in silicic acid ( $<2\ \mu mol\ L^{-1}$ ), but silicic acid concentrations and Chl *a* doubled at the last visit (M2-3) after a storm on the 10<sup>th</sup> March. Ammonium concentrations were higher at M2 than at off-plateau stations. Off-plateau stations sampled in HNLC waters presented higher nitrate, silicic acid, and phosphate concentrations than on-plateau (Table 1). Stations M1 and M4, south of the polar front, were characterized by lower temperature and higher silicic acid concentrations than M3, located in subantarctic waters north of the polar front (Fig. 1).

### Composition of phytoplankton communities

Haptophytes and diatoms contributed the most to Chl *a* at surface at all stations (36-70% and 18-40%, respectively: Fig. 2a, b). Chl *a* concentration strongly decreased between 75 and 125 m depending on the station. Down to 250 m, Chl *a* concentrations were low ( $0.01\ \mu g\ Chl\ a\ L^{-1}$ ) and diatoms accounted for 77-96% of total Chl *a*.

Vertical distribution of haptophyte's pigments and Phaeo/Chl *a* ratio differed between stations (Fig. 2a, b). At M2 and M1 stations, haptophyte pigments were abundant at surface but decreased rapidly with depth and almost disappeared below 75m. These stations were also characterized by Phaeo/Chl *a* ratios  $>1$  below 175m, indicating that pigments found below this depth were mostly degraded. At off-plateau

stations M3 and M4, haptophyte pigments signature extended deeper. Phaeo/Chl *a* ratio was approximately equal to 1 at 250m, reflecting a similar contribution of fresh and degraded pigments at this depth (Fig. 2b).

Sequencing data revealed that *Phaeocystis antarctica* (haptophyte) was the most abundant phytoplankton taxa in the small size fraction on- and off-plateau (up to 76% of the reads: Fig. 3). Other common non-silicified phytoplankton taxa of the small size fraction included chlorophytes *Prasinoderma* (Prasinococcales family, 34% of the reads at M3) and *Micromonas* (Mamiellaceae family, 3-13% of the reads at M2). CARD-FISH counts confirmed the importance of haptophytes (2-5 $\mu$ m in size) on- and off-plateau (735 – 4950 cells mL<sup>-1</sup>), and of prasinophytes (<2 $\mu$ m in size) on-plateau (Fig. S3). Members of the Pelagophyceae family were common at off-plateau stations, in particular *Pelagococcus* (23% of the reads at M3) and *Pelagomonas* (5-10% at M4 and M1, respectively). Diatoms contributed for 10-45% of the total number of reads in the small size fraction, with a higher contribution of raphid pennates (*Fragilariopsis* and unidentified raphid pennates) off- than on-plateau (8-30% and 4-6% of reads number respectively: Fig. 3).

Diatoms were the dominant phytoplankton class of the large size fraction (>20  $\mu$ m in size; 55-97% of the reads). Off-plateau, diatom communities were composed of pennate (*Fragilariopsis*, *Pseudo-nitzschia*) and centric diatoms (*Thalassiosira*, *Chaetoceros*, *Proboscia* and *Rhizosolenia*). On-plateau, large diatom communities were dominated by centric diatoms (*Eucampia* during the first visit and *Corethron* for the two last visits). *Phaeocystis* was abundant in read numbers in the large size fraction at M1 and M3-1 (40 and 21% of the reads respectively).

#### *C-based division rates of small and large cells*

Over 98% of the small cells measured with NanoSIMS were actively taking up carbon, at the exception of M1 where slightly less cells were active (92%: Fig. 4a). Division rates were significantly higher on- than off-plateau (mean from 0.33-0.38 and 0.18-0.26 division d<sup>-1</sup>, respectively: Fig. 4a). However, Nano2 cells were characterized by lower division rates than Pico and Nano1 on- and off-plateau (Fig. 4b). Nano2 also presented higher variability and higher Interquartile Range (IQR) of the division rates than the two other small cells groups. Interestingly, Nano2 was mostly composed of small diatoms off-plateau (70%), while non-silicified cells were the major contributors of this group on-plateau (81%). Division rates of small diatoms were significantly lower than those of non-silicified cells on-plateau (Mann-Whitney,  $P < 10^{-9}$ ), but they were not different off-plateau (Fig. S4). Division rates of small cells (Pico, Nano1 and Nano2) followed a symmetrical logistic distribution, very similar to the normal distribution (Fig. S5 a,b).

The mean division rates of larger diatoms (>20  $\mu$ m in size) were relatively low and showed great variability (0.11  $\pm$  0.14 and 0.09  $\pm$  0.11 division d<sup>-1</sup>). Mean division rates of large diatoms on-plateau were 0.17, 0.05 and 0.12 division d<sup>-1</sup> during the first, second and third visit at M2, respectively, while they ranged between 0.08 to 0.10 division d<sup>-1</sup> at off-plateau stations (Fig. 4c). The proportion of inactive diatoms varied from zero to 27% and 14 to 39 % on- and off-plateau, respectively. However, some active outliers (<7% of the diatoms measured with large-geometry SIMS) showed high division rates reaching 0.72 and 0.51 division d<sup>-1</sup> on- and off-plateau, respectively (Fig. 4c). As a consequence, the distribution best fitted to large diatoms' division rates was a log-normal distribution skewed towards low values (Fig. S5c).

### *CO<sub>2</sub>-fixation by small phytoplankton*

For small cells, the amount of carbon fixed at the single cell level (C-fix) scaled allometrically with cell volume (V) according to a power law  $C\text{-fix} = a \cdot V^\alpha$ , where the scaling exponent  $\alpha = 0.81$  and  $0.75$  on- and off-plateau respectively (Fig. 5). This relationship explained 66% of the variance observed in CO<sub>2</sub>-fixation of individual cells on-plateau and 54% off-plateau, where a few inactive cells departed from this relation. Consequently, mean daily CO<sub>2</sub>-fixation rates at each station were highest for Nano2, intermediate for Nano1 and the lowest for Pico-cells (Table S3). However, when normalized to cell volume, the volume-specific CO<sub>2</sub>-fixation rates were decreasing with size (Fig. S6).

Estimated contribution of the different small phytoplankton's size-groups to total CO<sub>2</sub>-fixation was important on- and off-plateau (41-61% and 43-70% on and off plateau respectively; Fig. 6a). Nano1 was the most important contributor within small autotrophs to CO<sub>2</sub>-fixation at all stations (17-34%) except M2-1 where Pico contribution was higher (21%). Total community CO<sub>2</sub>-fixation off-plateau varied between 0.20 and 0.44  $\mu\text{mol C L}^{-1}$  (Fig. 6b). The CO<sub>2</sub>-fixation on-plateau was slightly higher during the first two visits (0.37-0.48  $\mu\text{mol C L}^{-1}$ ) and doubled at the third visit (0.92  $\mu\text{mol C L}^{-1}$ ; Fig. 6b). The doubling of the CO<sub>2</sub>-fixation at the last visit at M2 was associated with the doubling of Chl *a* concentration as well as increases in abundances of the three small phytoplankton size-groups (Fig. S3; Table S2). Estimation of the contribution to CO<sub>2</sub>-fixation of large diatoms by extrapolation of their CO<sub>2</sub>-fixation rates was not possible because of: (i) the low number of large diatoms analyzed; and (ii) the variability observed in their division rates, with mean division rates very sensitive to the presence of active outliers.

## **Discussion**

We report here, for the first time, that small phytoplankton (mainly non-silicified) could represent 41 to 61% of the total CO<sub>2</sub>-fixation on the Kerguelen Plateau, a naturally iron-fertilized area previously characterized by the dominance of chain-forming and large diatoms. Previous estimates of small phytoplankton contribution to CO<sub>2</sub>-fixation in other naturally iron-fertilized regions of the SO were usually much lower (Table 2). This high contribution on- and off-plateau was achieved by different communities of small phytoplankton, mostly represented by non-silicified pico and nano-eukaryotes on-plateau, whereas small diatoms (3.8  $\square$  1.5  $\mu\text{m}$  equivalent spherical diameter; Fig. S7) were also abundant and active off-plateau (Fig. 4b). Complementary SIMS analysis revealed that many larger diatoms (>20  $\mu\text{m}$ ) were inactive at this time of the season and that most of the CO<sub>2</sub>-fixation within this group was achieved by a few cells only (Fig. 4c).

### *Drivers of small phytoplankton importance in CO<sub>2</sub>-fixation in contrasted areas*

In this study, small phytoplankton communities and CO<sub>2</sub>-fixation rates were different on and off-plateau (Fig. 4a,b), but small cells' contribution to CO<sub>2</sub>-fixation was comparable in these two areas (41-70%; Fig. 6a). In HNLC waters, high contribution of small phytoplankton to CO<sub>2</sub>-fixation is a commonly observed phenomenon (Table 2), attributed to the advantage of a reduced size in iron acquisition [60–62]. In our study, smaller cells showed higher volume-specific CO<sub>2</sub>-fixation rates than their larger counterparts, in line with their theoretical advantage of high surface/volume ratio for nutrient and light

uptake. This theoretical allometric relationship has not always been verified, as some studies have suggested that CO<sub>2</sub>-fixation could also scale isometrically with cell volume, and that larger cells could be as, or even more competitive, than smaller ones depending on the environmental conditions [63, 64]. During MOBYDICK, the allometric size-scaling relationship explained over half of the variability observed in CO<sub>2</sub>-fixation of small phytoplankton cells ranging over four orders of magnitude (66% on- and 54% off-plateau: Fig. 5). Other sources of variability in CO<sub>2</sub>-fixation may come from taxa-specific physiology adapted to on- and off-plateau conditions. For example, pelagophytes and small pennate diatoms were mostly present off-plateau and *Micromonas* on-plateau (Fig. 3). The lower C-based division rates observed at off-plateau stations (Fig. 4a) likely resulted from higher iron limitation, whereas iron is continuously supplied to surface waters by internal waves on-plateau [38]. Higher competitiveness with respect to iron acquisition may favor pelagophytes and pennate diatoms off-plateau. Hogle et al. (2018) observed over-expression of genes involved in iron metabolism in a metatranscriptomic study, suggesting pelagophytes were advantaged in HNLC waters [65]. As for pennate diatoms, they possess the iron storage protein ferritin, which enables them to store iron on the long term and to be very efficient in using pulsed iron inputs [66, 67]. On-plateau, higher ammonium and lower silicic acid concentrations were observed than off-plateau. The relatively high ammonium concentrations could have benefited to the growing *Micromonas* population (Fig. 3 & S3), since prasinophytes preference for ammonium could be 10-fold superior to other phytoplankton groups [68]. In contrast, silicic acid limitation could have limited small diatom's growth on-plateau in comparison to small non-silicified cells (Fig. S4) and explain why fewer small diatoms were observed on- than off-plateau (Fig. 4b). Finally, some of the variability observed in CO<sub>2</sub>-fixation of small cells may originate from physiological heterogeneity within a species. For example, *P. antarctica* which was the most abundant taxa on- and off-plateau is characterized by highly variable responses to iron limitation, even within clonal populations (i.e. size reduction, decrease of Chl *a* concentration; [69]).

Currently, little information is available on *in situ* division rates of small phytoplankton taxa in the SO, most of them been obtained from *Phaeocystis* cultures (Table S4). Despite the variability observed at the single cell level, mean division rates observed in our study on- and off-plateau were in the same range as the ones observed for *P. antarctica* in Fe-replete and Fe-limited cultures. Therefore, we suggest that the division rates measured in this study in natural communities composed of diverse phylogenetical groups could serve as a baseline to model small phytoplankton growth in HNLC (mean of  $0.22 \pm 0.09$  division d<sup>-1</sup>) and naturally-iron fertilized areas ( $0.37 \pm 0.13$  division d<sup>-1</sup>).

During MOBYDICK, many large diatoms (>20 μm) were not actively growing, while few cells showed high CO<sub>2</sub>-fixation (Fig. 4c). Most likely, division rates of large diatoms change considerably throughout the season in relation with silicic acid and iron availability. Silicic acid concentrations on-plateau can be as high as 19 μmol L<sup>-1</sup> in early spring at the onset of the bloom [70]. After the bloom, silicic acid concentrations were <2 μmol L<sup>-1</sup> during the first two visits at M2, a level which is considered as an empirical threshold to support diatoms' dominance over flagellates [71]. The high proportion of inactive large diatoms observed with SIMS was in line with microscopic observations of surface samples during MOBYDICK showing  $33 \pm 7$  % of empty/broken frustules (Lafond *et al.*, submitted). It is worthy to note that highly heterogeneous division rates have been observed in culture studies within large diatoms

(Table S4) in Fe-limited cultures (e.g. daily division rates from 0.03 to 0.43 d<sup>-1</sup>) and also within specific genera in Fe-replete conditions (e.g. daily division rates from 0.16 to 0.64 d<sup>-1</sup> for *Fragilariopsis* sp.). These intriguing results relative to the highly heterogeneous division rates of larger diatoms observed in our study highlight the need to further explore species-specific changes in CO<sub>2</sub>-fixation rates at the single cell level in response to contrasted environmental conditions.

#### *Indications on the fate of small phytoplankton*

Currently, export fluxes in the SO cannot be predicted based on global primary production and food web structure. Several studies conducted in the SO have revealed an inverse relationship between primary production and carbon export efficiency [72–74]. This decoupling between the carbon produced in the surface layer and the carbon export efficiency below 200m has also been documented on the Kerguelen Plateau, where high productivity regime during early spring was associated with low carbon export efficiency (1-2%), and moderate productivity in summer showed high export efficiency (26%; [75, 76]). In low productive HNLC waters of the Kerguelen Plateau, high carbon export efficiencies were observed in spring and summer (35% and 44% respectively; [75, 77]). Although the factors driving this inverse relationship between primary productivity and export efficiency are not fully understood, micro- and macrozooplankton-mediated grazing seem to be an efficient alternative pathway to export carbon in low productivity waters [74, 78]. Counter to the classical view that only large phytoplankton are exported due to their high sinking velocity [8], there is growing evidence that the relative contribution of small phytoplankton to total C-export is proportional to its contribution to total primary productivity, when indirect export pathways (such as grazing through the production of fecal pellets by higher trophic levels) were also considered [11]. Considering the important contribution of actively growing small cells to CO<sub>2</sub>-fixation in the surface layer in our study, their possible export pathways -in particular indirectly via grazing- deserve some attention. Interesting observations relative to grazing could shed light on the vertical pigment distribution observed during MOBYDICK where pigments of small non-silicified groups (haptophytes and prasinophytes mostly) were almost absent below 100 m.

Grazing measurements showed that microzooplankton grazed actively on phytoplankton at all stations with grazing rates exceeding phytoplankton growth rates (Christaki *et al.*, submitted). Consequently, an important part of the carbon fixed by small phytoplankton at the surface may have been channeled to higher trophic levels via microzooplankton grazing. Phaeo/Chl *a* ratio showed that grazing activity was intensified at stations M2 and M1 (Fig. 2a). These stations were characterized by higher productivity in the months before sampling, promoting the development of dense salps populations (*Salpa thompsoni*), making up 41-42 % of total micronekton biomass at these two stations while they were almost absent at M3 and M4 (Schenke *et al.*, submitted). Salps are major grazers of small phytoplankton in the SO [79] and produce easily fragmented fecal pellets in the upper mesopelagic layer [80], which could explain the pronounced Phaeo/Chl *a* ratio below the mixed layer at M2 and M1. Finally, molecular analysis of plankton communities at 300m revealed that 25% of the sequences recovered in HNLC waters in the >20 μm size fraction belonged to *P. antarctica*, confirming the contribution of small phytoplankton to carbon export through fecal pellet export and/or aggregation in low productive waters [81]. Our



observations underline that grazing and aggregation may be important pathways of small phytoplankton export in both productive and HNLC waters.

Concluding, this study has shown for the first time the importance of actively growing small (silicified and non-silicified) phytoplankton cells in iron-fertilized and HNLC waters of the SO during post-bloom conditions. Single cell analysis revealed higher homogeneity in CO<sub>2</sub>-fixation within small phytoplankton composed of diverse phylogenetically distant taxa (prymnesiophytes, prasinophytes and small diatoms) than within large diatoms which were likely limited by silicic acid and iron in post-bloom conditions. Considering the high inter-annual variability and limited duration (approx. 4 months) of diatom blooms, our data highlight the need to reassess the role of small phytoplankton in the SO. Further investigation of the indirect contribution of small phytoplankton to C-export via grazing is also needed as it may be an efficient export pathway especially in HNLC waters characterized by sparse productivity pulses. Data of phytoplankton division and CO<sub>2</sub>-fixation rates published here will also be useful for modelling parameterization of phytoplankton size-group contribution to the C-cycle in the SO.

### *Acknowledgement*

We thank B. Quéguiner, the PI of the MOBYDICK project, for providing us the opportunity to participate in this cruise; the captain and crew of the R/V Marion Dufresne for their enthusiasm and support aboard during the MOBYDICK–THEMISTO cruise (<https://doi.org/10.17600/18000403>) and the chief scientist I. Obernosterer.

We thank H  l  ne Timpano and Maria Ciobanu working at UNICELL platform, Orsay, for their help with flow cytometry sorting before NanoSIMS analysis. We also thank the NanoSIMS team of the French National Ion Microprobe Facility hosted by the Mus  um National d'histoire Naturelle (Paris) and the SIMS team from the Centre de Recherches P  trographiques et G  ochimiques (CRPG) in Nancy for precious advice and assistance during the analysis.

This work was supported by the French oceanographic fleet ("Flotte oc  anographique fran  aise"), the French ANR ("Agence Nationale de la Recherche", AAPG 2017 program, MOBYDICK Project number: ANR-17-CE01-0013), and the French Research program of INSU-CNRS LEFE/CYBER ("Les enveloppes fluides et l'environnement" – "Cycles biog  ochimiques, environnement et ressources"). We also thank the French Ministry of Higher Education and the Region des Hauts de France for funding the PhD grant to S. Irion.

The French Research program of INSU-CNRS LEFE/CYBER funded the project 'ACTIVEUK' that supported preliminary experiments that led to use of stable isotope tracers and the subsequent set up of protocols to concentrate cells for NanoSIMS analyses.

### *Competing Interests*

The authors declare no conflict of interest.

### **References**

1. Longhurst A, Sathyendranath S, Platt T, Caverhill C. An estimate of global primary production in the ocean from satellite radiometer data. *J Plankton Res* 1995; **17**: 1245–1271.

2. Field CB, Behrenfeld MJ, Randerson JT, Falkowski P. Primary production of the biosphere: Integrating terrestrial and oceanic components. *Science* 1998; **281**: 237–240.
3. Falkowski PG, Raven JA. Aquatic photosynthesis. 2013. Princeton University Press.
4. Falkowski PG, Barber RT, Smetacek V. Biogeochemical controls and feedbacks on Ocean primary production. *Science* 1998; **281**: 200–206.
5. Palmer JR, Totterdell IJ. Production and export in a global ocean ecosystem model. *Deep Sea Res Part Oceanogr Res Pap* 2001; **48**: 1169–1198.
6. Legendre L, Rivkin RB. Fluxes of carbon in the upper ocean: regulation by food-web control nodes. *Mar Ecol Prog Ser* 2002; **242**: 95–109.
7. Guidi L, Stemann L, Jackson GA, Ibanez F, Claustre H, Legendre L, et al. Effects of phytoplankton community on production, size, and export of large aggregates: A world-ocean analysis. *Limnol Oceanogr* 2009; **54**: 1951–1963.
8. Michaels AF, Silver MW. Primary production, sinking fluxes and the microbial food web. *Deep Sea Res Part Oceanogr Res Pap* 1988; **35**: 473–490.
9. Calbet A, Landry MR. Phytoplankton growth, microzooplankton grazing, and carbon cycling in marine systems. *Limnol Oceanogr* 2004; **49**: 51–57.
10. Jin X, Gruber N, Dunne JP, Sarmiento JL, Armstrong RA. Diagnosing the contribution of phytoplankton functional groups to the production and export of particulate organic carbon, CaCO<sub>3</sub>, and opal from global nutrient and alkalinity distributions. *Glob Biogeochem Cycles* 2006; **20**: GB2015.
11. Richardson TL, Jackson GA. Small phytoplankton and carbon export from the surface ocean. *Science* 2007; **315**: 838–840.
12. Uitz J, Claustre H, Griffiths FB, Ras J, Garcia N, Sandroni V. A phytoplankton class-specific primary production model applied to the Kerguelen Islands region (Southern Ocean). *Deep Sea Res Part Oceanogr Res Pap* 2009; **56**: 541–560.
13. Uitz J, Claustre H, Gentili B, Stramski D. Phytoplankton class-specific primary production in the world's oceans: Seasonal and interannual variability from satellite observations. *Glob Biogeochem Cycles* 2010; **24**.
14. Poulin FJ, Franks PJS. Size-structured planktonic ecosystems: constraints, controls and assembly instructions. *J Plankton Res* 2010; **32**: 1121–1130.
15. Ward BA, Dutkiewicz S, Jahn O, Follows MJ. A size-structured food-web model for the global ocean. *Limnol Oceanogr* 2012; **57**: 1877–1891.
16. Stoecker DK, Hansen PJ, Caron DA, Mitra A. Mixotrophy in the marine plankton. *Annu Rev Mar Sci* 2017; **9**: 311–335.
17. Tréguer P, Bowler C, Moriceau B, Dutkiewicz S, Gehlen M, Aumont O, et al. Influence of diatom diversity on the ocean biological carbon pump. *Nat Geosci* 2018; **11**: 27.
18. Lancelot C, Hannon E, Becquevort S, Veth C, De Baar HJW. Modeling phytoplankton blooms and carbon export production in the Southern Ocean: dominant controls by light and iron in the Atlantic sector in Austral spring 1992. *Deep Sea Res Part Oceanogr Res Pap* 2000; **47**: 1621–1662.

19. Wang S, Moore JK. Incorporating *Phaeocystis* into a Southern Ocean ecosystem model. *J Geophys Res Oceans* 2011; **116**.
20. Worthen DL, Arrigo KR. A coupled ocean-ecosystem model of the Ross Sea. Part 1: Interannual variability of primary production and phytoplankton community structure. *Biogeochemistry of the Ross Sea*. 2013. American Geophysical Union (AGU), pp 93–105.
21. Li WKW. Primary production of prochlorophytes, cyanobacteria, and eucaryotic ultraphytoplankton: Measurements from flow cytometric sorting. *Limnol Oceanogr* 1994; **39**: 169–175.
22. Jardillier L, Zubkov MV, Pearman J, Scanlan DJ. Significant CO<sub>2</sub> fixation by small prymnesiophytes in the subtropical and tropical northeast Atlantic Ocean. *ISME J* 2010; **4**: 1180–1192.
23. Rii YM, Duhamel S, Bidigare RR, Karl DM, Repeta DJ, Church MJ. Diversity and productivity of photosynthetic picoeukaryotes in biogeochemically distinct regions of the South East Pacific Ocean: Picophytoplankton diversity and productivity in the S. Pacific. *Limnol Oceanogr* 2016; **61**: 806–824.
24. Musat N, Halm H, Winterholler B, Hoppe P, Peduzzi S, Hillion F, et al. A single-cell view on the ecophysiology of anaerobic phototrophic bacteria. *Proc Natl Acad Sci* 2008; **105**: 17861–17866.
25. Foster RA, Kuypers MMM, Vagner T, Paerl RW, Musat N, Zehr JP. Nitrogen fixation and transfer in open ocean diatom–cyanobacterial symbioses. *ISME J* 2011; **5**: 1484.
26. Olofsson M, Robertson EK, Edler L, Arneborg L, Whitehouse MJ, Ploug H. Nitrate and ammonium fluxes to diatoms and dinoflagellates at a single cell level in mixed field communities in the sea. *Sci Rep* 2019; **9**: 1424.
27. Berthelot H, Duhamel S, L’Helguen S, Maguer J-F, Wang S, Cetinić I, et al. NanoSIMS single cell analyses reveal the contrasting nitrogen sources for small phytoplankton. *ISME J* 2019; **13**: 651–662.
28. Ploug H, Musat N, Adam B, Moraru CL, Lavik G, Vagner T, et al. Carbon and nitrogen fluxes associated with the cyanobacterium *Aphanizomenon* sp. in the Baltic Sea. *ISME J* 2010; **4**: 1215–1223.
29. Olofsson M, Kourtchenko O, Zetsche E-M, Marchant HK, Whitehouse MJ, Godhe A, et al. High single-cell diversity in carbon and nitrogen assimilations by a chain-forming diatom across a century. *Environ Microbiol* 2019; **21**: 142–151.
30. Zaoli S, Giometto A, Marañón E, Escrig S, Meibom A, Ahluwalia A, et al. Generalized size scaling of metabolic rates based on single-cell measurements with freshwater phytoplankton. *Proc Natl Acad Sci* 2019; **116**: 17323–17329.
31. Frölicher TL, Sarmiento JL, Paynter DJ, Dunne JP, Krasting JP, Winton M. Dominance of the Southern Ocean in anthropogenic carbon and heat uptake in CMIP5 models. *J Clim* 2014; **28**: 862–886.
32. Landschützer P, Gruber N, Haumann FA, Rödenbeck C, Bakker DCE, Heuven S van, et al. The reinvigoration of the Southern Ocean carbon sink. *Science* 2015; **349**: 1221–1224.
33. Martin JH. Glacial-interglacial CO<sub>2</sub> change: The Iron Hypothesis. *Paleoceanography* 1990; **5**: 1–13.

34. de Baar HJW, Jong JTM de, Bakker DCE, Löscher BM, Veth C, Bathmann U, et al. Importance of iron for plankton blooms and carbon dioxide drawdown in the Southern Ocean. *Nature* 1995; **373**: 412.
35. de Baar HJW, Boyd PW, Coale KH, Landry MR, Tsuda A, Assmy P, et al. Synthesis of iron fertilization experiments: From the Iron Age in the Age of Enlightenment. *J Geophys Res Oceans* 2005; **110**.
36. Weber LH, El-Sayed SZ. Contributions of the net, nano- and picoplankton to the phytoplankton standing crop and primary productivity in the Southern Ocean. *J Plankton Res* 1987; **9**: 973–994.
37. Froneman PW, Laubscher RK, Mcquaid CD. Size-fractionated primary production in the South Atlantic and Atlantic Sectors of the Southern Ocean. *J Plankton Res* 2001; **23**: 611–622.
38. Blain S, Quéguiner B, Armand L, Belviso S, Bombled B, Bopp L, et al. Effect of natural iron fertilization on carbon sequestration in the Southern Ocean. *Nature* 2007; **446**: 1070–1074.
39. Pollard R, Sanders R, Lucas M, Statham P. The Crozet Natural Iron Bloom and Export Experiment (CROZEX). *Deep Sea Res Part II Top Stud Oceanogr* 2007; **54**: 1905–1914.
40. Korb RE, Whitehouse MJ, Atkinson A, Thorpe SE. Magnitude and maintenance of the phytoplankton bloom at South Georgia: a naturally iron-replete environment. *Mar Ecol Prog Ser* 2008; **368**: 75–91.
41. Kopczyńska EE, Fiala M, Jeandel C. Annual and interannual variability in phytoplankton at a permanent station off Kerguelen Islands, Southern Ocean. *Polar Biol* 1998; **20**: 342–351.
42. Mosseri J, Quéguiner B, Armand L, Cornet-Barthaux V. Impact of iron on silicon utilization by diatoms in the Southern Ocean: A case study of Si/N cycle decoupling in a naturally iron-enriched area. *Deep Sea Res Part II Top Stud Oceanogr* 2008; **55**: 801–819.
43. Holmes RM, Aminot A, Kérouel R, Hooker BA, Peterson BJ. A simple and precise method for measuring ammonium in marine and freshwater ecosystems. *Can J Fish Aquat Sci* 1999; **56**: 1801–1808.
44. Aminot A, Kérouel R. Dosage automatique des nutriments dans les eaux marines: méthodes en flux continu. 2007. Editions Quae.
45. Ras J, Claustre H, Uitz J. Spatial variability of phytoplankton pigment distributions in the Subtropical South Pacific Ocean: comparison between *in situ* and predicted data. *Biogeosciences* 2008; **5**: 353–369.
46. Mackey MD, Mackey DJ, Higgins HW, Wright SW. CHEMTAX—a program for estimating class abundances from chemical markers: application to HPLC measurements of phytoplankton. *Mar Ecol Prog Ser* 1996; **144**: 265–283.
47. Wright SW, van den Enden RL, Pearce I, Davidson AT, Scott FJ, Westwood KJ. Phytoplankton community structure and stocks in the Southern Ocean (30–80 E) determined by CHEMTAX analysis of HPLC pigment signatures. *Deep Sea Res Part II Top Stud Oceanogr* 2010; **57**: 758–778.
48. van Leeuwe MA, Visser RJW, Stefels J. The pigment composition of *Phaeocystis antarctica* (Haptophyceae) under various conditions of light, temperature, salinity, and iron. *J Phycol* 2014; **50**: 1070–1080.

49. Szymczak-Żyła M, Kowalewska G, Louda JW. The influence of microorganisms on chlorophyll a degradation in the marine environment. *Limnol Oceanogr* 2008; **53**: 851–862.
50. Strom SL. Production of pheopigments by marine protozoa: results of laboratory experiments analysed by HPLC. *Deep Sea Res Part Oceanogr Res Pap* 1993; **40**: 57–80.
51. Roca-Martí M, Puigcorbé V, Iversen MH, van der Loeff MR, Klaas C, Cheah W, et al. High particulate organic carbon export during the decline of a vast diatom bloom in the Atlantic sector of the Southern Ocean. *Deep Sea Res Part II Top Stud Oceanogr* 2017; **138**: 102–115.
52. Bower SM, Carnegie RB, Goh B, Jones SR, Lowe GJ, Mak MW. Preferential PCR amplification of parasitic protistan small subunit rDNA from metazoan tissues. *J Eukaryot Microbiol* 2004; **51**: 325–332.
53. Guillou L, Bachar D, Audic S, Bass D, Berney C, Bittner L, et al. The Protist Ribosomal Reference database (PR2): a catalog of unicellular eukaryote Small Sub-Unit rRNA sequences with curated taxonomy. *Nucleic Acids Res* 2013; **41**: D597–D604.
54. Callahan BJ, McMurdie PJ, Rosen MJ, Han AW, Johnson AJA, Holmes SP. DADA2: High-resolution sample inference from Illumina amplicon data. *Nat Methods* 2016; **13**: 581–583.
55. Andersen KS, Kirkegaard RH, Karst SM, Albertsen M. ampvis2: an R package to analyse and visualise 16S rRNA amplicon data. *bioRxiv* 2018; 299537.
56. Not F, Simon N, Biegala IC, Vaultot D. Application of fluorescent *in situ* hybridization coupled with tyramide signal amplification (FISH CARD) to assess eukaryotic picoplankton composition. *Aquat Microb Ecol* 2002; **28**: 157–166.
57. Sun J, Liu D. Geometric models for calculating cell biovolume and surface area for phytoplankton. *J Plankton Res* 2003; **25**: 1331–1346.
58. Verity PG, Robertson CY, Tronzo CR, Andrews MG, Nelson JR, Sieracki ME. Relationships between cell volume and the carbon and nitrogen content of marine photosynthetic nanoplankton. *Limnol Oceanogr* 1992; **37**: 1434–1446.
59. R Core Team. R: A Language and Environment for Statistical Computing. 2018. R Foundation for Statistical Computing, Vienna, Austria.
60. Chisholm SW. Phytoplankton Size. In: Falkowski PG, Woodhead AD, Vivirito K (eds). *Primary Productivity and Biogeochemical Cycles in the Sea*. 1992. Springer US, Boston, MA, pp 213–237.
61. Marchetti A, Cassar N. Diatom elemental and morphological changes in response to iron limitation: a brief review with potential paleoceanographic applications. *Geobiology* 2009; **7**: 419–431.
62. Alderkamp A-C, Kulk G, Buma AGJ, Visser RJW, Van Dijken GL, Mills MM, et al. The effect of iron limitation on the photophysiology of *Phaeocystis antarctica* (prymnesiophyceae) and *Fragilariopsis cylindrus* (bacillariophyceae) under dynamic irradiance. *J Phycol* 2012; **48**: 45–59.
63. Marañón E. Inter-specific scaling of phytoplankton production and cell size in the field. *J Plankton Res* 2008; **30**: 157–163.
64. Huete-Ortega M, Cermeño P, Calvo-Díaz A, Marañón E. Isometric size-scaling of metabolic rate and the size abundance distribution of phytoplankton. *Proc R Soc B Biol Sci* 2012; **279**: 1815–1823.

65. Hogle SL, Dupont CL, Hopkinson BM, King AL, Buck KN, Roe KL, et al. Pervasive iron limitation at subsurface chlorophyll maxima of the California Current. *Proc Natl Acad Sci* 2018; **115**: 13300–13305.
66. Marchetti A, Parker MS, Moccia LP, Lin EO, Arrieta AL, Ribalet F, et al. Ferritin is used for iron storage in bloom-forming marine pennate diatoms. *Nature* 2009; **457**: 467–470.
67. Lampe RH, Mann EL, Cohen NR, Till CP, Thamatrakoln K, Brzezinski MA, et al. Different iron storage strategies among bloom-forming diatoms. *Proc Natl Acad Sci* 2018; **115**: E12275–E12284.
68. Litchman E, Klausmeier CA. Trait-based community ecology of phytoplankton. *Annu Rev Ecol Evol Syst* 2008; **39**: 615–639.
69. Luxem KE, Ellwood MJ, Strzepek RF. Intraspecific variability in *Phaeocystis antarctica*'s response to iron and light stress. *PLOS ONE* 2017; **12**: e0179751.
70. Closset I, Lasbleiz M, Leblanc K, Quéguiner B, Cavagna A-J, Elskens M, et al. Seasonal evolution of net and regenerated silica production around a natural Fe-fertilized area in the Southern Ocean estimated with Si isotopic approaches. *Biogeosciences* 2014; **11**: 5827–5846.
71. Egge J, Aksnes D. Silicate as regulating nutrient in phytoplankton competition. *Mar Ecol Prog Ser* 1992; **83**: 281–289.
72. Lam PJ, Bishop JKB. High biomass, low export regimes in the Southern Ocean. *Deep Sea Res Part II Top Stud Oceanogr* 2007; **54**: 601–638.
73. Maiti K, Charette MA, Buesseler KO, Kahru M. An inverse relationship between production and export efficiency in the Southern Ocean. *Geophys Res Lett* 2013; **40**: 1557–1561.
74. Le Moigne FAC, Henson SA, Cavan E, Georges C, PaborCARDva K, Achterberg EP, et al. What causes the inverse relationship between primary production and export efficiency in the Southern Ocean? *Geophys Res Lett* 2016; **43**: 4457–4466.
75. Christaki U, Lefèvre D, Georges C, Colombet J, Catala P, Courties C, et al. Microbial food web dynamics during spring phytoplankton blooms in the naturally iron-fertilized Kerguelen area (Southern Ocean). *Biogeosciences* 2014; **11**: 6739–6753.
76. Christaki U, Guenegues A, Liu Y, Blain S, Catala P, Colombet J, et al. Seasonal microbial food web dynamics in contrasting Southern Ocean productivity regimes. *Limnol Oceanogr* 2020; **accepted**.
77. Planchon F, Ballas D, Cavagna A-J, Bowie AR, Davies D, Trull T, et al. Carbon export in the naturally iron-fertilized Kerguelen area of the Southern Ocean based on the <sup>234</sup>Th approach. *Biogeosciences* 2015; **12**: 3831–3848.
78. Cassar N, Wright SW, Thomson PG, Trull TW, Westwood KJ, Salas M de, et al. The relation of mixed-layer net community production to phytoplankton community composition in the Southern Ocean. *Glob Biogeochem Cycles* 2015; **29**: 446–462.
79. Moline MA, Claustre H, Frazer TK, Schofield O, Vernet M. Alteration of the food web along the Antarctic Peninsula in response to a regional warming trend. *Glob Change Biol* 2004; **10**: 1973–1980.

80. Iversen MH, Pakhomov EA, Hunt BPV, van der Jagt H, Wolf-Gladrow D, Klaas C. Sinkers or floaters? Contribution from salp pellets to the export flux during a large bloom event in the Southern Ocean. *Deep Sea Res Part II Top Stud Oceanogr* 2017; **138**: 116–125.
81. Irion S, Jardillier L, Sassenhagen I, Christaki U. Marked spatiotemporal variations in small phytoplankton structure in contrasted waters of the Southern Ocean (Kerguelen area). *Limnol Oceanogr* 2020; **Early view**.
82. Seeyave S, Lucas MI, Moore CM, Poulton AJ. Phytoplankton productivity and community structure in the vicinity of the Crozet Plateau during austral summer 2004/2005. *Deep Sea Res Part II Top Stud Oceanogr* 2007; **54**: 2020–2044.
83. Lee SH, Kim BK, Lim YJ, Joo H, Kang JJ, Lee D, et al. Small phytoplankton contribution to the standing stocks and the total primary production in the Amundsen Sea. *Biogeosciences* 2017; **14**: 3705–3713.
84. Korb RE, Whitehouse M. Contrasting primary production regimes around South Georgia, Southern Ocean: large blooms versus high nutrient, low chlorophyll waters. *Deep Sea Res Part Oceanogr Res Pap* 2004; **51**: 721–738.
85. Gall MP, Strzepek R, Maldonado M, Boyd PW. Phytoplankton processes. Part 2: Rates of primary production and factors controlling algal growth during the Southern Ocean Iron RElease Experiment (SOIREE). *Deep Sea Res Part II Top Stud Oceanogr* 2001; **48**: 2571–2590.
86. Gervais F, Riebesell U, Gorbunov MY. Changes in primary productivity and chlorophyll *a* in response to iron fertilization in the Southern Polar Frontal Zone. *Limnol Oceanogr* 2002; **47**: 1324–1335.
87. Pauthenet E, Roquet F, Madec G, Guinet C, Hindell M, McMahon CR, et al. Seasonal meandering of the Polar Front upstream of the Kerguelen Plateau. *Geophys Res Lett* 2018; **45**: 9774–9781.

*Table 1: Main surface biogeochemical parameters of the stations sampled. Nutrients and Chl a concentration indicated in the table were sampled at 10 m for plateau stations and 25 m for off-plateau stations. The mean mixed layer depth (difference in sigma of 0.02 to the surface value) and euphotic layer depth (1% light depth) of all CTD casts performed during the occupation of the stations is given.*

	Station	Sampling date	Temperature (°C)	NH <sub>4</sub> <sup>+</sup> (nmol L <sup>-1</sup> )	NO <sub>3</sub> <sup>-</sup> (μmol L <sup>-1</sup> )	PO <sub>4</sub> <sup>3-</sup> (μmol L <sup>-1</sup> )	Si(OH) <sub>4</sub> (μmol L <sup>-1</sup> )	Mixed layer depth (m)	Euphotic layer (m)	Chl a (mg m <sup>-3</sup> )
Off plateau	M1	10/03/2018	5.08	421	24.76	1.63	6.49	27	80	0.31
	M3_1	05/03/2018	5.60	501	23.39	1.62	2.31	65	93	0.19
	M4_1	01/03/2018	4.49	354	25.50	1.72	4.13	49	96	0.18
	M4_2	10/03/2018	4.47	481	24.79	1.71	4.80	87	100	0.22
Plateau	M2_1	26/02/2018	5.21	704	21.62	1.45	1.17	62	64	0.28
	M2_2	07/03/2018	5.24	1090	21.25	1.47	1.29	61	61	0.32
	M2_3	17/03/2018	5.18	899	21.75	1.51	2.60	68	58	0.58

*Table 2: Contribution of small phytoplankton to CO<sub>2</sub>-fixation on and off iron-fertilized areas of the Southern Ocean. During artificial fertilization studies, the initial contribution of small phytoplankton corresponds to the HNLC value. This contribution decreased throughout the fertilization experiments as the contribution of larger phytoplankton increased.*

Study area (experiment name)	Type of Fe-fertilization	Small phytoplankton size	HNLC	Fe-fertilized	Month	Method	Source
Crozet (CROZEX)	Natural Fe	<20μm	66%	53%	November - January	Size-fractionation	[82]
Kerguelen (KEOPS1)	Natural Fe	<10μm	68%	10 - 20	February	Size-fractionation	[12]
Amundsen Sea	Natural Fe	<5μm	50.8%	14.9%	January	Size-fractionation	[83]
South Georgia	Natural Fe	<12μm	>60%	<20%	January	Size-fractionation	[84]
South of Australia (SOIREE)	Artificial	<20μm	>60%	decrease to <40% during the experiment	February	Size-fractionation	[85]
Atlantic sector of the so (EISENEX)	Artificial	<20μm	70-90%	decrease to <50% during the experiment	November	Size-fractionation	[86]
Kerguelen (MOBYDICK)	Natural Fe	<20μm	43-70%	41-61%	March	NanoSIMS	This study



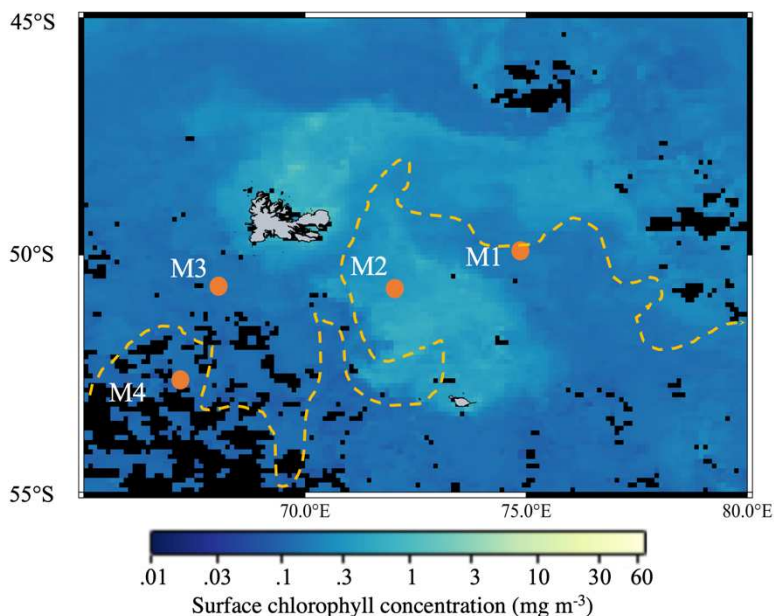


Fig. 1: Map of the study area. Surface chlorophyll *a* concentrations correspond to AQUA/MODIS average values for March 2018. The yellow dashed line indicates the position of the polar front after Pauthenet et al. (2018) [87].

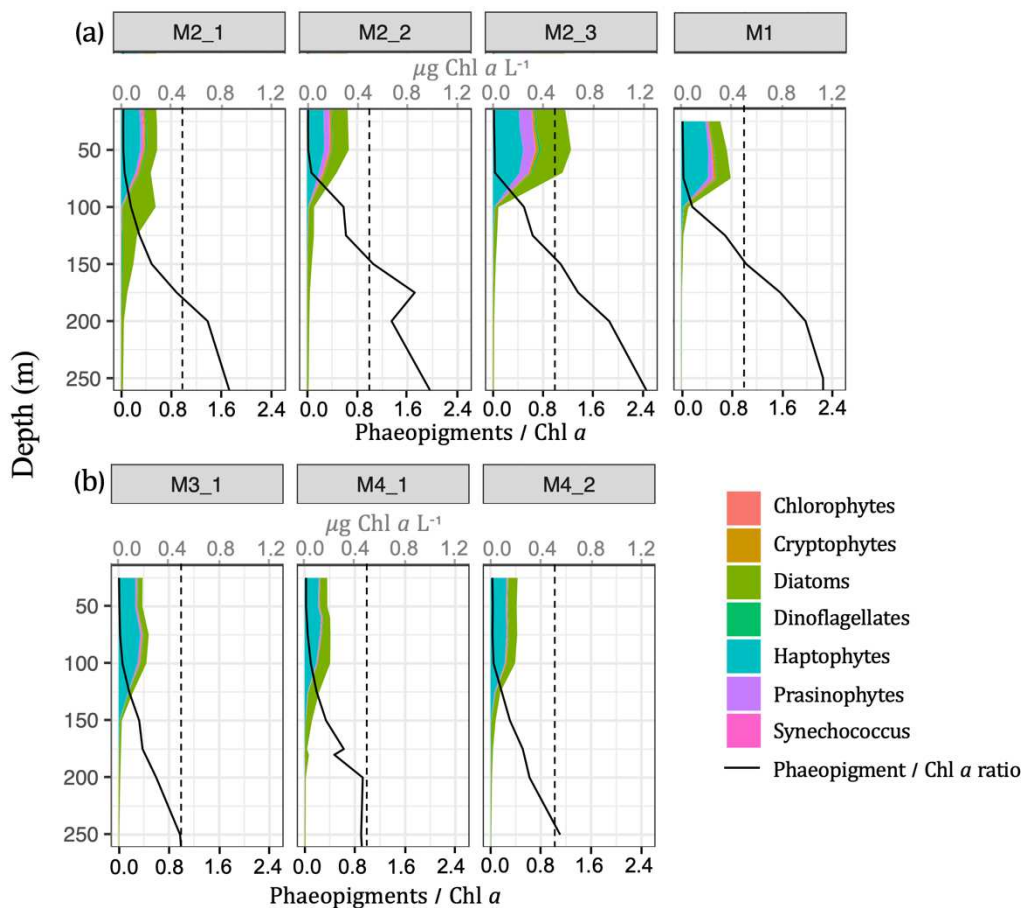


Fig. 2: Chemotaxonomic vertical profiles of the contribution of major phytoplankton groups to Chl *a* concentration. The black line indicates Phaeopigment:Chl *a* ratio. Phaeopigments correspond to degraded and Chl *a* to fresh pigment material. The dashed black line corresponds to a ratio of 1. In (a), stations have Phaeo/Chl *a* ratio above 1 at 200m depth, whereas in (b) stations the ratio is <1.

		0.2-20 $\mu\text{m}$						20-100 $\mu\text{m}$								
Haptophyta	Phaeocystis-	48	34	65	41	8	76	39	3	2	1	40	21	6	3	
	Emiliana-	2	4	0	1	4	0	2	0	0	0	0	1	0	0	
	Prymnesium-	0	0	0	0	0	0	0	0	0	0	0	1	0	0	
	Other prymnesiophyceae-	7	6	1	1	3	1	1	1	1	0	0	3	1	1	
	Clade HAP3-	0	0	0	1	1	0	0	0	0	0	0	0	0	0	
Chlorophyta	Prasinoderma-	4	5	0	0	34	0	0	0	0	0	0	3	0	0	
	Micromonas-	3	4	13	1	0	0	0	0	0	0	0	0	0	0	
	Pterosperma-	2	3	1	0	1	0	0	1	0	0	1	1	0	0	
	Bathycoccus-	1	1	1	0	0	0	0	0	0	0	0	0	0	0	
	Dunaliella-	1	0	0	0	0	0	0	0	0	0	0	1	0	0	
	Other chlorophyta-	1	0	0	0	0	0	0	0	0	0	0	0	0	0	
Pelagophyceae	Pelagococcus-	0	1	0	0	23	0	1	0	0	0	1	5	1	1	
	Pelagomonas-	1	1	2	7	1	5	10	0	0	0	0	1	0	0	
	Other pelagophyceae-	0	1	2	5	1	1	1	0	0	0	1	1	0	0	
Bacillariophyta	Radial centric	Corethron-	3	9	1	1	1	1	1	10	72	87	15	4	6	7
		Proboscia-	1	1	0	0	0	0	1	2	11	5	3	1	10	19
		Rhizosolenia-	1	1	0	0	0	0	0	5	1	1	0	0	3	15
		Guinardia-	2	1	0	0	0	0	0	2	6	1	0	0	0	0
		Other radial-centric-	3	5	0	0	0	0	4	1	0	0	0	0	0	2
	Polar centric	Eucampia-	2	3	1	0	0	0	0	62	1	1	0	1	0	0
		Thalassiosira-	3	3	1	3	3	1	6	1	1	1	12	14	16	7
		Chaetoceros-	1	1	1	15	1	1	1	4	1	0	2	4	13	18
		Dactyliosolen-	0	0	0	4	0	3	1	0	0	0	1	2	4	5
		Odontella-	1	1	0	0	0	0	0	3	1	0	0	0	0	0
	Raphid pennate	Other polar-centric-	4	1	4	8	0	0	0	0	0	0	3	0	2	1
		Fragilariopsis-	3	5	1	5	11	2	17	0	0	0	3	8	16	3
		Pseudo-nitzschia-	1	1	0	2	1	4	3	1	1	0	2	23	4	8
		Cylindrotheca-	0	0	0	0	0	0	0	0	0	0	0	1	2	0
		Un. raphid-pennate-	0	1	0	1	3	2	10	0	1	0	2	2	7	6
	Araphid pennate	Other raphid-pennate-	0	0	0	0	0	0	0	0	0	0	0	0	0	1
		Thalassiothrix-	0	0	0	0	0	0	0	0	0	0	2	0	0	0
		Thalassionema-	0	0	0	0	0	0	0	0	0	0	0	0	0	0
Un. araphid-pennate-		0	0	0	0	0	0	0	0	0	0	9	0	6	0	
Chrysophyceae	Un. chrysophyceae-	2	3	0	0	0	0	0	0	0	0	0	0	0	0	
Cryptophyceae	Teleaulax-	0	0	1	0	0	0	0	0	0	0	0	0	0	0	
	Plagioselmis-	1	1	0	0	0	0	0	0	0	0	0	0	0	0	
	Other cryptophyceae-	1	1	1	0	0	0	0	0	0	0	0	0	0	0	
Bolidophyceae	Parmales-	1	0	0	1	0	0	0	0	0	0	0	0	0	0	
MOCH	MOCH-	2	1	2	1	0	0	0	1	0	0	0	0	0	0	

M2-1 M2-2 M2-3 M1 M3-1 M4-1 M4-2 M2-1 M2-2 M2-3 M1 M3-1 M4-1 M4-2

Fig. 3: Heatmap of surface phytoplankton taxa in the small (0.2-20  $\mu\text{m}$ ) and large (20-100  $\mu\text{m}$ ) size-fraction. Taxa are grouped by division (Haptophyta, Chlorophyta) or class (Bacillariophyta, Pelagophyceae, Dinophyceae, Chrysophyceae, Cryptophyceae, Bolidophyceae and MOCH).

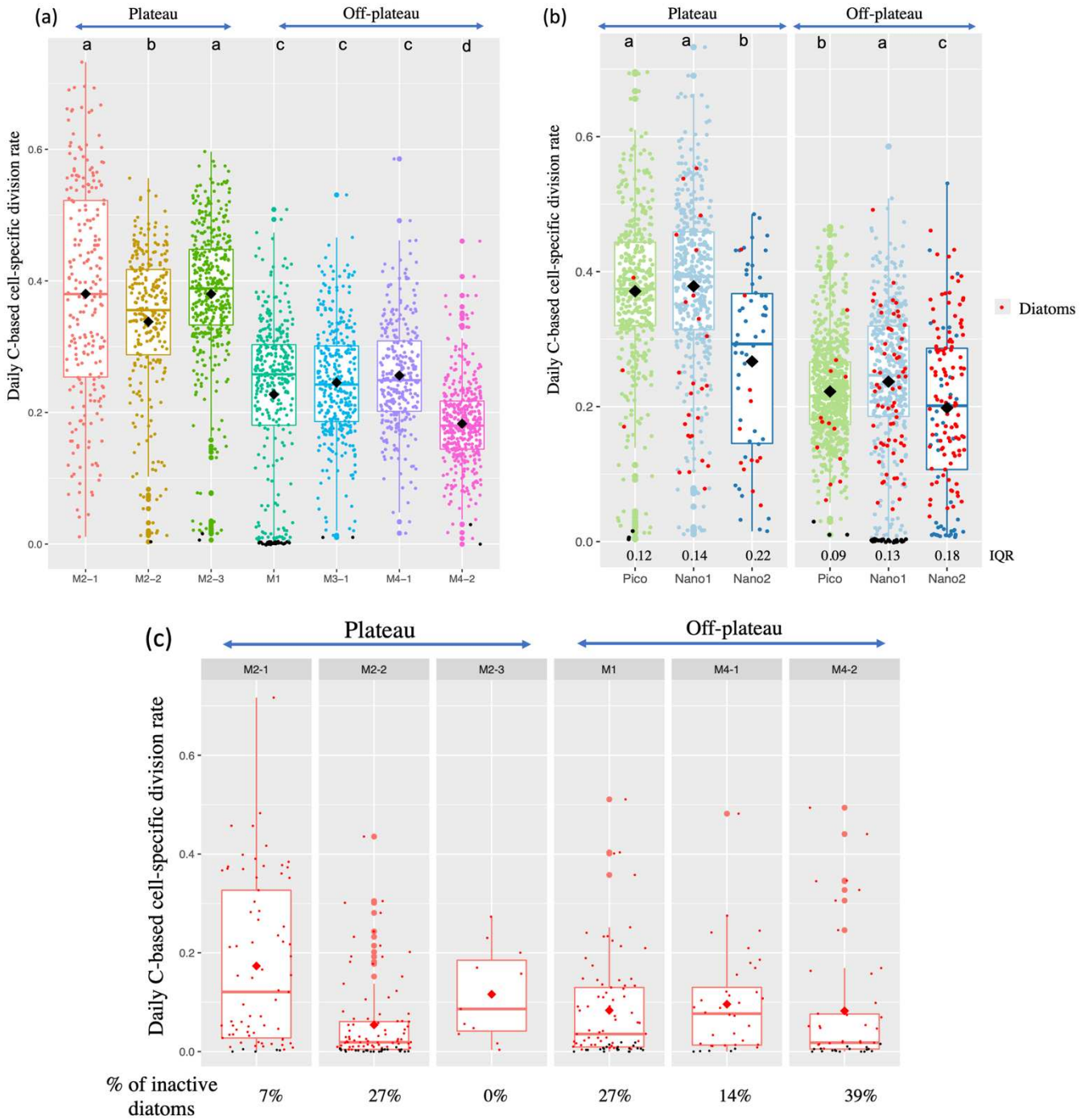


Fig. 4: Boxplot of the daily  $CO_2$ -based cell-specific division rates. Each dot corresponds to the division rate of a single cell measured with NanoSIMS for cells  $<20 \mu m$  (a,b) or with SIMS for diatoms  $>20 \mu m$  (c). Diamonds indicate mean division rates and inactive cells are colored in black. Significant differences (pairwise Mann-Whitney test with  $p < 0.05$ ) in division rates between stations (a) or between size-groups on- and off-plateau (b) are indicated by letters above the boxplots (ranked by alphabetical order from highest to lowest division rates). The interquartile range is indicated as a measure of dispersion of the division rates. Outliers correspond to the larger points.

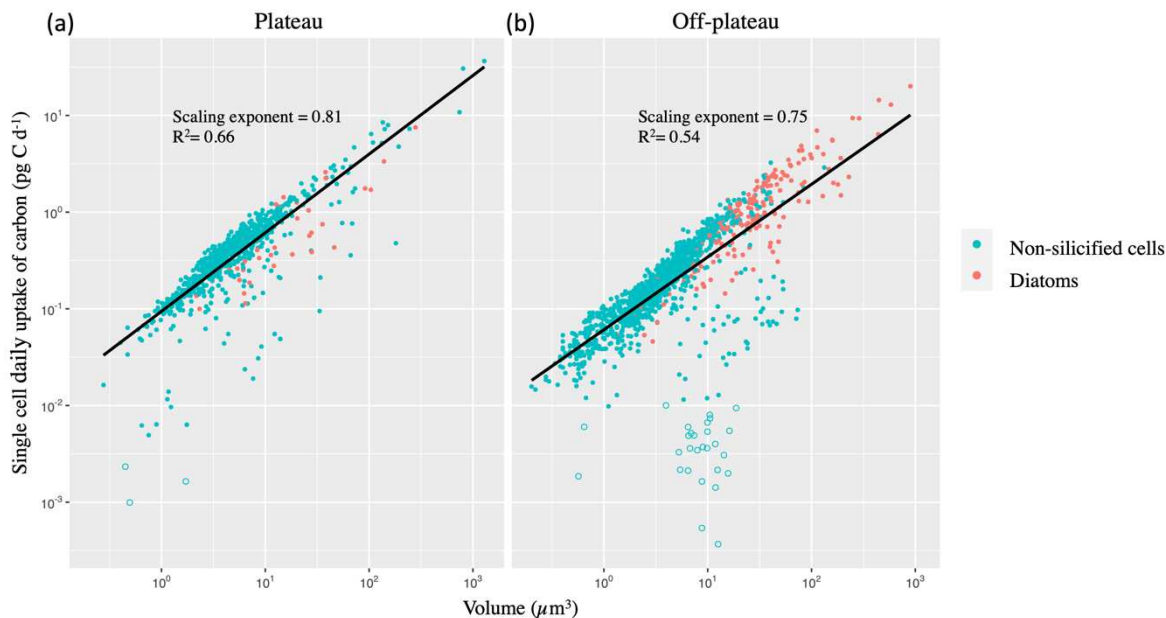


Fig. 5: Single-cell daily uptake rate of carbon ( $\text{pg C d}^{-1}$ ) vs. single-cell volume for diatoms and non-silicified cells measured with NanoSIMS on- (a) and off-plateau (b). Empty circles correspond to inactive cells. Scaling exponents have been obtained by linear least-squares fitting of log-transformed data. Consequently, the amount of  $\text{CO}_2$  fixed at the single cell level ( $C\text{-fix}$ ) scaled with cell volume ( $V$ ) according to the power law  $C\text{-fix} = a \cdot V^a$  where  $a$  is a constant that differed on- and off-plateau and  $a$  is the scaling exponent.

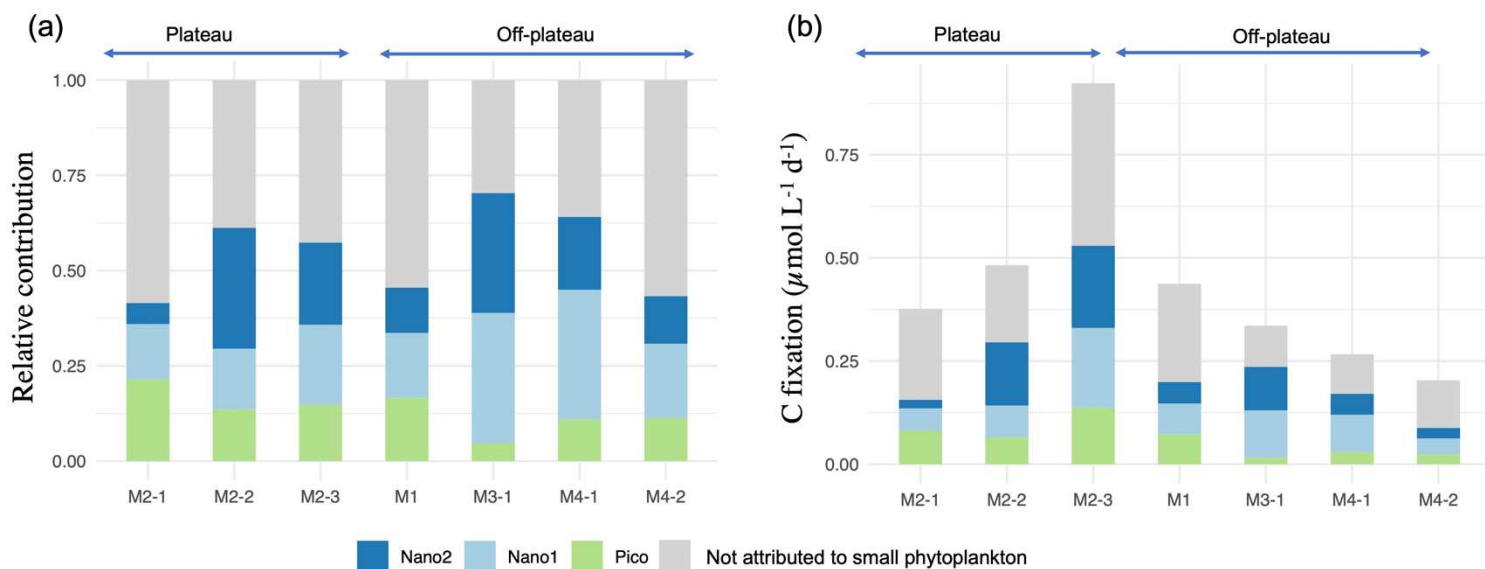


Fig. 6: Estimated relative (a) and absolute (b) contribution of the different groups of small phytoplankton to bulk  $\text{CO}_2$ -fixation (measured by EA-IRMS). Contribution of each group was obtained by multiplying mean  $\text{CO}_2$ -fixation rates (NanoSIMS) by the abundance of the groups (flow cytometry enumeration).

## Supplementary material

### Catalyzed reporter deposition of Fluorescent In Situ Hybridization (CARD-FISH)

Fluorescent in situ hybridization with horseradish peroxidase-labelled probes was performed as detailed in Not et al. [1] to quantify the abundances of the major phytoplankton phylogenetic groups. Diverse probes (EUK1209r, NCHLO01 and CHLO02) were combined to target all eukaryotes and a set of probes (PRAS04, PRYM02 and PELA01) were used separately to target most of the prasinophytes, prymnesiophytes, and pelagophytes [1–3]. In brief, filter pieces were incubated in the hybridization buffer (2  $\mu$ l of oligonucleotide probe at 50 ng  $\mu$ l<sup>-1</sup> stock, 40% formamide, 0.9 M NaCl, 20 mM pH 7.5 Tris-HCl, 0.01% (w/v) sodium dodecyl sulphate (SDS) - Sigma-Aldrich) and incubated at 35°C for 3 h. Filters were then washed twice at 37°C for 20 min with a washing buffer (56 mM NaCl, 5 mM EDTA, 0.01% (w/v) SDS, 20 mM Tris-HCl, pH 7.5) and equilibrated at room temperature for 15 min in TNT buffer (100 mM Tris-HCl, pH 7.5, 150 mM NaCl, 0.05% (v/v) Tween 20 - Sigma-Aldrich). CARD (fluorescein Tyramide reagent pack - Perkin Elmer) was performed in 20  $\mu$ l of CARD mix following manufacturer's recommendations for 30 min in the dark at room temperature. Finally, filters were transferred into a TNT buffer and incubated twice at 55°C for 20 minutes. Filters were then mounted in the anti-fading reagent AF1 (Citifluor, London, UK) mixed with propidium iodide (1  $\mu$ g mL<sup>-1</sup> final conc.). Samples were then stored at -20°C until analysis (<1 week) with a Zeiss imager M2 epifluorescence microscope.

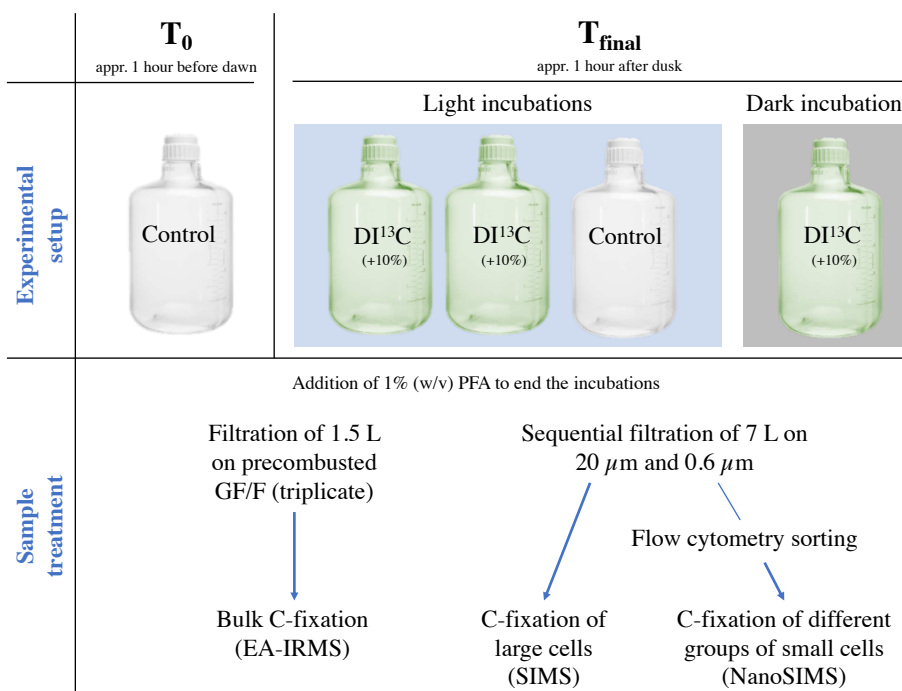


Fig. S1: Experimental setup of the study.

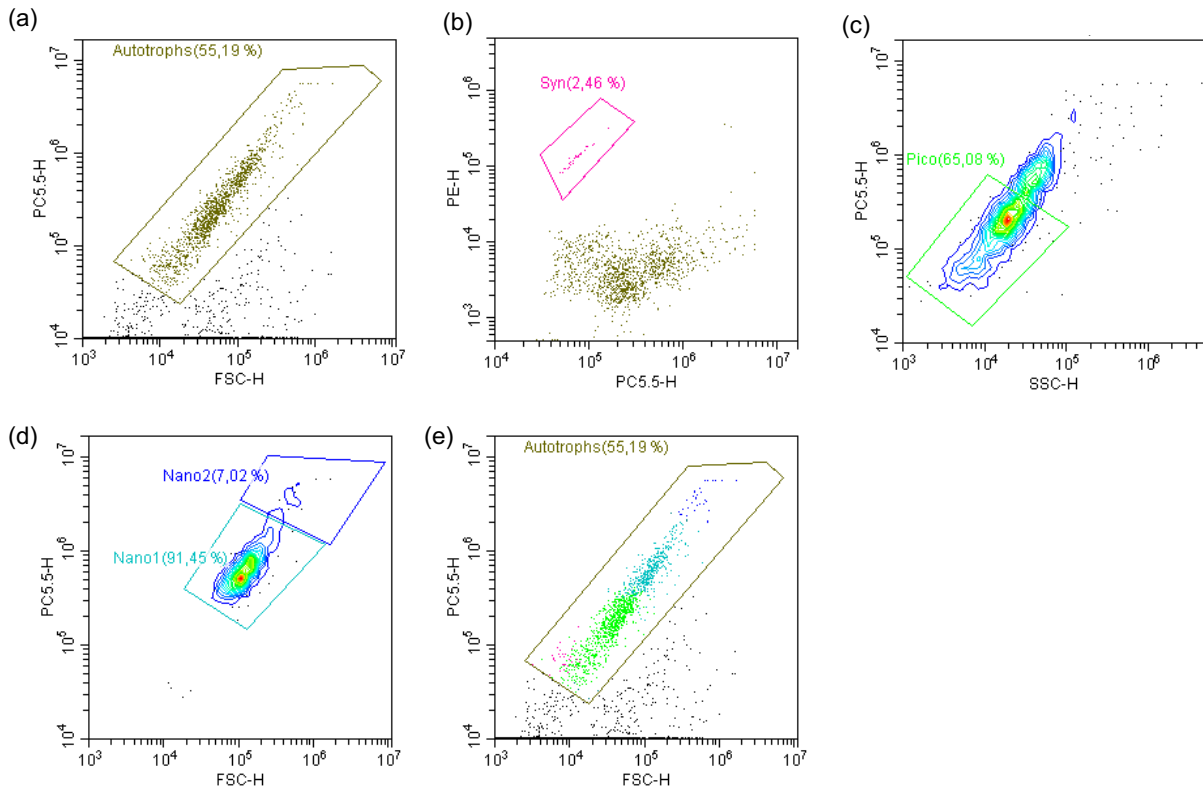


Fig. S2: Step by step protocol for the gating and sorting of small phytoplankton groups. Pigmented cells were first gated based on their chlorophyll (PC5.5-H) and forward scatter (FSC-H) (a). Only pigmented cells were plotted and Synechococcus cells gated based on their higher phycoerythrin signal (PE-H) (b). Pico group was created to group Synechococcus cells with pico-eukaryotes in the same size range (c). The rest of the autotrophs were separated in two groups (Nano1 and Nano2) based on their FSC-H (d). All groups were plotted based on their Chl a and forward scatter signal (Syn and pico-eukaryotes in pink and light green; Nano1 in turquoise and Nano2 in dark blue) (e).

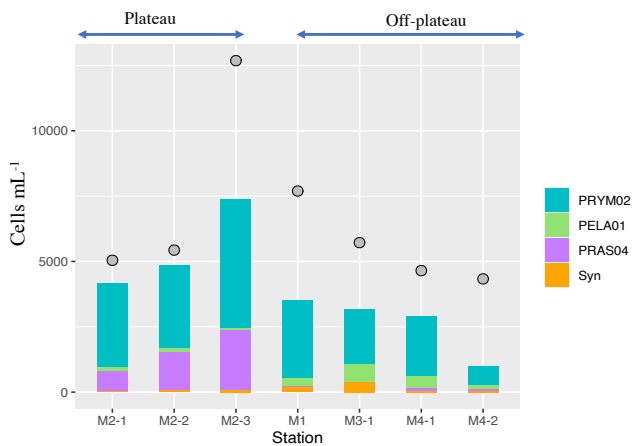


Fig. S3: Surface abundance of different groups of small non-silicified autotrophs assessed by CARD-FISH labeling with probes PRAS04 (prasinophytes, Mamiellaceae family), PRYM02 (haptophytes) and PELA01 (pelagophytes). Abundance of Synechococcus obtained by flow cytometry is also indicated (Syn). Total abundances of small autotrophs enumerated by flow cytometry are indicated at the top of each column with a grey dot. Counts with the CARD-FISH method confirmed the importance of haptophytes (2-5 $\mu$ m in size) on- and off-plateau (735 – 4950 cells mL<sup>-1</sup> depending on the station). Prasinophytes (<2 $\mu$ m in size) from the Mamiellaceae family were more abundant on-plateau (750-2300 and 70-115 cells mL<sup>-1</sup> respectively), while pelagophytes (appr. 3  $\mu$ m in size) were mostly observed off-plateau. These three groups accounted for 58-87% and 22-61% of small phytoplankton abundances enumerated by flow cytometry on- and off-plateau, respectively.

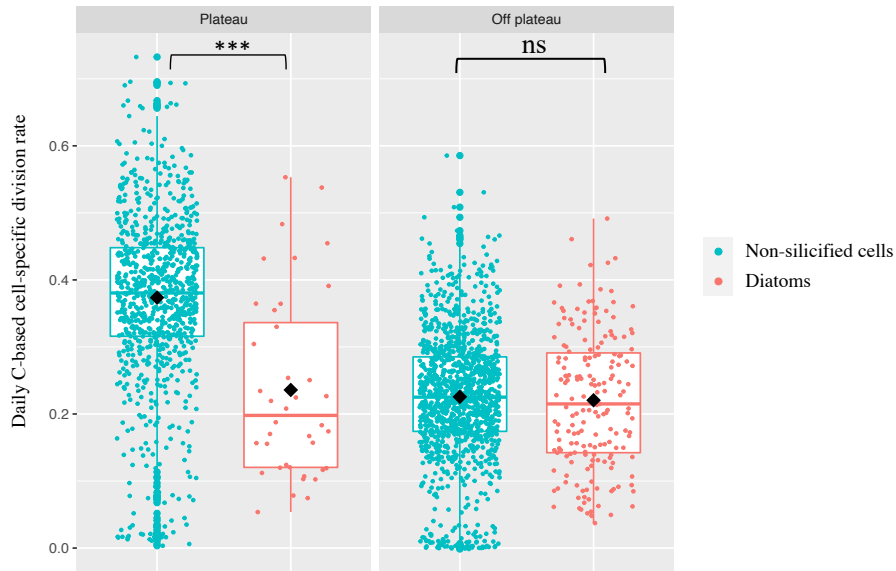


Fig. S4: C-based cell-specific division rates measured with NanoSIMS for small diatoms and non-silicified cells on and off plateau. Diatoms' division rates were significantly lower than those of non-silicified cells on-plateau (Kruskal-Wallis,  $P < 10^{-8}$ ; post-hoc pairwise Mann-Whitney,  $P < 10^{-9}$ ), but not off-plateau.

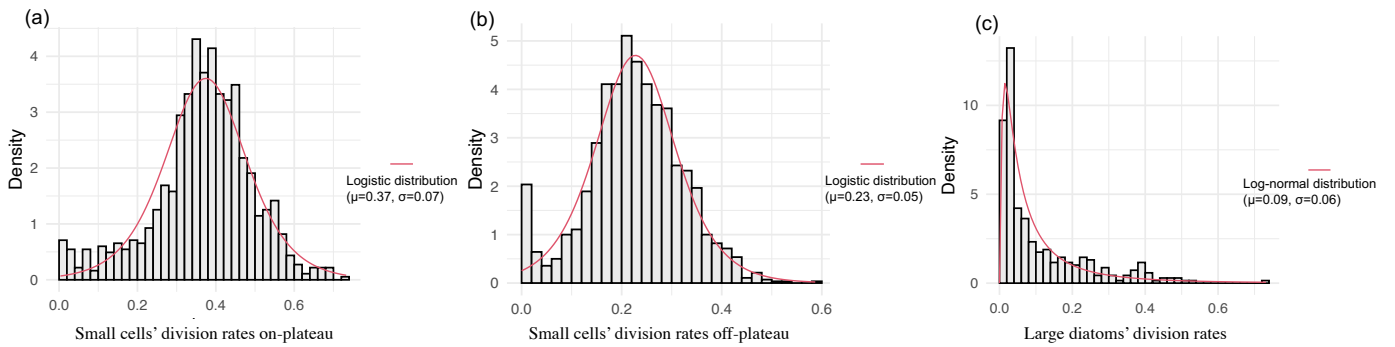


Fig. S5: Histogram of measured division rates of small cells on (a) and off-plateau (b) and large diatoms (c). The best distribution was selected from a predefined family of distributions (normal, logistic, exponential, log-normal, uniform, gamma) based on the lowest AIC. Division rates of small cells were best fitted by a logistic distribution on and off-plateau with mean division rates  $\mu=0.37$  and  $\mu=0.23$  on- and off-plateau respectively. Division rates of large diatoms fitted a log-normal distribution characterized by skewed distributions to the left (low division rates) with mean division rates  $\mu=0.09$ .

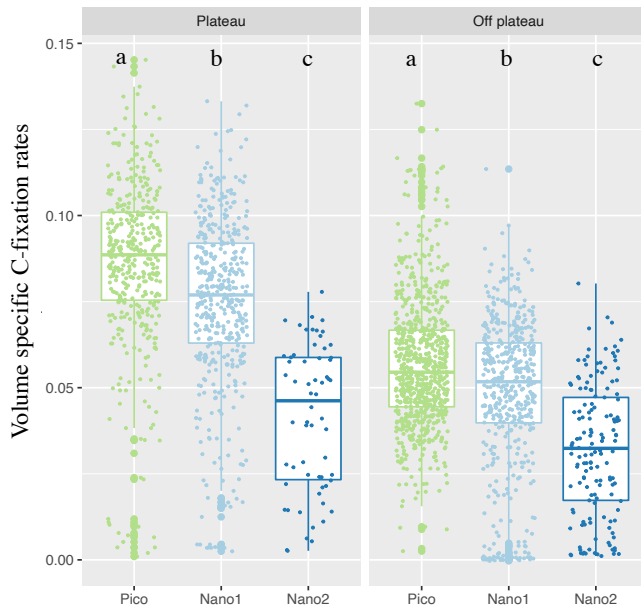


Fig. S6: Single-cell volume-specific C-fixation rates (i.e. the daily carbon fixation rate expressed in fg C divided by the cell volume). Significant differences are indicated by letters above the boxplots ranked by alphabetical order from highest to lowest mean volume-specific C-fixation rates (pairwise Mann-Whitney test with  $P < 0.05$ )

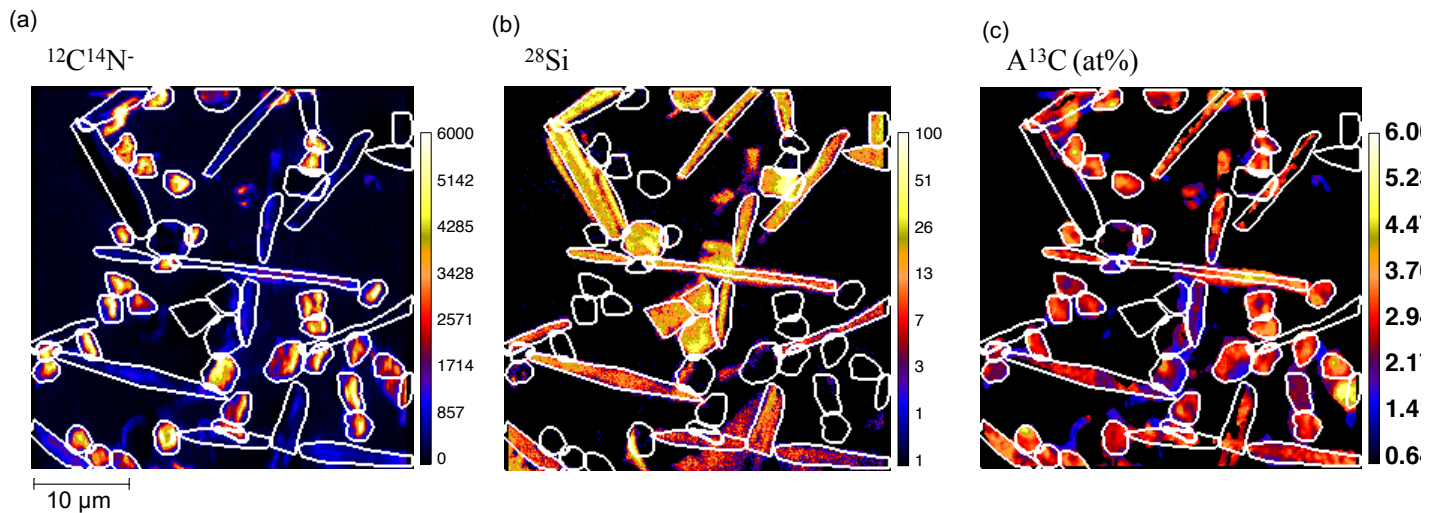


Fig. S7: Examples of NanoSIMS images showing the sum of  $^{12}\text{C}^{14}\text{N}^-$  (a) and  $^{28}\text{Si}$  ions detected (b), as well as the  $\text{A}^{13}\text{C}$  enrichment (c) for Nano1 at M4-1. The frustules of small diatoms are colored in (b).



Table S1: Summary of the <sup>13</sup>C fixation incubations' location and timing.

	Station	Longitude (degrees east)	Latitude (degrees north)	Incubation date	Start time	End time
Off-plateau	M1	74.9013	-49.8498	10/03/2018	03:20	20:15
	M3_1	68.0579	-50.6822	05/03/2018	05:40	20:15
	M4_1	67.1998	-52.6002	01/03/2018	05:20	20:10
	M4_2	67.1980	-52.6006	10/03/2018	04:30	20:15
Plateau	M2_1	72.0005	-50.6166	26/02/2018	05:20	20:15
	M2_2	72.0004	-50.6166	07/03/2018	05:10	20:30
	M2_3	71.9964	-50.6177	17/03/2018	03:40	19:55

Table S2: Details of the cells analyzed with NanoSIMS and SIMS.

Population	Station	Abundance (cells mL <sup>-1</sup> )	Cells analyzed	Diatoms analyzed	% diatoms	Nb of inactive cells	% Inactive cells	Mean diameter ( $\mu\text{m}$ +/- sd)	Mean division rate	Median division rate	Interquartile range (IQR)
Pico		3517	69	2	3%	-	-	1.78±0.16	0.41	0.43	0.21
Nano1		1190	153	16	10%	-	-	2.43±0.3	0.37	0.35	0.27
Nano2	M2-1	337	3	3	100%	-	-	3.71±0.04	0.15	0.12	0.05
Pico		3410	96	-	-	1	1%	1.76±0.16	0.34	0.35	0.14
Nano1		1603	145	9	6%	-	-	2.48±0.36	0.36	0.37	0.10
Nano2	M2-2	420	33	9	27%	-	-	5.62±2.03	0.25	0.28	0.24
NanoSIMS	Pico	8153	237	1	0%	2	1%	1.58±0.28	0.37	0.37	0.10
	Nano1	3753	155	-	-	-	-	2.43±0.35	0.41	0.43	0.11
	Nano2	M2-3	777	26	-	-	-	4.63±1.83	0.30	0.34	0.15

Pico		5090	123	3	2%	-	-	1.72±0.17	0.26	0.26	0.05
Nano1		2280	167	17	10%	29	17%	2.52±0.38	0.24	0.28	0.19
Nano2	M1	325	59	29	49%	-	-	4.8±1.74	0.14	0.12	0.21
Pico		2260	245	1	0%	2	1%	1.3±0.31	0.25	0.25	0.12
Nano1		2830	85	4	5%	-	-	2.61±0.45	0.23	0.23	0.10
Nano2	M3-1	630	20	13	65%	-	-	4.34±0.68	0.28	0.30	0.18
Pico		2380	115	2	2%	-	-	1.71±0.19	0.22	0.22	0.07
Nano1		2033	141	33	23%	-	-	2.6±0.4	0.28	0.28	0.11
Nano2	M4-1	237	36	31	86%	-	-	4.52±1.13	0.29	0.28	0.10
Pico		2603	277	7	3%	1	0%	1.61±0.2	0.18	0.18	0.06
Nano1		1510	98	12	12%	1	1%	2.43±0.36	0.19	0.19	0.09
Nano2	M4-2	220	34	31	91%	-	-	4.71±1.11	0.16	0.15	0.09

	Station	Number of diatoms	Nb of inactive cells	% Inactive cells	Mean diameter ( $\mu\text{m}$ +/- sd)	Mean division rate	Median division rate	Interquartile range (IQR)
SIMS	M1	81	22	27%	16.84±5.96	0.08	0.04	0.12
	M2-1	73	5	7%	12.36±7.37	0.17	0.12	0.30
	M2-2	97	26	27%	23.32±16.19	0.05	0.02	0.06
	M2-3	11	0	0%	60.89±16.28	0.12	0.09	0.14
	M4-1	36	5	14%	16.81±5.53	0.10	0.08	0.12
	M4-2	46	18	39%	14.15±5.59	0.08	0.02	0.07

Table S3: Mean amount of carbon fixed per cell, biomass and unit of carbon fixed per unit of biomass for each station and size-group. Biomass was calculated by converting the cell biovolume to carbon content according to Verity et al. (1992) [4].

Size-group	Station	Mean C-fixed (pgC cell <sup>-1</sup> )	Mean biomass (pgC cell <sup>-1</sup> )	Pg C-fixed / biomass
<b>Pico</b>	M2-1	0.28	1.12	0.25
	M2-2	0.23	1.09	0.21
	M2-3	0.20	0.86	0.23
	M1	0.17	1.03	0.17
	M3-1	0.08	0.54	0.15
	M4-1	0.15	1.02	0.14
	M4-2	0.11	0.88	0.12
<b>Nano1</b>	M2-1	0.55	2.55	0.22
	M2-2	0.57	2.71	0.21
	M2-3	0.62	2.58	0.24
	M1	0.39	2.85	0.14
	M3-1	0.49	3.16	0.15
	M4-1	0.54	3.10	0.17
	M4-2	0.32	2.59	0.12
<b>Nano2</b>	M2-1	0.74	7.41	0.10
	M2-2	4.37	28.10	0.16
	M2-3	3.08	17.82	0.17
	M1	1.92	18.71	0.10
	M3-1	2.01	11.63	0.17
	M4-1	2.58	14.04	0.18
	M4-2	1.39	15.27	0.09

Table S4: Compiled literature on division rates of open-ocean Southern Ocean phytoplankton depending on iron availability. When available, standard deviation is indicated in brackets.

	Species	Division rate [d <sup>-1</sup> ]		Method	Temperature	Comments	Reference
		Fe-replete	Fe-limited				
<b>Nano-sized flagellates</b>							
Haptophytes	Natural assemblage of small flagellates dominated by <i>P. antarctica</i>	0.37 (0.12)	0.23 (0.09)	<sup>13</sup> C incubations and NanoSIMS	4-5°C	incubation of nat. communities Fe-replete corresponds to plateau samples, Fe-limited to HNLC stations	This study
	<i>P. antarctica</i> (strain CCMP #1871)	0.38 (0.025)	0.19 (0.006)	Chl concentration <sup>a</sup>	2°C	culture	[5]
	<i>P. antarctica</i>	0.33	0.1	cell counts		incubation of nat. communities, Antarctic Circumpolar Current	[6]
	<i>Phaeocystis antarctica</i> (clone AA1)	0.52	0.28	cell counts	3°C	Cultures from isolates (Polar Frontal Zone, December 2001)	[7]
	<i>P. antarctica</i>	0.37-0.40	0.14-0.17	cell counts	0-4°C	cultures	[8]
	<i>Phaeocystis antarctica</i> (clone AA1)	0.50	0.20	cell counts	3°C	cultures	[9]
	<i>Phaeocystis antarctica</i> (clone AA1)	0.33	0.15	fluorometry	3°C	cultures	[10]
	<i>Phaeocystis antarctica</i> (clone SX9)	0.41	0.14	cell counts	3°C	cultures	[9]
	<i>P. antarctica</i>	0.36	0.24	cell counts	2°C	cultures	[11]
	<i>P. antarctica</i>	0.42	0.24	cell counts	2°C	cultures	[12]
Cryptophytes	<i>P. antarctica</i>	0.58	0.18	fluorometry	1°C	cultures	[13]
	<i>Geminigera cryophila</i>	0.26	0.05	cell counts	2°C	cultures	[14]
<b>Diatoms</b>							
	Natural assemblage of small diatoms (<20µm)	0.24 (0.14)	0.22 (0.1)	<sup>13</sup> C incubations and NanoSIMS	4-5°C	incubation of nat. communities Fe-replete corresponds to plateau samples, Fe-limited to HNLC stations	This study
	Natural assemblage of large diatoms (>20µm)	0.11 (0.14)	0.09 (0.11)	<sup>13</sup> C incubations and SIMS	4-5°C	incubation of nat. communities Fe-replete corresponds to plateau samples, Fe-limited to HNLC stations	This study
	<i>pennates</i>	0.2	0.16	cell counts	-	incubation of nat. communities, Ross sea (oceanic)	[6]
	<i>pennates</i>	0.27	0.2	cell counts		incubation of nat. communities, Antarctic Circumpolar Current	[6]
	<i>Fragilariopsis cylindrus</i>	0.33-0.64	0.2-0.43	cell counts	0-4°C	cultures	[8]
	<i>Fragilariopsis cylindrus</i>	0.16 (0.046)	0.05 (0.001)	Chl concentration <sup>a</sup>	2°C	cultures	[5]

<i>Fragilariopsis kerguelensis</i>	0.18	0.08	cell counts	3°C	cultures	[7]
<i>Fragilariopsis kerguelensis</i>	0.38	0.14	cell counts	4°C	cultures	[15]
<i>Pseudo-nitzschia</i>	0.67	0.27	fluorometry	1°C	cultures	[13]
<i>Pseudo-nitzschia subcurvata</i>	0.37-0.57	0.19-0.26	cell counts	0-4°C	cultures	[8]
<i>Thalassiosira</i>	0.28	0.08	cell counts	4°C	cultures	[15]
<i>Thalassiosira antarctica</i>	0.15	0.05	cell counts	3°C	cultures	[7]
<i>Eucampia antarctica</i>	0.34	0.19	cell counts	3°C	cultures	[7]
<i>Eucampia antarctica</i>	0.31	0.18	cell counts	3°C	cultures	[9]
<i>Eucampia antarctica</i>	0.26	0.14	fluorimetry	3°C	cultures	[10]
<i>Proboscia inermis</i>	0.47	0.29	cell counts	3°C	cultures	[7]
<i>Proboscia inermis</i>	0.56	0.34	cell counts	3°C	cultures	[9]
<i>Proboscia inermis</i>	0.44	0.30	fluorimetry	3°C	cultures	[10]
<i>Chaetoceros</i>	0.45-0.54	0.15-0.21	cell counts	0-4°C	cultures	[8]
<i>Chaetoceros brevis</i> (4-6µm)	0.39 (0.09)	0.39 (0.09)	cell counts	0-3°C	cultures	[16]
<i>Chaetoceros dichchaeta</i> (60-80µm)	0.55	0.12	cell counts	0-3°C	cultures	[16]
<i>Chaetoceros dichchaeta</i>	0.43	0.18	fluorometry	1°C	cultures	[13]
<i>Chaetoceros simplex</i>	0.5	0.23	cell counts	2°C	cultures	[14]
<i>Chaetoceros debilis</i>	0.37	0.19	cell counts	2°C	cultures	[12]
<i>Actinocyclus</i>	0.3	0.05	cell counts	4°C	cultures	[15]
<i>Corethron pennatum</i>	0.32	0.09	cell counts	4°C	cultures	[15]
<i>Corethron criophilum</i>	0.37	0.1	fluorometry	1°C	cultures	[13]
<i>Odontella</i>	0.23	0.03	fluorometry	1°C	cultures	[13]

#### Size fractionation

<5µm	0.5	0.2				
5-20µm	0.23	0.05	<sup>14</sup> C incubations	2.8°C	<i>In situ</i> incubations of an artificial Fe-fertilization experiment	[17]
>20µm	0.55	0.06				

1. Not F, Simon N, Biegala IC, Vaultot D. Application of fluorescent in situ hybridization coupled with tyramide signal amplification (FISH CARD) to assess eukaryotic picoplankton composition. *Aquat Microb Ecol* 2002; **28**: 157–166.
2. Simon N, Campbell L, Ornlfsdottir E, Groben R, Guillou L, Lange M, et al. Oligonucleotide probes for the identification of three algal groups by dot blot and fluorescent whole-cell hybridization. *J Eukaryot Microbiol* 2000; **47**: 76–84.
3. Not F, Latasa M, Marie D, Cariou T, Vaultot D, Simon N. A single species, *Micromonas pusilla* (Prasinophyceae), dominates the eukaryotic picoplankton in the Western English Channel. *Appl Environ Microbiol* 2004; **70**: 4064–4072.
4. Verity PG, Robertson CY, Tronzo CR, Andrews MG, Nelson JR, Sieracki ME. Relationships between cell volume and the carbon and nitrogen content of marine photosynthetic nanoplankton. *Limnol Oceanogr* 1992; **37**: 1434–1446.
5. Alderkamp A-C, Kulk G, Buma AGJ, Visser RJW, Van Dijken GL, Mills MM, et al. The effect of iron limitation on the photophysiology of *Phaeocystis antarctica* (prymnesiophyceae) and *Fragilariopsis cylindrus* (bacillariophyceae) under dynamic irradiance. *J Phycol* 2012; **48**: 45–59.
6. Coale KH, Wang X, Tanner SJ, Johnson KS. Phytoplankton growth and biological response to iron and zinc addition in the Ross Sea and Antarctic Circumpolar Current along 170°W. *Deep Sea Res Part II Top Stud Oceanogr* 2003; **50**: 635–653.
7. Strzepek RF, Maldonado MT, Hunter KA, Frew RD, Boyd PW. Adaptive strategies by Southern Ocean phytoplankton to lessen iron limitation: Uptake of organically complexed iron and reduced cellular iron requirements. *Limnol Oceanogr* 2011; **56**: 1983–2002.
8. Zhu Z, Xu K, Fu F, Spackeen JL, Bronk DA, Hutchins DA. A comparative study of iron and temperature interactive effects on diatoms and *Phaeocystis antarctica* from the Ross Sea, Antarctica. *Mar Ecol Prog Ser* 2016; **550**: 39–51.
9. Strzepek RF, Hunter KA, Frew RD, Harrison PJ, Boyd PW. Iron-light interactions differ in Southern Ocean phytoplankton. *Limnol Oceanogr* 2012; **57**: 1182–1200.
10. Strzepek RF, Boyd PW, Sunda WG. Photosynthetic adaptation to low iron, light, and temperature in Southern Ocean phytoplankton. *Proc Natl Acad Sci* 2019; **116**: 4388–4393.
11. Koch F, Beszteri S, Harms L, Trimborn S. The impacts of iron limitation and ocean acidification on the cellular stoichiometry, photophysiology, and transcriptome of *Phaeocystis antarctica*. *Limnol Oceanogr* 2019; **64**: 357–375.
12. Trimborn S, Thoms S, Bischof K, Beszteri S. Susceptibility of two Southern Ocean phytoplankton key species to iron limitation and high light. *Front Mar Sci* 2019; **6**.
13. Takeda S, Watanabe K. Growth response of Antarctic phytoplankton. 1997. pp 14–24.
14. Koch F, Trimborn S. Limitation by Fe, Zn, Co, and B12 results in similar physiological responses in two Antarctic phytoplankton species. *Front Mar Sci* 2019; **6**.
15. Timmermans KR, Wagt B van der, Baar HJW de. Growth rates, half-saturation constants, and silicate, nitrate, and phosphate depletion in relation to iron availability of four large, open-ocean diatoms from the Southern Ocean. *Limnol Oceanogr* 2004; **49**: 2141–2151.
16. Timmermans KR, Gerringa LJA, Baar HJW de, Wagt B van der, Veldhuis MJW, Jong JTM de, et al. Growth rates of large and small Southern Ocean diatoms in relation to availability of iron in natural seawater. *Limnol Oceanogr* 2001; **46**: 260–266.
17. Gall MP, Strzepek R, Maldonado M, Boyd PW. Phytoplankton processes. Part 2: Rates of primary production and factors controlling algal growth during the Southern Ocean Iron RElease Experiment (SOIREE). *Deep Sea Res Part II Top Stud Oceanogr* 2001; **48**: 2571–2590.

## Perspectives

### *Linking identity to CO<sub>2</sub>-fixation activity*

In this study, we managed to compare the variability in CO<sub>2</sub>-fixation rates between and within three different phytoplankton groups: small non-silicified cells, as well as small and large diatoms. More precise taxonomic identification of non-silicified cells or diatoms at the genus level were only inferred in parallel from metabarcoding or FISH data. Two methodological developments could help linking identity with function more directly.

The most direct method to link metabolic activity to phylogeny at the single-cell level is to couple FISH labelling of specific phylogenetic groups with NanoSIMS analysis (Behrens *et al.*, 2008; Li *et al.*, 2008; Musat *et al.*, 2008). In this procedure, labeled cells are discriminated from other cells by recording their coordinates with fluorescence microscopy, or marking their location with a laser microdissection microscope. This ensures that the same fields of interest are imaged by fluorescence microscopy and during NanoSIMS analysis (FISH-NanoSIMS) (e.g. McGlynn *et al.*, 2015). To avoid this two-step process (epifluorescence microscopy – NanoSIMS), direct visualization of hybridized cells during NanoSIMS analysis is also possible by using iodine- and fluorine-, or halogen labeled probes (EL-FISH-NanoSIMS, HISH-SIMS) (Behrens *et al.*, 2008; Li *et al.*, 2008). Considering the low sample throughput (5-10 images per day) and high measurement costs (500 euros per day) of NanoSIMS analysis, these two techniques are adapted only for abundant organisms, which explains why only prokaryotes have been studied this way. For rare taxa, a method developed recently consists in using the flow cytometry signal of the target group from pure cultures, and using this signal to sort populations in natural communities, before CARD-FISH and NanoSIMS analysis (Zimmermann *et al.*, 2015). A flow-FISH procedure to allow the sorting of particular microbial groups by flow cytometry was set up in 2017 by U. Christaki and L. Jardillier. This procedure is adequate for subsequent NanoSIMS analysis as it allowed to recover 90% of the target cells after CARD-FISH labelling, didn't damage the cells and did not seem to affect CO<sub>2</sub>-fixation rates measured after incubation with NaH<sup>14</sup>CO<sub>3</sub> (Jardillier, personal communication). Chemical manipulation of the cells during CARD-FISH was however shown to decrease profoundly the <sup>13</sup>C fraction in comparison to chemically untreated cells (Musat *et al.*, 2014). After paraformaldehyde (PFA) fixation, a reduction of the <sup>13</sup>C fraction from 94% to 90% was observed. PFA dissolves some lipids in cellular membranes, which slightly damages the cell membrane integrity (Cheng *et al.*, 2019), which may lead to leaking of labeled carbon that had not been fixed in high molecular weight molecules. Further decrease of the <sup>13</sup>C fraction to 80% was measured after FISH, while CARD-FISH decreased the fraction to 57% (Musat *et al.*, 2014). This was attributed by Musat *et al.* to the introduction of unlabeled carbon into the cells, diluting the <sup>13</sup>C proportion. The authors thus suggested to develop mathematical models to correct the reduction

of labeled carbon observed after CARD-FISH labeling and quantitatively assess the importance of specific populations to biochemical processes (Musat *et al.*, 2014).

To overcome the issues associated with chemical manipulation of the cells during CARD-FISH labelling, we could also imagine sequencing the three different size-groups sorted by flow cytometry. This would not enable to directly relate the function and identity of single cells like the first method considered, but it would give an idea of the key players within each size-group sorted. However, this was not possible during MOBYDICK as samples used for NanoSIMS were fixed with PFA.

#### *In situ CO<sub>2</sub>-fixation rates for model calibration*

Primary production rates attributed to different phytoplankton classes are key parameters required to validate or parameterize new biogeochemical models that explicitly incorporate distinct phytoplankton groups (Aumont and Bopp, 2006; Uitz *et al.*, 2009). In view of the relatively high homogeneity observed within small phytoplankton CO<sub>2</sub>-fixation rates, we suggested that mean fixation rates measured in this study for this size-class on and off-plateau could help to refine productivity models on and off naturally iron-fertilized areas of the SO. It would however be interesting to control the influence of specific abiotic factors on CO<sub>2</sub>-fixation rates, which were suggested to influence small phytoplankton taxonomic composition during MOBYDICK. We tried to model the influence of specific environmental parameters on growth rates, to explain the higher growth rates observed on-plateau in comparison to off-plateau. Nutrient concentrations (silicic acid, nitrate, phosphate) were lower on-plateau than off-plateau, but growth rates higher, which prevented to find any relation between nutrient concentration and growth rates. We thus assumed that the higher growth rates observed on-plateau were caused by continuous iron input. In Paper 1, we suggested iron, ammonium and silicic acid concentrations, could explain the spatial differences in the distribution of small phytoplankton taxa. The role of silicic acid depletion in limiting diatom's growth on-plateau was confirmed by the lower division rates of small diatoms in comparison to non-silicified cells (Paper 2; Fig. S4). The relative importance of iron, silicic acid and ammonium in controlling small phytoplankton growth and species composition could further be explored experimentally.

Our results do not allow to refine the parametrization of growth rates for large diatoms, considering the high heterogeneity observed from one cell to the other. More measures are needed to assess the influence of active outliers on mean division rates. It could also be interesting to investigate the variability at the single-cell level in CO<sub>2</sub>-fixation rates within specific species or groups depending on silicic acid and iron concentration. Such *in situ* experiments may for example allow to check if pennate are indeed advantaged over centric diatoms in iron-limited environments. Incubation experiments with Si isotopic tracers could also confirm the role of Si-limitation on-plateau in initiating the quasi-dominance of diatom communities by *Corethron inerme* on-plateau. More



importantly, understanding the drivers of the high variability observed in CO<sub>2</sub>-fixation rates within large diatoms would help calibrating models for this important group in SO productivity.

## D. Summary and discussion

Small phytoplankton dominates phytoplankton biomass and photosynthetic activity in vast areas of the global ocean where nutrient availability is limiting the growth of larger cells (Marañón *et al.*, 2009). This is the case in the SO, where phytoplankton communities are largely dominated by small cells (<20 μm) as a result of iron limitation in HNLC waters (e.g. 76% of phytoplankton biomass and 61% of CO<sub>2</sub>-fixation in the western Indian sector of the SO; Weber and El-Sayed, 1987). More recent studies found similar contribution of small cells to Chl *a* and underlined the dominance of haptophytes pigments in the small size fraction (Wright *et al.*, 2010; Iida and Odate, 2014; Nunes *et al.*, 2019). Consequently, model of primary production in the SO estimates that small phytoplankton contributes more to annual primary production (2.5 Gt C yr<sup>-1</sup>) than microphytoplankton (0.9 Gt C yr<sup>-1</sup>) (Uitz *et al.*, 2010).

A shift in dominance towards larger size classes, mainly diatoms, is occasionally observed at spring and summer in productive areas naturally fertilized with iron such as the Kerguelen Plateau (Korb and Whitehouse, 2004; Blain *et al.*, 2007). The magnitude and duration of these blooms dominated by large or chain-forming diatoms are dependent on seasonal factors (silicic acid and iron availability particularly), whereas small phytoplankton may constitute a more or less stable background community (Smetacek *et al.*, 1990) (Fig. D1).

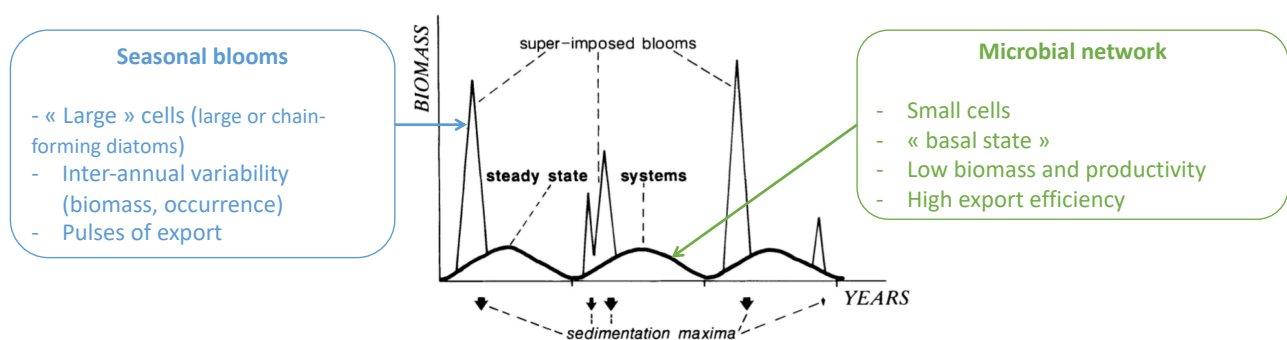


Fig. D1: Conceptual scheme demonstrating the relationship between seasonality of the microbial network (regenerating system, thick line) with superimposed "blooms" (thin lines). The latter exhibit more variability as they are induced by weather conditions operating on a scale of weeks. They are followed by correspondingly variable sedimentation pulses (arrows). The microbial network presents less variability in terms of biomass, productivity and export. Modified from (Smetacek *et al.* 1990)

Abundances of small phytoplankton rarely fall below concentrations of about  $2-4 \times 10^6$  cells L<sup>-1</sup>, which likely gives small phytoplankton a fundamental role within Antarctic food webs during winter and pre-bloom periods, when large and chain-forming diatoms are not abundant (Detmer and Bathmann, 1997). Thus, microbial food webs, where primary production mainly originates from small phytoplankton and is characterized by high grazing pressure of microzooplankton and salps,

may represent an important alternative energy flow to the classical food chain (diatoms—krill—whales) within marine ecosystems of the SO (Weber and El-Sayed, 1987; Smetacek *et al.*, 2004). Last but not least, higher carbon export efficiency was repeatedly measured in low productive ecosystems of the SO dominated by small phytoplankton in comparison with more productive ones dominated by large cells (Savoie *et al.*, 2008; Cavan *et al.*, 2015; Planchon *et al.*, 2015; Le Moigne *et al.*, 2016). Efficient carbon export via fecal pellets of grazers, low bacterial remineralization in the mesopelagic, or direct export of heavy-silicified diatoms in these low productive regions may explain the high export efficiency observed in low productive ecosystems of the SO (Smetacek *et al.*, 2004; Laurenceau-Cornec *et al.*, 2015b; Le Moigne *et al.*, 2016). Although the importance of small-sized protists in food webs, CO<sub>2</sub>-fixation and C-export in the SO is indisputable, only a few studies specifically explored their diversity (Díez *et al.*, 2004; Wright *et al.*, 2009; Thiele *et al.*, 2014), and no study explored how diversity of small phytoplankton could impact the carbon cycling. Deciphering which microorganisms are performing selected functions in the environment and what controls this function are among the most challenging tasks in microbial ecology (Madsen, 2005; Gutierrez-Zamora and Manefield, 2010). The two main objectives of this thesis – to explore the diversity of small phytoplankton communities and their contribution to CO<sub>2</sub>-fixation in contrasting environments – fit into this conceptual framework.

Three questions were addressed in this project to answer these two objectives:

1. Does small phytoplankton community composition differ on and off the naturally iron-fertilized plateau of Kerguelen after the diatom bloom?
2. What are the drivers of the balance between small cells and large diatoms throughout the season?
3. What is the contribution of different size and taxonomic groups of small cells to CO<sub>2</sub>-fixation on- and off-plateau in post-bloom conditions and what does this imply for the functioning of the biological carbon pump in the area?

In this chapter, I will briefly summarize the main conclusions of my different studies, widen the scope of the discussion in the context of global changes and draw a general scheme of the seasonal succession of phytoplankton communities and their influence on C-export around Kerguelen. Finally, general perspectives on the study of small phytoplankton in the C-cycling will be suggested.

## 1. First insights into small phytoplankton diversity around Kerguelen

The exploration of phytoplankton composition through the combination of pigment composition (CHEMTAX) and marker gene analyses (sequencing) clearly highlighted the important contribution of small phytoplankton -*Phaeocystis antarctica*- in particular, in phytoplankton communities on and off-plateau after the diatom bloom (Paper 1; Fig. 3, Fig. 6). *Phaeocystis* has been repeatedly

reported as a key player of phytoplankton communities in HNLC, as well as in naturally iron-fertilized waters of the SO (DiTullio *et al.*, 2000; Wright *et al.*, 2009). The success of *P. antarctica* may be linked to its polymorphic life stages as single cells or large colonies, that represent different adaptation strategies to contrasting environmental controls. In iron-fertilized waters, the capacity to build large colonies, allows *P. antarctica* to partly escape microzooplankton grazing and form large blooms (Schoemann *et al.*, 2005). Colony formation is triggered by iron availability (Bender *et al.*, 2018), but colony size can increase by 30% in the presence of grazers, which tends to confirm the ecological significance of colony formation as defense mechanism against small grazers (Tang *et al.*, 2008). As single cell, this species possesses different acclimation strategies to iron limitation by reducing its size, growth rate, chlorophyll *a* concentration and particulate organic carbon (POC) production (Bender *et al.*, 2018; Koch *et al.*, 2019). The importance of *Phaeocystis* under future oceanic conditions in the SO is likely to keep increasing as this species growth rates don't seem to be impacted by ocean acidification, CO<sub>2</sub> partial pressure and temperature increases (Zhu *et al.*, 2016; Koch *et al.*, 2019).

Metabarcoding of small protist communities was essential to reveal variations in the distribution of other small phytoplankton taxa on- and off-plateau. Although not quantitative, metabarcoding was useful in revealing the presence of distinct taxonomic groups that shared a common cortege of accessory pigments and couldn't be differentiated with CHEMTAX analysis. For instance, pelagophytes, usually characterized by the presence of 19'-butanoyloxyfucoxanthin, could not be included in the CHEMTAX analysis. This accessory pigment is shared with *Phaeocystis* (Wright and Jeffrey, 1987), which prevented CHEMTAX software to find an optimum solution when including pelagophytes. CHEMTAX relies on prior knowledge of phytoplankton communities in the region. It may thus overestimate the contribution of groups already described in the area, like *Phaeocystis*, and overlook the contribution to Chl *a* of taxa not described in the area before, such as pelagophytes, which accounted for 5 to 25% of phytoplankton reads in the small size fraction at off-plateau stations during MOBYDICK (Paper 2; Fig. 3). Moreover, CHEMTAX was not able to discriminate between different species within a broad taxonomic group. For example, diatoms accounted for 36% and 26% of Chl *a* during MOBYDICK on and off-plateau, respectively. However, sequencing data highlighted that diatoms assemblages were significantly different on- and off-plateau in relation with silicic acid availability (Paper 1; Fig. 4 & 5). On-plateau, silicic acid concentrations were depleted after the bloom, and the lightly silicified *Corethron inerme* dominated diatom community, while in HNLC waters, diatoms mainly consisted of a diverse assemblage of *Fragilariopsis*, *Thalassiosira*, *Chaetoceros* and unidentified pennates spanning a broad size-spectrum (Paper 1; Fig. 3 & 4). The importance of small-sized diatoms off-plateau was confirmed by NanoSIMS analysis that revealed abundant small diatoms ( $3.8 \pm 1.5 \mu\text{m}$  equivalent spherical diameter) in nano-sized groups (Paper 2, Fig. 4b).

The distribution of other non-silicified small phytoplankton taxa seemed influenced by contrasting ammonium and iron concentrations on- and off-plateau (Paper 1; Fig. 5). High ammonium concentrations on-plateau favored the presence of an active and growing population of pico-sized *Micromonas* (Paper 2; Fig. 3 & 4b), while iron limitation may explain the enriched contribution of pelagophytes off-plateau. These results are in line with pigment sampling at bloom end during CROZeX (Crozet Plateau, November to January 2004/05), that showed increasing contribution of pelagophytes to the pigment pool as iron was exhausted (Seeyave *et al.*, 2007), and with CARD-FISH counts and sequencing during the artificial iron fertilization experiment LOHAFEX (Thiele *et al.*, 2014). Thus, composition of small phytoplankton communities of the SO may change in relation to iron, ammonium and silicic acid concentrations.

Since no study explored in detail the taxonomic structure of small phytoplankton communities throughout the season before, we cannot exclude that different small phytoplankton may prevail later in the season. For example, PHYSAT model detected *Phaeocystis* in the SO mainly from November to March, whereas winter months were dominated by unspecified “nano” groups (Alvain *et al.*, 2008). Thus, even though *P. antarctica* didn't seem to be impacted by contrasting environmental conditions over our study area (Paper 1; Fig. 5), other small phytoplankton groups may be as or more competitive during autumn and winter. Mixed layer depth deepens considerably in the winter months and can be as deep as 185 m in August (Park *et al.*, 1998). In the Arctic, a seasonal succession within pico-sized prasinophytes is observed from winter to spring. *Bathycoccus* is more successful in winter than *Micromonas*, which is less adapted to dark winter conditions and more susceptible to viral suppression (Joli *et al.*, 2017). In our study, prasinophytes accounted for 20% of Chl *a* in October off-plateau (R-2), when mixed layer (ML) depth was still over 100 m. Sequencing of protist communities during KEOPS2 cruise (summer) indicated that these corresponded to a mixed assemblage of *Prasinoderma* and *Micromonas* (Georges *et al.*, 2014). Thus, specific groups of small phytoplankton, prasinophytes for example, may present special adaptations to low irradiance, enabling them to be as or even more competitive as *Phaeocystis* during winter. This study was the first assessment of the distribution of small phytoplankton taxa around Kerguelen and focused on the exploration of differences between the iron-fertilized plateau and HNLC waters. However, the localization of the Polar front (the natural boundary where Antarctic waters predominantly sink beneath the warmer sub-Antarctic waters) also likely drives small phytoplankton community composition at a smaller spatial scale in the area. Intriguingly, we observed different pelagophytes north and south of the Polar Front, with *Pelagomonas* being predominantly detected in Antarctic waters at M4 and M1 and *Pelagococcus* dominating in sub-Antarctic waters at M3 (Paper 2; Fig. 3). Prasinophytes species composition also differed between Antarctic and sub-Antarctic stations. *Micromonas* (Mamillellaceae family) was present at M2 in Antarctic waters south of the Polar Front, while *Prasinoderma* (Prasinococcales family) was observed north of the Polar Front at M3-1 (34% of the reads of small phytoplankton

taxa)(Paper 2; Fig. 3). These two prasinophytes belong to different families (Mamiellales and Prasinococcales) and could occupy different ecological niches. Alternatively, global oceanic circulation may favor their dispersion from their main habitat north or south of the Polar Front. *Prasinoderma* identified in our study presents a 100% similarity with sequences from *Prasinoderma singularis*. This species was described for the first time and sequenced since in the South-East Pacific Ocean (Jouenne *et al.*, 2011). In contrast, it was suggested that *Micromonas* in the SO was closely related to Arctic *Micromonas* and dispersed via deep currents and upwelling of deep waters on the Antarctic shelf in Antarctic waters (Simmons *et al.*, 2015). Further exploration of the biogeography and ecological drivers of small phytoplankton distribution in the SO is needed to explain these differences in species composition north and south of the Polar Front. As specific species of small phytoplankton, like *Micromonas*, could serve as “sentinels” of a warming ocean (Demory *et al.*, 2019), it may be interesting to further explore the detailed taxonomic composition of small phytoplankton taxa across frontal areas of the SO.

## 2. Seasonality and interannual variability of phytoplankton communities around Kerguelen

### 2.1. Seasonal succession from diatoms to small non-silicified cells

The comparison of MOBYDICK with KEOPS cruises enabled to describe the seasonal community succession from diatom to small non-silicified cells on-plateau (Paper 1, Fig. 6).

The bloom onset is triggered by a shallowing of the mixed layer, that reliefs phytoplankton from light limitation caused by deep mixing during winter (Venables and Moore, 2010). In a turbulent upper mixed layer, irradiance can fluctuate from full sunlight to complete darkness over just a few hours, limiting photosynthesis (MacIntyre *et al.*, 2000). Consequently, the bloom onset is correlated with the decrease of the mixed layer depth starting in October (Robinson *et al.*, 2016). At bloom onset, the combination of a relief in light limitation and maximum concentration of major inorganic nutrients and iron after winter mixing (maximum of 0.6 nM, reduced to 0.05 nM in summer) is expected to benefit both diatoms and small phytoplankton over the plateau (de Baar *et al.*, 2005; Moore *et al.*, 2007; Mongin *et al.*, 2008). However, small phytoplankton are efficiently grazed by rapidly growing microzooplankton, preventing accumulation of small phytoplankton biomass during the bloom onset. In our study, a strong decrease of the pigments associated with prymnesiophytes and prasinophytes was observed on-plateau during KEOPS2 from October to November (Paper 1; Fig. 6). At the same time, ciliates biomass increased 7-fold (Christaki *et al.*, 2015), exerting a strong control on small phytoplankton. The control of small phytoplankton biomass by microzooplankton was consistently observed over the different seasons. During the bloom decline, microzooplankton consumed daily up to 45% of the standing stock of small phytoplankton (KEOPS1), which represented more than small phytoplankton daily production (Brussaard *et al.*, 2008). During

MOBYDICK, grazing experiments also showed that phytoplankton net growth rate was lower than microzooplankton grazing rate (Paper 3; Christaki et al. submitted). Microzooplankton grazers were however strongly controlled by copepod predation (Fig. D2) that, in return, likely controlled their impact on phytoplankton mortality. This can explain why abundances of small phytoplankton did not decline below  $10^6$  cell  $L^{-1}$  despite the high potential of microzooplankton grazing (Paper 1; Fig. 6).

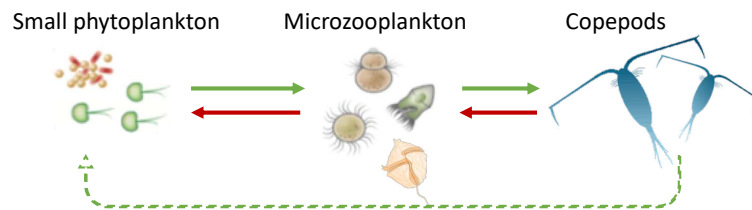


Fig. D2: Positive (green) and negative (red) feedbacks in small phytoplankton, microzooplankton and copepods interactions. By controlling microzooplankton populations, copepod predation exerts an indirect positive feedback on small phytoplankton abundances (dashed green arrow).

As the bloom progresses, the sinking of biogenic silica produced by diatoms to build up their frustules diminishes over time the standing stock of silicic acid at surface to concentrations  $<2 \mu\text{mol } L^{-1}$  (Closset *et al.*, 2014). The decrease of silicic acid concentrations during KEOPS1 and MOBYDICK was associated with a change in diatom community structure, shifting from an initial bloom of *Chaetoceros Hyalochaete* spp. to a quite monospecific bloom of *Eucampia antarctica* in February and *Corethron inerme* in March (Lafond *et al.*, submitted; Armand *et al.*, 2008; Lasbleiz *et al.*, 2016). The shallow mixed layer depth during MOBYDICK further limited the amount of nutrients -silicate and iron particularly- being brought to the surface from deep waters.

In addition to nutrient limitation, biotic interactions such as grazing and parasitism may speed up the bloom decline. During MOBYDICK, infection of microphytoplankton by parasitic Syndiniales was likely low after the bloom, although an important parasitic infection may have occurred before sampling (Paper 4; Sassenhagen *et al.* 2020). Indeed, a high proportion of parasitic Syndiniales (55-70% of the reads) was sequenced in the small size fraction during the first two visits on-plateau. These sequences may be attributed to Syndiniales spores released after the host death, potentially reflecting the end of a parasitic infection. Co-variance network analyses also suggested that Rhizaria may be important grazers of a wide range of diatom taxa. Although biotic interactions certainly played a role in controlling diatoms after the bloom, Chl *a* and associated diatom pigments doubled at the last visit on-plateau after a storm (Paper 1; Fig. 6), highlighting the main bottom-up control of phytoplankton communities in late summer and the importance of transient mixing events to occasionally help diatoms in overcoming Si- and iron limitation (Venables and Moore, 2010).

## 2.2. Interannual variability of the diatom bloom

The diatom bloom is characterized by a large interannual variability, shown by the high standard deviation in surface Chl *a* observed over the bloom period (Paper 1, Fig. 6a). To note that diatom blooms were more intense than usual during KEOPS1 and KEOPS2, as indicated by the Chl *a* concentrations well above the seasonal average during these cruises. The atypical importance of diatom blooms during KEOPS cruises may have contributed to overlook the role of small phytoplankton in CO<sub>2</sub>-fixation and ecosystem functioning of the region. The reasons for the high interannual variability of the bloom magnitude remain unclear, but may result from changes in the importance of iron and/or silicate supply in this area characterized by dynamic fronts (Mongin *et al.*, 2008; Robinson *et al.*, 2016). In this context, the position of the Polar Front North or South of the Kerguelen Plateau might be crucial, as sub-Antarctic waters north of the Polar Front are depleted in silicate. Indeed, the position of the Polar Front on the Kerguelen Plateau varies seasonally as warmer sub-Antarctic waters progress southward during summer (Pauthenet *et al.*, 2018). This southward shift is even more pronounced when warm sea surface temperature anomalies occur (Moore *et al.*, 1999). It will intensify in the future as waters will warm up and become more stratified due to climate change, shifting the position of fronts southward in the SO (Moore *et al.*, 1999; Deppeler and Davidson, 2017; Freeman *et al.*, 2018).

In contrast, Chl *a* interannual variability is low before and after the bloom, (Paper 1, Fig. 6a). Weather conditions in the SO constraint sampling in autumn and winter, but data from other cruises seem to confirm the dominance of small cells outside of bloom periods. For example, the deployment of BGC-Argo floats showed, based on optical properties of plankton communities, that nanophytoplankton dominated before the bloom on the plateau of Kerguelen (Rembauville *et al.*, 2017). Pico- and nanophytoplankton, mostly haptophytes and prasinophytes, also represented over 70% of the phytoplankton biomass before the diatom bloom in the Antarctic Peninsula (Rozema *et al.*, 2017) and in the marginal ice zone (Wright *et al.*, 2010). Thus, it is likely that before and after the bloom, productive ecosystems of the Southern Ocean are consistently dominated by overlooked small phytoplankton cells.

## 2.3. Ecological consequences of a shift towards smaller cells

Intensified stratification projected with southward shift in the position of the Polar Front will reduce the delivery of nutrients to surface water. This may shift the size-spectrum of phytoplankton towards smaller cells, as observed during MOBYDICK.

Changes in the frequency and magnitude of diatom blooms over the plateau is likely to impact the entire food chain. Similar shifts from diatoms to small non-silicified cells (cryptophytes) has caused a decline of krill populations and increase of gelatinous salps along the Antarctic Peninsula (Moline *et al.*, 2004). This trend has been confirmed by long term observations in the SO with negative feedbacks on the ecology of krill consumers, like penguins and seals (Atkinson *et al.*, 2004).

Our study showed that *Phaeocystis* is likely to be the winner in case of more intensified limitation of diatoms around Kerguelen. The impact of a shift towards smaller phytoplankton cells on higher trophic levels has not been explicitly investigated around Kerguelen yet. However, two elements indicate that such a shift may have similar ecological implications as the ones described in the above paragraph. First, salps populations during MOBYDICK were at least as abundant (up to 119 ind. 1000 m<sup>-3</sup> on-plateau) as more frequently sampled areas of the Southern Ocean, particularly at the most productive stations M2 and M1 (Henschke *et al.*, submitted). Similar abundances were described on-plateau during February and April 1987 and were associated with an influx of warmer sub-Antarctic waters. In the following summer (February 1988), the Polar Front passed to the north of the Kerguelen Islands, and salps abundances to the south-east of Kerguelen Islands were lower than the previous year (Hunt *et al.*, 2011). Secondly, past southward anomalies of the location of the Polar Front in link with warm sea surface temperatures were associated to decreasing breeding success of seabirds usually foraging in Antarctic waters, while opposite trends were observed for birds foraging in sub-Antarctic waters (Inchausti *et al.*, 2003). This suggests that increasing importance of small cells on the Kerguelen Plateau could deeply impact the food webs and affect the survival of emblematic predators of the area.

### 3. Impact of surface phytoplankton community structure and productivity regime on the biological carbon pump

#### 3.1. Importance of small phytoplankton in CO<sub>2</sub>-fixation rates during MOBYDICK and implications for C-export

During MOBYDICK, CO<sub>2</sub>-fixation rates showed that small cells were actively growing, whereas large diatoms presented low and heterogeneous growth rates (Paper 2; Fig. 4). These contrasted patterns of small phytoplankton and large diatoms photosynthetic activity provide a bottom-up explanation for the seasonal succession from large diatoms to smaller cells on-plateau. Increasing relative importance of small phytoplankton in CO<sub>2</sub>-fixation is mainly caused by diatoms limitation in post-bloom conditions, and not by increasing activity of small cells over the season. Indeed, mean growth rate of small cells were steady over the repeated visits at M2 ( $0.37 \pm 0.13$  division d<sup>-1</sup>) and compared well with growth rates of a 3 μm-sized phytoplankton population measured at bloom decline (KEOPS1) with the dilution technique (from 0.42 to 0.24 d<sup>-1</sup>) (Brussaard *et al.*, 2008). The ability of small cells to maintain steady growth rates -as opposed to large diatoms- explained the strong increase in the contribution of small cells to CO<sub>2</sub>-fixation from 10-20% at bloom decline (KEOPS1) (Uitz *et al.*, 2009) to 40-60% after the bloom during MOBYDICK (Paper 2; Fig. 6a). Two elements indicate that Si-limitation, rather than iron limitation, is the principal nutrient limiting diatom's growth on-plateau. First, higher growth rates of non-silicified cells were observed on-plateau in comparison to off-plateau stations (Paper 2; Fig. 4b). We can thus hypothesize that the



plateau still benefited from continuous iron input or regeneration that sustained primary production. Secondly, small diatoms were characterized by significantly lower division rates than small non-silicified cells on-plateau (Paper 2; Fig S4), confirming that Si-limitation was limiting diatom's growth on-plateau.

In theory, small cells dominating phytoplankton in the SO are assumed to be characterized by little export, because of rapid recycling of the bulk of organic matter in the euphotic zone (Smetacek *et al.*, 2004). As such, a larger contribution of small phytoplankton was expected to lower the C-export in comparison to previous cruises KEOPS1 and 2. Reduced export at 200m was observed during MOBYDICK in comparison to export at bloom decline (KEOPS1), but export after the bloom was higher than at bloom onset (KEOPS2) (7, 25 and 4 mmol m<sup>-2</sup> d<sup>-1</sup>, respectively) (Paper 5; Christaki *et al.* 2020). Thus, small phytoplankton may contribute to C-export, via grazing or aggregation mechanisms, as suggested by several findings in this thesis. The high proportion of *Phaeocystis* reads observed off-plateau at 300 m in the large size fraction (Paper 1; Fig. 3) indicated that this genus could be incorporated in the marine snow as aggregates or may be ingested by grazers in the mesopelagic. The study of pigment vertical distribution further suggested that small non-silicified taxa were rapidly ingested by grazers, especially on-plateau and at M1, where dense salps populations occurred (Paper 2; Fig. 2). To date, no technique can quantitatively assess the contribution of small phytoplankton to C-export. In contrast to large diatoms, for which the silica frustules can easily be observed in sediment traps or on polyacrylamide gels, small non-silicified cells lack characteristic features to identify them in the marine snow. Thus, most studies that discuss the contribution of small phytoplankton to C-export rely on indirect clues, based on modelling or qualitative observations.

“Vigorous” export (>50 mmol C m<sup>-2</sup> d<sup>-1</sup>) is thought to occur in summer in the sub-Antarctic zone south of Australia, a region dominated by small phytoplankton with few diatoms (Cassar *et al.*, 2010, 2015). In this area, grazing was positively correlated with export fluxes (Cassar *et al.*, 2015). The method used in these studies was however indirect, as it assumed that C-export equaled net community production (NCP). NCP corresponds to gross primary productivity (GPP) minus community respiration (i.e. the sum of auto- and heterotrophic respiration) within the surface ocean. When the organic carbon pool is at steady state, little particulate organic carbon is stored in the euphotic zone and it can be considered that NCP approximates organic C-export (Falkowski *et al.*, 2003). During MOBYDICK, NCP was appr. 4 to 14 times higher than export at 200 m on- and off-plateau (Paper 5; Christaki *et al.* 2020). Steady state conditions required for this method were likely not met around the Kerguelen Plateau, especially on-plateau, where rapid changes in autotrophic biomass were observed (Paper 1; Fig. 6a). Inverse food web models are another indirect way to evaluate the contribution of small phytoplankton to C-export (Richardson and Jackson, 2007). To our knowledge, this method hasn't been applied to evaluate the impact of phytoplankton size-structure on C-export in the SO yet. In the Arctic, inverse modelling highlighted that a shift from

diatoms to *Phaeocystis*/nanoflagellates dominated phytoplankton communities, would not necessarily lead to a reduction in C-export (Vernet *et al.*, 2017). However, the pathway of C-export through the food web should be longer when *Phaeocystis* dominated, with increasing importance of microzooplankton and detritus in carbon transfer to mesozooplankton (Vernet *et al.*, 2017). Observational techniques, such as identification of specific pigments or enumeration by flow cytometry of small cells in deep samples, provide direct evidence of the presence of small phytoplankton in sinking material (Roca-Martí *et al.*, 2017). However, these approaches are not quantitative as they underestimate the contribution of small phytoplankton to export via grazing or detritus. Only one study effectively showed, thanks to a combination of sediment trap gels, videography, and confocal microscopy, that a fraction of picoplankton was incorporated as abundant intact cells ( $1.15 \cdot 10^{11}$  prokaryotic picoplankton cells  $m^{-2} yr^{-1}$ ) into sinking organic aggregates via inefficient grazing from salps and copepods in sub-Antarctic HNLC waters (Waite *et al.*, 2000). This method presented the advantage unequivocally prove the contribution of small cells to export via both grazing and aggregation mechanisms, but can't be considered as quantitative, since it can only quantify cells incompletely digested. To conclude, a set of observations suggests that small phytoplankton is of importance in C-export where it dominates phytoplankton biomass and CO<sub>2</sub>-fixation, but for the moment, only models can propose estimates of small phytoplankton C-export. Output and accuracy of these models will however depend on detailed knowledge of production, growth, and grazing rates of all biological compartments included in the model, as well as experimental examination of the origin, composition, and fate of detrital material (Stukel and Landry, 2010).

### 3.2. Lessons from other Si-limited, iron-fertilized areas of the SO

Predicting the consequences of a more intense Si-limitation of larger diatoms on-plateau on CO<sub>2</sub>-fixation and C-export is challenging. Looking at past fertilization experiments in Si-limited waters can bring valuable insights. During LOHAFEX -an artificial iron fertilization in Si-limited waters ( $<2 \mu mol L^{-1}$ ) in the Atlantic region of the SO- Chl *a* and primary productivity doubled after artificial fertilization, mainly due to the increasing importance of small non-silicified cells, while diatoms accounted for  $<10\%$  of phytoplankton biomass (Martin *et al.*, 2013). The unusually high biomass attained and maintained by small flagellates was attributed to the initial absence of salps and to constraints on microzooplankton grazers by heavy predation exerted by the large copepod stock (Schulz *et al.*, 2018). The increase of primary production at surface did not enhance downward particle flux, that remained low throughout the experiment. Nevertheless, many small flagellates and coccoid cells, belonging to the pico- and nanoplankton, were found in sediment traps, and these small, soft-bodied cells probably contributed to the majority of downward POC flux via mesozooplankton grazing and fecal pellet export (Ebersbach *et al.*, 2014). During MOBYDICK, dense salp populations were observed on-plateau and at M1 (Henschke *et al.*, submitted),

potentially adding a one-step export pathway of small phytoplankton export as compared to LOHAFEX in addition to the two-step microzooplankton-copepod grazing and subsequent fecal pellet production (Paper 2).

Investigations of phytoplankton community structure, productivity and export in naturally iron-fertilized Si-limited waters around Crozet during CROZEX showed a more complex situation. In naturally iron-fertilized waters dominated by *Phaeocystis*, productivity was five times higher from early November to mid-December (Poulton *et al.*, 2007; Seeyave *et al.*, 2007) and C-export three times greater than in adjacent HNLC area (Pollard *et al.*, 2009). However, in both iron-enriched and iron-limited waters, most of the POC export over the season was the consequence of pulsed export of diatoms (Pollard *et al.*, 2009). It was suggested that the developing stage of the bloom, that occurred before the cruise, was dominated by large diatom *Eucampia antarctica* (Seeyave *et al.*, 2007). This species may have produced resting spores early in the season as a result of Si-limitation, that accounted for over 90% of the POC export (Salter *et al.*, 2012). Interestingly, in HNLC waters off Crozet, large, grazing resistant, heavy silicified diatoms also greatly contributed to C-export (Pollard *et al.*, 2009). “Giant” heavy silicified diatoms, developing slowly in HNLC waters like *Thalassiotrix* and *Fragilariopsis kerguelensis* were referred to as “silica sinkers” by Smetacek *et al.* (2004), as they allegedly contributed mostly to silicon export as empty cells and not to C-export. However, Quéguiner (2013) suggested they could rapidly sink as intact full cells in late summer and contribute significantly to C-export in HNLC waters. These observations underline the great contribution to export of heavy silicified and spore-producing diatoms in Si-limited environments. During MOBYDICK, *Odontella*, *Eucampia* and *Chaetoceros* were well represented in sequencing data below 125m, suggesting that these spore-producing genera were efficiently exported on-plateau. Off-plateau, large heavy silicified diatoms like *Fragilariopsis* and *Thalassiosira* were also common in sequencing results at 300m (Paper 1; Fig. 7). Thus, even when small phytoplankton greatly contributes to phytoplankton biomass and productivity, large diatoms may still contribute disproportionately to C-export.

### 3.3. Can phytoplankton assemblages predict C-export over the Kerguelen Plateau?

We showed that the contribution of small phytoplankton to CO<sub>2</sub>-fixation increased after the bloom due to silicic acid and iron limitation of large diatoms, and that both small phytoplankton and diatoms could contribute to C-export via direct sinking and indirect pathways through grazing. The fate of the carbon produced at surface by phytoplankton depends mainly on other biological processes involving a large diversity of trophic levels (e.g. prokaryotes, microzooplankton, mesozooplankton and higher trophic levels). In an attempt to understand the significance of this shift in phytoplankton community composition on the annual C-export over the Kerguelen Plateau, I summarized the available data collected during diverse cruises that occurred at different seasons over the last decades.

Prokaryotic communities on-plateau changed from bloom onset to bloom decline as a function of phytoplankton assemblages and community succession (Liu *et al.*, 2020). In addition to changes in bacterial composition, the efficiency of bacterially-mediated carbon transfer to higher trophic levels also shifted throughout seasons (Paper 5; Christaki *et al.* 2020). Marked losses of bacterial carbon were attributed to respiration and viral lysis during spring and summer, while grazing from heterotrophic nanoflagellates sustained a more efficient microbial food web after the bloom (Paper 5; Christaki *et al.* 2020). Microzooplankton community composition and biomass was also characterized by a high seasonality. A shift from large dinoflagellates (e.g. *Gyrodinium*, *Amphidinium* and *Proto-peridinium*), able to feed on large diatoms, to a dominance of small mixotrophic dinoflagellates like *Gymnodinium* was observed from bloom onset until bloom end (Paper 3; Christaki *et al.* submitted, 2015). This change in community composition affected microzooplankton biomass that strongly increased (10-fold) at bloom onset, but was back to pre-bloom levels during MOBYDICK (116 to 15.4 mmol C m<sup>2</sup>) (Paper 3; Christaki *et al.* submitted, 2015). Mesozooplankton biomass -mainly associated to copepods- increased continuously from mid-October to early February (×9 on-plateau and ×2.5 off-plateau), and may have constrained diatom and microzooplankton biomasses during the decline of the bloom (Carlotti *et al.*, 2015). At bloom onset, salps occurred in low numbers on-plateau and were almost absent off-plateau (Carlotti *et al.* 2015). They reached important densities during MOBYDICK (Henschke *et al.* submitted), although their importance on-plateau seems to vary from one year to the other depending on the position of the Polar Front (Hunt *et al.*, 2011).

The quality of the exported organic matter during the different seasons reflected the succession of phytoplankton and zooplankton assemblages. Phytoplankton aggregates were dominant at bloom onset (Laurenceau-Cornec *et al.*, 2015b), when grazers were still in a developing phase. Productivity regime was high (GCP 344 mmol m<sup>-2</sup> d<sup>-1</sup>) when export efficiency was very low (1%), suggesting a “retention” system characterized by high bacterial remineralization and biomass accumulation at surface (Laurenceau-Cornec *et al.*, 2015b; Christaki *et al.*, 2020). In contrast, large fecal pellets (>100 μm) dominated the export flux during bloom decline (KEOPS1), after important mesozooplankton communities had developed (Ebersbach and Trull, 2008). At this time, export efficiency over the plateau was maximum (26%). After the bloom (MOBYDICK), particles < 50 μm represented almost the whole POC biomass down to 300 m at all stations (Planchon, personal communication). This feature suggests a greater role in downward flux of fecal pellets of smaller grazers (microzooplankton and small copepods), as well as of easily fragmentable salp fecal pellets (Iversen *et al.*, 2017). Export efficiency dropped down to 5% in post-bloom conditions (Christaki *et al.*, 2020), which tends to confirm that export efficiency is lower when small phytoplankton and grazers are important, than when large diatoms and copepods dominate during bloom decline. This typical succession was confirmed by deployment of sediment traps over the season (Rembauville, Salter, *et al.*, 2015). This technique showed that fecal pellets contribution to annual carbon flux

reached its seasonal maximum in autumn and winter (>80%). Composition of fecal pellets types evolved throughout the season from small copepods in spring to large euphausiids and copepods in summer, to salps in autumn and winter (Rembauville, Salter, *et al.*, 2015).

Considering this seasonality, it could be tempting to associate characteristic phytoplankton and zooplankton assemblages to specific export regimes and export efficiencies and extrapolate these measures to an annual cycle. However, annual sediment traps also highlighted that *Chaetoceros* *Hyalochaete* spp. and *Thalassiosira antarctica* resting spores were responsible for more than 60% of the annual POC flux (Rembauville, Blain, *et al.*, 2015). Export pulses from resting spores of the same two species accounted for 42% of annual POC flux in the productive waters downstream of South Georgia, whereas diatom vegetative stages only contributed to 5% of POC fluxes (Rembauville *et al.*, 2016) and the importance of *Eucampia* spores in iron-fertilized waters off Crozet was already mentioned previously (Salter *et al.*, 2012). Integrative cruises like MOBYDICK are of great interest to understand pelagic ecology in contrasted productivity regimes and try to assess the impact of climate change on the different compartment of the ecosystem. However, temporal variability of C-export flux in the SO with importance of short flux events of a few diatom spore-resting species precludes extrapolation of discrete measurements to estimate seasonal or annual C-export (Rembauville *et al.* 2015a). As these fluxes can occur in Si-limited waters (Salter *et al.*, 2012), where diatoms growth is limited, it makes it even more speculative to predict the outcome on annual C-export of a shift in size of phytoplankton community composition from diatoms towards small non-silicified cells. This variability also highlights the idiosyncratic dimension of the links between pelagic ecology and ocean biogeochemistry and the difficulty for time-limited cruises to use natural or artificial fertilization experiments to understand the functioning of the biological carbon pump and serve as analogues for past and future climate-induced changes in C-export magnitude. Considering the remoteness and central role of the SO in the global C-cycle, this emphasizes the need to develop more remote automated sampling devices to explore the seasonality, recurrence and environmental links between phytoplankton surface communities and associated export.

#### 4. Outlook for future studies on the role of small phytoplankton in the marine C-cycle

Fully appreciating the links between phytoplankton community composition and biogeochemistry requires to (i) characterize phytoplankton diversity, that encompasses many taxonomic and functional groups, (ii) measure the activity of different functional groups, and (iii) understand the importance of these groups for other biological compartments and the feedbacks exerted by these other compartments on phytoplankton. Specific methods are associated with each of these issues,

and accessing at the same time diversity and measurable functions (in our case CO<sub>2</sub>-fixation) remains challenging in microbial ecology.

The advent of new sequencing technologies represented a huge technical advance to describe the diversity of small eukaryotes. Issues associated with PCR biases in metabarcoding studies will likely be circumvented in a near future by a more generalized use of metagenomic. For example, metagenomic studies can limit the common overestimation of dinoflagellates and underrepresentation of diatoms observed in metabarcoding studies (Genitsaris *et al.*, 2016). Identification of 18S rDNA sequences within metagenomes is a PCR-free alternative to metabarcoding to study microbial diversity, with the potential of also assessing functional and metabolic diversity. However, retrieving precise taxonomical classification from short Illumina metagenomic reads (100–250 bp) remains challenging, especially when targeting the 18S rDNA gene that contains a mosaic of conserved and highly variable regions (Breitwieser *et al.*, 2019). Nano-pore based sequencing has the potential to overcome limitations due to short reads by allowing for sequencing of long fragments (>10 000 bp) that potentially can contribute to higher taxonomic resolution and functional characterization (Reddington *et al.*, 2020). Methodological developments are still desirable to use this sequencing technology in complex environments, by deepening the sequence coverage, reducing the sequencing error rate and ensuring results replicability (Brown *et al.*, 2017). Another main limitation of metagenomic methods is the lack of reference sequences in databases, although the reconstruction of metagenome-assembled genomes from metagenomic data could partly overcome this issue.

Metagenomic or transcriptomic data can inform on metabolism of uncultured taxonomic groups and, therefore, shed light on their effects on biogeochemistry (Caron *et al.*, 2017; Grossart *et al.*, 2020). However, they do not inform on fluxes and need to be combined with *in situ* measurements to confirm hypothetic roles of taxonomic groups in the environment. In our study, we established that CO<sub>2</sub>-fixation was more homogeneously distributed within small cells belonging to various taxa, than within larger cells affiliated to the same taxonomic group (large diatoms). This suggests the validity of considering small phytoplankton as a unique compartment in primary production models. In contrast, taxonomy (at the species level) may be determinant for larger diatoms, for which species-specific responses to iron and silicic acid availability may significantly impact CO<sub>2</sub>-fixation rates. Once *in situ* measurements establish which descriptors are the best suited to accurately represent CO<sub>2</sub>-fixation by phytoplankton in the system, these can be used to calibrate models. We used single-cell data and scaled them up to understand the contribution of small phytoplankton to CO<sub>2</sub>-fixation around Kerguelen. The next step would be to incorporate such data into large-scale biogeochemical models (Mayali, 2020). *In situ* measurements of photosynthetic activity are relatively direct. They constitute the first step in understanding the functioning of the BCP but need to be concomitantly completed with *in situ* measures on micro- and mesozooplankton grazing to understand the processing of photosynthetically-fixed carbon by heterotrophs. Future research

should also focus on feedbacks of heterotrophic activity on bottom-up control of phytoplankton growth rates. Indeed, in addition to being a major cause of phytoplankton mortality, grazing was shown to largely control phytoplankton growth rates by recycling nutrients in the euphotic layer (Laws, 2013). For example, grazing by small copepods is considered in the SO as a major driver of iron recycling (Laglera *et al.*, 2017), whereas salps fast sinking fecal pellets could actively contribute to iron depletion in surface waters (Cabanès *et al.*, 2017). More integrative studies are needed to assess the transfer of elements throughout the food web and highlight possible competition or positive interactions between autotrophs and heterotrophs. This can for example be achieved by following with NanoSIMS and large-geometry SIMS the fixation and transfer of isotopic tracers between autotrophs and heterotrophs forming the basis of the food web (Adam *et al.*, 2016). Methodological considerations still limit our ability to assess directly the actual contributions of large and small phytoplankton to export flux. Direct measures of phytoplankton export as single cells or aggregate in sediment traps may help in assessing the relative contribution of small and large phytoplankton via sedimentation. Unsurprisingly, large cells are most commonly observed this way. Consequently, large cells are assumed in most models to contribute disproportionately to export in comparison with smaller ones. However, fecal pellets can contribute from <1 to 100% of export fluxes (Turner, 2015) and can constitute an important export pathway of small phytoplankton carbon. Inverse food-web models may be used to reconcile *in situ* measurements of primary production, grazing and export and provide a schematic overview of the processing of photosynthetically-fixed carbon via the BCP. These models highlighted the importance of small cells to export when they contributed importantly to net primary production (Richardson and Jackson, 2007; Stukel and Landry, 2010; Vernet *et al.*, 2017). However, sensitivity of model results to input parameters must be evaluated with care to potentially highlight important knowledge gaps, in particular regarding the origin, composition, and fate of detrital material of varying size (Stukel and Landry, 2010). More collaboration between scientists of different fields are needed to explore these promising research avenues that will contribute to a more mechanistic and predictive understanding of the links between phytoplankton diversity, structure and biogeochemical cycles.

## Related papers as co-author

In the frame of the MOBYDICK project, I was co-author on three papers, presented in this section as Paper 3, 4 and 5.

Paper 3 deals with microzooplankton diversity, grazing potential on phytoplankton and seasonal evolution. During MOBYDICK, microzooplankton community composition was similar on- and off-plateau and dominated by small cells ( $<20\mu\text{m}$ ). Microzooplankton grazing rates were higher than phytoplankton growth rates at all stations, but microzooplankton biomass low. Consequently, it was hypothesized that microzooplankton biomass was kept in check by copepod predation. This paper highlights the important role of microzooplankton for channeling the carbon produced by small phytoplankton to higher trophic levels.

Paper 4 explores the spatial structure and temporal dynamics of large-sized protist communities during MOBYDICK and identify potential abiotic and biotic drivers of these assemblages. Main findings of this study were that an important parasitic infection by Syndiniales may have occurred before MOBYDICK. Co-variance network analysis also suggested that Rhizaria may be important grazers of a wide range of diatom taxa and that Syndiniales may be associated with diatoms.

Paper 5 reviewed the seasonal dynamics of microbial loop fluxes in the Kerguelen area. During spring and summer, respiration and viral lysis represented important loss terms of bacterially-mediated carbon. After the bloom (MOBYDICK), grazing by heterotrophic nanoflagellates was the main loss process of heterotrophic bacterial production. This resulted in a more efficient transfer of primary production to bacteria, heterotrophic nanoflagellates and higher trophic levels.

### **Contributions:**

Paper 3: sequencing and pigment data analysis

Paper 4: help with developing the bioinformatic pipeline, analyzing and interpreting sequencing data.

Paper 5: flow cytometry enumeration of FLBs and viruses, analysis of environmental data.





22 ABSTRACT

23 Microzooplankton play an important role in aquatic food webs through their multiple interactions  
24 with other organisms and their impact on carbon export. They are major predators of phytoplankton  
25 and bacteria while preyed on by organisms from higher trophic levels. Microzooplankton diversity  
26 (Dinoflagellates, DIN and Ciliates, CIL), community structure, interaction with phytoplankton and its  
27 potential in channeling carbon to higher trophic levels were studied in contrasting productivity  
28 regimes (off- and on-plateau, the latter been naturally fertilized by iron) around the Kerguelen islands  
29 in the Southern Ocean (SO). Observations carried out in late summer (February-March 2018; project  
30 MOBYDICK) and at the onset-of the bloom (KEOPS2 cruise) are discussed here. DIN and CIL  
31 diversity was assessed by Illumina sequencing of 18S rDNA amplicons and microscopic observations.  
32 The diversity obtained by the two approaches could be compared at a relatively high taxonomic level  
33 (i.e. often to family level). In particular for DIN, relative abundances and ranking of dominant taxa  
34 differed between sequencing and microscopy observations. CIL were always recorded at  
35 considerably lower abundances than DIN, the median of their overall spatial (stations) and temporal  
36 (seasons) abundances being 350 and 1370 cells L<sup>-1</sup>, respectively. During late summer, DIN and CIL  
37 biomasses were about 1.5 times higher on- than in off-plateau waters, while community composition  
38 was spatially similar. The most abundant DIN at all stations and during both seasons were small  
39 *Gymnodinium* (<20µm). During late summer, ciliates *Lohmaniella oviformis* (<20µm) and  
40 *Cymatocylis antarctica* (20-40µm) were dominating on- and off-plateau, respectively. Dilution  
41 experiments suggested significant grazing of microzooplankton on phytoplankton as phytoplankton  
42 net growth (k) was lower than microzooplankton grazing (g) at all stations (mean k= 0.16±0.05 d<sup>-1</sup>,  
43 g=0.36±0.09 d<sup>-1</sup>) in late summer. Despite its great potential as phytoplankton grazer,  
44 microzooplankton occurred at low biomass and showed little temporal variability, suggesting that it  
45 was controlled by copepod predation. Microzooplankton is a key component of the SO as an  
46 intermediate trophic level mediating carbon transfer from primary producers to higher trophic levels.

47  
48 **Keywords:** dinoflagellates; ciliates; microscopy, metabarcoding, dilution experiments, Southern  
49 Ocean

50

51 [1. Introduction](#)

52 Dinoflagellates (DIN) and ciliates (CIL) represent the most abundant microzooplankton groups in  
53 planktonic food webs, where they play a pivotal role as phytoplankton consumers, food source for  
54 mesozooplankton and contributors to nutrient remineralization (e.g. [Calbet and Landry 2004](#); [Irigoien  
55 et al. 2005](#); [Sherr and Sherr 2007](#); [2009](#), [Caron and Hutchins 2013](#); [Steinberg and Landry 2017](#) and  
56 references therein). The proportion of carbon produced by the phytoplankton that is ingested by  
57 microzooplankton is highly variable and can exceed mesozooplankton consumption (e.g.. [Calbet and  
58 Landry 2004](#), [Schmoker et al. 2013](#); [Menden-Deuer et al. 2018](#)). Microzooplankton is able to closely  
59 track phytoplankton temporal dynamics because they overall share similar growth rates. Blooms, thus  
60 occur when particular phytoplankton taxa succeed to escape microzooplankton control ([Irigoien et al.  
61 2005](#); [Sherr and Sherr, 2009](#)). At a global scale, predatory protists and phytoplankton biomasses  
62 display a curvilinear relationship and the plateau observed at about  $50 \mu\text{g C L}^{-1}$  for phytoplankton has  
63 been attributed to predation by mesozooplankton ([Irigoien et al. 2005](#)). In fact, mesozooplankton  
64 preferentially grazes on microzooplankton (e.g. [Stoecker and Capuzzo 1990](#); [Kiorboe and Wisser  
65 1999](#); [Calbet and Saiz, 2005](#); [Vargas and Gonzalez 2004](#); [Campbell et al. 2009](#); [Sherr and Sherr  
66 2009](#)), releasing predation pressure on phytoplankton and favoring its blooming capacity (e.g.  
67 [Grattepanche et al. 2011a](#)). Due to the central position of microzooplankton in aquatic food webs and  
68 the direct interaction with primary producers, any change in its community structure and activity can  
69 have marked implications for multiple trophic levels and carbon export. A modeling study suggested  
70 that ocean warming will alter phytoplankton-microzooplankton equilibrium by enhancing loss of  
71 primary production to microzooplankton herbivory in chlorophyll rich waters ([Chen et al. 2012](#)).  
72 Theoretically, the trophic transfer of carbon produced by phytoplankton through microzooplankton  
73 rather than directly via mesozooplankton predation would result in lower C-export ([Hall and Safi  
74 2001](#); [Smetacek et al. 2004](#)). Despite several centuries of studies on protists, untangling the impact on  
75 carbon transfer of heterotrophic protists in plankton communities remains challenging due to their

76 fragility, lack of direct methods to accurately measure their growth rate, and time-consuming  
77 identification and counting (reviewed in [Caron et al. 2009; 2012; Caron and Hutchins 2013](#))

78 In the Southern Ocean (SO), diatoms and haptophytes are usually identified as the major primary  
79 producers and their diversity and role in the C-cycle have been described in detail in previous studies  
80 (e.g. [Smetacek et al. 2004; Poulton et al. 2007; Armand et al. 2008; Queguiner 2013; Wolf et al. 2014,](#)  
81 [Lasbleiz et al. 2016, Irion et al. 2020](#) among many others). By contrast, microbial heterotrophes and,  
82 in particular, phytoplankton predators, have been far less investigated ([Caron et al. 2000; Hall and](#)  
83 [Safi 2001; Saito et al. 2005; Henzes et al. 2007; Christaki et al. 2008; Poulton 2007, Christaki et al.](#)  
84 [2015](#)). In the SO, Kerguelen and Crozet islands are characterized by iron enrichment of surface  
85 waters. This results in large phytoplankton blooms in these waters that contrast with the surrounding  
86 HNLC (High Nutrients Low Chlorophyll) conditions ([Blain et al. 2007; Pollard et al. 2007, 2009](#)).  
87 The rare studies that provide information on microzooplankton community structure in the Crozet  
88 and Kerguelen areas reported a prevalence of DIN over CIL biomass ([Poulton 2007, Christaki et al.](#)  
89 [2015](#)). Microzooplankton was identified as a major consumer of phytoplankton during the onset and  
90 decline of the Kerguelen blooms ([Brussaard et al. 2008; Christaki et al. 2015](#)) and an important  
91 player in iron regeneration ([Sarhou et al. 2008](#)).

92 The present study was realized in the framework of the MOBYDICK project (Marine Ecosystem  
93 Biodiversity and Dynamics of Carbon around Kerguelen: an integrated view). MOBYDICK's aim  
94 was to trace C from its biological fixation and cycling within and across trophic levels at surface, as  
95 well as its export to depth under different productivity regimes of the Southern Ocean after the  
96 phytoplankton bloom, in late summer. The objective of this study was to provide information about  
97 the diversity and the community structure of microzooplankton (DIN and CIL) in relation to  
98 phytoplankton communities and to estimate their potential capacity for channeling carbon to higher  
99 trophic levels. The results obtained during the post-bloom period (MOBYDICK cruise) are discussed  
100 here along with observations from the onset-of a previous bloom (KEOPS2 cruise).

## 101 2. Material and Methods

### 102 2.1 Study site, Sample collection

103 The MOBYDICK cruise took place during the late Austral summer (from 19 February to 20 March  
104 2018), where samples were collected at four stations (M1, M2, M3, and M4. [Figure 1](#)). Station M2,  
105 above the Kerguelen plateau, was located in naturally iron-fertilized waters ([Blain et al. 2007](#)),  
106 characterized by intense phytoplankton blooms during spring and summer (e.g. [Mosseri et al. 2008](#);  
107 [Cavagna et al. 2014](#)). Stations M1, M3, and M4, situated off-plateau, were in an oceanic area of  
108 HNLC (High-nutrient, low-chlorophyll) waters ([Cavagna et al. 2015](#)). The sampling strategy  
109 included repeated visits at the different stations. Station M2 was sampled three-times at eight day  
110 intervals (M2-1, M2-2, and M2-3); stations M3 and M4 were sampled twice with two-week intervals  
111 (M3-1, M3-3, M4-1, and M4-2); and station M1 was sampled just once ([Table 1](#)). Samples were  
112 collected with 12L Niskin bottles mounted on a rosette equipped with CTD (SeaBird 911-plus).  
113 Pigments were analyzed using High Performance Liquid Chromatography (HPLC, [Ras et al. 2008](#)).  
114 CHEMTAX analysis was performed with CHEMTAX v1.95 ([Mackey et al. 1996](#)) to estimate the  
115 pigment:Chl *a* ratios for seven major phytoplanktonic groups: chlorophytes, prasinophytes,  
116 cyanobacteria, cryptophytes, diatoms, dinoflagellates, and haptophytes (detailed in [Irion et al. 2020](#)).  
117 Pigments and microzooplankton data (see below) from the onset of the bloom (early spring, October-  
118 November 2011, KEOPS2 cruise, [Georges et al. 2014](#), [Christaki et al. 2015](#)) were included here for  
119 comparison with post-bloom MOBYDICK period (this study); KEOPS2 pigments were analyzed  
120 with CHEMTAX as described above.

121

### 122 2.2 Molecular analysis

123 Water samples were collected at all stations (M1, M2, M3, and M4) at four depths (15 m, 60 m,  
124 125 m, and 300 m). The depths were chosen to correspond to the surface and the bottom of the mixed

125 layer (ML), the transition between surface and deeper waters (125 m), and the deep nutrient rich  
126 waters (300m). After pre-filtering through 100µm mesh to remove most of the metazoans, ten liters of  
127 seawater from each depth were filtered successively through 20µm and 0.2µm using a peristaltic  
128 pump ('large' and 'small' size fractions, respectively). Filters were stored at -80°C until DNA  
129 extraction. The extraction, PCR procedure, and downstream analysis are described in detail in  
130 [Sassenhagen et al. \(2020\)](#). Briefly, extraction was realized with PowerSoil DNA Isolation Kit  
131 (QIAGEN, Germany) following standard manufacturer's protocol. The 18S rDNA V4 region was  
132 amplified using EK-565F (5'-GCAGTTAAAAGCTCGTAGT) and UNonMet (5'-  
133 TTTAAGTTTCAGCCTTGCG) primers ([Bower et al. 2004](#)). Libraries were paired-end (2 x 300bp)  
134 Illumina MiSeq sequenced. The forward and reverse reads were demultiplexed using Qiime1 pipeline  
135 ([Caporaso et al. 2010](#)). The reads were further trimmed and filtered in the *R*-package DADA2  
136 ([Callahan et al. 2016](#)). The same package was used for identification of amplicon sequencing variants  
137 (ASV) and their taxonomical assignment based on the PR<sup>2</sup> database ([Guillou et al. 2013](#)). ASVs  
138 affiliated to Metazoa, Streptophyta, as well as rare ones with less than 15 reads in the whole data set,  
139 were removed with the *R*-package 'phyloseq' ([McMurdie and Holmes 2013](#)).

140 To investigate the phylogenetic relationship between the observed genera, the sequences generated in  
141 this study and additional sequences from the Genbank database were aligned using the software  
142 muscle 3.8.31 ([Edgar, 2004](#)) with default settings. The alignments were trimmed with the software  
143 trimAl v1.2 ([Capella-Gutiérrez et al. 2009](#)) applying a gap threshold of 0.6. Maximum likelihood  
144 trees were separately build for DIN and CIL with the software RAxML version 8.2.12 ([Stamatakis,](#)  
145 [2014](#)) using the substitution model "GTRCAT". The RAxML settings included rapid bootstrap  
146 analysis, while the number of distinct starting trees was based on bootstrapping criteria. The tree was  
147 visualized with the online application iTOL ([Letunic and Bork, 2016](#)).

148

149 2.3 Microscopic analysis

150 At each station, microzooplankton samples were taken from 10 to 12 depths between the surface and  
151 300m. Sample volume was 500ml from surface to 200m, and 1L at 300m. Samples were fixed with  
152 acid Lugol's solution (2% v/v). All samples were kept at 4°C in the dark until microscopy analysis.  
153 In the laboratory, samples were left to settle in graduated cylinders for four days, then the 100 ml  
154 bottom of each sample was transferred into settling chambers and left to settle for another 24h before  
155 examination under an inverted microscope (Nikon Eclipse TE2000-S; x400). DIN and CIL were  
156 identified based on their morphology at the lowest possible taxonomic level following (Tomas, 1997;  
157 McMinn and Scot 2005; Kofoid and Campbell, 1929; Schiller, 1931-1937; Petz, 2005; Hoppenrath *et*  
158 *al.* 2009, Georges *et al.* 2014). DIN and CIL were also classified into six size classes (<20, 20–40,  
159 40-60, 60-80, 80-100, and >100  $\mu\text{m}$ ). Linear dimensions were measured at x400 magnification using  
160 an image analyzer with a camera mounted on the microscope. Biovolume measurements were  
161 converted into biomass using a conversion factor of 190 fg C  $\mu\text{m}^{-3}$  (Putt and Stoecker, 1989) and  
162  $0.760 \times \text{volume}^{0.819}$  pg C  $\mu\text{m}^{-3}$ , respectively (Menden-Deuer and Lessard 2000).

163 2.4 Microzooplankton herbivory via dilution experiments

164 Dilution experiments were conducted at all stations following the protocol of Landry and Hassett  
165 (1982). However, due to a change in shipboard operational procedure at station M3-3, a significant  
166 increase in incubator water temperature occurred. Although samples were analyzed, (phytoplankton  
167 growth almost doubled while grazing remained of the same levels) the results are not been be  
168 presented here. Fifty liters of seawater were collected at 10-20m depth with Niskin bottles and gently  
169 screened through a 200 $\mu\text{m}$  sieve to remove metazoans. Twenty liters of 0.2  $\mu\text{m}$  filtered seawater  
170 (FSW) were prepared through low-pressure filtration (<50 mm Hg). Five different concentrations  
171 (10%, 25%, 50%, 75%, and 100%) were prepared by mixing <200 $\mu\text{m}$  and <0.2 $\mu\text{m}$  filtered seawater.  
172 For each treatment, three 2.4L polycarbonate bottles were filled to the rim by gently siphoning from

173 the carboys. All 15 bottles were incubated for 24h in an on-deck incubator connected to the flow-  
174 through sea surface-water system and covered with a lid that let 25% of PAR light through  
175 (equivalent light condition to in situ surface waters). Additionally, 2.4L were set aside for immediate  
176 sampling at T0. For Chl *a* measurement at the end of the incubation, 500-700ml from each bottle  
177 were filtered onto 0.2µm polycarbonate filters (ø 47mm). After filtration, each filter was placed into  
178 2ml cryotubes, flash frozen in liquid nitrogen and stored at -80°C. Chl *a* concentrations were  
179 estimated by fluorometry (Lorenzen, 1966). Filters were extracted overnight in 90% acetone at 4 °C.  
180 At the end of the extraction period, Chl *a* concentration was determined using a calibrated Turner  
181 Trilogy© fluorometer. Initial Chl *a* concentration for each dilution treatment was estimated by  
182 multiplying initial whole seawater Chl *a* concentrations by corresponding dilution factors. Assuming a  
183 phytoplankton exponential growth, Changes in Chl *a* concentration over the experiment were used to  
184 calculate the instantaneous phytoplankton growth ( $k$ ,  $d^{-1}$ ), and grazing mortality ( $g$ ,  $d^{-1}$ , [Landry and](#)  
185 [Hasset 1982, Figure A1](#)). Grazing pressure (% Chl *a* production  $d^{-1}$ ) has been calculated as the ratio  
186 between phytoplankton daily production ( $\mu g$  Chl *a*  $L^{-1} d^{-1}$ ) and microzooplankton daily consumption  
187 ( $\mu g$  Chl *a*  $L^{-1} d^{-1}$ ).

## 188 2.5 Data analysis

189 Co-inertia analysis (PCA-PCA COIA) was used to investigate the coupling between phytoplankton  
190 pigments and CIL and DIN communities ([Dolédéc and Chessel 1994](#), [Dray et al. 2003](#)). The  
191 abundances obtained through microscopic counts of the 16 most abundant genera (8 DIN and 8 CIL),  
192 representing >90 % of total abundance at each station were used. COIA consists in finding co-inertia  
193 axes by maximizing the covariance between the row coordinates of two matrices. It defines axes that  
194 simultaneously explain the highest possible variance in each of the two matrices and describes their  
195 closest possible common structure. A PCA (principal component analysis) was performed on each  
196 matrix prior to applying a COIA analysis ([Dray et al. 2003](#)). For PCA analysis, variables were  
197 standardized and PCA was performed using the R-package FactoMineR ([Lê et al. 2008](#)). COIA was



198 carried out with the ‘ade4’ package in R-software (Dray and Dufour 2007). To estimate the strength  
199 of the coupling between the two matrices, a multidimensional correlation coefficient (RV) was  
200 calculated, and statistical significance was tested using a Monte Carlo permutation procedure with  
201 1000 permutations. Finally, in order to define the variables that were the most important in  
202 structuring the COIA scatterplot, Pearson’s correlation coefficients were calculated between all  
203 variables and COIA coordinates. All statistical analyses were based on abundances from  
204 microscopical counts to avoid the biases of the sequencing data (see results and discussion sections).

205

### 206 3. Results

#### 207 3.1 Environmental Conditions and Phytoplankton composition

208 The four stations sampled during MOBYDICK were situated in different hydrological conditions.  
209 Station M1, which was situated in Antarctic waters and influenced by the polar front, was  
210 characterized by a shallow  $Z_{ML}$  (27 m, Table 1, Figs. 1 and 2). Stations M2 and M4, which were  
211 situated south of the polar front in Antarctic waters, presented a characteristic temperature minimum  
212 at 200m and showed the lowest surface temperature (at M4: 4.5°C) (Table 1, Figs. 1 and 2). Station  
213 M3, which was situated in sub-Antarctic waters (SAZ), showed the highest temperature in the ML  
214 (5.6° C, Table 1). The  $Z_{ML}$  deepened at all stations following a storm on the 10<sup>th</sup> of March 2018.  
215 Phosphate and nitrate concentrations were high at all stations while silicic acid was overall higher  
216 off-plateau (Table 1). For comparison with early spring (KEOPS2 cruise), stations A3 (on-plateau)  
217 and R (defined as the reference station off-plateau) are also shown in Fig. 1 and Table 1. Briefly, A3-  
218 1 was sampled in late October, just before the initiation of the bloom. A3-2 was explored about 3.5  
219 weeks later, during the onset of the bloom. During early spring, the  $Z_{ML}$  at these stations was >100m  
220 (Table 1, Christaki et al. 2014). During MOBYDICK, Chl a in the  $Z_{ML}$  doubled between the first and  
221 the third visit at M2 (from 0.27 to 0.58  $\mu\text{g L}^{-1}$ ). Chl a at the off-plateau stations ranged between 0.14  
222 and 0.35 (M3-3 and M1, respectively (Table 1, Fig. 1). The concentrations of group pigment

223 signatures analyzed with CHEMTAX illustrated the phytoplankton community structure. Diatoms  
224 and prymnesiophytes were always the two major groups. Their respective proportions varied between  
225 seasons (early spring or late summer) and positions (on- or off-plateau). Diatoms were dominating  
226 during early spring (74-94% of total Chl a in on-plateau water; Fig. 3a, b) while Prymnesiophytes  
227 were the most abundant phytoplankton group during late summer (37-53% and 59-70% of total Chl a  
228 in on- and off-plateau, respectively ; Fig. 3a, b). The third group contributing most to the  
229 phytoplankton biomass were pico- planktonic Prasinophytes that accounted for up to 21 % of Chl a  
230 during early spring in HNLC waters (R-2) and up-to 16.5 % of Chl a on the plateau during late  
231 summer (M2-3).

### 232 3.2 Microzooplankton communities

#### 233 3.2.1. Abundance, biomass distributions and morphological diversity

234 During MOBYDICK, microscopical observations allowed the identification, size measurement, and  
235 biomass estimation of dinoflagellates (DIN) and ciliates (CIL) (Fig. 4 a-f). Mean integrated  
236 abundance in the mixed layer showed that DIN were from 3 to 6 fold more abundant than CIL in the  
237 ML and varied between  $0.29$  and  $2.3 \times 10^3$  and  $0.28$  to  $0.45 \times 10^3$  cells  $L^{-1}$  for DIN and CIL,  
238 respectively (Fig. 4 a, c). During late summer, DIN were largely dominated by the  $<20 \mu m$  size  
239 fraction (63-85 % Fig. 4b) while CIL were mostly represented by the 20-40 and  $\mu m <20 \mu m$  size  
240 fractions (mean 50 and 32%, respectively, Fig. 4d). The biomass of DIN also prevailed by factors of  
241 1.3-2.3 at five out of the eight stations. DIN and CIL had, however, equal biomasses at M2-2, M1,  
242 and M3-3 (Fig. 4 e, f). The DIN+CIL biomass was slightly higher at M2 (mean  $3.5 \pm 0.2 \mu g L^{-1}$ ) than  
243 off-plateau ( $2.2 \pm 0.3 \mu g L^{-1}$ , Fig. 4e). The vertical profiles did not show any noticeable evolution  
244 over time at M2 or at the other stations (Fig. 5). A total of 40 morphotypes of DIN and CIL were  
245 identified by microscopy at the highest possible taxonomic level. The 23 identified DIN-morphotypes  
246 belonged to 13 genera. The genus *Gymnodinium* ( $<20\mu m$  in size) was the most abundant DIN and

247 largely prevailed at all stations (Fig. 6a). Other small sized DIN such as *Scripsiella*, *Prorocentrum*  
248 *compressum*, and *Amphidinium* were present and abundant at all stations. The larger size classes were  
249 represented by *Tripos* and *Dinophysis*, while a variety of *Protoperidinium* morphotypes belonged to  
250 small and larger size classes. As for abundance and biomass, DIN richness and community structure  
251 were similar at all stations on- and off-plateau (Fig. 6a). The 13 CIL-morphotypes covered 11 genera.  
252 *Lohmaniella oviformis* (<20µm in size) was the most abundant CIL at all stations, with the exception  
253 of M3 where the tintinnid *Cymatocylis antarctica* prevailed (Fig. 6b, Table 2). *Leegariella*,  
254 *Codoneopsis soyai*, *Salpingella acuminata*, and *Myrionecta* were present at all stations at variable  
255 low abundances. Finally, the large mixotrophic *Laboea* was relatively abundant during the last two  
256 visits at M2, while it was rare at the other stations (Fig. 6b)

### 257 3.2.2 Molecular diversity vs morphological diversity.

258 Heatmaps illustrating sequencing richness and abundance of DIN and CIL are presented on Figure  
259 6c, d. After downstream analysis and elimination of a few symbionts and parasites (e.g. *Blastodinium*  
260 and *Chytriodinium*), the class Dinophyceae was represented by 31 ASVs. (Fig. c). ASVs affiliated to  
261 *Tripos* were the most abundant ASVs among those affiliated to DIN (% of reads) in the large size  
262 fraction. In the small size fraction, *Tripos* and *Gymnodinium* ASVs were more or less equally  
263 represented (Fig. 6c). As in microscopy data, *Gyrodinium* and *Prorocentrum* were also among the  
264 most abundant in terms of proportions of reads. However, *Scripsiella* and *Amphidinium*, which were  
265 abundant in microscopy, were not found in sequencing data (Fig. 6a, c). A maximum likelihood tree  
266 (Fig. 7a) was constructed in order to visualize the relatedness of taxa identified by microscopy and  
267 sequencing. Besides sequences generated in this study, additional sequences from the Genbank  
268 database corresponding to missing genera observed only by microscopy (e.g. *Amphidinium* and  
269 *Scripsiella*) were included. The DIN genera *Oxytoxum* and *Katodinium*, which were observed by  
270 microscopy, were not represented by sequences in the Genbank or in the PR<sup>2</sup> (Guillou et al. 2012)  
271 databases. They were therefore not included in the tree (Fig. 7a). Most DIN genera in the maximum

272 likelihood tree did not cluster by order, which was especially evident for Gymnodiniales and  
273 Peridinales (Fig. 7a). The abundance ranking of taxa differed between sequencing and microscopy  
274 (Fig. 6a,c).

275 The ciliate ASVs were grouped into 40 approximate genera with often uncertain taxonomic  
276 affiliations below the class or order level (Fig. d). The maximum likelihood tree for CIL included  
277 sequences from this study and additional sequences from the Genbank database corresponding to  
278 missing genera observed only by microscopy (*Myrionecta*, *Scuticociliatia*, and *Laboea*). The CIL  
279 maximum likelyhood tree was better resolved than the tree for the DIN with almost all genera  
280 clustering by order. The microscopically observed CIL *Codoneopsis* and *Lohmaniella*, *L. oviformis*  
281 being the most abundant taxa based on microscopy, were lacking from the tree since they were not  
282 represented by sequences in public databases (Fig. 7b). At M3-1 and M3-3 an ASV affiliated to  
283 the tintinnid family Xystonellidae prevailed in the large size fraction (20-100  $\mu\text{m}$ ) while *Cymatocylis*  
284 *calyciformis* was the most abundant tintinnid in the microscopy dataset (Fig. 6 c, d). *Myrionecta* is a  
285 cosmopolitan CIL characterized by a particular morphology and also several morphotypes grouped  
286 into “scuticociliates” were observed by microscopy but were not retrieved in by sequencing.

### 287 3.3 Microzooplankton relation with pigment signatures.

288 COIA analysis was applied to test for spatiotemporal relation in DIN+CIL community composition  
289 and phytoplankton pigments (Fig. 8a-e). Hierarchical clustering and PCA of DIN+CIL abundances  
290 applied as the first step of the COIA analysis revealed that the on- and off- plateau MOBYDICK  
291 stations grouped together (Fig. 8a, c). A3-1, sampled in early spring before the onset of the bloom,  
292 grouped with the reference HNLC station (R, sampled during the same cruise), while A3-2 was  
293 highly differentiated from all stations in the PCA (Fig. 8a, c). In fact, PCA suggested that station A3-  
294 2 was characterized by the presence of the diatom consumers *Gyrodinium* and *Protoperidinium*. In  
295 contrast, all MOBYDICK stations were featuring *Gymnodinium*, *Leegardiella*, *Lohmaniella*,

296 *Scripsiella* and Tintinnids (Fig. 8c). Hierarchical clustering and PCA realized on pigment data  
297 indicated similar phytoplankton communities at off-plateau stations during the MOBYDICK cruise.  
298 The PCA highlighted a gradual change in pigment signature during the three visits at M2 related to  
299 an increase in prasinophyte pigment concentrations. The station A3 was uniquely characterized by  
300 high concentrations of diatom pigments and Chl *a* (Fig. 8b, d see also Fig. 3). The COIA  
301 multidimensional correlation coefficient (RV) used to estimate the strength of coupling between the  
302 pigment concentration and microzooplankton abundance was significant (RV= 0.602, p=0.005) and  
303 the first two axes explained 85.65 % of the projected variance (Fig. 8e). All the pigments showed  
304 significant correlations (p <0.05, Table A1) with at least one of the three first axes, while ten out of  
305 the sixteen genera used for the analysis showed significant correlations : *Gymnodinium*, *Gyrodinium*,  
306 *Scripsiella*, *Amphidinium*, *Tripos*, *Lohmaniella*, *Strombidium*, *Leegaardiella*, *Salpingella*, and  
307 *Myrionecta* (Table A1). The COIA scatterplot indicated the station position relative to their DIN, CIL  
308 and pigment variables. On the COIA scatterplot MOBYDICK off-plateau stations formed one group  
309 with M1 being slightly differentiated potentially due to the influence from the polar front. The  
310 position of station M1 also changed most between the two PCA-Biplots, as its microzooplankton  
311 community strongly resembled the communities at the other off-plateau stations, while its pigment  
312 signature was more similar to station M2-2. The first two visits at M2 were close together, while M2-  
313 3 was closer to the early spring reference station R, with which it shared a stronger prasinophyte  
314 signature. Station A3-2, uniquely representing typical bloom conditions with high diatom pigments  
315 and microphytoplankton grazers, was far apart from the other stations in this plot (Fig. 8e).

316

### 317 3.4 Microzooplankton herbivory via dilution experiments

318 In situ (10-20m depth) Chl *a* concentration measured at the beginning of the dilution experiment  
319 varied from 0.20 to 0.64  $\mu\text{g Chl } a \text{ L}^{-1}$  (M3-1 and M2-3, respectively). Dilution derived phytoplankton  
320 growth (*k*) and microzooplankton grazing (*g*) were significant at all stations (Table 2, Fig. A1).

321 Phytoplankton growth rate ( $k$ ) ranged from  $0.08 \pm 0.03 \text{ d}^{-1}$  at M4-1 to  $0.26 \pm 0.03 \text{ d}^{-1}$  at M2-3.  
322 Minimum microzooplankton grazing rates ( $g$ ) were measured at station M1 ( $0.28 \pm 0.03 \text{ d}^{-1}$ ) and the  
323 maximum value was at station M2-3 ( $0.52 \pm 0.05 \text{ d}^{-1}$ ). Phytoplankton mortality due to  
324 microzooplankton grazing was always higher than phytoplankton growth since it represented from  
325 130 to 428% of phytoplankton daily production at M1 and M4-1, respectively. Overall,  
326 phytoplankton growth rate increased at station M2 ( $0.13 \pm 0.03$  to  $0.26 \pm 0.03 \text{ d}^{-1}$ ) along with  
327 microzooplankton grazing ( $0.34 \pm 0.05$  to  $0.52 \pm 0.05 \text{ d}^{-1}$ , [Table 2](#)).

## 328 [4. Discussion](#)

### 329 4.1 Microzooplankton diversity, microscopy vs sequencing

330 Massive sequencing technologies such as Illumina MiSeq sequencing gain *in momentum* (e.g.  
331 [Pawlowski et al. 2012](#)) and are currently used to describe global patterns of plankton and even predict  
332 carbon export (e.g. [Guidi et al. 2016](#), [Obiol et al. 2020](#), among many others). The recent ASV  
333 approach is supposed to provide a more accurate image of the diversity by avoiding artificial  
334 similarity thresholds. Nevertheless, organisms differing by a few base pairs in their rDNA can belong  
335 to very different taxa and the threshold of differences in the rDNA sequence between species differs  
336 greatly from one taxonomic group to another one because of their evolution rate for example.  
337 Defining accurate taxonomy level based on the sequencing of rDNA remain a critical issue in  
338 microbial diversity investigations. In-depth sequencing and microscopical approaches are rarely  
339 confronted although they both 'miss' or 'misidentify' taxa due to the diverse biases inherent to each  
340 method (e.g. [Medinger et al. 2010](#); [Bachy et al. 2012](#); [Monchy et al. 2012](#); [Chavret et al. 2012](#); [Stern](#)  
341 [et al. 2018](#) and references therein). We thus address herein this crucial aspect by combining high  
342 throughput sequencing with microscopic observations to assess DIN and CIL diversity. Although  
343 microscopy and sequencing heatmaps ([Fig. 6a-d](#)) cannot be directly compared (different size  
344 fractions and water volumes analyzed for the two approaches), the diversity and abundance data  
345 obtained by the two approaches deserve to be discussed to understand whether these results are

346 conflicting or complementary. DIN were represented by 23 morphospecies in microscopy and 31  
347 ASVs in sequencing data. Microscopical identification of dinoflagellates based on broad  
348 morphological features is challenging. On the other hand, amplicon sequencing does not provide  
349 accurate taxonomic resolution because of the lack of cultured representatives to provide a detailed  
350 phylogeny. This is for example the case for dinoflagellate taxa that are under-represented in  
351 databases, resulting in approximate taxonomic identifications of sequences and diversity estimations  
352 (e.g. Bik et al. 2012). Most DIN genera did not cluster by order in the topologic tree, which was  
353 especially evident for Gymnodiniales and Peridinales (Fig. 7a). This insufficient resolution of DIN  
354 phylogeny might be due to the limited length and low variability of the V3-V4 region in the 18S  
355 rDNA (Daugbjerg et al. 2000; Mordret et al. 2018). A relatively good ‘correspondence’ was found  
356 between the two data sets in terms of diversity, but often at a higher taxonomic level, either at the  
357 family or order level (Fig. 6a, c). For example, the second most abundant genus found in microscopy  
358 identified as *Scrippsiella* was probably represented by the family level Thoracosphaeracea in  
359 sequencing data (Fig. 6a, c). However, no potential ‘relative’ for *Amphidinium* could be found in  
360 sequencing data (Fig. 7a). Sequencing complemented microscopy data in terms of diversity. Because  
361 the sample volume analyzed for microscopy counts is relatively limited, in contrast to the sequencing  
362 approach, low abundant taxa may not be observed by microscopy despite their characteristic  
363 morphological features. This was likely the case for the genus *Ornithocercus* (ASV 508) that was  
364 also retrieved in the vertically integrated plankton-net samples, where very large volumes of water  
365 were sampled (Karine Leblanc, <https://plankton.mio.osupytheas.fr/mobydick-other-microplankton/>).  
366 In addition, taxa relative abundance differed among sequencing and microscopy. It is well established  
367 that DIN are over-represented in sequencing data (e.g. Georges et al. 2014 and references therein).  
368 The dominance of *Tripos* in sequencing data -even in the small fraction- (Fig. 6c) highlighted that,  
369 even within the DIN population, specific taxa can be over-represented. As a consequence, using

370 relative abundances of DIN based on sequence data in numerical analysis and/or description of  
371 community structure might lead to biases.

372 CIL were represented by 17 morphospecies in microscopy and 40 genera in sequencing data. The  
373 difficulty to accurately identify CIL based on broad morphology is exacerbated by the distortion of  
374 soft CIL due to chemical fixation. Only tintinnids having a lorica preserve most of their features (e.g.  
375 [Dolan et al. 2012](#)). As for DIN, comparison of sequencing and microscopy data was challenging, in  
376 particular at the genus level, but could be attempted at higher taxonomic levels. Although, the CIL  
377 maximum likelihood tree had a better resolution than the topology of DIN, CIL sequencing and  
378 microscopy data could only be globally compared at a higher level than the DIN data (i.e. family,  
379 order, or class level). For example, *Lohmanniella oviformis*, which was the most abundant species in  
380 microscopy, was probably represented by *Leegardiella* in sequencing data (family Leegardiellidae,  
381 [Lynn and Montagnes, 1988](#)). *Strombidium* was the second most abundant genus in both data sets. At  
382 M3-1 and M3-3, the family Xystonellidae, order Tintinnida was prevailing in the large size fraction  
383 (20-100  $\mu\text{m}$ ) according to sequencing data. At the same stations, the dominant tintinnid in  
384 microscopy data was identified as *Cymatocylis calyciformis* that belongs to a different family  
385 (Ptychocylididae) but to the same order (Tintinnida) ([Fig. 6 b, d](#)). The organisms grouped into  
386 ‘scuticociliates’ in microscopy data probably belong to different families or classes. Within the CIL  
387 populations, there was no evidence of over-representation of specific taxa and the ranking of the  
388 different taxonomic groups obtained by sequencing corresponded more or less to the one by  
389 microscopy. The taxonomic resolution obtained by sequencing was lower than the one obtained by  
390 microscopy ([Fig. 6b, d](#)).

391 As a conclusion, applying both sequencing and microscopy analyses to DIN and CIL can  
392 complement and enrich our view on the population diversity. However, if available, microscopy  
393 based abundances seem more reliable for numeric analysis. Using DIN relative abundances (retrieved  
394 from sequencing data) for numerical analysis could lead to misinterpretations of the importance of



395 different taxa for ecosystem functioning. Therefore, morphological metadata can -and should- be  
396 collected parallel to sequencing of DIN and CIL.

#### 397 4.2 Late summer microzooplankton communities, relation to the phytoplankton

398 A first noteworthy observation during late summer was that DIN and CIL biomass was only about  
399 1.5 x higher on-plateau (M2) than off-plateau and that it showed little temporal variability (e.g. Fig.  
400 4). This observation contrasted with other components of the microbial food web that showed >2-3  
401 fold abundance and activity on the plateau and remained highly dynamic during the MOBYDICK  
402 cruise (Christaki et al. submitted). Microzooplankton community structures were expected to relate to  
403 shifts in phytoplankton community composition (e.g. Grattepanche et al. 2011a; Laurence and  
404 Menden-Deuer 2012). Chl a concentrations of  $\geq 0.6 \mu\text{g L}^{-1}$  in the ML of the SO are categorized as a  
405 phytoplankton-bloom situation, representing about two fold typical HNLC concentrations ( $\leq 0.3 \mu\text{g L}^{-1}$ )  
406 (Lasbleiz et al. 2016). During MOBYDICK, no phytoplankton bloom occurred, as indicated by the  
407 observed Chl a concentrations. However, Chl a concentrations showed temporal variability on the  
408 plateau, increasing by almost 2-fold and reaching  $0.58 \mu\text{g L}^{-1}$  during the third visit at M2 (Table 1).  
409 The COIA analysis showed that there was an overall significant relation between microzooplankton  
410 abundances and pigment concentrations ( $p=0.005$ , Fig. 8e). However, stations clustered differently  
411 based on pigment or microzooplankton data (Fig. 8a-d). The variability of the abundance of  
412 prasinophytes at M2, A3-1, R and the diatom increase at A3-2 were highlighted by the same analysis  
413 Fig. 8c, d). The correlation between DIN biomass and phytoplankton abundance was especially  
414 noticeable during the onset of the diatom bloom on the plateau (Lasbleiz et al. 2016, Figs. 3 and 8,  
415 KEOPS2). The abundance and biomass of DIN increased 8 and 7 fold, respectively, within 3.5 weeks  
416 between the visits at station A3. In particular, large dinoflagellates such as *Gyrodinium* (40-60  $\mu\text{m}$ ),  
417 *Amphidinium* (20-40 $\mu\text{m}$ ) and *Protoperidinium*, which feed on diatoms and can ingest prey cells of  
418 more than 10 x their own size (e.g. Saito et al. 2006, Grattepanche et al. 2011b), occurred in higher  
419 abundance after the intensification of the bloom (Figs. 6a, 8, Christaki et al. 2015).

420 During MOBYDICK a common feature of DIN and CIL communities was the relative importance of  
421 small cells (<40µm) which was particularly pronounced for DIN (Fig. 4b). Small sized *Gymnodinium*  
422 were the most abundant DIN taxa at all stations and during both seasons (<20µm, see also Christaki  
423 et al. 2015). *Gymnodinium* can grow in a wide range of environmental conditions due to two  
424 particular traits. Their mixotrophy allows them to switch between photosynthesis and grazing  
425 depending on present nutrient, prey and light conditions, while they can also feed on a wide range of  
426 prey (including other DIN, CIL, and bacteria)(e.g. Strom, 1991; Bockstalher and Coats, 1993; Sherr  
427 and Sherr, 2007; Sherr and Sherr, 2007; Jeong et al. 2010, 2018; Lee et al. 2014).

428 CIL abundances were considerably lower than those of DIN, the median for all stations and seasons  
429 being 350 and 1370 cells L<sup>-1</sup>, respectively (Figs. 4a,c, Fig. 5). DIN can graze on almost all planktonic  
430 organisms and are recognized as major microplankton predators (Sherr and Sherr, 2007). In contrast,  
431 naked CIL prefer prey of the 5-25 µm size-class (Hansen et al. 1994) and can also feed on bacteria  
432 (Sherr and Sherr, 1987; Christaki et al. 1998; 1999). The most abundant CIL during MOBYDICK  
433 was *Lohmaniella oviformis* belonging to the <20 µm size class. CIL abundances and biomasses were  
434 higher after the bloom than during the onset of the bloom. This pattern is likely related to the increase  
435 in abundance of their nanophytoplankton preys. However, while pico- and nanophytoplankton  
436 increased by about 15-fold between the onset and the post bloom periods in Kerguelen plateau waters  
437 (Christaki et al. 2014; Irion et al. 2020, CIL abundances increased only by about 1.4 and 2.5 on- and  
438 off-plateau, respectively (Fig. 6c). Also, during MOBYDICK, pico- and nanoplankton showed a 2.6-  
439 fold increase between the first and the third visit at M2 (Irion et al. 2020), while CIL slightly  
440 decreased (Fig. 4). The overall CIL abundance was always relatively low and never exceeded 450  
441 cells L<sup>-1</sup>. The absence of any clear relation between the abundances of CIL and their favorite preys  
442 was likely the result of the double top-down control on ciliates by both dinoflagellates and  
443 mesozooplankton (Calbet and Saiz, 2005; Franzé and Modigh, 2013). CIL have not been shown to  
444 effectively feed on large or chain-forming diatoms (Sherr and Sherr, 2007). Only tintinnid CIL can

445 feed on a large variety of small diatoms (Gowing and Garrison, 1992; Armbrecht et al. 2017). The  
446 tintinnids located in the Antarctic zone, delimited by the average location of the Polar Front, contain  
447 a large portion of wide-mouthed forms (Dolan et al. 2012). The ability of relatively large tintinnids in  
448 40-60  $\mu\text{m}$  and 60-100  $\mu\text{m}$  size-classes to ingest small diatoms is probably an advantage that allows  
449 them to form dense populations in SO (e.g. Alder and Boltovskoy 1991; Buck et al. 1992; Dolan et al.  
450 2012). Indeed, *Cymatocylis antarctica* was the second most abundant CIL and was particularly  
451 present at the HNLC M3-station where small diatoms (<20  $\mu\text{m}$ ) were also enhanced (*Fragilariopsis*,  
452 *Pseudo-nitzschia*, *Thalassiosira* and *Chaetoceros*, Irion et al. 2020).

#### 453 4.3 Potential role of Microzooplankton in carbon transfer in planktonic food webs

454 All existing methods assessing grazing are based on several assumptions and estimates. For example,  
455 dilution is a relatively simple method to estimate grazing rates based on phytoplankton growth in a  
456 gradient of grazing pressure. However, the main criticisms of the dilution method are its  
457 overestimation of grazing rates and its relative incapacity to detect very low grazing rates (e.g. Dolan  
458 et al. 2000; Dolan and McKeon 2005, Beckett and Weitz 2017). Indeed, dilution experiments may  
459 provide inconsistent abnormally for high and/or null grazing rates (e.g.. Calbet et al. 2011; Calbet and  
460 Saiz 2013). The phytoplankton growth rate ( $\mu$ ) and the microzooplankton grazing rate ( $g$ ) measured  
461 during MOBYDICK in the dilution experiments were within the range of previous studies in cold  
462 waters (e.g. Menden-Deuer et al. 2018; Schmoker et al. 2013 and references therein). Phytoplankton  
463 growth was lower than microzooplankton grazing at all stations (Table 2). In the Southern Ocean, the  
464 high variability of standing stock of phytoplankton grazed by microzooplankton ( from 0 to >100 %,   
465 median  $\approx$  50 %) remains mostly unexplained (Schmoker et al. 2013). Moreover, dilution results are  
466 rarely compared with *in situ* primary production measurements (e.g. Landry et al. 2016) and/or other  
467 measured fluxes (e.g. respiration, copepod consumption, and export). One question that needs to be  
468 addressed is, thus, the transfer of carbon to other components of the planktonic food web and  
469 exported to the ocean interior in the case microzooplankton processes >100 % of primary production.

470 During MOBIDICK and previous cruises during the onset and decline of the Kerguelen bloom  
471 (KEOPS2 and KEOPS 1, respectively), respiration measurements showed that community respiration  
472 accounted for about 20 to 90 % of the GCP, with heterotrophic bacteria processing large fractions of  
473 primary production in early spring (45%, [Christaki et al. 2014](#)) and in summer (100%, [Obernosterer  
474 et al. 2008](#)). This fraction substantially decreased in late summer (17%, [Christaki et al. submitted](#)).  
475 For comparison with dilution experiment results, the CD (Carbon Demand) of DIN and CIL as a  
476 proportion of GCP (Gross Community Production) was estimated based on their biomass stocks  
477 applying a conservative growth rate  $\mu = 0.2 \text{ d}^{-1}$  (e.g., [Bjørnsen and Kuparinen, 1991](#); [Verity et al.  
478 1993](#); [Neuer and Cowles, 1994](#); [Karayanni et al. 2008](#); [Rose et al. 2013](#)) and a growth efficiency (GE)  
479 of 30% (e.g. [Straile, 1997](#); [Strom, 1991](#); [Strom and Fredrickson, 2008](#)). According to these  
480 assumptions, the carbon demand of DIN and CIL accounted for 2 to 7 % of the GCP on- and off-  
481 plateau before and after the bloom. It was, however, considerably higher on the plateau during the  
482 onset of the bloom where it accounted for 18 % of the GCP (station A3-2, [Table 3](#)). The proportion  
483 of carbon corresponding to CD changed when NCP (Net Community Production) was taken into  
484 account due to the variability in DCR (Dark Community Respiration) among stations. Thus, the  
485 amount of NCP needed to cover the DIN+CIL carbon demand varied between 5-46 % ([Table 3](#)).  
486 These estimations should be considered also with caution since they are based on stocks and  
487 literature conversion factors. In addition, DIN+CIL do not graze exclusively on phytoplankton -  
488 intra-guild predation is common for these mixotrophic and heterotrophic organisms (e.g. [Franzé and  
489 Modigh 2013](#)).

490 Given all the above, we suggest that dilution grazing rates obtained here correspond to the maximum  
491 potential grazing rates under experimental conditions in the absence of higher trophic levels  
492 ([Schmoker et al. 2013](#)). Our results highlight the grazing potential of microzooplankton, suggesting  
493 that they could consume a substantial fraction of primary production and, in addition, have cascading  
494 effects on the whole trophic web if the top-down control on microzooplankton was reduced. After the

495 end of the bloom (MOBYDICK), the low nutritional quality of phytoplankton probably further  
496 enhanced top-down control on microzooplankton by copepods (Sherr et al. 2009; Tsuda et al. 2007).  
497 During MOBYDICK mesozooplankton abundance showed important variability (between 207 ind.  
498  $\text{m}^{-3}$  at M2-1 to 1636 ind.  $\text{m}^{-3}$  at M4-1, in particular at M2 where it showed 7-fold increase between  
499 the first and the second visit (1473 ind.  $\text{m}^{-3}$ ) at this station. However, grazing experiments showed  
500 insignificant grazing of copepods on phytoplankton and that their respiration requirements were  
501 never covered by phytoplankton ingestion (Delegrange et al. MOBYDICK data).  
502 Concluding, the present study provides two interesting observations: (i) dilution experiments  
503 indicated high microzooplankton grazing capacity on phytoplankton; and (ii) microzooplankton  
504 biomass remained low, suggesting a top-down feeding impact by copepods. We suggest that, DIN  
505 and CIL activities and thus their roles in the trophic web of surface SO waters are highly dynamic,  
506 however, this is not necessarily reflected in their stock variability. Microzooplankton cannot  
507 apparently prevent phytoplankton bloom initiations (Sherr and Sherr, 2009), likely due to substantial  
508 zooplankton predation on microzooplankton (Stoecker and Capuzzo, 1990). Our observations  
509 highlight the decoupling between microzooplankton stocks (abundance and biomass) and activities  
510 (C-transfer) in SO surface waters. Estimations of SO surface solely based on microzooplankton  
511 stocks will thus likely lead to uncorrect results. The strength of the microzooplankton-  
512 mesozooplankton relationship is rarely considered in plankton studies (e.g. Foreman et al. 1996;  
513 Calbet and Saiz, 2005) and typically neglected in the construction of carbon budgets. The question is  
514 therefore: How do we parametrize microzooplankton in ecosystem models? Strom and Fredrickson  
515 (2008) recommended to parametrize microzooplankton grazing as a ‘sometimes-on, frequently-off’  
516 response, rather than a low average. Microzooplankton biomass increase typically occur during brief  
517 periods of time -until copepod populations establish- as seen during the onset of the bloom when high  
518 DIN biomasses related to large diatom grazers were recorded on the plateau (Fig. 4, second visit at  
519 A3, Christaki et al. 2015). We suggest, that outside this period, when microzooplankton biomass

520 remains low, it continues to play a crucial role as they ‘repackage’ and ‘enrich’ phytoplankton carbon  
521 for higher trophic levels, and also contribute to nutrient and Fe regeneration (Sarhou et al. 2008).

522

523 **Acknowledgements** We thank B. Quéguiner, the PI of the MOBYDICK project, for providing us the  
524 opportunity to participate to this cruise, the captain and crew of the R/V Marion Dufresne for their  
525 enthusiasm and support aboard during the MOBYDICK–THEMISTO cruise  
526 (<https://doi.org/10.17600/18000403>) and the chief scientist I. Obernosterer. This work was supported  
527 by the French oceanographic fleet (“Flotte océanographique française”), the French ANR (“Agence  
528 Nationale de la Recherche”, AAPG 2017 program, MOBYDICK Project number: ANR-17-CE01-  
529 0013), and the French Research program of INSU-CNRS LEFE/CYBER (“Les enveloppes fluides et  
530 l’environnement” – “Cycles biogéochimiques, environnement et ressources”). This work was also  
531 supported by ULCO (Université du Littoral), CPER MARCO (<https://marco.univ-littoral.fr/>), the  
532 Region "Hauts de France" and CNRS LEFE-EC2CO through the project PLANKTON-PARTY. The  
533 authors clearly state there is no conflict of interests regarding this paper.

534

## 535 **References**

- 536 Alder, V.A., Boltovskoy, D., 1991. Microplanktonic distributional patterns west of the Antarctic  
537 Peninsula, with special emphasis on the Tintinnids. *Polar Biol* 11, 103–112.  
538 <https://doi.org/10.1007/BF00234272>
- 539 Armand, L.K., Cornet-Barthaux, V., Mosseri, J., Quéguiner, B., 2008. Late summer diatom biomass  
540 and community structure on and around the naturally iron-fertilised Kerguelen Plateau in the  
541 Southern Ocean. *Deep Sea Research Part II: Topical Studies in Oceanography* 55, 653–676.  
542 <https://doi.org/10.1016/j.dsr2.2007.12.031>
- 543 Armbrecht, L.H., Eriksen, R., Leventer, A., Armand, L.K., 2017. First observations of living sea-ice  
544 diatom agglomeration to tintinnid loricae in East Antarctica. *Journal of Plankton Research* 39,  
545 795–802. <https://doi.org/10.1093/plankt/fbx036>
- 546 Bachy, C., Dolan, J.R., López-García, P., Deschamps, P., Moreira, D., 2013. Accuracy of protist  
547 diversity assessments: morphology compared with cloning and direct pyrosequencing of 18S  
548 rRNA genes and ITS regions using the conspicuous tintinnid ciliates as a case study. *The*  
549 *ISME Journal* 7, 244–255. <https://doi.org/10.1038/ismej.2012.106>
- 550 Beckett, S.J., Weitz, J.S., 2017. Disentangling niche competition from grazing mortality in  
551 phytoplankton dilution experiments. *PLoS ONE* 12, e0177517.

552 <https://doi.org/10.1371/journal.pone.0177517>

553 Bik, H.M., Porazinska, D.L., Creer, S., Caporaso, J.G., Knight, R., Thomas, W.K., 2012. Sequencing  
554 our way towards understanding global eukaryotic biodiversity. *Trends in Ecology &*  
555 *Evolution* 27, 233–243. <https://doi.org/10.1016/j.tree.2011.11.010>

556 Bjørnsen, P.K., Kuparinen, J., 1991. Growth and herbivory by heterotrophic dinoflagellates in the  
557 Southern Ocean, studied by microcosm experiments. *Mar. Biol.* 109, 397–405.  
558 <https://doi.org/10.1007/BF01313505>

559 Blain, S., Quéguiner, B., Armand, L., Belviso, S., Bombled, B., Bopp, L., Bowie, A., Brunet, C.,  
560 Brussaard, C., Carlotti, F., Christaki, U., Corbière, A., Durand, I., Ebersbach, F., Fuda, J.-L.,  
561 Garcia, N., Gerringa, L., Griffiths, B., Guigue, C., Guillerm, C., Jacquet, S., Jeandel, C.,  
562 Laan, P., Lefèvre, D., Lo Monaco, C., Malits, A., Mosseri, J., Obernosterer, I., Park, Y.-H.,  
563 Picheral, M., Pondaven, P., Remenyi, T., Sandroni, V., Sarthou, G., Savoye, N., Scouarnec,  
564 L., Souhaut, M., Thuiller, D., Timmermans, K., Trull, T., Uitz, J., van Beek, P., Veldhuis, M.,  
565 Vincent, D., Viollier, E., Vong, L., Wagener, T., 2007. Effect of natural iron fertilization on  
566 carbon sequestration in the Southern Ocean. *Nature* 446, 1070–1074.  
567 <https://doi.org/10.1038/nature05700>

568 Blain, S., Capparos, J., Guéneuguès, A., Obernosterer, I., Oriol, L., 2015. Distributions and  
569 stoichiometry of dissolved nitrogen and phosphorus in the iron-fertilized region near  
570 Kerguelen (Southern Ocean). *Biogeosciences* 12, 623–635. [https://doi.org/10.5194/bg-12-](https://doi.org/10.5194/bg-12-623-2015)  
571 [623-2015](https://doi.org/10.5194/bg-12-623-2015)

572 Bockstahler, K.R., Coats, D.W., 1993. Grazing of the mixotrophic dinoflagellate *Gymnodinium*  
573 *sanguineum* on ciliate populations of Chesapeake Bay. *Marine Biology* 116, 477–487.  
574 <https://doi.org/10.1007/BF00350065>

575 Bower, S.M., Carnegie, R.B., Goh, B., Jones, S.R.M., Lowe, G.J., Mak, M.W.S., 2004. Preferential  
576 PCR Amplification of Parasitic Protistan Small Subunit rDNA from Metazoan Tissues. *J*  
577 *Eukaryotic Microbiology* 51, 325–332. <https://doi.org/10.1111/j.1550-7408.2004.tb00574.x>

578 Brussaard, C.P.D., Timmermans, K.R., Uitz, J., Veldhuis, M.J.W., 2008. Virioplankton dynamics and  
579 virally induced phytoplankton lysis versus microzooplankton grazing southeast of the  
580 Kerguelen (Southern Ocean) 14.

581 Buck, K.R., Garrison, D.L., Hopkins, T.L., 1992. Abundance and distribution of tintinnid ciliates in  
582 an ice edge zone during the austral autumn. *Antarctic science* 4, 3–8.  
583 <https://doi.org/10.1017/S0954102092000038>

584 Calbet, A., Landry, M.R., 2004. Phytoplankton growth, microzooplankton grazing, and carbon  
585 cycling in marine systems. *Limnol. Oceanogr.* 49, 51–57.  
586 <https://doi.org/10.4319/lo.2004.49.1.0051>

587 Calbet, A., Saiz, E., 2013. Effects of trophic cascades in dilution grazing experiments: from artificial  
588 saturated feeding responses to positive slopes. *Journal of Plankton Research* 35, 1183–1191.  
589 <https://doi.org/10.1093/plankt/fbt067>

590 Calbet, A., Saiz, E., 2005. The ciliate-copepod link in marine ecosystems. *Aquat. Microb. Ecol.* 38,  
591 157–167. <https://doi.org/10.3354/ame038157>

592 Calbet, A., Saiz, E., Almeda, R., Movilla, J.I., Alcaraz, M., 2011. Low microzooplankton grazing  
593 rates in the Arctic Ocean during a *Phaeocystis pouchetii* bloom (Summer 2007): fact or  
594 artifact of the dilution technique? *Journal of Plankton Research* 33, 687–701.  
595 <https://doi.org/10.1093/plankt/fbq142>

596 Calbet, A., Trepát, I., Almeda, R., Saló, V., Saiz, E., Movilla, J., Alcaraz, M., Yebra, L., Simó, R.,  
597 2008. Impact of micro- and nanograzers on phytoplankton assessed by standard and size-  
598 fractionated dilution grazing experiments. *Aquat. Microb. Ecol.* 50, 145–156.  
599 <https://doi.org/10.3354/ame01171>

600 Callahan, B.J., McMurdie, P.J., Rosen, M.J., Han, A.W., Johnson, A.J.A., Holmes, S.P., 2016.  
601 DADA2: High-resolution sample inference from Illumina amplicon data. *Nat Methods* 13,

581–583. <https://doi.org/10.1038/nmeth.3869>

602 Campbell, R.G., Sherr, E.B., Ashjian, C.J., Plourde, S., Sherr, B.F., Hill, V., Stockwell, D.A., 2009.  
603 Mesozooplankton prey preference and grazing impact in the western Arctic Ocean. *Deep Sea*  
604 *Research Part II: Topical Studies in Oceanography* 56, 1274–1289.  
605 <https://doi.org/10.1016/j.dsr2.2008.10.027>

606 Capella-Gutierrez, S., Silla-Martinez, J.M., Gabaldon, T., 2009. trimAl: a tool for automated  
607 alignment trimming in large-scale phylogenetic analyses. *Bioinformatics* 25, 1972–1973.  
608 <https://doi.org/10.1093/bioinformatics/btp348>

609 Caporaso, J.G., Kuczynski, J., Stombaugh, J., Bittinger, K., Bushman, F.D., Costello, E.K., Fierer,  
610 N., Peña, A.G., Goodrich, J.K., Gordon, J.I., Huttley, G.A., Kelley, S.T., Knights, D., Koenig,  
611 J.E., Ley, R.E., Lozupone, C.A., McDonald, D., Muegge, B.D., Pirrung, M., Reeder, J.,  
612 Sevinsky, J.R., Turnbaugh, P.J., Walters, W.A., Widmann, J., Yatsunencko, T., Zaneveld, J.,  
613 Knight, R., 2010. QIIME allows analysis of high-throughput community sequencing data. *Nat*  
614 *Methods* 7, 335–336. <https://doi.org/10.1038/nmeth.f.303>

615 Caron, D.A., Dennett, M.R., Lonsdale, D.J., Moran, D.M., Shalapyonok, L., 2000. Microzooplankton  
616 herbivory in the Ross Sea, Antarctica. *Deep Sea Research Part II: Topical Studies in*  
617 *Oceanography* 47, 3249–3272. [https://doi.org/10.1016/S0967-0645\(00\)00067-9](https://doi.org/10.1016/S0967-0645(00)00067-9)

618 Caron, D.A., Worden, A.Z., Countway, P.D., Demir, E., Heidelberg, K.B., 2009. Protists are  
619 microbes too: a perspective. *ISME J* 3, 4–12. <https://doi.org/10.1038/ismej.2008.101>

620 Caron, D.A., Countway, P.D., Jones, A.C., Kim, D.Y., Schnetzer, A., 2012. Marine Protistan  
621 Diversity. *Annu. Rev. Mar. Sci.* 4, 467–493. <https://doi.org/10.1146/annurev-marine-120709-142802>

622 Caron, D.A., Hutchins, D.A., 2013. The effects of changing climate on microzooplankton grazing  
623 and community structure: drivers, predictions and knowledge gaps. *Journal of Plankton*  
624 *Research* 35, 235–252. <https://doi.org/10.1093/plankt/fbs091>

625 Cavagna, A.J., Fripiat, F., Elskens, M., Dehairs, F., Mangion, P., Chirurgien, L., Closset, I., Lasbleiz,  
626 M., Flores–Leiva, L., Cardinal, D., Leblanc, K., Fernandez, C., Lefèvre, D., Oriol, L., Blain,  
627 S., Quéguiner, B., 2014. Biological productivity regime and associated N cycling in the  
628 vicinity of Kerguelen Island area, Southern Ocean. *Biogeosciences Discuss.* 11, 18073–  
629 18104. <https://doi.org/10.5194/bgd-11-18073-2014>

630 Cavagna, A.J., Fripiat, F., Elskens, M., Mangion, P., Chirurgien, L., Closset, I., Lasbleiz, M., Florez-  
631 Leiva, L., Cardinal, D., Leblanc, K., Fernandez, C., Lefèvre, D., Oriol, L., Blain, S.,  
632 Quéguiner, B., Dehairs, F., 2015. Production regime and associated N cycling in the vicinity  
633 of Kerguelen Island, Southern Ocean. *Biogeosciences* 12, 6515–6528.  
634 <https://doi.org/10.5194/bg-12-6515-2015>

635 Charvet, S., Vincent, W.F., Lovejoy, C., 2012. Chrysophytes and other protists in High Arctic lakes:  
636 molecular gene surveys, pigment signatures and microscopy. *Polar Biol* 35, 733–748.  
637 <https://doi.org/10.1007/s00300-011-1118-7>

638 Chen, B., Landry, M.R., Huang, B., Liu, H., 2012. Does warming enhance the effect of  
639 microzooplankton grazing on marine phytoplankton in the ocean? *Limnol. Oceanogr.* 57,  
640 519–526. <https://doi.org/10.4319/lo.2012.57.2.0519>

641 Christaki, U., Dolan, J.R., Pelegri, S., Rassoulzadegan, F., 1998. Consumption of picoplankton-size  
642 particles by marine ciliates: Effects of physiological state of the ciliate and particle quality.  
643 *Limnology and Oceanography* 43, 458–464. <https://doi.org/10.4319/lo.1998.43.3.0458>

644 Christaki, U., Jacquet, S., Dolan, J.R., Vaulot, D., Rassoulzadegan, F., 1999. Growth and grazing on  
645 Prochlorococcus and Synechococcus by two marine ciliates. *Limnol. Oceanogr.* 44, 52–61.  
646 <https://doi.org/10.4319/lo.1999.44.1.0052>

647 Christaki, U., Obernosterer, I., Van Wambeke, F., Veldhuis, M., Garcia, N., Catala, P., 2008.  
648 Microbial food web structure in a naturally iron-fertilized area in the Southern Ocean  
649 (Kerguelen Plateau). *Deep Sea Research Part II: Topical Studies in Oceanography* 55, 706–  
650 716. <https://doi.org/10.1016/j.dsr2.2008.10.027>



652 719. <https://doi.org/10.1016/j.dsr2.2007.12.009>

653 Christaki, U., Lefèvre, D., Georges, C., Colombet, J., Catala, P., Courties, C., Sime-Ngando, T.,  
654 Blain, S., Obernosterer, I., 2014. Microbial food web dynamics during spring phytoplankton  
655 blooms in the naturally iron-fertilized Kerguelen area (Southern Ocean). *Biogeosciences* 11,  
656 6739–6753. <https://doi.org/10.5194/bg-11-6739-2014>

657 Christaki, U., Georges, C., Genitsaris, S., Monchy, S., 2015. Microzooplankton community  
658 associated with phytoplankton blooms in the naturally iron-fertilized Kerguelen area  
659 (Southern Ocean). *FEMS Microbiology Ecology* 91. <https://doi.org/10.1093/femsec/fiv068>

660 Christaki, U., Guenegues, A., Liu, Y., Blain, S., Catala, C., Colombet, J., Debeljak, P., Jardillier, L.,  
661 Irion, S., Planchon, F., Sassenhagen, I., Sime-Ngando, T., Ingrid Obernosterer I., Seasonal  
662 microbial food web dynamics in contrasting Southern Ocean productivity regimes.  
663 *Limnology and Oceanography*. *submitted after minor revision*.

664 Closset, I., Lasbleiz, M., Leblanc, K., Quéguiner, B., Cavagna, A.-J., Elskens, M., Navez, J., Cardinal,  
665 D., 2014. Seasonal evolution of net and regenerated silica production around a natural Fe-  
666 fertilized area in the Southern Ocean estimated with Si isotopic approaches. *Biogeosciences*  
667 11, 5827–5846. <https://doi.org/10.5194/bg-11-5827-2014>

668 Daugbjerg, N., Hansen, G., Larsen, J., Moestrup, Ø., 2000. Phylogeny of some of the major genera of  
669 dinoflagellates based on ultrastructure and partial LSU rDNA sequence data, including the  
670 erection of three new genera of unarmoured dinoflagellates. *Phycologia* 39, 302–317.  
671 <https://doi.org/10.2216/i0031-8884-39-4-302.1>

672 Dolan, J., Gallegos, C., Moigis, A., 2000. Dilution effects on microzooplankton in dilution grazing  
673 experiments. *Mar. Ecol. Prog. Ser.* 200, 127–139. <https://doi.org/10.3354/meps200127>

674 Dolan, J.R., McKeon, K., 2005. The reliability of grazing rate estimates from dilution experiments:  
675 Have we over-estimated rates of organic carbon consumption by microzooplankton? *Ocean*  
676 *Sci.* 1, 1–7. <https://doi.org/10.5194/os-1-1-2005>

677 Dolan, J.R., Pierce, R.W., Yang, E.J., Kim, S.Y., 2012. Southern Ocean Biogeography of Tintinnid  
678 Ciliates of the Marine Plankton. *J. Eukaryot. Microbiol.* 59, 511–519.  
679 <https://doi.org/10.1111/j.1550-7408.2012.00646.x>

680 Doledec, S., Chessel, D., 1994. Co-inertia analysis: an alternative method for studying species-  
681 environment relationships. *Freshwater Biol* 31, 277–294. <https://doi.org/10.1111/j.1365-2427.1994.tb01741.x>

683 Dray, S., Chessel, D., Thioulouse, J., 2003. CO-INERTIA ANALYSIS AND THE LINKING OF  
684 ECOLOGICAL DATA TABLES. *Ecology* 84, 3078–3089. <https://doi.org/10.1890/03-0178>

685 Dray, S., Dufour, A.-B., 2007. The **ade4** Package: Implementing the Duality Diagram for Ecologists.  
686 *J. Stat. Soft.* 22. <https://doi.org/10.18637/jss.v022.i04>

687 Edgar, R.C., 2004. MUSCLE: multiple sequence alignment with high accuracy and high throughput.  
688 *Nucleic Acids Research* 32, 1792–1797. <https://doi.org/10.1093/nar/gkh340>

689 Franzé, G., Modigh, M., 2013. Experimental evidence for internal predation in microzooplankton  
690 communities. *Mar Biol* 160, 3103–3112. <https://doi.org/10.1007/s00227-013-2298-1>

691 Froneman, P., Pakhomov, E., Perissinotto, R., McQuaid, C., 1996. Role of microplankton in the diet  
692 and daily ration of Antarctic zooplankton species during austral summer. *Mar. Ecol. Prog.*  
693 *Ser.* 143, 15–23. <https://doi.org/10.3354/meps143015>

694 Georges, C., Monchy, S., Genitsaris, S., Christaki, U., 2014. Protist community composition during  
695 early phytoplankton blooms in the naturally iron-fertilized Kerguelen area (Southern Ocean).  
696 *Biogeosciences* 11, 5847–5863. <https://doi.org/10.5194/bg-11-5847-2014>

697 Gowing, M.M., Garrison, D.L., 1992. Abundance and feeding ecology of larger protozooplankton in  
698 the ice edge zone of the Weddell and Scotia Seas during the austral winter. *Deep Sea*  
699 *Research Part A. Oceanographic Research Papers* 39, 893–919. [https://doi.org/10.1016/0198-0149\(92\)90128-G](https://doi.org/10.1016/0198-0149(92)90128-G)

700

701 Grattepanche, J.-D., Breton, E., Brylinski, J.-M., Lecuyer, E., Christaki, U., 2011a. Succession of

702 primary producers and micrograzers in a coastal ecosystem dominated by *Phaeocystis globosa*  
703 blooms. *Journal of Plankton Research* 33, 37–50. <https://doi.org/10.1093/plankt/fbq097>

704 Grattepanche, J.-D., Vincent, D., Breton, E., Christaki, U., 2011b. Microzooplankton herbivory  
705 during the diatom–*Phaeocystis* spring succession in the eastern English Channel. *Journal of*  
706 *Experimental Marine Biology and Ecology* 404, 87–97.  
707 <https://doi.org/10.1016/j.jembe.2011.04.004>

708 Guidi, L., Chaffron, S., Bittner, L., Eveillard, D., Larhlimi, A., Roux, S., Darzi, Y., Audic, S.,  
709 Berline, L., Brum, J.R., Coelho, L.P., Espinoza, J.C.I., Malviya, S., Sunagawa, S., Dimier, C.,  
710 Kandels-Lewis, S., Picheral, M., Poulain, J., Searson, S., Stemmann, L., Not, F., Hingamp, P.,  
711 Speich, S., Follows, M., Karp-Boss, L., Boss, E., Ogata, H., Pesant, S., Weissenbach, J.,  
712 Wincker, P., Acinas, S.G., Bork, P., de Vargas, C., Iudicone, D., Sullivan, M.B., Raes, J.,  
713 Karsenti, E., Bowler, C., Gorsky, G., 2016. Plankton networks driving carbon export in the  
714 oligotrophic ocean. *Nature* 532, 465–470. <https://doi.org/10.1038/nature16942>

715 Guillou, L., Bachar, D., Audic, S., Bass, D., Berney, C., Bittner, L., Boutte, C., Burgaud, G., de  
716 Vargas, C., Decelle, J., del Campo, J., Dolan, J.R., Dunthorn, M., Edvardsen, B., Holzmann,  
717 M., Kooistra, W.H.C.F., Lara, E., Le Bescot, N., Logares, R., Mahé, F., Massana, R.,  
718 Montresor, M., Morard, R., Not, F., Pawlowski, J., Probert, I., Sauvadet, A.-L., Siano, R.,  
719 Stoeck, T., Vaultot, D., Zimmermann, P., Christen, R., 2012. The Protist Ribosomal Reference  
720 database (PR2): a catalog of unicellular eukaryote Small Sub-Unit rRNA sequences with  
721 curated taxonomy. *Nucleic Acids Research* 41, D597–D604.  
722 <https://doi.org/10.1093/nar/gks1160>

723 Hall, J.A., Safi, K., 2001. The impact of in situ Fe fertilisation on the microbial food web in the  
724 Southern Ocean. *Deep Sea Research Part II: Topical Studies in Oceanography* 48, 2591–  
725 2613. [https://doi.org/10.1016/S0967-0645\(01\)00010-8](https://doi.org/10.1016/S0967-0645(01)00010-8)

726 Henjes, J., Assmy, P., Klaas, C., Verity, P., Smetacek, V., 2007. Response of microzooplankton  
727 (protists and small copepods) to an iron-induced phytoplankton bloom in the Southern Ocean  
728 (EisenEx). *Deep Sea Research Part I: Oceanographic Research Papers* 54, 363–384.  
729 <https://doi.org/10.1016/j.dsr.2006.12.004>

730 Hoppenrath, M., Elbrächter, M., Drebes, G., 2009. *Marine Phytoplankton: Selected*  
731 *microphytoplankton species from the North Sea around Helgoland and Sylt. Kleine*  
732 *Senckenberg-Reihe* 49, Stuttgart: Schweitzerbart'sche Verlagsbuchhandlung.

733 Irigoien, X., Flynn, K.J., Harris, R.P., 2005. Phytoplankton blooms: a 'loophole' in  
734 microzooplankton grazing impact? *Journal of Plankton Research* 27, 313–321.  
735 <https://doi.org/10.1093/plankt/fbi011>

736 Irion, S., Jardillier, L., Sassenhagen, I., Christaki, U., 2020. Marked spatio-temporal variations in  
737 small phytoplankton structure in contrasted waters of the Southern Ocean (Kerguelen area).  
738 *Limnology and Oceanography*. <https://doi.org/10.1002/lno.11555> *in press*

739 Jeong, H.J., Yoo, Y.D., Kim, J.S., Seong, K.A., Kang, N.S., Kim, T.H., 2010. Growth, feeding and  
740 ecological roles of the mixotrophic and heterotrophic dinoflagellates in marine planktonic  
741 food webs. *Ocean Sci. J.* 45, 65–91. <https://doi.org/10.1007/s12601-010-0007-2>

742 Jeong, H.J., You, J.H., Lee, K.H., Kim, S.J., Lee, S.Y., 2018. Feeding by common heterotrophic  
743 protists on the mixotrophic alga *Gymnodinium smaydae* (Dinophyceae), one of the fastest  
744 growing dinoflagellates. *J. Phycol.* 54, 734–743. <https://doi.org/10.1111/jpy.12775>

745 Karayanni, H., Christaki, U., Van Wambeke, F., Thyssen, M., Denis, M., 2008. Heterotrophic  
746 nanoflagellate and ciliate bacterivorous activity and growth in the northeast Atlantic Ocean: a  
747 seasonal mesoscale study. *Aquat. Microb. Ecol.* 51, 169–181.  
748 <https://doi.org/10.3354/ame01181>

749 Kjørboe, T., Visser, A., 1999. Predator and prey perception in copepods due to hydromechanical  
750 signals. *Mar. Ecol. Prog. Ser.* 179, 81–95. <https://doi.org/10.3354/meps179081>

- 751 Kofoid, C.A., Campbell, A.S., 1929. A Conspectus of the Marine and Freshwater Ciliata Belonging  
752 to the suborder Tintinninea, with Descriptions of New Species Principally from the Agassiz  
753 Expedition to the Eastern Tropical Pacific 1904-1905. University of California Publications in  
754 Zoology, Berkley, Calif.
- 755 Landry, M.R., Hassett, R.P., 1982. Estimating the grazing impact of marine micro-zooplankton.  
756 *Marine Biology* 67, 283–288. <https://doi.org/10.1007/BF00397668>
- 757 Landry, M.R., Selph, K.E., Décima, M., Gutiérrez-Rodríguez, A., Stukel, M.R., Taylor, A.G.,  
758 Pasulka, A.L., 2016. Phytoplankton production and grazing balances in the Costa Rica Dome.  
759 *J. Plankton Res.* 38, 366–379. <https://doi.org/10.1093/plankt/fbv089>
- 760 Lasbleiz, M., Leblanc, K., Armand, L.K., Christaki, U., Georges, C., Obernosterer, I., Quéguiner, B.,  
761 2016. Composition of diatom communities and their contribution to plankton biomass in the  
762 naturally iron-fertilized region of Kerguelen in the Southern Ocean. *FEMS Microbiol Ecol*  
763 92. <https://doi.org/10.1093/femsec/fiw171>
- 764 Lawrence, C., Menden-Deuer, S., 2012. Drivers of protistan grazing pressure: seasonal signals of  
765 plankton community composition and environmental conditions. *Mar. Ecol. Prog. Ser.* 459,  
766 39–52. <https://doi.org/10.3354/meps09771>
- 767 Lê, S., Josse, J., Husson, F., 2008. **FactoMineR**: An R Package for Multivariate Analysis. *J. Stat.*  
768 *Soft.* 25. <https://doi.org/10.18637/jss.v025.i01>
- 769 Lee, K.H., Jeong, H.J., Jang, T.Y., Lim, A.S., Kang, N.S., Kim, J.-H., Kim, K.Y., Park, K.-T., Lee,  
770 K., 2014. Feeding by the newly described mixotrophic dinoflagellate *Gymnodinium smaydae*:  
771 Feeding mechanism, prey species, and effect of prey concentration. *Journal of Experimental*  
772 *Marine Biology and Ecology* 459, 114–125. <https://doi.org/10.1016/j.jembe.2014.05.011>
- 773 Letunic, I., Bork, P., 2016. Interactive tree of life (iTOL) v3: an online tool for the display and  
774 annotation of phylogenetic and other trees. *Nucleic Acids Res* 44, W242–W245.  
775 <https://doi.org/10.1093/nar/gkw290>
- 776 Lynn, D.H., Montagnes, D.J.S., 1988. Taxonomic Descriptions of Some Conspicuous Species of  
777 Strobilidiine Ciliates (Ciliophora: Choreotrichida) from the Isles of Shoals, Gulf of Maine.  
778 *Journal of the Marine Biological Association of the United Kingdom* 68, 639–658.  
779 <https://doi.org/10.1017/S0025315400028770>
- 780 Mackey, M., Mackey, D., Higgins, H., Wright, S., 1996. CHEMTAX - a program for estimating class  
781 abundances from chemical markers: application to HPLC measurements of phytoplankton.  
782 *Mar. Ecol. Prog. Ser.* 144, 265–283. <https://doi.org/10.3354/meps144265>
- 783 McMin, A., Scot, F. J., 2005. Dinoflagellates, in: Scott, F. J., Marchant H. W. (Eds), Antarctic  
784 marine protists. ABRs and AAD Publishers, Canberra, pp. 202-250.
- 785 McMurdie, P.J., Holmes, S., 2013. phyloseq: An R Package for Reproducible Interactive Analysis  
786 and Graphics of Microbiome Census Data. *PLoS ONE* 8, e61217.  
787 <https://doi.org/10.1371/journal.pone.0061217>
- 788 Medinger, R., Nolte, V., Pandey, R.V., Jost, S., Ottenwälder, B., Schlötterer, C., Boenigk, J., 2010.  
789 Diversity in a hidden world: potential and limitation of next-generation sequencing for  
790 surveys of molecular diversity of eukaryotic microorganisms. *Molecular Ecology* 19, 32–40.  
791 <https://doi.org/10.1111/j.1365-294X.2009.04478.x>
- 792 Menden-Deuer, S., Lawrence, C., Franzè, G., 2018. Herbivorous protist growth and grazing rates at  
793 in situ and artificially elevated temperatures during an Arctic phytoplankton spring bloom.  
794 *PeerJ* 6, e5264. <https://doi.org/10.7717/peerj.5264>
- 795 Menden-Deuer, S., Lessard, E.J., 2000. Carbon to volume relationships for dinoflagellates, diatoms,  
796 and other protist plankton. *Limnol. Oceanogr.* 45, 569–579.  
797 <https://doi.org/10.4319/lo.2000.45.3.0569>
- 798 Monchy, S., Grattepanche, J.-D., Breton, E., Meloni, D., Sancier, G., Chabé, M., Delhaes, L.,  
799 Viscogliosi, E., Sime-Ngando, T., Christaki, U., 2012. Microplanktonic Community Structure  
800 in a Coastal System Relative to a *Phaeocystis* Bloom Inferred from Morphological and Tag

801 Pyrosequencing Methods. PLoS ONE 7, e39924.  
802 <https://doi.org/10.1371/journal.pone.0039924>

803 Mordret, S., Piredda, R., Vaultot, D., Montresor, M., Kooistra, W.H.C.F., Sarno, D., 2018. DINOREF :  
804 A curated dinoflagellate (Dinophyceae) reference database for the 18S rRNA gene. Mol Ecol  
805 Resour 18, 974–987. <https://doi.org/10.1111/1755-0998.12781>

806 Mosseri, J., Quéguiner, B., Armand, L., Cornet-Barthaux, V., 2008. Impact of iron on silicon  
807 utilization by diatoms in the Southern Ocean: A case study of Si/N cycle decoupling in a  
808 naturally iron-enriched area. Deep Sea Research Part II: Topical Studies in Oceanography 55,  
809 801–819. <https://doi.org/10.1016/j.dsr2.2007.12.003>

810 Neuer, S., Cowles, T., 1994. Protist herbivory in the Oregon upwelling system. Mar. Ecol. Prog. Ser.  
811 113, 147–162. <https://doi.org/10.3354/meps113147>

812 Obernosterer, I., Christaki, U., Lefèvre, D., Catala, P., Van Wambeke, F., Lebaron, P., 2008. Rapid  
813 bacterial mineralization of organic carbon produced during a phytoplankton bloom induced  
814 by natural iron fertilization in the Southern Ocean. Deep Sea Research Part II: Topical Studies  
815 in Oceanography 55, 777–789. <https://doi.org/10.1016/j.dsr2.2007.12.005>

816 Obiol, A., Giner, C.R., Sánchez, P., Duarte, C.M., Acinas, S.G., Massana, R., 2020. A metagenomic  
817 assessment of microbial eukaryotic diversity in the global ocean. Mol Ecol Resour 20, 1755–  
818 0998.13147. <https://doi.org/10.1111/1755-0998.13147>

819 Pawlowski, J., Audic, S., Adl, S., Bass, D., Belbahri, L., Berney, C., Bowser, S.S., Cepicka, I.,  
820 Decelle, J., Dunthorn, M., Fiore-Donno, A.M., Gile, G.H., Holzmann, M., Jahn, R., Jirků, M.,  
821 Keeling, P.J., Kostka, M., Kudryavtsev, A., Lara, E., Lukeš, J., Mann, D.G., Mitchell, E.A.D.,  
822 Nitsche, F., Romeralo, M., Saunders, G.W., Simpson, A.G.B., Smirnov, A.V., Spouge, J.L.,  
823 Stern, R.F., Stoeck, T., Zimmermann, J., Schindel, D., de Vargas, C., 2012. CBOL Protist  
824 Working Group: Barcoding Eukaryotic Richness beyond the Animal, Plant, and Fungal  
825 Kingdoms. PLoS Biol 10, e1001419. <https://doi.org/10.1371/journal.pbio.1001419>

826 Petz, W., 2005. Ciliates. in: Scott, F. J., Marchant, H.J. (Eds.), Antarctic Marine Protists. ABRs and  
827 AAD Publishers, Canberra, pp. 347–448.

828 Pollard, R., Sanders, R., Lucas, M., Statham, P., 2007. The Crozet Natural Iron Bloom and Export  
829 Experiment (CROZEX). Deep Sea Research Part II: Topical Studies in Oceanography 54,  
830 1905–1914. <https://doi.org/10.1016/j.dsr2.2007.07.023>

831 Pollard, R.T., Salter, I., Sanders, R.J., Lucas, M.I., Moore, C.M., Mills, R.A., Statham, P.J., Allen,  
832 J.T., Baker, A.R., Bakker, D.C.E., Charette, M.A., Fielding, S., Fones, G.R., French, M.,  
833 Hickman, A.E., Holland, R.J., Hughes, J.A., Jickells, T.D., Lampitt, R.S., Morris, P.J.,  
834 Nédélec, F.H., Nielsdóttir, M., Planquette, H., Popova, E.E., Poulton, A.J., Read, J.F.,  
835 Seeyave, S., Smith, T., Stinchcombe, M., Taylor, S., Thomalla, S., Venables, H.J.,  
836 Williamson, R., Zubkov, M.V., 2009. Southern Ocean deep-water carbon export enhanced by  
837 natural iron fertilization. Nature 457, 577–580. <https://doi.org/10.1038/nature07716>

838 Poulton, A.J., Mark Moore, C., Seeyave, S., Lucas, M.I., Fielding, S., Ward, P., 2007. Phytoplankton  
839 community composition around the Crozet Plateau, with emphasis on diatoms and  
840 Phaeocystis. Deep Sea Research Part II: Topical Studies in Oceanography 54, 2085–2105.  
841 <https://doi.org/10.1016/j.dsr2.2007.06.005>

842 Putt, M., Stoecker, D.K., 1989. An experimentally determined carbon : volume ratio for marine  
843 “oligotrichous” ciliates from estuarine and coastal waters. Limnol. Oceanogr. 34, 1097–1103.  
844 <https://doi.org/10.4319/lo.1989.34.6.1097>

845 Quéguiner, B., 2013. Iron fertilization and the structure of planktonic communities in high nutrient  
846 regions of the Southern Ocean. Deep Sea Research Part II: Topical Studies in Oceanography  
847 90, 43–54. <https://doi.org/10.1016/j.dsr2.2012.07.024>

848 Ras, J., Claustre, H., Uitz, J., 2008. Spatial variability of phytoplankton pigment distributions in the  
849 Subtropical South Pacific Ocean: comparison between in situ and predicted data.  
850 Biogeosciences 5, 353–369. <https://doi.org/10.5194/bg-5-353-2008>

- 851 Rose, J.M., Fitzpatrick, E., Wang, A., Gast, R.J., Caron, D.A., 2013. Low temperature constrains  
852 growth rates but not short-term ingestion rates of Antarctic ciliates. *Polar Biol* 36, 645–659.  
853 <https://doi.org/10.1007/s00300-013-1291-y>
- 854 Saito, H., Suzuki, K., Hinuma, A., Ota, T., Fukami, K., Kiyosawa, H., Saino, T., Tsuda, A., 2005.  
855 Responses of microzooplankton to in situ iron fertilization in the western subarctic Pacific  
856 (SEEDS). *Progress in Oceanography* 64, 223–236.  
857 <https://doi.org/10.1016/j.pocean.2005.02.010>
- 858 Saito, H., Ota, T., Suzuki, K., Nishioka, J., Tsuda, A., 2006. Role of heterotrophic dinoflagellate  
859 *Gyrodinium* sp. in the fate of an iron induced diatom bloom. *Geophys. Res. Lett.* 33, L09602.  
860 <https://doi.org/10.1029/2005GL025366>
- 861 Sarthou, G., Vincent, D., Christaki, U., Obernosterer, I., Timmermans, K.R., Brussaard, C.P.D.,  
862 2008. The fate of biogenic iron during a phytoplankton bloom induced by natural fertilisation:  
863 Impact of copepod grazing. *Deep Sea Research Part II: Topical Studies in Oceanography* 55,  
864 734–751. <https://doi.org/10.1016/j.dsr2.2007.12.033>
- 865 Sassenhagen, I., Irion, S., Jardillier, L., Moreira, D., Christaki, U., 2020. Protist Interactions and  
866 Community Structure During Early Autumn in the Kerguelen Region (Southern Ocean).  
867 *Protist* 171, 125709. <https://doi.org/10.1016/j.protis.2019.125709>
- 868 Schiller, J., 1931–1937: Dinoflagellatae (Peridinineae) in monographischer Behandlung. in:  
869 Rabenhorst, L. (Eds.), *Kryptogamen-Flora von Deutschland, Österreichs und der Schweiz*.  
870 Akad. Verlag., Leipzig.
- 871 Schmoker, C., Hernández-León, S., Calbet, A., 2013. Microzooplankton grazing in the oceans:  
872 impacts, data variability, knowledge gaps and future directions. *Journal of Plankton Research*  
873 35, 691–706. <https://doi.org/10.1093/plankt/fbt023>
- 874 Sherr, B.F., Sherr, E.B., Fallon, R.D., 1987. Use of Monodispersed, Fluorescently Labeled Bacteria  
875 to Estimate In Situ Protozoan Bacterivory. *APPL. ENVIRON. MICROBIOL.* 53, 8.
- 876 Sherr, E., Sherr, B., 2007. Heterotrophic dinoflagellates: a significant component of  
877 microzooplankton biomass and major grazers of diatoms in the sea. *Mar. Ecol. Prog. Ser.* 352,  
878 187–197. <https://doi.org/10.3354/meps07161>
- 879 Sherr, E., Sherr, B., 2009. Capacity of herbivorous protists to control initiation and development of  
880 mass phytoplankton blooms. *Aquat. Microb. Ecol.* 57, 253–262.  
881 <https://doi.org/10.3354/ame01358>
- 882 Smetacek, V., Assmy, P., Henjes, J., 2004. The role of grazing in structuring Southern Ocean pelagic  
883 ecosystems and biogeochemical cycles. *Antarctic science* 16, 541–558.  
884 <https://doi.org/10.1017/S0954102004002317>
- 885 Stamatakis, A., 2014. RAxML version 8: a tool for phylogenetic analysis and post-analysis of large  
886 phylogenies. *Bioinformatics* 30, 1312–1313. <https://doi.org/10.1093/bioinformatics/btu033>
- 887 Steinberg, D.K., Landry, M.R., 2017. Zooplankton and the Ocean Carbon Cycle. *Annu. Rev. Mar.*  
888 *Sci.* 9, 413–444. <https://doi.org/10.1146/annurev-marine-010814-015924>
- 889 Stern, R., Kraberg, A., Bresnan, E., Kooistra, W.H.C.F., Lovejoy, C., Montresor, M., Morán, X.A.G.,  
890 Not, F., Salas, R., Siano, R., Vaultot, D., Amaral-Zettler, L., Zingone, A., Metfies, K., 2018.  
891 Molecular analyses of protists in long-term observation programmes—current status and  
892 future perspectives. *Journal of Plankton Research* 40, 519–536.  
893 <https://doi.org/10.1093/plankt/fby035>
- 894 Stoecker, D.K., Capuzzo, J.M., 1990. Predation on Protozoa: its importance to zooplankton. *J*  
895 *Plankton Res* 12, 891–908. <https://doi.org/10.1093/plankt/12.5.891>
- 896 Straile, D., 1997. Gross growth efficiencies of protozoan and metazoan zooplankton and their  
897 dependence on food concentration, predator-prey weight ratio, and taxonomic group. *Limnol.*  
898 *Oceanogr.* 42, 1375–1385. <https://doi.org/10.4319/lo.1997.42.6.1375>
- 899 Strom, S., 1991. Growth and grazing rates of the herbivorous dinoflagellate *Gymnodinium* sp. from  
900 the open subarctic Pacific Ocean. *Mar. Ecol. Prog. Ser.* 78, 103–113.

901 <https://doi.org/10.3354/meps078103>  
902 Strom, S.L., Fredrickson, K.A., 2008. Intense stratification leads to phytoplankton nutrient limitation  
903 and reduced microzooplankton grazing in the southeastern Bering Sea. *Deep Sea Research*  
904 *Part II: Topical Studies in Oceanography* 55, 1761–1774.  
905 <https://doi.org/10.1016/j.dsr2.2008.04.008>  
906 Tomas, C.R., 1997. *Identifying Marine Phytoplankton*. Elsevier, London.  
907 Tsuda, A., Takeda, S., Saito, H., Nishioka, J., Kudo, I., Nojiri, Y., Suzuki, K., Uematsu, M., Wells,  
908 M.L., Tsumune, D., Yoshimura, T., Aono, T., Aramaki, T., Cochlan, W.P., Hayakawa, M.,  
909 Imai, K., Isada, T., Iwamoto, Y., Johnson, W.K., Kameyama, S., Kato, S., Kiyosawa, H.,  
910 Kondo, Y., Levasseur, M., Machida, R.J., Nagao, I., Nakagawa, F., Nakanishi, T., Nakatsuka,  
911 S., Narita, A., Noiri, Y., Obata, H., Ogawa, H., Oguma, K., Ono, T., Sakuragi, T., Sasakawa,  
912 M., Sato, M., Shimamoto, A., Takata, H., Trick, C.G., Watanabe, Y.W., Wong, C.S., Yoshie,  
913 N., 2007. Evidence for the grazing hypothesis: Grazing reduces phytoplankton responses of  
914 the HNLC ecosystem to iron enrichment in the western subarctic pacific (SEEDS II). *J*  
915 *Oceanogr* 63, 983–994. <https://doi.org/10.1007/s10872-007-0082-x>  
916 Vargas, C., González, H., 2004. Plankton community structure and carbon cycling in a coastal  
917 upwelling system. I. Bacteria, microprotozoans and phytoplankton in the diet of copepods and  
918 appendicularians. *Aquat. Microb. Ecol.* 34, 151–164. <https://doi.org/10.3354/ame034151>  
919 Verity, P.G., Stoecker, D.K., Sieracki, M.E., Nelson, J.R., 1993. Grazing, growth and mortality of  
920 microzooplankton during the 1989 North Atlantic spring bloom at 47°N, 18°W. *Deep Sea*  
921 *Research Part I: Oceanographic Research Papers* 40, 1793–1814.  
922 [https://doi.org/10.1016/0967-0637\(93\)90033-Y](https://doi.org/10.1016/0967-0637(93)90033-Y)  
923 Wolf, C., Frickenhaus, S., Kiliyas, E.S., Peeken, I., Metfies, K., 2014. Protist community composition  
924 in the Pacific sector of the Southern Ocean during austral summer 2010. *Polar Biol* 37, 375–  
925 389. <https://doi.org/10.1007/s00300-013-1438-x>  
926

## 927 **Figure legends**

928 **Figure 1.** Location of stations Surface Chlorophyll *a* concentrations during MOBYDICK are the  
929 monthly means for March 2018 at a resolution of 4 km (Copernicus Marine Service,  
930 <http://marine.copernicus.eu/>). The black lines denote 1000 m bathymetry. The approximate position  
931 of the highly dynamic polar front (PF, blue line) during February-March 2018 was also drawn  
932 according to Pauthenet et al. (2018), gray zone around the polar front indicates variations in its  
933 trajectory. The position of the on-plateau A3 and reference HNLC R stations sampled during early  
934 spring (KEOPS2 cruise, October-November 2011) are also indicated on this map. KEOPS2 station  
935 A3 was named M2 during the MOBYDICK cruise and has the same coordinates.

936

937 **Figure 2.** Mean profiles of Temperature (°C), Salinity and Chl-*a* (derived from in vivo fluorescence)  
938 calculated from all the CTDs of each visit to a station. Shadows are standard deviations around the  
939 mean of all CTDs sampled at each station.

940

941 **Figure 3.** Mean contribution and relative contribution of pigments to total Chl. diat=diatoms,  
942 prymn=prymnesiophytes, pras=prasinophytes, crypt=cryptophytes, syn=*Synechococcus*,  
943 chlor=chlorophytes. A3-1, A3-2 and R: correspond to early spring data (KEOPS2, cruise). Late  
944 summer: MOBYDICK cruise.

945

946 **Figure 4.** Mean integrated abundances and relative abundance of dinoflagellate (DIN) size classes (a,  
947 b). Mean integrated abundances and relative abundance of ciliates (CIL) size classes (c, d) Mean  
948 integrated biomasses of DIN and CIL (e) and relative biomasses of DIN and CIL (f), in the mixed  
949 layer (ML).

950

951 **Figure 5.** Vertical profiles of dinoflagellates (DIN) and ciliates (CIL) during the MOBYDICK cruise.

952

953 **Figure 6.** Heatmaps illustrating microscopy (a, b) and sequencing (c,d) richness and abundance data  
954 during MOBYDICK. The microscopy data values are the mean integrated abundances of cells in the  
955 ML. The sequence data illustrate relative abundance of reads in the class Dinophyceae and the  
956 division Ciliophora for the 0.2-20 and 20-100 µm fractions.

957

958 **Figure 7.** Maximum likelihood trees for dinoflagellate (DIN)(a) and ciliate (CIL)(b) genera.  
959 Bootstrap values >50 are indicated on branches. Tree scales refer to the length of branches and  
960 indicate the mean number of substitutions per site. Genera are coloured by order. a) DIN topology.  
961 Purple = Noctilucales, blue = Gymnodiniales, green = Peridinales, orange = Gonyaulacales, red =

962 Dinophysiales, black = individual orders for each genus. b) CIL topology. Green = Tintinnida, red =  
963 Choreotrichia, purple = Colpodea, orange = Hypotrichia, blue = Strombidiida, black = Cyclotrichiida  
964 (Myrionecta), Scuticociliatia, Euplotia (Diophrys, Aspidisca).

965

966 **Figure 8.** Co-inertia analysis (PCA–PCA COIA) between the 16 most abundant DIN+CIL genera and  
967 characteristic pigments. Hierarchical Clustering Factor Maps indicating station grouping according to  
968 the DIN and CIL dominant genera and pigment present (a, b). Principal Component Analysis (PCA)  
969 of DIN+CIL and pigments with their contribution to the first to principal components (c, d). COIA  
970 synthesized results (e). The *x*-axes show projections of the first 3 PCA components from the  
971 pigments *y*-axes show those of the genera. The circles represent a view of the rotation needed to  
972 associate the 2 datasets. P-values were calculated using Monte Carlo permutation tests (1000  
973 permutations). The sample scatterplot shows how far apart the samples were relative to their pigment  
974 and taxonomic variables. The beginning of the arrow shows the position of the sample described by  
975 the pigments, and the end by the microzooplankton genera. RV: correlation coefficient between the 2  
976 tables ('R' for correlation and 'V' for vectorial) (e)

977 **Fig. A1.** Dilution experiment plots of apparent phytoplankton growth ( $\mu$ ) as a function of the fraction  
978 of bulk seawater (sieved on 200 $\mu$ m) in the dilution series for each station. Linear models have been  
979 associated to their 95% confidence interval (dark grey area). Calculated parameters are detailed on  
980 the plot (Ex). Apparent phytoplankton growth ( $\mu$ ) was obtained from measured chl a concentrations at  
981 each dilution by using the equation  $\mu = 1/t * \ln(Cf/C0)$  where *t* is the duration of the experiment (d),  
982 *Cf* and *C0* are the final and the initial chl a concentrations. The coefficients *k* and *g* have been  
983 determined from the best fit of the linear model linking apparent phytoplankton growth ( $\mu$ ) versus the  
984 dilution factor of whole seawater, *g* (microzooplankton grazing) being the negative slope and *k*  
985 (phytoplankton growth rate) the intercept of the linear model.



Table 1. Station description, coordinates and depth of the CTD "stock". The depth of the mixed layer ( $Z_{ML}$ ) is based on a difference in sigma of 0.02 to the surface value. The mean  $Z_{ML}$  and  $Z_e$  ( $Z_e=1\%$  light depth) of all CTD casts performed during the occupation of the stations is given. For the rest of the variables the mean $\pm$ SD is given for the mixed layer. **EARLY SPRING**: Onset of the bloom, KEOPS2 cruise (KErguelen Ocean and Plateau compared Study project, 2011), **LATE SUMMER** post-bloom MOBYDICK cruise (2018) on the plateau and ocean area of Kerguelen. The mean ML depth ( $Z_{ML}$ ) of all CTD casts performed during the occupation of the stations is given. For the rest of the variables the mean $\pm$ SD is given for the mixed layer except for GCP and NCP which is an integrated value in the ML. KEOPS2 station A3 was named M2 during the MOBYDICK cruise and has the same coordinates (cf Fig. 1). KEOPS 2, data from: [Blain et al. 2015](#), [Closset et al. 2014](#), [Christaki et al 2014](#), [Lasbleiz et al. 2016](#). MOBYDICK data of GCP and NCP for from [Christaki et al. submitted](#). NA: not available

	EARLY SPRING			LATE SUMMER							
	On-plateau		Off-plateau	On-plateau			Off-plateau				
Station	A3-1	A3-2	R	M2-1	M2-2	M2-3	M1	M3-1	M3-3	M4-1	M4-2
dates	20 Oct	16 Nov	26 Nov	6-8 Mar	16-17 Mar	8-9 Mar	3-5 Mar	18-20 Mar	28 Feb- 3 Mar	12-14 Mar	6-8 Mar
Long-Lat ( $^{\circ}$ E, $^{\circ}$ S)	72.1-50.6	72.1-50.6	50.3-66.7	72.0-50.4	72.0-50.4	72.0-50.4	74.5-49.5	68.0-50.4	68.0-50.4	67.1-52.3	67.1-52.3
Depth (m)	475	528	2450	520	519	527	2723	1000	1700	4186	4300
$Z_{ML}$ (m)	105	168	105	62	61	68	27	65	79	49	87
$Z_e$ (m)	N/A	38 38	92 92	64	61	58	80	93	107	96	100
Chlorophyll a ( $\mu$ g/L)	0.62 $\pm$ 0.17	2.03 $\pm$ 0.33	0.28 $\pm$ 0.04	0.27 $\pm$ 0.02	0.30 $\pm$ 0.04	0.58 $\pm$ 0.02	0.35 $\pm$ 0.040	0.20 $\pm$ 0.02	0.14 $\pm$ 0.00	0.18 $\pm$ 0.01	0.21 $\pm$ 0.00
NO <sub>3</sub> - + NO <sub>2</sub> - ( $\mu$ M)	29.7 $\pm$ 0.5	26.2 $\pm$ 0.4	26.0 $\pm$ 0.2	21.9 $\pm$ 0.12	21.79 $\pm$ 0.38	21.9 $\pm$ 0.08	25.2 $\pm$ 0.56	23.75 $\pm$ 0.31	23.34 $\pm$ 0.12	25.7 $\pm$ 0.05	24.8 $\pm$ 0.27
PO <sub>4</sub> <sup>3-</sup> ( $\mu$ M)	2.00 $\pm$ 0.03	1.78 $\pm$ 0.03	1.83 $\pm$ 0.03	1.47 $\pm$ 0.03	1.50 $\pm$ 0.04	1.50 $\pm$ 0.00	1.71 $\pm$ 0.11	1.65 $\pm$ 0.05	1.08 $\pm$ 0.92	1.70 $\pm$ 0.02	1.71 $\pm$ 0.01
Si(OH) <sub>4</sub> ( $\mu$ M)	23.7 $\pm$ 0.8	18.9 $\pm$ 0.5	12.3 $\pm$ 0.3	1.36 $\pm$ 0.41	1.72 $\pm$ 0.79	2.75 $\pm$ 0.27	8.38 $\pm$ 2.93	2.89 $\pm$ 1.01	2.31 $\pm$ 0.04	4.36 $\pm$ 0.35	4.80 $\pm$ 0.00
GCP (mmol C m <sup>-2</sup> )	N/A	344	134	105	213	83	121	nd	132	187	129
NCP (mmol C m <sup>-2</sup> )	N/A	237	57	30	100	44	52	nd	15	88	106

33

Table 2 : Dilution experiment derived phytoplankton growth and microzooplankton grazing parameters.

Station	On-plateau			Off-plateau			
	M2-1	M2-2	M2-3	M1	M3-1	M4-1	M4-2
Initial Chl a (10-20m depth, $\mu$ g L <sup>-1</sup> )	0.30	0.36	0.64	0.35	0.20	0.20	0.26
Phytoplankton growth rate (d <sup>-1</sup> )	0.13 $\pm$ 0.03	0.15 $\pm$ 0.02	0.26 $\pm$ 0.03	0.22 $\pm$ 0.02	0.17 $\pm$ 0.12	0.08 $\pm$ 0.03	0.18 $\pm$ 0.09
Microzooplankton grazing rate (d <sup>-1</sup> )	0.34 $\pm$ 0.05	0.37 $\pm$ 0.04	0.53 $\pm$ 0.05	0.28 $\pm$ 0.03	0.50 $\pm$ 0.20	0.38 $\pm$ 0.05	0.43 $\pm$ 0.15
Dilution determination coefficient (r <sup>2</sup> )	0.86***	0.90***	0.81***	0.89***	0.35*	0.83***	0.45*
Phytoplankton daily production ( $\mu$ g Chl a L <sup>-1</sup> d <sup>-1</sup> )	0.04 $\pm$ 0.009	0.05 $\pm$ 0.008	0.17 $\pm$ 0.02	0.08 $\pm$ 0.006	0.03 $\pm$ 0.02	0.02 $\pm$ 0.006	0.05 $\pm$ 0.02
Microzooplankton daily consumption ( $\mu$ g Chl a L <sup>-1</sup> d <sup>-1</sup> )	0.08 $\pm$ 0.01	0.13 $\pm$ 0.01	0.33 $\pm$ 0.03	0.10 $\pm$ 0.01	0.10 $\pm$ 0.04	0.07 $\pm$ 0.008	0.10 $\pm$ 0.04
Grazing pressure (%Chl a production d <sup>-1</sup> )	213.10	231.68	194.06	130.05	287.48	427.88	219.86

\*\*\* p<0.001 ; \*\* p<0.01 ; \* p<0.05

34

Table 3. Summary of seasonal characteristics above the plateau of Kerguelen and in HNLC waters calculated for the mixed layer (ML). GCP and NCP: Gross and Net community production (cf. Table 1), phytoplankton, dinoflagellates (DIN), ciliates (CIL) dominant genera.

	Productivity regime (GCP) mmol C m <sup>-2</sup> d <sup>-1</sup>	Community Respiration % of GCP	DIN+CIL biomass mmol C m <sup>-2</sup>	Phytoplankton	DIN	CIL	DIN+CIL carbon demand* as a % of GCP and NCP
<b>Kerguelen Bloom</b>							
Early spring	High <sup>1</sup> (344)	Low <sup>1</sup> 30%	High (116)	<i>Chaetoceros</i> <i>Thalassiosira</i> some <i>Phaeocystis</i> colonies <sup>3,4</sup>	<i>Gymnodinium</i> , <i>Protoperidinium</i> <i>Gyrodinium</i> <sup>3,6</sup>	<i>Strombidium</i> <i>Acanthostomella</i> <i>norvegica</i> <i>Codonellopsis</i> <i>soyai</i> <sup>4,6</sup>	18 % GCP 25% NCP (A3-2)
Late summer	Moderate (134) <sup>2</sup>	Moderate <sup>2</sup> 57 %	low (15.4)	<i>Corethron</i> , <i>Phaeocystis</i> free cells <i>Micromonas</i> <sup>5</sup>	<i>Gymnodinium</i> <i>Gyrodinium</i> <i>Prorocentrum</i>	<i>Lohmaniella oviformis</i> , <i>Strombidium</i>	5.3±2.4% GCP 14±9.8% NCP (mean±sd of the 3 visits at M2)
<b>HNLC</b>							
Early spring	Moderate (59) <sup>1</sup>	Moderate <sup>1</sup> 57%	low (17)	<i>Phaeocystis</i> <i>Fragilariopsis</i> <sup>3,4</sup>	<i>Gymnodinium</i> <i>Gyrodinium</i> <i>Scripsiella</i> <sup>4,6</sup>	<i>Strombidium</i> <i>Codonellopsis soyai</i> <sup>4,6</sup>	3 % GCP 8% NCP (R)
Late summer mean±sd of M1, M4-1, M4-2 and M3-3	Moderate (132) <sup>2</sup>	High <sup>2</sup> 89%	low (16)	<i>Phaeocystis</i> free cells small diatoms Pelagophytes <sup>5</sup>	<i>Gymnodinium</i> <i>Scripsiella</i> <i>Gyrodinium</i>	<i>Cymatocylis antarctica</i> , <i>Lohmaniella oviformis</i>	3.9±1.8 % GCP 6.8±2.2% NCP (mean±sd of M1, M4-1, M4-2) 5.2% GCP 46% NCP (M3-3)

\*Carbon demand is estimated based on biomass, 30% growth efficiency (e.g. Bjørnsen and Kuparinen, 1991; Verity et al. 1993; Neuer and Cowles, 1994; Karayanni et al. 2008) and  $\mu=0.2\text{ d}^{-1}$  corresponding roughly population generation time of about 3 days (Bjørnsen and Kuparinen, 1991; Verity et al. 1993; Neuer and Cowles, 1994; Karayanni et al. 2008).  
1.Christaki et al. 2014; 2. Christaki et al. submitted; 3. Lasbleiz et al. 2016; 4. Georges et al. 2014; 5. Irion et al. 2020; 6. Christaki et al. 2015

Table A1. Significant Pearson correlation between co-inertia axes and variables are highlighted with bold letters (p<0.05)

	axe1	axe2	axe3
Gymnodinium	-0.50563510	0.304129663	<b>-0.67727811</b>
Gyrodinium	0.49828359	0.481226933	-0.45085253
Scripsiella	<b>-0.91491628</b>	-0.003383030	-0.12224026
Prorocentrum	-0.52196271	-0.100576427	-0.46555616
Amphidinium	0.12412553	<b>0.694065230</b>	-0.10313589
Katodinium	-0.56273600	0.207027089	-0.35686930
Protoperidinium	0.35535326	<b>0.706082523</b>	0.29514842
Tripos	0.15099031	-0.389365386	-0.66223964
Lohmaniella	<b>-0.73329229</b>	-0.319589603	-0.54423781
Strombidium	-0.27722418	0.564209822	<b>-0.64544930</b>
Cymatocylis	-0.41318569	0.168130159	0.21346582
Leegaardiella	-0.59748443	0.008128098	<b>-0.65963309</b>
Codonellopsis	-0.07381567	-0.392015027	-0.33990282
Salpingella	<b>-0.73867635</b>	-0.083404745	0.02006962
Laboea	0.14926345	-0.375836980	-0.59724940
Myrionecta	<b>0.72419475</b>	0.532171341	0.07215646
	axe1	axe2	axe3
diat	<b>0.9076259</b>	-0.08972795	-0.20646614
prymn	-0.1780910	<b>-0.71742385</b>	-0.34364613
pras	0.5544056	<b>-0.83415468</b>	-0.01453556
crypt	<b>0.8845281</b>	-0.45060719	-0.13261950
Syn	<b>0.7408795</b>	-0.03714631	-0.71035252
chlor	0.3045928	0.44763322	<b>-0.81309706</b>
Chla	<b>0.9186115</b>	-0.17271963	-0.24602134

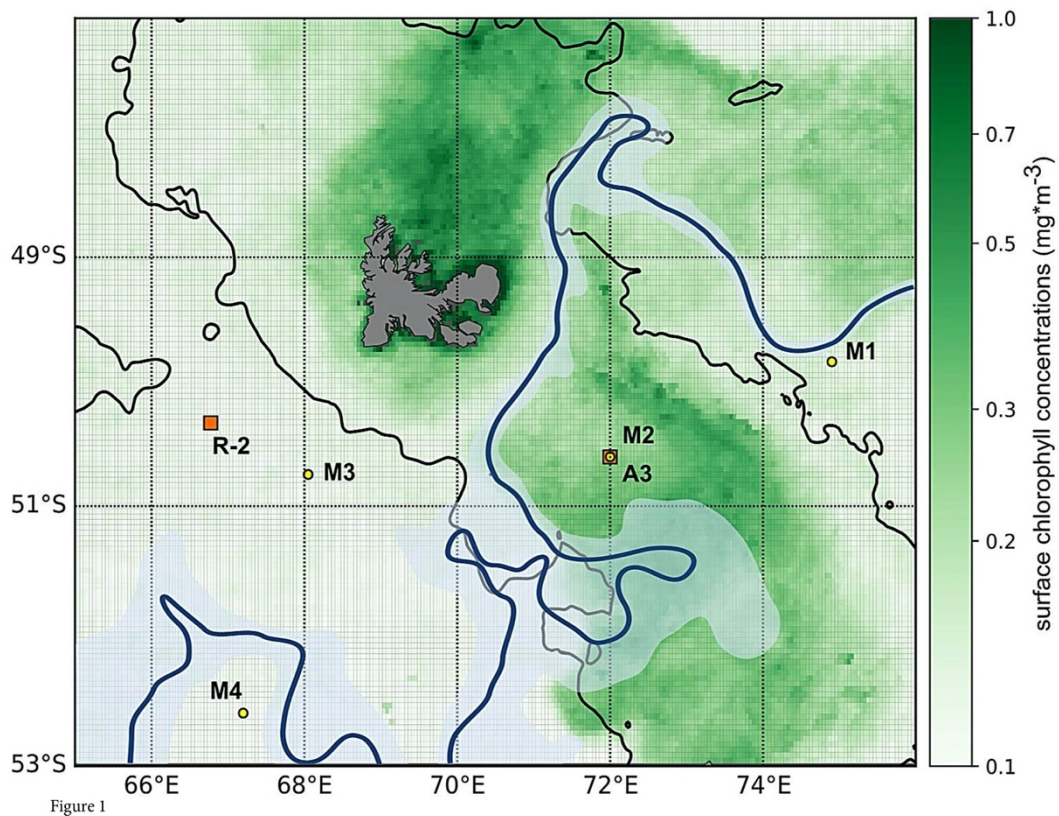


Figure 1

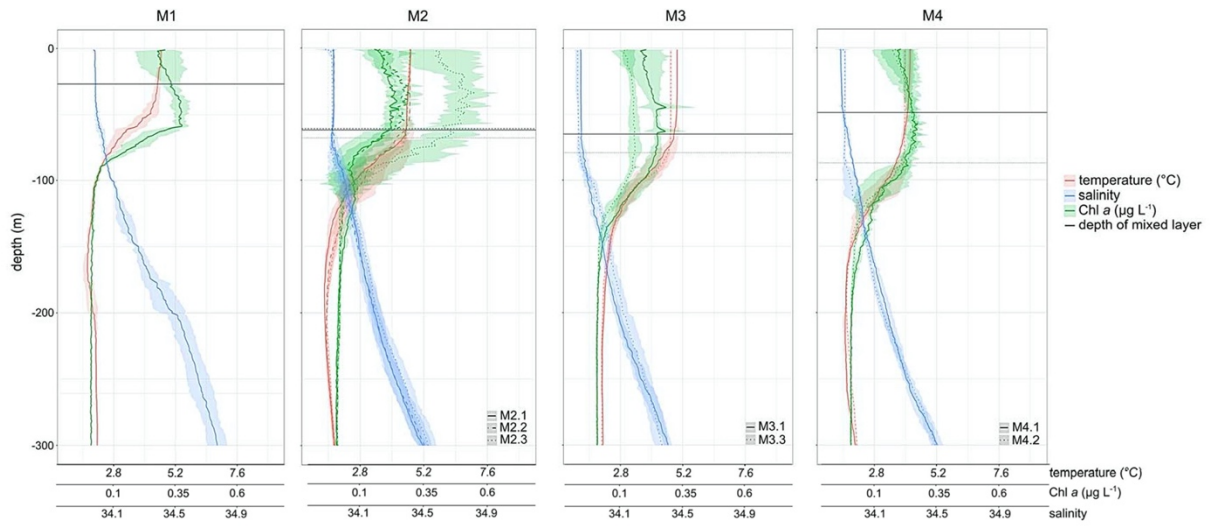


Figure 2

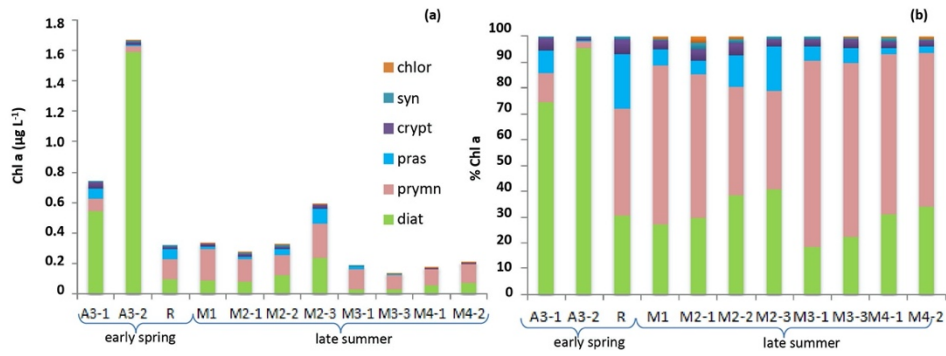


Figure 3

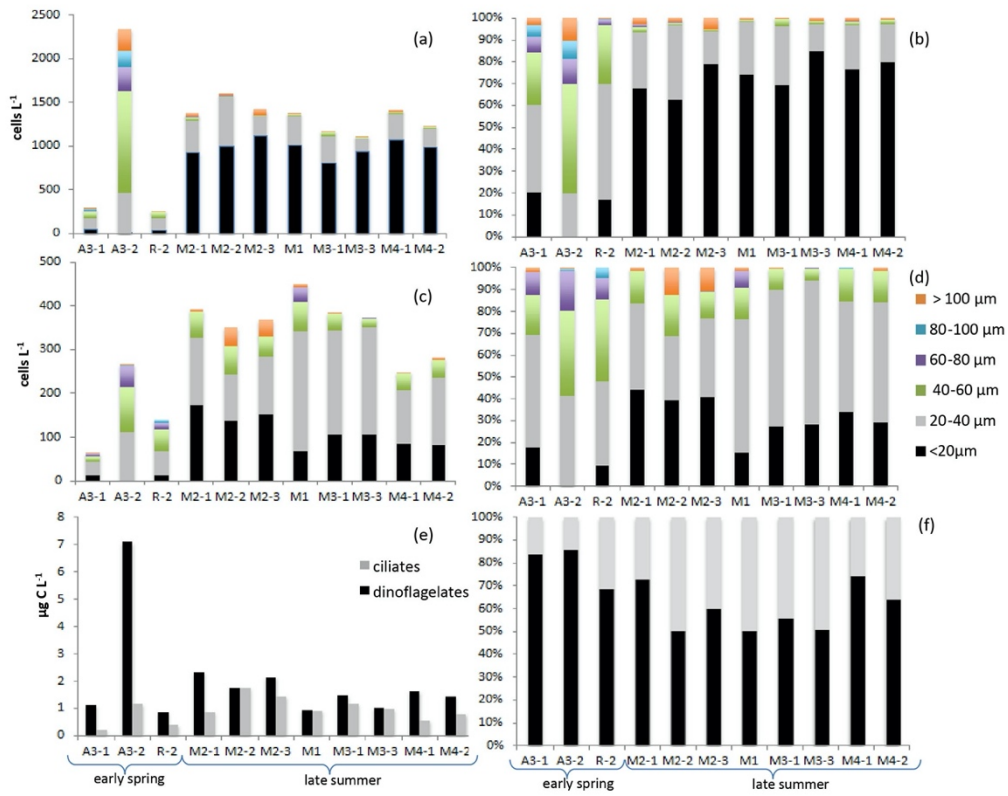


Figure 4

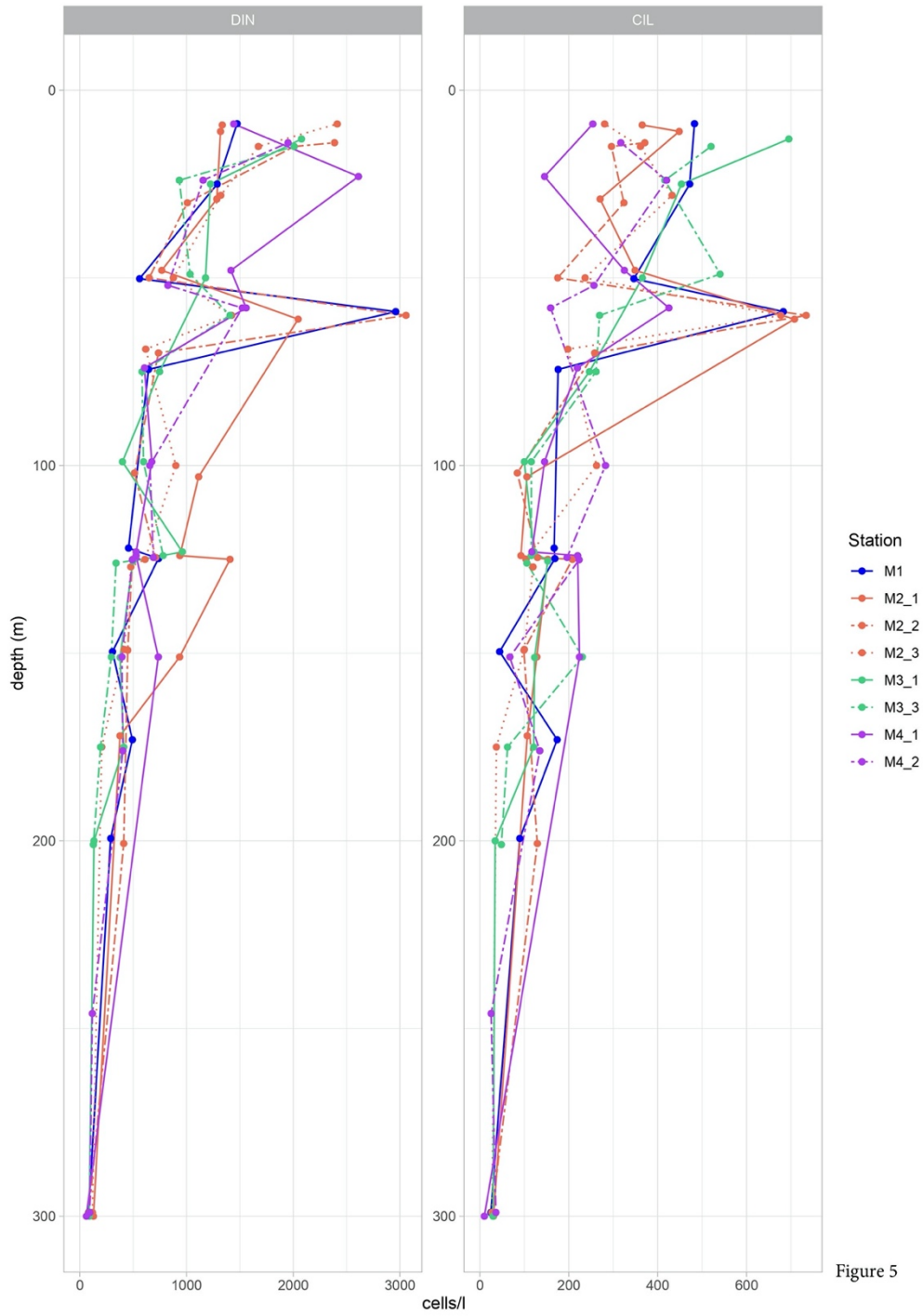


Figure 5



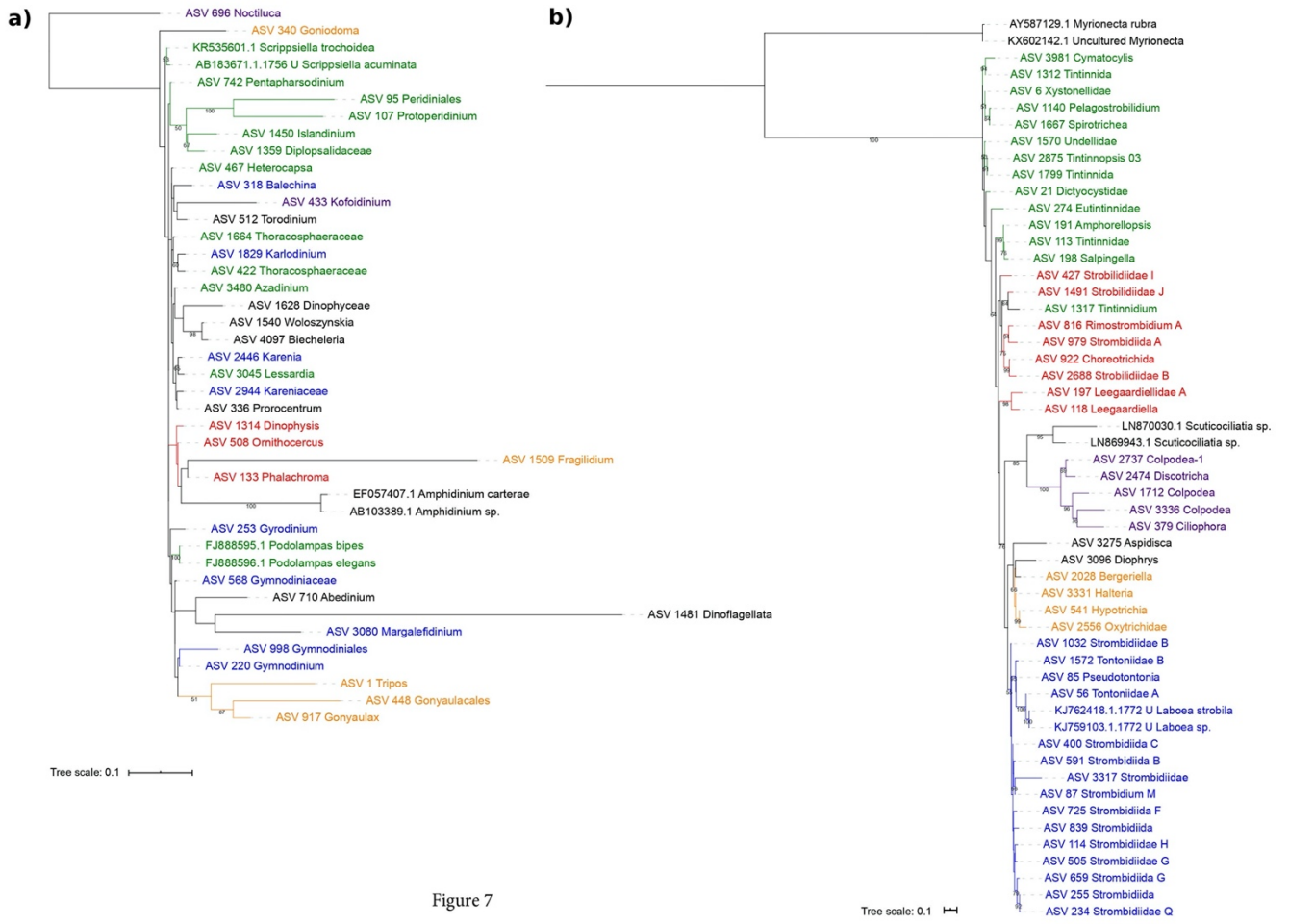


Figure 7

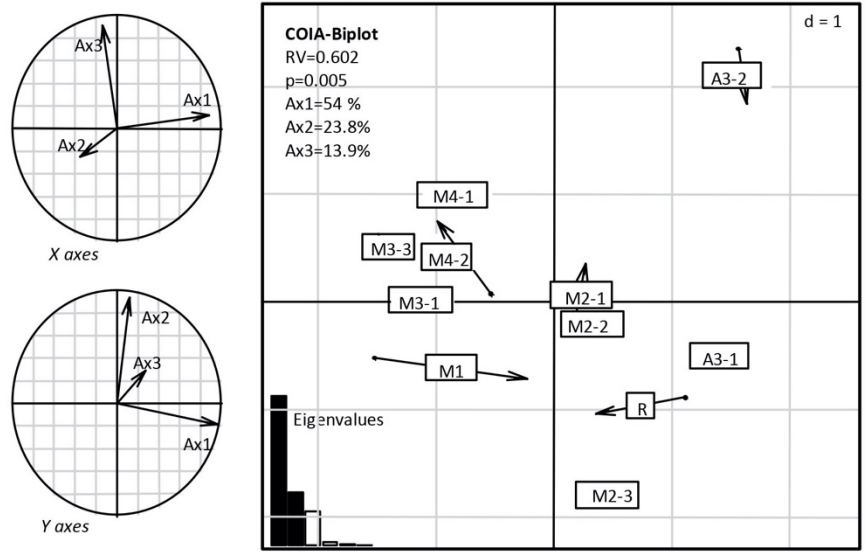
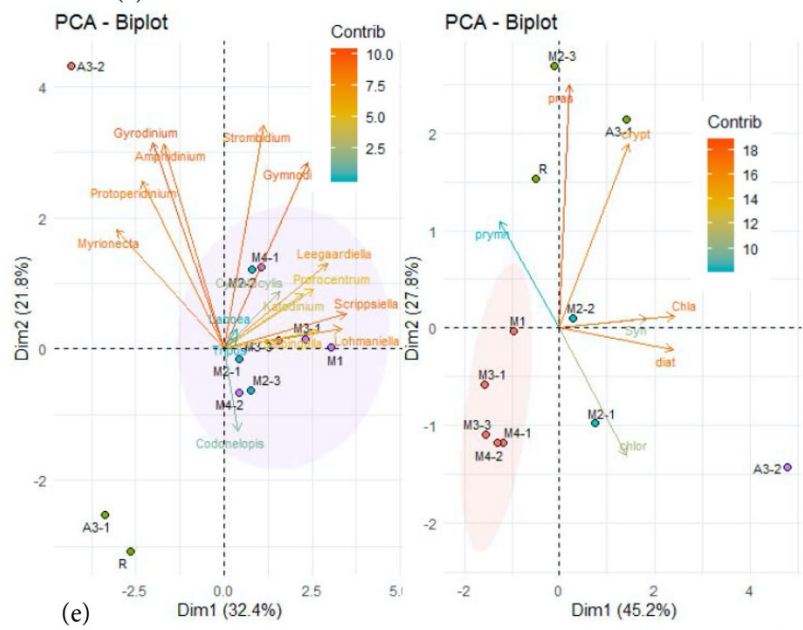
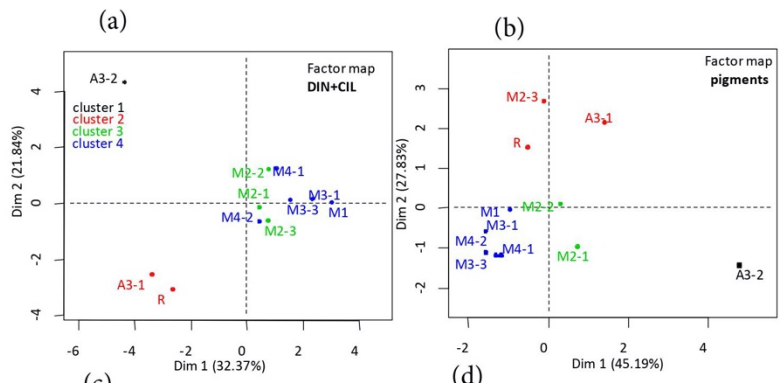


Figure 8



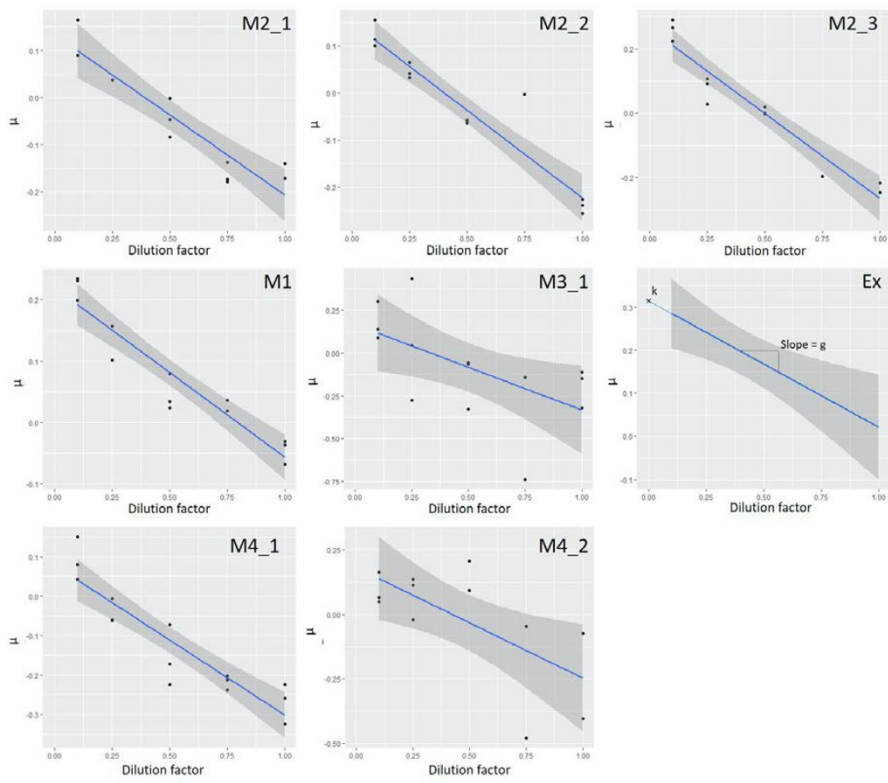


Figure A1

ORIGINAL PAPER

## Protist Interactions and Community Structure During Early Autumn in the Kerguelen Region (Southern Ocean)



Ingrid Sassenhagen<sup>a,1</sup>, Solène Irion<sup>a</sup>, Ludwig Jardillier<sup>b</sup>,  
David Moreira<sup>b</sup>, and Urania Christaki<sup>a</sup>

<sup>a</sup>Laboratoire d'Océanologie et Géosciences, UMR CNRS 8187, Université du Littoral Côte d'Opale, 32 Avenue du Maréchal Foch, 62930 Wimereux, France

<sup>b</sup>Unité d'Ecologie, Systématique et Evolution, Université Paris-Sud, CNRS, AgroParisTech, Université Paris-Saclay, Rue du doyen A. Guinier bât. 360, 91405 Orsay Cedex, France

Submitted August 19, 2019; Accepted December 1, 2019  
Monitoring Editor: Laure Guillou

**This study investigated protist community composition and biotic interactions focusing on microplankton at four distinct sites around the Kerguelen Islands (Southern Ocean) after the summer phytoplankton bloom. Protist diversity in different size fractions, sampled with Niskin bottles and plankton nets, was assessed by sequencing of the V4 18S rDNA region. Combining different approaches, i.e. sequencing of different plankton size fractions, and isolation and sequencing of single cells, provided new insights into microbial interactions in protist communities. The communities displayed high variability, including short-term fluctuations in relative abundance of large protists (>35  $\mu\text{m}$ ) highlighted by the plankton net samples. Size fractionation of protist communities showed high concentrations of free Syndiniales spores but relatively few Syndiniales associated with microplankton, suggesting low parasitic infection in early autumn. Co-variance network analyses and sequencing of individually isolated single cells highlighted the important role of Rhizaria as consumers of a wide range of different diatom taxa. The data also raised the hypothesis that different Syndiniales clades might be directly or indirectly associated with some diatom genera, thus suggesting a potentially wider host range of these parasites than has been previously reported. These associations and the potential impact on carbon fluxes are discussed.**

© 2019 Elsevier GmbH. All rights reserved.

**Key words:** Southern Ocean; single cell sequencing; co-variance analysis; biotic interactions; parasitic Syndiniales; predation.

### Introduction

Although the Southern Ocean is considered a high-nutrient low-chlorophyll (HNLC) area, massive and recurrent phytoplankton blooms are observed over

and eastward of the Kerguelen plateau. Massive, annual diatom blooms cover an area of approx. 45.000 km<sup>2</sup> within the otherwise HNLC Southern Ocean, last three to four months and play a major role in carbon export in this area (e.g. Blain et al. 2007). This phenomenon is explained by intense vertical mixing through eddies east of the Kerguelen Islands that transports deep, iron-rich water onto

<sup>1</sup>Corresponding author  
e-mail [ingrid.sassenhagen@gmail.com](mailto:ingrid.sassenhagen@gmail.com) (I. Sassenhagen).

the plateau (Blain et al. 2007; d'Ovidio et al. 2015; Park et al. 2014), resulting in spatially restricted natural iron fertilization that sustains very high production rates (Cavagna et al. 2015). In contrast, areas off the plateau largely represent less productive HNLC waters typical for the Southern Ocean. This spatial heterogeneity gives rise to highly differentiated phytoplankton communities and corresponding differences in higher trophic levels due to cascading effects (Georges et al. 2014; Lasbleiz et al. 2016).

Previous cruises in the Kerguelen area focused on the onset and decline of the diatom bloom and the associated carbon export (cruises KEOPS2 and KEOPS1, Blain et al. 2007; Christaki et al. 2014; and references therein). The cruise for this study took place in February and March 2018, approximately one month after the decline of the high biomass diatom summer bloom, and was part of the MOBYDICK (Marine Ecosystem Biodiversity and Dynamics of Carbon around Kerguelen: an integrated view) project. Outside the bloom season, phytoplankton communities in the Southern Ocean are typically dominated by autotrophic pico- and nanophytoplankton (Detmer and Bathmann 1997). An increase of predators, including various Rhizaria, phagotrophic dinoflagellates and ciliates (Gowing and Garrison 1992; Matsuoka 2007; Pierce and Turner 1992; Sherr and Sherr 2007), at the end of the phytoplankton bloom contributes significantly to the decline of the diatom community in the Kerguelen area and other polar regions (Christaki et al. 2015; Levinsen et al. 1999, 2000; Lovejoy et al. 2002; Nielsen and Hansen 1995). Furthermore, several recent studies emphasized the potential importance of parasitism in aquatic plankton communities (e.g. Hudson et al. 2006; Jephcott et al. 2016; Lafferty et al. 2006; Lepère et al. 2008). Parasites have the potential to strongly influence community composition and nutrient cycling in an ecosystem by e.g. terminating phytoplankton blooms (Chambouvet et al. 2008; Velo-Suárez et al. 2013) or favoring the growth of one species through the infection of its grazers or competitors (Coats and Heisler 1989; Kimmerer and McKinnon 1990; Skovgaard and Saiz 2006). Recent studies of marine microbial communities, using 18S rDNA sequencing, showcased extremely high diversity and abundance (as deduced from sequence numbers) of Syndiniales in a variety of marine ecosystems (e.g. Christaki et al. 2017; Guillou et al. 2008; López-García et al. 2001). These parasites, phylogenetically related to dinoflagellates (Guillou et al. 2008), also represented the majority of Alveolata sequences in

a previous study in this area of the Southern Ocean (KEOPS2, Georges et al. 2014). Despite their potentially large impact upon ecosystem functioning, information about cell densities and host range of Syndiniales remains very limited due to difficulties with microscopic counts and culturing of these organisms.

Biotic interactions such as predation and parasitism may have an important role in shaping protist community composition in the Austral autumn after the diatom summer bloom. However, estimating cell abundance and impact of parasites and large grazers through amplicon sequencing of entire microbial communities is challenging. Cell numbers of large organisms ( $>20\ \mu\text{m}$ ) in volumes of approx. 10L are usually not representative due to their patchy distribution and often low abundance (Omori and Hamner 1982). On the other hand, the proportion of Syndiniales might be overestimated due to their potentially high rRNA gene copy numbers (Not et al. 2009). In addition, classical sequencing data sets from whole water communities do not allow distinguishing between different parasitic life-stages, such as free-living spores ( $3\text{--}10\ \mu\text{m}$ ) and infecting stages associated with larger cells ( $>20\ \mu\text{m}$ ). In contrast, plankton net tows process large amounts of water over an integrated depth, concentrate large and potentially infected organisms, and exclude small cells like free-living parasitic spores. To gain insights into plankton community composition focusing especially on large protists and their interactions in the Southern Ocean around the Kerguelen Islands, we compared the  $>35\ \mu\text{m}$  size fraction of the protist community from plankton net tows (125 m depth to surface) with the  $0.2\text{--}20\ \mu\text{m}$  and  $20\text{--}100\ \mu\text{m}$  fractions from Niskin bottles taken at discrete depths (10, 60 and 125 m). The objectives of this study were to assess the spatial structure and temporal dynamics of protist communities in this region after the diatom summer bloom and identify potential abiotic and biotic drivers of protist assemblages. The sequencing data showed clear spatial differences in protist diversity in the Kerguelen area, as well as high, short-term variability in relative abundance of large protists after the diatom summer bloom. Furthermore, our sampling strategy revealed many Syndiniales reads in smaller size fractions ( $0.2\text{--}20\ \mu\text{m}$ ) likely representing free-living spores, but suggested lower prevalence (% of infected host cells) of parasitic infections in large cells. Co-variance network analysis and single cell sequencing confirmed Rhizaria as important predators and suggested potential associations between diatoms and parasitic Syndiniales.

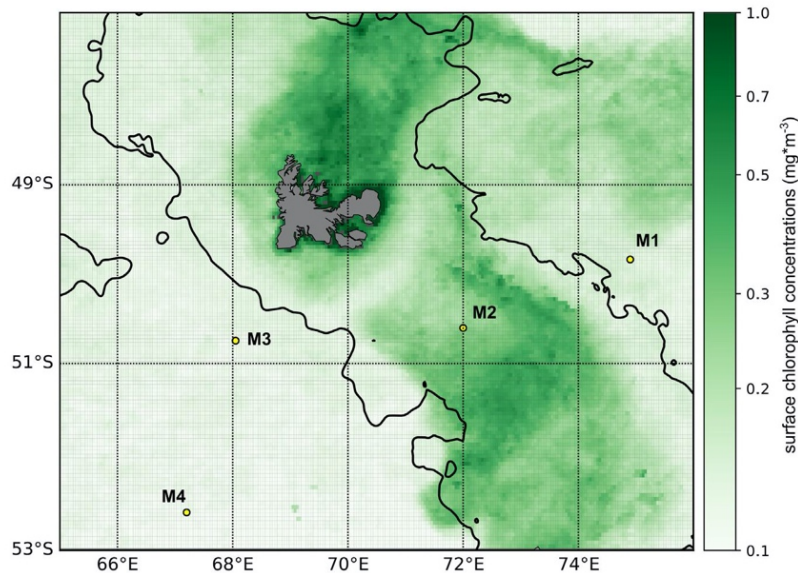


**Figure 1.** Map of sampling stations around the Kerguelen Islands in the Southern Ocean. Surface chlorophyll concentrations are Reprocessed Global Ocean Satellite Observations (Copernicus-GlobColour) from Copernicus Marine Service (<http://marine.copernicus.eu/>). Chlorophyll concentrations are the monthly means for March 2018 at a resolution of 4 km. The black lines denote 1000 m bathymetry.

## Results

### Environmental and Hydrographic Conditions

During the MOBYDICK oceanographic cruise in 2018, we sampled four sites around the Kerguelen Islands. The site M2 was located in the highly productive, iron fertilized waters on the plateau of the Kerguelen Islands corresponding to station A3 in previous KEOPS1 and KEOPS2 cruises (Blain et al. 2007, 2008; Closset et al. 2014). During the MOBYDICK cruise, this station was characterized by Antarctic water masses. The sites M1 and M4 were both situated very close to the Polar Front (Pauthenet et al. 2018), but still in the Antarctic zone, north and south-west of the plateau respectively. In contrast, the site M3 was located in Sub-Antarctic water masses north of the Polar Front. The depth of the mixed layer ( $Z_{ML}$ ) varied from 27 m at M1 to 87 m at M4.2 and it deepened at all stations visited after a storm that occurred in the region on March 10<sup>th</sup> 2018 (Table 1). Mean concentrations of Chl *a* in the mixed layer doubled within the three weeks between the first and the third visit at M2 (from 0.26 to 0.58  $\mu\text{g L}^{-1}$ ). The stations off the plateau displayed slightly lower Chl *a* concentrations with the exception of M1, which showed intermediate Chl *a* concentrations (0.35  $\mu\text{g L}^{-1}$ ).

Temperature was highest at M3 indicating the influence of the Sub-Antarctic zone. In the mixed layer of all stations, the macronutrients  $\text{NO}_3$  and  $\text{PO}_4$  were abundant,  $\text{NH}_4$  showed an increase between the first and the second visit at M2, while  $\text{SiOH}_4$  was lowest at M2 and slightly increased over the three visits at this station (Table 1).

### Protist Diversity in Different Size Fractions

In total, 61 samples were collected using either plankton nets or Niskin bottles. Between 5,594 and 140,900 reads remained per sample after demultiplexing, filtering of reads and removal of ASVs affiliated to Metazoa, Excavata and Amoebozoa. The remaining sequences were clustered into 3,320 ASVs that belonged to 408 different genera.

The different sampling approaches yielded distinct protist communities (Fig. 3). A total of 314 different genera were recorded in the small size fraction (<20  $\mu\text{m}$ ) from the Niskin bottles, out of which 15 genera were classified as abundant by representing more than 1% of all reads in this fraction. These samples were dominated, in terms of number of reads, by ASVs affiliated with Synidiales, Prymnesiophyceae (mainly *Phaeocystis*), *Telonemia* and the small diatom *Chaetoceros* (Table 2). The 20–100  $\mu\text{m}$  size fraction comprised 338 different genera, out of which 21 were abun-

**Table 1.** Sampling locations, dates and times of the plankton net samples. Isolation, amplification and sequencing success of single cells (SC) from one plankton net sample per station. Only successful sequenced SC, i.e. retrieval of a sequence from the anticipated isolated taxon, are listed. Depth of mixed layer ( $Z_{ML}$ ) and environmental parameters assessed by CTD or manual measurements from Niskin bottles at most 19h before or after the net sampling. Environmental parameters represent averages of discrete samples from surface to 75 m depth. Chl *a* concentrations are based on CTD fluorescence data.

Net Station	Longitude (°E)	Latitude (°S)	Date	Sampling time	isolated SC	amplified SC	sequenced SC	T (°C)	$Z_{ML}$ (m)	Sal	Chl <i>a</i> ( $\mu\text{g L}^{-1}$ )	$\text{NH}_4$ ( $\mu\text{M}$ )	$\text{PO}_4$ ( $\mu\text{M}$ )	$\text{Si(OH)}_4$ ( $\mu\text{M}$ )	$\text{NO}_2$ ( $\mu\text{M}$ )	$\text{NO}_3$ ( $\mu\text{M}$ )
PN01 M2.1	72.0004	50.3697	26.02.2018	15:00–15:30	24	20	14	5.18	61	33.86	0.29	0.75	1.47	1.36	0.27	21.72
PN02			26.02.2018	18:45–19:10				5.17	61	33.86	0.29	0.75	1.47	1.36	0.27	21.72
PN03			01.03.2018	14:45–15:05	17	10	0	4.60	49	33.84	0.18	0.37	1.71	4.37	0.25	25.47
PN04 M4.1	67.1198	52.3601	01.03.2018	18:20–18:45				4.60	49	33.84	0.18	0.37	1.71	4.37	0.25	25.47
PN05 M3.1	68.0347	50.4095	04.03.2018	06:00–06:45	35	11	1	5.49	65	33.82	0.19	0.63	1.65	2.90	0.25	23.50
PN06			04.03.2018	19:05–19:20				5.48	65	33.82	0.19	0.63	1.65	2.90	0.25	23.50
PN07 M2.2	72.0099	50.3769	06.03.2018	17:20–17:35	48	24	5	5.21	62	33.86	0.33	1.12	1.50	1.72	0.28	21.51
PN08 M1	74.5406	49.5098	09.03.2018	16:10–16:30	30	22	18	4.42	27	33.90	0.31	0.80	1.72	8.39	0.33	24.93
PN09			12.03.2018	16:45–17:05	28	9	2	4.47	87	33.85	0.21	0.48	1.72	4.80	0.27	24.58
PN10 M4.2	67.1228	52.3610	13.03.2018	10:45–11:00				4.42	87	33.85	0.21	0.48	1.72	4.80	0.27	24.58
PN11			16.03.2018	12:25–12:45				5.14	68	33.86	0.6	0.95	1.51	2.76	0.30	21.68
PN12 M2.3	72.0013	50.3700	16.03.2018	17:55–18:15	39	19	8	5.14	68	33.86	0.6	0.95	1.51	2.76	0.30	21.68
PN13			17.03.2018	19:25–19:45				5.16	68	33.86	0.6	0.95	1.51	2.76	0.30	21.68
PN14 M3.3	68.0302	50.4193	19.03.2018	15:00–15:30	30	14	4	5.28	79	33.81	0.14	0.73	1.08	2.31	0.16	15.41

**Table 2.** List of abundant protist genera, which represent more than 1% of the reads in each size fraction.

	Niskin bottle 0.2–20 µm		Niskin bottle 20–100 µm		plankton net 35–100 µm	
# samples	23		24		14	
# genera abundant	314		338		270	
Genera (>1% of reads)	15		21		14	
	Syndiniales	Group-I-Clade-1	Bacillariophyta	Corethron	Bacillariophyta	Corethron
	Pymnesiophyceae	Phaeocystis	Dinophyceae	NA	Dinophyceae	Triplos
	Dinophyceae	NA	Spirotrichea	NA	Bacillariophyta	Thalassiosira
	Syndiniales	Group-I-Clade-4	Bacillariophyta	Acantharea	Bacillariophyta	Eucampia
	Syndiniales	Group-II-Clade-10&11	Acantharea	Acanthomeiron	Bacillariophyta	Chaetoceros
	Bacillariophyta	Chaetoceros	Syndiniales	Group-I-Clade-1	Acantharea	Acanthomeiron
	Dinophyceae	Dinophyceae	Dinophyceae	Triplos	Bacillariophyta	NA
	Bacillariophyta	Fragiliariopsis	Bacillariophyta	Proboscia	Dinophyceae	Protooperidinium
	Acantharea	Acanthomeiron	Bacillariophyta	Eucampia	Dinophyceae	NA
	MAST	MAST-1C	Pymnesiophyceae	Phaeocystis	Bacillariophyta	NA
	Telonemia	Telonemia-Group-2	Bacillariophyta	Chaetoceros	Bacillariophyta	Odontella
	Telonemia	Telonemia-Group-1	Spirotrichea	Dictyocystidae	Syndiniales	Hematodinium
	Bacillariophyta	NA	Bacillariophyta	Odontella	Bacillariophyta	Proboscia
	RAD-B	RAD-B-Group-IV	Bacillariophyta	NA	Bacillariophyta	NA
	Pelagophyceae	Pelagomonas	Bacillariophyta	Pseudo-nitzschia		
			Dinophyceae	Radiolaria		
			Radiolaria	Group-II-Clade-10&11		
			Syndiniales	NA		
			Bacillariophyta	Fragiliariopsis		
			Bacillariophyta	Leegaardella		
			Spirotrichea			

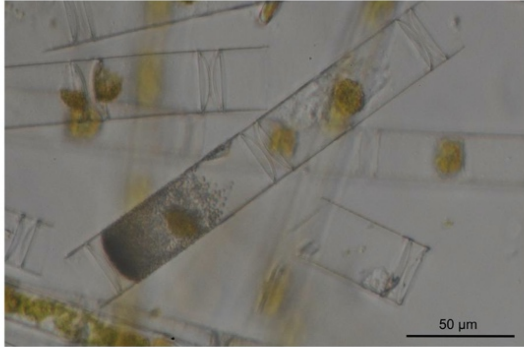


**Figure 2.** Photograph of the dominant diatom on the plateau (M2) *Corethron inerme* filled with small, round, intracellular features.

dant. These samples were also characterized by high read numbers of *Phaeocystis* (Prymnesiophyceae), different ciliate and Syndiniales genera, but most reads were affiliated with large diatoms, dinoflagellates and Radiolaria. In contrast, the plankton net samples (35–100  $\mu\text{m}$ ) contained much fewer reads of small protist taxa such as *Phaeocystis* and Syndiniales, but illustrated the dominance of diatoms such as *Corethron* and *Thalassiosira*, and the dinoflagellate *Tripos* in a few samples. These samples only contained 270 different genera, of which 14 were abundant. Although up to 35 genera were exclusively found in one of the three size fractions, they were always rare, contributing to, at most, 0.02% of reads to their respective size fraction.

The plankton net samples contained very few Syndiniales reads (<10% at each station) compared to the 0.2–20  $\mu\text{m}$  size fraction from the Niskin bottles (up to 70%) (Fig. 2). Despite these overall differences in read numbers, Syndiniales Group I clade 1 was the most abundant Syndiniales taxon at all stations and in all size fractions (Fig. 4). Syndiniales Group II clade 10 and 11 was similarly abundant in both size fractions from the Niskin bottles (<20  $\mu\text{m}$  and 20–100  $\mu\text{m}$ ), but represented only few reads in the plankton net samples. Syndiniales Group I clade 4 reached relatively high read numbers in the small size fraction of the Niskin bottles, but was much less abundant in both larger size fractions. In contrast, *Hematodinium* (Group IV) and Group II clade 4 contributed a high proportion of reads to many plankton net samples (35–100  $\mu\text{m}$ ), but were often absent in smaller size fractions. The relative abundance of Syndiniales in all size fractions declined over time at all sites that were

repeatedly sampled during the cruise (M2, M3 and M4) (Fig. 3).

### Community Structure of Large Protists (Plankton Net Samples)

Plankton net samples collected at M2 showed high variability in diversity indices with lowest richness at M2.1 (193 ASVs) and highest richness at M2.3 (341 ASVs) (Fig. 5). Interestingly, while M2.3 showed the highest richness, it also displayed the lowest Simpson, Shannon and Pielou evenness indices. In contrast, M4.1 showed the highest evenness. This higher evenness in the protist community at M4.1 was also illustrated by the shape of rank abundance curves, which displayed a much more linear relationship between ranked taxa and their relative abundance compared to M2.3 (Supplementary Material Fig. S2). However, individual plankton nets from M4.1 varied noticeably in richness, PN03 (afternoon sample from M4.1) containing much higher number of ASVs than PN04 (evening sample from M4.1), which also represented the plankton net sample with the lowest sequencing depth (6944 reads in PN04 vs. >14000 reads in other PN). Evenness indices varied also significantly between samples from M3.1, PN06 being much less diverse than PN05. Samples collected in the morning or afternoon were usually more diverse than samples collected in the evening, especially based on the Shannon index (M2.1: PN01 > PN02, M4.1: PN03 > PN04, M3.1: PN05 > PN06).

In a dendrogram based on weighted unifrac distances, the protist communities sampled with plankton nets at M2.3 clustered together (>90% similarity) and were highly differentiated from all other plankton net samples (Fig. 6). The composition of protist communities collected at M4 was also highly similar (approx. 80% similarity) and formed a “south-western” cluster with most plankton net samples from M3. This cluster was further characterized by relatively high diversity (i.e. evenness). The third cluster in the dendrogram was formed by plankton nets from earlier visits at M2 (M2.1 and M2.2), M3.1 and M1.1, from here on referred to as the “mixed” cluster, and displayed intermediate diversity. These three clusters were significantly differentiated from each other based on overall PERMANOVA ( $F=6.56$ ,  $p=0.002$ ) and multilevel pairwise comparisons (adj.  $p<0.05$ ). Grouping the plankton net samples by site or location relative to the plateau also revealed significant differences among the groups ( $p<0.006$ ), but only one pairwise comparison turned out to be significant (M2 vs. M4, plateau vs. south-west) in each analysis. Interest-

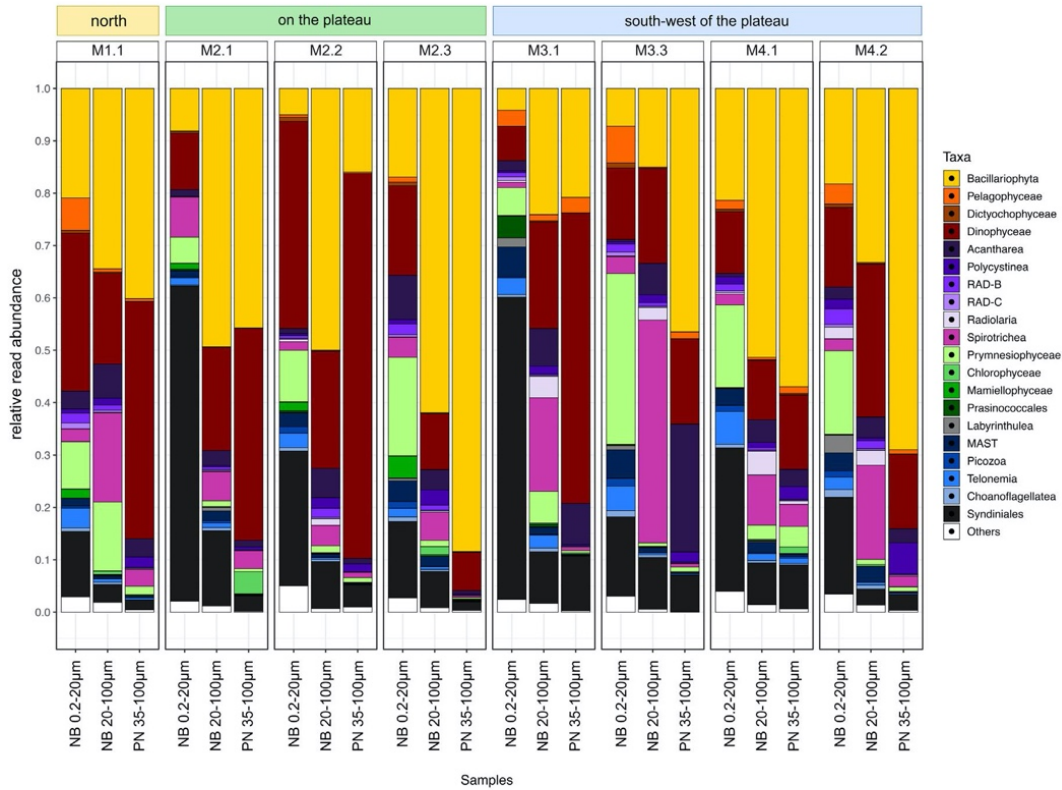


**Figure 3.** Barplot illustrating the relative read abundance of the 20 most common protist classes present in the 0.2–20  $\mu\text{m}$  fraction and 20–100  $\mu\text{m}$  fraction from Niskin bottles (NB), and plankton net samples (PN) at all stations.

ingly, plankton nets collected at M3.1 thirteen hours apart from each other appeared to be highly distinct and belonged to different dendrogram clusters.

A heatmap of relative protist abundance in the plankton net samples (35–100  $\mu\text{m}$  size fraction) (Fig. 6) further emphasized the high variability in community composition at the plateau sampling site M2. During the first two visits (M2.1 – PN01 and PN02, M2.2 – PN07), the samples were characterized by high numbers of reads from the dinoflagellate *Tripes* similar to samples collected north of the plateau (M1.1 – PN08) and in the evening of the first visit at M3 (PN06). Furthermore, the diatom *Eucampia* was highly abundant in samples taken at M2.1. In contrast, *Corethron* reads dominated the samples from the third visit at M2 (M2.3 – PN11, PN12 and PN13). The stations M3 and M4 south of the plateau were dominated by reads from *Thalassiosira*, the second most abundant diatom genus in this sequencing dataset. Furthermore, the diatom *Chaetoceros* and other unidentified diatoms were highly abundant at sta-

tion M4. Plankton net samples from M3 contained also a high number of reads from the radiolarian genus *Acanthometron*. The Syndiniales genus *Hematodinium* represented 20% of the reads from the plankton net sample taken in the morning of the first visit at M3 (PN05, Fig. 6). In all other plankton net samples, Syndiniales were significantly less abundant based on number of reads. *Hematodinium* contributed at most 3% of reads to the community data at all other stations. Syndiniales Group I represented at most 6% of reads at M4.1 while Group II reached at most 4% of reads at the same station. Overall, our sequencing data suggested the highest prevalence of parasites associated with large cells at the stations M3 and M4.1.

In the plankton net samples, Syndiniales Group I was more abundant in terms of number of reads than Group II (Figs 4, 6). However, Group II displayed more phylogenetic diversity by representing six different clades in contrast to only three clades in Group I (Fig. 7), according to classification by



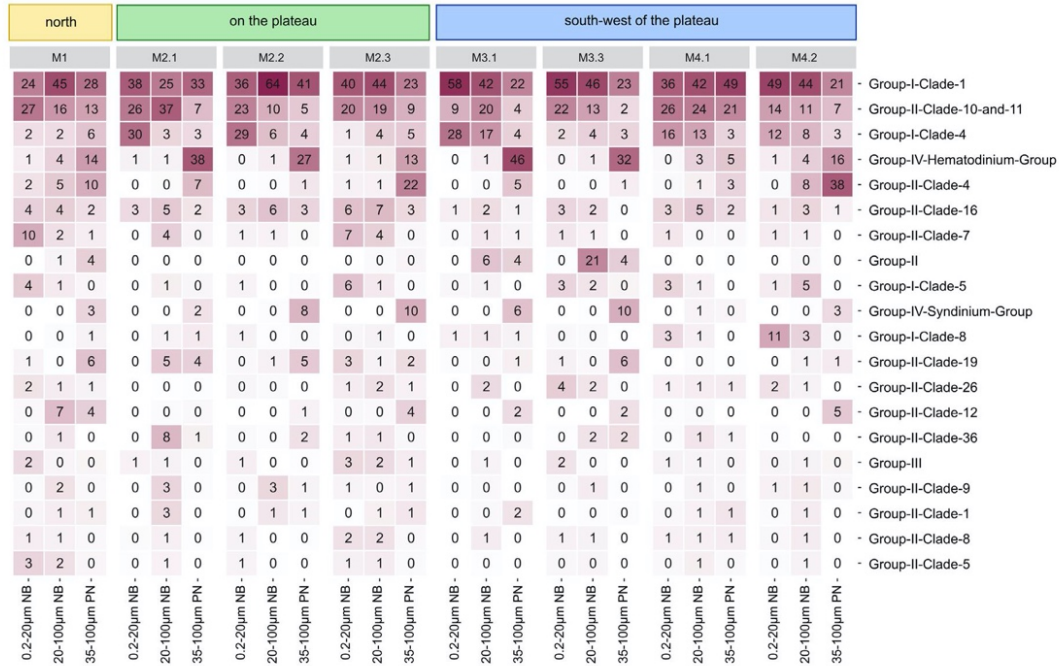


**Figure 4.** Heatmap illustrating the read numbers of the 20 most common Syndiniales families out of the total, rarefied protist communities present in the 0.2–20 µm fraction, 20–100 µm fraction from Niskin bottles (NB) and plankton net samples (PN) at all stations.

Guillou et al. (2008). The phylogenetic tree of the 25 most abundant Syndiniales sequences in the 0.2–20 µm size fraction from the Niskin bottles, the plankton nets and the single cell isolates showed that the majority of ASVs and OTUs from Group II belonged to the dominant clade 10 and 11. Two single cell OTUs (OTU27 & OTU76) and four ASVs from plankton net communities belonged to clade 4 and were closely related to the genus *Amoebophrya* (Fig. 7). Furthermore, Syndiniales belonging to clade 7, 12, 16 and 19 in Group II were also found. The majority of Group I Syndiniales belonged to clade 1, but few ASVs and OTUs were part of clade 4 and closely related to *Euduboscquella*. Some Syndiniales sequenced in this study belonged to Group IV and likely represented the genus *Hematodinium*. Furthermore, ASV383 was highly similar to sequences of the genus *Syndinium* (Fig. 7).

#### Relation with Environmental Variables

Spearman correlations between relative abundance of individual protist genera and environmental variables suggested that the diatoms *Pseudo-nitzschia*, *Dactyliosolen* and *Fragilariopsis* were positively correlated to phosphate and

silicate concentrations ( $R > 0.83$ , adj.  $p < 0.005$ ). The diatoms *Odontella* and *Eucampia* occurred in higher salinity water masses ( $R > 0.8$ , adj.  $p < 0.02$ ), which characterized the area on and to the north of the plateau at the beginning of the cruise (M1, M2.1, M2.2). Read numbers of the ciliate *Salpingella* and the diatoms *Odontella* and *Corethron* rose with increasing nitrite concentrations ( $R > 0.77$ , adj.  $p < 0.03$ ), while the Syndiniales genus *Syndinium* was negatively correlated to oxygen concentrations ( $R = -0.88$ , adj.  $p < 0.0001$ ). However, when performing a CCA of all plankton net samples (all ASVs) to assess the impact of environmental conditions on protist community composition in the mixed layer, only ammonium concentrations were significantly related to the sequencing data (AIC = 164.91,  $F = 2.7229$ ,  $p = 0.005$ ). Ammonium concentrations explained approximately 18.5% of the variation independent of the taxonomic level and abundance threshold applied to the taxa. The plotted ordination (Fig. 8), limited for better readability to genera representing  $> 0.1\%$  of the reads, illustrated also that samples collected at M2.3 were characterized by the diatom genera *Corethron* and *Rhizosolenia*, and a Syndiniales genus belonging to Group II clade 4. The mixed cluster was characterized

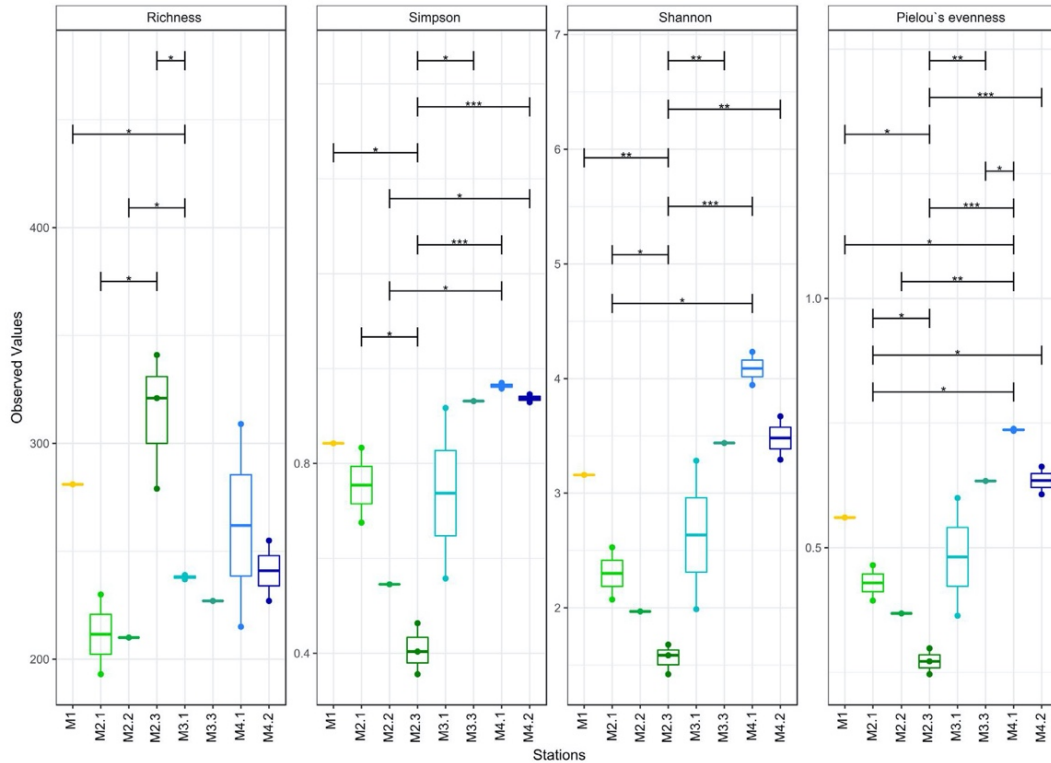


**Figure 5.** Alpha diversity indices of plankton net communities pooled by sampling stations. Horizontal lines with stars indicate significant differences in diversity indices between individual stations. M2.1 contains the net samples PN01 & PN02, while M2.3 represents PN11, PN12 & PN13. M3.1 contains PN05 and PN06. M4.1 consists of two net samples (PN03 & PN04), while M4.2 represents PN09 & PN10. M1, M2.2 and M3.3 consist of one net sample each.

by high amounts of reads from the dinoflagellate *Tripes*, the ciliate *Salpingella*, a radiolarian, the chlorophyte *Dunaliella*, a Syndiniales strain belonging to Group I clade 1 and the diatoms *Eucampia* and *Odontella*, emphasizing again the high variability at the plateau station M2. The protist community in the south-western cluster (M4 and most of M3) could be distinguished from other samples based on the higher read abundance of the ciliate *Leegardiella*, a radiolarian, the dinoflagellate *Protoperdinium* and diatoms such as *Chaetoceros*, *Thalassiosira* and *Dactyliosolen* (Fig. 8).

### Co-variance Network Analysis

The amount of significantly contributing nodes and edges in the networks generated with PLNmodels decreased with increasing taxonomic clustering rank (i.e. species > genera > family). When merging ASVs at the family level, highly diverse families such as diatoms vanished from the network likely

due to conflicting occurrence patterns among different taxa within this family. On the other hand, when clustering at the species level, more co-variance appeared among incompletely identified taxa likely belonging to the same species. The network that we presented was, therefore, a compromise based on ASVs merged, when possible, at the taxonomic rank of genera. Excluding indirect effects through co-variation of protist community composition in plankton net samples with ammonium concentrations increased the Bayesian Information Criterion (control for  $\text{NH}_4$ :  $\text{BIC} = -5163.8$ ; no control:  $\text{BIC} = -5239.6$ ) of the model suggesting a better fit when controlling for this environmental parameter. The plankton net network consisted of 38 nodes (genera) and 77 edges (co-variances) (Fig. 9). It displayed relatively low density. Only 11% of the possible connections were inferred indicating that each node was only connected to a limited number other nodes (Supplementary Material Table

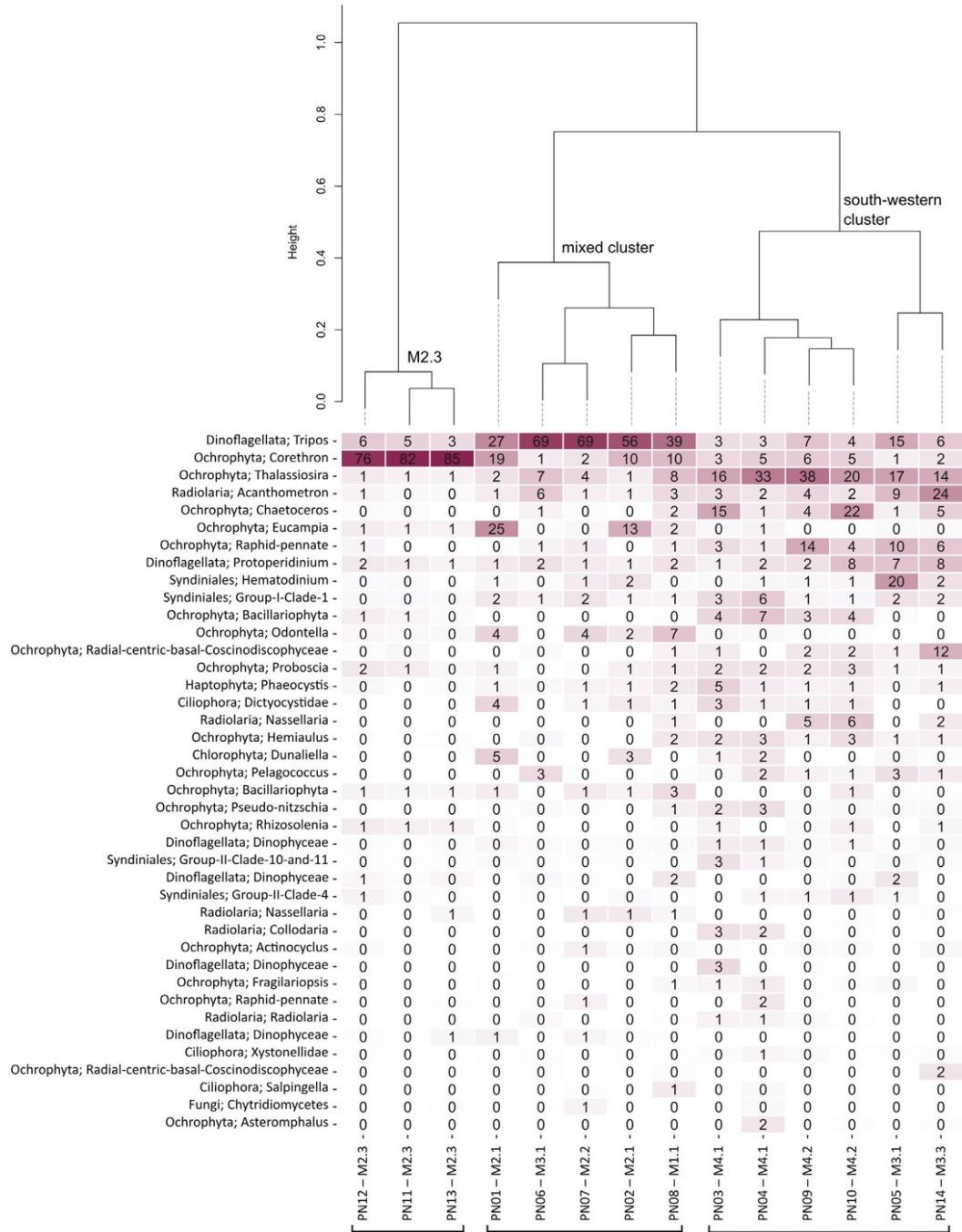


**Figure 6.** Heatmap and dendrogram from weighted unifracs distances illustrating community composition and clustering of plankton net samples (35–100 μm size fraction) based on the relative read abundance (%) of protist genera.

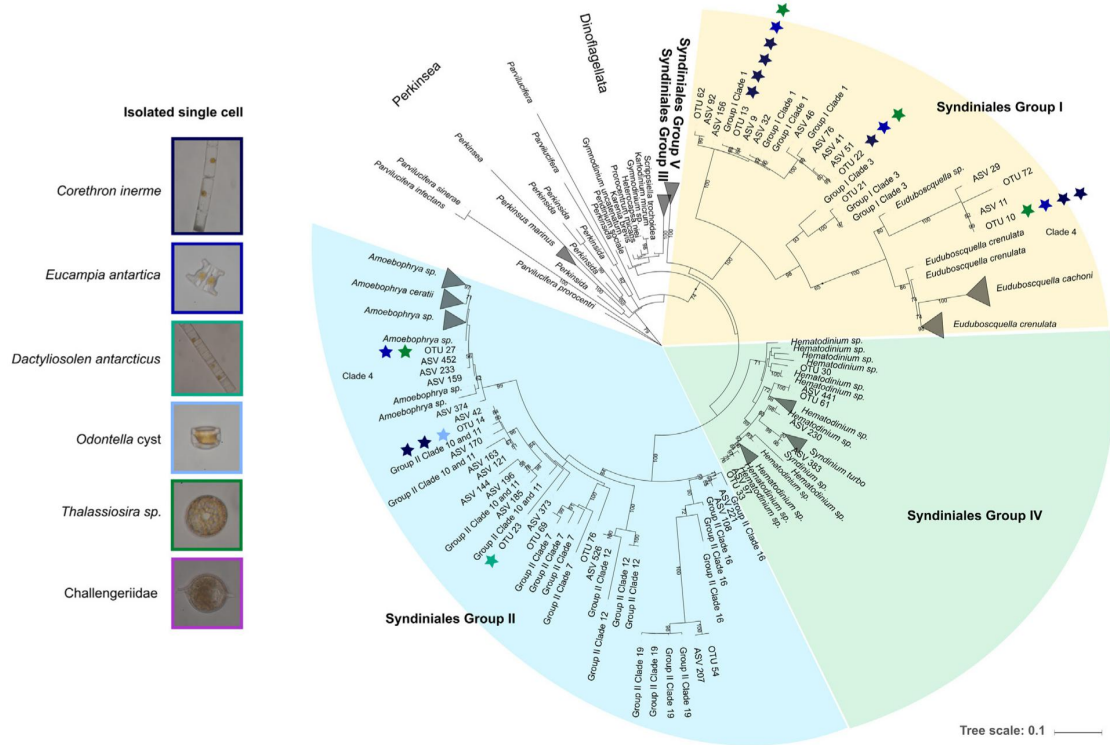


**Figure 7.** Maximum Likelihood phylogeny of 18S rDNA sequences of Syndiniales built with RAxML. Sequences marked with ASV originate from community sequencing data of the 0.2–20  $\mu\text{m}$  Niskin bottle and 35–100  $\mu\text{m}$  plankton net size fractions, while OTUs were sequenced with single cell isolates. All other sequences represent references from PR<sup>2</sup> and NCBI. The colour of stars refers to the manually isolated organisms on the left side of the figure, with which the Syndiniales OTUs were associated.

S1). However, this network was notably different from randomized networks (Kolmogorov–Smirnov statistic test avg.  $D=0.346$ ). The clustering coefficient ( $C(p)=0.302$ ) for example was higher than in the randomized networks ( $C(p)=0.023–0.165$ ) suggesting that some nodes were connected to most components of the network. Furthermore, neighborhood connectivity was noticeably different between the original network and the random networks (Kolmogorov–Smirnov test statistic  $D=0.66$ ) due to a strong decline of neighborhood connectivity with increasing number of neighbors in the original network (Supplementary Material Fig. S3). This pattern indicated that nodes with low connectivity were often associated with highly connected nodes in the network (Maslov and Sneppen 2002). Due to these features, i.e. high local clustering of nodes but also short path lengths between elements, the network was classified as a “small world” ( $\sigma=4.71$ ).

Several genera with different ecological functions were central to this network of protists from plankton net samples (Fig. 9). Syndiniales from Group II clade 12, Radiolaria belonging to Arthracanthida-Symphycanthida and Nassellaria, the diatom *Rhizosolenia* and a tintinnid (*Amphorellopsis*) represented the most connected taxa. Syndiniales from Group II clade 12 were negatively related to two ciliate genera (Dictyocystidae and Tontoniidae), and diatoms such as *Odontella* and *Eucampia*, but positively co-varied with other Syndiniales, radial-centric Coscinodiscophyceae and *Pelagococcus*. *Hematodinium* (Group IV) displayed, in contrast, only a negative relation to the diatom *Rhizosolenia*, while Syndiniales from Group II clade 4 negatively co-varied with the dinoflagellate *Phalacroma*. The radiolarian Arthracanthida-Symphycanthida were negatively related to three diatom genera (*Chaetoceros*, polar-centric Mediophyceae, *Rhizosolenia*) and other radiolarians

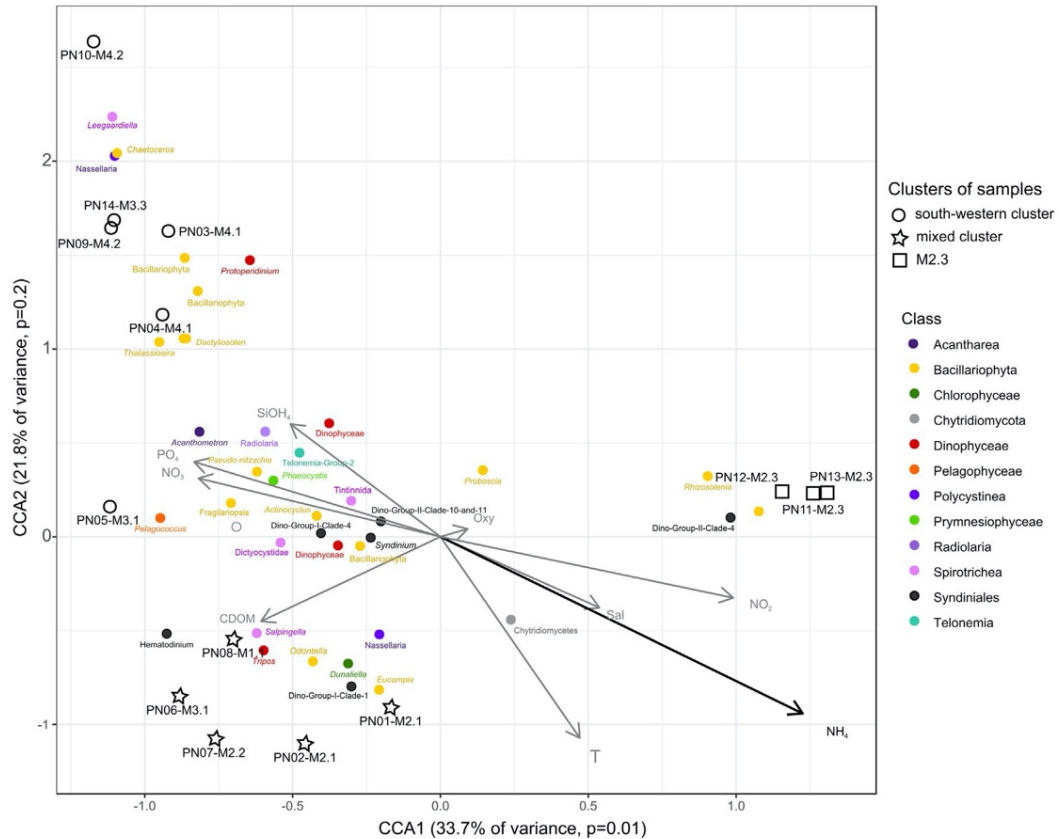


**Figure 8.** This CCA illustrates the impact of environmental conditions on protist community composition collected by plankton nets (35–100  $\mu\text{m}$ ) in surface waters. For better readability, the ordination only includes genera with >0.1% read contribution. Taxa are colored by phylogenetic class and labeled when possible by genus. Cluster assignments of plankton net samples are based on the dendrogram from weighted unifrac distances (Fig. 3). Only  $\text{NH}_4$  explained a significant proportion of the variance in sequencing data between the 14 samples ( $p = 0.005$ , 18.5% of variance).

(*Nassellaria*), but co-occurred with other diatoms (radial-centric *Coscinodiscophyceae*, *Eucampia*), *Chlorophyceae* and the dinoflagellate *Goniodoma*. The diatom *Rhizosolenia* co-varied with several other autotrophic genera (diatoms, *Prymnesiophyceae*), but was negatively related to the *Syndiniales* genus *Hematodinium* and the radiolarian taxon *Arthracanthida-Symphyacanthida*. The tintinnid *Amphorellopsis* co-varied with two dinoflagellates (*Tripos* and *Phalacrothrix*), two diatoms (*Eucampia* and *Odontella*), another tintinnid, parasitic *Chytridiomycetes* and the radiolarian taxon *Arthracanthida-Symphyacanthida*, but was negatively related to another ciliate (*Leegaardiella*) and polar-centric *Coscinodiscophyceae*. The few

chytrids found in this study co-varied with very few protists genera in the network, which might be caused by the tight correlation of their read numbers with ammonium concentrations (see Fig. 8).

The co-variance network of protists in the small size fraction (0.2–20  $\mu\text{m}$ ) was dominated by *Rhizaria* and parasites such as *Syndiniales*, *Cryothecomonas*, *Labyrinthulaceae*, *Endomyxa* and *Blastodinium* (Supplementary Material Fig. S4). Group I clade 2 *Syndiniales* represented the most connected taxon in this network, co-varying with several other *Syndiniales*, *Rhizaria* and *Stramenopiles*. Very few autotrophic genera or dinoflagellates were included in the network due to lack of significant co-variation.

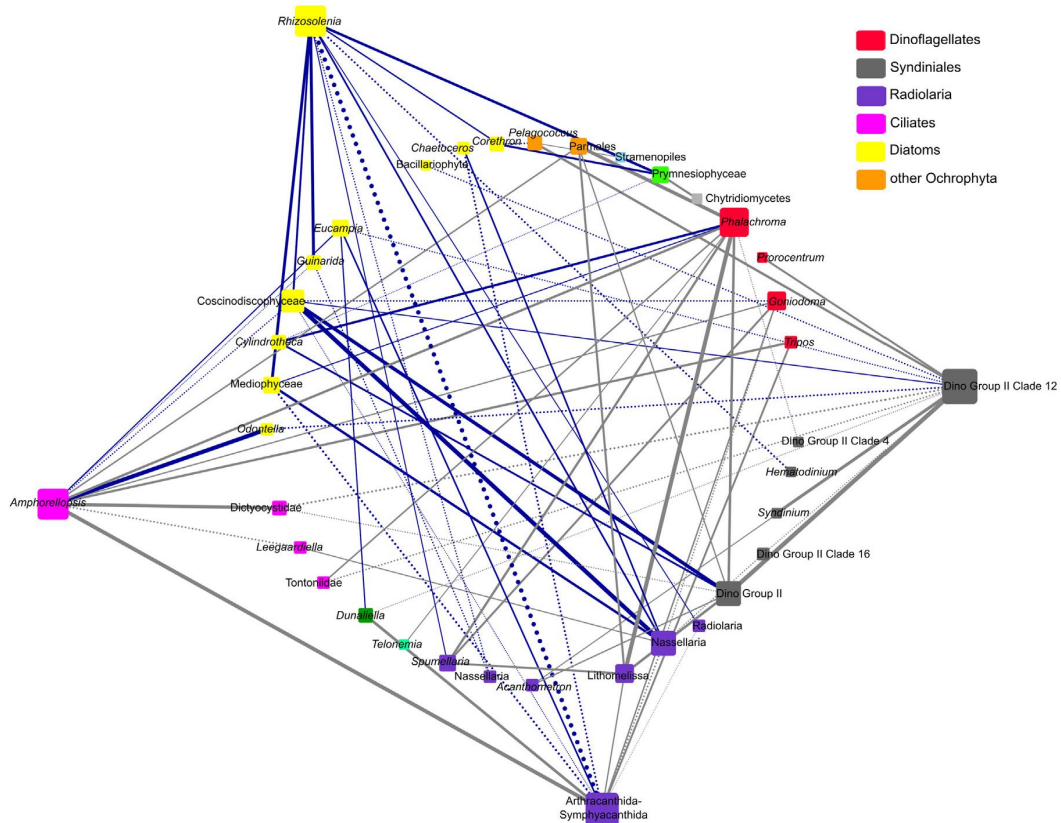


**Figure 9.** Co-variance network based on PLNmodels of protist genera with >0.02% abundance from the plankton net samples. Solid lines indicate positive covariation, while dotted lines indicate negative covariation. The width of lines corresponds to the strength of the covariation. The size of the boxes, which are coloured by division and labeled when possible by genus, corresponds to number of co-variances each nodes is displaying. Potential indirect effects between taxa due to covariation with  $\text{NH}_4$  concentrations are removed from the network. Co-variances with diatoms are emphasized in blue. (For interpretation of the references to colour in this figure legend, the reader is referred to the web version of this article).

### Single Cell Sequencing

From the plankton net samples, the 18S rDNA of 129 individually isolated protists cells was amplified and sequenced (Table 1). The isolated taxa comprised diatoms, dinoflagellates, Rhizaria and ciliates. The taxonomic classification by sequencing agreed in 55 of these single cell samples with morphological identification based on microscopy (Supplementary Material Table S2). Out of these 55 successfully sequenced isolates, 13 contained OTUs affiliated with Syndiniales, which belonged to the groups I, II and IV (Fig. 7). Almost all Syndiniales OTUs were retrieved with isolates of diatoms such as *Corethron*, *Eucampia* and *Thalassiosira*. One Syndiniales OTU was detected in association with a rhizarian cell (Cercozoa, Pheo-

darea). However, no Syndiniales were identified along the 20 sequenced dinoflagellate cells (mostly *Tripos*). Sequencing success of the dinoflagellate *Protoperdinium* was low as only one cell morphologically identified as this genus yielded a sequence in agreement with this affiliation. Individual single cell isolates (e.g. *Corethron*, *Eucampia* etc.) sometimes yielded, in particular at M2.2, sequences of different Syndiniales OTUs (Supplementary Material Table S2), suggesting simultaneous association of one protist cell with different parasitic taxa. Most rhizarian cells (8x Challengeriidae and 4x *Acanthometron*) were associated with sequences of potential prey or symbiont cells (Supplementary Material Table S2). Parasitic Syndiniales and fungi, *Pelagococcus* and diatoms were identified with Challengeriidae cells (Cercozoa, Pheodarea). The

haptophyte *Phaeocystis*, parasitic fungi (Exobasidiomycetes) and diatoms such as *Odontella*, *Dactyliosolen*, *Chaeotoceros* and *Eucampia* were recorded with *Acanthometron* cells (Radiolaria, Acantharea).

## Discussion

### Comparison of Size Fractions

Previous studies in the Southern Ocean around the Kerguelen Islands focused on the onset and decline of the diatom bloom highlighting contrasting chlorophyll *a* concentrations and phytoplankton communities, with generally large diatoms dominating on the plateau and nanophytoplankton in HNLC areas (Armand et al. 2008; Georges et al. 2014; Hashihama et al. 2008; Iida and Odate 2014; Lasbleiz et al. 2016). The present study explored protist communities after the diatom bloom, when chlorophyll concentrations were relatively low in the whole area and the contribution of small sized phytoplankton notably increased on the plateau of the Kerguelen Islands. The different sampling approaches employed in this study provided complementary insights into protist community composition and putative interactions between microbial eukaryotes. The Niskin bottle samples showcased the high diversity of small protists (0.2–20  $\mu\text{m}$ ) such as Prymnesiophyta, Telonemia and Syndiniales. However, short term fluctuations in abundance of large protists (>35  $\mu\text{m}$ ) that might contribute significantly to primary production (i.e. large diatoms) or carbon transfer to higher trophic levels (i.e. Rhizaria), were hardly visible in Niskin bottle samples. Variations in Syndiniales abundance among the different sampling methods were also noticeable. Free-living dinospores of Syndiniales range from 3 to 10  $\mu\text{m}$  in size (Chambouvet et al. 2011; Coats and Park 2002; Velo-Suárez et al. 2013). Syndiniales sequences in the small size fraction from the Niskin bottles (0.2–20  $\mu\text{m}$ ) should, thus, mainly represent free-living dinospores, although infections of host cells smaller than 20  $\mu\text{m}$  might also occur. Sequences in the other samples are expected to mainly correspond to parasites associated with larger cells (>20  $\mu\text{m}$ ). However, cells undergoing parasitic infections can be fragile, and the technique used to separate the <20  $\mu\text{m}$  fraction from the 20–100  $\mu\text{m}$  fraction could rupture them, which could in turn skew the relative abundance of free-living spores. The large differences observed between relative abundance of potential parasitic spores in the small

size fraction (0.2–20  $\mu\text{m}$ ) and parasites likely associated to other cells in the plankton nets potentially reflected the end of a parasitic infection. Several hundred spores are released from each dying host cell (Chambouvet et al. 2008; Coats and Park 2002), but depending on environmental conditions and their short survival time in the water column (Coats and Park 2002), only a small fraction of these free spores will successfully infect a new host cell (<20%, Coats and Park 2002). The eventual lack of host cells following a massive infection will further increase the ratio of spores to parasites associated with hosts.

### Spatial and Temporal Community Dynamics of Large Protists (Plankton Nets)

The protist communities in the plankton net samples were characterized by numerous diatom taxa, some dinoflagellates and radiolarians, and several different Syndiniales taxa. Most protist genera observed in this study have also been reported from previous cruises in the Southern Ocean around Kerguelen Islands (KEOPS 1 and KEOPS 2) (Armand et al. 2008; Christaki et al. 2015; Georges et al. 2014; Lasbleiz et al. 2016). The four chosen sampling sites revealed highly variable protist communities, in particular site M2 on the plateau displayed strong temporal dynamics and rapid community changes. Plankton net samples collected at M2 at the beginning of the cruise (M2.1 and M2.2) displayed a relatively diverse community characterized by the dinoflagellates *Tripos* and *Protoperidinium*, the diatoms *Corethron*, *Eucampia* and *Odontella*, and ciliates similar to samples from M1 and M3.1 (PN06). In contrast, samples collected 10 days later at M2.3 were dominated by reads from the chain-forming diatom *Corethron inerme*. A similar shift in community composition was also observed in the sequencing data from the large size fraction of the Niskin bottles (20–100  $\mu\text{m}$ ), although the dominance of *C. inerme* at M2.3 was more emphasized in plankton net samples. On the other hand, sequencing data from the Niskin bottles and microscopic counts (pers. comm. Leblanc and Lafond) suggested a pronounced increase of *C. inerme* already at station M2.2 contradicting the relatively low read numbers from this species in the sequencing data from the plankton net. Microscopic investigations of the plankton net samples revealed high proportions of broken and infected diatom cells at station M2.2 (Supplementary Material Fig. S1), meaning that only approx. 50% of the cells were viable

(pers. comm. Leblanc and Lafond). This low viability might have reduced the amplification success of *C. inermis* cells in this sample. Furthermore, the high amount of rRNA gene copies in dinoflagellates (Prokopowich et al. 2003), such as *Tripos*, likely exaggerated the actual abundance of these organisms and might have suppressed amplification of other taxa, e.g. at the stations M1, M3.1, M2.1 and M2.2.

The community of large protists sampled at the sites M3 and M4 south-west of the plateau was very distinct from the protist community on and to the north of the plateau (M1 and M2). The samples collected at M3 and M4 were characterized by overall high diversity of diatoms, *Thalassiosira* being the most abundant genus (Fig. 6). Significant differences in plankton community composition between plankton net samples just taken 13 hours apart from each other at M3.1 were driven by large fluctuations in relative abundance of *Tripos*. These fluctuations were potentially caused by heterogeneous distribution of this dinoflagellate population due to aggregation of cells in horizontal and vertical patches (e.g. Breier et al. 2018) that are most likely evidenced by net tows rather than Niskin bottle sampling. Furthermore, diel vertical migration of this dinoflagellate, as it has been previously observed on the Southern California shelf and in the Southern Benguela upwelling system (Eppley et al. 1984; Pitcher et al. 1998), might have contributed to high variability in relative abundance of this genus as well. In this study, the abundance of *Tripos* was higher in the surface layer (<125 m depth) in the afternoon and evening than in the morning suggesting vertical migration through phototaxis (Kamykowski 1995). Vertical migration allows balancing photosynthetic requirements for light and uptake of nutrients over a relatively large part of the water column, a behavior that is especially beneficial in oligotrophic, stratified environments. Diel variability in protist community composition might be very common in marine ecosystems and needs to be considered in sampling designs of future studies.

### Impact of Environmental Conditions on Protist Community Composition

To assess potential drivers of this community variability, relationships between environmental conditions and community composition were investigated. The canonical correspondence analysis (CCA) indicated a significant impact of ammonium concentrations on the community composition in the plankton net samples. Ammonium concentra-

tions were always highest at the plateau station M2, but increased even further over the course of the cruise from 0.75 to >1  $\mu\text{M}$ . Bacterial growth rates and grazing increased between the first and third visit at M2.2, likely contributing to intensified remineralization of organic nitrogen and increased ammonium concentrations (Goeyens et al. 1995; Mosseri et al. 2008). Ammonium represents the preferred nitrogen source of most phytoplankton species in the ocean (Mosseri et al. 2008; Smith and Harrison 1991). As silicate was relatively low but not depleted at any station during this cruise (>1.3  $\mu\text{M}$ ), the large, lightly silicified diatom *C. inermis* might have been able to significantly increase its growth rate under these favorable conditions and successfully compete with smaller phytoplankton species (Owens et al. 1991). However, ammonium concentrations, although significant, only explained 18.5% of the variation in plankton community composition among the net samples suggesting that biotic interactions, such as predation or parasitism, might be the main structural drivers of protist assemblages (Christaki et al. 2017; Genitsaris et al. 2015; Lima-Mendez et al. 2015; Steele et al. 2011). In agreement with this result, the “small world” characteristics ( $\sigma = 4.71$ ) of the co-variance network suggested that the protist community structure might be relatively resistant to abiotic variations, but more affected by the removal of highly associated taxa (Humphries and Gurney 2008; Watts and Strogatz 1998).

### Interactions Between Rhizaria and other Protists

Many Rhizaria are well known predators in plankton communities that feed on a wide range of different organisms. Microscopic studies of Phaeodarea (Cerczoa) indicated that these organisms are omnivorous generalists feeding on prokaryotes as well as on other protists such as diatoms, dinoflagellates, chlorophytes and chrysophytes (Parmales) (Gowing 1986, 1989). Also Acantharea (Radiolaria) are known to ingest a wide range of organisms, while preferentially preying on tintinnids (Swanberg and Caron 1991). In contrast, previous studies (Matsuoka 2007) suggested that polycystine Radiolaria (Nassellaria and Spumellaria) are more limited to smaller prey organisms such as small flagellates and prokaryotes. The acantharian *Acanthometron* contributed most reads of all Rhizaria to the sequencing data from the plankton net samples in this study. However, the network analysis did not identify any significant co-variance of this radiolarian genus with other protists potentially due



to its consistent high abundance in sequencing data and wide range of prey organisms. Although several Phaeodarea cells were isolated from plankton nets for this study, sequencing of plankton net communities yielded only very low read numbers of this taxon, which suggested low DNA extraction or amplification success for these Cercozoa. Instead, the network analysis indicated a large impact of a radiolarian genus belonging to the order Acantharea-Symphyacanthida on protist community composition. This taxon was negatively related to the diatoms *Chaetoceros*, *Rhizosolenia* and radial-centric Mediophyceae indicating potential grazing pressure on these primary producers. Radiolarian Nassellaria (Polycystinea) were negatively related to the diatom *Guinardia* indicating another potential predator-prey relationship. Furthermore, the network analysis inferred positive co-variance between Radiolaria and other protists, such as the chlorophyte *Dunaliella*, the dinoflagellate *Goniodoma*, the diatoms *Eucampia* and radial-centric Coscinodiscophyceae, the dinoflagellate *Phalochroma* and Parmales. This co-variation suggested that the Radiolaria increased in abundance along with their potential prey.

Complementing the network analysis, the single cell sequencing data provided insights into interactions of the dominant rhizarian taxa *Acanthometron* (Radiolaria, Acantharea) and Challengeriiidae (Cercozoa, Phaeodarea) with other protists. Both taxa were associated with sequences from several different diatom genera, which might indicate preferential predation on these abundant organisms. As the number of successfully sequenced single cells was relatively low in this study (20%), this approach was likely not able to identify the full prey range of Rhizaria at the sampled stations. The low success rate of this approach was partly caused by difficulties with extracting sufficient, good quality DNA from single cells. Some cell walls were very difficult to lyse, while the DNA of other cells might have been damaged due to their poor physiological state or parasitic infections. Furthermore, some disagreements between sequencing data and morphological identification of isolates by microscopy likely resulted from contamination by free, environmental DNA. However, such contaminations occurred in a fraction of isolates from all taxonomic groups (e.g. ciliates, dinoflagellates, diatoms). Although diatom frustules are suspected to attract more free DNA due to their silica content, contaminations in diatom isolates did not correspond to the genetic diversity of the surrounding community. Stringent exclusion of isolates without sequences from the anticipated genus and with

contaminations by unexpected taxa resulted in the final low amount of single cells retained for further analyses (Table 1). Nevertheless, the sequencing data of isolated Rhizaria cells emphasized the important role of these organisms as predators of diatoms in the Southern Ocean transferring organic carbon from primary production to higher trophic levels (Burki and Keeling 2014; Fenchel 1988).

Radiolaria are also well known to contain photosymbionts such as dinoflagellates, prasinophytes and prymnesiophytes (Gast and Caron 2001), which transfer photosynthetically derived organic substances to the host organism (Takahashi et al. 2003). Several studies have shown that Acantharea live in symbiosis with the genus *Phaeocystis* (Decelle et al. 2012), but some studies have also identified other Prymnesiophyceae as symbionts (Mars Brisbin et al. 2018). Such an association between *Acanthometron* and the haptophyte *Phaeocystis* was also suggested by the single cell sequencing data (Supplementary Material Table S1). The network analysis in this study did not infer any associations between Radiolaria and prymnesiophytes, but indicated positive co-variation with other autotrophs such as chlorophytes, diatoms and dinoflagellates. In light of the common mutualistic relationships found in Radiolaria, these autotrophic genera might represent photosymbionts instead of ingested prey. Overall, the complementary methods used in this study suggested similar patterns and provided a more complete description of potential biotic interactions among Radiolaria and other protists than the individual approaches would have offered.

### Well-established Host-parasite Associations

Several previous studies suggested an important role of parasites such as Syndiniales in shaping microbial community composition. Prevalence of infections and host range of most parasites, however, are still largely unknown. 18S rDNA sequencing of entire microbial communities (e.g. 0.2–100  $\mu\text{m}$ ) has revealed extremely high relative abundance of Syndiniales in many marine ecosystems (e.g. Christaki et al. 2017; Georges et al. 2014; Guillou et al. 2008; López-García et al. 2001). However, protist communities collected by plankton nets in this study were characterized by lower proportion of Syndiniales reads compared to smaller size fractions suggesting relatively low abundance of parasitic infections in large protist cells and likely higher concentrations of parasitic spores.

Nevertheless, parasitic Syndiniales represented well-connected nodes in the co-variance network indicating host-parasite interactions that were affirmed by previous studies. The network analysis identified an association between Syndiniales Group II clade 4, which are closely related to *Amoebophrya*, and the dinoflagellate genus *Phalacroma*. This association was supported by previous studies, which suggested that *Amoebophrya*, the most studied parasite genus in Syndiniales Group II, mainly infects dinoflagellates (Alves-de-Souza et al. 2012; Siano et al. 2011). However, no Syndiniales were associated with any other dinoflagellates, such as *Tripos*, *Protoperdinium*, *Goniodom*, *Gonyaulax* or *Gyrodinium*, based on co-variance network analysis of plankton net samples. Repeated sequencing of individual *Tripos* cells did also not indicate any parasitic infections, despite such observations in previous studies (Gárate Lizárraga and Siqueiros Beltrones 2003; Park et al. 2013). Small dinoflagellates such as *Gymnodinium*, *Scripsiella*, *Heterocapsa* or *Prorocentrum* present in the 0.2–20 µm size fraction might also represent potential hosts for Group II Syndiniales, although the co-variance network analysis of the small size fraction (Supplementary Material Fig. S4) did not suggest such associations.

Past studies identified tintinnids as common hosts of *Euduboscquella* (Bachvaroff et al. 2012), which belongs to Syndiniales Group I. In the network analysis, however, two tintinnid genera (Tontoniidae and Dictyocystidae) were negatively related to Syndiniales Group II clade 12. Due to a lack of direct evidence or support through the literature, the cause of this association remains uncertain. It could result from either preying of the ciliates on the free-living dinospores of this Syndiniales clade or from parasitism suggesting a wider range of parasites in tintinnids than previously known. Furthermore, an association between Syndiniales Group I clade 1 and Rhizaria (Phaeodarea, Challengeriidae) was detected through single cell sequencing, despite the limited sample size in this analysis. Syndiniales taxa from the same clade were previously found associated to the Nassellaria *Androcyclas gamphonyca* in a Norwegian fjord (Dolven et al. 2007; Guillou et al. 2008). Single cell sequencing studies focusing on Rhizaria further emphasized the frequent interactions of Spumellaria, Nassellaria and Phaeodaria with both Group I and Group II Syndiniales (Bråte et al. 2012; Dolven et al. 2007). *Syndinium* (Group IV) was sequenced in several plankton net samples, but neither the co-variance analysis nor the single cell sequencing suggested any interactions of

this parasite with other protists. Copepods were very abundant in plankton net samples before filtration through the 100 µm mesh and could have suffered from parasitic infections. The *Syndinium* cells were, therefore, likely associated with broken copepods or nauplii, well known hosts of this parasite (Skovgaard and Saiz 2006), that passed the 100 µm mesh.

### Unexpected Associations of Syndiniales with Diatoms

Both co-variance analysis and single cell sequencing data pointed towards a common association of Syndiniales with diatoms in the Southern Ocean. In the co-variance network, Syndiniales Group II clade 12 was negatively related to several diatom genera such as *Eucampia* and *Odontella*. Although the R package PLNmodels is supposed to exclude indirect effects, tintinnids infected by Syndiniales, as discussed above, and preying on diatoms might have resulted in indirect co-variation in the network analysis. However, the single cell sequencing data indicated associations between several clades of Syndiniales Group II, including OTUs in clade 4 closely related to *Amoebophrya*, and diatoms such as *Corethron inerme*, *Eucampia antarctica* and *Thalassiosira sp.* These findings suggest that Syndiniales Group II might not be restricted to infecting dinoflagellates and Rhizaria, but may display an even wider host range in some ecosystems like the Southern Ocean.

The most abundant Syndiniales ASVs in all size fractions in this study belonged to Group I and were either closely related to *Euduboscquella* or formed a separate clade within this group. However, Syndiniales from Group I were not represented in the co-variance network, which might indicate very low host specificity of these taxa. Parasites that are not specialized on few host species but infect a wide range of different organisms would likely not follow the population dynamics of one specific species and cause its decline due to exhaustive parasitic load. Instead, the infection of a wide range of hosts might result in relatively stable population size of such a generalist parasite taxon preventing the detection of significant co-variations in network analyses. On the other hand, species- or genotype-specific associations might play an important role in protist community composition, but were not resolved in the co-variance analysis. In the single cell sequencing data, Syndiniales Group I OTUs, including OTUs closely affiliated with *Euduboscquella*, were consistently found to be associated with at least three different diatom

species (*Corethron inerme*, *Eucampia antarctica*, *Thalassiosira* sp.) supporting this hypothesized low host specificity. The third abundant Syndiniales group (Syndiniales Group IV) was closely related to the parasite *Hematodinium*, which is known to infect crustaceans such as crabs and lobsters (Small et al. 2006, 2007). However, sequences of this group were frequently found in the plankton net samples, which did not contain any sequences of benthic crustaceans. The hosts of this Syndiniales group in the plankton net samples remain, thus, uncertain, as the network analysis only identified negative co-variation of *Hematodinium* with the diatom *Rhizosolenia*.

Although Syndiniales are reported to have a large host range (Coats 1999; Park et al. 2013), there is no evidence from literature of Syndiniales infections in diatoms. Based on the limited single cell data in this study and the results from the covariance analysis, we can, however, hypothesize that these parasites might have a wider host range than previously reported, which needs to be verified in the future. Parasitic infection of diatoms was further supported by microscopic observation of small round features inside several *Corethron inerme* cells at the plateau station M2 (Fig. 2, Supplementary Material Fig. S1). This potential parasitic infection, which is not taxonomically identified yet, was easily visible due to the comparatively thin silica frustules of this species (Quéguiner et al. 1997). Direct microscopic identification of these features with fluorescence in-situ hybridization (FISH) would provide definitive proof of Syndiniales infecting diatoms. Unfortunately, this approach was hampered by the lack of suitable FISH probes for Group I Syndiniales, the dominant Syndiniales group in the Southern Ocean. Despite the lack of direct evidence, the findings in this study suggest an association of these organisms, demanding more attention for such potential biotic interaction in future studies. Differences between our findings and observed host ranges reported in previous studies might be caused by adaptation of parasite populations to the local protist community composition and preferential infection of highly abundant taxa.

#### Potential Impact of Syndiniales on Protist Diversity and Carbon Flux During Austral Autumn

In general, this study suggested that free-living dinospores represented the majority of Syndiniales in the Southern Ocean around the Kerguelen Islands after the diatom bloom. Furthermore,

detailed analysis of the relative abundance of individual Syndiniales clades in the different size fractions revealed potential differences in composition of free-living dinospore and intracellular parasite populations. Syndiniales Group IV and taxa closely related to *Amoebophrya* were mainly sequenced from plankton net or single cell samples, suggesting that these taxa were usually associated with larger cells (i.e. potential hosts) during time of sampling. Representatives of clade 10 and 11 in Syndiniales Group II were, on the contrary, predominantly found in the 0.2–20 µm size fraction, which is likely dominated by free-living dinospores. These findings indicated that many free-living dinospores potentially represent parasite populations, which have passed their prevalence peak likely due to the decline of their host populations. In contrast, concentrations of free-living spores from parasite populations with abundant hosts and higher prevalence could, in general, be low due to rapid infection of new host cells (Alves-de-Souza et al. 2012; Chambouvet et al. 2008). Syndiniales predominantly present in the small size fraction did, thus, potentially infect dominant taxa during the Austral summer bloom, but their spores did not encounter suitable host cells after its decline. This hypothesis is supported by the overall drop in relative abundance of Syndiniales in all size fractions at the stations sampled at the end of the cruise (Fig. 3).

The parasite spores represent valuable prey for zooplankton (e.g. ciliates), thus, contributing to the carbon flux to higher trophic levels (Kagami et al. 2011) in an ecosystem which is usually characterized by relatively short trophic chains (Hempel 1985). Furthermore, even low occurrence of parasitic infections might have a significant impact on protist community composition. Several studies have suggested that parasitism can enhance species richness and the number of trophic levels (Hudson et al. 2006; Kagami et al. 2007). The bursting of dying host cells at the end of a parasitic infection would release organic carbon into the environment from often grazer-protected primary producers, e.g. heavily silicified diatoms like *Eucampia antarctica*, *Thalassiosira* sp. and *Odonotella* sp. (Assmy et al. 2013; Liu et al. 2016). This organic carbon could be taken up by bacteria resulting in the high bacterial growth rates on the plateau measured during the cruise (Christaki et al., unpubl. observ.) and intense grazing of bacteria by other microorganisms (Christaki et al., unpubl. observ.; Haraldsson et al. 2018). The relatively high number of Syndiniales reads in the plankton net samples collected south-west of the plateau (see Fig. 3) sug-

gesting higher number of parasitic infections, could, thus, result in additional trophic pathways and more carbon transfer to higher trophic levels (Agha et al., 2016; Grami et al. 2011; Haraldsson et al. 2018). Furthermore, by infecting highly abundant taxa, parasites might decrease the competitiveness of their hosts resulting in an increase of less abundant taxa and higher evenness (Frainer et al. 2018). The higher diversity (Simpson and Shannon) in communities of large protists south-west of the plateau of the Kerguelen Islands, as well as the higher relative abundance of reads from the radiolarian *Acanthometron* and ciliates, as suggested by our data from the 20–100  $\mu\text{m}$  fraction, might reflect this hypothesized effect of parasitism on microbial community composition.

## Conclusions

Overall, the plankton net samples revealed high spatial and temporal variability in community composition of large protists in the Southern Ocean around the Kerguelen Islands. Even in the Austral autumn when protist communities are usually dominated by nano- and picophytoplankton (Hashihama et al. 2008; Iida and Odate 2014), changes in nutrient concentrations can result in a rapid increase in relative abundance of large diatom species such as *Corethron inerme*. Furthermore, combining different approaches, i.e. sequencing of different size fractions, and isolation and sequencing of single cells, provided new insights into microbial interactions in protist communities. The data from this study suggested that parasitism by Syndiniales and grazing by Rhizaria might be related to different diatom genera, due to as yet unconfirmed direct or indirect associations, in this polar ecosystem. Relatively numerous associations of parasites with large protist cells in HNLC waters south-west of the plateau might have made additional carbon available to the microbial community and, thus, enhanced species diversity at these stations.

## Methods

**Sampling:** Samples for this study were taken onboard of the R/V *Marion Dufresne* at four sampling sites (M1, M2, M3, M4) in the Southern Ocean close to the Kerguelen Islands (Fig. 1) as part of the MOBYDICK research cruise from February 19<sup>th</sup> to March 26<sup>th</sup> 2018. Each site was visited up to three times during the cruise resulting in eight sampling stations (M1.1, M2.1, M2.2, M2.3, M3.1, M3.3, M4.1, M4.2).

Microplankton (>35  $\mu\text{m}$ ) was collected up to three times at each station with plankton net (PN) (Spartel, UK) tows from 125 m depth to surface resulting in 14 plankton net samples

(Table 1). Although this study aimed at investigating protists and the plankton net was designed for phytoplankton and microzooplankton sampling, several Metazoa were also captured. To remove the majority of easily visible copepods, which can strongly bias the sequencing, from the plankton net samples, the samples were pre-filtered through a 100  $\mu\text{m}$  nylon mesh (SEFAR FYLTIS, France). Ten to 30 ml of concentrated plankton net samples were collected on 0.2  $\mu\text{m}$  25 mm diameter polycarbonate filters (Whatman, UK). These samples were preserved with RNAsafeguard Reagent (BIOER Technology, China) and stored at  $-80^{\circ}\text{C}$ . Seventeen to 48 individual protist cells were isolated by micromanipulation under an inverted microscope (Nikon Eclipse TS100, Japan) from one pre-filtered plankton net sample per station. At the stations M2.2 and M2.3, several *Corethron inerme* cells filled with small (approx. 1–3  $\mu\text{m}$ ), black, round features were noticed (Fig. 2, Supplementary Material Fig. S1) and the isolation effort was focused on these cells. After three washing steps with sterile filtered sea water, the individual cells were photographed at 200x magnification, transferred with minimal amounts of water to 0.2 ml sterile PCR tubes and stored at  $-80^{\circ}\text{C}$ .

At the same stations, twelve liter samples were taken with Niskin bottles (NB) at 10, 60 and 125 m depth. To size fractionate the microbial community in these samples (0.2–20  $\mu\text{m}$  and 20–100  $\mu\text{m}$ ), the water was serially filtered through 100  $\mu\text{m}$  nylon mesh, 20  $\mu\text{m}$  47 mm diameter and 0.2  $\mu\text{m}$  90 mm diameter polycarbonate filters (Whatman, UK). These filters were cut into quarters using an ethanol cleaned scalpel, each quarter was placed into sterile cryovials (Thermo Scientific, Massachusetts, USA) and stored at  $-80^{\circ}\text{C}$ .

Environmental variables (temperature, salinity, colored dissolved organic matter, chlorophyll a fluorescence, dissolved oxygen) were measured at every sampling depth by CTD Seabird911-plus and a WET labs Eco Triplet sensor (Sea-Bird Scientific, Washington, USA), which were mounted on a rosette of 24 Niskin bottles. Additionally, ammonium, phosphate, silicate, nitrite and nitrate were measured in water samples from rosette bottles at every sampling depth during one CTD cast at each station by fluorescence measurements (Holmes et al. 1999) and colorimetric detection using a segmented flow analyzer (Aminot and K erouel 2007), respectively.

**DNA extraction, amplification and sequencing of rDNA fragments:** To comprehensively assess protist community composition in small (<20  $\mu\text{m}$ ) and large size fractions (>20  $\mu\text{m}$  from Niskin bottles and >35  $\mu\text{m}$  from plankton net tows) at the eight sampling station in the Southern Ocean, DNA was extracted from half of each plankton net filter and an eighth of each Niskin bottle filter. The filters were cut with flame sterilized scalpels into small pieces before they were further processed with the DNA Power Soil kit (Qiagen, Germany) according to manufacturer's instructions. The V4 region of the 18S rDNA (527 bp) was four times amplified from the extracted DNA of each sample using a universal eukaryote primer set biased against metazoans (EK-565F - GCAGTTAAAAAGCTCGTAGT and UNonMet - TTTAAGTTTCAGCCTTGCG, Bower et al., 2004). Forward and reverse primers were tagged with 96 distinct 10 bp barcodes to allow multiplexing of PCR products from the different samples. Samples were amplified in 20  $\mu\text{l}$  reactions using the DreamTaqGreen master mix (Thermo Scientific, Vilnius, Lithuania) with the following PCR settings: 95  $^{\circ}\text{C}$  for 2 min, 30 cycles including 95  $^{\circ}\text{C}$  for 30 sec, 51  $^{\circ}\text{C}$  for 30 sec, 72  $^{\circ}\text{C}$  for 1 min, and a final elongation step of 5 min at 72  $^{\circ}\text{C}$ . Successful amplification was confirmed on 1% agarose gels. The four PCR products from each sample were pooled and purified together using the QIAquick PCR purification kit (Qiagen, Germany). DNA concentrations after purification were measured

with a Qubit 2.0 fluorometer (Invitrogen, Massachusetts, USA) and adjusted to  $30 \text{ ng } \mu\text{l}^{-1}$ .

To identify physically associated cells, the isolated single cells were defrosted at room temperature,  $8 \mu\text{l}$  of  $400 \text{ ng } \mu\text{l}^{-1}$  Proteinase K (Fisher Scientific, Germany) were added to each tube and the samples were frozen again at  $-20^\circ\text{C}$  for at least 1 hour. Afterwards, the cells were lysed by activating the enzyme at  $55^\circ\text{C}$  for 30 min followed by denaturation at  $95^\circ\text{C}$  for 5 min. These digested samples were used as templates for amplification of the 18S rDNA, ITS and partial 28S rDNA (3160 bp) in  $20 \mu\text{l}$  reactions with Phusion polymerase master mix (Thermo Scientific, Lithuania) using the primers EK-42F (CTCAARGAYTAAGCCATGCA) and 25-R1 (CTTGGTCCGTGTTCAAGAC). The PCR settings were as follows:  $98^\circ\text{C}$  for 30 sec, 30 cycles including  $98^\circ\text{C}$  for 10 sec,  $61^\circ\text{C}$  for 15 sec,  $72^\circ\text{C}$  for 90 sec, and a final elongation step of 10 min at  $72^\circ\text{C}$ . With a nested PCR and barcoded primers, the same 18S rDNA fragment as targeted in the plankton net and Niskin bottle samples was amplified from the long PCR product using DreamTaqGreen master mix. The entire PCR products were loaded on agarose gels to confirm successful amplification and to purify the products using the QIAquick gel purification kit (Qiagen, Germany). Five or ten different single cell amplicons were pooled during this process, depending on amplification success, to increase DNA concentrations per isolate. DNA concentrations of these pools were measured with a Qubit fluorometer. All single cell samples together contributed the same amount of DNA as one plankton net or Niskin bottle sample to the final Illumina sequencing library. To allow for even sequencing depth of all isolates, the contributing volume from each single cell pool to this library was accordingly adjusted. The library was paired-end sequenced ( $2 \times 300 \text{ bp}$ ) on an Illumina MiSeq lane at the genomics service company Genewiz (South Plainfield, NJ, USA).

**Processing of sequences:** The forward and reverse sequences were demultiplexed after orienting all reads based on their primer sequence and extraction of barcodes using the Qiime1 pipeline (Caporaso et al. 2010). The plankton net and Niskin bottle samples were further processed with the DADA2 pipeline (Callahan et al. 2016, 2) in R-3.5.1. At most six errors were allowed during filtering, while 19 bp were trimmed from the end of the forward and 30 bp from the end of the reverse reads to remove barcodes and primers. The minimum allowed read length was set to 210 bp. After dereplicating forward and reverse reads, the DADA2 pipeline identified amplicon sequence variants (ASV) in the dataset. The forward and reverse reads were merged and chimeras were identified and removed based on matches with combinations of 3'- and 5'-segments of different sequences. The taxonomy of the ASVs was assigned with the naïve Bayesian classifier method implemented in DADA2 based on the PR<sup>2</sup> database (Guillou et al. 2013).

The forward and reverse reads from single cell samples were joined after demultiplexing in Qiime2-2018.8. After dereplication, the reads were clustered with the UPARSE-OTU algorithm in USEARCH v11 (Edgar 2013) into OTUs based on 97% similarity. USEARCH and OTU clustering was chosen for the single cell sequencing data, as this approach consists of several stand-alone modules that could be individually applied to this unconventional dataset. Furthermore, OTU clustering is likely less sensitive to amplification errors arising from repeated PCR compared to ASV clustering. The taxonomy of the OTUs was predicted using the Sintax algorithm in USEARCH v11 based on the PR<sup>2</sup> database. Only taxa with at least 5 reads per individual isolate were kept for further analyses. Taxa with less reads were considered to be noise and discarded.

**Analysis of ASV diversity and distribution:** All downstream processing of the sequencing data was done in R-3.5.1 usually using the packages phyloseq, vegan and ggplot2 (McMurdie and Holmes 2013; Oksanen et al. 2016; Wickham 2016). The 119 ASVs affiliated to Metazoa and Streptophyta were removed from the data set before downstream analyses, as they likely represent broken individuals that passed through the  $100 \mu\text{m}$  mesh and are, therefore, not representative for the population. Four ASVs affiliated to Amoebozoa and Excavata were also filtered out of the data set as these ASVs only occurred in one sample each. To remove noise from potential PCR and sequencing errors, 15 reads per ASV, which represents the median number of reads per ASV in this data set, were chosen as a threshold for identification of reliable ASVs. Samples with less than 1000 reads were also removed to allow for unbiased presentation of the present diversity in all samples.

Heatmaps and barplots were built with the R packages ampvis2 (Andersen et al. 2018) and phyloseq to illustrate the overall protist community composition and distribution of the most common genera in all samples. Alpha diversity indices (Richness, Simpson, Shannon and Pielou's evenness) were calculated for the plankton net samples after rarefying the read numbers per sample using the R package microbiomeSeq (Ssekagiri et al. 2018). Plankton net samples were clustered into a dendrogram based on weighted unifrac distances implementing Ward's algorithm. Significance of differentiation among dendrogram clusters, sites and location relative to the plateau were investigated with a Permutational Multivariate Analysis of Variance (PERMANOVA) using weighted unifrac distances between plankton net samples with the adonis2 and pairwise.adonis functions in the R package vegan implementing Bonferroni adjustment of p-values.

Environmental variables measured at discrete depths in the mixed layer (0–75 m depth) were averaged and normalized ( $V_{\text{norm}} = (\text{value} - \text{mean}) / \text{stdev}$ ) for further analyses. The relationship between genetic biodiversity and normalized environmental variables was assessed with a canonical correspondence analysis (CCA) using the R package vegan (Oksanen et al. 2016). The best model was selected based on automatic stepwise model building using the function "ordisstep" in the R package vegan starting with a model that included only the intercept, and adding all environmental variables afterwards. CCAs were calculated for the entire dataset, ASVs merged at the genus or family level as well as only including taxa representing at least 0.01% or 0.1% of all reads. Ordinations were visualized using phyloseq and ggplot2 packages. Spearman correlations were calculated between the read numbers of the 30 most common genera in the plankton net samples and environmental variables from CTD casts. P-values were Bonferroni corrected and the results were visualized with microbiomeSeq.

**Co-variance network analyses:** Co-variance analyses were conducted separately for plankton net samples and small size fraction (0.2–20  $\mu\text{m}$ ) samples from the Niskin bottles. ASVs representing less than 0.02% of all reads and occurring in less than three samples were removed from the dataset. To identify consistency of co-variance across multiple taxonomic levels, several input datasets were created with reads of ASVs merged at common species, genus and family levels. Co-variance of taxa was assessed using the R package PLNmodels (Chiquet et al. 2018), which utilizes a multivariate Poisson lognormal model to infer networks. This approach allows identification and exclusion of co-variance between nodes due to indirect effects, e.g. susceptibility to the same predatory species or correlation with the same environmental variable. In this study, the model was first applied without considering any environmental

parameters. In a second scenario for the plankton net samples, ammonium concentrations were included, as the CCA identified a significant impact of this environmental parameter on community composition. Partial correlation coefficients (normalized, inverse sigma) from the final model were visualized in a network with cytoscape 3.7.0 (Shannon et al., 2003). Network Randomizer 1.1.3 (Tosadori et al. 2017) was used to generate random networks based on the Erdos-Renyi model using the same number of nodes and edges as in the original network. Topological parameters of each network were calculated in cytoscape and compared using the Kolmogorov–Smirnov test implemented in the Network Randomizer.

The “small world” coefficient ( $\sigma$ ) of the network was calculated following Humphries and Gurney (2008):  $\sigma = (C/C_r)/(L/L_r)$ , where C and  $C_r$  are the observed and random Clustering Coefficients and L and  $L_r$  the observed and random Characteristic Path Lengths. A  $\sigma$  coefficient larger than 1 ( $C \gg C_r$  and  $L \approx L_r$ ) indicates “small world” characteristics in the network (Humphries and Gurney 2008; Watts and Strogatz 1998).

**Analysis of Syndiniales sequences:** The sequences of all Syndiniales OTUs from the single cell samples as well as the 20 most abundant Syndiniales ASVs from the plankton net samples and from the small size fraction of the Niskin bottle samples (0.2–20  $\mu\text{m}$ ) were aligned with Muscle 3.8.425 in Geneious (Kearse et al. 2012) and trimmed with trimAl (Capella-Gutiérrez et al. 2009) using a gap threshold of 0.5. Reference sequences of Perkinsea and dinoflagellates were added from GenBank database as well as Syndiniales sequences from the PR<sup>2</sup> database. The phylogenetic relationships of these parasites was investigated by building a Maximum Likelihood tree with RAxML (Stamatakis 2014) using the substitution model “GTRCAT”. The RAxML settings included rapid bootstrap analysis while the number of distinct starting trees was based on bootstrapping criteria. The tree was visualized with the online application iTOL (Letunic and Bork 2016).

## Data Accessibility

All data for this study are accessible in the Moby-Dick database (<http://www.obs-vlfr.fr/proof/php/mobydick/mobydick.php#SA>). Raw sequencing files in fastq format are available at [http://www.obs-vlfr.fr/proof/ftptree/mobydick/db/DATA/PAR\\_2251/](http://www.obs-vlfr.fr/proof/ftptree/mobydick/db/DATA/PAR_2251/). Single cell sequencing data can be found at [http://www.obs-vlfr.fr/proof/ftptree/mobydick/db/DATA/PAR\\_1089/](http://www.obs-vlfr.fr/proof/ftptree/mobydick/db/DATA/PAR_1089/).

## Conflict of interest

We declare that all authors of this manuscript do not have any conflict of interest.

## Author Contribution Statement

UC and LJ conceived and designed the study with contribution from IS. IS, LJ and UC took the samples during the cruise. IS and SI extracted the DNA and prepared the samples for sequencing. IS per-

formed the bioinformatic and statistical analyses of the samples with support from SI. IS interpreted the data with contributions from SI, LJ, DM and UC. IS wrote the manuscript, all co-authors read it and provide comments.

## Acknowledgements

We thank B. Quéguiner, the PI of the MOBY-DICK project, for providing us the opportunity to participate on the cruise, the chief scientist I. Obernosterer and the crew of the R/V Marion Dufresne for their enthusiasm and help aboard during the MOBYDICK–THEMISTO cruise (<https://doi.org/10.17600/18000403>). This work was supported by the French oceanographic fleet (Flotte océanographique française), the French ANR (Agence Nationale de la Recherche, AAPG 2017 program, MOBYDICK Project number: ANR-17-CE01-0013), and the French Research program of INSU-CNRS LEFE-CYBER (Les enveloppes fluides et l’environnement – Cycles biogéochimiques, environnement et ressources). This research was funded by CNRS LEFE-EC2CO through the projects PLANKTON-PARTY, Aktiv-Euk, and an ULCO (Université du Littoral) and CPER MARCO (<https://marco.univ-littoral.fr/>) postdoctoral fellowship for I. Sassenhagen. We are grateful to Elisa Thebault for introducing us to co-variance analyses. Constructive comments from the editor and the reviewers improved this manuscript.

## Appendix A. Supplementary Data

Supplementary material related to this article can be found, in the online version, at doi:10.1016/j.protis.2019.125709.

## References

- Agha R, Saebelfeld M, Manthey C, Rohrlack T, Wolinska J (2016) Chytrid parasitism facilitates trophic transfer between bloom-forming cyanobacteria and zooplankton (*Daphnia*). *Sci Rep* 6:35039
- Alves-de-Souza C, Varela D, Iriarte J, González H, Guillou L (2012) Infection dynamics of Amoebozoa parasitoids on harmful dinoflagellates in a southern Chilean fjord dominated by diatoms. *Aquat Microb Ecol* 66:183–197
- Aminot A, Kérouel R (2007) Dosage automatique des nutriments dans les eaux marines: méthodes en flux continu. *Editions Quae*. GIE, 188 p

- Andersen KS, Kirkegaard RH, Karst SM, Albertsen M** (2018) ampvis2: an R package to analyse and visualise 16S rRNA amplicon data. bioRxiv, <http://dx.doi.org/10.1101/299537>
- Armand LK, Cornet-Barthaux V, Mosseri J, Quéguiner B** (2008) Late summer diatom biomass and community structure on and around the naturally iron-fertilised Kerguelen Plateau in the Southern Ocean. *Deep Sea Res Part II Top Stud Oceanogr* **55**:653–676
- Assmy P, Smetacek V, Montresor M, Klaas C, Henjes J, Strass VH, et al.** (2013) Thick-shelled, grazer-protected diatoms decouple ocean carbon and silicon cycles in the iron-limited Antarctic Circumpolar Current. *Proc Natl Acad Sci USA* **110**:20633–20638
- Bachvaroff TR, Kim S Guillou L, Delwiche CF, Coats DW** (2012) Molecular diversity of the syndinean genus *Euduboscquella* based on single-cell PCR analysis. *Appl Environ Microbiol* **78**:334–345
- Blain S, Quéguiner B, Trull T** (2008) The natural iron fertilization experiment KEOPS (KErguelen Ocean and Plateau compared Study): An overview. *Deep Sea Res Part II Top Stud Oceanogr* **55**:559–565
- Blain S, Quéguiner B, Armand L, Belviso S, Bombled B, Bopp L, Bowie A, Brunet C, Brussaard C, Carlotti F, et al.** (2007) Effect of natural iron fertilization on carbon sequestration in the Southern Ocean. *Nature* **446**:1070–1074
- Bower SM, Carnegie RB, Goh B, Jones SRM, Lowe GJ, Mak MWS** (2004) Preferential PCR amplification of parasitic protistan small subunit rDNA from Metazoan tissues. *J Eukaryot Microbiol* **51**:325–332
- Bråte J, Krabberød AK, Dolven JK, Ose RF, Kristensen T, Bjørklund KR, et al.** (2012) Radiolaria associated with large diversity of marine alveolates. *Protist* **163**:767–777
- Breier RE, Lalescu CC, Waas D, Wilczek M, Mazza MG** (2018) Emergence of phytoplankton patchiness at small scales in mild turbulence. *Proc Natl Acad Sci USA* **115**:12112–12117
- Burki F, Keeling PJ** (2014) Rhizaria. *Curr Biol* **24**:R103–R107
- Callahan BJ, McMurdie PJ, Rosen MJ, Han AW, Johnson AJA, Holmes SP** (2016) DADA2: High-resolution sample inference from Illumina amplicon data. *Nat Methods* **13**:581–583
- Capella-Gutiérrez S, Silla-Martínez JM, Gabaldón T** (2009) trimAl: a tool for automated alignment trimming in large-scale phylogenetic analyses. *Bioinformatics* **25**:1972–1973
- Caporaso JG, Kuczynski J, Stombaugh J, Bittinger K, Bushman FD, Costello EK, et al.** (2010) QIIME allows analysis of high-throughput community sequencing data. *Nat Methods* **7**:335–336
- Cavagna A, Fripiat F, Elskens M, Mangion P, Chirugien L, Closset I, et al.** (2015) Production regime and associated N cycling in the vicinity of Kerguelen Island, Southern Ocean. *Biogeosciences* **12**:6515–6528
- Chambouvet A, Morin P, Marie D, Guillou L** (2008) Control of toxic marine dinoflagellate blooms by serial parasitic killers. *Science* **322**:1254–1257
- Chambouvet A, Alves-de-Souza C, Cuff V, Marie D, Karpov S, Guillou L** (2011) Interplay between the parasite *Amoebophrya* sp. (Alveolata) and the cyst formation of the red tide dinoflagellate *Scrippsiella trochoidea*. *Protist* **162**:637–649
- Chiquet J, Mariadassou M, Robin S** (2018) Variational inference for sparse network reconstruction from count data. ArXiv180603120 Stat, Available at: <http://arxiv.org/abs/1806.03120> [Accessed February 14, 2019]
- Christaki U, Georges C, Genitsaris S, Monchy S** (2015) Microzooplankton community associated with phytoplankton blooms in the naturally iron-fertilized Kerguelen area (Southern Ocean). *FEMS Microbiol Ecol* **91**:fiv068
- Christaki U, Genitsaris S, Monchy S, Li LL, Rachik S, Breton E, et al.** (2017) Parasitic eukaryotes in a meso-eutrophic coastal system with marked *Phaeocystis globosa* blooms. *Front Mar Sci* **4**:416
- Christaki U, Lefèvre D, Georges C, Colombet J, Catala P, Courties C, et al.** (2014) Microbial food web dynamics during spring phytoplankton blooms in the naturally iron-fertilized Kerguelen area (Southern Ocean). *Biogeosciences* **11**:6739–6753
- Closset I, Lasbleiz M, Leblanc K, Quéguiner B, Cavagna A-J, Elskens M, et al.** (2014) Seasonal evolution of net and regenerated silica production around a natural Fe-fertilized area in the Southern Ocean estimated with Si isotopic approaches. *Biogeosciences* **11**:5827–5846
- Coats DW** (1999) Parasitic life styles of marine dinoflagellates. *J Eukaryot Microbiol* **46**:402–409
- Coats DW, Heisler JJ** (1989) Spatial and temporal occurrence of the parasitic dinoflagellate *Duboscquella cachoni* and its tintinnine host *Eutintinnus pectinis* in Chesapeake Bay. *Mar Biol* **101**:401–409
- Coats DW, Park MG** (2002) Parasitism of photosynthetic dinoflagellates by three strains of *Amoebophrya* (Dinophyta): Parasite survival, infectivity, generation time, and host specificity. *J Phycol* **38**:520–528
- d'Ovidio F, Della Penna A, Trull TW, Nencioli F, Pujol M-I, Rio M-H, et al.** (2015) The biogeochemical structuring role of horizontal stirring: Lagrangian perspectives on iron delivery downstream of the Kerguelen Plateau. *Biogeosciences* **12**:5567–5581
- Decelle J, Probert I, Bittner L, Desdevises Y, Colin S, de Vargas C, et al.** (2012) An original mode of symbiosis in open ocean plankton. *Proc Natl Acad Sci USA* **109**:18000–18005
- Detmer AE, Bathmann UV** (1997) Distribution patterns of autotrophic pico- and nanoplankton and their relative contribution to algal biomass during spring in the Atlantic sector of the Southern Ocean. *Deep Sea Res Part II Top Stud Oceanogr* **44**:299–320
- Dolven JK, Lindqvist C, Albert VA, Bjørklund KR, Yuasa T, Takahashi O, et al.** (2007) Molecular diversity of alveolates associated with neritic North Atlantic radiolarians. *Protist* **158**:65–76
- Edgar RC** (2013) UPARSE: highly accurate OTU sequences from microbial amplicon reads. *Nat Methods* **10**:996–998
- Eppley RW, Reid FMH, Cullen JJ, Winant CD, Stewart E** (1984) Subsurface patch of a dinoflagellate (*Ceratium tripos*) off Southern California: Patch length, growth rate, associated vertically migrating species. *Mar Biol* **80**:207–214

- Fenchel T** (1988) Marine plankton food chains. *Annu Rev Ecol Syst* **19**:19–38
- Frainer A, McKie BG, Amundsen P-A, Knudsen R, Lafferty KD** (2018) Parasitism and the biodiversity-functioning relationship. *Trends Ecol Evol* **33**:260–268
- Gárate Lizárraga I, Siqueiros Beltrones DA** (2003) Infection of *Ceratium furca* by the parasitic dinoflagellate *Amoebophyra ceratii* (Amoebophryidae) in the Mexican Pacific. *Acta Botánica Mex* **65**:1–9
- Gast RJ, Caron DA** (2001) Photosymbiotic associations in planktonic foraminifera and radiolaria. *Hydrobiologia* **461**:1–7
- Genitsaris S, Monchy S, Viscogliosi E, Sime-Ngando T, Ferreira S, Christaki U** (2015) Seasonal variations of marine protist community structure based on taxon-specific traits using the eastern English Channel as a model coastal system. *FEMS Microbiol Ecol* **91**:fiv034
- Georges C, Monchy S, Genitsaris S, Christaki U** (2014) Protist community composition during early phytoplankton blooms in the naturally iron-fertilized Kerguelen area (Southern Ocean). *Biogeosciences* **11**:5847–5863
- Goeyens L, Tréguer P, Baumann MEM, Baeyens W, Dehairs F** (1995) The leading role of ammonium in the nitrogen uptake regime of Southern Ocean marginal ice zones. *J Mar Syst* **6**:345–361
- Gowing MM** (1986) Trophic biology of phaeodarian radiolarians and flux of living radiolarians in the upper 2000 m of the North Pacific central gyre. *Deep Sea Res Part Oceanogr Res Pap* **33**:655–674
- Gowing MM** (1989) Abundance and feeding ecology of Antarctic phaeodarian radiolarians. *Mar Biol* **103**:107–118
- Gowing MM, Garrison DL** (1992) Abundance and feeding ecology of larger protozooplankton in the ice edge zone of the Weddell and Scotia Seas during the austral winter. *Deep Sea Res Part Oceanogr Res Pap* **39**:893–919
- Grami B, Rasconi S, Niqul N, Jobard M, Saint-Béat B, Sime-Ngando T** (2011) Functional effects of parasites on food web properties during the spring diatom bloom in Lake Pavin: a linear inverse modeling analysis. *PLoS ONE* **6**:e23273
- Guillou L, Bachar D, Audic S, Bass D, Berney C, Bittner L, et al.** (2013) The Protist Ribosomal Reference database (PR2): a catalog of unicellular eukaryote Small Sub-Unit rRNA sequences with curated taxonomy. *Nucleic Acids Res* **41**:D597–D604
- Guillou L, Viprey M, Chambouvet A, Welsh RM, Kirkham AR, Massana R, et al.** (2008) Widespread occurrence and genetic diversity of marine parasitoids belonging to Syndiniales (Alveolata). *Environ Microbiol* **10**:3349–3365
- Haraldsson M, Gerphagnon M, Bazin P, Colombet J, Techio S, Sime-Ngando T, et al.** (2018) Microbial parasites make cyanobacteria blooms less of a trophic dead end than commonly assumed. *ISME J* **12**:1008–1020
- Hashihama F, Hirawake T, Kudoh S, Kanda J, Furuya K, Yamaguchi Y, et al.** (2008) Size fraction and class composition of phytoplankton in the Antarctic marginal ice zone along the 140°E meridian during February–March 2003. *Polar Sci* **2**:109–120
- Hempel G** (1985) Antarctic Marine Food Webs. In Siegfried WR, Condy PR, Laws RM (eds) *Antarctic Nutrient Cycles and Food Webs*. Springer, Berlin, Heidelberg, pp 266–270
- Holmes RM, Aminot A, Kérouel R, Hooker BA, Peterson BJ** (1999) A simple and precise method for measuring ammonium in marine and freshwater ecosystems. *Can J. Fish Aquat Sci* **56**:1801–1808
- Hudson PJ, Dobson AP, Lafferty KD** (2006) Is a healthy ecosystem one that is rich in parasites? *Trends Ecol Evol* **21**:381–385
- Humphries MD, Gurney K** (2008) Network ‘Small-World-Ness’: A quantitative method for determining canonical network equivalence. *PLoS ONE* **3**:e0002051
- Iida T, Odate T** (2014) Seasonal variability of phytoplankton biomass and composition in the major water masses of the Indian Ocean sector of the Southern Ocean. *Polar Sci* **8**:283–297
- Jephcott TG, Alves-de-Souza C, Gleason FH, van Ogtrop FF, Sime-Ngando T, Karpov SA, et al.** (2016) Ecological impacts of parasitic chytrids, syndiniales and perkinsids on populations of marine photosynthetic dinoflagellates. *Fungal Ecol* **19**:47–58
- Kagami M, Helmsing NR, van Donk E** (2011) Parasitic chytrids could promote copepod survival by mediating material transfer from inedible diatoms. *Hydrobiologia* **659**:49–54
- Kagami M, de Bruin A, Ibelings BW, Donk EV** (2007) Parasitic chytrids: their effects on phytoplankton communities and food-web dynamics. *Hydrobiologia* **578**:113–129
- Kamykowski D** (1995) Trajectories of autotrophic marine dinoflagellates. *J Phycol* **31**:200–208
- Kearse M, Moir R, Wilson A, Stones-Havas S, Cheung M, Sturrock S, et al.** (2012) Geneious Basic: An integrated and extendable desktop software platform for the organization and analysis of sequence data. *Bioinformatics* **28**:1647–1649
- Kimmerer WJ, McKinnon AD** (1990) High mortality in a copepod population caused by a parasitic dinoflagellate. *Mar Biol* **107**:449–452
- Lafferty KD, Dobson AP, Kuris AM** (2006) Parasites dominate food web links. *Proc Natl Acad Sci USA* **103**:11211–11216
- Lasbleiz M, Leblanc K, Armand LK, Christaki U, Georges C, Obernosterer I, et al.** (2016) Composition of diatom communities and their contribution to plankton biomass in the naturally iron-fertilized region of Kerguelen in the Southern Ocean. *FEMS Microbiol Ecol* **92**:fiw171
- Lepère C, Domaizon I, Debroas D** (2008) Unexpected importance of potential parasites in the composition of the freshwater small-eukaryote community. *Appl Environ Microbiol* **74**:2940–2949
- Letunic I, Bork P** (2016) Interactive tree of life (iTOL) v3: an online tool for the display and annotation of phylogenetic and other trees. *Nucleic Acids Res* **44**:W242–W245
- Levinsen H, Nielsen TG, Hansen BW** (1999) Plankton community structure and carbon cycling on the western coast of Greenland during the stratified summer situation. II. Heterotrophic dinoflagellates and ciliates. *Aquat Microb Ecol* **16**:217–232



- Levinsen H, Nielsen TG, Hansen BW** (2000) Annual succession of marine pelagic protozoans in Disko Bay, West Greenland, with emphasis on winter dynamics. *Mar Ecol Prog Ser* **206**:119–134
- Lima-Mendez G, Faust K, Henry N, Decelle J, Colin S, Carcillo F, et al.** (2015) Determinants of community structure in the global plankton interactome. *Science* **348**:1262073
- Liu H, Chen M, Zhu F, Harrison PJ** (2016) Effect of diatom silica content on copepod grazing, growth and reproduction. *Front Mar Sci* **3**:89
- López-García P, Rodríguez-Valera F, Pedrós-Alió C, Moreira D** (2001) Unexpected diversity of small eukaryotes in deep-sea Antarctic plankton. *Nature* **409**:603–607
- Lovejoy C, Legendre L, Price NM** (2002) Prolonged diatom blooms and microbial food web dynamics: experimental results from an Arctic polynya. *Aquat Microb Ecol* **29**:267–278
- Mars Brisbin M, Mesrop LY, Grossmann MM, Mitarai S** (2018) Intra-host symbiont diversity and extended symbiont maintenance in photosymbiotic Acantharea (Clade F). *Front Microbiol* **9**:1998
- Maslov S, Sneppen K** (2002) Specificity and stability in topology of protein networks. *Science* **296**:910–913
- Matsuoka A** (2007) Living radiolarian feeding mechanisms: new light on past marine ecosystems. *Swiss J Geosci* **100**:273–279
- McMurdie PJ, Holmes S** (2013) phyloseq: An R package for reproducible interactive analysis and graphics of microbiome census data. *PLoS ONE* **8**:e61217
- Mosseri J, Quéguiner B, Armand L, Cornet-Barthaux V** (2008) Impact of iron on silicon utilization by diatoms in the Southern Ocean: A case study of Si/N cycle decoupling in a naturally iron-enriched area. *Deep Sea Res Part II Top Stud Oceanogr* **55**:801–819
- Nielsen TG, Hansen B** (1995) Plankton community structure and carbon cycling on the western coast of Greenland during and after the sedimentation of a diatom bloom. *Mar Ecol Prog Ser* **125**:239–257
- Not F, del Campo J, Balagué V, de Vargas C, Massana R** (2009) New insights into the diversity of marine picoeukaryotes. *PLoS ONE* **4**:e7143
- Oksanen J, Blanchet FG, Friendly M, Kindt R, Legendre P, McGilinn D, et al.** (2016) vegan: Community Ecology Package, Available at: <http://CRAN.R-project.org/package=vegan>
- Omori M, Hamner WM** (1982) Patchy distribution of zooplankton: Behavior, population assessment and sampling problems. *Mar Biol* **72**:193–200
- Owens NJP, Priddle J, Whitehouse MJ** (1991) Variations in phytoplanktonic nitrogen assimilation around South Georgia and in the Bransfield Strait (Southern Ocean). *Mar Chem* **35**:287–304
- Park MG, Kim S, Shin E-Y, Yih W, Coats DW** (2013) Parasitism of harmful dinoflagellates in Korean coastal waters. *Harmful Algae* **30**:S62–S74
- Park Y-H, Durand I, Kestenare E, Rougier G, Zhou M, d'Ovidio F, et al.** (2014) Polar front around the Kerguelen Islands: An up-to-date determination and associated circulation of surface/subsurface waters. *J Geophys Res Oceans* **119**:6575–6592
- Pauthenet E, Roquet F, Madec G, Guinet C, Hindell M, McMahon CR, et al.** (2018) Seasonal meandering of the polar front upstream of the Kerguelen Plateau. *Geophys Res Lett* **45**:9774–9781
- Pierce RW, Turner JT** (1992) Ecology of planktonic ciliates in marine food webs. *Rev Aquat Sci* **6**:139–181
- Pitcher GC, Boyd AJ, Horstman DA, Mitchell-Innes BA** (1998) Subsurface dinoflagellate populations, frontal blooms and the formation of red tide in the southern Benguela upwelling system. *Mar Ecol Prog Ser* **172**:253–264
- Prokopowich CD, Gregory TR, Crease TJ** (2003) The correlation between rDNA copy number and genome size in eukaryotes. *Genome* **46**:48–50
- Quéguiner B, Tréguer P, Peeken I, Scharek R** (1997) Biogeochemical dynamics and the silicon cycle in the Atlantic sector of the Southern Ocean during austral spring 1992. *Deep Sea Res Part II Top Stud Oceanogr* **44**:69–89
- Shannon P, Markiel A, Ozier O, Baliga NS, Wang JT, Ramage D, et al.** (2003) Cytoscape: A software environment for integrated models of biomolecular interaction networks. *Genome Res* **13**:2498–2504
- Sherr EB, Sherr BF** (2007) Heterotrophic dinoflagellates: a significant component of microzooplankton biomass and major grazers of diatoms in the sea. *Mar Ecol Prog Ser* **352**:187–197
- Siano R, Alves-de-Souza C, Foulon E, Bendif EM, Simon N, Guillou L, et al.** (2011) Distribution and host diversity of Amoebozoa parasites across oligotrophic waters of the Mediterranean Sea. *Biogeosciences* **8**:267–278
- Skovgaard A, Saiz E** (2006) Seasonal occurrence and role of protistan parasites in coastal marine zooplankton. *Mar Ecol Prog Ser* **327**:37–49
- Small HJ, Shields JD, Hudson KL, Reece KS** (2007) Molecular detection of *Hematodinium* sp. infecting the blue crab, *Callinectes sapidus*. *J Shellfish Res* **26**:131–139
- Small HJ, Neil DM, Taylor AC, Atkinson RJA, Coombs GH** (2006) Molecular detection of *Hematodinium* spp. in Norway lobster *Nephrops norvegicus* and other crustaceans. *Dis Aquat Organ* **69**:185–195
- Smith WO, Harrison WG** (1991) New production in polar regions: the role of environmental controls. *Deep Sea Res Part Oceanogr Res Pap* **38**:1463–1479
- Ssekagiri A, Sloan WT, Ijaz UZ** (2018) microbiomeSeq: An R package for microbial community analysis in an environmental context, Available at <http://www.github.com/umerijaz/microbiomeSeq>
- Stamatakis A** (2014) RAxML version 8: a tool for phylogenetic analysis and post-analysis of large phylogenies. *Bioinformatics* **30**:1312–1313
- Steele JA, Countway PD, Xia L, Vigil PD, Beman JM, Kim DY, et al.** (2011) Marine bacterial, archaeal and protistan association networks reveal ecological linkages. *ISME J* **5**:1414–1425

**Swanberg NR, Caron DA** (1991) Patterns of sarcodine feeding in epipelagic oceanic plankton. *J Plankton Res* **13**:287–312

**Takahashi O, Mayama S, Matsuoka A** (2003) Host-symbiont associations of polycystine Radiolaria: epifluorescence microscopic observation of living Radiolaria. *Mar Micropaleontol* **49**:187–194

**Tosadori G, Bestvina I, Spoto F, Laudanna C, Scardoni G** (2017) Creating, generating and comparing random network models with NetworkRandomizer. *F1000 Research* **5**:2524

**Velo-Suárez L, Brosnahan ML, Anderson DM, McGillicuddy DJ Jr** (2013) A quantitative assessment of the role of the parasite *Amoebophrya* in the termination of *Alexandrium fundyense* blooms within a small coastal embayment. *PLoS ONE* **8**:e81150

**Watts DJ, Strogatz SH** (1998) Collective dynamics of 'small-world' networks. *Nature* **393**:440–442




**Wickham H** (2016) ggplot2: Elegant Graphics for Data Analysis. 2nd edn Springer, New York

Available online at [www.sciencedirect.com](http://www.sciencedirect.com)

**ScienceDirect**



## Seasonal microbial food web dynamics in contrasting Southern Ocean productivity regimes

Urania Christaki <sup>1\*</sup>, Audrey Gueneugues,<sup>2</sup> Yan Liu,<sup>2</sup> Stéphane Blain <sup>2</sup>, Philippe Catala,<sup>2</sup> Jonathan Colombet,<sup>3</sup> Pavla Debeljak,<sup>2</sup> Ludwig Jardillier,<sup>4</sup> Solène Irion <sup>1</sup>, Fred Planchon,<sup>5</sup> Ingrid Sassenhagen,<sup>1</sup> Telesphore Sime-Ngando,<sup>3</sup> Ingrid Obernosterer<sup>2</sup>

<sup>1</sup>Univ. Littoral Côte d'Opale ULCO, CNRS, Univ. Lille, UMR 8187, LOG, Laboratoire d'Océanologie et de Géosciences, F-Code postal Ville, France

<sup>2</sup>Sorbonne Université, CNRS, Laboratoire d'Océanographie Microbienne (LOMIC), Banyuls-sur-Mer, France

<sup>3</sup>Laboratoire Microorganismes: Génome et Environnement (LMGE), UMR CNRS 6023, Clermont Université Blaise Pascal, Aubière Cedex, France

<sup>4</sup>Unité d'Ecologie, Systématique et Evolution, Université Paris-Sud, CNRS, AgroParisTech, Université Paris-Saclay, Orsay Cedex, France

<sup>5</sup>University of Brest, Laboratoire des Sciences de l'Environnement (LEMAR), UMR6539 CNRS/UBO/IFREMER/IRD, Technopôle Brest Iroise, Plouzané, France

### Abstract

Spatial and seasonal dynamics of microbial loop fluxes were investigated in contrasting productivity regimes in the Indian sector of the Southern Ocean. Observations carried out in late summer (February–March 2018; project MOBYDICK) revealed higher microbial biomasses and fluxes in the naturally iron-fertilized surface waters of Kerguelen island in comparison to surrounding off-plateau waters. Differences were most pronounced for bacterial heterotrophic production (2.3-fold), the abundance of heterotrophic nanoflagellates (HNF; 2.7-fold). Independent of site, grazing by HNF was the main loss process of bacterial production (80–100%), while virus-induced mortality was low (< 9%). Combining these results with observations from previous investigations during early spring and summer allowed us to describe seasonal patterns in microbial food web fluxes and to compare these to carbon export in the iron-fertilized and high-nutrient, low-chlorophyll (HNLC) Southern Ocean. Our data suggest an overall less efficient microbial food web during spring and summer, when respiration and viral lysis, respectively, represent important loss terms of bacterially-mediated carbon. In late summer, primary production is more efficiently transferred to bacterial biomass and HNF and thus available for higher trophic levels. These results provide a new insight into the seasonal variability and the quantitative importance of microbial food web processes for the fate of primary production in the Southern Ocean.

The Southern Ocean plays a major role in the global carbon cycle, yet there are still major gaps in our understanding of how it fully functions (e.g., Gruber et al. 2009; Gray et al. 2018). Investigations into biogenic C-export in the Southern Ocean suggest an inverse relationship between primary production and carbon export efficiency (Lam and Bishop 2007; Maiti et al. 2013; LeMoigne et al. 2016).

\*Correspondence: urania.christaki@univ-littoral.fr

This is an open access article under the terms of the Creative Commons Attribution-NonCommercial License, which permits use, distribution and reproduction in any medium, provided the original work is properly cited and is not used for commercial purposes.

Additional Supporting Information may be found in the online version of this article.

Urania Christaki and Ingrid Obernosterer have equal contribution.

Differences in phytoplankton community composition may affect trophic structure, grazing intensity and/or microbial remineralization (e.g., Maiti et al. 2013; LeMoigne et al. 2016). At present, no model can reasonably calculate carbon export in the Southern Ocean, partly because, neither primary production nor food web structure can predict these fluxes (Rembauville et al. 2015; LeMoigne et al. 2016; Deppeler and Davidson 2017). Observational studies of planktonic communities and their activities in this remote ocean can thus offer essential information in understanding the current and future state of the mechanisms that link planktonic communities with carbon export (Rembauville et al. 2015).

The Southern Ocean is the largest high-nutrient, low-chlorophyll (HNLC) zone where the limitation of primary production by iron is spatially heterogeneous (Blain et al. 2007). In this context, the contrasting iron-fertilized and HNLC areas around the Kerguelen and Crozet islands provide an excellent

environment to investigate the spatial and temporal heterogeneity of planktonic C-fluxes in the Southern Ocean (Blain et al. 2007; Pollard et al. 2007, 2009). The extensive phytoplankton blooms occurring in iron-fertilized waters, mainly characterized by diatom communities (e.g., Poulton et al. 2007; Lasbleiz et al. 2016), have higher primary production rates (Seeyave et al. 2007; Cavagna et al. 2015) and higher carbon export in contrast to the surrounding HNLC waters (Savoie et al. 2008; Planchon et al. 2015). The Kerguelen bloom, -despite being a major carbon sink with high CO<sub>2</sub> sequestration per unit of iron (Blain et al. 2007), follows the “High Biomass Low Export” paradigm (Lam and Bishop 2007) of the Southern Ocean (Mosseri et al. 2008; Savoie et al. 2008; Cavagna et al. 2015; Planchon et al. 2015).

Microbial food web processes determine to a large extent what fraction of primary production is remineralized or available for higher trophic levels or export. The fraction of primary production consumed by heterotrophic bacteria is highly variable in polar oceans (Kirchman et al. 2009), likely resulting from variable degrees of phytoplankton-bacteria coupling (Morán et al. 2006). In Kerguelen plateau waters, heterotrophic bacteria respond rapidly to the phytoplankton bloom and process a considerable fraction of the primary production (Obernosterer et al. 2008; Christaki et al. 2014). Protists channel prokaryotic carbon to higher trophic levels through bacterivory while viruses return dissolved and small particulate prokaryotic carbon forms to the water column via the viral shunt. Theoretically, grazing should therefore enhance carbon export while viral lysis would enhance respiration and reduce prokaryote growth efficiency. Viral activity in the Southern Ocean could be crucial for iron regeneration, especially in HNLC areas (Strzepek et al. 2005; Evans and Brussaard 2012). This said, integrative studies of microbial stocks (viruses, heterotrophic bacteria, heterotrophic and phototrophic flagellates) and fluxes (bacterial production, respiration, grazing and viral lysis) along with community production and C-export measurements are necessary to describe the role of bacteria in C-flux variability.

The present study was undertaken in the framework of the MOBYDICK project (Marine Ecosystem Biodiversity and Dynamics of Carbon around Kerguelen: an integrated view). MOBYDICK's objective was to trace C from its biological fixation, cycling within and across trophic levels, and its export to depth, under different productivity regimes of the Southern Ocean in late summer. Our aim here was to compare C-fluxes mediated by microbes at the surface to carbon export to deeper layers and carbon availability for higher trophic levels at the surface. Seasonal dynamics of bacterial carbon processing in iron-fertilized and HNLC waters and its implications for ecosystem functioning is described during three periods, separated by 7 to 13 yr: early spring (onset of the bloom, October–November 2011, KEOPS2 cruise), summer (decline of the bloom, January–February 2005, KEOPS1 cruise 2005), and end of summer (post-bloom period, February–March 2018, MOBYDICK cruise).

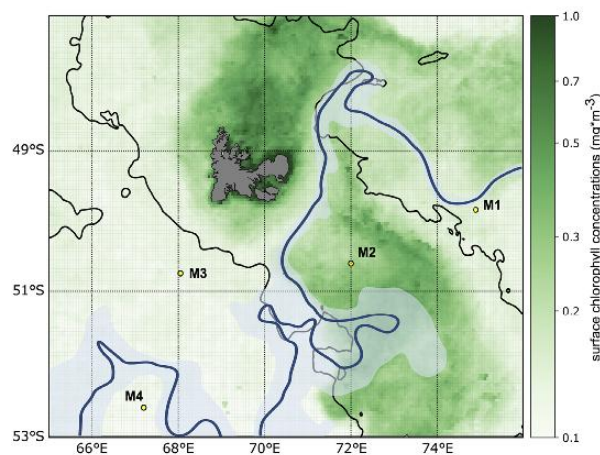


**Fig 1.** Map of the MOBYDICK station locations. Surface chlorophyll *a* (Chl *a*) concentrations were Reprocessed Global Ocean Satellite Observations (Copernicus-GlobColour). Data were provided by Copernicus Marine Service (<http://marine.copernicus.eu/>). Chl *a* concentrations are the monthly means for March 2018 at a resolution of 4 km. The black lines denote 1000 m bathymetry. The approximate position of the highly dynamic polar front during February–March 2018 was also drawn according to Pauthenet et al. (2018). The polar front is the dark, thick, blue line, gray zone around the polar front indicates variations in its trajectory.

## Materials and methods

### Sample collection

Samples were collected at four stations (M1, M2, M3, and M4) in the region of Kerguelen island in the Indian sector of the Southern Ocean during late austral summer (19 February to 20 March 2018; MOBYDICK cruise) (Fig. 1). The timing of the visits corresponded to about one month after the seasonal maximum in chlorophyll *a* (Chl *a*) (Figs. S1, S2). Sta. M2 was located above the Kerguelen plateau and is the “historical” A3 station of the previous KEOPS1 and KEOS2 cruises (Figs. 1, S1). This site is located in naturally iron-fertilized waters and characterized by high primary production during spring and summer (Lefèvre et al. 2008; Mosseri et al. 2008; Cavagna et al. 2015). Sta. M1, M3, and M4 were located off the plateau characterized by lower seasonal primary production (Fig. S1). Sta. M2 was sampled three times with an eight day interval between visits (M2-1, M2-2, M2-3; Table 1). Sta. M3 (M3-1, M3-3) and M4 (M4-1, M4-2) were both sampled twice with a 2-week interval each, and Sta. M1 was visited once (Table 1). All water samples were collected with 12L Niskin bottles mounted on a rosette equipped with CTD (SeaBird 911-plus). Microbial parameters were sampled at selected depths throughout the water column (Table 2).

### Viral and microbial abundance

Pico- and nanophytoplankton, virus-like particles, heterotrophic bacteria (sensu-stricto includes *Archaea* and *Bacteria*), and heterotrophic nanoflagellates (HNF) were enumerated

**Table 1.** Station description. The depth of the mixed layer ( $Z_{ML}$ ) is based on a difference in sigma of 0.02 to the surface value. The mean  $Z_{ML}$  and euphotic layer ( $Z_e = 1\%$  light depth) of all CTD casts performed during the occupation of the stations is given. For the rest of the variables the mean  $\pm$  SD is given for the mixed layer.

Sta.	Date (2018)	Long (°E)*	Lat (°S)*	Depth (m)*	$Z_{ML}$ (m)	$Z_e$ (m)	T (°C)	Chlorophyll $a$ ( $\mu\text{g L}^{-1}$ )	$\text{NO}_3^- + \text{NO}_2^-$ ( $\mu\text{M}$ )	$\text{NH}_4^+$ ( $\mu\text{M}$ )	$\text{PO}_4^{3-}$ ( $\mu\text{M}$ )	SI ( $(\text{OH})_4$ (nM))
M2-1	26–28 Feb	72.0004	50.3697	520	62	64	5.10 $\pm$ 0.06	0.27 $\pm$ 0.02	21.9 $\pm$ 0.12	0.75 $\pm$ 0.07	1.47 $\pm$ 0.03	1.36 $\pm$ 0.41
M2-2	6–8 Mar	72.0099	50.3769	519	61	61	5.24 $\pm$ 0.00	0.30 $\pm$ 0.04	21.79 $\pm$ 0.38	1.12 $\pm$ 0.02	1.50 $\pm$ 0.04	1.72 $\pm$ 0.79
M2-3	16–17 Mar	72.0013	50.3700	527	68	58	5.11 $\pm$ 0.07	0.58 $\pm$ 0.02	21.9 $\pm$ 0.08	0.95 $\pm$ 0.05	1.50 $\pm$ 0.00	2.75 $\pm$ 0.27
M1	8–9 Mar	74.5406	49.5098	2723	27	80	4.99 $\pm$ 0.10	0.35 $\pm$ 0.040	25.2 $\pm$ 0.56	0.56 $\pm$ 0.20	1.71 $\pm$ 0.11	8.38 $\pm$ 2.93
M3-1	3–5 Mar	68.0347	50.4095	1000	65	93	5.6 $\pm$ 0.00	0.20 $\pm$ 0.02	23.75 $\pm$ 0.31	0.50 $\pm$ 0.03	1.65 $\pm$ 0.05	2.89 $\pm$ 1.01
M3-3	18–20 Mar	68.0302	50.4193	1700	79	107	5.31 $\pm$ 0.02	0.14 $\pm$ 0.00	23.34 $\pm$ 0.12	0.73 $\pm$ 0.01	1.08 $\pm$ 0.92	2.31 $\pm$ 0.04
M4-1	28 Feb–3 Mar	67.1198	52.3601	4186	49	96	4.45 $\pm$ 0.06	0.18 $\pm$ 0.01	25.7 $\pm$ 0.05	0.37 $\pm$ 0.03	1.70 $\pm$ 0.02	4.36 $\pm$ 0.35
M4-2	12–14 Mar	67.1228	52.3610	4300	87	100	4.46 $\pm$ 0.00	0.21 $\pm$ 0.00	24.8 $\pm$ 0.27	0.48 $\pm$ 0.01	1.71 $\pm$ 0.01	4.80 $\pm$ 0.00

\* Coordinates and depth of the CTD “stock.”

from surface to 450–1000 m. Samples for virus-like particles and heterotrophic bacteria (2.5 mL) were fixed with 1% v/v glutaraldehyde. Samples for HNF were fixed with 1% v/v paraformaldehyde prepared on board. Samples were stored at 4°C for 40 min, flash frozen in liquid nitrogen and then kept at –80°C until analysis. Counts for heterotrophic bacteria were made after staining with SYBRGreen I by flow cytometric analysis on a BD FACS Canto. Two heterotrophic bacteria populations were discriminated, one with high fluorescence called “high nucleic acid” and one with low fluorescence called “low nucleic acid”. Pico-nanophytoplankton and cyanobacteria of the genus *Synechococcus* were discriminated based on their side scatter and red fluorescence. HNF and virus-like particles were enumerated after staining with SYBRGreen I on a Cytoflex Beckman-Coulter flow cytometer, following Christaki et al. (2011) and Brussaard (2004), respectively. As for bacteria, two populations of virus-like particles could be distinguished based on their fluorescence intensity. Ciliates and dinoflagellates were counted in acid Lugol’s (2% v/v) fixed samples (500 mL) under an inverted microscope (Nikon Eclipse TE2000-S  $\times$ 400).

### Bacterial production

Heterotrophic bacterial production was measured from surface to 500 m with the  $^3\text{H}$ -leucine incorporation method. At each depth 20 mL triplicate samples and a formalin killed control (2% v/v) were spiked with a mixture of nonradioactive (19 nM) and L-[4,5- $^3\text{H}$ ] leucine (Perkin Elmer, 120 Ci/mmol). The concentration of radioactive leucine was 1 nM in the mixed layer and 2 nM below the mixed layer. Concentration kinetics were checked at 25 and 250 m with 4, 6, 12, 20, and 40 nM of leucine, to ensure that there was no isotopic dilution. The incubation times were 2 h in the 0–150 m layer, 4 h in the 150–200 m layer, and 8 h in the 250–500 m layer. Time kinetics were tested for 10, 125, 250, and 500 m (0, 3, 6, 8, 10 h) and were found linear for the applied incubation times. Samples were incubated in the dark at in situ temperature. Incubations were terminated with formalin (2% v/v). Samples were filtered onto 0.22  $\mu\text{m}$  Nuclepore filters, after filtration ice-cold 5% trichloroacetic acid (10 mL) was added on the filters for 10 min. The filters were rinsed 3 times with 4 mL ice-cold 5% trichloroacetic acid, placed in scintillation vials where 8 mL of scintillation cocktail (Ultima Gold—Packard) was added and radioassayed on board. Incorporation rates of leucine into carbon were calculated using a theoretical conversion factor of 1.55 kg of C mol $^{-1}$  (Kirchman 1993).

### Dark community and bacterial respiration, net community production, and gross community production

Rates of dark community respiration, bacterial respiration and net community production were determined from changes in the concentration of dissolved oxygen ( $\text{O}_2$ ) during 24 h light and dark incubations as described previously (Lefèvre et al. 2008). For dark community respiration and net

**Table 2.** Parameters sampled. Virus-like particles (VLP), heterotrophic bacteria (HB), heterotrophic nanoflagellates (HNF), phototrophic pico- and nanoplankton (PNP), bacterial heterotrophic production (BP), bacterial respiration (BR), gross community production (GCP), dark community respiration (DCR), net community production (NCP), virus induced bacterial mortality (VIBM), grazing induced bacterial mortality (GIBM), photosynthetically active radiation (PAR).

Parameter	Sta.	Depth (m)
VLP, HB, HNF, PNP	All	10, 15 or 20, 30, 50, 60, 70, 100, 125, 150, 175, 200, 350, 450, 500 (except M2, 450 m)
BP	All	Same as above
BR	All, except M3-1	50%, 1% PAR level
GCP, DCR, NCP	All, except M3-3	50%, 25%, 4%, 1% PAR level
VIBM	All	10, 60, 125, 300 m
GIBM	All, except M3-3, M4-2	30 m

community production, seawater was collected at four depths corresponding to 1%, 4%, 25%, and 50% of photosynthetically active radiation levels of surface values. Unfiltered seawater was transferred to 125 mL borosilicate glass bottles and incubated in an on-deck incubator at the respective photosynthetically active radiation levels using optical density filters (Nickel screens). The outdoor incubators were connected with a running seawater system to maintain the incubation bottles at the temperature of the mixed layer zone. The 1% light depth (euphotic depth) was at the bottom of the mixed layer at Sta. M2, but the euphotic depth was well below the mixed layer at the off-plateau sites (Table 1). Gross community production was calculated as the sum of dark community respiration and net community production. For bacterial respiration, seawater from two depths corresponding to the 1% and 50% surface photosynthetically active radiation levels were filtered through 0.8  $\mu\text{m}$  polycarbonate filters (Nuclepore) and the subsequent filtrate was incubated in 125 mL borosilicate bottles in the dark at in situ temperature for 1–3 days (Obenosterer et al. 2008). All incubations were done in five replicates. Dissolved oxygen ( $\text{O}_2$ ) concentration was determined by spectrophotometric detection of iodine following the Winkler reaction, using a Hitachi U-3010 Spectrophotometer equipped with a sipper system.

#### Grazing induced bacterial mortality

Bacterial mortality due to protists was evaluated in the mixed layer (30 m) using the principle of fluorescently labeled bacteria (FLB) as prey analogues (Sherr et al. 1987). The FLB were prepared with a culture of *Brevundimonas diminuta* (CECT 313) following the protocol of Sherr et al. (1987). Triplicate glass Schott bottles of 2 L were filled with 60  $\mu\text{m}$  screened water directly from the Niskin bottle and one control with 0.2  $\mu\text{m}$  filtered sea water were inoculated with FLB at a final concentration of approx.  $0.7 \times 10^5 \text{ mL}^{-1}$  in a refrigerated room (4°C). The expected FLB to bacteria ratio-based on bacterial abundances during previous cruises was expected to be around 20%. Because of increased bacteria abundances during

MOBYDICK, this ratio was of 6–14%. After addition of labeled preys in all bottles, samples for FLB, heterotrophic bacteria and HNF counts were immediately withdrawn for  $T_0$  counts. Incubations were performed in an on-deck incubator with surface seawater circulation, covered with a screen providing 50% light attenuation. Grazing on bacteria was measured by counting both the number of ingested FLB in food vacuoles by microscopy and FLB disappearing by flow cytometry. The food vacuole observation approach allows visual observation of the proportion and the morphology of protists that ingested FLB. Both approaches are based on several assumptions which will be further discussed in the paper.

#### Food vacuole analysis

After 4 h of incubation, 45 mL samples were retrieved from the bottles, fixed with glutaraldehyde (1% final conc.) and filtered on 0.8  $\mu\text{m}$  Nuclepore filters before being stained with DAPI (4',6-diamidino-2-phenylindole). They were then kept frozen at  $-80^\circ\text{C}$  until they were observed with a Zeiss AX10 epifluorescence microscope. Prokaryotes were identified by their blue fluorescence when excited with UV radiation, while DTAF (4,6-dichlorotriazinyl-aminofluorescein) stained FLB were identified by their yellow-green fluorescence when excited with blue light. The ingestion rate (IR:  $\text{FLB HNF}^{-1} \text{ h}^{-1}$ ) was calculated according to Dolan and Šimek (1998) as:

$$\text{IR} = \text{VC} \times k, \quad (1)$$

where VC is vacuole content at steady state, and  $k$  is a conservative digestion rate of  $0.92\% \text{ cell content min}^{-1}$ , which corresponds to a  $t_{1/2}$  digestion time of 75 min. For comparison, a higher  $k$  of  $1.1\%$  was also calculated ( $t_{1/2}$  digestion time of 63 min).

#### Fluorescently labeled bacteria disappearance

Bottles were incubated for approximately 50 h. Samples for prokaryotes, FLB, and HNF abundances were taken every 10–12 h. Samples were fixed and stored for flow cytometry as

described above. Triplicate counts by flow cytometry were performed for each sample. Bacterial grazing rates were obtained by measuring the rate of disappearance of FLB after subtracting the FLB disappearance in the “control.” The abundance of FLB was plotted vs. time, and the calculation of grazing rates ( $g, h^{-1}$ ) of FLB corresponds to the slope of the abundance of FLB as a function of time. The decrease of FLB abundance was linear for the first 40–48 h, at the exception of M2-3 where it was linear only for the first 24 h. The “control” bottles showed no decrease of FLB during the incubations. In the experimental bottles, the abundances of bacteria and nanophytoplankton did not show significant increases or decreases for the first 40 h. The impact of protists on bacteria was calculated as the % of the bacterial production consumed, assuming that FLB were grazed at the same rates as natural bacteria (Sherr et al. 1987).

For comparison with FLB disappearance and vacuole content analysis, the potential consumption of bacteria by HNF and ciliates was also estimated assuming a clearance rate of  $10^5$  cell volume  $h^{-1}$  (Fenchel 1982). For all approaches, the % of bacterial production consumed was calculated from the number of bacterial cells produced as determined by leucine incorporation (see above).

#### Virus-induced bacterial mortality

Triplicate 4.5 mL samples, collected at each depth (Table 2), were fixed and stored as for flow cytometry (see

above). Upon analysis, they were pooled and ultracentrifuged in order to harvest the bacterial cells for transmission electron microscope observations (detailed in Christaki et al. 2014). Virus induced bacterial mortality (VIBM) was calculated as (Eq. 2, Binder 1999; Eq. 3, Weinbauer et al. 2002):

$$VIBM = (FIC + 0.6 \times FIC^2) / (1 - 1.2 \times FIC) \quad (2)$$

$$FIC = 9.524 \times FVIC - 3.256 \quad (3)$$

where FIC is the frequency of infected cells, and FVIC is the frequency of visibly infected cells (i.e., cells that contain five or more phages).

#### Statistical analyses

Principal component analysis (PCA) and hierarchical clustering on principle components was performed on environmental variables with R-software, version 3.5.1 using the package FactoMineR (Lê et al. 2008). Before these analyses, environmental variables were standardized to zero mean using function “decostand” in the package vegan (Oksanen 2017).

## Results

#### Environmental context

The hydrological context of the stations was characterized by the location of the polar front during the MOBYDICK

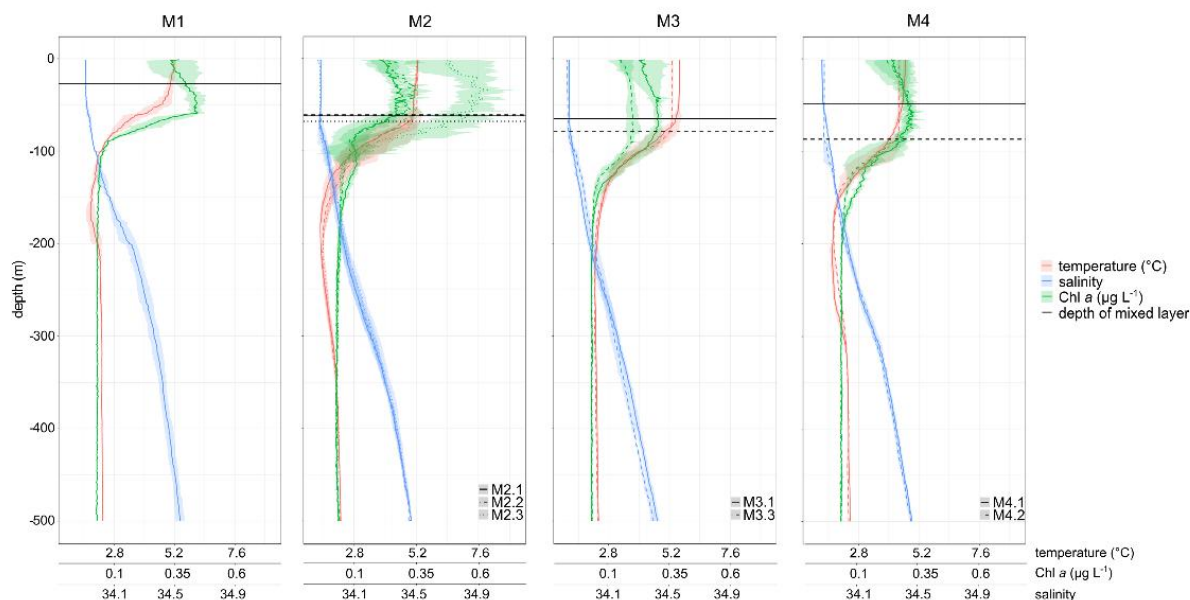


**Fig 2.** Temperature ( $^{\circ}C$ ), salinity and chlorophyll *a* (Chl *a*) (derived from in vivo fluorescence) profiles for all the visits at the four stations. The mean profiles were calculated from all the CTDs of each visit to a station, the shadows around the mean profiles are standard deviations.

cruise. Sta. M1, situated in Antarctic waters, was influenced by the highly dynamic polar front (Pauthenet et al. 2018), resulting in a shallow mixed layer (27 m, Table 1, Figs. 1, 2). Sta. M2 and M4 were located south of the polar front in Antarctic waters with a characteristic temperature minimum zone close to 200 m (Figs. 1, 2) and a mixed layer varying between 61–68 m, and 49–87 m, respectively (Table 1, Fig. 2). Sta. M3 was situated in the sub-Antarctic zone outside the influence of the polar front (mixed layer depth, 65–79 m). Temperature in the mixed layer was lowest at Sta. M4 (4.5°C) and highest at Sta. M3 (5.6°C, Table 1). The mixed layer deepened at all stations after a storm that occurred on the 10<sup>th</sup> of March 2018. The greatest increase in the mixed layer depth induced by the

storm was observed at Sta. M4 (77%, from 49 to 87 m) while at stations M2 and M3 the increase of the mixed layer depth was moderate (10% and 20%, respectively, Table 1).

Average Chl *a* concentrations in the mixed layer ranged from 0.14 (M3-3) to 0.58  $\mu\text{g L}^{-1}$  (Sta. M2-3). Chl *a* in the mixed layer doubled from the first to the third visit at Sta. M2 3 weeks later (from 0.27 to 0.58  $\mu\text{g L}^{-1}$  Table 1, Fig. 2). Phosphate and nitrate were abundant in the mixed layer at all stations, while the highest ammonium concentrations were observed on the plateau at Sta. M2 (0.75–1.12  $\mu\text{M}$ ). Silicic acid concentration was overall higher off the plateau (2.3–8.4  $\mu\text{M}$ ) than in surface waters on the Kerguelen plateau (1.4–2.8  $\mu\text{M}$ , Table 1). The first two components of the principal

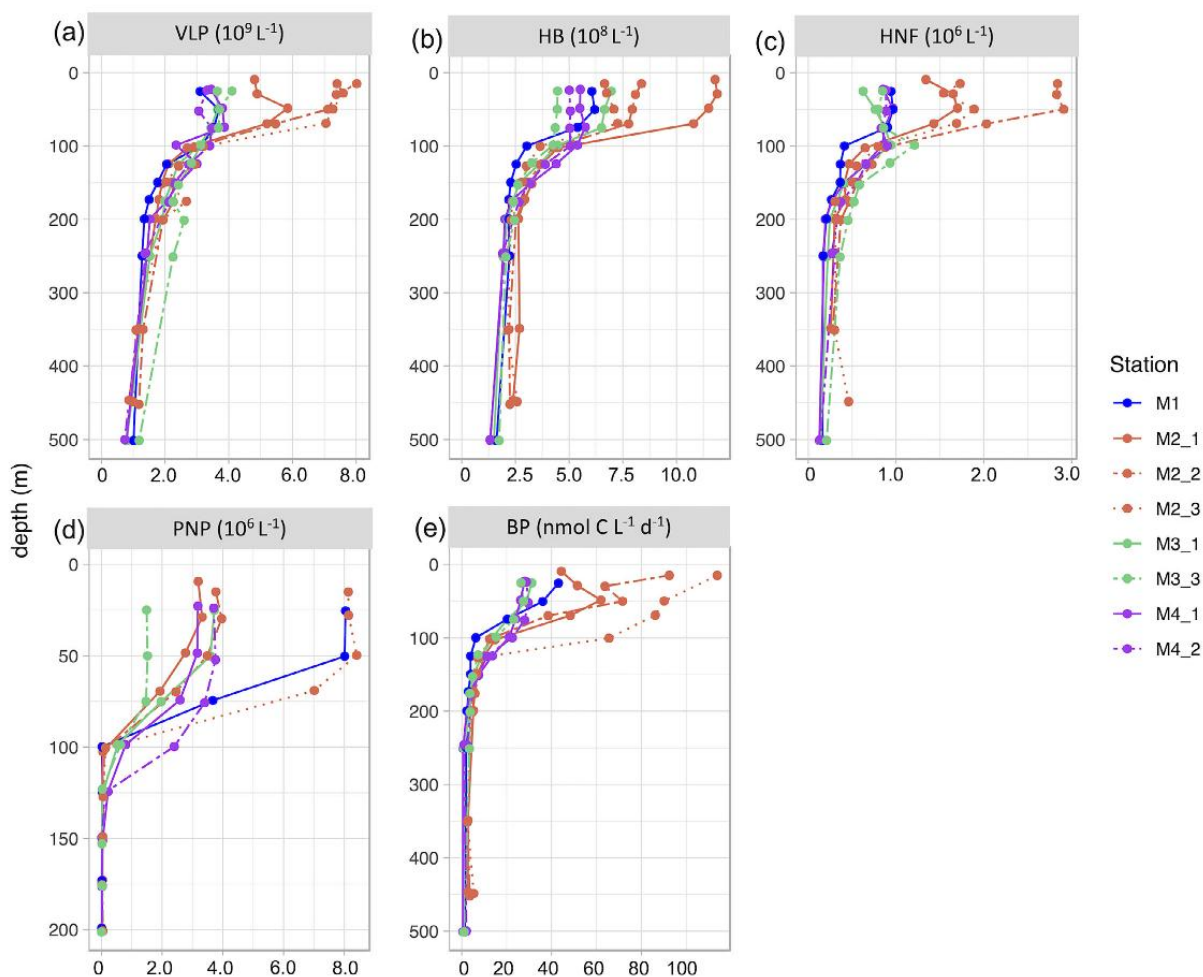


**Fig 3.** Vertical profiles of viral-like particles (VLP) (a), heterotrophic bacteria (HB) (b), heterotrophic nanoflagellates (HNF) (c), phototrophic pico- and nanoplankton (PNP) (d), and bacterial production (BP) (e).



**Table 3.** Mean  $\pm$  SD values of all visits at the M2 plateau station and the off-plateau stations (M1, M3, and M4). heterotrophic bacteria (HB), % of high and low DNA bacteria as defined by flow cytometry (%“high nucleic acid”, %“low nucleic acid”), virus like particles (VLP), % of low and high green fluorescence VLP (VLP1 VLP2), heterotrophic nanoflagellates (HNF), pico- and nanophytoplankton (PNP) and *Synechococcus* spp. at on-plateau (M2) and the off-plateau stations (M1, M3, M4).

Layer	HB ( $10^8 \text{ L}^{-1}$ )		HB “high nucleic acid” %		HB “low nucleic acid” %	
	M2	Off plateau	M2	Off plateau	M2	Off plateau
Mixed layer ( $Z_{ML}$ )	8.8 $\pm$ 2.1	5.3 $\pm$ 1.1	56 $\pm$ 2	41 $\pm$ 3	44 $\pm$ 4	59 $\pm$ 3
$Z_{ML}$ -200 m	4.1 $\pm$ 2.3	3.1 $\pm$ 1.0	57 $\pm$ 2	52 $\pm$ 4	43 $\pm$ 4	58 $\pm$ 4
200-500 m	2.4 $\pm$ 0.2	1.5 $\pm$ 0.6	52 $\pm$ 5	46 $\pm$ 2	46 $\pm$ 3	54 $\pm$ 2

Layer	VLP ( $10^9 \text{ L}^{-1}$ )		%VLP1		%VLP2	
	M2	Off plateau	M2	Off plateau	M2	Off plateau
Mixed layer ( $Z_{ML}$ )	6.46 $\pm$ 0.9	3.35 $\pm$ 0.07	90 $\pm$ 1	89 $\pm$ 3	10 $\pm$ 1	11 $\pm$ 3
$Z_{ML}$ -200 m	2.41 $\pm$ 0.05	2.26 $\pm$ 0.06	86 $\pm$ 3	85 $\pm$ 2	14 $\pm$ 3	15 $\pm$ 2
200-500 m	1.17 $\pm$ 0.05	1.24 $\pm$ 0.04	86 $\pm$ 6	84 $\pm$ 2	14 $\pm$ 6	16 $\pm$ 2

Layer	HNF ( $10^6 \text{ L}^{-1}$ )		PNP ( $10^6 \text{ L}^{-1}$ )		<i>Synechococcus</i> ( $10^3 \text{ L}^{-1}$ )	
	M2	Off plateau	M2	Off plateau	M2	Off plateau
Mixed layer ( $Z_{ML}$ )	1.96 $\pm$ 0.5	0.83 $\pm$ 0.13	4.71 $\pm$ 1.9	3.33 $\pm$ 2.1	73 $\pm$ 16	111 $\pm$ 88
$Z_{ML}$ -200 m	0.51 $\pm$ 0.1	0.53 $\pm$ 0.27	0.52 $\pm$ 0.31	0.22 $\pm$ 0.52	10 $\pm$ 5	12 $\pm$ 16
200-500 m	0.25 $\pm$ 0.08	0.19 $\pm$ 0.08	-	-	-	-

component analysis (PCA) of environmental parameters in the mixed layer explained 76% of the variability of the data (Fig. S3). Phosphate, nitrate and ammonium were the most important variables for the principal component axis formation. Sta. M2 was associated with higher ammonium concentrations while Sta. M4 presented the highest nitrate,

phosphate and silicic acid concentrations, and Sta. M1 was associated to high dissolved oxygen concentrations (Fig. S3).

#### Stocks and fluxes of microbial components

During the late Austral summer, abundances of virus-like particles, heterotrophic bacteria, bacterial production,

**Table 4.** Bacterial production (BP), Bacterial respiration (BR), cell-specific BP and BR, growth rate ( $\mu$ ) and growth efficiency (BGE) measured at 10 and 60 m. Mean values  $\pm$  SD for BP, BGE) and  $\pm$  SE for BR. Bacterial respiration rates have been converted from  $\text{O}_2$  into C units using a RQ value of 1. No respiration measurements at M3-1.

Sta.	Depth (m)	BP ( $\text{nmol C L}^{-1} \text{ d}^{-1}$ )	BR ( $\mu\text{mol C L}^{-1} \text{ d}^{-1}$ )	Cell-specific BP ( $\text{fmol C cell}^{-1} \text{ d}^{-1}$ )	Cell-specific BR ( $\text{fmol C cell}^{-1} \text{ d}^{-1}$ )	$\mu$ ( $\text{d}^{-1}$ )	BGE %
M2-1	10	44.0 $\pm$ 0.2	0.68 $\pm$ 0.63	0.042	0.64	0.041	6 $\pm$ 5
	60	62.0 $\pm$ 11.6	2.37 $\pm$ 0.24	0.057	2.16	0.055	3 $\pm$ 1
M2-2	10	92.5 $\pm$ 12.8	0.41 $\pm$ 0.29	0.110	0.49	0.107	18 $\pm$ 10
	60	71.6 $\pm$ 3.2	0.48 $\pm$ 0.13	0.090	0.60	0.088	13 $\pm$ 3
M2-3	10	113.8 $\pm$ 4.0	0.35 $\pm$ 0.07	0.157	0.40	0.154	28 $\pm$ 4
	60	86.2 $\pm$ 1.6	0.35 $\pm$ 0.07	0.122	0.45	0.119	21 $\pm$ 3
M1	10	43.1 $\pm$ 4.0	0.11 $\pm$ 0.09	0.078	0.20	0.076	28 $\pm$ 16
	60	27.5 $\pm$ 2.4	0.11 $\pm$ 0.09	0.075	0.22	0.073	25 $\pm$ 15
M3-3	10	26.4 $\pm$ 2.0	0.29 $\pm$ 0.13	0.048	0.352	0.046	8 $\pm$ 4
	60	27.5 $\pm$ 2.4	0.32 $\pm$ 0.06	0.057	0.66	0.056	8 $\pm$ 2
M4-1	10	28.0 $\pm$ 3.6	0.91 $\pm$ 0.15	0.040	1.30	0.039	3 $\pm$ 1
	60	26.2 $\pm$ 2.4	0.41 $\pm$ 0.32	0.043	0.67	0.042	6 $\pm$ 4
M4-2	10	28.8 $\pm$ 4.0	0.22 $\pm$ 0.11	0.052	0.39	0.050	12 $\pm$ 5
	60	29.6 $\pm$ 4.0	0.38 $\pm$ 0.15	0.053	0.68	0.052	7 $\pm$ 3

heterotrophic nanoflagellates (HNF), and phototrophic pico- and nanophytoplankton were higher on the plateau (Sta. M2) than at the off-plateau stations (M1, M3, and M4, Fig. 3a–e). These differences were more pronounced in the mixed layer and were attenuated at depth. The proportion of “high nucleic acid” bacteria was slightly higher on the plateau (56%) than off the plateau (44%, Table 3). The proportion of the two virus-like particles populations identified based on their fluorescence was similar at all sites, with low fluorescence virus-like particles dominating throughout the water column (84–90%) (Table 3). *Synechococcus* was found at low abundances of a magnitude of  $10^4$  cells  $L^{-1}$  (Table 3). Bacterial production, averaged over the three visits, was about 2-fold higher in the mixed layer at Sta. M2 than the off-plateau stations (Table 3). Bacterial respiration in the mixed layer on the plateau (mean  $0.45 \pm 0.14 \mu\text{mol O}_2 L^{-1} d^{-1}$ ) was not different to that determined off the plateau (mean  $0.38 \pm 0.26 \mu\text{mol O}_2 L^{-1} d^{-1}$ ), with the exception of one high value recorded during the first visit of Sta. M2 (Table 4). As a consequence, bacterial growth efficiency was substantially higher on the plateau during the 2<sup>nd</sup> and 3<sup>rd</sup> visit (mean  $20 \pm 6\%$ ) than off the plateau at Sta. M3 and M4 (mean  $7 \pm 3\%$ ). Bacterial growth rates were also higher during the 2<sup>nd</sup> and 3<sup>rd</sup> visit of Sta. M2 ( $0.12 \pm 0.03 d^{-1}$ ) as compared to the off-plateau stations ( $0.05 \pm 0.00 d^{-1}$ ) (Table 4).

#### Loss of bacteria due to grazing and viral lysis

As revealed by microscopic observations, HNF and ciliates were ingesting FLB (Fig. S4). Because of their higher abundance when compared to ciliates ( $0.2\text{--}0.5 \times 10^3$  ciliates  $L^{-1}$ ), HNF ( $10^6$  HNF  $L^{-1}$ ) were the major bacterial grazers. On average, 60% (range 38–87%) of the HNF ingested in most cases 1–3 FLB. The few ciliates observed on the filters contained 5 to  $> 10$  FLB  $CIL^{-1}$ . Small dinoflagellate *Gymnodinium* spp. cells of  $10\text{--}20 \mu\text{m}$  accounted for  $0.7\text{--}1.0 \times 10^3$  cells  $L^{-1}$  (data not shown) and they occasionally contained 1–3 FLB *Gymnodinium*<sup>-1</sup>. Finally, FLB ingestion occurred in less than 1% of nanophytoplankton observed on the filters (cf. Fig. S4). Based on all observations, the ingestion rate was of about 1–3 bact grazer<sup>-1</sup> h<sup>-1</sup> (mean 1.4, median 1.3 bact grazer<sup>-1</sup> h<sup>-1</sup>, Fig. 4a). The loss of bacterial production induced by grazing was calculated based on the estimated ingestion rate multiplied by the number of grazers. Grazing on bacteria was higher at Sta. M2 (median 105%) than off-plateau stations (median 80%) (Fig. 4b). By contrast, the virus-induced mortality was comparatively low, varying from undetectable values at M2-3 to 15% at M2-2 (median 9% for all stations) (Fig. 4c).

#### Short-term temporal variability

The higher microbial stocks and fluxes measured on the plateau at Sta. M2 were also accompanied by a more pronounced variability between the three visits as compared to off-plateau waters. Concentrations of Chl *a* and the abundance of pico- and nanophytoplankton in the mixed layer

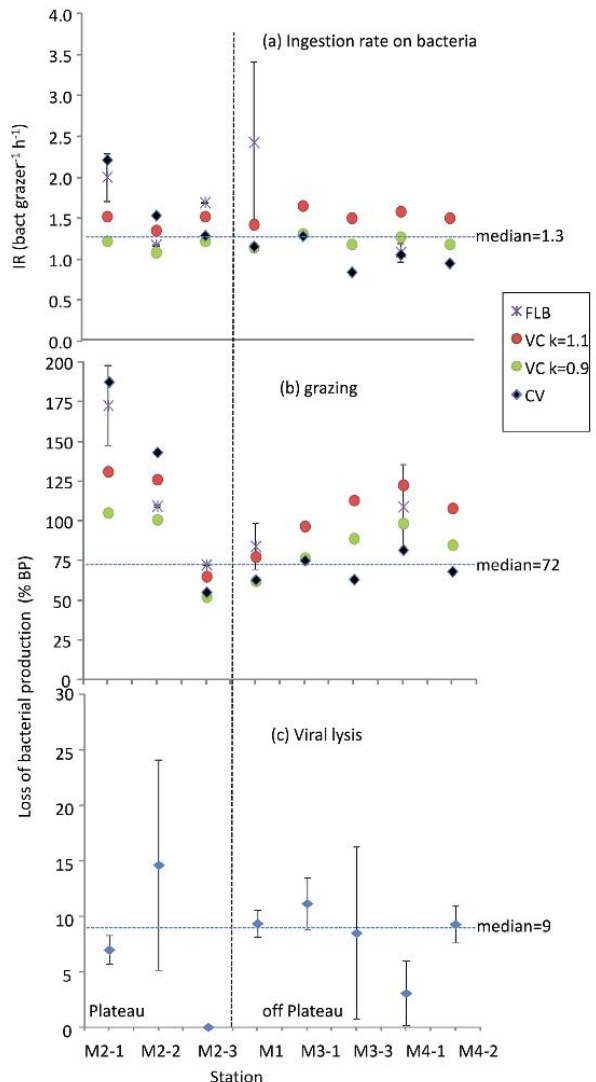


**Fig 4.** Mean ingestion rates on bacteria (a), proportion (%) of bacterial production loss due to grazing (b) and proportion (%) of bacterial production loss due to viral lysis (c). FLB: based on FLB disappearance, error bars for FLB indicate standard deviation (SD) between replicates. The estimation based on vacuole content (VC) analysis was calculated for digestion times  $k = 1.1$  and  $k = 0.9$ . The estimation based on cell volume (CV) was calculated assuming a clearance rate of  $10^5$  cell volume  $h^{-1}$  of grazers (for more details see M&M section). Error bars indicate SD between replicates for grazing and between different depths in the mixed layer for viral lysis.

increased between the first to the third visit by factors of 2.0 and 2.6, respectively. A similar pattern was observed for bacterial production (3-fold increase, Fig. 3e), while the abundance of heterotrophic bacteria decreased by 1.9-fold during this

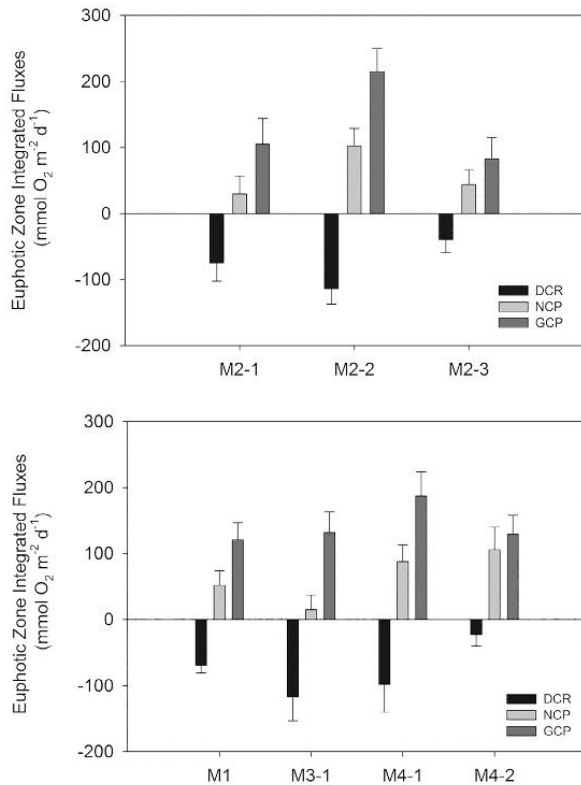


**Fig 5.** Integrated euphotic layer, gross community production (GCP), dark community respiration (DCR) and net community production (NCP) ( $\text{mmol O}_2 \text{ m}^{-2} \text{ d}^{-1}$ ). Error bars represent standard errors.

3-week time period (Fig. 3b). The inverse temporal pattern in bacterial production and heterotrophic bacteria abundance resulted in a 3.7 and 2-fold increase in the bacterial growth rate ( $\mu$ ) and cell-specific bacterial production, respectively (Table 4). Concomitant with the decrease in heterotrophic bacteria abundance, bacterial grazers (HNF) and virus-like particles increased by 2- and 1.5-fold between the first and the second visit of Sta. M2 (Fig. 3a–c). All three bacterivory estimation approaches used in this study revealed higher grazing during the first visit (>100%) and grazing decreased to 50–75% of the bacterial production during the third visit (Fig. 4b). Off the Kerguelen plateau, the short-term variability was much less pronounced. Noticeable decreases between consecutive visits were observed for the abundance of heterotrophic bacteria and pico- and nanophytoplankton at Sta. M3.

#### Net community production, dark community respiration, and gross community production

Above the Kerguelen plateau, at Sta. M2, net community production fluxes integrated over the euphotic zone varied

between 30 and 44  $\text{mmol O}_2 \text{ m}^{-2} \text{ d}^{-1}$  during the 1<sup>st</sup> and 3<sup>rd</sup> visit. Net community production was substantially higher during the 2<sup>nd</sup> visit (100  $\text{mmol O}_2 \text{ m}^{-2} \text{ d}^{-1}$ ) (Fig. 5), which could explain the observed increase in the Chl *a* concentrations about 1 week later (Table 1). Off-plateau, highest net community production fluxes were determined at Sta. M4 (88–106  $\text{mmol O}_2 \text{ m}^{-2} \text{ d}^{-1}$ ). Euphotic zone integrated fluxes of dark community respiration varied between 75 and 113  $\text{mmol O}_2 \text{ m}^{-2} \text{ d}^{-1}$  during the first two visits at Sta. M2 and dark community respiration decreased to 39  $\text{mmol O}_2 \text{ m}^{-2} \text{ d}^{-1}$  during the 3<sup>rd</sup> visit. Fluxes of dark community respiration off-plateau ranged between 69 and 117  $\text{mmol O}_2 \text{ m}^{-2} \text{ d}^{-1}$ , with the exception of the last visit at Sta. M4 (23  $\text{mmol O}_2 \text{ m}^{-2} \text{ d}^{-1}$ ) (Fig. 5), which corresponded to a deepening of the mixed layer following the storm event. Highest depth-integrated fluxes of gross community production were recorded during the 2<sup>nd</sup> visit at Sta. M2 (215  $\text{mmol O}_2 \text{ m}^{-2} \text{ d}^{-1}$ ) while gross community production ranged between 121 and 187  $\text{mmol O}_2 \text{ m}^{-2} \text{ d}^{-1}$  off-plateau (Fig. 5). Comparison of the volumetric rates of oxygen consumption in unfiltered and < 0.8  $\mu\text{m}$  filtered seawater revealed that above the Kerguelen plateau bacterial respiration accounted for  $41 \pm 2\%$  and  $87 \pm 24\%$  of community respiration at 10 and 60 m, respectively. Off-plateau, bacterial respiration accounted for 100% of community respiration during both visits.

## Discussion

### Late summer microbial food web

We observed that the microbial standing stocks and fluxes, apart from microbial respiration, were higher in the mixed layer of the iron-fertilized area above the Kerguelen plateau as compared to surrounding HNLC waters, even one month after the decline of the phytoplankton bloom. Our results thereby complement previous observations during the onset and the decline of the Kerguelen bloom (e.g., Table 4 in Christaki et al. 2014). A comparison of the different phases of the bloom reveals, however, distinct features at the end of summer. While the enhancement of Chl *a* and bacterial production on- vs. off-plateau ratios exceeded by 2–4-fold that of the other parameters in early spring and summer, their on- vs. off-plateau ratios were in a similar range during the post bloom period (Table S1, Fig. 6). Pico- and nanophytoplankton were characterized by marked increases in their abundance (about 15-fold) and contribution to total Chl *a* (10–53%) between the onset and the post bloom periods in Kerguelen plateau waters (Table S1). In addition, the ratio of pico- and nanophytoplankton in fertilized vs. HNLC waters was < 1 during the onset and decline of the bloom and > 1 after the bloom (Fig. 6). This observation is in line with previous studies in the Kerguelen area indicating that pico- and nanophytoplankton dominate communities on the plateau before (Christaki et al. 2014) and after the bloom (Uitz

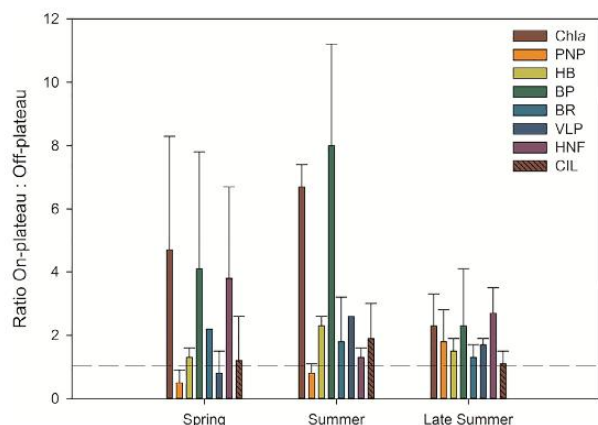


**Fig 6.** On- vs. off-plateau ratios of microbial parameters in the mixed layer. Chlorophyll *a* (Chl *a*), heterotrophic bacteria (HB), phototrophic pico- and nanoplankton (PNP), bacterial production (BP), bacterial respiration (BR), virus like particles (VLP), heterotrophic nanoflagellates (HNF), and ciliates (CIL).

et al. 2010). Furthermore, estimates of mean annual primary production reveal that pico- and nanophytoplankton ( $2.5 \text{ Gt C yr}^{-1}$ ) have a higher contribution as compared to microphytoplankton ( $0.9 \text{ Gt C yr}^{-1}$ , Uitz et al. (2010), underlying their importance in Southern Ocean waters.

Heterotrophic bacteria reached  $1.0 \times 10^9 \text{ cells L}^{-1}$  during the post bloom period, and their biomass was about 2 to 3-fold higher as compared to those recorded at this station during the onset and decline of the bloom (Table S1). The most important heterotrophic bacterial mortality factors HNF and virus-like particles revealed opposite seasonal trends. While HNF had higher on-/off-plateau ratios during early spring and late summer, virus-like particles revealed highest on-/off-plateau differences in summer (Fig. 6). These observations are coherent with estimates of grazing and viral lysis of heterotrophic bacteria. Grazing was identified as the dominant loss process of heterotrophic bacteria during late summer, and a similar scenario has been observed in early spring (Christaki et al. 2014). The intense bacterial grazing seemed to co-occur with the  $\text{NH}_4$  increase between the first and the second visit at Sta. M2 (Table 1, Figs. 4, S3). The methods assessing grazing are based on several assumptions. In the present study, we used three experimental and theoretical approaches to better frame the lower and upper limits of bacterial mortality attributed to grazing. The grazing estimations based on volume specific clearance rates (Fenchel 1982) or digestion times (Dolan and Šimek 1998) were determined in cultures, and even though they are not a direct measure of grazing, they provide representative patterns of the potential of HNF to ingest bacteria. At Sta. M2-1, the obtained values from the different approaches showed the highest variability, however, all values

had a consistent pattern in that grazing exceeded bacterial production (Sta. M2-1, CV 26%, Fig. 4). The mean ingestion rates obtained by all methods ( $1\text{--}3 \text{ bact. grazer}^{-1} \text{ h}^{-1}$ ) varied within a narrow range, being consistent at all stations and similar to previous observations (e.g., Christaki et al. 2008, 2014; Gast et al. 2018). This mean ingestion rate corresponds to the ingesting capacity of HNF since they were one order of magnitude more abundant than ciliates and *Gymnodinium* spp. despite the higher number of cells they ingest. Few studies have considered grazing by protists and viral mortality simultaneously, particularly in the Southern Ocean (Guixa-Boixereu et al. 2002; Malits et al. 2014; Vaqué et al. 2017). Prey consumption by grazers is expected to be more important than viral activity during early stages of phytoplankton blooms, which could explain the delay between bacterial production and the increase in abundances (Brum et al. 2016). Confirming this hypothesis, in our study, predation was the dominant cause of bacterial mortality during the onset and after the bloom, while viral lysis dominated during the decline of the bloom. During summer (decline of the bloom), virus induced mortality accounted on average  $72 \pm 72$  and  $27 \pm 19\%$  of bacterial production inside and outside the bloom, respectively. Lysogenic infected bacteria could be detected only in 7 out of 15 essays and ranged from 0 to 31% of infected bacteria on the plateau and from 0 to 4% in HNLC waters, without any significant difference between the two areas (Malits et al. 2014). In the Southern Ocean, a number of studies taking into account viral infection have found consistent high viral lytic production (e.g., Guixa-Boixereu et al. 2002; Evans and Brussaard 2012; Vaqué et al. 2017 and references therein) while lysogeny was varying greatly (e.g., Evans and Brussaard 2012; Vaqué et al. 2017).

Mixotrophy of unicellular eukaryotes is widespread (e.g., Zubkov and Tarran 2008; Stoecker et al. 2017), including in the Southern Ocean (Moorthi et al. 2009; Gast et al. 2018), but the possible triggering factors such as light or nutrient limitation remain largely unresolved. Even though pico- and nanophytoplankton were abundant at all stations during MOBYDICK, we observed insignificant uptake of FLB by nanophytoplankton. It was therefore impossible to evaluate accurately mixotrophic activity in the present study. In oligotrophic systems, pico- and nanophytoplankton can account for up to 95% of bacterivory (Zubkov and Tarran 2008). In this case, phagocytosis might be advantageous to photosynthetic organisms as it provides an increased access to limiting nutrients. This could suggest that the nutrient and light conditions were optimal for pico- and nanophytoplankton growth during late summer in the Kerguelen region, and phototrophic cells did not need to complement their diet by ingesting bacteria. However, in a study in the eastern Mediterranean (Christaki et al. 1999) it was found that 12% of nanophytoplankton ingested small spherical FLB called "minicells" (*E. coli* X-1488,  $0.65 \mu\text{m}$  in diameter), while only 6% ingested larger elongated

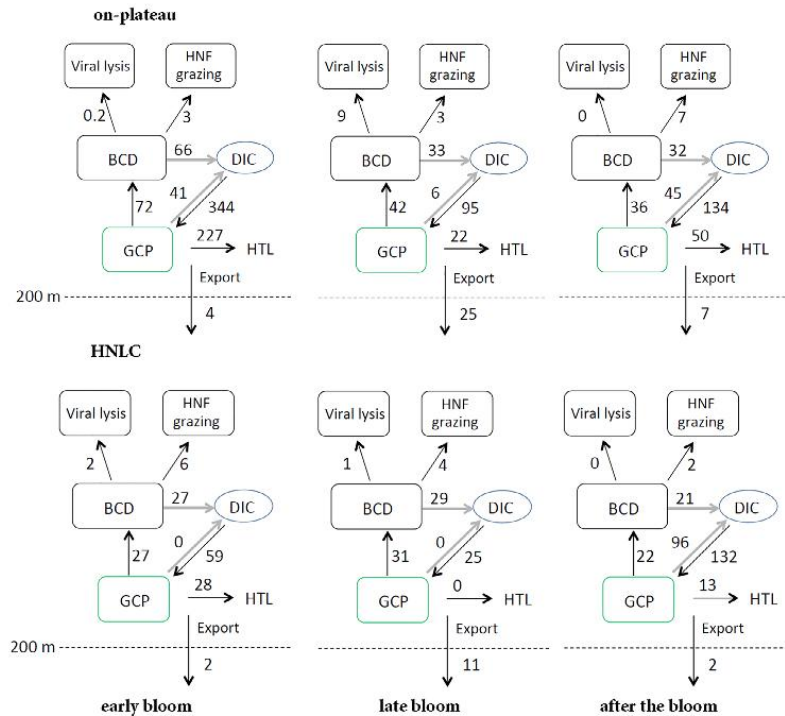


**Fig 7.** Mixed layer integrated carbon flow within the microbial food web. From left to right: during early (KEOPS2), late (KEOPS1), and after the diatom bloom (MOBYDICK). KEOPS2 and KEOPS1 on-plateau stations were redrawn from Christaki et al. 2014 (and references therein). Values from MOBYDICK refer to the mean of the three visits at M2. All fluxes are integrated in the mixed layer and units are  $\text{mmol C m}^{-2} \text{d}^{-1}$ . Arrows in gray indicate rates of bacterial respiration (BR) and dark community respiration (DCR). Bacterial carbon demand (BCD) defined as  $\text{BCD} = \text{bacterial production (BP)} + \text{bacterial respiration (BR)}$ , dissolved inorganic carbon (DIC), gross community production (GCP), biomass available for higher trophic levels (HTL), defined as  $\text{HTL} = \text{GCP} - (\text{DCR} + \text{BCD} + \text{export})$ . MOBYDICK export data were calculated based on the  $^{234}\text{Th}$  approach (Planchon pers. comm., the method is described in detail in Planchon et al. 2015). Late bloom (KEOPS1) data from Carlotti et al. (2008), Christaki et al. (2008), Lefèvre et al. (2008), Obernosterer et al. (2008), Savoye et al. (2008) and Malits et al. (2014). Early bloom data (KEOPS 2) from Planchon et al. (2015) and Carlotti et al. (2015), Christaki et al. (2014).

FLB (approx.  $0.8 \mu\text{m}$  ESD: equivalent spherical diameter) as the ones used here (Fig. S4). Thus, selection against the FLB is also a possibility and it most likely depends on the prevailing taxonomic groups. During MOBYDICK, nanophytoplankton were dominated at all stations by the prymnesiophyte *Phaeocystis antarctica* (> 70% based on pigment and microscopic data; Irion et al. 2020), which is known to be widespread in the Southern Ocean (Poulton et al. 2007; Gast et al. 2018). Contrary to many prymnesiophytes, mixotrophic activity has not been reported so far for *P. antarctica* (Gast et al. 2018). We therefore suggest one of the following possibilities, or a combination of them, to explain our results on mixotrophy: (i) a selection against the FLB used in this study; (ii) environmental conditions leading to low bacterivory by phototrophs; and (iii) the dominance of non-mixotrophic cells such as *P. antarctica*.

### Seasonal microbial dynamics and ecosystem functioning

Combining the observations made during late summer (MOBYDICK project) with those from previous projects carried out in early spring (KEOPS2) and summer (KEOPS1) has allowed us to draw a seasonal scenario for microbial food web fluxes in iron-fertilized and HNLC waters. In Kerguelen plateau waters, the three observation periods corresponded to the onset, decline, and post phytoplankton bloom phase (Fig. 7, Table 5). In early spring, the system is highly productive, with low carbon export and carbon export efficiency, resulting in a large amount of phytoplankton carbon potentially available for higher trophic levels. During the decline of the bloom, gross community production decreases by 3-fold as compared to early spring. The system is characterized by high carbon export and carbon export efficiency while phytoplankton carbon potentially available for higher trophic levels is 10-fold

**Table 5.** Seasonal ecosystem characteristics and microbial food web dynamics above the Fe-fertilized Kerguelen plateau and in HNLC waters. Productivity regime refers to gross community production (GCP), export efficiency is the ratio of carbon exported below 200 m to GCP, bacterial growth efficiency (BGE), heterotrophic nanoflagellates (HNF). Early spring and summer BGE and microbial food web fluxes from Lefèvre et al. 2008; Obermosterer et al. 2008, Christaki et al. 2014; Malits et al. 2014 (see also Fig. 7).

	Productivity regime	Export efficiency	Biomass available for higher trophic levels	Microbial food web fluxes (MFW)
Kerguelen plateau				
Early spring: Onset of the bloom	High (344)	Low (1%)	High (227)	Moderate fraction of C channeled through MFW (21%) Low BGE (9%) Transfer to HNF (50%) dominates over viral lysis (3%)
Summer: Decline of the bloom	Moderate (95)	High (26%)	Low (22)	High fraction of C channeled through MFW (44%) High BGE (18%) Viral lysis dominates (>80%) over HNF (34%)
Late summer: Post bloom	Moderate (134)	Low (4%)	Moderate (50)	Moderate fraction of C channeled through MFW (27%) High BGE (17%) Transfer to HNF dominates (76%) over viral lysis (7%)
HNLC waters				
Early spring	Moderate (59)	Low (3%)	Moderate (30)	High fraction of C channeled through MFW (46%) Low BGE (3%) Transfer to HNF (69%) dominates over viral lysis (20%)
Summer	Low (25)	High (44%)	Low (0)	High fraction of C channeled through MFW (100%) Low BGE (8%) Transfer to HNF (95%) dominates over viral lysis (10%)
Late summer	Moderate (132)	Low (2%)	Low (12)	Moderate fraction of C channeled through MFW (17%) Low BGE (8%) Transfer to HNF (97%) dominates over viral lysis (11%)

lower as compared to spring. During the post-bloom phase, gross community production is similar to that determined during the declining bloom phase. However, carbon export and export efficiency are again low, resulting in biomass available for higher trophic levels roughly 2-fold higher as compared to the bloom decline (Fig. 7, Table 5).

Heterotrophic bacteria contribute substantially to carbon processing during all stages. The fraction of total biomass available for higher trophic levels accounted for by bacteria is minor during early spring (< 1%) and it increases up to 14% during the declining and post-bloom phases (Fig. 7, Table 5). In addition, bacteria have a substantial contribution to microbial community respiration (42% and 85% of dark community respiration). The role of the microbial food web for carbon processing varies during the three stages (Table 5). In early spring, a moderate fraction of primary production is channeled through bacteria (21%) and due to a low bacterial growth efficiency (9%) this organic matter is mainly respired. During the decline of the bloom, heterotrophic bacteria process a higher fraction of primary production (44%) with a more efficient bacterial biomass production as compared to spring (bacterial growth efficiency of 18%, Table S1). The importance of viral lysis in carbon losses results in an inefficient transfer of bacterial biomass to HNF. During the post

bloom phase, organic carbon is processed with a bacterial growth efficiency (17%) similar to the declining bloom phase, and the transfer to HNF dominates over the loss by viral lysis. Taken together, these observations suggest an overall less efficient microbial food web during early spring and summer with respiration and viral lysis, respectively, representing important loss terms. During the post bloom period, roughly 30% of the gross community production are efficiently transferred to bacterial biomass and HNF, suggesting a good functioning of the microbial loop.

In HNLC waters, a seasonal pattern similar to that in iron-fertilized waters can be depicted, though with fluxes that are less variable among periods (Fig. 7, Table 5). In contrast to iron-fertilized waters, most of the gross community production is remineralized, leading to lower export and biomass available for higher trophic levels. Heterotrophic bacteria dominate microbial community respiration in early spring and summer, and their contribution decreases to 18% at the end of the season. Similarly, bacteria process large fractions of primary production in early spring (45%) and in summer (100%), and this fraction substantially decreases in late summer (17%). Despite the low bacterial growth efficiency (3–8%), the carbon processed by bacteria supports the microbial food web as grazing by HNF dominates over viral lysis. These

observations illustrate the quantitative importance of microbial food web processes across seasons and productivity regimes in the Southern Ocean.

What are the potential consequences of climate-driven environmental changes on the role of microbes in food webs of cold-water environments? The Southern Ocean is a major storage reservoir of heat, thus the warming of surface waters is expected to affect microbial communities (Morán et al. 2010; Kim and Ducklow 2016). Temperature and the supply of bioavailable dissolved organic matter were identified as key factors for bacterial biomass and growth in polar waters (Kirchman et al. 2009). Warming is expected to increase total and dissolved phytoplankton primary production (Morán et al. 2006; Boyd et al. 2016; Deppeler and Davidson 2017), which could result in a stronger coupling to bacteria through the utilization of dissolved organic matter (Vaqué et al. 2019). These observations suggest an increasingly important role of heterotrophic bacteria. In this context, our data provide two interesting observations. Firstly, the high contribution of bacteria to community respiration, and secondly the amount of carbon transferred in the form of bacterial biomass to HNF, which is in the same range as the carbon export ( $2\text{--}7\text{ mmol C m}^{-2}\text{ d}^{-1}$ ) in early spring and late summer. Thus, the predicted changes could lead to an increase in the amount of phytoplankton-derived organic matter consumed by bacteria. Temperature effects on the bacterial growth efficiency are uncertain (López-Urrutia and Morán 2007), leaving the question on the quantitative importance of organic carbon remineralization open (Sarmiento et al. 2010). The increased flow of carbon to bacterial biomass and HNF could support higher trophic levels, but in turn lead to a weakening of the Southern Ocean capacity to sequester organic carbon.

## References

- Binder, B. 1999. Reconsidering the relationship between virally induced bacterial mortality and frequency of infected cells. *Aquat. Microb. Ecol.* **18**: 207–215. doi:10.3354/ame018207
- Blain, S., et al. 2007. Effect of natural iron fertilization on carbon sequestration in the Southern Ocean. *Nature* **446**: 1070–1074. doi:10.1038/nature05700
- Boyd, P. W., and others. 2016. Physiological responses of a Southern Ocean diatom to complex future ocean conditions. *Nat. Clim. Change* **6**: 207–213. doi:10.1038/nclimate2811
- Brum, J. R., B. L. Hurwitz, O. Schofield, H. W. Ducklow, and M. B. Sullivan. 2016. Seasonal time bombs: dominant temperate viruses affect Southern Ocean microbial dynamics. *ISME J.* **10**: 437–449. doi:10.1038/ismej.2015.125
- Brussaard, C. P. D. 2004. Optimization of procedures for counting viruses by flow cytometry. *Appl. Environ. Microbiol.* **70**: 1506–1513. doi:10.1128/AEM.70.3.1506-1513.2004
- Carlotti, F., et al. 2015. Mesozooplankton structure and functioning during the onset of the Kerguelen phytoplankton bloom during the KEOPS2 survey. *Biogeosciences* **12**: 4543–4563. doi:10.5194/bg-12-4543-2015
- Carlotti, F., D., Thibault-Botha, A. Nowaczyk, and D. Lefèvre. 2008. Zooplankton community structure, biomass and role in carbon fluxes during the second half of a phytoplankton bloom in the eastern sector of the Kerguelen Shelf (January–February 2005). *Deep Sea Research Part II: Topical Studies in Oceanography* **55**: 720–733. doi:10.1016/j.dsr2.2007.12.010
- Cavagna, A. J., and others. 2015. Production regime and associated N cycling in the vicinity of Kerguelen Island, Southern Ocean. *Biogeosciences* **12**: 6515–6528. doi:10.5194/bg-12-6515-2015
- Christaki, U., F. Van Wambeke, and J. Dolan. 1999. Nanoflagellates (mixotrophs, heterotrophs and autotrophs) in the oligotrophic eastern Mediterranean: standing stocks, bacterivory and relationships with bacterial production. *Mar. Ecol. Prog. Ser.* **181**: 297–307. doi:10.3354/meps181297
- Christaki, U., I. Obernosterer, F. Van Wambeke, M. Veldhuis, N. Garcia, and P. Catala. 2008. Microbial food web structure in a naturally iron-fertilized area in the Southern Ocean (Kerguelen Plateau). *Deep Sea Res. Part II: Top. Stud. Oceanogr.* **55**: 706–719. doi:10.1016/j.dsr2.2007.12.009
- Christaki, U., C. Courties, R. Massana, P. Catala, P. Lebaron, J. M. Gasol, and M. V. Zubkov. 2011. Optimized routine flow cytometric enumeration of heterotrophic flagellates using SYBR Green I: FC analysis of HF. *Limnol. Oceanogr.: Methods* **9**: 329–339. doi:10.4319/lom.2011.9.329
- Christaki, U., and others. 2014. Microbial food web dynamics during spring phytoplankton blooms in the naturally iron-fertilized Kerguelen area (Southern Ocean). *Biogeosciences* **11**: 6739–6753. doi:10.5194/bg-11-6739-2014
- Deppeler, S. L., and A. T. Davidson. 2017. Southern Ocean phytoplankton in a changing climate. *Front. Mar. Sci.* **4**: 40. doi:10.3389/fmars.2017.00040
- Dolan, J. R., and K. Šimek. 1998. Ingestion and digestion of an autotrophic picoplankter, *Synechococcus*, by a heterotrophic nanoflagellate, *Bode salians*. *Limnol. Oceanogr.* **43**: 1740–1746. doi:10.4319/lo.1998.43.7.1740
- Evans, C., and C. P. D. Brussaard. 2012. Regional variation in lytic and lysogenic viral infection in the Southern Ocean and its contribution to biogeochemical cycling. *Appl. Environ. Microbiol.* **78**: 6741–6748. doi:10.1128/AEM.01388-12
- Fenchel, T. 1982. Ecology of heterotrophic microflagellates. IV: Quantitative occurrence and importance as bacterial consumers. *Mar. Ecol. Prog. Ser.* **9**: 35–42. doi:10.3354/meps009035
- Gast, R. J., S. A. Fay, and R. W. Sanders. 2018. Mixotrophic activity and diversity of antarctic marine protists in austral summer. *Front. Mar. Sci.* **5**: 13. doi:10.3389/fmars.2018.00013

- Gray, A. R., and others. 2018. Autonomous biogeochemical floats detect significant carbon dioxide outgassing in the high-latitude Southern Ocean. *Geophys. Res. Lett.* **45**: 9049–9057. doi:10.1029/2018GL078013
- Gruber, N., et al. 2009. Oceanic sources, sinks, and transport of atmospheric CO<sub>2</sub>: Oceanic sources, sinks and transport of CO<sub>2</sub>. *Global Biogeochem. Cycles* **23**. doi:10.1029/2008GB003349
- Guixa-Boixereu, N., D. Vaqué, J. M. Gasol, J. Sánchez-Cámara, and C. Pedrós-Alió. 2002. Viral distribution and activity in Antarctic waters. *Deep-Sea Res. Part II: Top. Stud. Oceanogr.* **49**: 827–845. doi:10.1016/S0967-0645(01)00126-6
- Irion, S., L. Jardillier, I. Sassenhagen, and U. Christaki. 2020. Marked spatio-temporal variations in small phytoplankton structure in contrasted waters of the Southern Ocean (Kerguelen area). *Limnol. Oceanogr.* **9999**: 1–18. doi:10.1002/lno.11555
- Kim, H., and H. W. Ducklow. 2016. A decadal (2002–2014) analysis for dynamics of heterotrophic bacteria in an Antarctic coastal ecosystem: Variability and physical and biogeochemical forcings. *Front. Mar. Sci.* **3**: 214. doi:10.3389/fmars.2016.00214
- Kirchman, D. L. 1993. Leucine incorporation as a measure of biomass production by heterotrophic bacteria, p. 509–512. *In* P. F. Kemp, B. F. Sherr, E. B. Sherr, and J. J. Cole [eds.], *Handbook of methods in aquatic microbial ecology*. Boca Raton, FL: Lewis Publishers.
- Kirchman, D. L., X. A. G. Morán, and H. Ducklow. 2009. Microbial growth in the polar oceans—role of temperature and potential impact of climate change. *Nat. Rev. Microbiol.* **7**: 451–459. doi:10.1038/nrmicro2115
- Lam, P. J., and J. K. B. Bishop. 2007. High biomass, low export regimes in the Southern Ocean. *Deep-Sea Res. Part II: Top. Stud. Oceanogr.* **54**: 601–638. doi:10.1016/j.dsr2.2007.01.013
- Lasbleiz, M., K. Leblanc, L. K. Armand, U. Christaki, C. Georges, I. Obernosterer, and B. Quéguiner. 2016. Composition of diatom communities and their contribution to plankton biomass in the naturally iron-fertilized region of Kerguelen in the Southern Ocean. *FEMS Microbiol. Ecol.* **92**: fiw171. doi:10.1093/femsec/fiw171
- Lê, S., J. Josse, and F. Husson. 2008. FactoMineR: An R package for multivariate analysis. *J. Stat. Softw.* **25**: 1–18.
- Lefèvre, D., C. Guigue, and I. Obernosterer. 2008. The metabolic balance at two contrasting sites in the Southern Ocean: The iron-fertilized Kerguelen area and HNLC waters. *Deep-Sea Res. Part II: Top. Stud. Oceanogr.* **55**: 766–776. doi:10.1016/j.dsr2.2007.12.006
- LeMoigne, F. A. C., et al. 2016. What causes the inverse relationship between primary production and export efficiency in the Southern Ocean? *Geophys. Res. Lett.* **43**: 4457–4466. doi:10.1002/2016GL068480
- López-Urrutia, Á., and X. A. G. Morán. 2007. Resource limitation of bacterial production distorts the temperature dependence of oceanic carbon cycling. *Ecology* **88**: 817–822.
- Maiti, K., M. A. Charette, K. O. Buesseler, and M. Kahru. 2013. An inverse relationship between production and export efficiency in the Southern Ocean. *Geophys. Res. Lett.* **40**: 1557–1561. doi:10.1002/grl.50219
- Malits, A., U. Christaki, I. Obernosterer, and M. G. Weinbauer. 2014. Enhanced viral production and virus-mediated mortality of bacterioplankton in a natural iron-fertilized bloom event above the Kerguelen Plateau. *Biogeosciences* **11**: 6841–6853. doi:10.5194/bg-11-6841-2014
- Moorthi, S., D. Caron, R. Gast, and R. Sanders. 2009. Mixotrophy: a widespread and important ecological strategy for planktonic and sea-ice nanoflagellates in the Ross Sea, Antarctica. *Aquat. Microb. Ecol.* **54**: 269–277. doi:10.3354/ame01276
- Morán, X. A. G., M. Sebastián, C. Pedrós-Alió, and M. Estrada. 2006. Response of Southern Ocean phytoplankton and bacterioplankton production to short-term experimental warming. *Limnol. Oceanogr.* **51**: 1791–1800. doi:10.4319/lo.2006.51.4.1791
- Morán, X. A. G., Á. López-Urrutia, A. Calvo-Díaz, and W. K. W. Li. 2010. Increasing importance of small phytoplankton in a warmer ocean. *Glob. Change Biol.* **16**: 1137–1144. doi:10.1111/j.1365-2486.2009.01960.x
- Mosseri, J., B. Quéguiner, L. Armand, and V. Cornet-Barthaux. 2008. Impact of iron on silicon utilization by diatoms in the Southern Ocean: A case study of Si/N cycle decoupling in a naturally iron-enriched area. *Deep-Sea Res. Part II: Top. Stud. Oceanogr.* **55**: 801–819. doi:10.1016/j.dsr2.2007.12.003
- Obernosterer, I., U. Christaki, D. Lefèvre, P. Catala, F. Van Wambeke, and P. Lebaron. 2008. Rapid bacterial mineralization of organic carbon produced during a phytoplankton bloom induced by natural iron fertilization in the Southern Ocean. *Deep-Sea Res. Part II: Top. Stud. Oceanogr.* **55**: 777–789. doi:10.1016/j.dsr2.2007.12.005
- Oksanen, J. and others. 2017. *vegan: Community Ecology Package*. R package version 2.3-0. 2015.
- Pauthenet, E., F. Roquet, G. Madec, C. Guinet, M. Hindell, C. R. McMahon, R. Harcourt, and D. Nerini. 2018. Seasonal Meandering of the Polar front upstream of the Kerguelen plateau. *Geophys. Res. Lett.* **45**: 9774–9781. doi:10.1029/2018GL079614
- Planchon, F., and others. 2015. Carbon export in the naturally iron-fertilized Kerguelen area of the Southern Ocean based on the <sup>234</sup>Th approach. *Biogeosciences* **12**: 3831–3848. doi:10.5194/bg-12-3831-2015
- Pollard, R., R. Sanders, M. Lucas, and P. Statham. 2007. The Crozet natural iron bloom and export experiment (CROZEX). *Deep-Sea Res. Part II: Top. Stud. Oceanogr.* **54**: 1905–1914. doi:10.1016/j.dsr2.2007.07.023
- Pollard, R. T., and others. 2009. Southern Ocean deep-water carbon export enhanced by natural iron fertilization. *Nature* **457**: 577–580. doi:10.1038/nature07716



- Poulton, A. J., C. Mark Moore, S. Seeyave, M. I. Lucas, S. Fielding, and P. Ward. 2007. Phytoplankton community composition around the Crozet Plateau, with emphasis on diatoms and Phaeocystis. *Deep-Sea Res. Part II: Top. Stud. Oceanogr.* **54**: 2085–2105. doi:10.1016/j.dsr2.2007.06.005
- Rembauville, M., S. Blain, L. Armand, B. Quéguiner, and I. Salter. 2015. Export fluxes in a naturally iron-fertilized area of the Southern Ocean—Part 2: Importance of diatom resting spores and faecal pellets for export. *Biogeosciences* **12**: 3171–3195. doi:10.5194/bg-12-3171-2015
- Sarmiento, H., J. M. Montoya, E. Vázquez-Domínguez, D. Vaqué, and J. M. Gasol. 2010. Warming effects on marine microbial food web processes: How far can we go when it comes to predictions? *Philos. Trans. R. Soc. B* **365**: 2137–2149. doi:10.1098/rstb.2010.0045
- Savoye, N., T. W. Trull, S. H. M. Jacquet, J. Navez, and F. Dehairs. 2008. <sup>234</sup>Th-based export fluxes during a natural iron fertilization experiment in the Southern Ocean (KEOPS). *Deep-Sea Res. Part II: Top. Stud. Oceanogr.* **55**: 841–855. doi:10.1016/j.dsr2.2007.12.036
- Seeyave, S., M. I. Lucas, C. M. Moore, and A. J. Poulton. 2007. Phytoplankton productivity and community structure in the vicinity of the Crozet Plateau during austral summer 2004/2005. *Deep-Sea Res. Part II: Top. Stud. Oceanogr.* **54**: 2020–2044. doi:10.1016/j.dsr2.2007.06.010
- Sherr, B. F., E. B. Sherr, and R. D. Fallon. 1987. Use of mono-dispersed, fluorescently labeled bacteria to estimate in situ protozoan bacterivory. *Appl. Environ. Microbiol.* **53**: 8.
- Stoecker, D. K., P. J. Hansen, D. A. Caron, and A. Mitra. 2017. Mixotrophy in the marine plankton. *Annu. Rev. Mar. Sci.* **9**: 311–335. doi:10.1146/annurev-marine-010816-060617
- Strzepek, R. F., M. T. Maldonado, J. L. Higgins, J. Hall, K. Safi, S. W. Wilhelm, and P. W. Boyd. 2005. Spinning the “Ferroous Wheel”: The importance of the microbial community in an iron budget during the FeCycle experiment: Microbial Iron Recycling. *Glob. Biogeochem. Cycles* **19**. doi:10.1029/2005GB002490
- Uitz, J., H. Claustre, B. Gentili, and D. Stramski. 2010. Phytoplankton class-specific primary production in the world’s oceans: Seasonal and interannual variability from satellite observations: Phytoplankton class-specific production. *Glob. Biogeochem. Cycles* **24**. doi:10.1029/2009GB003680
- Vaqué, D., et al. 2017. Viruses and protists induced-mortality of prokaryotes around the Antarctic Peninsula during the Austral summer. *Front. Microbiol.* **8**: 214. doi:10.3389/fmicb.2017.00241
- Vaqué, D., and others. 2019. Warming and CO<sub>2</sub> enhance arctic heterotrophic microbial activity. *Front. Microbiol.* **10**: 494. doi:10.3389/fmicb.2019.00494
- Weinbauer, M., C. Winter, and M. Höfle. 2002. Reconsidering transmission electron microscopy based estimates of viral infection of bacterioplankton using conversion factors derived from natural communities. *Aquat. Microb. Ecol.* **27**: 103–110. doi:10.3354/ame027103
- Zubkov, M. V., and G. A. Tarran. 2008. High bacterivory by the smallest phytoplankton in the North Atlantic Ocean. *Nature* **455**: 224–226. doi:10.1038/nature07236

#### Acknowledgments

We thank B. Quéguiner, the PI of the MOBYDICK project, for providing us the opportunity to participate to this cruise, the captain and crew of the R/V Marion Dufresne for their enthusiasm and support aboard during the MOBYDICK–THEMISTO cruise (<https://doi.org/10.17600/18000403>) and the chief scientist I. Obemosterer. This work was supported by the French oceanographic fleet (“Flotte océanographique française”), the French ANR (“Agence Nationale de la Recherche”, AAPG 2017 program, MOBYDICK Project number: ANR-17-CE01-0013), and the French Research program of INSU-CNRS LEFE/CYBER (“Les enveloppes fluides et l’environnement”—“Cycles biogéochimiques, environnement et ressources”). This work was also supported by ULCO (Université du Littoral) and CPER MARCO (<https://marco.univ-littoral.fr/>). We thank three anonymous reviewers and the editors for their comments which helped to improve this work.

#### Conflict of Interest

None declared.

Submitted 20 March 2020

Revised 03 June 2020

Accepted 16 July 2020

Associate editor: Leila Hamdan

## References

- Ackermann, M. (2013) Microbial individuality in the natural environment. *ISME J* **7**: 465–467.
- Adam, B., Klawonn, I., Svedén, J.B., Bergkvist, J., Nahar, N., Walve, J., et al. (2016) N<sub>2</sub>-fixation, ammonium release and N-transfer to the microbial and classical food web within a plankton community. *ISME J* **10**: 450–459.
- Adl, S.M., Simpson, A.G.B., Farmer, M.A., Andersen, R.A., Anderson, O.R., Barta, J.R., et al. (2005) The new higher level classification of eukaryotes with emphasis on the taxonomy of protists. *J Eukaryot Microbiol* **52**: 399–451.
- Alderkamp, A.-C., Kulk, G., Buma, A.G.J., Visser, R.J.W., Van Dijken, G.L., Mills, M.M., and Arrigo, K.R. (2012) The effect of iron limitation on the photophysiology of *Phaeocystis antarctica* (prymnesiophyceae) and *Fragilariopsis cylindrus* (bacillariophyceae) under dynamic irradiance. *J Phycol* **48**: 45–59.
- Alvain, S., Moulin, C., Dandonneau, Y., and Loisel, H. (2008) Seasonal distribution and succession of dominant phytoplankton groups in the global ocean: a satellite view. *Glob Biogeochem Cycles* **22**:
- Amato, A., Kooistra, W.H.C.F., Ghiron, J.H.L., Mann, D.G., Pröschold, T., and Montresor, M. (2007) Reproductive isolation among sympatric cryptic species in marine diatoms. *Protist* **158**: 193–207.
- Anderson, R., Charvet, S., and Hansen, P.J. (2018) Mixotrophy in chlorophytes and haptophytes—effect of irradiance, macronutrient, micronutrient and vitamin limitation. *Front Microbiol* **9**:
- Arandia-Gorostidi, N., Weber, P.K., Alonso-Sáez, L., Morán, X.A.G., and Mayali, X. (2017) Elevated temperature increases carbon and nitrogen fluxes between phytoplankton and heterotrophic bacteria through physical attachment. *ISME J* **11**: 641–650.
- Armand, L.K., Cornet-Barthaux, V., Mosseri, J., and Quéguiner, B. (2008) Late summer diatom biomass and community structure on and around the naturally iron-fertilised Kerguelen Plateau in the Southern Ocean. *Deep Sea Res Part II Top Stud Oceanogr* **55**: 653–676.
- Arrigo, K.R., Mills, M.M., Kropuenske, L.R., van Dijken, G.L., Alderkamp, A.-C., and Robinson, D.H. (2010) Photophysiology in two major Southern Ocean phytoplankton taxa: photosynthesis and growth of *Phaeocystis antarctica* and *Fragilariopsis cylindrus* under different irradiance levels. *Integr Comp Biol* **50**: 950–966.
- Assmy, P., Henjes, J., Klaas, C., and Smetacek, V. (2007) Mechanisms determining species dominance in a phytoplankton bloom induced by the iron fertilization experiment EisenEx in the Southern Ocean. *Deep Sea Res Part Oceanogr Res Pap* **54**: 340–362.
- Atkinson, A., Siegel, V., Pakhomov, E., and Rothery, P. (2004) Long-term decline in krill stock and increase in salps within the Southern Ocean. *Nature* **432**: 100–103.
- Aumont, O. and Bopp, L. (2006) Globalizing results from ocean *in situ* iron fertilization studies. *Glob Biogeochem Cycles* **20**:
- de Baar, H.J.W., Boyd, P.W., Coale, K.H., Landry, M.R., Tsuda, A., Assmy, P., et al. (2005) Synthesis of iron fertilization experiments: from the iron age in the age of enlightenment. *J Geophys Res Oceans* **110**:
- Bachy, C., Dolan, J.R., López-García, P., Deschamps, P., and Moreira, D. (2013) Accuracy of protist diversity assessments: morphology compared with cloning and direct pyrosequencing of 18S rRNA genes and ITS regions using the conspicuous tintinnid ciliates as a case study. *ISME J* **7**: 244–255.

- Bar-On, Y.M., Phillips, R., and Milo, R. (2018) The biomass distribution on Earth. *Proc Natl Acad Sci* **115**: 6506.
- de-Bashan, L.E., Mayali, X., Bebout, B.M., Weber, P.K., Detweiler, A.M., Hernandez, J.-P., et al. (2016) Establishment of stable synthetic mutualism without co-evolution between microalgae and bacteria demonstrated by mutual transfer of metabolites (NanoSIMS isotopic imaging) and persistent physical association (Fluorescent in situ hybridization). *Algal Res* **15**: 179–186.
- Behrenfeld, M.J. and Milligan, A.J. (2013) Photophysiological expressions of iron stress in phytoplankton. *Annu Rev Mar Sci* **5**: 217–246.
- Behrens, S., Lösekann, T., Pett-Ridge, J., Weber, P.K., Ng, W.-O., Stevenson, B.S., et al. (2008) Linking microbial phylogeny to metabolic activity at the single-cell level by using enhanced element labeling-catalyzed reporter deposition fluorescence *in situ* hybridization (EL-FISH) and NanoSIMS. *Appl Environ Microbiol* **74**: 3143–3150.
- Bekker, A., Holland, H.D., Wang, P.-L., Rumble, D., Stein, H.J., Hannah, J.L., et al. (2004) Dating the rise of atmospheric oxygen. *Nature* **427**: 117–120.
- Bender, S.J., Moran, D.M., McIlvin, M.R., Zheng, H., McCrow, J.P., Badger, J., et al. (2018) Colony formation in *Phaeocystis antarctica*: connecting molecular mechanisms with iron biogeochemistry. *Biogeosciences* **15**: 4923–4942.
- Berthelot, H., Duhamel, S., L'Helguen, S., Maguer, J.-F., Wang, S., Cetinić, I., and Cassar, N. (2019) NanoSIMS single cell analyses reveal the contrasting nitrogen sources for small phytoplankton. *ISME J* **13**: 651–662.
- Biard, T., Bigeard, E., Audic, S., Poulain, J., Gutierrez-Rodriguez, A., Pesant, S., et al. (2017) Biogeography and diversity of Collodaria (Radiolaria) in the global ocean. *ISME J* **11**: 1331–1344.
- Blain, S., Quéguiner, B., Armand, L., Belviso, S., Bombled, B., Bopp, L., et al. (2007) Effect of natural iron fertilization on carbon sequestration in the Southern Ocean. *Nature* **446**: 1070–1074.
- Bonnet, S., Berthelot, H., Turk-Kubo, K., Cornet-Barthaux, V., Fawcett, S., Berman-Frank, I., et al. (2016) Diazotroph derived nitrogen supports diatom growth in the South West Pacific: a quantitative study using nanoSIMS. *Limnol Oceanogr* **61**: 1549–1562.
- Bopp, L., Aumont, O., Cadule, P., Alvain, S., and Gehlen, M. (2005) Response of diatoms distribution to global warming and potential implications: a global model study. *Geophys Res Lett* **32**:
- Bopp, L., Monfray, P., Aumont, O., Dufresne, J.-L., Le Treut, H., Madec, G., et al. (2001) Potential impact of climate change on marine export production. *Glob Biogeochem Cycles* **15**: 81–99.
- Bopp, L., Resplandy, L., Orr, J.C., Doney, S.C., Dunne, J.P., Gehlen, M., et al. (2013) Multiple stressors of ocean ecosystems in the 21st century: projections with CMIP5 models. *Biogeosciences* **10**: 6225–6245.
- Bower, S.M., Carnegie, R.B., Goh, B., Jones, S.R., Lowe, G.J., and Mak, M.W. (2004) Preferential PCR amplification of parasitic protistan small subunit rDNA from metazoan tissues. *J Eukaryot Microbiol* **51**: 325–332.
- Boyd, P.W. (2002) Environmental factors controlling phytoplankton processes in the Southern Ocean. *J Phycol* **38**: 844–861.
- Boyd, P.W., Crossley, A.C., DiTullio, G.R., Griffiths, F.B., Hutchins, D.A., Queguiner, B., et al. (2001) Control of phytoplankton growth by iron supply and irradiance in the subantarctic

- Southern Ocean: experimental results from the SAZ Project. *J Geophys Res Oceans* **106**: 31573–31583.
- Boyd, P.W., Jickells, T., Law, C.S., Blain, S., Boyle, E.A., Buesseler, K.O., et al. (2007) Mesoscale iron enrichment experiments 1993–2005: synthesis and future directions. *Science* **315**: 612–617.
- Boyd, P.W., Strzepek, R., Fu, F., and Hutchins, D.A. (2010) Environmental control of open-ocean phytoplankton groups: Now and in the future. *Limnol Oceanogr* **55**: 1353–1376.
- Boyd, P.W., Watson, A.J., Law, C.S., Abraham, E.R., Trull, T., Murdoch, R., et al. (2000) A mesoscale phytoplankton bloom in the polar Southern Ocean stimulated by iron fertilization. *Nature* **407**: 695–702.
- Breitwieser, F.P., Lu, J., and Salzberg, S.L. (2019) A review of methods and databases for metagenomic classification and assembly. *Brief Bioinform* **20**: 1125–1136.
- Brown, B.L., Watson, M., Minot, S.S., Rivera, M.C., and Franklin, R.B. (2017) MinION™ nanopore sequencing of environmental metagenomes: a synthetic approach. *GigaScience* **6**:
- Brun, P., Vogt, M., Payne, M.R., Gruber, N., O’Brien, C.J., Buitenhuis, E.T., et al. (2015) Ecological niches of open ocean phytoplankton taxa. *Limnol Oceanogr* **60**: 1020–1038.
- Brussaard, C.P.D., Timmermans, K.R., Uitz, J., and Veldhuis, M.J.W. (2008) Virioplankton dynamics and virally induced phytoplankton lysis versus microzooplankton grazing southeast of the Kerguelen (Southern Ocean). *Deep Sea Res Part II Top Stud Oceanogr* **55**: 752–765.
- Buesseler, K.O., Andrews, J.E., Pike, S.M., Charette, M.A., Goldson, L.E., Brzezinski, M.A., and Lance, V.P. (2005) Particle export during the Southern Ocean Iron Experiment (SOFEX). *Limnol Oceanogr* **50**: 311–327.
- Buesseler, K.O. and Boyd, P.W. (2003) Will ocean fertilization work? *Science* **300**: 67–68.
- Cabanes, D.J.E., Norman, L., Santos-Echeandía, J., Iversen, M.H., Trimborn, S., Laglera, L.M., and Hassler, C.S. (2017) First evaluation of the role of salp fecal pellets on iron biogeochemistry. *Front Mar Sci* **3**:
- Callahan, B.J., McMurdie, P.J., and Holmes, S.P. (2017) Exact sequence variants should replace operational taxonomic units in marker-gene data analysis. *ISME J* **11**: 2639–2643.
- Callahan, B.J., McMurdie, P.J., Rosen, M.J., Han, A.W., Johnson, A.J.A., and Holmes, S.P. (2016) DADA2: High-resolution sample inference from Illumina amplicon data. *Nat Methods* **13**: 581–583.
- Calvo-Díaz, A., Díaz-Pérez, L., Suárez, L.Á., Morán, X.A.G., Teira, E., and Marañón, E. (2011) Decrease in the autotrophic-to-heterotrophic biomass ratio of picoplankton in oligotrophic marine waters due to bottle enclosure. *Appl Environ Microbiol* **77**: 5739–5746.
- Carlotti, F., Jouandet, M.-P., Nowaczyk, A., Harmelin-Vivien, M., Lefèvre, D., Guillou, G., et al. (2015) Mesozooplankton structure and functioning during the onset of the Kerguelen phytoplankton bloom during the KEOPS2 survey. *Biogeosciences Discuss* **12**: 2381–2427.
- Caron, D.A., Alexander, H., Allen, A.E., Archibald, J.M., Armbrust, E.V., Bachy, C., et al. (2017) Probing the evolution, ecology and physiology of marine protists using transcriptomics. *Nat Rev Microbiol* **15**: 6–20.
- Caron, D.A., Countway, P.D., Savai, P., Gast, R.J., Schnetzer, A., Moorthi, S.D., et al. (2009) Defining DNA-based operational taxonomic units for microbial-eukaryote ecology. *Appl Environ Microbiol* **75**: 5797–5808.

- Caron, D.A., Dennett, M.R., Lonsdale, D.J., Moran, D.M., and Shalapyonok, L. (2000) Microzooplankton herbivory in the Ross Sea, Antarctica. *Deep Sea Res Part II Top Stud Oceanogr* **47**: 3249–3272.
- Caruso, V., Song, X., Asquith, M., and Karstens, L. (2019) Performance of microbiome sequence inference methods in environments with varying biomass. *mSystems* **4**:
- Cassar, N., DiFiore, P.J., Barnett, B.A., Bender, M.L., Bowie, A.R., Tilbrook, B., et al. (2010) The influence of iron and light on net community production in the Subantarctic and Polar Frontal Zones. *Biogeosciences Discuss* **7**: 5649–5674.
- Cassar, N., Wright, S.W., Thomson, P.G., Trull, T.W., Westwood, K.J., Salas, M. de, et al. (2015) The relation of mixed-layer net community production to phytoplankton community composition in the Southern Ocean. *Glob Biogeochem Cycles* **29**: 446–462.
- Cavan, E.L., Moigne, F.A.C.L., Poulton, A.J., Tarling, G.A., Ward, P., Daniels, C.J., et al. (2015) Attenuation of particulate organic carbon flux in the Scotia Sea, Southern Ocean, is controlled by zooplankton fecal pellets. *Geophys Res Lett* **42**: 821–830.
- Chang, F.H., Marquis, E.C., Chang, C.W., Gong, G.C., and Hsieh, C.H. (2013) Scaling of growth rate and mortality with size and its consequence on size spectra of natural microphytoplankton assemblages in the East China Sea. *Biogeosciences* **10**: 5267–5280.
- Cheng, R., Zhang, F., Li, M., Wo, X., Su, Y.-W., and Wang, W. (2019) Influence of fixation and permeabilization on the mass density of single cells: a surface plasmon resonance imaging study. *Front Chem* **7**:
- Chisholm, S.W. (1992) Phytoplankton Size. In *Primary Productivity and Biogeochemical Cycles in the Sea*. Falkowski, P.G., Woodhead, A.D., and Vivirito, K. (eds). Boston, MA: Springer US, pp. 213–237.
- Chisholm, S.W. (2000) Stirring times in the Southern Ocean. *Nature* **407**: 685–687.
- Christaki, U., Georges, C., Genitsaris, S., and Monchy, S. (2015) Microzooplankton community associated with phytoplankton blooms in the naturally iron-fertilized Kerguelen area (Southern Ocean). *FEMS Microbiol Ecol* **91**:
- Christaki, U., Guenegues, A., Liu, Y., Blain, S., Catala, P., Colombet, J., et al. (2020) Seasonal microbial food web dynamics in contrasting Southern Ocean productivity regimes. *Limnol Oceanogr* **Early view**:
- Christaki, U., Lefèvre, D., Georges, C., Colombet, J., Catala, P., Courties, C., et al. (2014) Microbial food web dynamics during spring phytoplankton blooms in the naturally iron-fertilized Kerguelen area (Southern Ocean). *Biogeosciences* **11**: 6739–6753.
- Christaki, U., Skouroliakou, D.-I., Delegrange, A., Irion, S., Courcot, L., Jardillier, L., and Sassenhagen, I. (submitted) Microzooplankton diversity and role in carbon cycle in contrasting Southern Ocean productivity regimes. *J Mar Syst* **submitted**:
- Clarke, L.J. and Deagle, B.E. (2018) Eukaryote plankton assemblages in the southern Kerguelen axis region: ecological drivers differ between size fractions. *Deep Sea Res Part II Top Stud Oceanogr*.
- Closset, I., Lasbleiz, M., Leblanc, K., Quéguiner, B., Cavagna, A.-J., Elskens, M., et al. (2014) Seasonal evolution of net and regenerated silica production around a natural Fe-fertilized area in the Southern Ocean estimated with Si isotopic approaches. *Biogeosciences* **11**: 5827–5846.
- Coale, K.H., Johnson, K.S., Chavez, F.P., Buesseler, K.O., Barber, R.T., Brzezinski, M.A., et al. (2004) Southern Ocean Iron Enrichment Experiment: carbon cycling in high- and low-Si Waters. *Science* **304**: 408–414.

- Coupel, P., Matsuoka, A., Ruiz-Pino, D., Gosselin, M., Marie, D., Tremblay, J.-É., and Babin, M. (2015) Pigment signatures of phytoplankton communities in the Beaufort Sea. *Biogeosciences* **12**: 991–1006.
- DeLong, E.F., Wickham, G.S., and Pace, N.R. (1989) Phylogenetic stains: ribosomal RNA-based probes for the identification of single cells. *Science* **243**: 1360–1363.
- Delwiche, C.F. (1999) Tracing the thread of plastid diversity through the tapestry of life. *Am Nat* **154**: S164–S177.
- Demory, D., Baudoux, A.-C., Monier, A., Simon, N., Six, C., Ge, P., et al. (2019) Picoeukaryotes of the *Micromonas* genus: sentinels of a warming ocean. *ISME J* **13**: 132–146.
- Deppeler, S.L. and Davidson, A.T. (2017) Southern Ocean phytoplankton in a changing climate. *Front Mar Sci* **4**:
- Detmer, A.E. and Bathmann, U.V. (1997) Distribution patterns of autotrophic pico- and nanoplankton and their relative contribution to algal biomass during spring in the Atlantic sector of the Southern Ocean. *Deep Sea Res Part II Top Stud Oceanogr* **44**: 299–320.
- Díez, B., Massana, R., Estrada, M., and Pedrós-Alió, C. (2004) Distribution of eukaryotic picoplankton assemblages across hydrographic fronts in the Southern Ocean, studied by denaturing gradient gel electrophoresis. *Limnol Oceanogr* **49**: 1022–1034.
- DiTullio, G.R., Grebmeier, J.M., Arrigo, K.R., Lizotte, M.P., Robinson, D.H., Leventer, A., et al. (2000) Rapid and early export of *Phaeocystis antarctica* blooms in the Ross Sea, Antarctica. *Nature* **404**: 595–598.
- Ducklow, H.W., Fraser, W.R., Meredith, M.P., Stammerjohn, S., Doney, S.C., Martinson, D.G., et al. (2013) West Antarctic peninsula: an ice-dependent coastal marine ecosystem in transition. *Oceanography* **26**: 190–203.
- Dutkiewicz, S., Hickman, A.E., Jahn, O., Gregg, W.W., Mouw, C.B., and Follows, M.J. (2015) Capturing optically important constituents and properties in a marine biogeochemical and ecosystem model. *Biogeosciences* **12**: 4447–4481.
- Ebersbach, F., Assmy, P., Martin, P., Schulz, I., Wolzenburg, S., and Nöthig, E.-M. (2014) Particle flux characterisation and sedimentation patterns of protistan plankton during the iron fertilisation experiment LOHAFEX in the Southern Ocean. *Deep Sea Res Part Oceanogr Res Pap* **89**: 94–103.
- Ebersbach, F. and Trull, T.W. (2008) Sinking particle properties from polyacrylamide gels during the Kerguelen Ocean and Plateau compared Study (KEOPS): zooplankton control of carbon export in an area of persistent natural iron inputs in the Southern Ocean. *Limnol Oceanogr* **53**: 212–224.
- Edwardsen, B., Eikrem, W., Green, J.C., Andersen, R.A., Staay, S.Y.M. der, and Medlin, L.K. (2000) Phylogenetic reconstructions of the Haptophyta inferred from 18S ribosomal DNA sequences and available morphological data. *Phycologia* **39**: 19–35.
- Elbrecht, V. and Leese, F. (2015) Can DNA-based ecosystem assessments quantify species abundance? Testing primer bias and biomass—sequence relationships with an innovative metabarcoding protocol. *PLOS ONE* **10**: e0130324.
- Falkowski, P.G. (2004) The Evolution of Modern Eukaryotic Phytoplankton. *Science* **305**: 354–360.
- Falkowski, P.G., Barber, R.T., and Smetacek, V. (1998) Biogeochemical controls and feedbacks on Ocean primary production. *Science* **281**: 200–206.
- Falkowski, P.G., Laws, E.A., Barber, R.T., and Murray, J.W. (2003) Phytoplankton and their role in primary, new, and export production. In *Ocean Biogeochemistry*. Fasham, M.J.R. (ed). Berlin, Heidelberg: Springer Berlin Heidelberg, pp. 99–121.

- Fiala, M., Kopczynska, E.E., Jeandel, C., Oriol, L., and Vétion, G. (1998) Seasonal and interannual variability of size-fractionated phytoplankton biomass and community structure at station Kerfix, off the Kerguelen Islands, Antarctica. *J Plankton Res* **20**: 1341–1356.
- Field, C.B., Behrenfeld, M.J., Randerson, J.T., and Falkowski, P. (1998) Primary production of the biosphere: integrating terrestrial and oceanic components. *Science* **281**: 237–240.
- Finkel, Z.V. (2001) Light absorption and size scaling of light-limited metabolism in marine diatoms. *Limnol Oceanogr* **46**: 86–94.
- Finkel, Z.V., Beardall, J., Flynn, K.J., Quigg, A., Rees, T.A.V., and Raven, J.A. (2010) Phytoplankton in a changing world: cell size and elemental stoichiometry. *J Plankton Res* **32**: 119–137.
- Fitzwater, S.E., Knauer, G.A., and Martin, J.H. (1982) Metal contamination and its effect on primary production measurements. *Limnol Oceanogr* **27**: 544–551.
- Flegontova, O., Flegontov, P., Malviya, S., Audic, S., Wincker, P., de Vargas, C., et al. (2016) Extreme diversity of diplomonad eukaryotes in the Ocean. *Curr Biol* **26**: 3060–3065.
- Freeman, N.M., Lovenduski, N.S., Munro, D.R., Krumhardt, K.M., Lindsay, K., Long, M.C., and Maclennan, M. (2018) The variable and changing Southern Ocean silicate front: insights from the CESM Large Ensemble. *Glob Biogeochem Cycles* **32**: 752–768.
- Frölicher, T.L., Sarmiento, J.L., Paynter, D.J., Dunne, J.P., Krasting, J.P., and Winton, M. (2014) Dominance of the Southern Ocean in anthropogenic carbon and heat uptake in CMIP5 models. *J Clim* **28**: 862–886.
- Froneman, P.W., Pakhomov, E.A., and Balarin, M.G. (2004) Size-fractionated phytoplankton biomass, production and biogenic carbon flux in the eastern Atlantic sector of the Southern Ocean in late austral summer 1997–1998. *Deep Sea Res Part II Top Stud Oceanogr* **51**: 2715–2729.
- Geider, R.J. (1987) Light and temperature dependence of the carbon to chlorophyll a ratio in microalgae and cyanobacteria: implications for physiology and growth of phytoplankton. *New Phytol* **106**: 1–34.
- Geisen, S., Vaulot, D., Mahé, F., Lara, E., Vargas, C. de, and Bass, D. (2019) A user guide to environmental protistology: primers, metabarcoding, sequencing, and analyses. *bioRxiv* 850610.
- Genitsaris, S., Monchy, S., Denonfoux, J., Ferreira, S., Kormas, K.A., Sime-Ngando, T., et al. (2016) Marine microbial community structure assessed from combined metagenomic analysis and ribosomal amplicon deep-sequencing. *Mar Biol Res* **12**: 30–42.
- Gentil, J., Hempel, F., Moog, D., Zauner, S., and Maier, U.G. (2017) Review: origin of complex algae by secondary endosymbiosis: a journey through time. *Protoplasma* **254**: 1835–1843.
- Georges, C., Monchy, S., Genitsaris, S., and Christaki, U. (2014) Protist community composition during early phytoplankton blooms in the naturally iron-fertilized Kerguelen area (Southern Ocean). *Biogeosciences* **11**: 5847–5863.
- Gieskes, W.W.C., Kraay, G.W., and Baars, M.A. (1979) Current <sup>14</sup>C methods for measuring primary production: gross underestimates in oceanic waters. *Neth J Sea Res* **13**: 58–78.
- Gjøsæter, J., Lekve, K., Stenseth, N.C., Leinaas, H.P., Christie, H., Dahl, E., et al. (2000) A long-term perspective on the *Chrysochromulina* bloom on the Norwegian Skagerrak coast 1988: a catastrophe or an innocent incident? *Mar Ecol Prog Ser* **207**: 201–218.
- Glibert, P.M. (2016) Margalef revisited: a new phytoplankton mandala incorporating twelve dimensions, including nutritional physiology. *Harmful Algae* **55**: 25–30.

- Gong, W. and Marchetti, A. (2019) Estimation of 18S gene copy number in marine eukaryotic plankton using a next-generation sequencing approach. *Front Mar Sci* **6**.
- González, H.E. (1992) Distribution and abundance of minipellets around the Antarctic peninsula. Implications for protistan feeding behaviour. *Mar Ecol Prog Ser* **90**: 223–236.
- Grande, K.D., Williams, P.J.LeB., Marra, J., Purdie, D.A., Heinemann, K., Eppley, R.W., and Bender, M.L. (1989) Primary production in the North Pacific gyre: a comparison of rates determined by the  $^{14}\text{C}$ ,  $\text{O}_2$  concentration and  $^{18}\text{O}$  methods. *Deep Sea Res Part Oceanogr Res Pap* **36**: 1621–1634.
- Granéli, E., Edvardsen, B., Roelke, D.L., and Hagström, J.A. (2012) The ecophysiology and bloom dynamics of *Prymnesium* spp. *Harmful Algae* **14**: 260–270.
- Grob, C., Jardillier, L., Hartmann, M., Ostrowski, M., Zubkov, M.V., and Scanlan, D.J. (2015) Cell-specific  $\text{CO}_2$  fixation rates of two distinct groups of plastidic protists in the Atlantic Ocean remain unchanged after nutrient addition. *Environ Microbiol Rep* **7**: 211–218.
- Grossart, H.-P., Massana, R., McMahon, K.D., and Walsh, D.A. (2020) Linking metagenomics to aquatic microbial ecology and biogeochemical cycles. *Limnol Oceanogr* **65**: S2–S20.
- Guidi, L., Stemann, L., Jackson, G.A., Ibanez, F., Claustre, H., Legendre, L., et al. (2009) Effects of phytoplankton community on production, size, and export of large aggregates: a world-ocean analysis. *Limnol Oceanogr* **54**: 1951–1963.
- Guillou, L., Bachar, D., Audic, S., Bass, D., Berney, C., Bittner, L., et al. (2013) The Protist Ribosomal Reference database (PR2): a catalog of unicellular eukaryote Small Sub-Unit rRNA sequences with curated taxonomy. *Nucleic Acids Res* **41**: D597–D604.
- Guillou, L., Eikrem, W., Chrétiennot-Dinet, M.-J., Le Gall, F., Massana, R., Romari, K., et al. (2004) Diversity of picoplanktonic prasinophytes assessed by direct nuclear SSU rDNA sequencing of environmental samples and novel isolates retrieved from oceanic and coastal marine ecosystems. *Protist* **155**: 193–214.
- Gutiérrez-Rodríguez, A., Latasa, M., Scharek, R., Massana, R., Vila, G., and Gasol, J.M. (2011) Growth and grazing rate dynamics of major phytoplankton groups in an oligotrophic coastal site. *Estuar Coast Shelf Sci* **95**: 77–87.
- Gutierrez-Zamora, M.-L. and Manefield, M. (2010) An appraisal of methods for linking environmental processes to specific microbial taxa. *Rev Environ Sci Biotechnol* **9**: 153–185.
- Harrison, P.J., Thompson, P.A., and Calderwood, G.S. (1990) Effects of nutrient and light limitation on the biochemical composition of phytoplankton. *J Appl Phycol* **2**: 45–56.
- Hart, T.J. (1934) On the phytoplankton of the South-west Atlantic and the Bellingshausen Sea, 1929-1931.
- Hartmann, M., Gomez-Pereira, P., Grob, C., Ostrowski, M., Scanlan, D.J., and Zubkov, M.V. (2014) Efficient  $\text{CO}_2$  fixation by surface *Prochlorococcus* in the Atlantic Ocean. *ISME J* **8**: 2280.
- Harvey, M.J., Law, C.S., Smith, M.J., Hall, J.A., Abraham, E.R., Stevens, C.L., et al. (2011) The SOLAS air–sea gas exchange experiment (SAGE) 2004. *Deep Sea Res Part II Top Stud Oceanogr* **58**: 753–763.
- Henschke, N., Blain, S., Chérel, Y., Cotte, C., Espinasse, B., Hunt, B.P.V., and Pakhomov, E. (submitted) Distribution, abundance and population demographics of *Salpa thompsoni* on the Kerguelen Plateau. *J Mar Syst*.
- Henson, S.A., Sanders, R., and Madsen, E. (2012) Global patterns in efficiency of particulate organic carbon export and transfer to the deep ocean. *Glob Biogeochem Cycles* **26**.



- Hilst, C.M. van and Jr, W.O.S. (2002) Photosynthesis/irradiance relationships in the Ross Sea, Antarctica, and their control by phytoplankton assemblage composition and environmental factors. *Mar Ecol Prog Ser* **226**: 1–12.
- Hoffmann, L.J., Peeken, I., and Lochte, K. (2008) Iron, silicate, and light co-limitation of three Southern Ocean diatom species. *Polar Biol* **31**: 1067–1080.
- Huete-Ortega, M., Cermeño, P., Calvo-Díaz, A., and Marañón, E. (2012) Isometric size-scaling of metabolic rate and the size abundance distribution of phytoplankton. *Proc R Soc B Biol Sci* **279**: 1815–1823.
- Hunt, B.P.V., Pakhomov, E.A., and Williams, V. (2011) Comparative analysis of the 1980s and 2004 microzooplankton composition and distribution in the vicinity of Kerguelen and Heard Islands: seasonal cycles and oceanographic forcing of long-term change. In *The Kerguelen Plateau: Marine Ecosystems and Fisheries*. pp. 79–92.
- Iida, T. and Odate, T. (2014) Seasonal variability of phytoplankton biomass and composition in the major water masses of the Indian Ocean sector of the Southern Ocean. *Polar Sci* **8**: 283–297.
- Inchausti, P., Guinet, C., Koudil, M., Durbec, J.-P., Barbraud, C., Weimerskirch, H., et al. (2003) Inter-annual variability in the breeding performance of seabirds in relation to oceanographic anomalies that affect the Crozet and the Kerguelen sectors of the Southern Ocean. *J Avian Biol* **34**: 170–176.
- Irigoien, X., Flynn, K.J., and Harris, R.P. (2005) Phytoplankton blooms: a ‘loophole’ in microzooplankton grazing impact? *J Plankton Res* **27**: 313–321.
- Ito, T. and Follows, M.J. (2005) Preformed phosphate, soft tissue pump and atmospheric CO<sub>2</sub>. *J Mar Res* **63**: 813–839.
- Iversen, M.H., Pakhomov, E.A., Hunt, B.P.V., van der Jagt, H., Wolf-Gladrow, D., and Klaas, C. (2017) Sinkers or floaters? Contribution from salp pellets to the export flux during a large bloom event in the Southern Ocean. *Deep Sea Res Part II Top Stud Oceanogr* **138**: 116–125.
- Jakobsen, H.H. and Markager, S. (2016) Carbon-to-chlorophyll ratio for phytoplankton in temperate coastal waters: seasonal patterns and relationship to nutrients. *Limnol Oceanogr* **61**: 1853–1868.
- Jardillier, L., Zubkov, M.V., Pearman, J., and Scanlan, D.J. (2010) Significant CO<sub>2</sub> fixation by small prymnesiophytes in the subtropical and tropical northeast Atlantic Ocean. *ISME J* **4**: 1180–1192.
- Jiao, N., Luo, T., Zhang, R., Yan, W., Lin, Y., Johnson, Z.I., et al. (2014) Presence of *Prochlorococcus* in the aphotic waters of the western Pacific Ocean. *Biogeosciences* **11**: 2391–2400.
- Joli, N., Monier, A., Logares, R., and Lovejoy, C. (2017) Seasonal patterns in Arctic prasinophytes and inferred ecology of *Bathycoccus* unveiled in an Arctic winter metagenome. *ISME J* **11**: 1372–1385.
- Jouenne, F., Eikrem, W., Le Gall, F., Marie, D., Johnsen, G., and Vaultot, D. (2011) *Prasinoderma singularis* sp. nov. (Prasinophyceae, Chlorophyta), a solitary coccoid prasinophyte from the South-East Pacific Ocean. *Protist* **162**: 70–84.
- Katz, M.E., Fennel, K., and FALKOWSKI, P.G. (2007) Geochemical and biological consequences of phytoplankton evolution. In *Evolution of primary producers in the sea*. Elsevier, pp. 405–430.

- Kawachi, M., Inouye, I., Maeda, O., and Chihara, M. (1991) The haptonema as a food-capturing device: observations on *Chrysochromulina hirta* (Prymnesiophyceae). *Phycologia* **30**: 563–573.
- Kleiber, M. (1947) Body size and metabolic rate. *Physiol Rev* **27**: 511–541.
- Koch, F., Beszteri, S., Harms, L., and Trimborn, S. (2019) The impacts of iron limitation and ocean acidification on the cellular stoichiometry, photophysiology, and transcriptome of *Phaeocystis antarctica*. *Limnol Oceanogr* **64**: 357–375.
- Kopczyńska, E.E., Fiala, M., and Jeandel, C. (1998) Annual and interannual variability in phytoplankton at a permanent station off Kerguelen Islands, Southern Ocean. *Polar Biol* **20**: 342–351.
- Korb, R.E. and Whitehouse, M. (2004) Contrasting primary production regimes around South Georgia, Southern Ocean: large blooms versus high nutrient, low chlorophyll waters. *Deep Sea Res Part Oceanogr Res Pap* **51**: 721–738.
- Korb, R.E., Whitehouse, M.J., Atkinson, A., and Thorpe, S.E. (2008) Magnitude and maintenance of the phytoplankton bloom at South Georgia: a naturally iron-replete environment. *Mar Ecol Prog Ser* **368**: 75–91.
- Korb, R.E., Whitehouse, M.J., Ward, P., Gordon, M., Venables, H.J., and Poulton, A.J. (2012) Regional and seasonal differences in microplankton biomass, productivity, and structure across the Scotia Sea: implications for the export of biogenic carbon. *Deep Sea Res Part II Top Stud Oceanogr* **59–60**: 67–77.
- Kunin, V., Engelbrektsen, A., Ochman, H., and Hugenholtz, P. (2010) Wrinkles in the rare biosphere: pyrosequencing errors can lead to artificial inflation of diversity estimates. *Environ Microbiol* **12**: 118–123.
- Laender, F.D., Oevelen, D.V., Soetaert, K., and Middelburg, J.J. (2010) Carbon transfer in a herbivore- and microbial loop-dominated pelagic food webs in the southern Barents Sea during spring and summer. *Mar Ecol Prog Ser* **398**: 93–107.
- Lafond, A., Leblanc, K., Cornet, V., Legras, J., and Queguiner, B. (submitted) The structure of diatom communities constrains biogeochemical properties in surface waters of the Southern Ocean (Kerguelen Plateau). *J Mar Syst*.
- Laglera, L.M., Tovar-Sánchez, A., Iversen, M.H., González, H.E., Naik, H., Mangesh, G., et al. (2017) Iron partitioning during LOHAFEX: copepod grazing as a major driver for iron recycling in the Southern Ocean. *Mar Chem* **196**: 148–161.
- Lamb, P.D., Hunter, E., Pinnegar, J.K., Creer, S., Davies, R.G., and Taylor, M.I. (2019) How quantitative is metabarcoding: a meta-analytical approach. *Mol Ecol* **28**: 420–430.
- Landry, M.R., Constantinou, J., Latasa, M., Brown, S.L., Bidigare, R.R., and Ondrusek, M.E. (2000) Biological response to iron fertilization in the eastern equatorial Pacific (IronEx II). III. Dynamics of phytoplankton growth and microzooplankton grazing. *Mar Ecol Prog Ser* **201**: 57–72.
- Landschützer, P., Gruber, N., Haumann, F.A., Rödenbeck, C., Bakker, D.C.E., Heuven, S. van, et al. (2015) The reinvigoration of the Southern Ocean carbon sink. *Science* **349**: 1221–1224.
- Lange, M., Chen, Y.-Q., and Medlin, L.K. (2002) Molecular genetic delineation of *Phaeocystis* species (Prymnesiophyceae) using coding and non-coding regions of nuclear and plastid genomes. *Eur J Phycol* **37**: 77–92.
- Lasbleiz, M., Leblanc, K., Armand, L.K., Christaki, U., Georges, C., Obernosterer, I., and Quéguiner, B. (2016) Composition of diatom communities and their contribution to plankton biomass in the naturally iron-fertilized region of Kerguelen in the Southern Ocean. *FEMS Microbiol Ecol* **92**:

- Latasa, M., Landry, M.R., Louise, S., and Bidigare, R.R. (1997) Pigment specific growth and grazing rates of phytoplankton in the central equatorial Pacific. *Limnol Oceanogr* **42**: 289–298.
- Latasa, M., Morán, X.A.G., Scharek, R., and Estrada, M. (2005) Estimating the carbon flux through main phytoplankton groups in the northwestern Mediterranean. *Limnol Oceanogr* **50**: 1447–1458.
- Laurenceau-Cornec, E.C., Trull, T.W., Davies, D.M., Bray, S.G., Doran, J., Planchon, F., et al. (2015a) The relative importance of phytoplankton aggregates and zooplankton fecal pellets to carbon export: insights from free-drifting sediment trap deployments in naturally iron-fertilised waters near the Kerguelen Plateau. *Biogeosciences* **12**: 1007–1027.
- Laurenceau-Cornec, E.C., Trull, T.W., Davies, D.M., Bray, S.G., Doran, J., Planchon, F., et al. (2015b) The relative importance of phytoplankton aggregates and zooplankton fecal pellets to carbon export: insights from free-drifting sediment trap deployments in naturally iron-fertilised waters near the Kerguelen Plateau.
- Laws, E.A. (2013) Evaluation of *in situ* phytoplankton growth rates: a synthesis of data from varied approaches. *Annu Rev Mar Sci* **5**: 247–268.
- Laws, E.A., D'Sa, E., and Naik, P. (2011) Simple equations to estimate ratios of new or export production to total production from satellite-derived estimates of sea surface temperature and primary production. *Limnol Oceanogr Methods* **9**: 593–601.
- Le Moigne, F.A.C., Henson, S.A., Cavan, E., Georges, C., Pabortsava, K., Achterberg, E.P., et al. (2016) What causes the inverse relationship between primary production and export efficiency in the Southern Ocean? *Geophys Res Lett* **43**: 4457–4466.
- Lee, C.K., Herbold, C.W., Polson, S.W., Wommack, K.E., Williamson, S.J., McDonald, I.R., and Cary, S.C. (2012) Groundtruthing next-gen sequencing for microbial ecology-biases and errors in community structure estimates from PCR amplicon pyrosequencing. *PLoS One* **7**: e44224.
- van Leeuwe, M.A., Kattner, G., van Oijen, T., de Jong, J.T.M., and de Baar, H.J.W. (2015) Phytoplankton and pigment patterns across frontal zones in the Atlantic sector of the Southern Ocean. *Mar Chem* **177**: 510–517.
- van Leeuwe, M.A., Visser, R.J.W., and Stefels, J. (2014) The pigment composition of *Phaeocystis antarctica* (Haptophyceae) under various conditions of light, temperature, salinity, and iron. *J Phycol* **50**: 1070–1080.
- Legendre, L. and Le Fèvre, J. (1995) Microbial food webs and the export of biogenic carbon in oceans. *Aquat Microb Ecol* **9**: 69–77.
- Leliaert, F., Smith, D.R., Moreau, H., Herron, M.D., Verbruggen, H., Delwiche, C.F., and De Clerck, O. (2012) Phylogeny and molecular evolution of the green algae. *Crit Rev Plant Sci* **31**: 1–46.
- Leynaert, A., Bucciarelli, E., Claquin, P., Dugdale, R.C., Martin-Jézéquel, V., Pondaven, P., and Ragueneau, O. (2004) Effect of iron deficiency on diatom cell size and silicic acid uptake kinetics. *Limnol Oceanogr* **49**: 1134–1143.
- Li, T., Wu, T.-D., Mazéas, L., Toffin, L., Guerquin-Kern, J.-L., Leblon, G., and Bouchez, T. (2008) Simultaneous analysis of microbial identity and function using NanoSIMS. *Environ Microbiol* **10**: 580–588.
- Li, W.K.W. (1994) Primary production of prochlorophytes, cyanobacteria, and eucaryotic ultraphytoplankton: measurements from flow cytometric sorting. *Limnol Oceanogr* **39**: 169–175.

- Li, W.K.W., McLaughlin, F.A., Lovejoy, C., and Carmack, E.C. (2009) Smallest algae thrive as the Arctic Ocean freshens. *Science* **326**: 539.
- Litchman, E. and Klausmeier, C.A. (2008) Trait-based community ecology of phytoplankton. *Annu Rev Ecol Evol Syst* **39**: 615–639.
- Litchman, E., Klausmeier, C.A., Schofield, O.M., and Falkowski, P.G. (2007) The role of functional traits and trade-offs in structuring phytoplankton communities: scaling from cellular to ecosystem level. *Ecol Lett* **10**: 1170–1181.
- Litchman, E., Pinto, P. de T., Edwards, K.F., Klausmeier, C.A., Kremer, C.T., and Thomas, M.K. (2015) Global biogeochemical impacts of phytoplankton: a trait-based perspective. *J Ecol* **103**: 1384–1396.
- Liu, H., Probert, I., Uitz, J., Claustre, H., Aris-Brosou, S., Frada, M., et al. (2009) Extreme diversity in noncalcifying haptophytes explains a major pigment paradox in open oceans. *Proc Natl Acad Sci* **106**: 12803–12808.
- Liu, L., Liu, M., Wilkinson, D.M., Chen, H., Yu, X., and Yang, J. (2017) DNA metabarcoding reveals that 200-  $\mu$ m-size-fractionated filtering is unable to discriminate between planktonic microbial and large eukaryotes. *Mol Ecol Resour* **17**: 991–1002.
- Liu, Y., Blain, S., Crispi, O., Rembauville, M., and Obernosterer, I. (2020) Seasonal dynamics of prokaryotes and their associations with diatoms in the Southern Ocean as revealed by an autonomous sampler. *Environ Microbiol* **In press**.
- Logares, R., Audic, S., Bass, D., Bittner, L., Boutte, C., Christen, R., et al. (2014) Patterns of rare and abundant marine microbial eukaryotes. *Curr Biol* **24**: 813–821.
- Losa, S.N., Dutkiewicz, S., Losch, M., Oelker, J., Soppa, M.A., Trimborn, S., et al. (2019) On modeling the Southern Ocean phytoplankton functional types, Biogeochemistry: Open Ocean.
- MacIntyre, H.L., Kana, T.M., and Geider, R.J. (2000) The effect of water motion on short-term rates of photosynthesis by marine phytoplankton. *Trends Plant Sci* **5**: 12–17.
- Mackey, M.D., Mackey, D.J., Higgins, H.W., and Wright, S.W. (1996) CHEMTAX—a program for estimating class abundances from chemical markers: application to HPLC measurements of phytoplankton. *Mar Ecol Prog Ser* **144**: 265–283.
- Madsen, E.L. (2005) Identifying microorganisms responsible for ecologically significant biogeochemical processes. *Nat Rev Microbiol* **3**: 439–446.
- Maiti, K., Charette, M.A., Buesseler, K.O., and Kahru, M. (2013) An inverse relationship between production and export efficiency in the Southern Ocean. *Geophys Res Lett* **40**: 1557–1561.
- Manno, C., Stowasser, G., Enderlein, P., Fielding, S., and Tarling, G.A. (2015) The contribution of zooplankton faecal pellets to deep-carbon transport in the Scotia Sea (Southern Ocean). *Biogeosciences* **12**: 1955–1965.
- Maranger, R., Bird, D.F., and Price, N.M. (1998) Iron acquisition by photosynthetic marine phytoplankton from ingested bacteria. *Nature* **396**: 248–251.
- Marañón, E., Steele, J., Thorpe, A., and Turekian, K. (2009) Phytoplankton size structure. *Elem Phys Oceanogr Deriv Encycl Ocean Sci* **85**.
- Marchetti, A., Parker, M.S., Moccia, L.P., Lin, E.O., Arrieta, A.L., Ribalet, F., et al. (2009) Ferritin is used for iron storage in bloom-forming marine pennate diatoms. *Nature* **457**: 467–470.
- Marra, J. (2009) Net and gross productivity: weighing in with  $^{14}\text{C}$ . *Aquat Microb Ecol* **56**: 123–131.
- Martin, J.H. (1990) Glacial-interglacial  $\text{CO}_2$  change: The Iron Hypothesis. *Paleoceanography* **5**: 1–13.

- Martin, P., Loeff, M.R. van der, Cassar, N., Vandromme, P., d'Ovidio, F., Stemmann, L., et al. (2013) Iron fertilization enhanced net community production but not downward particle flux during the Southern Ocean iron fertilization experiment LOHAFEX. *Glob Biogeochem Cycles* **27**: 871–881.
- Massana, R., del Campo, J., Sieracki, M.E., Audic, S., and Logares, R. (2014) Exploring the uncultured microeukaryote majority in the oceans: reevaluation of ribogroups within stramenopiles. *ISME J* **8**: 854–866.
- Massana, R. and Pedrós-Alió, C. (2008) Unveiling new microbial eukaryotes in the surface ocean. *Curr Opin Microbiol* **11**: 213–218.
- Mayali, X. (2020) NanoSIMS: microscale quantification of biogeochemical activity with large-scale impacts. *Annu Rev Mar Sci* **12**: 449–467.
- McGlynn, S.E., Chadwick, G.L., Kempes, C.P., and Orphan, V.J. (2015) Single cell activity reveals direct electron transfer in methanotrophic consortia. *Nature* **526**: 531–535.
- McKie-Krisberg, Z.M., Gast, R.J., and Sanders, R.W. (2015) Physiological responses of three species of Antarctic mixotrophic phytoflagellates to changes in light and dissolved nutrients. *Microb Ecol* **70**: 21–29.
- McKie-Krisberg, Z.M. and Sanders, R.W. (2014) Phagotrophy by the picoeukaryotic green alga *Micromonas*: implications for Arctic Oceans. *ISME J* **8**: 1953–1961.
- Mendes, C.R.B., Tavano, V.M., Dotto, T.S., Kerr, R., de Souza, M.S., Garcia, C.A.E., and Secchi, E.R. (2018) New insights on the dominance of cryptophytes in Antarctic coastal waters: a case study in Gerlache Strait. *Deep Sea Res Part II Top Stud Oceanogr* **149**: 161–170.
- Michaels, A.F. and Silver, M.W. (1988) Primary production, sinking fluxes and the microbial food web. *Deep Sea Res Part Oceanogr Res Pap* **35**: 473–490.
- Mills, M.M., Kropuenske, L.R., van Dijken, G.L., Alderkamp, A.-C., Berg, G.M., Robinson, D.H., et al. (2010) Photophysiology in two Southern Ocean phytoplankton taxa: photosynthesis of *Phaeocystis antarctica* (prymnesiophyceae) and *Fragilariopsis cylindrus* (Bacillariophyceae) under simulated mixed-layer irradiance. *J Phycol* **46**: 1114–1127.
- Mine Berg, G., Glibert, P.M., and Chen, C.-C. (1999) Dimension effects of enclosures on ecological processes in pelagic systems. *Limnol Oceanogr* **44**: 1331–1340.
- Moline, M.A., Claustre, H., Frazer, T.K., Schofield, O., and Vernet, M. (2004) Alteration of the food web along the Antarctic Peninsula in response to a regional warming trend. *Glob Change Biol* **10**: 1973–1980.
- Mongin, M., Molina, E., and Trull, T.W. (2008) Seasonality and scale of the Kerguelen plateau phytoplankton bloom: a remote sensing and modeling analysis of the influence of natural iron fertilization in the Southern Ocean. *Deep Sea Res Part II Top Stud Oceanogr* **55**: 880–892.
- Moore, C.M., Seeyave, S., Hickman, A.E., Allen, J.T., Lucas, M.I., Planquette, H., et al. (2007) Iron–light interactions during the CROZet natural iron bloom and EXport experiment (CROZEX) I: Phytoplankton growth and photophysiology. *Deep Sea Res Part II Top Stud Oceanogr* **54**: 2045–2065.
- Moore, J.K., Abbott, M.R., and Richman, J.G. (1999) Location and dynamics of the Antarctic Polar Front from satellite sea surface temperature data. *J Geophys Res Oceans* **104**: 3059–3073.
- Moran, M.A. (2015) The global ocean microbiome. *Science* **350**:
- Morard, R., Darling, K.F., Mahé, F., Audic, S., Ujiie, Y., Weiner, A.K.M., et al. (2015) PFR2: a curated database of planktonic foraminifera 18S ribosomal DNA as a resource for studies of plankton ecology, biogeography and evolution. *Mol Ecol Resour* **15**: 1472–1485.

- Mordret, S., Piredda, R., Vaultot, D., Montresor, M., Kooistra, W.H.C.F., and Sarno, D. (2018) dinoref: a curated dinoflagellate (Dinophyceae) reference database for the 18S rRNA gene. *Mol Ecol Resour.*
- Moreira, D. and López-García, P. (2002) The molecular ecology of microbial eukaryotes unveils a hidden world. *Trends Microbiol* **10**: 31–38.
- Mosseri, J., Quéguiner, B., Armand, L., and Cornet-Barthaux, V. (2008) Impact of iron on silicon utilization by diatoms in the Southern Ocean: a case study of Si/N cycle decoupling in a naturally iron-enriched area. *Deep Sea Res Part II Top Stud Oceanogr* **55**: 801–819.
- Musat, N., Foster, R., Vagner, T., Adam, B., and Kuypers, M.M.M. (2012) Detecting metabolic activities in single cells, with emphasis on nanoSIMS. *FEMS Microbiol Rev* **36**: 486–511.
- Musat, N., Halm, H., Winterholler, B., Hoppe, P., Peduzzi, S., Hillion, F., et al. (2008) A single-cell view on the ecophysiology of anaerobic phototrophic bacteria. *Proc Natl Acad Sci* **105**: 17861–17866.
- Musat, N., Stryhanyuk, H., Bombach, P., Adrian, L., Audinot, J.-N., and Richnow, H.H. (2014) The effect of FISH and CARD-FISH on the isotopic composition of <sup>13</sup>C- and <sup>15</sup>N-labeled *Pseudomonas putida* cells measured by nanoSIMS. *Syst Appl Microbiol* **37**: 267–276.
- Needham, D.M., Sachdeva, R., and Fuhrman, J.A. (2017) Ecological dynamics and co-occurrence among marine phytoplankton, bacteria and myoviruses shows microdiversity matters. *ISME J* **11**: 1614–1629.
- Not, F., Latasa, M., Marie, D., Cariou, T., Vaultot, D., and Simon, N. (2004) A single species, *Micromonas pusilla* (Prasinophyceae), dominates the eukaryotic picoplankton in the Western English Channel. *Appl Environ Microbiol* **70**: 4064–4072.
- Not, F., Simon, N., Biegala, I.C., and Vaultot, D. (2002) Application of fluorescent *in situ* hybridization coupled with tyramide signal amplification (FISH TSA) to assess eukaryotic picoplankton composition. *Aquat Microb Ecol* **28**: 157–166.
- Nunes, S., Latasa, M., Delgado, M., Emelianov, M., Simó, R., and Estrada, M. (2019) Phytoplankton community structure in contrasting ecosystems of the Southern Ocean: South Georgia, South Orkneys and western Antarctic Peninsula. *Deep Sea Res Part Oceanogr Res Pap* **151**: 103059.
- Nuñez, J., Renslow, R., Cliff, J.B., and Anderton, C.R. (2017) NanoSIMS for biological applications: current practices and analyses. *Biointerphases* **13**: 03B301.
- Nutman, A.P., Bennett, V.C., Friend, C.R.L., Van Kranendonk, M.J., and Chivas, A.R. (2016) Rapid emergence of life shown by discovery of 3,700-million-year-old microbial structures. *Nature* **537**: 535–538.
- Nygaard, K. and Tobiesen, A. (1993) Bacterivory in algae: a survival strategy during nutrient limitation. *Limnol Oceanogr* **38**: 273–279.
- O’Kelly, C.J., Sieracki, M.E., Thier, E.C., and Hobson, I.C. (2003) A transient bloom of *Ostreococcus* (Chlorophyta, Prasinophyceae) in West Neck Bay, Long Island, New York. *J Phycol* **39**: 850–854.
- Olofsson, M., Robertson, E.K., Edler, L., Arneborg, L., Whitehouse, M.J., and Ploug, H. (2019) Nitrate and ammonium fluxes to diatoms and dinoflagellates at a single cell level in mixed field communities in the sea. *Sci Rep* **9**: 1424.
- Orphan, V.J., House, C.H., Hinrichs, K.U., McKeegan, K.D., and DeLong, E.F. (2001) Methane-consuming archaea revealed by directly coupled isotopic and phylogenetic analysis. *Science* **293**: 484–487.
- Palmer, J.R. and Totterdell, I.J. (2001) Production and export in a global ocean ecosystem model. *Deep Sea Res Part Oceanogr Res Pap* **48**: 1169–1198.

- Park, Y.-H., Charriaud, E., Pino, D.R., and Jeandel, C. (1998) Seasonal and interannual variability of the mixed layer properties and steric height at station KERFIX, southwest of Kerguelen. *J Mar Syst* **17**: 571–586.
- Park, Y.-H., Roquet, F., Durand, I., and Fuda, J.-L. (2008) Large-scale circulation over and around the Northern Kerguelen Plateau. *Deep Sea Res Part II Top Stud Oceanogr* **55**: 566–581.
- Pasulka, A.L., Thamatrakoln, K., Kopf, S.H., Guan, Y., Poulos, B.R., Moradian, A., et al. (2017) Interrogating marine virus-host interactions and elemental transfer with BONCAT and nanoSIMS-based methods. *Environ Microbiol* **20**: 671–692.
- Pauthenet, E., Roquet, F., Madec, G., Guinet, C., Hindell, M., McMahon, C.R., et al. (2018) Seasonal meandering of the Polar Front upstream of the Kerguelen Plateau. *Geophys Res Lett* **45**: 9774–9781.
- Pedrés-Alió, C. (2007) Dipping into the rare biosphere. *Science* **315**: 192–193.
- Pei, S. and Laws, E.A. (2013) Does the <sup>14</sup>C method estimate net photosynthesis? Implications from batch and continuous culture studies of marine phytoplankton. *Deep Sea Res Part Oceanogr Res Pap* **82**: 1–9.
- Penna, A.D., Trull, T.W., Wotherspoon, S., Monte, S.D., Johnson, C.R., and d’Ovidio, F. (2018) Mesoscale variability of conditions favoring an iron-induced diatom bloom downstream of the Kerguelen Plateau. *J Geophys Res Oceans* **123**: 3355–3367.
- Peperzak, L., Colijn, F., Gieskes, W.W.C., and Peeters, J.C.H. (1998) Development of the diatom-*Phaeocystis* spring bloom in the Dutch coastal zone of the North Sea: the silicon depletion versus the daily irradiance threshold hypothesis. *J Plankton Res* **20**: 517–537.
- Pérez, V., Fernández, E., Marañón, E., Morán, X.A.G., and Zubkov, M.V. (2006) Vertical distribution of phytoplankton biomass, production and growth in the Atlantic subtropical gyres. *Deep Sea Res Part Oceanogr Res Pap* **53**: 1616–1634.
- Pernthaler, A., Pernthaler, J., and Amann, R. (2002) Fluorescence in situ hybridization and catalyzed reporter deposition for the identification of marine bacteria. *Appl Environ Microbiol* **68**: 3094–3101.
- Pierella Karlusich, J.J., Ibarbalz, F.M., and Bowler, C. (2020) Phytoplankton in the Tara Ocean. *Annu Rev Mar Sci* **12**: 233–265.
- Planchon, F., Ballas, D., Cavagna, A.-J., Bowie, A.R., Davies, D., Trull, T., et al. (2015) Carbon export in the naturally iron-fertilized Kerguelen area of the Southern Ocean based on the <sup>234</sup>Th approach. *Biogeosciences* **12**: 3831–3848.
- Ploug, H., Musat, N., Adam, B., Moraru, C.L., Lavik, G., Vagner, T., et al. (2010) Carbon and nitrogen fluxes associated with the cyanobacterium *Aphanizomenon* sp. in the Baltic Sea. *ISME J* **4**: 1215–1223.
- Pollard, R.T., Salter, I., Sanders, R.J., Lucas, M.I., Moore, C.M., Mills, R.A., et al. (2009) Southern Ocean deep-water carbon export enhanced by natural iron fertilization. *Nature* **457**: 577–580.
- Polovina, J.J., Howell, E.A., and Abecassis, M. (2008) Ocean’s least productive waters are expanding. *Geophys Res Lett* **35**.
- Poulin, F.J. and Franks, P.J.S. (2010) Size-structured planktonic ecosystems: constraints, controls and assembly instructions. *J Plankton Res* **32**: 1121–1130.
- Poulton, A.J., Holligan, P.M., Hickman, A., Kim, Y.-N., Adey, T.R., Stinchcombe, M.C., et al. (2006) Phytoplankton carbon fixation, chlorophyll-biomass and diagnostic pigments in the Atlantic Ocean. *Atl Merid Transect* **53**: 1593–1610.

- Poulton, A.J., Mark Moore, C., Seeyave, S., Lucas, M.I., Fielding, S., and Ward, P. (2007) Phytoplankton community composition around the Crozet Plateau, with emphasis on diatoms and *Phaeocystis*. *Deep Sea Res Part II Top Stud Oceanogr* **54**: 2085–2105.
- Prodan, A., Tremaroli, V., Brolin, H., Zwinderman, A.H., Nieuwdorp, M., and Levin, E. (2020) Comparing bioinformatic pipelines for microbial 16S rRNA amplicon sequencing. *PLoS ONE* **15**:
- Pruesse, E., Quast, C., Knittel, K., Fuchs, B.M., Ludwig, W., Peplies, J., and Glöckner, F.O. (2007) SILVA: a comprehensive online resource for quality checked and aligned ribosomal RNA sequence data compatible with ARB. *Nucleic Acids Res* **35**: 7188–7196.
- Quéguiner, B. (2013) Iron fertilization and the structure of planktonic communities in high nutrient regions of the Southern Ocean. *Deep Sea Res Part II Top Stud Oceanogr* **90**: 43–54.
- Quéré, C.L., Rödenbeck, C., Buitenhuis, E.T., Conway, T.J., Langenfelds, R., Gomez, A., et al. (2007) Saturation of the Southern Ocean CO<sub>2</sub> sink due to recent climate change. *Science* **316**: 1735–1738.
- Quigg, A., Finkel, Z.V., Irwin, A.J., Rosenthal, Y., Ho, T.-Y., Reinfelder, J.R., et al. (2003) The evolutionary inheritance of elemental stoichiometry in marine phytoplankton. *Nature* **425**: 291–294.
- Quince, C., Lanzen, A., Davenport, R.J., and Turnbaugh, P.J. (2011) Removing noise from pyrosequenced amplicons. *BMC Bioinformatics* **12**: 38.
- Raven, J.A. (1987) The role of vacuoles. *New Phytol* **106**: 357–422.
- Raven, J.A. (1998) The twelfth Tansley Lecture. Small is beautiful: the picophytoplankton. *Funct Ecol* **12**: 503–513.
- Reddington, K., Eccles, D., O’Grady, J., Drown, D.M., Hansen, L.H., Nielsen, T.K., et al. (2020) Metagenomic analysis of planktonic riverine microbial consortia using nanopore sequencing reveals insight into river microbe taxonomy and function. *GigaScience* **9**:
- Rembauville, M., Blain, S., Armand, L., Quéguiner, B., and Salter, I. (2015) Export fluxes in a naturally iron-fertilized area of the Southern Ocean – Part 2: importance of diatom resting spores and faecal pellets for export. *Biogeosciences* **12**: 3171–3195.
- Rembauville, M., Briggs, N., Ardyna, M., Uitz, J., Catala, P., Penkerch, C., et al. (2017) Plankton assemblage estimated with BGC-Argo Floats in the Southern Ocean: implications for seasonal successions and particle export. *J Geophys Res Oceans* **122**: 8278–8292.
- Rembauville, M., Manno, C., Tarling, G.A., Blain, S., and Salter, I. (2016) Strong contribution of diatom resting spores to deep-sea carbon transfer in naturally iron-fertilized waters downstream of South Georgia. *Deep Sea Res Part Oceanogr Res Pap* **115**: 22–35.
- Rembauville, M., Salter, I., Leblond, N., Gueneugues, A., and Blain, S. (2015) Export fluxes in a naturally iron-fertilized area of the Southern Ocean – Part 1: seasonal dynamics of particulate organic carbon export from a moored sediment trap. *Biogeosciences* **12**: 3153–3170.
- Richardson, T.L. (2018) Mechanisms and pathways of small-phytoplankton export from the surface ocean. *Annu Rev Mar Sci* **11**: 57–74.
- Richardson, T.L. and Jackson, G.A. (2007) Small phytoplankton and carbon export from the surface ocean. *Science* **315**: 838–840.
- Rii, Y.M., Karl, D.M., and Church, M.J. (2016) Temporal and vertical variability in picophytoplankton primary productivity in the North Pacific Subtropical Gyre. *Mar Ecol Prog Ser* **562**: 1–18.



- Riou, V., Périot, M., and Biegala, I.C. (2017) Specificity re-evaluation of oligonucleotide probes for the detection of marine picoplankton by Tyramide Signal Amplification-Fluorescent In Situ Hybridization. *Front Microbiol* **8**:
- Robinson, J., Popova, E.E., Srokosz, M.A., and Yool, A. (2016) A tale of three islands: downstream natural iron fertilization in the Southern Ocean. *J Geophys Res Oceans* **121**: 3350–3371.
- Roca-Martí, M., Puigcorbé, V., Iversen, M.H., van der Loeff, M.R., Klaas, C., Cheah, W., et al. (2017) High particulate organic carbon export during the decline of a vast diatom bloom in the Atlantic sector of the Southern Ocean. *Deep Sea Res Part II Top Stud Oceanogr* **138**: 102–115.
- Rodríguez-Martínez, R., Labrenz, M., del Campo, J., Forn, I., Jürgens, K., and Massana, R. (2009) Distribution of the uncultured protist MAST-4 in the Indian Ocean, Drake Passage and Mediterranean Sea assessed by real-time quantitative PCR. *Environ Microbiol* **11**: 397–408.
- Rousseaux, C. and Gregg, W. (2013) Interannual variation in phytoplankton primary production at a global scale. *Remote Sens* **6**: 1–19.
- Roy, S., Llewellyn, C.A., Egeland, E.S., and Johnsen, G. (2011) Phytoplankton pigments: characterization, chemotaxonomy and applications in oceanography, Cambridge University Press.
- Roy, S., Sathyendranath, S., Bouman, H., and Platt, T. (2013) The global distribution of phytoplankton size spectrum and size classes from their light-absorption spectra derived from satellite data. *Remote Sens Environ* **139**: 185–197.
- Rozema, P.D., Biggs, T., Sprong, P.A.A., Buma, A.G.J., Venables, H.J., Evans, C., et al. (2017) Summer microbial community composition governed by upper-ocean stratification and nutrient availability in northern Marguerite Bay, Antarctica. *Deep Sea Res Part II Top Stud Oceanogr* **139**: 151–166.
- Sáez, A.G., Probert, I., Geisen, M., Quinn, P., Young, J.R., and Medlin, L.K. (2003) Pseudo-cryptic speciation in coccolithophores. *Proc Natl Acad Sci* **100**: 7163.
- Salter, I., Kemp, A.E.S., Moore, C.M., Lampitt, R.S., Wolff, G.A., and Holtvoeth, J. (2012) Diatom resting spore ecology drives enhanced carbon export from a naturally iron-fertilized bloom in the Southern Ocean. *Glob Biogeochem Cycles* **26**:
- Sánchez-Baracaldo, P., Raven, J.A., Pisani, D., and Knoll, A.H. (2017) Early photosynthetic eukaryotes inhabited low-salinity habitats. *Proc Natl Acad Sci* **114**: E7737–E7745.
- Sarmiento, J.L., Slater, R., Barber, R., Bopp, L., Doney, S.C., Hirst, A.C., et al. (2004) Response of ocean ecosystems to climate warming. *Glob Biogeochem Cycles* **18**: n/a-n/a.
- Sarthou, G., Timmermans, K.R., Blain, S., and Tréguer, P. (2005) Growth physiology and fate of diatoms in the ocean: a review. *J Sea Res* **53**: 25–42.
- Sassenhagen, I., Irion, S., Jardillier, L., Moreira, D., and Christaki, U. (2020) Protist interactions and community structure during early autumn in the Kerguelen Region (Southern Ocean). *Protist* **171**: 125709.
- Savoie, N., Trull, T.W., Jacquet, S.H.M., Navez, J., and Dehairs, F. (2008) <sup>234</sup>Th-based export fluxes during a natural iron fertilization experiment in the Southern Ocean (KEOPS). *Deep Sea Res Part II Top Stud Oceanogr* **55**: 841–855.
- Schoemann, V., Becquevort, S., Stefels, J., Rousseau, V., and Lancelot, C. (2005) *Phaeocystis* blooms in the global ocean and their controlling mechanisms: a review. *J Sea Res* **53**: 43–66.

- Schulz, I., Montresor, M., Klaas, C., Assmy, P., Wolzenburg, S., Gauns, M., et al. (2018) Remarkable structural resistance of a nanoflagellate-dominated plankton community to iron fertilization during the Southern Ocean experiment LOHAFEX. *Mar Ecol Prog Ser* **601**: 77–95.
- Seeyave, S., Lucas, M.I., Moore, C.M., and Poulton, A.J. (2007) Phytoplankton productivity and community structure in the vicinity of the Crozet Plateau during austral summer 2004/2005. *Deep Sea Res Part II Top Stud Oceanogr* **54**: 2020–2044.
- Sheik, A.R., Brussaard, C.P.D., Lavik, G., Foster, R.A., Musat, N., Adam, B., and Kuypers, M.M.M. (2013) Viral infection of *Phaeocystis globosa* impedes release of chitinous star-like structures: quantification using single cell approaches: single cell view on virally infected *P. globosa*. *Environ Microbiol* **15**: 1441–1451.
- Sherr, E.B. and Sherr, B.F. (2009) Capacity of herbivorous protists to control initiation and development of mass phytoplankton blooms. *Aquat Microb Ecol* **57**: 253–262.
- Sicko-Goad, L.M., Schelske, C.L., and Stoermer, E.F. (1984) Estimation of intracellular carbon and silica content of diatoms from natural assemblages using morphometric techniques. *Limnol Oceanogr* **29**: 1170–1178.
- Simmons, M.P., Bachy, C., Sudek, S., van Baren, M.J., Sudek, L., Ares, M., and Worden, A.Z. (2015) Intron invasions trace algal speciation and reveal nearly identical Arctic and Antarctic *Micromonas* populations. *Mol Biol Evol* **32**: 2219–2235.
- Simon, N., Campbell, L., Ornlófsdóttir, E., Groben, R., Guillou, L., Lange, M., and Medlin, L.K. (2000) Oligonucleotide probes for the identification of three algal groups by dot blot and fluorescent whole-cell hybridization. *J Eukaryot Microbiol* **47**: 76–84.
- Sitch, S., Friedlingstein, P., Gruber, N., Jones, S.D., Murray-Tortarolo, G., Ahlström, A., et al. (2015) Recent trends and drivers of regional sources and sinks of carbon dioxide. *Biogeosciences* **12**: 653–679.
- Smetacek, V. (2008) Are declining Antarctic krill stocks a result of global warming or of the decimation of the whales? In *Impacts of global warming on Polar ecosystems*. Bilbao: Fundación BBVA.
- Smetacek, V., Assmy, P., and Henjes, J. (2004) The role of grazing in structuring Southern Ocean pelagic ecosystems and biogeochemical cycles. *Antarct Sci* **16**: 541–558.
- Smetacek, V., Klaas, C., Strass, V.H., Assmy, P., Montresor, M., Cisewski, B., et al. (2012) Deep carbon export from a Southern Ocean iron-fertilized diatom bloom. *Nature* **487**: 313–319.
- Smetacek, V., Scharek, R., and Nöthig, E.-M. (1990) Seasonal and regional variation in the pelagial and its relationship to the life history cycle of krill. In *Antarctic Ecosystems*. Kerry, K.R. and Hempel, G. (eds). Springer Berlin Heidelberg, pp. 103–114.
- Smith, W.O., Dennett, M.R., Mathot, S., and Caron, D.A. (2003) The temporal dynamics of the flagellated and colonial stages of *Phaeocystis antarctica* in the Ross Sea. *Deep Sea Res Part II Top Stud Oceanogr* **50**: 605–617.
- Sournia, A., Chrdtinnot-Dinet, M.-J., and Ricard, M. (1991) Marine phytoplankton: how many species in the world ocean? *J Plankton Res* **13**: 1093–1099.
- Steeemann Nielsen, E. (1955) The interaction of photosynthesis and respiration and its importance for the determination of <sup>14</sup>C-discrimination in photosynthesis. *Physiol Plant* **8**: 945–953.
- Steeemann Nielsen, E. (1952) The use of radio-active carbon (C<sup>14</sup>) for measuring organic production in the sea. *ICES J Mar Sci* **18**: 117–140.
- Stoecker, D.K., Hansen, P.J., Caron, D.A., and Mitra, A. (2017) Mixotrophy in the marine plankton. *Annu Rev Mar Sci* **9**: 311–335.

- Stoll, H. (2020) 30 years of the iron hypothesis of ice ages. *Nature* **578**: 370–371.
- Strom, S.L., Macri, E.L., and Olson, M.B. (2007) Microzooplankton grazing in the coastal Gulf of Alaska: Variations in top-down control of phytoplankton. *Limnol Oceanogr* **52**: 1480–1494.
- Stukel, M.R. and Landry, M.R. (2010) Contribution of picophytoplankton to carbon export in the equatorial Pacific: a reassessment of food web flux inferences from inverse models. *Limnol Oceanogr* **55**: 2669–2685.
- Sunagawa, S., Coelho, L.P., Chaffron, S., Kultima, J.R., Labadie, K., Salazar, G., et al. (2015) Structure and function of the global ocean microbiome. *Science* **348**:
- Sunda, W.G. and Huntsman, S.A. (1997) Interrelated influence of iron, light and cell size on marine phytoplankton growth. *Nature* **390**: 389–392.
- Sutherland, K.R., Madin, L.P., and Stocker, R. (2010) Filtration of submicrometer particles by pelagic tunicates. *Proc Natl Acad Sci* **107**: 15129.
- Symondson, W.O.C. and Harwood, J.D. (2014) Special issue on molecular detection of trophic interactions: unpicking the tangled bank. *Mol Ecol* **23**: 3601–3604.
- Tang, K.W., Jr, W.O.S., Elliott, D.T., and Shields, A.R. (2008) Colony size of *Phaeocystis antarctica* (Prymnesiophyceae) as influenced by zooplankton grazers. *J Phycol* **44**: 1372–1378.
- Teira, E., Mouriño, B., Marañón, E., Pérez, V., Pazó, M.J., Serret, P., et al. (2005) Variability of chlorophyll and primary production in the Eastern North Atlantic Subtropical Gyre: potential factors affecting phytoplankton activity. *Deep Sea Res Part Oceanogr Res Pap* **52**: 569–588.
- Thiele, S., Wolf, C., Schulz, I.K., Assmy, P., Metfies, K., and Fuchs, B.M. (2014) Stable composition of the nano- and picoplankton community during the ocean iron fertilization experiment LOHAFEX. *PLOS ONE* **9**: e113244.
- Thompson, A.W., Foster, R.A., Krupke, A., Carter, B.J., Musat, N., Vaultot, D., et al. (2012) Unicellular cyanobacterium symbiotic with a single-celled eukaryotic alga. *Science* **337**: 1546–1550.
- Tilstone, G.H., Lange, P.K., Misra, A., Brewin, R.J.W., and Cain, T. (2017) Micro-phytoplankton photosynthesis, primary production and potential export production in the Atlantic Ocean. *Atl Merid Transect Programme 1995-2016* **158**: 109–129.
- Tréguer, P., Bowler, C., Moriceau, B., Dutkiewicz, S., Gehlen, M., Aumont, O., et al. (2018) Influence of diatom diversity on the ocean biological carbon pump. *Nat Geosci* **11**: 27–37.
- Tréguer, P.J. (2014) The Southern Ocean silica cycle. *Comptes Rendus Geosci* **346**: 279–286.
- Tsuji, Y. and Yoshida, M. (2017) Chapter seven - Biology of haptophytes: complicated cellular processes driving the global carbon cycle. In *Advances in Botanical Research*. Secondary Endosymbioses. Hirakawa, Y. (ed). Academic Press, pp. 219–261.
- Turner, J.T. (2015) Zooplankton fecal pellets, marine snow, phytodetritus and the ocean's biological pump. *Prog Oceanogr* **130**: 205–248.
- Tyrrell, T. and Merico, A. (2004) *Emiliania huxleyi*: bloom observations and the conditions that induce them. In *Coccolithophores*. Springer, pp. 75–97.
- Uitz, J., Claustre, H., Gentili, B., and Stramski, D. (2010) Phytoplankton class-specific primary production in the world's oceans: seasonal and interannual variability from satellite observations. *Glob Biogeochem Cycles* **24**:
- Uitz, J., Claustre, H., Griffiths, F.B., Ras, J., Garcia, N., and Sandroni, V. (2009) A phytoplankton class-specific primary production model applied to the Kerguelen Islands region (Southern Ocean). *Deep Sea Res Part Oceanogr Res Pap* **56**: 541–560.

- Venables, H. and Moore, C.M. (2010) Phytoplankton and light limitation in the Southern Ocean: learning from high-nutrient, high-chlorophyll areas. *J Geophys Res Oceans* **115**:
- Verity, P.G., Robertson, C.Y., Tronzo, C.R., Andrews, M.G., Nelson, J.R., and Sieracki, M.E. (1992) Relationships between cell volume and the carbon and nitrogen content of marine photosynthetic nanoplankton. *Limnol Oceanogr* **37**: 1434–1446.
- Vernet, M., Richardson, T.L., Metfies, K., Nöthig, E.-M., and Peeken, I. (2017) Models of plankton community changes during a warm water anomaly in Arctic waters show altered trophic pathways with minimal changes in carbon export. *Front Mar Sci* **4**:
- Waite, A.M., Safi, K.A., Hall, J.A., and Nodder, S.D. (2000) Mass sedimentation of picoplankton embedded in organic aggregates. *Limnol Oceanogr* **45**: 87–97.
- Wang, S., Bailey, D., Lindsay, K., Moore, J.K., and Holland, M. (2014) Impact of sea ice on the marine iron cycle and phytoplankton productivity. *Biogeosciences* **11**: 4713–4731.
- Ward, B.A., Dutkiewicz, S., Jahn, O., and Follows, M.J. (2012) A size-structured food-web model for the global ocean. *Limnol Oceanogr* **57**: 1877–1891.
- Ward, B.A., Marañón, E., Sauterey, B., Rault, J., and Claessen, D. (2017) The size dependence of phytoplankton growth rates: a trade-off between nutrient uptake and metabolism. *Am Nat* **189**: 170–177.
- Weber, L.H. and El-Sayed, S.Z. (1987) Contributions of the net, nano- and picoplankton to the phytoplankton standing crop and primary productivity in the Southern Ocean. *J Plankton Res* **9**: 973–994.
- Wilson, S. and Steinberg, D. (2010) Autotrophic picoplankton in mesozooplankton guts: evidence of aggregate feeding in the mesopelagic zone and export of small phytoplankton. *Mar Ecol Prog Ser* **412**: 11–27.
- Wisecaver, J.H. and Hackett, J.D. (2011) Dinoflagellate genome evolution. *Annu Rev Microbiol* **65**: 369–387.
- Wolf, C., Frickenhaus, S., Kiliyas, E.S., Peeken, I., and Metfies, K. (2014) Protist community composition in the Pacific sector of the Southern Ocean during austral summer 2010. *Polar Biol* **37**: 375–389.
- Worden, A.Z., Follows, M.J., Giovannoni, S.J., Wilken, S., Zimmerman, A.E., and Keeling, P.J. (2015) Rethinking the marine carbon cycle: factoring in the multifarious lifestyles of microbes. *Science* **347**:
- Wright, S.W., van den Enden, R.L., Pearce, I., Davidson, A.T., Scott, F.J., and Westwood, K.J. (2010) Phytoplankton community structure and stocks in the Southern Ocean (30–80 E) determined by CHEMTAX analysis of HPLC pigment signatures. *Deep Sea Res Part II Top Stud Oceanogr* **57**: 758–778.
- Wright, S.W., Ishikawa, A., Marchant, H.J., Davidson, A.T., van den Enden, R.L., and Nash, G.V. (2009) Composition and significance of picophytoplankton in Antarctic waters. *Polar Biol* **32**: 797–808.
- Wright, S.W. and Jeffrey, S.W. (1987) Fucoxanthin pigment markers of marine phytoplankton analysed by HPLC and HPTLC. *Mar Ecol Prog Ser* **38**: 259–266.
- Wright, S.W., Thomas, D., Marchant, H., Higgins, H., Mackey, M., and Mackey, D. (1996) Analysis of phytoplankton of the Australian sector of the Southern Ocean: comparisons of microscopy and size frequency data with interpretations of pigment HPLC data using the CHEMTAX matrix factorisation program. *Mar Ecol Prog Ser* **144**: 285–298.
- Yoon, J.-E., Yoo, K.-C., Macdonald, A.M., Yoon, H.-I., Park, K.-T., Yang, E.J., et al. (2018) Reviews and syntheses: Ocean iron fertilization experiments – past, present, and future looking to

- a future Korean Iron Fertilization Experiment in the Southern Ocean (KIFES) project. *Biogeosciences* **15**: 5847–5889.
- Zaoli, S., Giometto, A., Marañón, E., Escrig, S., Meibom, A., Ahluwalia, A., et al. (2019) Generalized size scaling of metabolic rates based on single-cell measurements with freshwater phytoplankton. *Proc Natl Acad Sci* **116**: 17323–17329.
- Zhu, Z., Xu, K., Fu, F., Spackeen, J.L., Bronk, D.A., and Hutchins, D.A. (2016) A comparative study of iron and temperature interactive effects on diatoms and *Phaeocystis antarctica* from the Ross Sea, Antarctica. *Mar Ecol Prog Ser* **550**: 39–51.
- Zimmermann, M., Escrig, S., Hübschmann, T., Kirf, M.K., Brand, A., Inglis, R.F., et al. (2015) Phenotypic heterogeneity in metabolic traits among single cells of a rare bacterial species in its natural environment quantified with a combination of flow cell sorting and NanoSIMS. *Front Microbiol* **6**: 1–11.
- Zubkov, M.V. and Tarran, G.A. (2008) High bacterivory by the smallest phytoplankton in the North Atlantic Ocean. *Nature* **455**: 224–226.



